

RHEOLOGY AND STABILITY OF MAGNETITE DENSE MEDIA

by

BERNHARD KLEIN

B.A.Sc, The University of British Columbia, 1985

**A THESIS SUBMITTED IN PARTIAL FULFILMENT OF
THE REQUIREMENTS FOR THE DEGREE OF
DOCTOR OF PHILOSOPHY**

in

THE FACULTY OF GRADUATE STUDIES

Department of Mining and Mineral Process Engineering

We accept this thesis as conforming
to the required standard

THE UNIVERSITY OF BRITISH COLUMBIA

May 1992

© Bernhard Klein, 1992

National Library
of Canada

Canadian Theses Service

Bibliothèque nationale
du Canada

Service des thèses canadiennes

NOTICE

THE QUALITY OF THIS MICROFICHE
IS HEAVILY DEPENDENT UPON THE
QUALITY OF THE THESIS SUBMITTED
FOR MICROFILMING.

UNFORTUNATELY THE COLOURED
ILLUSTRATIONS OF THIS THESIS
CAN ONLY YIELD DIFFERENT TONES
OF GREY.

AVIS

LA QUALITE DE CETTE MICROFICHE
DEPEND GRANDEMENT DE LA QUALITE DE LA
THESE SOUMISE AU MICROFILMAGE.

MALHEUREUSEMENT, LES DIFFERENTES
ILLUSTRATIONS EN COULEURS DE CETTE
THESE NE PEUVENT DONNER QUE DES
TEINTES DE GRIS.

In presenting this thesis in partial fulfilment of the requirements for an advanced degree at the University of British Columbia, I agree that the Library shall make it freely available for reference and study. I further agree that permission for extensive copying of this thesis for scholarly purposes may be granted by the head of my department or by his or her representatives. It is understood that copying or publication of this thesis for financial gain shall not be allowed without my written permission.

Department of Mining & Mineral Process Engineering

The University of British Columbia
Vancouver, Canada

Date May 6, 1992

ABSTRACT

The efficiency of the dense medium separation process is known to depend on the rheology and stability of the medium. In particular, the medium should exhibit a low viscosity and a high settling stability. Despite this knowledge, little information existed on these medium properties. The lack of information stems partially from the difficulties associated with measuring the rheological properties of unstable suspensions. In order to measure these properties, it was necessary to design a rheometer for settling suspensions. Once this was achieved, the rheology and stability of magnetite suspensions were characterized and the influences of various medium parameters on these properties were investigated.

Settling experiments revealed that magnetite dense media exhibit bulk zone settling properties that are characterized by the presence of (from top to bottom): a supernatant, a transition zone, a constant density zone and a sediment. The constant density zone was found to have a solids content that was the same as that of the initial suspension. Test results indicated that the suspension mudline settled at approximately the same rate as the constant density zone and should therefore provide a good indication of the media stability.

Based on knowledge of the settling properties of magnetite suspensions, a rheometer fixture was designed that could be used to measure the rheological properties of such suspensions. The fixture is an elongated double gap concentric cylinder cup and bob arrangement that positions the bob in the constant density zone of the settling suspension during measurements.

Rheological measurements revealed that magnetite dense media exhibits yield shear thinning and thixotropic flow properties. The Casson flow curve model was found to fit the rheological flow curves for these suspensions better than other well known models.

Investigations into the effects of various parameters on medium rheology and stability revealed that solids content, magnetite particle size and, in the presence of clays, pH are the most important suspension variables. Other parameters that significantly affect the suspension properties include magnetization, dispersing agents and the presence of clay and fine coal contaminants. Several of these parameters significantly affected the Casson yield stress, while only a few parameters affected the Casson viscosity, indicating that the yield stress is the most controllable rheological parameter. In addition, over the tested shear rate range, the yield stress term contributed much more to the apparent viscosity of the suspensions than the Casson viscosity term, and is therefore the most important rheological property. It was also found that the yield stress is inversely related to the mudline settling rate such that when the yield stress is high the settling rate is low and vice versa.

Investigations into the effect of particle size distribution on the properties of magnetite dense media revealed that media properties can be improved by using bimodal particle size distributions. In particular, at low medium densities, where stability is of concern, the size ratio of the two particle fractions and the proportion of fine magnetite particles were found to have a large effect on the settling rate. At high medium densities, where the media can be excessively viscous, optimum size ratios and proportions of fine particles can be selected to reduce the suspension Casson yield stress.

TABLE OF CONTENTS

ABSTRACT	ii
TABLE OF CONTENTS	iv
LIST OF TABLES	x
LIST OF FIGURES	xii
TABLE OF SYMBOLS	xix
ACKNOWLEDGEMENTS	xxii
CHAPTER 1: INTRODUCTION	1
CHAPTER 2: OBJECTIVES	2
CHAPTER 3: SCOPE AND IMPORTANCE	3
A: LITERATURE REVIEW	4
CHAPTER 4: DENSE MEDIUM SEPARATION	4
4.1 Applications and Importance	4
4.2 Principle of Separation	6
4.3 Process Flowsheets	12
4.4 Factors Affecting Separation Performance	15
4.5 Effect of Medium Properties on Separation Performance	16
4.5.1 Static Separators	17
4.5.2 Dynamic Separators	20
CHAPTER 5: MAGNETITE CHARACTERIZATION	26
5.1 Introduction	26
5.2 Mineralogy and Geological Deposition	26
5.3 Craigmont Magnetite Production	28
5.4 Physical and Chemical Properties	28
CHAPTER 6: RHEOLOGICAL MEASUREMENTS	34
6.1 Rheological Measuring Devices	34
6.2 Concentric Cylinder Rheometry	36
6.2.1 Flow Geometry	36
6.2.2 Measurement Errors	41
6.2.2.1 Effect of Particle Settling	41

	6.2.2.2 Other Errors	44
6.3	Yield Stress Measurements	47
CHAPTER 7:	RHEOLOGY OF SUSPENSIONS	51
7.1	Introduction	51
7.2	Time Independent Flow	52
7.2.1	Characterization of Flow Behaviour	52
7.2.2	Flow Curve Modelling	55
	7.2.2.1 Newton's Viscosity Law	57
	7.2.2.2 The Power-Law Model	58
	7.2.2.3 The Cross Model	59
	7.2.2.4 The Carreau Model	61
	7.2.2.5 The Bingham Plastic Model	62
	7.2.2.6 The Herschel Bulkley Model	63
	7.2.2.7 The Casson Model	64
7.3	Time Dependent Flow	65
7.4	Visco-elasticity	68
CHAPTER 8:	CONTROL OF RHEOLOGICAL PROPERTIES	69
8.1	Introduction	69
8.2	Micro-rheology	69
	8.2.1 Hydrodynamic Effects	70
	8.2.2 Granuloviscous Effects	73
	8.2.3 Electroviscous Effects	73
	8.2.4 Aggregation Effects	74
8.3	Physico-mechanical Parameters	78
	8.3.1 Solids Content	78
	8.3.2 Particle Density	83
	8.3.3 Particle Shape	85
	8.3.4 Particle Size	87
	8.3.5 Particle Size Distribution	90
8.4	Physico-chemical Parameters	94
	8.4.1 pH and Dissolved Ions	94
	8.4.2 Dispersing Agents	96
CHAPTER 9:	RHEOLOGY OF MAGNETITE DENSE MEDIA	98
9.1	Introduction	98
9.2	Characterization	98
9.3	Control of Medium Properties	99
	9.3.1 Physico-Mechanical Parameters	100
	9.3.1.1 Solids Content	100
	9.3.1.2 Particle Size	101
	9.3.1.3 Particle Size Distribution	103
	9.3.1.4 Particle Roughness and Shape	103

9.3.2	Physico-Chemical Parameters	104
9.3.2.1	pH and Dissolved Ions	104
9.3.2.2	Dispersing Agents	105
9.3.2.3	Magnetization	106
9.3.3	Contamination	108
CHAPTER 10:	STABILITY OF MAGNETITE DENSE MEDIA	110
10.1	Introduction	110
10.2	Settling in Suspensions	110
10.3	Measurement of Stability	114
10.4	Settling Properties of Magnetite Dense Media	115
CHAPTER 11:	SUMMARY OF LITERATURE REVIEW	117
SECTION B:	EXPERIMENTAL PROGRAM	120
CHAPTER 12:	EXPERIMENTAL PLAN	120
12.1	Introduction	120
12.2	Measuring Rheological Properties of Settling Suspensions	120
12.3	Rheology and Stability of Magnetite Dense Media	121
12.4	Effect of Parameters on Medium Properties	122
12.5	Effect of Particle Size Distribution on Medium Properties	123
CHAPTER 13:	SAMPLE PREPARATION AND CHARACTERIZATION OF MATERIALS	125
13.1	Introduction	125
13.2	Magnetite Characterization Procedures	125
13.2.1	Density Determination	125
13.2.2	Size Analyses	126
13.2.3	Magnetics Content	128
13.2.4	Electrophoretic Mobility	128
13.2.5	Chemical Composition	129
13.2.6	Magnetic Properties	129
13.3	Magnetite Sample	130
13.3.1	Preparation of Magnetite Sample	130
13.3.2	Characterization of Upgraded Magnetite Sample	132
13.3.2.1	Magnetite Density	132
13.3.2.2	Particle Size Distribution	135
13.3.2.3	Electrophoretic Mobility	139
13.3.2.4	Magnetics Content	142
13.3.2.5	Elemental Analyses	142
13.3.2.6	Magnetic Properties	146
13.3.3	Preparation of Size Fractions	148
13.3.4	Characterization of Size Ranges	150

	13.3.4.1 Size Analysis of Size Fractions	151
	13.3.4.2 Density of Size Fractions	151
	13.3.4.3 Elemental Composition of the Size Fractions	151
	13.3.5 Preparation of Narrow Size Fractions	155
	13.3.6 Characterization of Narrow Size Fractions	155
	13.3.6.1 Size Analyses of the Narrow Size Fractions	157
	13.3.6.2 Densities of Narrow Size Fractions	157
	13.3.6.3 Elemental Composition of Size Fractions	157
13.4	Chemical Reagents and Medium Contaminants	162
	13.4.1 pH Modifiers	162
	13.4.2 Organic Dispersants	162
	13.4.3 Inorganic Dispersants	163
	13.4.4 Medium Contaminants	163
CHAPTER 14:	SETTLING PROPERTIES OF MAGNETITE DENSE MEDIA	165
14.1	Introduction	165
14.2	Mudline Falling Rate	165
	14.2.1 Procedure for Mudline Falling Rate Determinations	165
	14.2.2 Results of Interface Settling Tests	166
14.3	Solids Concentration Profile	169
	14.3.1 Procedure for Solids Concentration Profile Determinations	169
	14.3.2 Solids Concentration Profile Results	170
14.4	Conclusions	174
CHAPTER 15:	RHEOMETER FIXTURE FOR SETTLING SUSPENSIONS	175
15.1	Introduction	175
15.2	Details of the Fixture Design	177
15.3	Fixture Dimensions	182
15.4	Calibration of the Fixture	183
15.5	Fixture Evaluation	185
	15.5.1 Effect of Shaft and Spokes on Measured Stresses	187
	15.5.2 Particle Settling in the Elongated Fixture	191
15.6	The Rheological Measurement Procedures	203
	15.6.1 Measurement Time Periods	203
	15.6.2 Shear Rate Measurement Range	205
	15.6.3 Non-Newtonian Shear Rate Corrections	206
15.7	Conclusions	209
CHAPTER 16:	RHEOLOGICAL PROPERTIES OF MAGNETITE DENSE MEDIA	210
16.1	Introduction	210
16.2	Flow Behaviour of Magnetite Dense Media	210
16.3	Flow Curve Modelling	211
	16.3.1 Model Fitting	214
	16.3.2 Model Discrimination	221

16.4	Time Dependent Flow Properties	224
16.5	Conclusions	228
CHAPTER 17:	EFFECT OF PHYSICO-MECHANICAL AND PHYSICO-CHEMICAL PARAMETERS ON MEDIUM PROPERTIES	229
17.1	Introduction	229
17.2	Determination of Parameter Levels	229
17.3	Experimental Design	240
17.4	Sample Preparation	244
17.5	Characterization of Medium Properties	247
17.6	Evaluation of the Effects on Medium Properties	251
17.7	Results of Experimental Program	252
17.7.1	Analyses of Measured Responses	254
17.7.2	Effects of Suspension Parameters on Medium Properties ..	258
17.7.2.1	Effect of Solids Concentration	259
17.7.2.2	Effect of Particle Size	260
17.7.2.3	Effect of Suspension pH	262
17.7.2.4	Effect of Magnetization	264
17.8	Conclusions	264
CHAPTER 18:	EFFECT OF PARTICLE SIZE DISTRIBUTION ON MEDIUM PROPERTIES	266
18.1	Introduction	266
18.2	Experimental Design	266
18.3	Experimental Procedure	270
18.4	Modelling the Effects of Particle Size Distribution	271
18.5	Analyses of Regression Models	274
18.5.1	Effect of Particle Size Distribution on the Casson Yield Stress	278
18.5.2	Effect of Particle Size Distribution on the Casson Viscosity	283
18.5.3	Effect of Particle Size Distribution on the Settling Rate ..	286
18.5.4	Optimization of Medium Properties	290
18.6	Conclusions	291
CHAPTER 19:	CONCLUSIONS AND RECOMMENDATIONS FOR FURTHER WORK	293
19.1	Conclusions	293
19.2	Recommendations For Further Work	299
REFERENCES	302
APPENDIX I	Publications Related to this Thesis	322

APPENDIX II	Program For Shear Rate Corrections	324
APPENDIX III	Simplex Optimization Program for Modelling Rheological Flow Curve Data	332
APPENDIX IV	Model Discrimination Program to Compare Fits of Rheological Flow Curve Models	345
APPENDIX V	Settling Curves and Modelled Rheological Flow Curves for Investigations into the Effects of Various Parameters on Media Properties	351
APPENDIX VI	Settling Curves and Modelled Rheological Flow Curves for Investigations into the Effects of Particle Size Distribution on Media Properties	412
APPENDIX VII	Statistical Analyses of Modelled Media Properties	429

LIST OF TABLES

Table 5.1	Recommended specifications for magnetite used in dense media (Osborne, 1988).	30
Table 8.1	Models describing relative viscosity as a function of solids content and maximum packing fraction.	81
Table 13.1	Magnetite samples considered for use in test work.	131
Table 13.2	Comparison of density measurement results for upgraded magnetite using wet pycnometer, air pycnometer and volumetric flask methods.	134
Table 13.3	Size analysis results for upgraded magnetite, determined using Horiba PSA, Elzone PSA and Cyclosizer.	137
Table 13.4	Elemental analyses of upgraded magnetite sample.	145
Table 13.5	Magnetic properties of the -400 mesh upgraded magnetite sample.	147
Table 13.6	Size analyses of -45 µm, -30 µm and -15 µm size fractions determined using the Horiba Particle Size Analyzer.	152
Table 13.7	Densities of the -45 µm, -30 µm and -15 µm size fractions determined using air pycnometer.	154
Table 13.8	Elemental analyses of the -45 µm, -30 µm and -15 µm size fractions.	156
Table 13.9	Size analyses of narrow size fractions determined using Elzone PSA and RRB size and distribution moduli.	158
Table 13.10	Densities of narrow size fractions determined using air pycnometer.	160
Table 13.11	Elemental analyses of the narrow size fractions.	161
Table 16.1	Rheological flow curve equations used to model flow curve data for magnetite suspensions.	215
Table 16.2	Coefficients of fitted rheological flow curve equations and R ² values.	216
Table 16.3	Results of model discrimination procedure to determine which flow curve equation best fit the rheological data.	223
Table 17.1	Levels of -325 mesh (45 µm) contaminants in dense media.	239
Table 17.2	Alias structure for fractional factorial design showing the confounded main effects, two factor interaction effects and three factor interaction effects.	243
Table 17.3	Coded levels for 2 ⁹⁻⁵ _{III} fractional factorial experimental design used to investigate the effects of suspension variables on rheology and stability.	245
Table 17.4	Variable levels corresponding to coded levels.	246
Table 17.5	Responses of rheological properties and settling properties for each of the experimental runs.	249
Table 17.6	Multiple index of determination values for each of the rheological equations fit to the measured flow curve data from the experimental program.	250
Table 17.7	Estimated effects of each variable for each of the determined responses.	253
Table 17.8	Statistically significant estimates of the effects in order of magnitude.	255
Table 18.1	Coded variable levels for central composite experimental design.	269

Table 18.2	Variable levels corresponding to coded levels.	269
Table 18.3	Settling rate, Casson yield stress and Casson viscosity responses for experimental program.	272
Table 18.4	Casson yield stress, Casson viscosity and settling rate coefficients for fitted second order models.	273
Table VII.1	Statistical analysis of the model for the Casson yield stress as a function of particle size distribution parameters.	430
Table VII.2	Statistical analysis of the model for the Casson viscosity as a function of particle size distribution parameters.	431
Table VII.3	Statistical analysis of the model for settling velocity as a function of particle size distribution parameters.	432

LIST OF FIGURES

Figure 4.1	Typical coal preparation process flowsheet using dense media separation.	13
Figure 4.2	Typical magnetite dense media recovery circuit (Osborne, 1988).	14
Figure 6.1	Geometry of a conventional cup and bob rheometer fixture.	37
Figure 6.2	Schematic showing settling of particles in a cup and bob rheometer fixture.	43
Figure 7.1	Schematic showing various types of flow behaviours a) Newtonian, b) Bingham plastic, c) shear thinning, d) yield shear thinning, e) dilatant, and f) yield dilatant.	54
Figure 7.2	Plot of two different flow curves that could be characterized by the same apparent viscosity.	56
Figure 8.1	Typical potential energy curve at the surface of a mineral particle.	76
Figure 13.1	Process flow sheet showing the procedure that was used to upgrade the magnetite sample.	133
Figure 13.2	RRB particle size distribution of upgraded magnetite sample measured using a) Horiba PSA, b) Elzone PSA and c) Cyclosizer.	138
Figure 13.3	Electrophoretic mobility of -10 μ m magnetite sample showing an iso-electric point in the pH range of 2.3.	141
Figure 13.4a	Scanning electron micrograph of magnetite particles.	143
Figure 13.4b	Energy dispersive x-ray analyzer spectrum for magnetite particles showing an iron peak and a distinct silica peak.	144
Figure 13.6	Scanning electron micrographs of a) magnetized (-75 μ m + 38 μ m) magnetite particles and b) magnetized -75 μ m magnetite particles.	149
Figure 13.7	RRB particle size distributions of -45 μ m, -30 μ m and -15 μ m magnetite samples determined using the Horiba PSA.	153
Figure 13.8	RRB particle size distributions for narrow size fractions of magnetite particles from Elzone PSA data.	159
Figure 14.1	Settling suspension of magnetite particles with a solids volume fraction of 15%. The photograph shows that the magnetite settles with a sharp supernatant/ suspension interface.	167
Figure 14.2	Magnetite suspension mudline interface height versus settling time showing three sets of data (solids volume fraction = 0.15, pH = 8.24, temperature = 25°C).	168
Figure 14.3	Volume solids fraction versus height in column of settling magnetite particles for settling times of zero minutes to ten minutes (solids volume fraction = 0.15, pH = 8.52, temperature = 25°C).	172
Figure 14.4	Magnetite volume solids content as a function of height and settling time showing settling zones (solids volume fraction - 0.15, pH = 8.52, temp.= 25°C).	173
Figure 15.1	Rheologic laboratory facility showing a) the Haake RV20 controller, b) the M5 viscometer, c) the PC and d) the temperature controller.	176
Figure 15.2	Rheometer fixture for settling suspensions showing the bob positioned	

	in the constant density zone of a settling suspension.	178
Figure 15.3	Plan view of a double concentric cylinder viscometer fixture.	181
Figure 15.4	Rheometer fixture for measuring rheological properties of settling suspensions showing a) the bob, b) the inner cylinder, and c) the cup.	184
Figure 15.5	Flow curves produced with the developed rheometer fixture, for 9.5 mPa.s and 50 mPa.s standard viscosity oils. Three sets of data were plotted for each oil.	186
Figure 15.6a	Photographs of the rheometer components: a) entire fixture, and b) shaft, spokes and cylindrical ring.	188
Figure 15.6b	Photographs of the rheometer components: c) shaft and spokes, and d) shaft.	189
Figure 15.7	Flow curves produced for 10 mPa.s standard viscosity oil using a) the entire bob, b) the shaft, spokes and cylindrical ring, c) the shaft and spokes, and d) the shaft.	190
Figure 15.8	Rheometer fixture for settling suspensions showing sampling points for solids content determinations during rheological measurements.	192
Figure 15.9	Constructed rheometer fixture for solids content determinations during rheological measurements.	193
Figure 15.10a	Solids concentration profile in the rheometer fixture at a settling time of 2 minutes determined while the bob was not rotating.	195
Figure 15.10b	Solids concentration profile in the rheometer fixture at a settling time of 4 minutes determined while the bob was not rotating.	196
Figure 15.10c	Solids concentration profile in the rheometer fixture at a settling time of 6 minutes determined while the bob was not rotating.	197
Figure 15.10d	Solids concentration profile in the rheometer fixture at a settling time of 8 minutes determined while the bob was not rotating.	198
Figure 15.11a	Solids concentration profile in the rheometer fixture at a settling time of 2 minutes determined while the bob was rotating at a shear rate of 500 s^{-1} .	199
Figure 15.11b	Solids concentration profile in the rheometer fixture at a settling time of 4 minutes determined while the bob was rotating at a shear rate of 500 s^{-1} .	200
Figure 15.11c	Solids concentration profile in the rheometer fixture at a settling time of 6 minutes determined while the bob was rotating at a shear rate of 500 s^{-1} .	201
Figure 15.11d	Solids concentration profile in the rheometer fixture at a settling time of 8 minutes determined while the bob was rotating at a shear rate of 500 s^{-1} .	202
Figure 15.12	Measurement of shear stress at shear rate equal to 500 s^{-1} versus time for a magnetite suspension with a solids volume fraction of 0.15.	204
Figure 15.13	Rheological flow curve for a magnetite suspension with 15% solids by volume showing apparent dilatant flow behaviour at shear rates greater than approximately 40 s^{-1} .	207
Figure 15.14	Flow curve for magnetite suspension (solids volume fraction = 0.15)	

	with uncorrected shear rate data (AB8), and corrected shear rate data (RAB8).	208
Figure 16.1a	Flow curve for magnetite suspension with a solids volume fraction of 0.15 showing a band of data points produced from three consecutive measurements on the same suspension.	212
Figure 16.1b	Apparent viscosity versus shear rate for a magnetite suspension with a solids volume fraction of 0.15 showing data points for three consecutive measurements on the same suspension.	213
Figure 16.2a	Rheological flow curve for a magnetite suspension with a solids volume fraction of 0.15 and fitted Casson model.	217
Figure 16.2b	Rheological flow curve for a magnetite suspension with a solids volume fraction of 0.15 and fitted Herschel Bulkley model.	218
Figure 16.2c	Rheological flow curve for a magnetite suspension with a solids volume fraction of 0.15 and fitted Carreau model.	219
Figure 16.2d	Rheological flow curve for a magnetite suspension with a solids volume fraction of 0.15 and fitted Cross model.	220
Figure 16.3	Flow curve hysteresis for demagnetized magnetite suspension with a solids volume fraction of 0.15.	225
Figure 16.4	Flow curve hysteresis for a suspension of magnetized magnetite particles (volume solids fraction = 0.15).	227
Figure 17.1	Effect of magnetite solids content on the settling rate.	231
Figure 17.2	Effect of particle size on settling rate of magnetite suspensions (volume solids fraction = 0.15).	232
Figure 17.3	Supernatant/slurry interface height as a function of time for magnetized and demagnetized magnetite suspensions with a solids volume fraction of 0.15.	233
Figure 17.4	The effect of pH on the settling rates of magnetite suspensions (volume solids fraction = 0.15).	235
Figure 17.5	Effect of carboxymethyl cellulose and dextran on the settling rates of magnetite suspensions (volume solids fraction = 0.15).	236
Figure 17.6	Effect of sodium hexametaphosphate and sodium silicate on the settling rates of magnetite suspensions (volume solids fraction = 0.15).	237
Figure 17.7	Effect of coal fines, kaolinite and bentonite content on the settling rate of magnetite suspensions with a volume solids fraction of 0.15.	241
Figure 17.8	Relationship between the Casson yield stress and the settling rate.	257
Figure 18.1	Predicted versus estimated Casson yield stress responses.	275
Figure 18.2	Predicted versus estimated Casson viscosity responses.	276
Figure 18.3	Predicted versus estimated settling rate responses.	277
Figure 18.4	Response contours of the Casson yield stress as a function of size ratio and fine fraction (magnetite volume solids content = 0.15).	279
Figure 18.5	Response contours of the Casson yield stress as a function of size ratio on fine fraction (magnetite volume solids content = 0.25).	280
Figure 18.6	Response contours of the Casson viscosity as a function of size ratio and volume solids fraction.	284

Figure 18.7	Response contours of the settling rate as a function of size ratio and fine fraction (magnetite volume solids fraction = 0.125).	287
Figure 18.8	Response contours of the settling rate as a function of size ratio and fine fraction(magnetite volume solids fraction = 0.175).	288
Figure 18.9	Relationship between the Casson yield stress and the settling rate.	289
Figure AV.1	Settling curve interface height as a function of time for experimental Run #1.	352
Figure AV.2	Rheological flow curve with fitted a) Herschel Bulkley and b) Casson models for experimental Run #1.	353
Figure AV.3	Rheological flow curve with fitted a) Carreau and b) Cross models for experimental Run #1.	354
Figure AV.4	Settling curve interface height as a function of time for experimental Run #2.	355
Figure AV.5	Rheological flow curve with fitted a) Herschel Bulkley and b) Casson models for experimental Run #2.	356
Figure AV.6	Rheological flow curve with fitted a) Carreau and b) Cross models for experimental Run #2.	357
Figure AV.7	Settling curve interface height as a function of time for experimental Run #3.	358
Figure AV.8	Rheological flow curve with fitted a) Herschel Bulkley and b) Casson models for experimental Run #3.	359
Figure AV.9	Rheological flow curve with fitted a) Carreau and b) Cross models for experimental Run #3.	360
Figure AV.10	Settling curve interface height as a function of time for experimental Run #4.	361
Figure AV.11	Rheological flow curve with fitted a) Herschel Bulkley and b) Casson models for experimental Run #4.	362
Figure AV.12	Rheological flow curve with fitted a) Carreau and b) Cross models for experimental Run #4.	363
Figure AV.13	Settling curve interface height as a function of time for experimental Run #5.	364
Figure AV.14	Rheological flow curve with fitted a) Herschel Bulkley and b) Casson models for experimental Run #5.	365
Figure AV.15	Rheological flow curve with fitted a) Carreau and b) Cross models for experimental Run #5.	366
Figure AV.16	Settling curve interface height as a function of time for experimental Run #6.	367
Figure AV.17	Rheological flow curve with fitted a) Herschel Bulkley and b) Casson models for experimental Run #6.	368
Figure AV.18	Rheological flow curve with fitted a) Carreau and b) Cross models for experimental Run #6.	369
Figure AV.19	Settling curve interface height as a function of time for experimental Run #7.	370
Figure AV.20	Rheological flow curve with fitted a) Herschel Bulkley and b) Casson	

	models for experimental Run #7.	371
Figure AV.21	Rheological flow curve with fitted a) Carreau and b) Cross models for experimental Run #7.	372
Figure AV.22	Settling curve interface height as a function of time for experimental Run #8.	373
Figure AV.23	Rheological flow curve with fitted a) Herschel Bulkley and b) Casson models for experimental Run #8.	374
Figure AV.24	Rheological flow curve with fitted a) Carreau and b) Cross models for experimental Run #8.	375
Figure AV.25	Settling curve interface height as a function of time for experimental Run #9.	376
Figure AV.26	Rheological flow curve with fitted a) Herschel Bulkley and b) Casson models for experimental Run #9.	377
Figure AV.27	Rheological flow curve with fitted a) Carreau and b) Cross models for experimental Run #9.	378
Figure AV.28	Settling curve interface height as a function of time for experimental Run #10.	379
Figure AV.29	Rheological flow curve with fitted a) Herschel Bulkley and b) Casson models for experimental Run #10.	380
Figure AV.30	Rheological flow curve with fitted a) Carreau and b) Cross models for experimental Run #10.	381
Figure AV.31	Settling curve interface height as a function of time for experimental Run #11.	382
Figure AV.32	Rheological flow curve with fitted a) Herschel Bulkley and b) Casson models for experimental Run #11.	383
Figure AV.33	Rheological flow curve with fitted a) Carreau and b) Cross models for experimental Run #11.	384
Figure AV.34	Settling curve interface height as a function of time for experimental Run #12.	385
Figure AV.34	Rheological flow curve with fitted a) Herschel Bulkley and b) Casson models for experimental Run #12.	386
Figure AV.36	Rheological flow curve with fitted a) Carreau and b) Cross models for experimental Run #12.	387
Figure AV.37	Settling curve interface height as a function of time for experimental Run #13.	388
Figure AV.38	Rheological flow curve with fitted a) Herschel Bulkley and b) Casson models for experimental Run #13.	389
Figure AV.39	Rheological flow curve with fitted a) Carreau and b) Cross models for experimental Run #13.	390
Figure AV.40	Settling curve interface height as a function of time for experimental Run #14.	391
Figure AV.41	Rheological flow curve with fitted a) Herschel Bulkley and b) Casson models for experimental Run #14.	392
Figure AV.42	Rheological flow curve with fitted a) Carreau and b) Cross models for	

	experimental Run #14.	393
Figure AV.43	Settling curve interface height as a function of time for experimental Run #15.	394
Figure AV.44	Rheological flow curve with fitted a) Herschel Bulkley and b) Casson models for experimental Run #15.	395
Figure AV.45	Rheological flow curve with fitted a) Carreau and b) Cross models for experimental Run #15.	396
Figure AV.46	Settling curve interface height as a function of time for experimental Run #16.	397
Figure AV.47	Rheological flow curve with fitted a) Herschel Bulkley and b) Casson models for experimental Run #16.	398
Figure AV.48	Rheological flow curve with fitted a) Carreau and b) Cross models for experimental Run #16.	399
Figure AV.49	Settling curve interface height as a function of time for experimental Run #17.	400
Figure AV.50	Rheological flow curve with fitted a) Herschel Bulkley and b) Casson models for experimental Run #18.	401
Figure AV.51	Rheological flow curve with fitted a) Carreau and b) Cross models for experimental Run #17.	402
Figure AV.52	Settling curve interface height as a function of time for experimental Run #18.	403
Figure AV.53	Rheological flow curve with fitted a) Herschel Bulkley and b) Casson models for experimental Run #18.	404
Figure AV.54	Rheological flow curve with fitted a) Carreau and b) Cross models for experimental Run #18.	405
Figure AV.55	Settling curve interface height as a function of time for experimental Run #19.	406
Figure AV.56	Rheological flow curve with fitted a) Herschel Bulkley and b) Casson models for experimental Run #19.	407
Figure AV.57	Rheological flow curve with fitted a) Carreau and b) Cross models for experimental Run #19.	408
Figure AV.58	Settling curve interface height as a function of time for experimental Run #20.	409
Figure AV.59	Rheological flow curve with fitted a) Herschel Bulkley and b) Casson models for experimental Run #20.	410
Figure AV.60	Rheological flow curve with fitted a) Carreau and b) Cross models for experimental Run #20.	411
Figure AVI.1	a) Settling curve and b) fitted (Casson model) flow curve for experimental Run #1 ($\phi_{sv}=0.25$, $\phi_f=0.40$, $d_s/d_i=0.39$, pH=8.08).	413
Figure AVI.2	a) Settling curve and b) fitted (Casson model) flow curve for experimental Run #2 ($\phi_{sv}=0.25$, $\phi_f=0.40$, $d_s/d_i=0.13$, pH=8.33).	414
Figure AVI.3	a) Settling curve and b) fitted (Casson model) flow curve for experimental Run #3 ($\phi_{sv}=0.25$, $\phi_f=0.25$, $d_s/d_i=0.39$, pH=8.38).	415
Figure AVI.4	a) Settling curve and b) fitted (Casson model) flow curve for	

	experimental Run #4 ($\phi_{sv}=0.25$, $\phi_r=0.25$, $d_s/d_i=0.13$, $pH=8.21$).	416
Figure AVL.5	a) Settling curve and b) fitted (Casson model) flow curve for experimental Run #5 ($\phi_{sv}=0.15$, $\phi_r=0.40$, $d_s/d_i=0.39$, $pH=8.17$).	417
Figure AVL.6	a) Settling curve and b) fitted (Casson model) flow curve for experimental Run #6 ($\phi_{sv}=0.15$, $\phi_r=0.40$, $d_s/d_i=0.13$, $pH=8.78$).	418
Figure AVL.7	a) Settling curve and b) fitted (Casson model) flow curve for experimental Run #7 ($\phi_{sv}=0.15$, $\phi_r=0.25$, $d_s/d_i=0.39$, $pH=8.42$).	419
Figure AVL.8	a) Settling curve and b) fitted (Casson model) flow curve for experimental Run #8 ($\phi_{sv}=0.15$, $\phi_r=0.25$, $d_s/d_i=0.13$, $pH=8.85$).	420
Figure AVL.9	a) Settling curve and b) fitted (Casson model) flow curve for experimental Run #9 ($\phi_{sv}=0.20$, $\phi_r=0.325$, $d_s/d_i=0.67$, $pH=8.25$).	421
Figure AVL.10	a) Settling curve and b) fitted (Casson model) flow curve for experimental Run #10 ($\phi_{sv}=0.20$, $\phi_r=0.325$, $d_s/d_i=0.09$, $pH=8.63$).	422
Figure AVL.11	a) Settling curve and b) fitted (Casson model) flow curve for experimental Run #11 ($\phi_{sv}=0.20$, $\phi_r=0.451$, $d_s/d_i=0.22$, $pH=8.35$).	423
Figure AVL.12	a) Settling curve and b) fitted (Casson model) flow curve for experimental Run #12 ($\phi_{sv}=0.20$, $\phi_r=0.199$, $d_s/d_i=0.22$, $pH=8.29$).	424
Figure AVL.13	a) Settling curve and b) fitted (Casson model) flow curve for experimental Run #13 ($\phi_{sv}=0.284$, $\phi_r=0.325$, $d_s/d_i=0.22$, $pH=8.27$).	425
Figure AVL.14	a) Settling curve and b) fitted (Casson model) flow curve for experimental Run #14 ($\phi_{sv}=0.116$, $\phi_r=0.325$, $d_s/d_i=0.22$, $pH=8.41$).	426
Figure AVL.15	a) Settling curve and b) fitted (Casson model) flow curve for experimental Run #15 ($\phi_{sv}=0.20$, $\phi_r=0.325$, $d_s/d_i=0.22$, $pH=8.42$).	427
Figure AVL.16	a) Settling curve and b) fitted (Casson model) flow curve for experimental Run #16 ($\phi_{sv}=0.20$, $\phi_r=0.325$, $d_s/d_i=0.22$, $pH=8.94$).	428

TABLE OF SYMBOLS

a, b, c, d, e, f	model coefficients
A	shear stress factor
A_i	model coefficient
C_D	particle drag coefficient
d	particle diameter
d_s	mean diameter of small particle fraction
d_l	mean diameter of large particle fraction
D	convective diffusion coefficient
D_r	rotational diffusion coefficient
D_t	translational diffusion coefficient
F_a	accelerating force
F_b	buoyant force
F_d	drag force
$F(d)$	cumulative per cent passing size d
$d_{63,2}$	size modulus
d_l	large particle diameter
d_s	small particle diameter
E_p	probable error
g	gravitational acceleration
m	distribution modulus
M	shear rate factor
h, h_b	bob height
H	column height
H	induced magnetic field
H_b	height from cup bottom to bob top
k, n	power law model coefficients
k_f, k_r	rate constant of structure formation and rupture, respectively
k_0, k_1	rate constants for rupture of linkages due to Brownian motion and shearing
\hat{l}_i	is the estimated values of the effect,
\hat{l}_0	is the mean effect,
L_i	value of effect
m	mass
m	polydispersity material constant

M	intensity of magnetization
N, \dot{N}	Krieger's parameters for shear rate calculation
p	Nguyen's parameter for shear rate calculation
Pe_r	rotational Peclet number
Pe_t	translational Peclet number
r	radius
r_1	inner radius of inner gap
r_2	outer radius of inner gap
r_3	inner radius of outer gap
r_4	outer radius of outer gap
r^*	shearing radius
R_b	bob radius
R_c	cup radius
Re	average particle Reynolds number
Re_{crit}	critical Reynolds number for turbulence between cup and bob
R_1	bob radius
R_2	cup radius
R^2	coefficient of multiple determination
S	measured particle surface area
\hat{S}	calculated surface area based on size
t	time
$t_{v,1-\alpha}$	t-statistic
T	torque
v	velocity
v_{tc}	settling rate transition zone/constant density zone interface
v_{cs}	settling rate constant density zone/sediment interface
v_t	tangential velocity
v_r	radial velocity
v_T	terminal velocity
$V(\hat{l}_i)$	variance of the estimated effects
V_b	bob peripheral velocity
V_{sb}	bob slip velocity
V_{sc}	cup slip velocity
X	magnetic susceptibility
X_i	level of variable i

Y	observed value
Y_i	measured response value for run i
\hat{Y}_1, \hat{Y}_2	predicted values from model one and two, respectively
Z	model discrimination variable
α	material constant
δ_{50}	separation density
ε	error
η	viscosity
η_{ap}	apparent Newtonian viscosity
γ	shear rate
η_C	Casson viscosity
η_N	Newtonian coefficient of viscosity
η_{pl}	plastic viscosity
η_r	relative viscosity
η_o	viscosity at zero shear rate
η_∞	viscosity at infinite shear rate
λ	structural factor
ρ_f	feed medium density
ρ_l	liquid density
ρ_p	particle density
ρ_u	underflow medium density
ϕ_f	fine fraction of total solids
ϕ, ϕ_{sv}	volume solids fraction
ϕ_{eff}	effective volume solids fraction
ϕ_m	maximum packing volume solids fraction
τ	shear stress
τ_{BY}	Bingham yield stress
τ_C	Casson yield stress
τ_{HB}	Herschel Bulkley yield stress
ω	angular velocity

ACKNOWLEDGEMENTS

The experiences gained during the time spent as a graduate student have been rewarding, interesting and enjoyable. The greatest reward was to become acquainted with the people that I have met and worked with. There is no doubt that without the support and assistance of these people, this document would never have been completed.

I am deeply indebted to Professor Janusz Laskowski whose guidance, drive and support were critical to the completion of this thesis. I would like to express sincere thanks to Professor Andrew Mular for his guidance with the statistical aspects of the experimental program. I would also like to thank Professor Ken Pinder for his useful comments and discussions regarding the subject of rheology and Professor George Poling whose comment "keep it short" sticks in my mind as I prepare to submit this volume.

I will miss the times spent working with Dr. Susan Partridge whose knowledge and input complemented by her personality made performing this work an enjoyable experience. For these reasons I am deeply indebted to her.

I would also like to thank: Mr. Frank Schmidiger for the precision in which he constructed the viscometer fixture; Mrs. Sally Finora for her technical assistance and for making sure I drank enough coffee; my class mates Andrew Burkert and Richard Senior who knew little about my subject which allowed us to talk about something else for a change; Miss Cindy Thom who proofread several sections of this document and who helped to prepare the figures; Mr. Reini Klein, my brother, who prepared the photographs for me; Dr. W. Gordon Bacon for allowing me to use the BDA facilities to write up the thesis; and Mary Gelinas, Tali Afgin and Dave Clark

who made time during the Christmas rush to assist in typing and assembling this document.

I would like to express my appreciation to the Natural Sciences and Engineering Research Council of Canada for providing the research grant and equipment grant that were necessary for this research program. I would also like to express my gratitude to Mr. W. Murray of the M7 group for providing the magnetite samples for the test work.

Finally, I would like to express appreciation to my wife, parents and siblings for their love and support. I dedicate this thesis to my wife, Maren Klein, without whom I would have not had a cause to work for.

CHAPTER 1: INTRODUCTION

Suspensions of fine magnetite in water are used in dense medium separation processes. These suspensions behave like dense liquids to relatively coarse mineral particles which, depending on their density, either float or sink. The properties of dense media, however, differ from those of a true liquid; they exhibit non-Newtonian rheology and the magnetite particles tend to settle producing non-homogeneous conditions.

Media rheology and sedimentation stability are known to influence separation performance of both static and dynamic separators. The rheology describes the resistance that a solid particle experiences as it moves towards the appropriate separator outlet; a greater resistance results in a lower separation efficiency. The stability describes the degree of stratification of magnetite particles in the separator. Particle settling causes the formation of density gradients and zones of varying medium density which can impair a sharp separation and thereby reduces the separation efficiency. It is therefore desirable to control both of these media properties so that the process performance can be optimized.

The rheology and stability of magnetite dense medium are affected by physico-mechanical and physico-chemical parameters, and the presence of contaminants. While physico-mechanical parameters describe the physical components of the system, the physico-chemical parameters describe the conditions that influence the inter-particle forces of attraction and repulsion. Contaminants, such as coal fines or clays, have a significant effect on the medium properties and must therefore also be considered. It is important to note that the rheology and stability can be controlled by manipulating the parameters, however, manipulating parameters to improve one of

the medium properties usually has an adverse effect on the other. It is therefore necessary to consider the effects of these parameters on both the rheology and stability.

While it is simple to measure and characterize settling properties, it is more difficult to measure the rheological properties of unstable suspensions. The stability can be characterized by the settling rate of the supernatant-slurry interface; a high stability corresponds to a low settling rate and vice versa. However, since particle settling leads to the formation of a solids concentration gradient in the measuring region of standard cup and bob rotational viscometers, it affects rheological measurements.

Since the overall objective of the dense medium related projects in the Department of Mining and Mineral Process Engineering included studies of the effect of media rheology on dense medium separation performance, improved methods of measuring dense media rheology and a better understanding of this subject were needed.

CHAPTER 2: OBJECTIVES

1. To develop a method to measure the rheology of settling suspensions.
2. To model and characterize the rheology of magnetite dense medium suspensions.
3. To characterize the stability of magnetite dense medium suspensions.
4. To study the relative significance of important controllable parameters that influence the dense medium rheology and stability.
5. To investigate the influence of particle size distribution on the dense medium rheology and stability.

CHAPTER 3: SCOPE AND IMPORTANCE

The research objectives, as outlined above, are to provide basic information that is needed to study further the relationship between magnetite suspension properties and dense medium separation performance. Specifically, a full and accurate characterization of the rheological properties of dense media will assist in determining their effect on process performance. Once the effects of these properties are understood, knowledge of how they can be manipulated will assist in optimizing the process efficiency. The ability to optimize separation efficiency through the control of media properties should benefit the processing of difficult-to-treat and fine coals.

The development of a method to measure accurately the rheological properties of settling suspensions may also significantly aid processing and handling of many industrially important disperse systems such as coal water slurries, flotation concentrates and tailings, and cyanidation pulps.

A: LITERATURE REVIEW

CHAPTER 4: DENSE MEDIUM SEPARATION

4.1 Applications and Importance

Due to the high efficiency and capacity of dense medium separation, it has become one of the most important processes for cleaning coal and concentrating mineral ores. In particular, the process has the capacity to produce sharp separations even in cases when the density difference between the products is small and when the ore contains large amounts of near density material (Osborne, 1988). In addition, dense medium separation is used to process efficiently a wide range of particle sizes. The ore feed size typically ranges from 0.5 mm to 12 mm for dynamic separators and from 12 mm to 75 mm for static ones (Burt, 1984). It has been shown that dynamic separators can be used efficiently to clean coal particles as fine as 75 μm (King and Juckes, 1984) and efforts to clean coal as fine as 15 μm have proven to be successful.

In addition to its application in coal preparation, dense medium separation is also used to process iron, diamond, potash, industrial mineral and sulphide and oxide base metal ores (Burt, 1984). For many of these applications, the process is used as a pre-concentration step (Burt, 1984, Aplan, 1989).

It was reported (Osborne, 1988) that in 1980, over 35% of all coal cleaned in Canada and the United States was processed using dense medium separation. In the United States, the application of the process for cleaning coal increased from 27.2% in 1975 to 39.0% in 1988

(Aplan, 1989). This trend is expected to continue because of the ability of the process to deal with fine coals at high separation efficiencies. The use of the process has increased worldwide as a result of the mining of more difficult-to-clean coals and the need to produce cleaner coal (Osborne, 1988).

The medium density is determined by the total mass of fine solids and water divided by their total volume. Magnetite (density = 4800 kg m^{-3} to 5200 kg m^{-3}) is typically used for medium with densities up to 2500 kg m^{-3} . At higher densities the medium becomes excessively viscous due to the high magnetite solids content. In this case higher density ferrosilicon (density 6700 kg m^{-3} to 6900 kg m^{-3}) is used to produce medium with densities up to 4000 kg m^{-3} . Mixtures of magnetite and ferrosilicon have also been used to produce a medium with suitable viscous properties while minimizing costs; ferrosilicon is significantly more expensive than magnetite. For coal preparation, where medium densities range from 1300 kg m^{-3} to 1900 kg m^{-3} , magnetite is typically used.

There is considerable interest in using dense medium separation to process fine coal ($-500 \mu\text{m}$) as a result of the need for an efficient process that can handle these fine sizes. This is particularly important for upgrading more difficult-to-clean coals, the removal of liberated pyrite, the deeper cleaning of coal to be used as coal/water slurries and coal/oil mixture fuels and the upgrading of oxidized coal fines. In addition, mechanized mining methods produce more fine coal than traditional methods resulting in an increased yield of fine material to be processed (Fourie et al, 1980, Killmeyer, 1982, Lathioor and Osborne, 1984, King and Juckes, 1984, 1988).

Several plants have demonstrated the successful application of the "cleaning to zero" concept using dense medium separation (Lathioor and Osborne, 1984, Burch and Stone, 1985).

The efficiency is, however, very dependent on the properties of the medium (Ferrara and Schena, 1988). Stoessner (1987) showed that cleaning the -500 μm fraction separately from the +500 μm fraction has many advantages with respect to separation efficiency because the medium properties could be better controlled for the specific size ranges.

The second largest application of the dense medium separation process is in concentrating iron ore. The high capacity of the process and its ability to make separations at high densities make it suitable for this application (Burt, 1984). In addition, the very high recovery efficiency of the process has resulted in its extensive use for diamond concentration in South Africa (Chaston and Napier-Munn, 1976). As mentioned, DMS has found specific applications for the processing of sulphide and oxide base metal ores and industrial mineral ores. Recently, there has been an increased interest to use dense medium separation to process potash ores (White and Littman, 1987). It was suggested that most new potash processing plants would install a dense medium circuit to produce a coarse grade product. The medium used for this application is a suspension of magnetite in brine.

4.2 Principle of Separation

It has long been known that suspensions of fine particles in water exhibit many properties that are similar to those of a dense liquid. In particular, such a suspension has the ability to allow particles with a lower density than the medium to float and those with a higher density to sink (DeVaney, Shelton, 1940). The first commercial application of this concept was the Chance process developed in 1918 (Chance, 1924). The process was advanced considerably with the

introduction of the Dutch State Mines dense medium cyclone in 1945 (Dreissen and Jennekens, 1982) that introduced centrifugal forces to the separation process. Dreissen and Jennekens (1982), Burt (1984) and Osborne (1988) provide a summary of chronological developments in the dense medium separation processes.

The forces responsible for the movement of particles in the medium are the accelerating force, the buoyancy force and the viscous drag force. The predominant accelerating force in static separators is due to gravity and in dynamic separators it is the result of centrifugal flow. From Newton's second law, the force balance on a solid particle in a dense suspension can be described by Equation 4.1.

$$m \frac{dv}{dt} = F_b + F_a + F_d \quad (4.1)$$

where, F_b is the buoyant force,

F_a is the accelerating force,

F_d is the drag force,

m is the mass of the particle, and

$\frac{dv}{dt}$ is the particle acceleration.

The buoyant and gravitational forces acting on a particle can be calculated from its volume and density. The drag force is described by the Navier-Stokes equation. However, because of the complexity of determining a rigorous solution to this equation, drag coefficients are used to describe these forces. Assuming the particle is spherical, the force balance in a gravitational field can be rewritten as in Equation 4.2.

$$m \frac{dv}{dt} = \frac{\pi d^3 g (\rho_p - \rho_l)}{6} - \frac{C_D \rho_l v^2 A}{2} \quad (4.2)$$

where d is the particle diameter,

g is the acceleration due to gravity,

ρ_p and ρ_l are the particle and liquid density,

C_D is the drag coefficient,

v is the particle velocity,

A is the surface area.

The terminal velocity, v_T , can be calculated from Equation 4.2 by setting the acceleration term to zero.

$$v_T = \left(\frac{4(\rho_p - \rho_l)gd}{3\rho_l C_D} \right)^{1/2} \quad (4.3)$$

where, $C_D = 24/Re$ for $Re < 0.1$

$C_D = 18.5/Re^{3/5}$ for $0.1 < Re < 1000$

$C_D = 0.445$ for $Re > 1000$ and,

$Re = \rho d v / \eta$, average particle Reynolds number (Schlichting, 1979).

For dynamic separators the predominant accelerating forces are due to centrifugal flow.

The force balance for particles in these separators can be written as follows (Yopps et al 1987):

$$m \frac{dv}{dt} = \frac{\pi d^3 v_r (\rho_p - \rho_l)}{6r} - C_D \rho_l v_r^2 A \quad (4.4)$$

where, r is radial position in the cyclone,

v_r is the radial velocity, and

v_t is the tangential velocity.

In dynamic separators, the particle radial velocity determines whether the particle reports to the overflow or to the underflow products. The terminal radial velocity can be determined by setting the acceleration term in equation (4.4) to zero ($dv/dt = 0$) (Equation 4.5).

$$v_r = \left(\frac{4(\rho_p - \rho_l)dv_t^2}{3\rho_l C_D r} \right)^{1/2} \quad (4.5)$$

These equations of motion describe the ideal movement of particles in a separator. The drag coefficient for an accelerating particle is, however, greater than that for a particle moving at steady terminal velocity (Schlichting, 1979). Since the time required to reach the terminal velocity is small, the velocity equation will adequately describe the movement of the particles. Based on appropriate estimates of the parameters, the equations can be used to estimate the Reynolds numbers for ore particles in dense media separators. Such an exercise reveals that in both static and dynamic separators the Reynolds numbers for small and near density particles are in the intermediate range ($0.1 < Re < 1000$) where viscosity is important to particle movement (Napier-Munn, 1990). Calculations also indicate that large particles with densities significantly greater than the medium experience turbulent flow. Napier-Munn (1990) fit of the form of Stokes equation to performance criteria (probable error and separation density). He found that the values of the fitted exponents for the viscosity and particle size terms were between values that represent laminar and turbulent flow regimes. These results therefore support the conclusion

that most particles move in the intermediate flow regime where viscosity is important.

The medium in both static and dynamic separators is constantly moving and flowing. As a result eddy flows are produced which affect the motion of coal/ore particles in the separator. The above equations do not account for this type of movement in the medium and therefore represent an ideal situation which may be quite different to that in separators.

In addition, the above equations have been derived for spherical particles moving in a Newtonian fluid. However, coal/ore particles are not spherical and dense media exhibits non-Newtonian properties. The correction for the non-spherical shape can be determined using a volume equivalent diameter and shape factor. The settling of a particle through a non-Newtonian fluid is a more complicated subject; the drag coefficient is a function of the apparent viscosity which changes with shear rate. The effective shear rate experienced by a spherical particle moving through a Newtonian fluid at low Reynolds numbers can be shown to equal $12v_T/d$. Based on this expression, the effective shear rates for small and near density particles (in static and dynamic separators) are in the range ($<100 \text{ s}^{-1}$) where the apparent viscosity is very dependent on shear rate.

Du Plessis and Ansley (1967) determined the relation between the drag coefficient and Bingham equation parameters (Equation 4.6). The relationship implies that the yield stress affects particle movement through its contribution to the apparent viscosity of the medium.

$$C_D = f \left(\frac{\frac{\eta_{pl} v}{d} + \tau_{BY}}{\rho_f v^2} \right) \quad (4.6)$$

where, η_{pl} the plastic viscosity, and

τ_{BY} is the Bingham yield stress according to the Bingham equation,

$$\tau = \tau_{BY} + \eta_{pl}\dot{\gamma} \quad (4.7)$$

where, τ is the shear stress and $\dot{\gamma}$ is the shear rate.

Lockyer et al (1980) determined the drag force as a function of the coefficients (k and n) for a power law fluid.

$$\tau = k\dot{\gamma}^n \quad (4.8)$$

$$F_d = 12\pi k A^2 \left(\frac{v}{2d} \right)^n f(n) \quad (4.9)$$

These expressions emphasize the need to relate separator performance to the complete rheological properties rather than to some estimate of a suitable apparent viscosity.

The magnitude of the forces on particles depends on the design of the separator and the operating conditions. Various static separators have been developed including the dense medium drum, vessel and bath in which the separating forces on the particles are due to gravitational acceleration. In dynamic separators, the centrifugal forces depend on the geometry of the separator. The main types of dynamic separators are the Dutch State Mines (DSM) cyclone, the Dynawhirlpool, the Tri-Flo, the Larcodem and the Vorsyl. A description of these separators can be found in Burt (1986) and Osborne (1988).

4.3 Process Flowsheets

Both static and dynamic dense medium separators are used in coal preparation plants. The static separators are applied to upgrade the coarse coal and dynamic separators have found applications in treating the intermediate size coal. The flowsheet for a typical coal preparation plant using both types of separators is shown in Figure 4.1. The flowsheet shows that the raw coal is classified into size fractions before feeding the separators. The coarse fraction +12 mm is fed to static separators, the 0.5 mm x 12 mm material is fed to dynamic separators and the fines (-0.5 mm) are upgraded using other processes such as water-only cyclones and flotation. It is important to de-slime the feed to the dense medium separators since fine material, such as clays, can adversely affect separation performance. Following upgrading, the products must be de-watered prior to shipping.

The dense medium is recovered for re-use in a dense media recovery circuit (Figure 4.2). The magnetite is recovered for re-use in correct medium and dilute medium circuits. The medium is drained from the separator products on screens and then flows to the medium sump. Medium not recovered at this stage is rinsed from the product with water through a second set of screens. This diluted medium is then upgraded and de-watered with the use of magnetic separators and densifying cyclones. The concentrated magnetite product is then added to the medium sump. The medium density is controlled at the outlet of the medium sump, where water is added as required. A feedback controller is used to manipulate this water flow based on a signal from a nuclear density gauge.

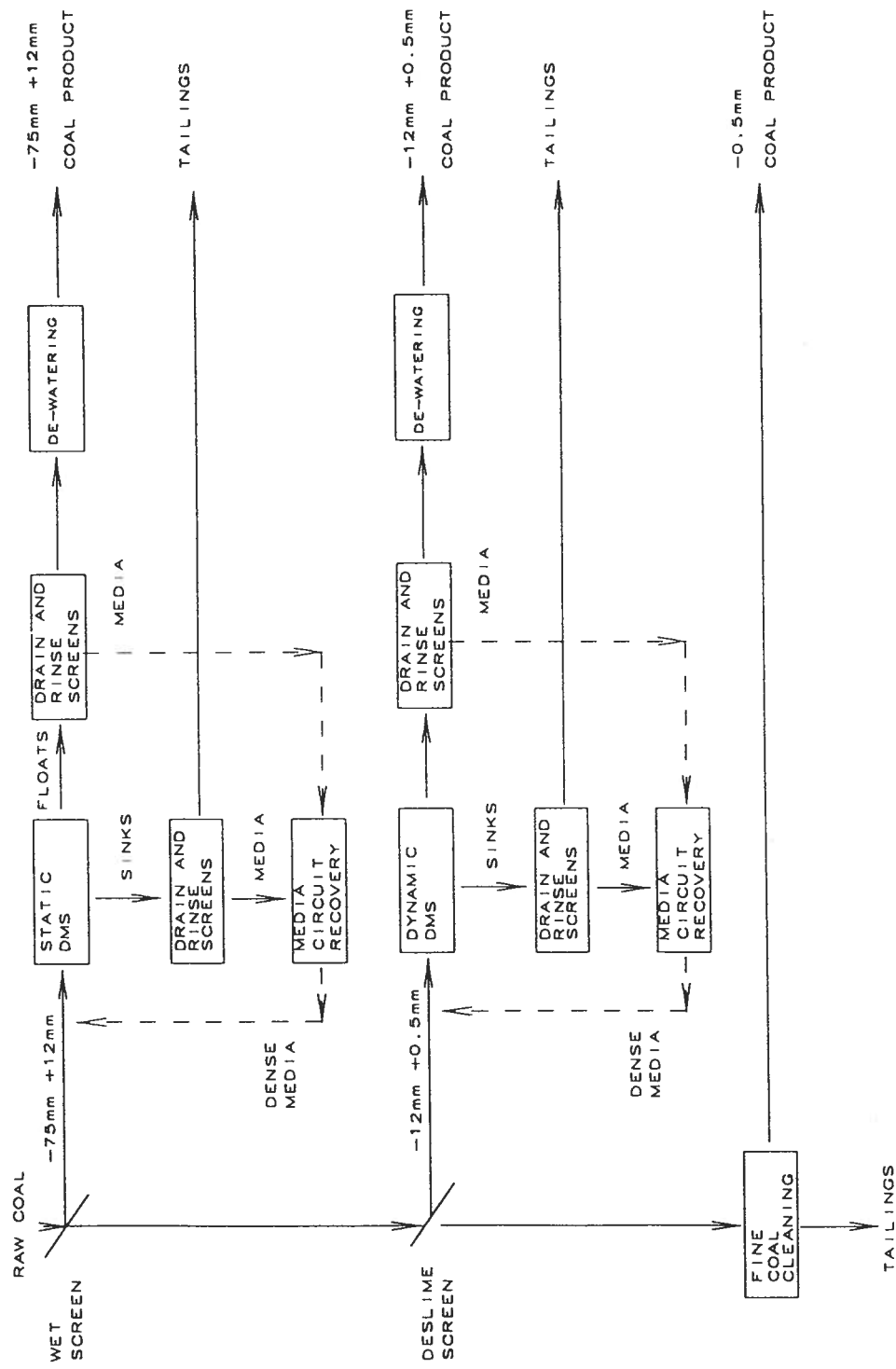


Figure 4.1 Typical coal preparation process flowsheet using dense media separation.

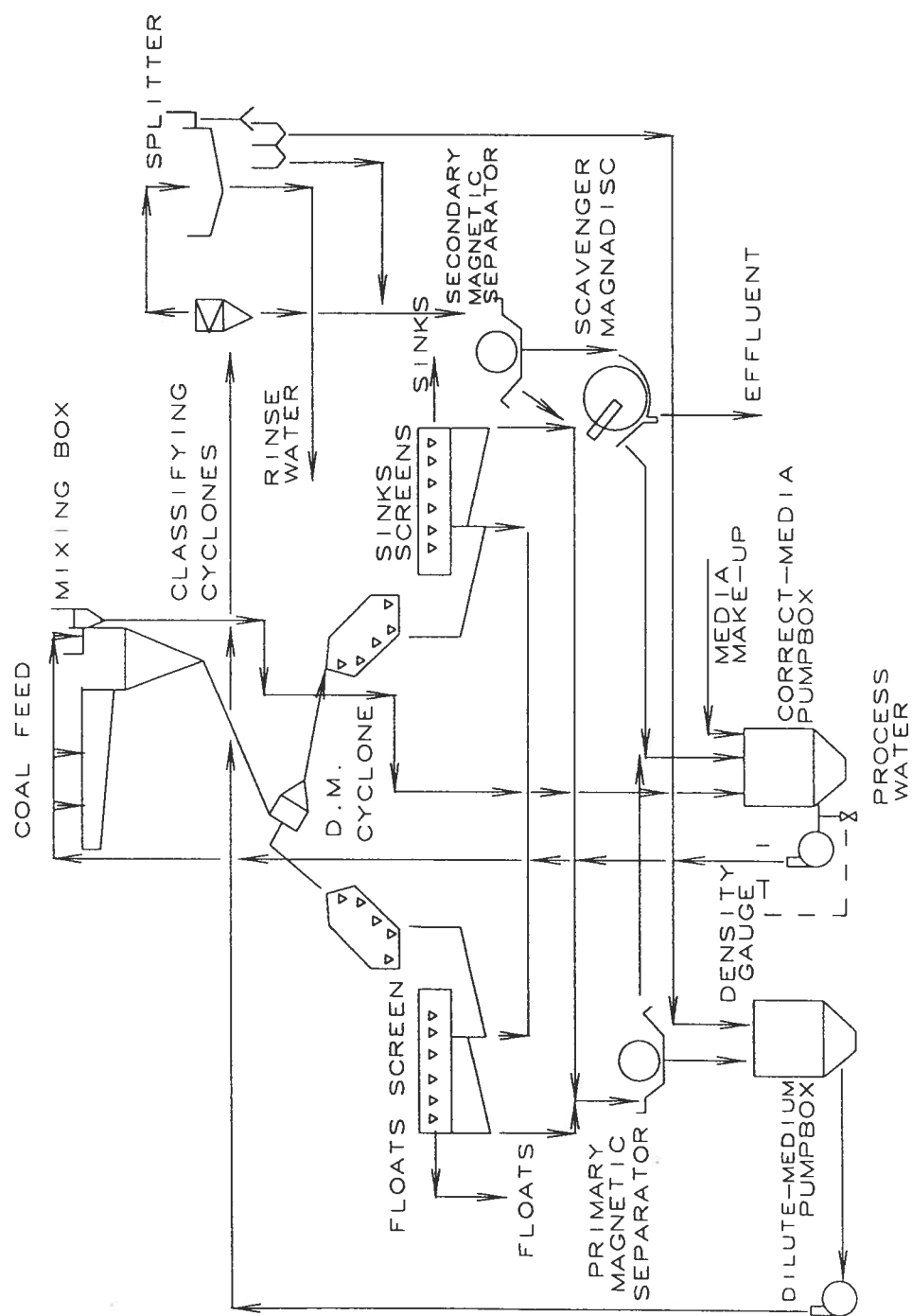


Figure 4.2 Typical magnetite dense media recovery circuit (Osborne, 1988).

4.4 Factors Affecting Separation Performance

The performance of both static and dynamic dense medium separators depends on the properties of the medium, the design of the separating device and the operating conditions. The design features of importance are specific to each type of separator; these have been described elsewhere (Hudy, 1968, Deurbrouck and Hudy, 1972, Burt, 1984, Napier-Munn, 1983, Osborne, 1988). The operating conditions include throughput, medium to coal ratio, feed particle size and for dynamic separators inlet pressure; the effects of which have been reviewed by several researchers (Chaston and Napier-Munn, 1974, Napier-Munn, 1983, Osborne, 1988).

The medium properties of interest are the density and some measure of both the stability and the rheology. The density is set between the densities of the two products by controlling the magnetite content. The stability describes the degree of stratification that occurs as a result of the settling of the medium particles. This stratification results in the formation of zones of varying density which can affect the sharpness of separation. The rheology describes the resistance that a particle experiences as it moves towards a separator outlet. In general media with low stabilities have low viscosities and vice versa. Both properties depend on the levels of physico-mechanical parameters, physico-chemical parameters and the presence of contaminants. It is therefore desirable to control these parameters in order produce a medium exhibiting a low viscosity and a high stability.

The partition curve is conventionally used to characterize separation performance for most gravity separation processes. The probable error, E_p , the cut density, δ_{50} , the amount of material short circuiting to the overflow and the amount of material short circuiting to the underflow can

be determined from this curve (King and Juckes, 1988). For dense medium cyclones, Scott et al (1986) defined the pivot parameters which are the medium split to separator underflow and the medium density in the separation region of the cyclone. These parameters are obtained from the point of intersection of partition curves produced for particles in different size ranges.

4.5 Effect of Medium Properties on Separation Performance

There is a difference of opinion concerning the importance of viscosity in dense medium separation. Many researchers (Schranz, 1954, Geer et al, 1957, Whitmore, 1958, Collins et al, 1983, Napier-Munn, 1983, Scott et al, 1987, Davis, 1987, Ferrara and Schena, 1988) have provided evidence to show the viscosity of the medium is an important process variable. Other researchers (King and Juckes, 1988) believe that because of the turbulent conditions in separators, the viscosity has little effect. Although turbulent flow in the separator likely influences particle movement, the flow regime of the particle relative to medium determines the role of viscosity. As presented in Section 4.2, estimated Reynolds numbers for small and near density particles are in an intermediate range between laminar and turbulent flow regimes in which viscosity is important.

Several investigators (Govier et al, 1957, Whitmore, 1958, Berghofer, 1959) have shown that magnetite dense media exhibit non-Newtonian rheological properties that can be modelled with the Bingham plastic equation. These non-Newtonian properties make it difficult to estimate the drag force that a particle experiences as it moves through the medium (see section 4.2). Specifically, the role and relative importance of the yield stress and plastic viscosity are not

known. In addition, the rheological properties influence the medium stability which in turn affects separation performance (Napier-Munn, 1990).

4.5.1 Static Separators

One of the first investigations showing that media viscosity affects the performance of dense medium separators was performed by Schranz (1954). He used a surfactant (wetting agent coco-amino-acetate) to reduce the consistency (viscosity) of barite and calcite media. The reduction in viscosity resulted in improved separation performance (lower E_p) when cleaning coal in a small scale dense medium vessel. The improved performance was more pronounced for small (1.0-0.5 mm) particles than for larger ones. The study also showed that the separation performance was better when using a "stable" barite medium with reduced viscosity than when using a low viscosity but "unstable" magnetite medium.

Geer et al (1957) cleaned four different coals in a pilot scale drum separator using magnetite dense medium with bentonite to control viscosity. Increasing the viscosity resulted in an increased E_p ; however, the magnitude of the increase was very dependent on the characteristics of the coal. In particular, the viscosity affected E_p most when the coal was fine or when the coal contained a large amount of near density particles. In a related investigation Yancey et al (1958) characterized the rheological properties of the medium using the Bingham plastic model. It was found that the yield stress was positively correlated with the plastic viscosity which made it difficult to determine the respective roles of the two properties. To attempt to determine which property had the greater affect on separation performance (E_p), critical viscosity and critical yield

stress values were estimated from force balances. The critical viscosity is the viscosity that would prevent particles from settling a sufficient amount for separation and the critical yield stress is the yield value that would support particles and prevent them from settling. Based on the calculations, it was found that the critical viscosities were much greater than the measured plastic viscosities. The changes in E_p could therefore not be explained by the changes in viscosity. The calculated critical yield stress values were, however, within the range of the measured values implying that it affected process performance.

Whitmore (1958) modelled the rheological properties of various types of dense media (barite, flotation tailings, shale, magnetite, galena) with the Bingham plastic equation. Using dense medium baths to clean coal, he found that the E_p was affected by the plastic viscosity but was independent of the Bingham yield stress (Equation 4.10). As is indicated by Equation 4.10, the E_p also increased as particle size (d) decreased. The value of the exponent for the particle diameter term (0.5) implies that the flow around the particles is turbulent. According to Napier-Munn (1990), however, the exponent value of 0.5 for the viscosity term indicates that the flow is in the intermediate flow regime.

$$E_p = k \left(\frac{\eta_{pl}}{d} \right)^{1/2} \quad (4.10)$$

where k is a proportionality constant.

In a subsequent investigation, Valentik and Whitmore (1964) showed that the yield stress affected particle settling and thereby influenced separation performance. It was demonstrated that small and near density particles do not exert sufficient stress on the medium to overcome the

yield stress and therefore do not settle. As a result, particles of different sizes have different separation densities. For example, for a top fed separator, the separation density for small particles is greater than the separation density for large particles. It was also observed that large sinking particles drag small float particles in their wake. Once at the bottom of the separators, these small particles were trapped by the yield stress and therefore reported to the sinks. The effect of the yield stress was reduced by vibrating the settling vessel; the vibration was added to simulate conditions in an industrial separator. As a result of this investigation, it was recommended that control medium parameters be controlled (magnetization, clay content, particle size, etc.) in order to reduce the yield stress. It was also stated that any increase in plastic viscosity, resulting from changes in these parameters, would be small compared to the effect of a yield stress.

In order to develop a better understanding of the respective roles of the yield stress and plastic viscosity, Valentik and Whitmore (1965) developed a model for the settling of particles through a Bingham plastic fluid. In their model they assumed that usual drag forces experienced by a moving body in a Newtonian fluid are supplemented by an additional force ($= \pi^2 d^2 \tau_{BY} / 4$) to overcome the yield stress.

Scott et al (1987) used tracers to study the effect of medium viscosity on the processing of iron ore in a bottom fed Wemco drum separator. The apparent viscosity of the ferrosilicon medium was monitored with a Debex on-line viscometer and was adjusted by increasing the medium density (solids content), by adding magnetite and by allowing contaminant levels to increase. As the viscosity increased, the E_p increased and the separation density increased. The effect of viscosity was more pronounced for small particles than for large ones. It was also

observed that the separation density for small particles was lower than the separation density for large ones. If it can be assumed that the yield stress contributed more to the effective apparent viscosity than the plastic viscosity, these results support those predicted by Valentik and Whitmore (1964).

Results indicate that not only is medium viscosity important to the performance of static separators, but more specifically the non-Newtonian properties are important. The roles and relative importance of the yield stress and plastic viscosity are, however, not known. Valentik and Whitmore (1964) suggested that yield stress contributes an additional component to the drag force such that once the yield stress is overcome the plastic viscosity determines the movement of the particle. As presented in Section 4.2, the view of Du Plessis and Ansley (1967) is that the yield stress contributes to the drag coefficient implying that it affects separation performance through its contribution to the apparent viscosity. In either case, the yield stress must be considered to be important to the movement of the particles.

4.5.2 Dynamic Separators

Based on direct and indirect evidence from the literature, Napier-Munn (1983) concluded that for dense medium cyclones, "the characteristics and behaviour of the medium are process determining". The relationship between separation performance and the medium viscosity and stability are, however, complicated by the non-Newtonian properties of the medium. Napier-Munn (1990) concluded that the viscosity effects separation performance by two mechanisms:

1. it influences the motion of the coal/ore particles, and

2. it controls medium behaviour (stability) which in turn influences separation performance.

Researchers (Fern, 1952, Chaston and Napier-Munn, 1974) have believed for a long time that a high medium viscosity resists the motion of particles and thereby has a deleterious effect on separation performance. Several investigators (Lilge et al, 1957, Collins et al, 1974, Napier-Munn, 1980, Collins et al, 1983, Napier-Munn, 1984, Stoessner, 1987, Davis, 1987, Scott, 1988) have provided evidence to support this belief. The investigations have shown that the separation of small and near density particles are most affected by the medium viscosity. In addition, the effect is more significant for the high density (solids content) separation of minerals than it is for the low density separation of coal (Napier-Munn, 1990). Very few investigations have been performed to study the importance of the non-Newtonian properties of the medium.

It has been established that dense media exhibit non-Newtonian flow properties which implies that the apparent viscosity will change with shear rate. Lilge et al (1957) related the tangential velocities of the medium at different radii in a cyclone to the shear rates. Apparent viscosities were then determined for different radii from rheological flow curves and the calculated shear rates. For magnetite dense medium, which exhibited pseudoplastic properties, the apparent viscosity was determined to be highest near the periphery of the cone and lowest near the centre. It should be noted, however, that since particles (coal/ore) move with the medium, the calculated shear rates (and therefore apparent viscosities) do not necessarily represent those experienced by the particles. Specifically, particles of different size and density will move at different velocities (shear rates) relative to the medium and therefore experience different apparent viscosities.

To investigate the importance of viscosity independently of stability, Napier-Munn (1980) used a medium containing fine quartz in a dense liquid. Since the liquid had a density equal to that of the quartz, the viscosity could be controlled by varying the amount of quartz in the suspension. It was shown that a high medium viscosity resulted in a low separation efficiency. When a yield stress existed, the partition curve became horizontal over a density range close to the medium density. It was suggested that the stress exerted by near density particles on the medium did not exceed the yield stress and therefore no density separation occurred. An alternate explanation is that at low shear rates, such as would be experienced by near density particles, a yield stress produces a high apparent viscosity that in turn resists particle movement. This result opposes the belief of some investigators (Ferrara and Schena, 1988) that a yield stress would not influence the performance of dynamic separators due to the high shear stresses.

From classifying hydrocyclone models that are based on the equilibrium orbit theory (Bradley, 1965), it can be shown that the separation density should increase with medium viscosity (Napier-Munn, 1980). This trend was confirmed by tests performed with a dense medium cyclone using a "stable" medium composed of a quartz in a dense liquid (Napier-Munn, 1984). It was shown that the separation density increased with both the plastic viscosity and the Bingham yield stress. Several investigators (Napier-Munn, 1983, Napier-Munn, 1984, Scott et al, 1987, Davis and Napier-Munn, 1987) have observed, however, that increasing the viscosity of "unstable" media results in a decrease in the separation density. The discrepancy was attributed to the unstable nature of the medium.

Collins et al (1983) related medium stability to separation performance in tests with DSM cyclones and Vorsyl separators. The media were composed of mixtures of ferrosilicon and

magnetite and the stability (density differential between cyclone overflow and underflow) was controlled by varying the magnetite content. It was found that separation performance was optimum when the density differential was in the range of 200 kg m^{-3} to 500 kg m^{-3} . The optimum differential was found to be slightly higher for the separation of fine particles and lower for the separation of coarse particles. As the medium viscosity was increased, the differential decreased such that a very stable medium (differential $< 200 \text{ kg m}^{-3}$) had an excessively high viscosity which in turn reduced separation efficiency. At differentials below 800 kg m^{-3} , the separation density was found to be approximately equal to the underflow density, while, at higher differentials it dropped off sharply. Napier-Munn (1984) and Davis (1987) found that the separation density was close to but slightly higher than the underflow density.

Scott et al (1986) believe that a low medium stability results in the formation of density zones; a high density zone forming near the apex of the cyclone and a low density zone forming near the vortex. As a result, near density particles remain trapped in the cyclone; they are not dense enough to penetrate the high density zone of the apex and are too dense to report to the overflow. When a large amount of near density material is present in the feed, it builds up in the cyclone overloading it and eventually causing it to surge. In addition, the build up of solids causes particle crowding which may impede particle movement resulting in a loss in separation efficiency (Ferrara and Schena, 1987).

The results and observations described above imply that the relationship between separation density and viscosity can be explained as follows. For an unstable medium, increasing the viscosity reduces the underflow medium density. If it can be assumed that the underflow density is approximately equal to the medium density in the zone near the cyclone apex, the

reduced underflow density corresponds to a lower density in this zone. As observed by Collins et al (1983), Napier-Munn (1984) and Davis (1987), the separation density is close to the underflow density implying that particles with lower densities cannot penetrate the zone around the apex and are therefore forced to report to the overflow. Increasing the viscosity, therefore results in a lower medium density near the cyclone apex which in turn decreases the separation density.

Collins et al (1983) and Napier-Munn (1984) consider that the bulk of the medium in the separator is of constant density except when low viscosities and high differentials exist. Under these conditions the cyclone acts as a size classifier for medium particles (Ferrara and Schena, 1988). As viscosity increases, size classification effects are reduced revealing a positive correlation between viscosity and stability. Studies (Yopps et al, 1987) with hydrocyclones have also shown that the sharpness of size classification decreases as suspension viscosity increases. This relationship implies that the same mechanisms that are responsible for an increase in viscosity are also responsible for an increase in stability (decrease in size classification efficiency).

Horsley and Allen (1987) studied the relationship between the non-Newtonian properties of suspensions and size classification in hydrocyclones. They showed that when the suspension exhibited a yield stress, the size classification efficiency was low. Increasing the yield stress resulted in a higher cut size and a reduction in classification efficiency. The existence of a yield stress was attributed to particle aggregation. It was explained that fine particles that were trapped in the aggregates reported to the cyclone underflow which resulted in a lower sizing efficiency. Since dense media exhibit a yield stress, similar mechanisms may be responsible for media

stability in dense medium cyclones.

Researchers have shown that medium properties are process determining. Specifically, trends in process performance have been related to the viscosity and stability of the medium. In order to understand the mechanisms that relate medium properties to separation performance, however, it is necessary to have knowledge of the complete rheology.

CHAPTER 5: MAGNETITE CHARACTERIZATION

5.1 Introduction

During the development of the dense medium separation process, the importance of the properties of the suspended solids became apparent. DeVaney and Shelton (1940) compared the properties of various solids that could be used as the medium solids. The factors considered to be important included cost, density, shape of particles, resistance to abrasion, resistance to corrosion, chemical inertness, and physical and chemical properties that affect the recoverability for re-use. Magnetite is readily available and its properties meet the requirements listed above.

The greater understanding of the role of the medium rheology and stability on dense medium separation performance, warrants investigations into the magnetite properties that influence these medium properties. The important properties of the magnetite depend largely on its mineralogical composition, but they can be controlled to some extent. Properties such as liberation size and chemical purity depend on the geological environment in which the magnetite was formed. The grade and particle size distribution are, however, determined by how the material is processed. The suitability of a particular source of magnetite is therefore partly inherent and partly controlled by how it is prepared.

5.2 Mineralogy and Geological Deposition

Magnetite, Fe_3O_4 , is an iron oxide mineral that belongs to the spinel group having the

chemical formula $[\text{Fe}^{2+}][\text{Fe}^{3+}]_2[\text{O}^{2-}]_4$. It has a cubic structure with oxygen atoms forming the lattice in a cubic close packed arrangement. Octahedral and tetrahedral interstices are occupied by the ferrous, Fe^{2+} , and ferric, Fe^{3+} , cations (Cann, 1979).

Impurities affect the important physical and chemical properties of magnetite. The impurities may be present in three forms:

- i. as a result of iso-morphous substitutions of metal ions for Fe^{2+} and Fe^{3+} ;
- ii. as mineral inclusions formed by exsolution during cooling; and
- iii. as inclusions formed during crystallization.

The conditions of mineralogical deposition are important for the substitution and exsolution processes. The exsolved minerals typically contain the elements Ti, V, Mn, Mg and Cr. Substitution is dependent on temperature, pressure, composition of the environment and properties of the ions. Substitution of Fe^{2+} is commonly by Ca^{2+} , Mn^{2+} , Mg^{2+} , Ni^{2+} , Co^{2+} and Zn^{2+} , and substitution of Fe^{3+} can be by Cr^{3+} and V^{3+} . In addition, at high temperatures, there may be coupled substitution of Ti^{4+} and Fe^{2+} for 2Fe^{3+} (Cann, 1979).

Magnetite is commonly found in skarn, differentiated magmatic, stratabound, ultramafic and placer deposits. In British Columbia, the largest and most common deposits are skarns. Many of these deposits have been mined for iron ore; examples include Texada Island Iron Mines, the Brynnor Mine at Kennedy Lake, and the Jedway and Wesfrob mines on South Moresby Island. Many other mines contained significant amounts of magnetite, although most did not produce it as a secondary product with the exception of the Craigmont Mine. The stock piles from the Craigmont Mine are the main source of magnetite for western Canadian coal producers.

5.3 Craigmont Magnetite Production

The Craigmont mine produced magnetite as a secondary product from its copper iron skarn deposit. The mine is located 200 kilometres north east of Vancouver, B.C.. From the beginning of the operation in 1961 to closing in 1982 the mine produced 426,000 tonnes of copper from 36,750,000 tonnes of ore with an average grade of 1.28 per cent copper (Shewchuk, 1983). Production of magnetite began in 1969 due to the demand by Kaiser Resources who needed it for their dense medium separation process at their Fernie coal mine (Shewchuk, 1983). It is presently the main source of magnetite for use in dense medium by coal preparation plants throughout British Columbia and Alberta. The ore-body had an average iron grade of 19.8 per cent which is accounted for by its magnetite grade of 14 per cent and hematite grade of 12 per cent. In total, approximately one million tonnes of magnetite was concentrated from the raw ore and the reprocessed tailings. Annual shipments of approximately 50,000 tonnes to coal mines were reported in 1982 (Hancock, 1988). Presently 430,000 tonnes remain in stockpiles. Magnetite recovery, from tailings material, grading 15% magnetite, where a further 600,000 tonnes may be recovered, should commence in 1991 to increase the stockpile at a production rate of 50,000 tonnes per year (Murray, 1990).

5.4 Physical and Chemical Properties

The suitability of a particular source of magnetite depends on its physical and chemical properties. The most important properties include particle density, particle size and size

distribution, particle shape, magnetic characteristics, magnetics content, elemental composition, surface chemistry and moisture content (Osborne, 1988). To determine the suitability of a particular supply of magnetite, standard measuring procedures and property levels have been established (Jonker, 1984; Anon, 1985; Osborne, 1986, 1988).

Various organizations have set specifications for magnetite used in dense medium separation. These specification (Table 5.1) are based on the original standards set by the British coal mining industry (Jonker, 1984; Osborne, 1986, 1988) and since they are quite general, they should only be considered as guidelines.

The magnetite density determines the solids volume concentration required to produce a specified medium density which is the total mass of magnetite and water divided by their total volume. The higher the density of the magnetite, the lower is the medium solids volume concentration. The concentration of magnetite in suspension affects the medium rheology and stability; at high concentrations the medium becomes viscous while at low concentrations it has a poor stability. The density of the magnetite is also an indicator of its chemical purity. Pure magnetite has a density of 5180 kg m^{-3} (Hancock, 1988); densities lower than this indicate the presence of some form of impurities.

The magnetite particle size and size distribution depends on the natural grain size. If the grain size is very small, fine grinding may be necessary to liberate the magnetite from other minerals. Small magnetite particles ($-10 \text{ }\mu\text{m}$) are difficult to recover for re-use and can produce a viscous medium. If the liberation size is large, it is possible to produce particle sizes and size distributions that are easy to recover and that produce desirable media characteristics.

Table 5.1 Recommended specifications for magnetite used in dense media (Osborne, 1988).

Physical Properties	Specification
Relative density	≥ 4.85
Magnetics Content	$\geq 97\%$
Moisture Content	$\leq 10\%$
% Passing 40 μm	95%
% Passing 10 μm	$\leq 10\%$
Magnetic Properties	
Initial Susceptibility, K_{30} (emu/g)	> 0.050
Susceptibility at 800 oersteds, k_{800} (emu/g)	> 0.053
Saturation Moment, M_{sat} (emu/g)	> 80
Coercive Force, H_c (oersteds)	< 50

Particle shape is largely determined by the fracture characteristics of the magnetite and by the type of comminution process used to reduce the particle size. Most magnetite is ground using conventional rod and ball mills producing angular and irregularly shaped particles. Alternatively, magnetite particles from steel smelter fly-ash (Osborne, 1988) and from placer deposits have more rounded particle shapes. It has been shown that rounded ferrosilicon particles provide superior medium properties, with respect to viscosity, particularly at high solids content (Collins et al, 1974).

Magnetite is ferromagnetic and since it is recovered by magnetic separators and is recycled, its magnetic properties are very important. The magnetic properties are characterized by the magnetic susceptibility, the saturation moment, and the coercive force.

The magnetic susceptibility and saturation moment are indicators of the force exerted on a particle in a magnetic field. A greater magnetic force results in an improved recovery in magnetic separators. Mineralogical replacement of ferrous cations in the magnetite lattice structure by other ions results in an inferior susceptibility and saturation moment. Mineral inclusions, such as finely disseminated quartz, also reduce the magnetic strength of the material.

The coercive force describes the state of magnetization of the particles. A high coercive force corresponds to a high remnant magnetism resulting in magnetic aggregation of the particles in the medium. Aggregation has a negative influence on both the rheology and the stability of the medium. When the magnetite has a high coercive force or remnant magnetism, demagnetizing coils have been installed in dense medium recovery circuits to reduce the amount of magnetic aggregation (Hartig et al 1951; Osborne, 1986, 1988).

Once the magnetite is introduced into a magnetic field, its magnetic domains align in the

direction of the applied field. By removing the magnetic field, the domains realign to a state of lowest energy where the net magnetic effects of the domains cancel one another. If the magnetite exhibits remnant magnetic properties, the domains remain partially aligned which causes the particles to behave like small magnets. The coercive force has been attributed to the replacement of iron ions in the lattice structure. For example, these properties are particularly high when titanium, (Ti^{4+}), is present in the ore. The coupled substitution of titanium, (Ti^{4+}), and ferrous iron, (Fe^{2+}), ions for two ferric ions, (2Fe^{3+}), which have a similar ionic radius, can take place during crystallization (Cann, 1979). Under these conditions the titanium ions are not as mobile as the ferric ions which seems to inhibit the dis-alignment of the domains. Therefore, when the magnetic field is removed the particles have a net magnetic force (Graham et al, 1982). Titaniferrous magnetite is characterized by high remnant magnetism that usually makes it unsuitable for use in dense medium.

The "magnetics content" is a measure of the amount of magnetic material that is recoverable with a magnetic separator and it can be considered as a magnetite grade. Measured values depend on the type of measuring equipment used (Davis Tube, Magnachute etc.) and, to some extent, on the equipment operator; the results are, therefore, difficult to compare. The non-magnetic fraction is typically magnetite grains locked with other minerals, very small magnetite particles that are difficult to recover and non-magnetic minerals that were trapped between magnetite particles during recovery from the run-of-mine ore (Osborne, 1988).

The elemental composition of a magnetite sample, as discussed above, describes its purity and determines the sample density, magnetic properties, magnetics content and surface chemistry. The elements of most interest are: ferric and ferrous iron; cations that typically replace the iron

ions in the lattice structure; and elements that may be present in associated minerals.

Surface chemistry of magnetite has received little attention in the dense media related research. The surface chemistry, however, influences inter-particle forces of attraction and repulsion that affect particle aggregation which is very important to the properties of the medium. The iso-electric point (i.e.p.) for iron oxide minerals is typically between pH 6.0 and 7.0 (Leja, 1983). The exact value of the i.e.p. can vary and it depends on the types and quantities of impurities in the sample. To control the state of aggregation, dispersing agents can be used.

Many of the properties of magnetite are interrelated. The suitability of a potential source may therefore be determined from some basic mineralogical information. It should be noted that so far little effort has been given to the tailoring of a magnetite supply to optimize the dense medium separation processes.

CHAPTER 6: RHEOLOGICAL MEASUREMENTS

6.1 Rheological Measuring Devices

The most widely used devices developed to measure rheological properties of fluids and suspensions include rotational viscometers and capillary (tube) viscometers (Nguyen, 1983, Cheng, 1980). Van Wazer (1963) and Whorlow (1980) described many of the devices that have been developed.

The function of each device is to produce data that describe the flow behaviour of fluids or suspensions in terms of shear stress and shear rate. Usually, one of either shear stress or shear rate is controlled while the other parameter is measured. The most appropriate device for a specific application depends on the rheological properties of interest such as viscosity, yield stress, thixotropy and visco-elasticity. The rotational viscometers are the most versatile and can be used to measure all of these properties. Based on a review of rheological measuring devices, Graham and Lamb (1982) recommended rotational viscometers for measuring the rheological properties of magnetite dense medium.

The tube viscometers have also been widely used to measure the rheology of suspensions (Nguyen, 1983). Van Wazer et al, (1963), Whorlow (1980), and Hanks (1981) have reviewed several of these instruments. The two main concerns in using these viscometers are that they can not be used to measure time dependent flow properties (Whorlow, 1980, Nguyen, 1983) and that for suspensions, measurement errors are produced as a result of particle migration in the tube (Whitmore, 1957, Seshadri and Suter, 1970, Whorlow, 1980, Graham and Lamb, 1982). Tube

viscometers are, however, relatively inexpensive in comparison to rotational viscometers and can provide some useful information if the data are treated properly (Whorlow, 1980).

There are two main types of rotational viscometers; these are referred to as controlled stress and controlled rate viscometers. As is implied, in a controlled stress rheometer, the shear stress is controlled and the corresponding shear rate is measured. The best known manufacturers of these devices are Rheometrics, Carri-Med and Bohlin. In the controlled rate viscometer, such as the Haake Rotovisco, the shear rate is controlled and the corresponding shear stress is measured.

Each instrument has some specific advantages over the other. Both use similar measuring fixtures, either concentric cylinders or cone and plate. For suspensions that settle, cone and plate fixtures are impractical because the sample in the measuring area would sediment before any measurements could be taken. Particle settling in concentric cylinder devices also causes measurement errors.

The two basic types of concentric cylinders are the Couette type in which the cup rotates around a stationary bob, and the Searle type where the bob rotates in a stationary cup. Couette instruments are better for high shear rate measurements because in the Searle instruments, turbulence forms at relatively low shear rates (Schlichting, 1968). Significant advances have been made in the measurement and control of shear stresses and rates making these instruments very accurate for a wide variety of fluids and suspensions. Van Wazer et al (1963) and Whorlow (1980) have reviewed many of the instruments that have been developed.

6.2 Concentric Cylinder Rheometry

The flow behaviour of a fluid or suspension is described in terms of a rheological flow curve. This is a relationship between the shear rate and shear stress for the sample. In a concentric cylinder viscometer, one cylinder rotates relative to the other; the rate of shear being proportional to the angular velocity. The shear stress is usually measured as a torque on one of the cylinders. Figure 6.1 shows the geometry of a conventional concentric cylinder arrangement. The main assumptions required to determine the shear stress and shear rate from the torque and angular velocity, respectively, are (Van Wazer, 1963):

- i. steady, laminar flow only in the direction of cylinder rotation;
- ii. no wall slippage;
- iii. no end effects; and
- iv. shear rate, $\dot{\gamma}$, is a function of shear stress, τ , only (Equation 6.1).

$$\dot{\gamma} = f(\tau) \quad (6.1)$$

6.2.1 Flow Geometry

The shear stress and the shear rate depend on the geometry of the fixture and the rotational speed. Derivations of expressions that relate the shear stress to the shear rate can be found in Van Wazer (1963) and Whorlow (1980). For a simple cup and bob fixture the shear stress can be described by Equation 6.2.

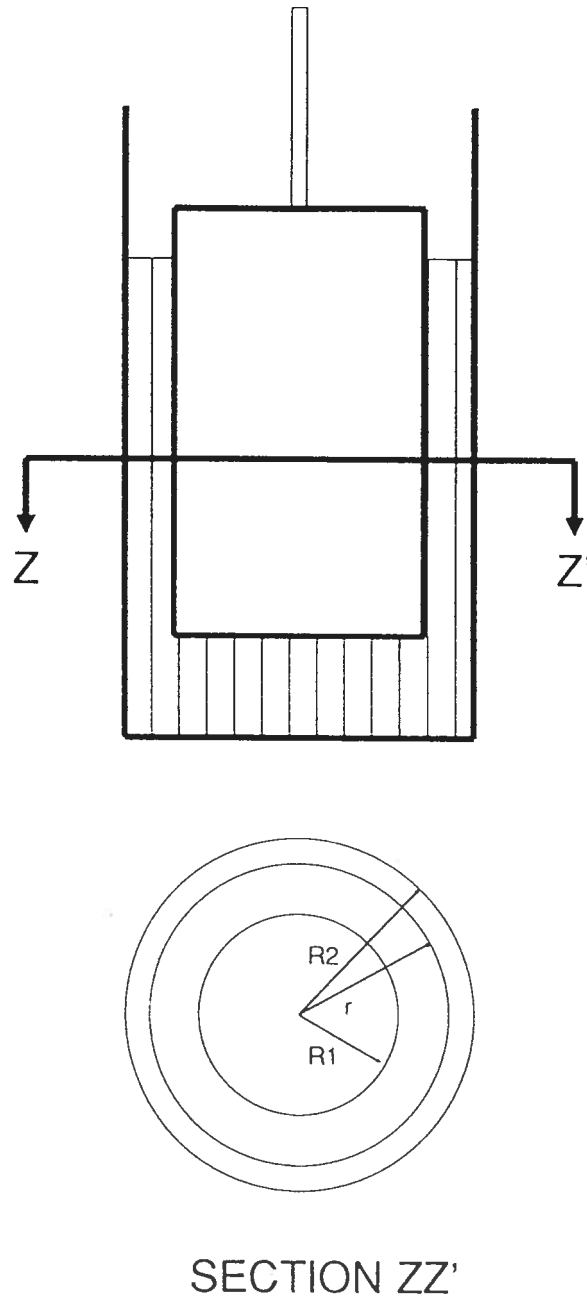


Figure 6.1 Geometry of a conventional cup and bob rheometer fixture.

$$\tau = \frac{T}{2\pi r^2 h} \quad (6.2)$$

where, T is the measured torque,

r is the bob radius, and

h is the bob height

The shear rate can be described by Equation 6.3.

$$\dot{\gamma} = r \frac{\delta \omega}{\delta r} \quad (6.3)$$

where, ω is angular velocity

The shear rate can be related to the shear stress by Equation 6.4.

$$\dot{\gamma} = -2\tau \frac{\delta \omega}{\delta \tau} = f(\tau) \quad (6.4)$$

For a Newtonian fluid, the relation between shear rate and shear stress is by definition:

$$\tau = \eta_N \dot{\gamma} = \frac{T}{2\pi h r^2} \quad (6.5)$$

where, η_N is the Newtonian viscosity coefficient.

In this case the shear rate can be calculated by Equation 6.6.

$$\dot{\gamma} = \frac{2\omega R_2^2}{R_2^2 - R_1^2} \quad (6.6)$$

where, R_1 is the radius of the bob, and

R_2 is the radius of the cup.

Several methods have been developed to determine the relation between shear stress and shear rate for fluids with unknown flow properties. Krieger and Elrod (1951, 1952) developed a method of calculating the shear rate from measurements with a single fixture as compared to other methods requiring several fixture geometries. Krieger (1968a, 1968b) then modified the relations from his original work. The following expression describes the shear rate relation with respect to shear stress and rotational velocity:

$$\dot{\gamma}(\tau) = \frac{2N\omega}{1-s^{-2N}} \left(1 + \frac{\dot{N}}{N^2} f(t)\right) \quad (6.7)$$

where,

$$N = \frac{\delta \ln(\tau)}{\delta \ln(\omega)} \quad (6.8)$$

$$\dot{N} = \frac{\delta N}{\delta \ln(\omega)} \quad (6.9)$$

and,

$$f(t) = t^2/12 \left(1 - \frac{t}{2} + \frac{t^2}{15} \dots\right) \quad (6.10)$$

where,

$$t = 2 \ln(s) \quad (6.11)$$

and (see Figure 6.1),

$$s = \frac{R_2}{R_1} \quad (6.12)$$

If the suspension exhibits a yield stress, there may be a small error in the shear rates as

calculated by Krieger's equations. At low shear rates, the stress at the cup surface may be too small to cause the suspension to shear as the suspension will only shear out to the radius where the shear stress exceeds the yield stress. Therefore, the gap is effectively smaller than that determined by the geometry of the cup and the bob (Horie and Pinder, 1979).

The shear stresses at the cup and bob surfaces are related to their radii by the equation:

$$\frac{\tau_1}{\tau_2} = \left(\frac{R_2}{R_1} \right)^2 \quad (6.13)$$

The radius to which the suspension will be sheared can be calculated by:

$$r^* = R_1 \sqrt{\left(\frac{\tau_1}{\tau_y} \right)} \quad (6.14)$$

The gap is, therefore, effectively reduced to the difference:

$$Gap = r^* - R_1 \quad (6.15)$$

Nguyen (1983) proposed a different solution to the shear rate calculation for the case where the yield stress exceeds the stress at the cup surface (Equations 6.16 and 6.17).

$$\dot{\gamma} = \frac{\pi \omega}{15 p} \quad (6.16)$$

where,

$$p = \frac{\delta \ln(\tau)}{\delta \ln(\omega)} \quad (6.17)$$

The error obtained by using Krieger's method depends on the magnitude of the yield stress. Nguyen (1983) showed for drilling fluid with a high yield stress, low shear rate values, calculated using Krieger's method, were in error by less than 2%.

6.2.2 Measurement Errors

There are several measurement errors that occur when making rheological measurements on non-Newtonian suspensions. These errors are the result of particle movement such as settling and migration away from the device surfaces.

6.2.2.1 Effect of Particle Settling

Settling of particles make measurements in concentric cylinder fixtures difficult. In a typical cup and bob, the particles settle during measurement. This settling results in the formation of a particle depleted zone in the upper annulus between concentric cylinders and a sludge at the bottom of the cup. The particle depleted zone will have a lower resistance to flow than a homogeneous suspension resulting in a low shear stress measurement. At the same time, the sludge build up at the bottom of the cup may contact the bob and impede its rotation (see Figure 6.2). These problems are most severe for suspensions of fast settling large, high density particles at low solids content.

Several devices have been developed to measure rheological properties of settling suspensions. In most, methods were developed to maintain a homogeneous suspension in the

annular gap. Overand et al (1984) used a cup with slots on its walls and an open bottom which is placed in a mixing bowl containing the suspension. The mixed suspension flows into the annular gap through the slots in the cup wall and thereby maintains the composition of the suspension in the annular gap. They showed, using Newtonian fluids, that at low agitation rates within the mixing bowl, results compared well to values obtained with no mixing. Clarke (1967) positioned a cup with an opened bottom in a stirred vessel. The impeller at the bottom of the vessel caused the mixed suspension to circulate up through baffles in the walls of the vessel into the top of the cup and down through the annular gap between the cylinders. Purohit and Roy (1965) developed a similar arrangement using paddles.

Haake developed a bob with a helical groove which, when rotated supplies a lift to settling particles. Haake also developed an arrangement with a pump which forces the suspension up through the annular gap at a rate greater than the settling rate of the fastest settling particles (Haake, 1988). Similarly, Valentyik (1971), Ferrini et al (1979), Reeves and Roy (1985, 1990) and Klemblowski et al (1988), supplied the suspension to the top of the cup, allowing it to flow through the annular gap and out through the bottom during the measurements. Each of these methods, however, introduced undefined components to the shear rate experienced by the suspension. While these devices may have produced good results under some conditions, for non-Newtonian suspensions with possibly time-dependent properties the undefined shear rate likely influences the measured values.

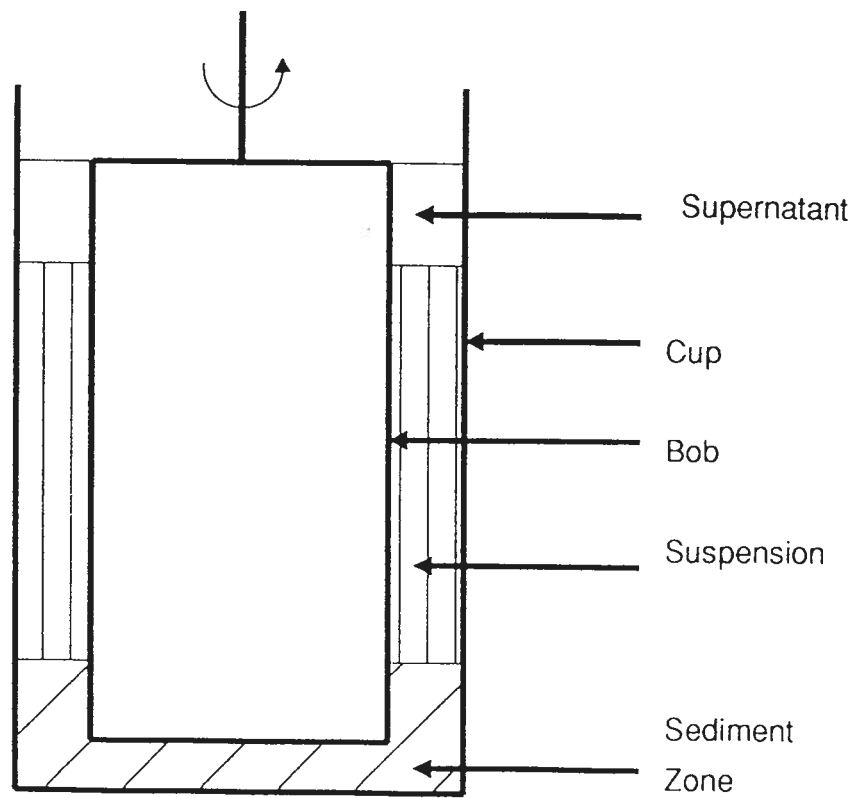


Figure 6.2 Schematic showing settling of particles in a cup and bob rheometer fixture.

6.2.2.2 Other Errors

Several possible effects may increase overall errors in measurements with concentric cylinder fixtures. Possible sources of error include end effects, wall slip, turbulence and temperature effects. These can be corrected or minimized by the adjustment of the data and the proper design of the fixture.

The end effect is due to the shearing of the suspension by the bottom surface of the bob which contributes to the measured torque and is not accounted for. End effect errors can be reduced by:

- i. minimizing the sheared surface area of the bottom of the bob,
- ii. arranging the geometry, so that the shear rate is the same at the bottom of the bob as that between the cylindrical surfaces, and
- iii. adding an extra effective length to the bob in calculations to account for the additional stress (Van Wazer et al 1963, Whorlow, 1980).

In a double gap arrangement the area of the bottom of the bob is small, therefore the end effects may be considered to be negligible (Moore and Davies, 1956).

Wall slip occurs in suspensions when a layer of liquid forms at the surface of the bob due to the migration of particles away from the surface (Whitmore, 1957; Horie and Pinder, 1979; Mannheimer 1982, 1985; Leighton and Acrivos 1987). Since the liquid has a lower resistance than the suspension, much of the shearing may take place in this layer resulting in a low shear stress measurement. Particle migration may occur due to the centrifugal forces acting on them by the rotating flow. In addition, since it is physically not possible for particles to penetrate the

surface, they are displaced away from the wall, creating a layer with a lower particle concentration (Whorlow, 1980). The effect may be more pronounced for non-Newtonian suspensions and at high shear rates (Wein et al, 1988). These type of effects may produce flow results that can be mistaken as thixotropy since the particle migration takes place with time (Leighton and Acrivos 1987).

Oldroyd (1956) mathematically described the effect of wall slip on the rotational speed (Equation 6.18).

$$\omega = \frac{V_{sc}}{R_c} + \frac{V_{sb}}{R_b} + \frac{1}{2} \frac{\dot{\gamma}(\tau)}{\tau} \delta \tau \quad (6.18)$$

where, V_{sc} and V_{sb} are slip velocities for the cup and bob surfaces respectively.

Several methods have been developed to correct for wall slip (Oldroyd, 1956, Mannheimer, 1985, Schlegel, 1986, 1988, Hanks ,1988, Yoshimura and Prud'homme et al 1988). These methods rely on various assumptions about the flow of the suspension in the annular gap that may or may not apply. Roughening of the wall surface has also been shown to minimize the wall slip effect (Cheng , 1978, Nguyen, 1983, Cheng, 1984).

Searle type concentric cylinder viscometers have a low limiting maximum shear rate beyond which turbulent flow will prevail. The turbulence results from moving fluid near the inner rotating cylinder that tries to move outward due to momentum and centrifugal forces. This outward flow causes the formation of Taylor vortices, which is an intermediate stage between laminar and turbulent flow (Duty and Reid, 1964, Graebel, 1964, Purohit and Roy, 1965,

Schlichting, 1968, Sun, 1972, Whorlow, 1980, Cheng, 1988). These vortices can be observed visually as horizontal bands in the annular gap (Purohit and Roy, 1965). The result is an increase in the measured shear stress at high shear rates which is often mistaken for dilatancy in the suspension. Taylor (1923) determined that the formation of this type of flow is a function of the geometry of the fixture and the viscosity of the fluid. The critical Reynolds number, Re_{crit} , for the onset of the Taylor vortices formation can be determined from Equation 6.19 (Taylor, 1923).

$$Re_{crit} = V_b(R_c - R_b)\eta > 41.3 \frac{R_c}{R_c - R_b} \quad (6.19)$$

where, V_b is the peripheral velocity of bob.

The transition to turbulent flow has been studied in more detail by Harris and Reid (1964), Krueger et al (1966) and Hocquart et al (1988). In Couette flow, where the cup rotates, the centrifugal forces stabilize the flow allowing for measurements at much higher shear rates while maintaining a laminar flow regime.

At high shear rates the temperature of the sample may increase significantly with time. This may lead to errors in measurements, particularly for fluids and solutions whose viscosity is strongly dependent on temperature. For suspensions, in which the rheology is more dependent on particle interactions than on the viscosity of the suspending fluid, temperature is less significant (Van Wazer et al, 1963, Whorlow, 1980). The temperature is commonly kept constant by surrounding the fixture with a temperature controlled water jacket.

6.3 Yield Stress Measurements

The yield stress is defined as the threshold stress that must be applied before permanent deformation occurs. Cheng (1985) described yield stress as a time dependent property that has a static and dynamic value. The static yield stress is greater than the dynamic value and it is measured after the sample has had sufficient time to develop its structure fully. The dynamic yield stress is measured after the sample has been sheared at which time the structure is at some equilibrium value. According to Tung et al (1989) the static yield stress is measured at a high Deborah number and the dynamic yield stress at a low Deborah number, where the Deborah number is defined as the ratio of characteristic relaxation time to the time of observation. The type of yield stress measured depends on the technique used. Cheng (1985) suggested using an observation time that best suits the characteristic time of the particular process. The existence of a yield stress has been the subject of many debates (Mannheimer, 1988). It is argued that given sufficient time, applying a small stress will cause a fluid with an apparent yield stress to deform.

Several techniques and devices have been developed to measure the yield stress, many of which have been summarized by Nguyen (1983), Nguyen and Boger (1983), Cheng (1985), and Tung et al (1988). These can be divided into two major groups, direct methods and indirect methods (Nguyen, 1983). The most common direct methods include the stress relaxation, the vane and the applied shear stress techniques. Indirect methods involve extrapolating flow curve data or fitting the data with an appropriate model to find the zero shear rate intercept of the shear stress axis. Mewis and Spaul (1976) refer to a yield value determined in this way as an apparent

yield stress.

The controlled stress technique of making direct yield stress measurements involves slowly increasing the stress in a sample until it begins to flow and reducing it until it ceases to flow. In this case, the yield stress is approached from both static and dynamic conditions. It was found that the time allowed to observe flow at a particular stress influences the determined yield stress value. In particular, the longer the time allowed to observe flow, the lower is the yield stress (Cheng 1985). A controlled stress rheometer must be used to make these measurements.

The vane method of direct yield stress measurement uses a special fixture of blades attached to a spindle with the blades set at equal angles around the spindle. This fixture is positioned in a cup containing the suspension. At very low shear rates the torque measured through the shaft will increase from zero as force is applied. When the sample begins to shear, a maximum torque will be measured which decays with time to an equilibrium value. It is assumed that the suspension is sheared along a cylindrical surface defined by the dimensions of the blades. The yield stress may then be determined from the maximum torque and the area of the sheared surface (Nguyen, 1983, Nguyen and Boger, 1983, Nguyen, 1985, Tung et al 1989).

The stress relaxation technique for determining yield stress involves shearing a suspension at a constant rate and reducing the rate to zero either suddenly or slowly. The remnant stress exerted by the sample on the bob, preventing it from returning to a position of zero stress, is considered to be the yield stress (Nguyen and Boger, 1983, Nguyen, 1983). Wall slip may allow this stress to decay with time, resulting in a lower than actual yield stress measurement (Nguyen, 1983).

The accuracy of indirect yield stress determinations depends on the accuracy and number

of data points in the low shear rate range. The low shear rate data can be extrapolated to the shear stress axis with the shear stress axis intercept being the yield value. For visco-plastic fluids, the shear stress drops off very quickly at low shear rates. For some fluids it may be found that if measurements can be made at sufficiently low shear rates no yield stress is found at all (Cheng, 1985). Cheng (1985) recommended constructing an equilibrium flow curve by measuring the equilibrium stress with time at various shear rates and then extrapolating equilibrium flow curve data. Using a model to fit such data provides a good approximation of the yield stress. The model chosen must, however, be suitable to describe the flow behaviour of the particular suspension at low shear rates. In this case, the estimate of yield stress is considered to be better than the value obtained by extrapolating the data (Nguyen, 1985).

The yield values determined using different techniques are difficult to compare as wide variations in the results are often observed (Tung et al, 1985, 1986, 1986, 1989). It is known that these variations may be due to the type of yield stress being measured, the time of measurement, the history of the sample and any errors associated with the technique. Comparisons of these methods have been made by Nguyen (1983), who found a good correlation between the values predicted by the fitted models using nonlinear equations (such as the Casson and Herschel-Bulkley equations) and direct methods such as stress relaxation and the vane method. The Bingham Plastic model was found to estimate a high yield stress, particularly at high suspension solids concentrations. Tung et al, (1986, 1989) found that yield stress values obtained using the vane method were twice as large as values obtained by the model fitting techniques. The results could be explained by the difference between static and dynamic yield stresses (Cheng, 1985). They also found that the stress relaxation method predicted values that were

much lower than values obtained by using other methods. These lower values were attributed to wall slip.

In general, the more methods used to measure the yield stress, the more definite are the results. However, because of time dependence, shear history and the differences between the measuring techniques, the results may be difficult to compare. A method that best suits the application in which the suspension is used is the most appropriate (Cheng, 1985).

CHAPTER 7: RHEOLOGY OF SUSPENSIONS

7.1 Introduction

Suspensions of fine magnetite in water have many of the same mechanical properties as a liquid. These mechanical properties are the responses to the application of stress and are referred to as rheological properties (Harris, 1977, Hanks, 1981). When shear stress is applied to a suspension, the suspension deforms irreversibly and begins to flow according to a shear stress-shear rate relationship (Equation 7.1).

$$\tau = f(\dot{\gamma}) \quad (7.1)$$

This relationship can be graphically plotted as a flow curve, the most common of which are shown in Figure 7.1. The shapes of the curves depend on the micro-rheology which describes the types and magnitude of interactions between the components of a suspension (Goldsmith and Mason, 1967). The interactions are often responsible for the formation of a structure that may complicate the flow behaviour by making it time dependent (Cheng, 1985). In this case, the shear stress depends on both the shear rate and on time (Equation 7.2).

$$\tau = g(\dot{\gamma}, t) \quad (7.2)$$

The influence of the interactions can be controlled by manipulating the physical and

chemical characteristics of the suspension (Tadros, 1980). In this way the rheological properties of suspensions can then be controlled.

7.2 Time Independent Flow

Flow curves are used to characterize the rheological properties of fluids and suspensions. In order to apply this information, it is important to describe these curves mathematically. Several flow curve models have been developed to characterize flow curve shapes. The coefficients from these models can then be used as dependent variables to represent the rheological properties.

7.2.1 Characterization of Flow Behaviour

The basic flow curve shapes (Figure 7.1) or combinations of them, can be used to characterize the rheology of most suspensions. These flow behaviours can be categorized into two groups;

- i. those exhibiting only viscous properties, and
- ii. those exhibiting visco-plastic properties.

In an ideal viscous fluid, any strain resulting from the application of stress results in instantaneous flow. In visco-plastic fluids, a yield stress must be overcome before any strain is relieved by flow.

The simplest flow behaviour is exhibited by fluids that obey Newton's Viscous Law; these

are referred to as Newtonian fluids and they are characterized by a shear stress that is directly proportional to the time derivative of strain. This flow behaviour is shown as flow curve (a) in Figure 7.1 which is a straight line passing through the origin of the shear stress - shear rate plot. The slope of the line is the viscosity which fully characterizes the flow behaviour of these fluids. Many dilute suspensions exhibit these Newtonian properties (Boger et al, 1978, Tadros, 1980, Hanks, 1981).

Fluids or suspensions characterized by flow curves that deviate from that of a Newtonian fluid are referred to as non-Newtonian. Curve (c) of Figure 7.1 represents shear thinning or pseudoplastic properties. These curves exhibit a higher differential viscosity at low shear rates than at high shear rates. The differential viscosity is merely the slope of a tangent to the curve at a specific shear rate. Coarse particle suspensions and suspensions with asymmetric particle shapes are often characterized by this behaviour (Horie and Pinder, 1979, Cheng 1980b).

The second class of non-Newtonian viscous fluids are dilatant or shear thickening (presented as curve (e) in Figure 7.1). The most common example of a suspension exhibiting these properties is quick sand (Hanks, 1981). Upon shearing, such a system becomes less fluid. This type of flow behaviour is less common than shear thinning. Griskey (1989) has summarized what is known about suspensions exhibiting this type of flow behaviour. Dilatant behaviour has also been observed at high shear rates for suspensions that are shear thinning at low rates (Hanks, 1981).

The plastic properties exhibited by many suspensions have been explained in terms of the interactions between particles. These interactions are responsible for the formation of a structure that will, upon the application of stress, resist flow (Hunter and Firth, 1981; Hunter, 1985a). The

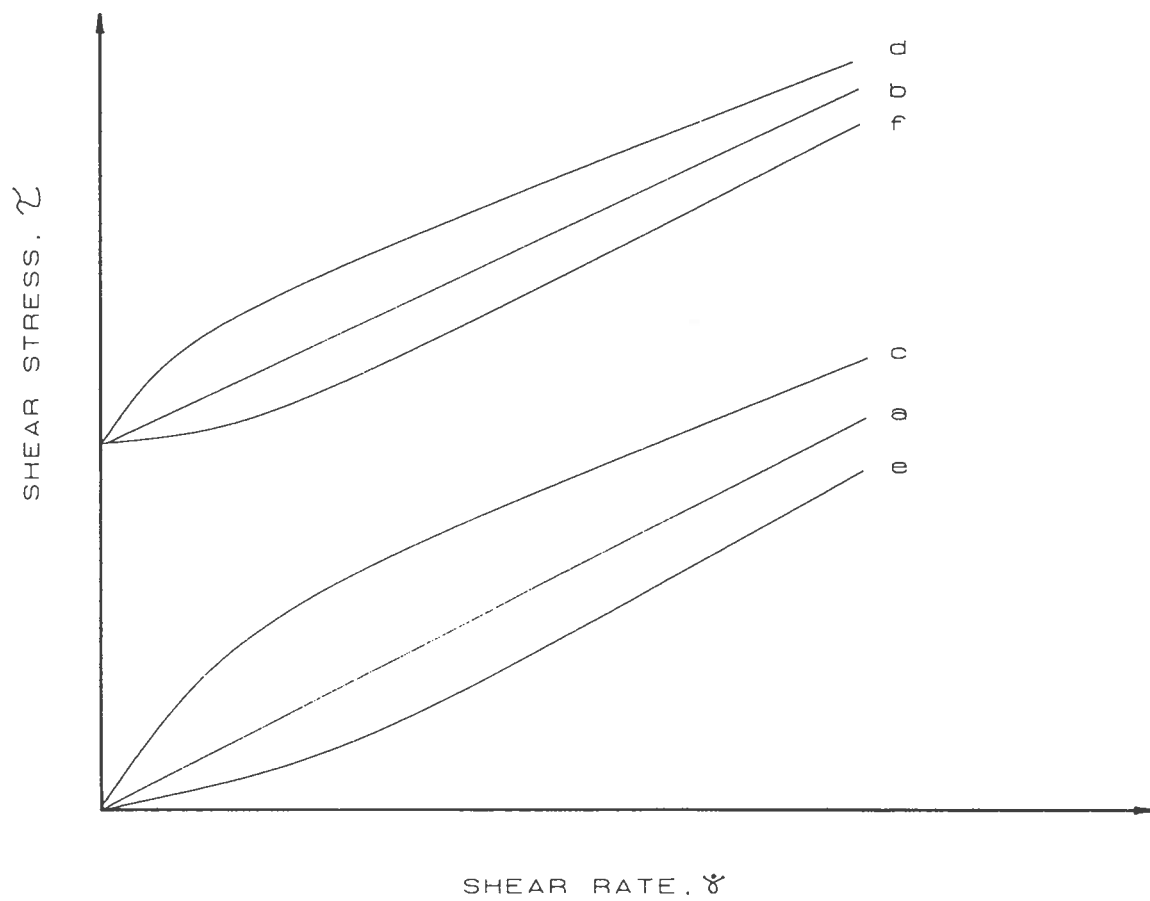


Figure 7.1 Schematic showing various types of flow behaviours a) Newtonian, b) Bingham plastic, c) shear thinning, d) yield shear thinning, e) dilatant, and f) yield dilatant.

minimum stress required to initiate flow is referred to as the yield value. Upon further application of stress, visco-plastic fluids flow in the same manner as the viscous fluids already described. Curves (b), (d) and (f) are examples of Bingham plastic, yield shear thinning and yield shear thickening flow curves, respectively. Concentrated suspensions of interacting particles often exhibit Bingham plastic or yield shear thinning properties (Nguyen, 1983, Nguyen and Boger, 1983, Renehan, 1988b).

Apparent viscosity is often used to characterize the rheology of suspensions. The apparent viscosity represents the viscosity of a suspension at a particular shear rate (Van Wazer, 1963). Figure 7.2 shows two flow curves with the same apparent viscosity. Clearly, apparent viscosity does not fully describe the flow behaviour of these fluids. In addition, it can be misleading as it characterizes both the flow behaviours as being the same when they are different.

7.2.2 Flow Curve Modelling

In order to describe the flow curves mathematically, several rheological models have been developed. Mechanistic approaches are, however, difficult to apply because of the diversity of properties responsible for the rheological behaviour. More commonly, empirical models have been used to describe the characteristics of the flow behaviour.

Several empirical equations relating shear stress to shear rate have been developed to model the basic flow curve shapes. The criteria for the suitability of a model are:

- i. it should fit the data over a wide range of shear rates,
- ii. it should be simple with a minimum number of independent constants,

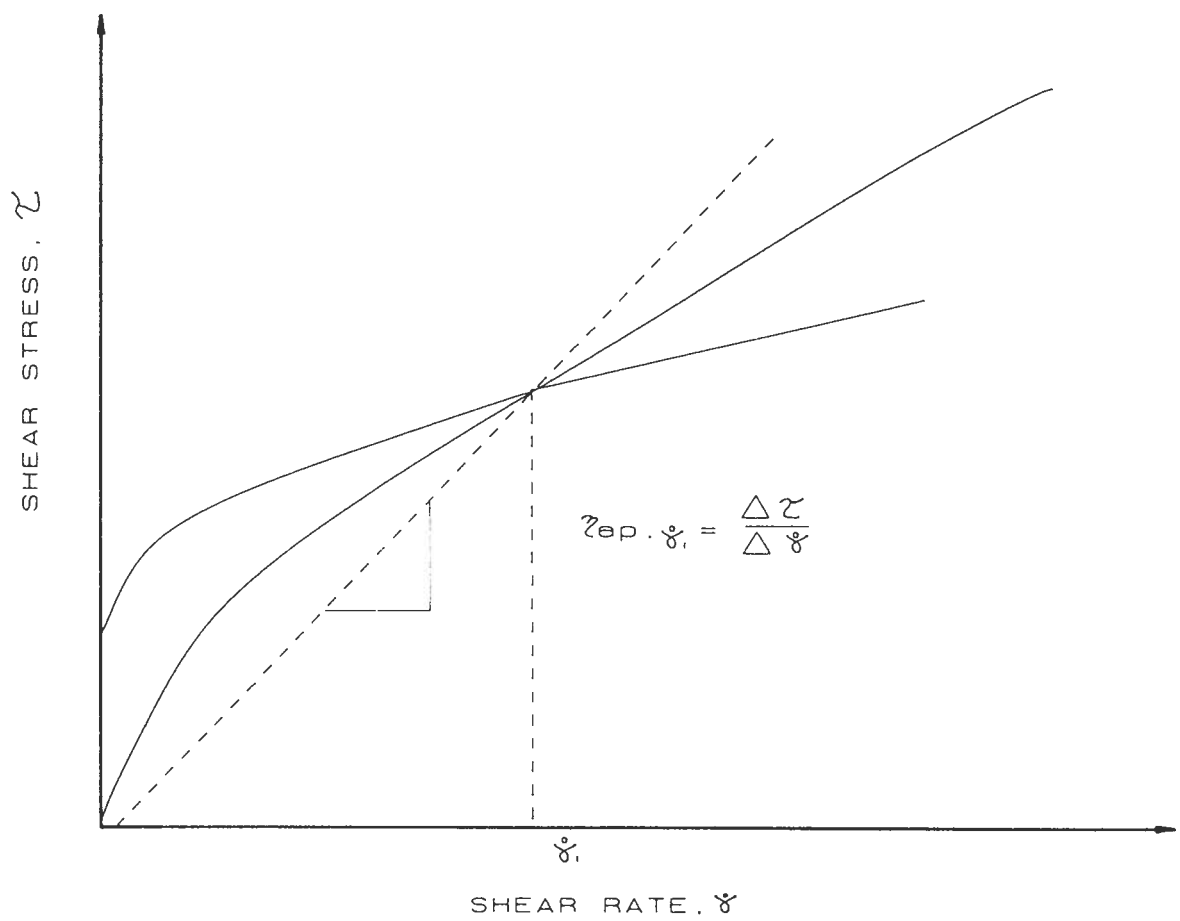


Figure 7.2 Plot of two different flow curves that could be characterized by the same apparent viscosity.

- iii. its' constants should be easily determined and,
- iv. the constants should have some physical significance.

Regression methods may be used to fit the equations to the rheological data. The fit of these equations can then be compared using statistical methods. Many of the equations were developed for specific systems for which their coefficients have physical significance. In particular, coefficients may describe various viscosities or yield stress values which help to explain the types of interactions responsible for the rheological properties. Models with the smallest number of coefficients are preferred because they are usually simple to use.

The following describes some of the models commonly used to represent the rheological properties of suspensions. Included are Newton's Viscosity Law, three models that can be used to characterize shear thinning properties and three models that describe plastic flow properties. The shear thinning properties are often characterized using the Power-Law Model, the Cross Model and the Carreau Model. Models that describe plastic flow properties must have a yield stress term such as the Bingham Plastic Model, the Herschel Bulkley Model and the Casson Model.

7.2.2.1 Newton's Viscosity Law

The flow behaviour of Newtonian fluids can be described by Newton's Law of Viscosity (Equation 7.3).

$$\tau = \eta_N \dot{\gamma} \quad (7.3)$$

where η_N is the Newtonian coefficient of viscosity.

According to Hanks (1981), this equation is not a law but rather an empirical rheological equation of state. It has been used to describe the rheology of dilute suspensions of non-interacting spheres in Newtonian liquids (Einstein, 1905, Harris, 1977, Boger, 1978, Tadros, 1980, Hanks, 1981, Czaban, 1988). Above a critical solids concentration, suspensions exhibit non-Newtonian properties (Nguyen and Boger, 1984, Czaban, 1988). The onset of non-Newtonian flow is believed to be due to the particle-particle interactions that become significant with increasing solids concentrations (Smoluchowski, 1916, Tadros, 1980, 1985). The critical solids concentration, above which interactions cause the flow to become non-Newtonian, has been found to decrease with decreasing particle sizes and with increasing asymmetry of particle shapes.

7.2.2.2 The Power-Law Model

The power law model originated from empirical observations by Ostwald who noticed that rheological data plotted a straight line on log-log plots (Hanks, 1981). The model (Equation 7.4) is also referred to as the Ostwald-De Waele model.

$$\tau = k\dot{\gamma}^n \quad 7.4$$

This equation can be used to model all three basic viscous flow behaviours. The coefficients k and n are referred to as the fluid consistency index and flow behaviour index,

respectively (Boger et al, 1978, Nguyen, 1983). A high k value implies that the suspension has a high viscosity. The deviation of n from unity is a measure of the non-Newtonian behaviour. Clearly, at n equal to unity, the equation becomes Newton's viscous law and k becomes η_N . For n less than unity, the model describes pseudoplastic flow and, for n greater than one it describes dilatant flow.

The model fails to fit the flow behaviours of many suspensions accurately at very low and very high shear rates (Van Wazer, 1963, Boger et al, 1978, Hanks, 1981, Nguyen, 1983). Another criticism is that, based on dimensional analysis, the coefficients have little physical significance (Van Wazer, 1963, Harris, 1977). Despite these misgivings, it is likely the most widely used model for describing pseudoplastic behaviour (Harris, 1977). It has been used to characterize coal-oil mixtures (Alessandrini et al, 1983), kaolinite suspensions (Czaban, 1988), quartz and feldspar slurries (Aarnio and Laapas, 1988) as well as other mineral slurries (Boger et al, 1978).

7.2.2.3 The Cross Model

The Cross model (Equation 7.5) was developed based on the assumption that pseudoplastic flow is due to the process of the formation and rupture of linkages in chains of particles. This process is believed to occur in aggregated systems where links between particles result in the formation of chain-like aggregates which rupture due to Brownian motion and shearing (Cross 1965, 1970).

$$\eta_{ap} = \eta_{\infty} + \frac{(\eta_0 - \eta_{\infty})}{(1 - \alpha \dot{\gamma}^m)} \quad (7.5)$$

where η_{ap} is the apparent viscosity,

η_{∞} is the apparent viscosity at infinite shear rate,

η_0 is the apparent viscosity at zero shear rate,

α is a material constant associated with rupture of linkages, and

m is a parameter that depends on the polydispersity.

The material constant α is defined as k_1/k_0 where k_0 is the rate constant associated with rupture due to Brownian movement and k_1 is the rate constant for ruptures resulting from shearing.

Studies with calcite mineral suspensions revealed that values of η_0 and α were very large. The high α value is attributed to the relative insignificance of the effect of Brownian movement on the linkage rupture as compared to the effect of shearing. Therefore the ratio of the respective rate constants is very high. This could be expected for most coarse suspensions. In the case of high initial viscosity, η_0 , and relatively coarse particles, the Cross model can be simplified (Equation 7.6).

$$\eta = \eta_{\infty} + \alpha \dot{\gamma}^{-m} \quad (7.6)$$

A value of m equal to $2/3$ was found to be suitable for many pseudoplastic systems which reduces the number of coefficients in the equation to two (Cross, 1965). The Cross model has been applied to suspensions that exhibit pseudoplastic behaviour (Mewis and Spaul, 1976).

7.2.2.4 The Carreau Model

The Carreau model (Equation 7.7) was developed to describe the pseudoplastic properties of polymer solutions and melts. It is based on molecular network theory which describes the non-Newtonian flow with respect to the creation and loss of segments. The rate of the creation and loss of these segments is a function of shear rate and results in the non-Newtonian response to shear. At a high deformation rate there is a simultaneous increase in rate of segment formation due to increased contacts, and an increased rate of junction breakage due to shearing (Carreau 1972, 1979a, 1979b).

$$\eta = \eta_o(1 + (A\dot{\gamma})^2)^{-s} \quad (7.7)$$

where, A is a time constant,

η_o is the zero shear rate viscosity, and

s is associated with the power law behaviour.

According to this equation, at high shear rates the viscosity approaches zero which is a flaw of the model. To correct this flaw, a high shear rate viscosity term, η_∞ , can be added to the equation as indicated in Equation 7.8.

$$\frac{(\eta - \eta_\infty)}{(\eta_o - \eta_\infty)} = \eta_o(1 + (A\dot{\gamma})^2)^s \quad (7.8)$$

This equation has been successfully applied to numerous polymer solutions (Carreau,

1972,1979; Tam, 1988). It is a flexible, meaningful and simple model that is an improvement over the power-law model (Carreau, 1979).

7.2.2.5 The Bingham Plastic Model

The Bingham Plastic model (Equation 7.9) describes the simplest type of visco-plastic flow. The model characterizes the ideal case in which a complete structure breakdown occurs once the yield stress has been exceeded. Once the yield stress is exceeded a linear relationship exists between the shear stress and shear rate (Nguyen, 1983).

$$\tau = \tau_{BY} + \eta_{pl}\dot{\gamma} \quad (7.9)$$

where, τ_{BY} is the Bingham yield stress, and

η_{pl} is the plastic viscosity.

For most real systems, once the yield stress has been exceeded, the suspensions exhibit a non-linear flow behaviour. In this case the model may be adequate for fitting only the very high shear rate data (Nguyen, 1983). However, using this equation to predict yield stress can be very inaccurate. The lack of data at low shear rates often results in a high estimate of the true yield stress if the Bingham model is used. The model can even predict a yield stress where none exists (Nguyen, 1983 Nguyen and Boger, 1983). Therefore, the Bingham yield stress should be considered to be a model parameter rather than a true yield value (Mewis and Spaul, 1976).

The Bingham model is widely used because of its simplicity. The equation is based on

observations made with paints and clay suspensions. Nguyen found that this equation fits flow curves for red mud suspensions with low solids concentrations (<20% by volume) better than those with high concentrations. Other suspensions that have been modelled with this equation include suspensions of kaolinite clays (Nicol and Hunter, 1970, Czaban, 1988), drilling mud (Nguyen, 1983, Nguyen and Boger, 1984), flocculated brewing yeast suspensions (Speers, 1989) and many other mineral suspensions (Mewis and Spaull, 1976, Hanks, 1981).

7.2.2.6 The Herschel Bulkley Model

The Herschel Bulkley model (Equation 7.10) is a combination of the Ostwald-De Waele power law model and the Bingham plastic model. As the yield stress term becomes small, the equation assumes the form of the power-law model and, as the power coefficient, n , approaches unity, it becomes the Bingham plastic model.

$$\tau = \tau_{HB} + k\dot{\gamma}^n \quad (7.10)$$

where, τ_{HB} is the yield value, and

k and n have the same meaning as described for the power law equation.

This model fits the curvature at low shear rates and therefore provides better estimates of yield stress than the Bingham model. Yield stress values determined using this equation compare well with the values determined using direct measurement methods (Nguyen, 1983, Nguyen and Boger, 1983). This simple, versatile and practical empirical model has been widely

used to characterize both dilute and concentrated suspensions (Mewis and Spaull, 1976, Mun and Boger, 1988). Examples of the applications include coal slurries (Alessandrini et al, 1983, Casassa et al, 1984), red mud (Nguyen, 1983, Nguyen and Boger, 1984), drilling fluids (Alderman et al ,1988), kaolin suspensions (Czaban, 1988), highly concentrated ceramic suspensions (Doraiswamy et al, 1988), and paraffin wax in oil solutions (Al-Farris and Pinder, 1987).

7.2.2.7 The Casson Model

The Casson model (Equation 7.11) is a simple two parameter model that has a physical basis and is derived from structural arguments. It is proposed that particles form chain-like aggregates, the dimensions of which control the viscosity. Under conditions of flow, disruptive stresses develop which are a function of shear rate and particle aggregate size. The disruptive stresses are responsible for the break up of these aggregates such that for a particular shear rate there is a mean aggregate size. The formation of the aggregates is the result of net inter-particle attraction forces. The contribution of these aggregates to the viscosity depends on their shape and orientation. It is assumed that the aggregates form chains that can be treated as cylindrical rods. The contribution of hydrodynamic effects involving these rods to the energy dissipation was used to develop the Casson model (Casson, 1959).

$$\tau = (\tau_{CY}^{1/2} + (\eta_C \dot{\gamma})^{1/2})^2 \quad (7.11)$$

where, τ_{CY} is the Casson yield stress, and

η_C is the limiting viscosity at high shear rates.

The coefficients are related to the suspension solids concentration, the viscosity of the suspended liquid and various parameters describing the rod size and orientation. Since the Casson yield stress is the flow curve intercept with the shear stress axis and the Casson viscosity is the slope of the flow curve at high shear rates, the coefficients are easy to determine. In addition, the coefficients have physical significance since they have stress (Pa.) and viscosity (mPa.s) units. Tadros (1980) developed a similar equation from fundamental principles of particle aggregation. Mills and Snabre (1988) applied fractal concepts to describe particle interactions and also obtained a similar expression. This model is capable of fitting low shear rate curvature and therefore its estimates of the yield stress compare well to values obtained from direct measurement methods (Nguyen and Boger, 1983, Tung et al, 1989). Casson developed the model for suspensions of pigments in varnishes. Examples of its applications include, kaolin suspensions, drilling fluids (Czaban, 1988), yeast suspensions (Speers et al, 1989), coal suspensions (Renehan, 1988a) red mud (Nguyen, 1983, Nguyen and Boger, 1983) and magnetite suspensions (Klein et al, 1990).

7.3 Time Dependent Flow

Many suspensions exhibit time dependent flow properties. For such suspensions shearing at a constant rate results either in an increase or in a decrease in shear stress with time. A stress increase over time is referred to as rheopexy and it is usually found in suspensions with dilatant

properties. If a stress decrease occurs over time, the suspension is thixotropic; this stress decrease is commonly found in pseudoplastic suspensions (Van Wazer, 1963). Both types of time dependent flow behaviour are exhibited by suspensions that have a yield stress. Thixotropy is much more common than rheopexy.

The time dependent flow behaviours have been described in terms of a structure within the suspension. The structure is formed by the attachment of particles creating aggregates that may be bonded together. These same attachments may also be responsible for a yield stress (Van Wazer, 1963, Cheng, 1971, Nguyen, 1989). Upon shearing, the structure changes with time resulting in the increase or decrease in stress at steady shear. Shearing causes inter-particle and inter-floc attachments to either break, if the attachments already exist, or to form due to shear induced collisions. A net breakage of attachments, producing smaller aggregates or dispersed particles, is responsible for thixotropic behaviours. The opposite, net formation of attachments, is caused by shear induced collisions and is responsible for rheopexy. At a particular shear rate, the stress will typically initially change sharply and with time will asymptotically approach an equilibrium value. At this equilibrium stress, the number of attachments being broken equals the number being formed. If the equilibrium stress is reached very quickly, it may not be possible to observe the time dependence. This process may or may not be reversible.

Time dependent properties have also been observed in suspensions of non-interacting asymmetric particles. Flow causes elongated particles to align in the direction of shear, creating a state of lower energy dissipation. In this case, the time required for the particles to align is responsible for the measured thixotropic stress decay (Pinder, 1964, Brown and Pinder, 1971). This shape effect increases with particle aspect ratio to a limit (Pinder, 1964).

The breakdown and formation of structure has been modelled using a reversible kinetic chemical rate equation. The level of an equilibrium structure is dependent on the rate of structure breakage and formation (Pinder, 1964). The rate of structure breakdown can be described by Equation 7.12.

$$\frac{\delta \eta}{\delta t} = k_f \eta^m - k_r (\eta_o - \eta)^n \quad (7.12)$$

where, k_r and k_f are rate constants for structure rupture and formation,

η_o is the maximum apparent viscosity,

η is the apparent viscosity at time t , and

n and m are exponent parameters.

This structure may also be expressed in terms of other rheological parameters such as yield stress. Several researchers have used this equation to model time dependent flow properties of suspensions. Various orders, m and n , have been tested and the best fit to stress decay data was found to depend on the type of suspension (Pinder, 1964, Brown and Pinder, 1971, Horie and Pinder, 1979, Nguyen, 1983).

Cheng (1971) modelled time dependent flow properties using an equation of state along with a rate equation. The equation of state (Equation 7.13) describes the shear stress as a function of shear rate for a particular level of structure. The rate equation (Equation 7.14) describes the change in structure with time in terms of shear rate and the instantaneous amount of structure present.

$$\tau = \eta_{sp}(\lambda, \dot{\gamma}) \dot{\gamma} \quad (7.13)$$

$$\frac{\delta \lambda}{\delta t} = g(\lambda, \dot{\gamma}) \quad (7.14)$$

where, g is the rate of structural build up, and λ is a structural factor.

The rate constant, g , is negative if structure breakdown occurs and positive for structure formation. The magnitude of the rate constant is a function of the magnitude of the difference between the instantaneous and equilibrium structures (Cheng, 1971, Mewis and Spaul, 1976, Cheng, 1985).

The degree of time dependency can also be characterized by the hysteresis produced from increasing the shear rate to a given value and then decreasing it to zero. The area between the increasing and decreasing shear rate curves is a measure of thixotropy or rheopexy which can be compared providing that a consistent measuring procedure is used. In this way the influence of suspension variables on thixotropy can be determined (Moore and Davies, 1956, Saunders, 1976, Mehta et al, 1983, Windhab et al, 1986, Alderman et al, 1988, Chen et al, 1988).

7.4 Visco-elasticity

Visco-elastic properties have been measured in very fine and highly concentrated suspensions (Tadros, 1980, 1988, 1990, Ahuja and Isganitis, 1988, Ohl, 1988, Doraiswamy et al, 1988). In such suspensions, the structure, resulting from inter-particle interactions, may deform elastically under small stresses. When high stresses are applied the suspension flows irreversibly. Measurement of elastic properties provides information on the type of structure that exists.

CHAPTER 8: CONTROL OF RHEOLOGICAL PROPERTIES

8.1 Introduction

Micro-rheological effects determine the rheological properties of a suspension. The micro-rheological effects include hydrodynamic effects, electroviscous effects, aggregation effects and granulo-viscous effects. The magnitude of each of these micro-rheological factors depends on the physico-mechanical and physico-chemical properties of the suspension. Physico-mechanical parameters describe the physical components of the suspension and include solids concentration and properties of the particles such as density, shape, size and size distribution. Physico-chemical parameters that influence the inter-particle forces of attraction and repulsion include pH, dissolved ions, magnetization and chemicals such as dispersing agents. Both types of parameters can be altered to control the micro-rheological factors and thereby the flow behaviour of the suspension.

8.2 Micro-rheology

The macroscopic rheological properties of a suspension can be predicted from a detailed description of behaviour of elements from which it is composed; this is referred to as the micro-rheology (Goldsmith and Mason, 1967). In particular, energy dissipation due to hydrodynamic, electroviscous, aggregation and granulo-viscous effects are responsible for the macroscopic rheological properties of suspensions. Hydrodynamic effects describe energy

dissipation resulting from the movement of particles in the liquid (Brenner, 1972). Granuloviscous effects describe the physical interactions between particles in dense suspensions that dissipate energy via friction (Cheng, 1978). There are three electroviscous effects; these result from electrostatic forces of repulsion and influence how the particles interact (Smoluchowski, 1916, Tadros, 1980, Goodwin, 1981). The aggregation effects describe the energy dissipated from the rupture and formation of bonds that result from attractive forces between particles (Papenhuijzen, 1972, Firth and Hunter, 1976).

8.2.1 Hydrodynamic Effects

Particle movement in liquid results in viscous energy dissipation which is given off as heat. Einstein (1905) derived an expression for the rheological properties of dilute suspensions from the energy dissipated due to fluid flow past hard, spherical, non-interacting particles. The expression obtained for the relative viscosity includes the first two terms on the right side of Equation 8.1 in which the coefficient equal to 2.5 is referred to as the intrinsic viscosity. The value of the intrinsic viscosity will vary depending on the size and shape of the particles (Goldsmith and Mason, 1967, Goodwin, 1981).

$$\eta_r = \frac{\eta_s}{\eta_o} = 1 + 2.5\phi + k_2\phi^2 + k_3\phi^3 + \dots \quad (8.1)$$

where η_r is the relative viscosity,

η_s is the suspension viscosity,

η_o is the viscosity of the suspending fluid,

ϕ is the volume solids fraction, and

k_i are coefficients.

At higher solids concentrations, greater than approximately 1% by volume, hydrodynamic particle interactions contribute to the relative viscosity; their contributions are described by the higher order terms in Equation 8.1. Several investigators have used both theoretical and empirical methods to derive the values of these higher order coefficients; most of these terms have been summarized by Rutgers (1962a, 1962b) and Thomas (1965).

Particle movement and interaction dynamics are related to flow behaviour (Goldsmith and Mason, 1965, Brenner, 1972). In particular Brownian motion, particle shape and particle deformation influence the particle motion (ie. translation, rotation and orientation) in a flow field. The particles will tend to adopt that motion which corresponds to the least dissipation of viscous energy (Goldsmith and Mason, 1967).

The influence of interactions on the viscous dissipation is more difficult to describe. Krieger and Dougherty (1959) described the viscous properties of concentrated suspensions by considering the contribution of doublets. Doublets form as two rotating particles approach each other; because of the viscous resistance between the approaching rotating particles, the particles will rotate about each other before separating and continuing on their path of movement. The viscosity was considered to be related to the concentration of doublets which in turn depends on the rate of their formation and separation. Shearing forces contribute to the breakage of the doublets thus explaining the shear thinning properties of concentrated suspensions.

Frankel and Acrivos (1967) used lubrication theory to describe the energy dissipation associated with the extrusion of fluid from the gap between two approaching particles. They

claimed that this type of hydrodynamic energy dissipation was much greater than that resulting from particles sliding past each other. While many of the types of hydrodynamic interactions that contribute to the viscosity have been identified, it is difficult to quantitatively assess their importance.

For small particles (-10µm) and under low shearing conditions, Brownian movement dominates the translatory and rotational motion of particles. It acts to disperse the particles and it randomizes their position and orientation distributions (Goodwin 1981, Mewis and Spaul 1976). Brownian movement is significant at low rotary and translational Peclet numbers, where the rotary Peclet number is the ratio of convective to Brownian rotation, Pe_r , (Equation 8.2) and the translational Peclet number is the ratio of inertial to Brownian translation, Pe_t , (Equation 8.3). Particles coarser than 10 µm are not strongly affected by Brownian movement because of the greater influence of the convective and inertial forces. With increasing shear rate, the ordering effect of flow will become more important than the thermal energy (Mewis and Spaul, 1976).

$$Pe_r = \frac{D}{D_r} \quad (8.2)$$

$$Pe_t = r^2 \frac{D}{D_t} \quad (8.3)$$

where, D is the convective diffusion coefficient,

D_r is the rotational diffusion coefficient,

D_t is the translational diffusion coefficient, and

r is the particle radius.

8.2.2 Granuloviscous Effects

For dense suspensions, with solids concentration greater than 35% and approaching the maximum packing fraction, rheological responses have been related to granuloviscous effects (Cheng, 1978). At these high concentrations particle packing structure can strongly influence the flow properties of the suspension. The packing structure can change in response to: the type of flow (extensional versus simple shear), the rate of shear and the physico-mechanical and physico-chemical conditions. Frictional energy is dissipated as the result of particles sliding past each other (Clarke, 1967).

The granuloviscous effects are responsible for shear thinning and time dependent properties, since packing structures change with shear rate over time contributing to the variance in the measured rheological responses. While granuloviscous effects are more significant at high solids concentrations, the frictional energy dissipation also contributes to the viscosity of less concentrated suspensions (Cheng 1978, 1980, 1984).

8.2.3 Electroviscous Effects

Inter-particle electrostatic repulsion forces are responsible for viscous energy dissipation via the three electroviscous effects. In suspensions with high particle zeta potential and low counter-ion concentration (high electrostatic repulsion) the electrical double layer may have a substantial thickness. Under these conditions, soft particle interactions will influence the flow behaviour (Smoluchowski, 1916, Tadros, 1980, 1985, Goodwin, 1981).

The primary electroviscous effect accounts for the dissipation of energy that results from the deformation of the diffuse part of the electrical double layer during flow (Smoluchowski, 1916, Tadros, 1980, 1985, Goodwin, 1981). It contributes to the intrinsic viscosity term in Equation 8.1 (Papenhuijzen, 1972) and is responsible for elastic properties which result from the tendency of the double layer to reform to a spherical shape around a particle (Smoluchowski, 1916, Goodwin, 1981, Tadros, 1985).

The secondary electroviscous effect results from inter-particle repulsion that adds to the effective radius of the particles and decreases the excluded volume of the suspension. The magnitude of the effect is related to the thickness of the double layer and it becomes much greater than the primary effect with increasing solids concentration (Russel, 1980). It influences the paths of approaching particles and causes doublets to separate (Goodwin, 1981), thus contributing to the second order hydrodynamic interaction coefficient, k_2 , in Equation 8.1 (Papenhuijzen, 1972).

The tertiary electroviscous effect results in the deformation of the particle as a result of the repulsive forces which causes them to change in size and shape (Mewis and Spaul, 1976). This effect may be neglected for suspensions of rigid particles (Tadros, 1985).

8.2.4 Aggregation Effects

The presence of aggregates in a suspension strongly influences the flow behaviour. Aggregates form as a result of net attractive forces between particles. London's Van der Waals and electrostatic forces are responsible for particle aggregation or dispersion. The theory

developed by Derjaguin, Landau (1941), Verwey and Overbeek, (1948), "DLVO theory", describes the net potential energy of attraction and repulsion as a function of distance between particles. A typical potential energy curve is presented in Figure 8.1 which shows the primary and secondary minimum potential energy wells at which distances two particles would attach. Aggregation of particles in the primary minimum energy well is referred to as irreversible coagulation. Comparatively small shear forces are needed to disperse particles aggregated in the secondary minimum and this is therefore referred to as reversible coagulation.

In addition to the forces described above, remnant magnetic attractive forces will influence the shape of the potential energy curve. Magnetized particles behave like small magnets with a north and south pole. When these particles are aggregated, the particle positions are aligned as the result of the attraction of opposite poles and the repulsion of like poles. These forces are long range and may be quite strong.

Aggregation effects are the most complex ones that contribute to the rheological properties. Papenhuijzen (1972) described the viscous, elastic and thixotropic properties of suspensions in terms of a network model. The network consists of particles arranged in chains that are stretched during deformation until the bonds are broken. At high shear rates the structure is broken and non-interacting aggregates make up the dispersed phase. The elastic properties are associated with the stretching of the chains, the viscous properties are related to the flow around the aggregates and the thixotropic properties are related to the time required to break and form the structural units.

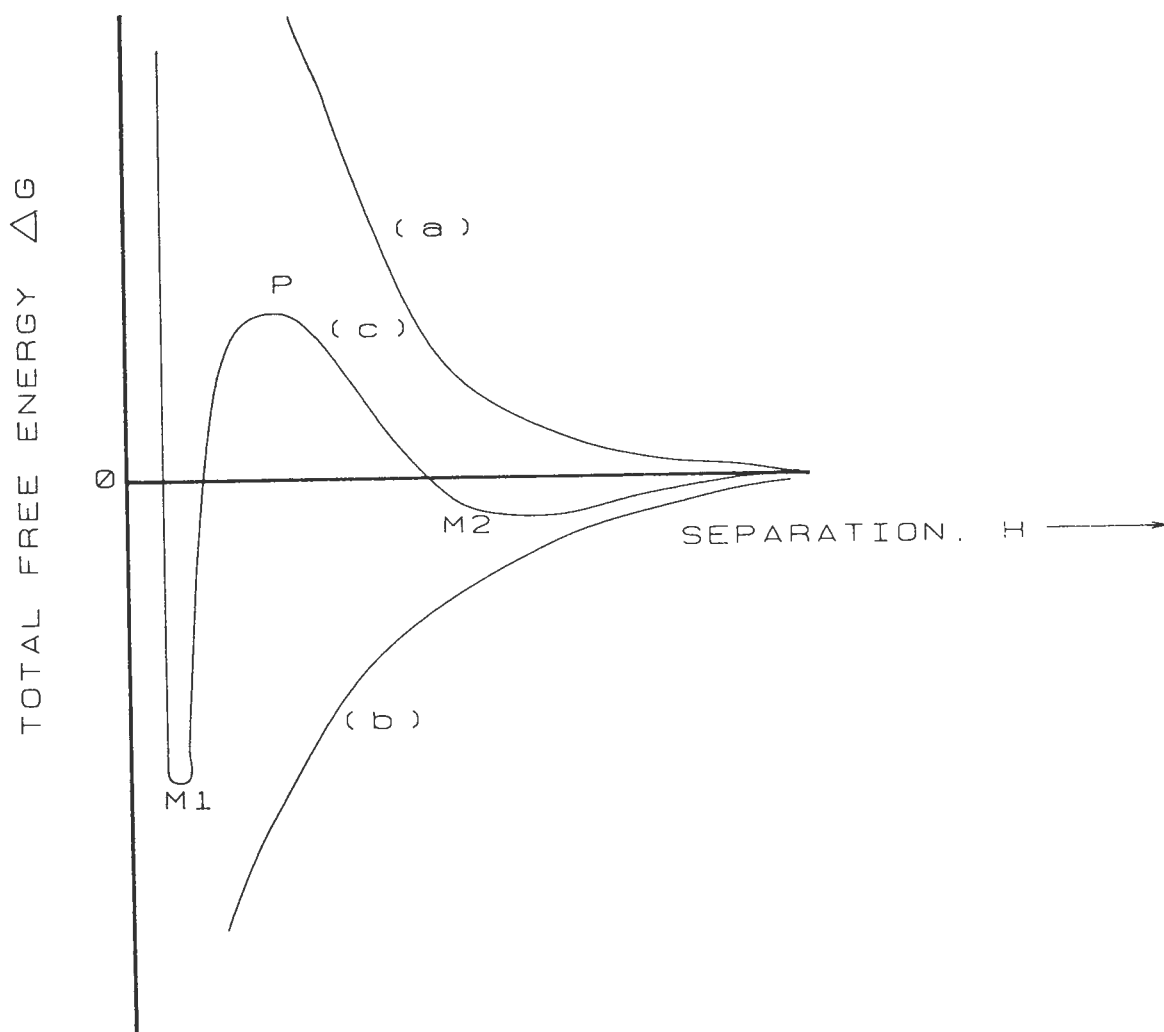


Figure 8.1 Typical potential energy curve at the surface of a mineral particle.

Firth and Hunter (1976) developed the elastic floc model that describes the rheological properties of aggregated suspensions in terms of the contributions to energy dissipation resulting from viscosity of the fluid, floc rotation, bond rupture and formation, and doublet rupture and formation. The energy dissipated from doublet rupture consists of the energy to rupture links between the flocs, to stretch links within a floc, and to move liquid inside a floc. In describing this model the term floc refers to a coagulated group of particles. Van de Ven and Hunter (1977) found that the viscous dissipation transmitted by the particle movement within a floc, together with the viscous flow around flocs, described most of the total energy dissipation. Expressions describing these types of energy dissipations are used to develop equations that estimate values for the plastic viscosity, Bingham yield stress and critical shear rate. The plastic viscosity was related to the hydrodynamic energy dissipation resulting from flow around the aggregates using Einstein's (1905) equation and more suitably Krieger's (1971) equation, which applies to more concentrated suspensions. The yield value is determined from the energy dissipated from fluid flow in a floc. The critical shear rate, above which no doublets exist and the flow curve is linear, is determined from the number and strength of the inter-floc bonds. Many of the assumptions of the model restrict its application to colloidal dispersions and it only predicts the shear stress at shear rates that are greater than the critical one (Hunter, 1985a).

Van de Ven and Hunter (1977) suggested that suspensions that are weakly coagulated (ie. reversible secondary minimum coagulation) become dispersed at low shear rates. At higher shear rates, primary minimum coagulation can be induced to form doublets. At yet higher rates, the kinetic energy may be large enough to cause these primary doublets to disperse (Russel 1980, Goodwin 1981).

8.3 Physico-mechanical Parameters

Physico-mechanical parameters that affect the rheological properties of suspensions include the solids content and the density, shape, size and size distribution of the particles.

8.3.1 Solids Content

Several studies have shown that the viscosity of suspensions increase in an exponential manner with solids concentration and becomes infinite at the maximum packing fraction. For dilute suspensions of non-interacting spherical particles (volume solids contents less than a few percent), Einstein (1905) derived a linear equation, based on the viscous energy dissipated by the flow around a sphere, relating the relative viscosity to solids content. With increasing solids concentrations, there is a greater number of particle interactions; these are responsible for the exponentially increasing viscosity. These interactions result in energy dissipation that can be described in terms of the hydrodynamic, granuloviscous, electroviscous and aggregation effects (see Section 8.2). These effects are also responsible for the increased non-Newtonian behaviour that is found at higher solids concentrations.

The number of hydrodynamic particle interactions increases with solids content. These interactions dissipate energy by extruding and shearing fluid as particles approach and slide past each other (Frankel and Acrivos, 1967). If the particles are rotating, they will form doublets with a concentration that is proportional to the solids concentration. Since these dissipate more energy than two separated particles, they help to explain the exponentially increasing viscosity (Krieger

and Dougherty, 1959). Their concentration is also proportional to the shearing conditions, since high shearing causes the break up of doublets; this break up can explain the shear thinning properties exhibited by concentrated suspensions (Krieger and Dougherty, 1959, Krieger, 1971).

At high solids concentrations, (greater than 30% by volume) granuloviscous effects determine the frictional energy dissipation that results from crowded particles sliding past each other (Cheng, 1978). At high solids concentrations, these effects dominate the flow behaviour. When these suspensions are sheared, the packing arrangement can change causing the suspension to exhibit time dependent and non-Newtonian properties.

Secondary electroviscous effects result in an increase in the effective solids content of a suspension and thereby enhance the contribution of the hydrodynamic interactions described above (Goodwin, 1981). Primary electroviscous effects, that are the result of the deformation of the electrical double layer, are responsible for viscoelastic properties (Tadros, 1985). These effects become more pronounced as particle crowding increases.

When aggregation effects exist, the aggregates may be considered to be the suspended units in the suspension. This results in an increase in the effective solids content as the aggregates will trap liquid (Lewis and Neilson, 1968). The size of the aggregates depends on the types of attractive forces, the shearing conditions and the solids concentration in the suspension (Firth and Hunter, 1976). At high solids concentrations, the aggregates may interconnect to form a network structure that is often associated with a yield stress (Papenhuijzen, 1972). The main source of energy dissipation has been attributed to the viscous resistance by fluid movement in the deforming aggregates (Van de Ven and Hunter, 1977).

Many of these effects have been considered in the evaluation of the coefficients of the

"general power formula" (Rutgers 1962a, 1962b). This model, which is an extension of Einstein's equation, applies only to moderately concentrated suspensions and does not cover the entire solids concentration range (Rutgers 1962b, Thomas 1965). A number of equations have been developed that relate the viscosity to the maximum solids packing fraction, Table 8.1. As solids contents approach the maximum packing fraction, the suspension viscosity becomes infinite.

Eilers (1941) used the maximum solids content as an upper limit in relating relative viscosity to solids fraction for bitumen emulsions. Chong (1971) modified Eilers equation to correlate the relative viscosity to solids content for poly-disperse suspensions. Mooney (1951) considered the crowding effects of mono-disperse spheres to obtain his equation. He also showed how this approach could be extended to bimodal and poly-disperse suspensions (Mooney 1951). Krieger and Dougherty (1959) also used particle crowding, in a similar manner, to derive their equation. Simha (1952) used a cage model to describe the extent to which particles beyond nearest neighbours can hydrodynamically interact to derive his equation. Frankel and Acrivos (1967) obtained an expression for the energy dissipated between two approaching particles and applied it to obtain an expression for concentrated suspensions of spherical particles.

Ting and Luebber (1957) considered the effects of liquid-solid density ratio, particle size distribution and particle shape on packing arrangements to derive an empirical relation between relative viscosity and some function of these parameters for varying solids contents. Sherman (1965) derived an expression relating the relative viscosity to the solids content, maximum packing fraction and mean particle size. He recognized the non-Newtonian behaviour of

Table 8.1 Models describing relative viscosity as a function of solids content and maximum packing fraction.

Eiler (1941)

$$\eta_r = \left[\left(1 + \frac{1}{2} [\eta] \phi \right) / \left(1 - \frac{\phi}{\phi_m} \right) \right]^2$$

Mooney (1951)

$$\eta_r = \exp \left[[\eta] \phi / \left(1 - \frac{\phi}{\phi_m} \right) \right]$$

Simha (1952)

$$\eta_r = \left(\frac{54}{5f^3} \right) \left[\phi^2 / \left(1 - \frac{\phi}{\phi_m} \right)^3 \right], f = \text{packing parameter}$$

Ting & Luebbers (1957)

$$\eta_r = \frac{\phi_{v,\infty}}{(\phi_{v,\infty} - \phi)}, \phi_{v,\infty} = f \left(\phi_{\max}, \frac{\rho_l}{\rho_s}, d \right)$$

Krieger & Dougherty (1959)

$$\eta_r = \left(1 - \frac{\phi}{\phi_m} \right)^{-\phi m[\eta]}$$

Table 8.1 Models describing relative viscosity as a function of solids content and maximum packing fraction. (Continued)

Sherman (1965)

$$\eta_r = \exp \left[0.036 d_m / \left(\frac{\phi_m}{\phi - 1} \right)^{\frac{1}{3}} - 0.15 \right]$$

Frankel & Acrivos (1967)

$$\eta_r = \frac{9}{8} \left[\left(\frac{\phi}{\phi_m} \right)^{\frac{1}{3}} / \left(1 - \left(\frac{\phi}{\phi_m} \right)^{\frac{1}{3}} \right) \right]$$

Chong et al (1971)

$$\eta_r = \left[1 + 0.75 \left(\frac{\phi}{\phi_m} \right) / \left(1 - \frac{\phi}{\phi_m} \right) \right]^2$$

Mills & Snabre (1988)

$$\eta_r = (1 - \phi_{eff}) / \left(\frac{1 - \phi_{eff}}{\phi_m} \right)^2, \quad \phi_{eff} = f(\tau)$$

suspensions in his derivation as being related to the particle size through its effects on aggregation and interaction energy. Mills and Snabre (1988) describe the non-Newtonian flow behaviour of suspensions of aggregated particles by considering the radius of fractal clusters in simple shear.

The equations described above are some of the better known ones. Many more models have been developed, some of which have been summarized by Rutgers (1962a, 1962b). Although most were derived for mono-disperse suspensions of spherical particles, they have been successfully applied to systems such as non-Newtonian coal slurries (Castillo and Williams, 1979, Ogden and Rutter, 1984, Wildemuth and Williams, 1985) and various other mineral suspensions that contain poly-disperse and aggregated particles in a variety of physico-chemical environments (Lewis and Neilson, 1968, Fedors, 1973,1975, Renehan, 1988b). Examination of these models reveals that the viscosity of suspensions can be minimized by maximizing the packing density of the suspension. The packing density is a function of the effective particle size distribution and the state of aggregation.

8.3.2 Particle Density

In many industrial suspensions the solids density is greater than the fluid density. In these suspensions, shear forces and gravitational forces influence the behaviour of the particles by creating inertia. This inertial force is countered by the viscous forces exerted by the fluid on the particles.

In the case of a suspension of high density particles in a low viscosity fluid, the particle

motion will be strongly influenced by the inertial forces. Such particles would collide more frequently and with more impact than low density particles and therefore dissipate more energy. This effect will be enhanced with increasing particle size (Clarke 1967, Brenner 1972, Concha et al, 1990). In addition, the effect becomes more pronounced at high solids concentrations where these types of interactions dominate the flow behaviour (Purohit and Roy, 1965, Clarke, 1967). Clarke (1976) observed that the viscosity of settling suspensions increased with particle size and he attributed this to inertial effects.

At low solids concentrations, the high density particles will move more freely and therefore dissipate more viscous energy. This results in an increased intrinsic viscosity with increasing particle relative density. Ferrini et al (1979) measured the intrinsic viscosity for suspensions of coal (density = 2000 kg m^{-3}) and magnetite (density = 4900 kg m^{-3}) as 4 mPa.s and 5.8 mPa.s, respectively. Inertia can also influence the measured intrinsic viscosity through its effect on the particle orientation distribution (Brenner, 1972). As particles align with the shear flow or orientate as they settle, the magnitude of the viscous energy dissipation will change and thereby change the intrinsic viscosity.

The greater number of particle interactions in settling suspensions than in stable ones, helps to explain their non-Newtonian flow behaviour (Clarke 1967, Brenner 1972, Laapas 1985). These suspensions typically exhibit shear thinning or yield shear thinning properties. Clarke (1976) found that the solids concentration above which the suspension exhibits non-Newtonian properties is lower for suspensions containing particles with a higher relative density. Laapas (1985) obtained a relationship between yield stress and relative density. As the relative density increased, the yield stress increased.

Clarke (1967) also found that at high shear rates suspensions of settling particles exhibited dilatant properties. At high shear rates Purohit and Roy (1965) observed the formation of horizontal bands in their transparent rotational viscometer. Taylor (1923) has described similar bands by the onset of turbulence. This turbulence explained the dilatant properties found by Clarke (1967) at high shear rates. In particular, the shear forces induce inertia into the particles in the Couette flow. As the particle velocity increases the particles tend to move to the outside of the annular gap and thereby form the well known Taylor vortices. Kirchberg et al (1975) observed similar results and suggested that a solids concentration gradient forms in the annular gap with more particles concentrated near the outside wall.

8.3.3 Particle Shape

For a given suspension, particle shape is a difficult parameter to try to control. It depends on the physical properties of the solid and on the environment in which the particles were formed. Despite this, an understanding of how particle shape influences suspension rheology is necessary for the interpretation of measured rheological responses.

In most natural systems the particle shapes vary from perfect spheres to rods and discs. The movement of these particles in a flowing fluid depends on a balance between opposing viscous stresses and Brownian movement (Goldsmith and Mason, 1967, Brenner, 1972). The viscous stress aligns particles, such that their longest dimension is parallel to the flow (Horie and Pinder, 1979), which reduces the energy dissipation and therefore the viscosity. At low shear rates, Brownian movement randomizes the orientation of smaller particles. Laapas (1982)

described the flow curves for suspensions of elongated particles using the Bingham plastic model; and he found that with increasing particle anisotropy the plastic viscosity increased. Laapas (1985) described the particle shapes in terms of sphericity as defined by Equation 8.4.

$$\text{Sphericity} = \frac{\hat{S}}{S} \quad (8.4)$$

where, \hat{S} is the calculated surface area based on the particle diameter, and
 S is the measured surface area.

For dilute suspensions, the particle shape contributes to the relative viscosity through its effect on the intrinsic viscosity term (Ting and Luebbbers, 1957, Goldsmith and Mason, 1967, Brenner, 1972). In suspensions containing elongated particles the intrinsic viscosity is highest at low shear rates where the particle orientation is random and it is lowest at high shear rates where the particles are aligned with the flow. The magnitude of the difference between the low and high shear states is proportional to the particle aspect ratio (Goldsmith and Mason, 1967).

In concentrated suspensions, particle shape affects the maximum packing density and thereby influences the relative viscosity (Ting and Luebbbers, 1957, Wildemuth and Williams, 1985). Unlike most models (described in the last section), the model developed by Ting and Luebbbers (1957) considered the effect of particle shape on the maximum packing fraction. Wildemuth and Williams (1985) also considered the effect of particle shape through its effect on maximum packing density as related to relative viscosity using the Eilers (1941) and Krieger and Dougherty (1959) equations. The relationship between specific particle shapes and packing density were, however, not determined.

Suspensions containing elongated particles have been observed to exhibit time dependent properties (thixotropy). Horie and Pinder (1979) observed that with increasing aspect ratio there is an increase in the amount of thixotropy. However, the rate of change of thixotropic break down and recovery in these suspensions decreased with increasing aspect ratio. They also observed that as the aspect ratio increased, the relative viscosity and the yield stress of concentrated suspensions also increased. The time dependent properties can be explained in terms of the time required for particle orientation to occur. As the particles align with the flow the viscosity decreases. With higher aspect ratios this orientation requires a long time period.

8.3.4 Particle Size

The size of particles in a suspension has been shown to have a strong influence on its' rheological properties. In particular, it has been shown that suspensions with very large ($+100\text{ }\mu\text{m}$) or very small ($-10\text{ }\mu\text{m}$) particles have a higher viscosity than suspensions containing intermediately sized particles ($+10\text{ }\mu\text{m}$ - $100\text{ }\mu\text{m}$) (Purohit and Roy 1965, Clarke, 1967, Renehan, 1988a). These differences in viscosities can be explained by the contributions of the electroviscous, aggregation, hydrodynamic and granuloviscous effects. Each effect contributes to the viscosity to a greater or lesser degree depending on the size of the particles.

Many investigators have reported an increase in viscosity with a decrease in particle size (Williams, 1951, Roscoe, 1952, Sweeney and Geckler, 1954, Sherman, 1965, Clark, 1967, Parkinson et al, 1970, Saraf and Khullar, 1975, Rukin et al, 1977, Tsai 1986, Schreuder 1986). This increase in viscosity has been attributed to the electroviscous and aggregation effects that

dominate fine particle behaviour (Eveson, 1957, Sherman, 1965, Thomas, 1965, Saunders 1967, Krieger 1971, Renehan, 1988a). Inter-particle forces of attraction and repulsion are responsible for these effects which dominate the movement of colloidal size particles (Thomas 1965, Renehan 1988a). The magnitude of these forces may be large enough to influence the movement of coarse particles. Renehan (1988a) showed that the movement of coal particles as coarse as 200 μm were influenced by surface charge related effects that were large enough to contribute to the rheological properties. The maximum particle size affected by surface charge related effects was referred to as the reactive size limit. Sweeney and Geckler (1954) suggested that the contribution from electroviscous effects to the rheological properties of fine particle suspensions can be very significant. They showed that the viscosity of a suspension of glass spheres in an ionic suspending fluid, where electroviscous effects should be large, was greater than the viscosity of a suspension of the same glass spheres in a non-ionic fluid, in which electroviscous effects should be small.

For suspensions of glass and polystyrene spheres, Williams (1951), Saunders (1967) and Parkinson et al (1970) explained the increases in non-Newtonian behaviour, yield stress and thixotropy with decreasing particle size, by the contribution of aggregation effects. Inter-particle forces of attraction dominate over inertial forces for small particles which makes them more susceptible to aggregation than coarse ones. With increasing shear rate the attachments break resulting in a more dispersed suspension. As the particle became dispersed the apparent viscosity decreased resulting in the shear thinning properties (Sherman, 1965, Laapas 1982,1985). Since this dispersion with shearing is not instantaneous, at a given shear rate the apparent viscosity will decay with time resulting in the thixotropic characteristics of such suspensions. The structure that

forms as a result of the aggregation of the fine particles contributes to the yield stress. Below a critical solids concentration the structure may not be continuous and therefore no yield stress may be present (Sherman, 1965, Laapas 1982,1985). The effects of particle size are therefore more pronounced at high solids concentrations than at low ones.

The magnitude of the hydrodynamic effects is proportional to the specific surface area of the particles. Since the specific surface area increases with decreasing particle size, the contribution of hydrodynamic effects also increases (Yucel and Hughes, 1984). Therefore the increase in viscosity of suspensions resulting from decreasing particle sizes can be explained by the greater amount of hydrodynamic energy dissipation (Sherman, 1965, Saunders 1967).

The results of several investigations have shown that an increase in viscosity occurs as particle size increases (Eveson, 1957, Purohit and Roy 1965, Clarke, 1967, Saraf and Khullar 1975, Renehan 1988a). This result has been explained by the energy dissipated due to physical particle interactions as described by granuloviscous effects. Since coarse particles have a greater inertia than fine ones they will collide rather than slip past each other. The physical collisions dissipate energy through friction and loss of translational and rotational momentum (Thomas, 1965).

Saraf and Khullar (1975) showed that the viscosities of quartz particle suspensions increased as the mean particle size was increased from 37 μm to 74 μm . Clark (1967) obtained similar results by increasing the size of quartz particles from 30 μm to 180 μm . Similar results were obtained for suspensions of hematite and quartz by Purohit and Roy (1965) who also measured the viscosity of coal suspensions which did not increase with particle size. Since the coal has a significantly lower density than the quartz and hematite, the differences in the results

can be explained by the differences in particle inertia. The denser quartz and hematite particles have a greater inertia than the coal and therefore dissipate more energy through collisions. Therefore, the size effects contribute to the rheological properties via inertial effects.

The contributions of the four effects (electroviscous, granuloviscous, aggregation and hydrodynamic) clearly depend on the size of the particles. In order to minimize the viscosity, it seems that an optimum particle size exists that is not too large and not too small. Clarke (1967) determined this optimum size to be approximately 16 μm for suspensions of quartz particles.

8.3.5 Particle Size Distribution

It is well known that particle size distribution influences the rheological properties of suspensions. The explanation for this influence is, however, not well understood. Researchers have demonstrated that suspensions composed of particles with a wide size distribution are less viscous than suspensions with a narrow size distribution (Castillo and Williams 1979). Other researchers have shown that suspensions with particle size distributions that have a high packing solids fraction are less viscous than those with distributions that have a low packing fraction. In order to exploit this result, investigators have applied particle packing theory to produce size distributions that have a maximum packing density in order to produce suspensions with a minimum viscosity. Despite these investigations, there is little explanation of the physical reasons for the observed results. Moreover, none of these results have been explained in terms of the micro-rheological interactions that occur between particles of different sizes.

Castillo and Williams (1979) showed that the relative viscosities of concentrated coal suspensions with narrow size distributions are greater than the viscosities of suspensions with wide distributions. They related this result to the higher packing fractions of suspensions with a wide distributions than those with narrow distributions.

Zheng et al (1984) found that coal suspensions had a minimum viscosity and maximum packing fraction when the particle size distribution was characterized by a Rosin Rammler Bennett (RRB) distribution coefficient equal to 0.7 - 0.8. Similarly, Rukin et al (1977) found the optimum value of the RRB distribution coefficient to be approximately 1.0. Kikkawa et al (1984) showed that a minimum viscosity and a corresponding maximum packing fraction was achieved when the Gates Gaudin Schuhmann size distribution modulus equalled 0.4 - 0.5. These results support the conclusion that the viscosity of a suspension can be reduced by manipulating the particle size distribution to increase the solids packing fraction.

The effect of solids packing fraction has been incorporated into several rheological equations that relate relative viscosity to the maximum solids packing fraction. Many of these empirical equations have been presented in Table 8.1. Each equation contains terms of the form:

$$\eta_r = f\left(\frac{\phi}{\phi_{\infty}}\right) \quad (8.6)$$

where, ϕ is the suspension solids fraction, and

ϕ_{∞} is the maximum solids packing fraction.

As can be seen in the equation, at a given solids concentration, the relative viscosity can be decreased by increasing the solids packing fraction. The solids packing fraction is a function

of particle size distribution.

Mooney (1951) considered the effect of particle size distribution on particle crowding. In particular, he assumed that large spheres are not crowded by small ones and that the small spheres are crowded into the spaces between large ones. Ting and Luebbbers (1957) suggested that the small particles fill the voids between the large particles which increases the packing fraction and thereby reduces the viscosity. Clarke (1967) explained that the small particles move in the voids between the large ones, the net effect being a decrease in the number of inter-particle impacts and therefore a decrease in viscosity.

Sweeny and Geckler (1954) considered the effect of the ratio of small to large particle diameters in a bimodal distribution on the packing fraction and viscosity. By increasing the size ratio, the packing fraction decreased and the viscosity increased. Several investigators (Eveson 1953, Chong et al, 1971 and Round and Hessari, 1984) explained the effect of size ratio as follows. As the size ratio decreases, there is an increase in the number of small spheres. These small spheres may act as ball bearings between the large particles which thereby reduces the viscosity. In addition, below a size ratio of approximately 0.1, the small particles behave like fluid to the large particles.

Fidleris and Whitmore (1961) observed that large spheres move through a suspension of fine spheres as if it were a liquid with the same viscosity and density as the fine particle suspension. As the size ratio of small to large particle diameters was increased to greater than 0.1, the large spheres began to move in a zigzag motion indicating that interactions between the fine and coarse particles became more significant. Farris (1968) considered these interactions in his model by including a crowding factor that increased as the size ratio increased.

Farris (1968) also showed that the viscosities of suspensions decreased with the increase in the number of component sizes; that is multi-modal suspensions are less viscous than bimodal suspensions which in turn are less viscous than mono-modal suspensions. These results can be explained by expressions developed by Gillespie (1963) which describe the rate constants of collisions for particles of different sizes. The expressions indicate that poly-dispersity reduces the rate constant for shear induced collisions. This result is supported by observations made by Wildemuth and Williams (1985) who observed that differences in the viscosities between suspensions composed of particles with a wide size distribution and those composed of a narrow size distribution became more pronounced at high shear rates. At high shear rates, the shear induced collisions would contribute more to the rheological properties than they would at low shear rates.

Not only is the size ratio important to the viscosity, but so are the proportions of each of the component sizes. For bimodal suspensions, the optimum proportion of small particles was reported to be between 0.25 and 0.45 (Parkinson et al, 1970, Chong et al, 1971, Round and Hessari, 1984 and Ferrini et al, 1984). The optimum proportion of fines was considered to be the proportion that can fill the voids between the packed coarse particles without adding to the total volume of a packed bed of solids. Such a size distribution would clearly result in a high packing fraction.

Lee (1970) as well as Ferrini et al (1984) used particle packing theory in order to select the optimum size distributions. The optimum size distributions can be calculated from relationships between packing arrangements and the particle shape (Westman and Hugill, 1930, Furnas, 1931, White and Walton, 1937, McGeary, 1961 and Fedors, 1979a, 1979b, 1979c).

Ferrini (1984) determined from packing theory that for a coal slurry with a top particle size of 300 μm and a minimum particle size of 1 μm , the optimum particle size distribution would be bimodal. The mean size ratio used was set at 0.2 because of practical considerations of producing the component sizes. The optimum proportion of fines was determined to range from 0.35 to 0.45. It was also learned that the effect of size distribution became much more pronounced at high suspension solids concentrations.

8.4 Physico-chemical Parameters

Physico-chemical parameters are the properties of the suspensions that influence the inter-particle forces of attraction and repulsion. As described by DLVO theory (Overbeek, 1952, Derjaguin, 1989), London's Van der Waals and electrostatic forces are responsible for particle aggregation and stabilization. The magnitude of each of these forces depends on the chemical composition of the particles, the concentration of potential determining ions in the suspending fluid, the type and concentration of indifferent electrolyte in solution, the type and concentration of dispersing agents and for ferromagnetic particles the state of magnetization.

8.4.1 pH and Dissolved Ions

Surface chemistry strongly influences the rheological properties of suspensions of colloidally sized particles. In particular, the magnitude of electrostatic repulsive forces determines the state of dispersion of the suspension which affects the contributions to the

rheological properties from electroviscous and aggregation effects (Atlas et al, 1985). The electrostatic repulsive forces in turn depend on the surface chemistry of the particles and on the type and concentration of dissolved ions (Overbeek, 1952, Derjaguin, 1989).

The surface of oxide minerals, such as magnetite, is covered by hydroxyl groups. These surface hydroxyl groups are amphoteric and behave as acids or bases; their ionization is controlled by the pH. As a result, at low pH most oxide minerals become positively charged and at high pH they become negatively charged. The point of zero charge (p.z.c.), varies from mineral to mineral and in practice also depends on the impurities present in the mineral (Kitchener 1969, Atlas et al, 1985). Since electrokinetic measurements are more common than titration techniques used to determine the p.z.c., the iso-electric point (i.e.p.) is more practically measured. These two points are identical in the absence of specifically adsorbing ions.

At a pH near the i.e.p., electrostatic repulsion is at a minimum. This allows particles to approach each other to a distance at which Van der Waals forces of attraction are large and as a result the particles coagulate into a primary minimum. Several investigations have shown that near such a pH value, the flow behaviour of suspensions becomes shear thinning and a yield stress develops. This rheological behaviour has been explained in terms of aggregation effects; the particle aggregation results in the formation of a structure which when sheared breaks down (Atlas et al, 1985, Leong and Boger, 1988, 1990).

At pH values higher and lower than the i.e.p., the aggregates disperse due to increased electrostatic repulsive forces. As a result, the viscosity decreases and the flow resumes Newtonian behaviour. However, with a further increase or decrease in the pH the viscosity increases. This result can be explained by the increase in the magnitude of the electroviscous

effects (Smoluchowski, 1916, Leong and Boger, 1990). Therefore, a minimum suspension viscosity exists at pH levels above and below the i.e.p.

Coagulation can also be initiated by a high concentration of electrolyte. Under such conditions, double layers surrounding particles are compressed and this leads to a reduction in the range of the electrostatic repulsion forces resulting in aggregation and the formation of a structure. Such a structure is responsible for increased viscosity, shear thinning flow properties and the presence of a yield stress (Friend and Kitchener, 1973, Atlas et al, 1985, Meagher et al, 1988).

8.4.2 Dispersing Agents

Dispersing agents can be classified into: (i) inorganic compounds, and (ii) polymeric dispersants (natural and synthetic) (Laskowski, 1988, Laskowski and Pugh, 1992). While inorganic dispersants are used primarily to control the charge density at the solid/liquid interface, the polymeric compounds also provide a steric hindrance.

As described in the previous Section (8.2.4), suspensions of aggregated particles can exhibit a yield stress and typically have shear thinning flow properties (Aarnio and Laapas, 1988, Jones and Chandler, 1989). Dispersing the particles results in a more Newtonian flow behaviour and a reduced apparent viscosity. It should be noted, however, that by increasing electrostatic repulsion, electroviscous effects can also become more important (Aarnio and Laapas, 1988) resulting in greater apparent viscosities.

Organic reagents typically used in iron ore processing are polysaccharides such as starch

and carboxyl methyl cellulose which are used to flocculate hematite (Iwasaki et al, 1969, Lin et al, 1988). The effectiveness of these reagents depends on the nature of the reagents, the particle surface chemistry, the types of dissolved ions and the pH. Typical inorganic dispersing agents are sodium polyphosphates and sodium silicates (Laskowski, 1988, Yang, 1988, Jones and Chandler, 1989). These dispersing agents are widely used in the processing of iron ores.

CHAPTER 9: RHEOLOGY OF MAGNETITE DENSE MEDIA

9.1 Introduction

It has been established that the rheological properties of magnetite dense media are important to the process separation efficiency. As discussed in Section 4.5, recent investigations have confirmed that these medium properties affect the performance of both static and dynamic separators (Napier-Munn, 1990). While some information exists on the rheological properties of magnetite suspensions, a better understanding of how physico-mechanical and physico-chemical parameters affect the medium properties is required.

9.2 Characterization

It was established in early publications that magnetite suspensions exhibit non-Newtonian flow properties (Eveson, 1953). In particular, the rheological properties of magnetite suspensions have been described as Newtonian at low solids contents, becoming pseudo-plastic with increasing solids contents (Govier et al, 1957, Lilge et al, 1957, Berghofer, 1959). This flow behaviour has been described with the Bingham plastic equation (Yancey et al 1958, Berghofer, 1959, Klassen et al, 1964, 1966, Valentyik, 1972, Valentyik and Patton, 1976, Graham and Lamb 1982, 1988) which implies that a yield stress exists. The available data indicate that the Bingham equation fits the data poorly at low shear rates (Berghofer, 1959). In particular, at low shear rates measured stress values are lower than the stresses predicted by the Bingham equation. In

addition, the Bingham yield stress is usually greater than yield values determined by using other methods.

Apparent viscosity values have been used to provide an indication of the viscous resistance of various magnetite suspensions. While this indicator of viscosity may be useful, such data are difficult to compare when values are obtained from different types of instruments at various shear rate conditions. Furthermore, an apparent viscosity value does not represent viscosities over the range of shear conditions that are found in a dense media separator.

As discussed in Section 6.3.2, measurements of the rheological properties of settling suspensions require that careful consideration be given to various potential errors. Since most viscosity measurements have been made without accounting for these errors, much of the available rheological data are suspect. These data do, however, provide valuable information concerning the type of flow behaviour and trends associated with the levels of various parameters such as solids content and particle size.

9.3 Control of Medium Properties

As stated, once it is understood how the physico-mechanical and physico-chemical parameters influence the rheological properties of magnetite dense media, these parameters can be manipulated to control the rheological properties. In this way, the rheological properties can be optimized to improve separation performance.

9.3.1 Physico-Mechanical Parameters

Physico-mechanical parameters, that affect the rheological properties of a suspension, include the solids content, and the density, size, size distribution, shape and roughness of the particles.

Since magnetite is a natural occurring mineral, its density varies with the types and amounts of impurities present. Typically, magnetite used in dense media must have a density greater than approximately 4800 kg m^{-3} (pure magnetite has a density that is close to 5180 kg m^{-3}). The density of the magnetite determines the solids content required to produce a specific medium density. Since this parameter is a difficult parameter to control, it will not be discussed further.

9.3.1.1 Solids Content

The effective medium density is determined by the density of the magnetite particles and the solids content of the suspension. For coal preparation, media densities range from 1350 kg m^{-3} to 1800 kg m^{-3} , requiring approximately 10% to 20% of magnetite by volume, respectively (Osborne 1988). For mineral separations, media densities as high as 2500 kg m^{-3} (Burt, 1984), requiring a solids content of approximately 40% magnetite by volume, have been used.

It is well known that the suspension viscosity increases with solids concentration. Several investigators found that the apparent viscosity of magnetite suspensions increases proportionally with magnetite content up to approximately 25% by volume and then rises sharply in an

exponential manner at higher solids content (DeVaney and Shelton, 1940, Geer et al, 1957, Chakravarti et al, 1958). Also, with increasing solids concentration the flow behaviours of magnetite dense media become more non-Newtonian (Govier et al. 1957) and a yield stress becomes more pronounced. In fact, the exponential increase in apparent viscosity above 25% solids by volume can be attributed to the sharp increase in the Bingham yield stress, although the plastic viscosity also rises with solids concentrations (Berghofer, 1959). The sharp increase in rheological parameters at these high solids concentrations was attributed to energy dissipation resulting from particle collisions and friction between particles (Berghofer, 1959). Clearly, it is not practical to use magnetite suspensions for separation densities that require high solids concentrations due to the excessively viscous properties of the media.

9.3.1.2 Particle Size

The size of magnetite particles used in dense media suspensions is typically in the range of 90% -45 μm with less than 30% -10 μm (Osborne, 1988). This particle size range has been selected based on considerations of:

- i. magnetite recoverability,
- ii. magnetite grindability,
- iii. medium sedimentation stability and,
- iv. medium rheology (Graham, Lamb, 1988).

Despite evidence that medium rheology influences separation performance, it has received very little attention in industrial applications.

Early investigations by DeVaney and Shelton (1940) revealed that as the mean particle size of the magnetite was decreased from 51.7 μm to 15.8 μm , the apparent viscosity of the medium increased. This trend was attributed to the increase in particle surface area with decreasing mean particle size. In particular, liquid becomes trapped in the irregularities of the particle surface, thereby increasing the effective particle volume and therefore the effective solids concentration. Since the amount of immobile liquid present is proportional to the particle surface area, its amount increases with decreasing particle size. Therefore, the effective solids concentration and thereby the apparent viscosity increase with decreasing particle size (Eveson, 1958). Berghofer (1959) investigated the effect of particle size on the coefficients of the fitted Bingham Plastic equation. He found that the effect of particle size on these coefficients was more pronounced at a high volume solids content ($> 25\%$) than at low ones (15%). In addition, the yield stress was much more affected than the plastic viscosity. These results were explained in terms of the energy dissipation resulting from inter-particle interactions. In particular, at high solids concentrations, inter-particle interactions are the major source of viscous energy dissipation. With decreasing particle size, there is a corresponding increase in the number of particles that interact and dissipate energy.

In order to maintain a low medium viscosity, it is therefore recommended to use coarse magnetite particles at high solids contents and to use fine particles at low solids contents (Chakravarti et al, 1958, Graham and Lamb, 1982). Since the apparent viscosity increases with decreasing particle size, it is expected that media composed of micronized magnetite ($-10 \mu\text{m}$), used for the dense media separation of fine coal ($600 \times 38 \mu\text{m}$) (Klima and Killmeyer, 1990), may be prohibitively viscous.

9.3.1.3 Particle Size Distribution

Although investigations have shown that particle size distribution affects the rheological properties of various suspensions (see Section 8.3.5), no similar work has been carried out with magnetite. DeVaney and Shelton (1940) and Eveson (1953) suggested, however, that particle size distribution could affect the rheological properties of magnetite dense media. In particular, it was suggested that magnetite suspensions could exhibit the same rheological trends as tested model systems. The main differences are that the solids concentrations of magnetite dense media are lower than those of the systems investigated, the particles have irregular shapes, and the particles interact as a result of physico-chemical effects.

9.3.1.4 Particle Roughness and Shape

Magnetite particles are generated by grinding in conventional rod and ball mills. These grinding procedures produce irregularly shaped rough angular particles. It is known that particle roughness and shape affect the rheological properties of a suspension (see Section 8.3.3). Several investigations with ferrosilicon dense media (Aplan and Spedden, 1964, Collins et al, 1974, Ferrara and Schena, 1986) have shown that medium composed of spherical atomized particles has a lower viscosity than media composed of irregularly shaped ground material. In this case, atomized ferrosilicon is often used in dense media separation applications where high medium densities are needed and viscosity is of concern.

The effect of particle shape on viscosity has been explained by the ease with which round

smooth particles can roll and slide past each other as compared to the wedging and interlocking of uneven angular particles (DeVaney and Shelton, 1940).

Some smoothing and rounding of magnetite particles occurs as result of pumping and flow in a dense media circuit. The abrasion resulting from this flow removes sharp edges from the particles which over time produces rounded and less angular particles (Eveson, 1958, Graham and Lamb, 1988). Alternative sources of magnetite such as fly-ash from smelters (Osborne, 1988) and naturally eroded particles from placer deposits (Klein et al, 1988) have been considered. Particles from both of these sources are smoother and rounder than ground material and the viscosities of corresponding media would likely be lower.

9.3.2 Physico-Chemical Parameters

It is well known that physico-chemical parameters strongly influence the rheological properties of magnetite dense media. Specifically, in order to improve the rheological properties, it is recommended to install demagnetizing coils in dense media recovery circuits and to add dispersing agents to the medium when clays or slimes are present. Despite this knowledge, there have been few investigations into the effects of these parameters on the medium properties.

9.3.2.1 pH and Dissolved Ions

As discussed in Section 8.4.1, the pH and dissolved ion concentration affect rheological properties through their effect on the zeta potential of particles. In particular, the zeta potential

of the suspended solid is dependent on the pH and on the types and concentration of dissolved ions. When the zeta potential is large, strong electrostatic repulsion facilitates particle dispersion. Since rheological properties are influenced by the state of aggregation, the pH and dissolved ions can influence the medium rheological properties (Graham and Lamb, 1982, 1988).

While the main component of the medium is the magnetite, the effect of pH and dissolved ions on the zeta potential of clays and other slimes can have a large effect on the rheological properties of the medium (Aplan and Spedden, 1964). No data are available on the effect of dissolved ions and pH on the rheological properties of magnetite dense medium.

9.3.2.2 Dispersing Agents

While it is believed that the rheological properties of magnetite dense media can be improved by the addition of dispersing agent, few studies have been carried out. Klassen et al (1966) found that sodium hexametaphosphate was effective in reducing the viscosity of magnetite dense media contaminated with clay. In particular, from two coal plant studies it was found that the additions of 3-5 grams of sodium hexametaphosphate per tonne of medium reduced the plastic viscosity and the Bingham yield stress. The addition of this dispersant also improved the medium stability. The net result was a decreased product ash content and a decreased magnetite consumption.

Graham and Lamb (1988) compared the effects of various inorganic and organic dispersing agents on the zeta potential of fine magnetite. It was shown that sodium hexametaphosphate increased the zeta potential value more than the other dispersants. From

rheological measurements, it was found that the addition of sodium hexametaphosphate had little effect on the yield stress and even less effect on the plastic viscosity of pure magnetite suspensions. When slimes were present, however, the addition of dispersant significantly reduced the yield stress.

9.3.2.3 Magnetization

Magnetite particles are composed of a ferromagnetic material that, once introduced to a magnetic field, often exhibits remnant magnetic properties (see Section 4.2.3). This remnant magnetism causes the particles to aggregate and thereby influences the rheological properties of magnetite suspensions.

The magnitude of remnant magnetic forces vary with the composition and structure of the magnetite particles. These forces can be strong as compared to electrostatic repulsive forces, in which case it is not possible to disperse the particles using chemical methods (Meerman, 1958). The particles can be dispersed by demagnetizing them. This can be achieved by raising the temperature above the Curie point (approximately 770 °C for iron) or by passing the magnetite through an alternating current (AC) magnetic field (Onstad, 1954). The demagnetization randomizes the orientation of magnetic domains within the particles such that the domains cancel each other leaving the particle with no net magnetic force (Tipler, 1979).

Magnetically aggregated particles form chain structures whose size depend on the strength of the magnetic forces and the shearing conditions in the suspension (Voet and Suriani, 1950, Kamiyama and Satoh, 1989). With shear, the magnetic attachments can break thereby reducing

the size of the aggregates. When such structures form, the suspensions exhibit pseudoplastic properties and can have a yield stress. Kamiyama and Satoh (1989) found that the apparent viscosity increased with increasing number of particles in the aggregates. Demagnetizing the particles results in the dispersion of the particles and a more Newtonian flow behaviour (Meerman, 1958).

The effect of particle magnetization on the rheological properties of magnetite dense media was investigated by Erten (1964). He observed that by magnetizing a suspension of magnetite, the yield stress increased although the plastic viscosity did not change significantly. Graham and Lamb (1982) explained such an increase in yield stress by the stress required to break aggregates of particles resulting from remnant magnetism (see Section 8.4.3). The strength of the remnant magnetic forces depends on the types and amounts of impurities in the lattice structure of the magnetite.

Erten (1964) also showed that the yield stress of a magnetized suspension could be reduced to its original state by passing it through a demagnetizing coil. Napier-Munn et al (1990) suggested that a coil with a larger field strength is required to demagnetize particles with high remnant magnetism and to demagnetize small particles. Despite the understanding of the effect of magnetization on media properties, many coal operations do not use their demagnetizing coils; many plants do not have coils at all.

9.3.3 Contamination

Fine coal, mineral and clay particles that enter dense media are referred to as contaminants. Inefficient de-sliming of the feed to the separators results in the introduction of such contaminants into the medium. In addition, the abrasion of the coal particles in the separator generates fines (DeVaney and Shelton, 1940) that also enter the medium. These contaminants are almost always present in dense media and due to their small particle sizes, influence the rheological properties.

As with magnetite, the physico-mechanical and physico-chemical properties of the contaminants determine how they influence the medium rheology. For example, since contaminants typically have a lower density than magnetite, a higher medium solids content is required to achieve a specified medium density. Therefore contaminated media has a higher solids content and corresponding higher viscosity than uncontaminated media (DeVaney and Shelton, 1940). In addition, contaminating particles change the effective medium particle size distribution. A reduction in the effective medium particle sizes can result in an increase in the medium viscosity (Ferrara et al, 1988).

Fine coal particles, with sizes ranging from a few micrometers to approximately 100 μm , practically increase the effective solids concentration of the medium. At low solids contents, coal suspensions exhibit Newtonian rheological properties and have a low viscosity (Castillo and Williams, 1979, Wildemuth and Williams, 1985). However, the addition of a small amount of fine material to a viscous suspension can result in a large increase in suspension viscosity (Thomas, 1965). The contribution of the coal fines to the rheological properties of the dense

medium, therefore, depends on the rheological properties of the pure magnetite suspension and on the amount of fine coal that contaminates it.

The surface properties of the contaminating particles may have a large effect on the medium rheology. This is especially true in the case of clays. Bentonite and to a lesser extent kaolinite, swell in aqueous suspensions to create a "card house" structure. Even at low concentrations, this structure can result in a large increase in media viscosity (DeVaney and Shelton, 1940, Geer et al 1957, Chakravarti et al, 1958).

Clay suspensions typically exhibit a yield shear thinning flow behaviour (Nicol and Hunter, 1970, Czaban et al, 1986) and thixotropy (Speers et al, 1987, Chen et al, 1988). The rheological properties are attributed to the structures formed by the fine aggregated particles. Kaolinite and montmorillonite form an extensive "card house structure" at neutral and acidic pH levels with negatively charged cleavage surfaces attached to positively charged edge surfaces of the particles (Street, 1956). In the acidic to neutral pH range, these attachments can break during shearing and reform which accounts for the yield stress and thixotropic properties of clay suspensions. Such structures are strongly influenced by pH, dissolved ion concentration and the addition of dispersants (Klassen et al, 1966, Nicol and Hunter, 1970, Chen et al, 1988, Graham and Lamb, 1988, Helfricht and Schatz, 1989). These rheological properties are found even in dilute suspensions of clay particles (volume solids fraction less than 3%).

The levels of contaminants found in magnetite dense medium vary widely and depend on the softness of the coal, the amount of clay present and the design of the feed preparation and dense media recovery stages. Levels of contaminants have been reported to range from 0.1% (DeVaney and Shelton, 1940) to 15.4% by weight (Graham and Lamb, 1988).

CHAPTER 10: STABILITY OF MAGNETITE DENSE MEDIA

10.1 Introduction

The medium stability, (settling) has been shown to be an important media parameter that influences the performance of both static and dynamic dense media separators (See Section 4.5). The stability is a measure of the suspensions ability to remain homogeneous with respect to medium density; it has also been defined as the degree of stratification of particles in the separator (Graham and Lamb, 1988). Gravitational and centrifugal acceleration, however, cause media particles to settle or segregate, creating a non-homogeneous environment.

Both the physico-mechanical and physico-chemical parameters affect settling properties of dense media. Magnetite dense medium is a concentrated poly-disperse suspension of interacting, irregularly shaped particles. Specifically, the solids concentrations range of magnetite dense media is typically between 10% and 25% solids by volume, the particle sizes typically range from a few μm to 75 μm , and the magnetite particle density varies from 4800 to 5180 kg m^{-3} . The remnant magnetism exhibited by magnetite particles as well as colloidal forces, may affect media stability via formation of aggregates.

10.2 Settling in Suspensions

The settling in a suspension depends on the same physico-mechanical and physico-chemical parameters that influence the rheological properties (Chapter 8).

Stokes (1891) developed an equation for the settling rate of non-interacting, spherical particles in a dilute (solids content less than a few percent) suspensions at low Reynolds numbers (Equation 10.1).

$$v = \frac{d^2(\rho_s - \rho_f)g}{18\eta} \quad (10.1)$$

This equation shows the relationship between the settling velocity, v , and particle size, d , particle density, ρ_s , fluid density, ρ_f , accelerating field, g , and fluid viscosity, η .

Steinour (1944) considered that with increasing solids concentration, the particle settling velocity is lower than predicted by Stoke's equation due to hindering effects which include:

- i. particle-particle collisions causing particles to lose momentum and,
- ii. hydrostatic pressures caused by the upward flowing fluid that is displaced by the settling particles (Richardson and Zaki, 1954, Garside and Al-Dibouni 1977, Zimmels, 1985).

Several equations have been developed to relate the settling velocities of particles to the suspension volume solids fraction. Steinour (1944) developed an equation that is an extension of Stoke's equation. Similarly and more recently Zimmels (1985) developed an equation that is also an extensions of Stokes equation (1891) as follows.

$$v = \frac{d^2(\rho_s - \rho_f)ng}{18\eta_f} \frac{(1-\phi)}{\left(1 + \phi^{\frac{1}{3}} \exp\left(\frac{5}{3} \frac{\phi}{1-\phi}\right)\right)} \quad (10.2)$$

where, ϕ is the solids volume fraction, and

n is a multiple of the gravitational acceleration.

For poly-disperse systems, large particles settle faster than small ones; this leads to differential settling. The amount of differential settling depends on the solids content in the suspension. At intermediate solids concentrations, large particles displace small ones along with the fluid; the result is a reduced or even a negative settling velocity for the small particles. In addition, the small particles and fluid provide "carrier" properties to the large particles thereby hindering their settling. These carrier properties have been explained by the buoyancy and viscosity exerted on large particles by the suspension of smaller ones (Selim et al, 1983, Williams and Amarasinghe, 1989). At high solids concentrations, these hindering effects prevent differential settling and the suspension settles with constant composition (Williams and Amarasinghe, 1989).

A concentrated poly-disperse suspension settling in a column forms four distinct zones (Greenspan and Ungarish, 1982). As the particles settle, a supernatant will form at the top of the column. This region extends vertically to the position of the smallest settling particle that was originally at the top of the column. Below this position is the transition region, which is characterized by an increasing particle size with depth. This region, also has an increasing solids concentration with depth. Below the transition region is the constant density zone, which has a solids concentration and size distribution approximately equal to that of the original suspension. Immediately below this zone is the consolidation zone in which the settling particles form a sediment. With increasing solids concentrations, the transition zone will diminish in size such that at high solids content it will not exist.

In the above discussion, the effects of physico-chemical parameters have not been considered. When a net attraction occurs between the particles, aggregates form. These

aggregates are composed of particles and trapped liquid which reduces the effective density of the unit and increases the effective solids concentration of the suspension. At high solids concentrations these aggregates interact and may form a network resulting in a lower settling rate than in a suspension of individual particles. At such high concentrations, the suspensions settle with homogeneous size and solids compositions through the vertical extent of a column (Cheng, 1980a). In the low to intermediate solids concentration range, however, the increased effective diameter of the settling unit results in a higher settling rate than in a suspension of dispersed particles (Michaels and Bolger, 1962, Zimmels, 1985). In addition, at low solids concentrations differential settling occurs, that is large aggregates settle faster than small ones (Cheng, 1980a). The critical solids concentration, beyond which the suspension settles slower than a suspension of non-interacting particles, may range from 15% to 45% and is a function of the physico-mechanical and physico-chemical conditions in the suspension.

Sadowski et al (1978) and Sadowski and Laskowski (1980) related the settling rates of quartz, calcite, dolomite and magnesite suspensions to the surface properties of the minerals. In particular, it was shown that at a pH near the iso-electric point (i.e.p.) for the minerals, the settling rate increased due to coagulation. It was also observed that for very small particles (2-4 μm), which can only experience primary minimum coagulation, the pH at which the settling rate began to increase was close to reported i.e.p. ranges. For larger particles (12-18 μm), settling rates began to increase at pH values further away from the i.e.p. These results demonstrate the importance of physico-chemical parameters to the settling of suspensions.

In magnetite dense media, particle sizes range from the colloidal size to about 75 μm . For particles in the colloidal size range, the forces responsible for aggregation may have a

significant effect on their settling properties. In such a case, the reactive small particles and the liquid can form a structure that acts to support the large particles thereby increasing the suspension stability (Yucel and Hughes, 1984, Renehan et al, 1988a).

10.3 Measurement of Stability

Several techniques for measuring and characterizing the settling properties of suspensions have been developed. The most commonly used method involves measuring the height of the supernatant - suspension interface (mud line) with time from which a settling rate can be calculated. From the above discussion, it is clear that this measurement does not provide a complete description of the settling properties. In systems where conditions are such that the suspension settles with constant composition throughout its extent, the method does provide a good indication of the relative stability of suspensions (Williams and Amarasinghe, 1989).

Graham and Lamb (1988) showed that magnetite dense media exhibits zone settling properties. It was found that little differential settling occurred and that a constant density zone existed that had a composition equal to that of the original suspension. They therefore suggested that interface falling rate is an accurate measure of stability for the static separation process. The shear conditions and accelerating forces are, however, very different in dynamic separators from those in static ones. As a result, aggregation effects that are likely to contribute to the settling properties of magnetite in a settling column, are probably less significant in dynamic separators. Collins et al (1983) suggested, however, that this settling rate does provide an indication of the medium stability in dynamic separators.

The magnetite settling properties are also characterized by the "F5 index". This F5 index was recommended to determine the relative stability of magnetite dense media (Graham and Lamb, 1982), and it is calculated from the ratio of the solids drawn from the upper and lower section of settling column after a standard settling time. According to Williams et al, 1990, this method is of little use for diagnostic analyses.

10.4 Settling Properties of Magnetite Dense Media

The effect of various physico-mechanical and physico-chemical parameters on the stability of magnetite dense media has been the subject of several publications. In particular, the effects of the physico-mechanical parameters (solids concentration, particle size and particle density), the physico-chemical parameters (magnetization and dispersants) and of fine contaminating particles (coal fines and clays) have been considered. However, no data were found on the effects of particle size distribution, particle shape, pH or dissolved ions. The following summarizes the available results.

It is clear from Equation 10.1 that magnetite particles with a density close to 5000 kg m^{-3} , will settle quickly in water. It has been shown that the settling rate of magnetite increases in an exponential manner with decreasing solids content (DeVaney and Shelton, 1940, Berghofer, 1959). Therefore, at low solids concentrations (low medium densities) stability is of greater concern. In particular, at low solids concentrations, large particles settle faster than small ones resulting in differential settling and poor medium stability properties (Berghofer, 1959). For low medium densities it has been shown that fine grades of magnetite provide greater stability

(DeVaney and Shelton, 1940). Fine size grades (95% -45 μm) are therefore recommended for low density separations (1200 - 1500 kg m^{-3}), while coarser grades (95% -53 μm) can be used at high densities (1400 kg m^{-3} to 2000 kg m^{-3}) (Graham and Lamb, 1988).

As has been discussed (Section 3.2.3), the remnant magnetism in magnetite particles may result in the formation of aggregates. This magnetic aggregation increases the settling rate of the medium. The effect of aggregation depends on the strength of the magnetic forces which is specific to the sample. The effect of magnetic aggregation on the medium stability in dynamic separators is not clear. Some investigators believe that the shear forces in a dynamic separator will break up the aggregates and reduce such effects. Graham and Lamb (1988) found that shearing a suspension of magnetically aggregated particles had little effect on subsequent settling results and concluded that either the shearing did not break the aggregates or the aggregates quickly reformed. It has therefore been suggested to install demagnetizing coils for dynamic processes as well (Graham and Lamb, 1988, Napier-Munn, 1990).

The effect of a variety of dispersing agents on medium settling properties has been studied. It was found that they did not significantly influence the stability of pure suspensions. They have, however, been shown to affect significantly the settling properties of dense medium containing fine clays. Aplan and Spedden (1964) found that sodium hexametaphosphate was effective in dispersing clay which lowered the structure and resulted in higher settling rates. The dispersants did, however, reduce the medium viscosity. Since clays such as bentonite and kaolinite can be added to dense medium to improve stability (DeVaney and Shelton, 1940, Aplan and Spedden, 1964, Graham and Lamb, 1988), the addition of dispersing agents can be used to control their effects on medium viscosity.

CHAPTER 11: SUMMARY OF LITERATURE REVIEW

Dense medium separation is one of the most important processes used to upgrade coal and mineral ores. It is expected that the use of the process will increase in the future as a result of new applications such as for the cleaning of fine coal. To extend the use of dense medium separation to such applications, it is necessary to optimize the medium properties. Specifically, for optimum separation performance, the medium should exhibit a low viscosity and a good stability. The viscosity affects separation performance via two mechanisms: i. it influences the motion of coal/ore particles, and ii. it controls the medium stability. The relationship between medium properties and separation performance is complicated by its non-Newtonian flow behaviour. Investigations with both static and dynamic separators have indicated that a yield stress has a deleterious effect on the separation of small or near density particles. In addition, results from tests with hydrocyclones revealed that the existence of a yield stress impedes size classification suggesting that the yield stress is related to medium stability. Based on the meagre data that is available, it is apparent that in order to understand the relationship between medium properties and separation performance it is necessary to have knowledge of the complete rheology.

Many studies have been carried out to characterize the rheological properties of magnetite dense media. Due to the different types of instruments that have been used and the difficulties associated with accurately measuring the rheological properties of settling suspensions, results have been difficult to compare. Several viscometers have been developed for measuring the rheological properties of settling suspensions. Each device applies an undefined shear to inhibit

particle settling during the measurement. This undefined shear produces a measurement error that may be significant particularly for suspensions exhibiting non-Newtonian and time dependent properties. A method that does not apply an undefined shear to maintain the particles in the suspension would therefore be considered an improvement over existing methods. Other errors associated with measuring the rheological properties of suspensions can be reduced by properly designing the rheometer and by treating the rheological data.

Magnetite dense media exhibit non-Newtonian rheological properties that have been modelled with the Bingham plastic equation. Examination of available flow curve data revealed that the Bingham equation does not fit the low shear rate data. Since the viscous properties at low shear rates may determine the separation efficiency of fine and near density particles, better fitting models are needed.

Various suspension parameters influence the rheological properties of magnetite suspensions. How and to what extent these parameters influence the rheological properties is, however, unknown. From investigations with other coarse suspensions it has been shown that physico-mechanical and physico-chemical parameters can be manipulated to control the medium properties. For example, it has been shown that suspension viscosity can be minimized by using a specific bimodal particle size distribution. Experiments were therefore designed to investigate the influence of these parameters on the rheology and stability of magnetite suspensions.

A considerable amount research has been carried out to study the rheological properties of suspensions of coarse hard particles. The rheological properties of these suspensions have been explained in terms of micro-rheological effects which describe the different types of particle interactions that are responsible for viscous energy dissipation. The same theory can be used to

develop a better understanding of the rheological properties of magnetite dense media.

Since medium rheology is interrelated with stability and since both properties are important to process performance, any study of the medium rheology should include a simultaneous study of the stability. The medium stability is affected by the same parameters as the rheology. In most cases, changing parameter levels to increase the stability also results in a detrimental increase in the viscosity. Medium stability is typically characterized by a mudline settling rate. However, it is not known how the mudline settling rate relates to the stability in a separator. Some investigators believe that the medium exhibits differential settling properties although recent studies indicate that it exhibits bulk zone settling properties.

SECTION B: EXPERIMENTAL PROGRAM

CHAPTER 12: EXPERIMENTAL PLAN

12.1 Introduction

Following the literature review (Section A), an experimental program was designed to achieve each of the objectives. These objectives include:

- i. Development of a method to measure the rheological properties of settling suspensions such as magnetite dense media;
- ii. Characterization of the rheological and settling (stability) properties of magnetite dense media;
- iii. Investigation of the effects of physico-mechanical and physico-chemical parameters on the medium properties; and
- iv. Examination of the effects of particle size distribution on the medium properties.

12.2 Measuring Rheological Properties of Settling Suspensions

The errors associated with measuring the rheological properties of settling suspensions were reviewed in Section 6.2.2. A suitable method should minimize these errors. Therefore, the first objective of the thesis was to develop a new method of measuring the rheological properties of settling suspensions.

The development of a device used to measure the rheological properties of sedimenting suspensions involved:

- i. Designing a modified device based on known theory;
- ii. Working out details of the design from experiments;
- iii. Constructing a prototype; and
- iv. Calibrating the device.

The new device was then evaluated to check assumptions used to design the device, and to determine the magnitude of potential errors.

The design and evaluation of the measuring device are discussed in Chapter 15.

12.3 Rheology and Stability of Magnetite Dense Media

Once a method of measuring the rheological properties of settling suspensions was established, the rheological properties of magnetite dense media were measured using the developed procedure. The settling properties of the suspensions served as an indicator of dense media stability. The first step was to select and prepare a magnetite sample and to characterize its physical and chemical properties.

The magnetite sample was obtained from the Craigmont Mine stock pile, which is the main source of magnetite used by western Canadian coal operations for dense media separation. The material was first upgraded and subsequently characterized with respect to:

- i. Elemental composition;
- ii. Density;

- iii. Size distribution;
- iv. Surface properties (electrophoretic mobility);
- v. Magnetic properties; and
- vi. Per cent magnetics.

The medium settling properties were characterized by determining the solids concentration profile as a function of time. In addition, the supernatant - suspension interface was measured with time to determine a settling rate.

The rheological properties were studied:

- i. Using the developed device to measure a rheological flow curve;
- ii. Fitting the flow curve data to several rheological models using a simplex optimization non-linear regression program,
- iii. Determining the best fitting equation using a model discrimination program.

The coefficients from the selected model were used to characterize the rheological properties of the suspension. The time dependent properties were characterized by the flow curve hysteresis method.

12.4 Effect of Parameters on Medium Properties

The effects of various physico-mechanical and physico-chemical parameters on the properties of suspensions were discussed in Chapter 8. In Section 9.3, the effects of these parameters on magnetite dense media properties were also analyzed. However, much of the available data for magnetite dense media were obtained using rheological measuring devices that

could not be considered accurate. The objective of this section is, therefore, to determine accurately the effects of these parameters by using the measuring device referred to in Section 12.2.

A fractional factorial experimental design was used to determine the relative importance of these parameters to the rheological and settling properties of magnetite dense media.

The first step was to determine the levels of the variables over which the experiments should be carried out. This was achieved by using parameter levels reported in the literature, and by consulting with coal mining operations and carrying out preliminary experiments.

Once the parameter levels had been determined and the suspensions had been prepared, the rheological and settling tests were carried out. The rheological data were modelled using various equations to fit the flow curve. The best fitting model was then selected. A simplex optimization non-linear regression program and a model discrimination program were written to fit the flow curve models to the data and then to compare the fits of the models, respectively.

The relative significance of suspension variables to the measured responses (model coefficients, settling rate and sediment solids content) were determined from the magnitude of their effects. The variable effects were then discussed.

12.5 Effect of Particle Size Distribution on Medium Properties

From the reviewed literature, it was shown that it is possible to manipulate particle size distribution in order to control and therefore optimize suspension viscosity and stability (see Section 8.3.5). Specifically, it was shown that suspension properties can be improved by using

a bimodal particle size distribution. The effect of particle size distribution was found to be most significant at high solids concentrations. To investigate the effect of these variables on the properties of magnetite dense media a central composite experimental design was used.

From the results of this investigation, second order models were fitted to responses that characterized the suspension stability and rheology. The second order models were then plotted to show minimum and maximum responses and corresponding variable levels. The responses included the coefficients of the fitted flow curve equation and the suspension settling rate.

To achieve the objectives, the following work was undertaken:

- i. Samples of narrow particle size fractions were prepared and characterized;
- ii. An experimental design was selected and set up;
- iii. Appropriate variable levels were established;
- iv. Media settling and rheological properties were measured;
- v. The rheological data were modelled; and
- vi. The rheological model coefficients and the settling rate were modelled as a function of the suspension variables.

CHAPTER 13: SAMPLE PREPARATION AND CHARACTERIZATION OF MATERIALS

13.1 Introduction

To perform the proposed experimental program, it was necessary to obtain a suitable sample of magnetite and prepare it to meet the required specifications. In addition, samples of fine coal and clays, as well as various chemical reagents (pH modifiers and dispersing agents) were used to carry out the experimental program.

13.2 Magnetite Characterization Procedures

The following summarizes the procedures set by ISO (Anon, 1985) and Mintek (Jonker, 1984) that were used to determine the magnetite properties.

13.2.1 Density Determination

Magnetite density was determined using three separate methods:

- i. The wet pycnometer method;
- ii. The air pycnometer method; and
- iii. The volumetric flask method.

For the wet pycnometer method, a known weight of solids is added to distilled water in a pycnometer bottle. The magnetite density was then determined from the total weight and

volume of the solids. To ensure particle wetting, sodium hexametaphosphate was added to the suspension. Complete de-aeration was difficult to achieve as air appeared to be trapped between the particles. To solve this problem, the bottle was tapped and evacuated in a desiccator.

The air pycnometer method (Beckman Model 930) involved placing a known weight of magnetite into a pycnometer cup. The cup was then placed in an air pycnometer containing two chambers with pistons one of which contained the sample. A differential pressure indicator connected the two chambers. As the pistons were moved to increase the pressure in the two chambers, the pressure differential was maintained at zero. When the piston in the chamber without the sample displaced a defined volume, the volume of the sample was read from a calibrated indicator.

The volumetric flask method is similar to the wet pycnometer method except that a one litre volumetric flask was used instead of the pycnometer bottle. To ensure that trapped air was removed, the magnetite and water were heated to almost boiling and the suspension was lightly agitated. After allowing the suspension to cool, the magnetite density was then calculated from the weight of magnetite, the weight of solids plus distilled water and the flask volume. Results produced from the three procedures are compared in Section 13.3.2.1.

13.2.2 Size Analyses

Two different instruments were used to perform particle size analyses of the magnetite samples, a Horiba Particle Size Analyzer (PSA) and an Elzone PSA. Results produced from these two instruments were compared to results produced by a Warman Cyclosizer which is more

commonly used by industry. The Horiba and Elzone PSA's were used because they can provide more detailed size information than the cyclosizer. This was considered important particularly when characterizing samples with very narrow size distributions and samples with particle sizes smaller than the limits of the cyclosizer.

The Horiba CAPA 700 PSA relates light transmittance through a settling suspension to particle size distribution (Allen, 1990). Since coarse particles settle faster than fine particles, the transmittance changes with time in a manner proportional to the particle sizes. The absorbence is determined and related to the particle areas and number of particles. The particle areas are then converted to volumes from which Stokes diameters are determined. As with most methods that rely on particle settling to determine particle sizes, particle shape can have a large influence on the results. The Horiba PSA is capable of running in gravitational mode or, for measurements of very fine ($\sim 10\text{ }\mu\text{m}$) particles, in centrifugal mode.

The Elzone PSA uses the electrical sensing zone method of particle size determination (the Coulter principle). The principle of the method is that a particle in an electrolyte solution passing through a small orifice with electrodes on each side will change the impedance across the orifice. The change in impedance will produce a voltage pulse that has an amplitude which is proportional to the particle volume (Allen, 1990). The pulses are counted to produce a cumulative particle frequency versus particle size (volume diameter) plot. The accuracy of the Elzone depends on the careful preparation of the sample to ensure that it is well dispersed in a conductive electrolyte solution (Berg, 1958).

The Warman Cyclosizer consists of a series of five inverted classifying cyclones that are designed for sizing particles in the sub-sieve size range (~ 400 mesh). During a run, each of the

cyclone oversize products are collected and subsequently weighed. Since the undersize from the last cyclone in the series is not usually collected, its weight is calculated from the difference between the feed and product weights. Since the size increments (Stokes diameters) are quite large, the instrument is not well suited to samples with narrow size distributions. In addition, since the finest cut size is approximately 10 μm , the instrument does not provide detailed size information for very fine samples.

13.2.3 Magnetics Content

The magnetics content of the sample was determined with a Davis Tube. The method involves passing an aqueous suspension of magnetite and water through a tube surrounded by a magnet. The tube rocks back and forth while water is washed through the sample to remove any non-magnetic particles. The magnetics content can then be calculated as the weight of material trapped by the magnet divided by the total weight of the sample fed to the tube.

13.2.4 Electrophoretic Mobility

A Zeta Meter was used to determine the electrophoretic mobility (EPM) of the magnetite particles as a function of pH. The measurements involved determining the rate of particle movement in a capillary in an electrical field. The electrophoretic mobility of particles is proportional to the applied potential. One difficulty associated with using the zeta meter in measurements with suspensions is that the instrument was designed to determine the zeta

potential for particles in the colloidal size range. Therefore, to determine the electrophoretic mobility of the magnetite, fine ($\sim 10 \mu\text{m}$) particles had to be separated from a magnetite sample. To insure that the particles were dispersed, they were demagnetized which can be difficult for small particles.

13.2.5 Chemical Composition

The chemical composition of the magnetite samples was determined by using gravimetric and atomic absorption procedures. The samples were analyzed for the content of the following elements: total iron, ferrous iron, silica, titanium, manganese, copper, aluminum, calcium, magnesium, chromium and sulphur.

13.2.6 Magnetic Properties

The magnetic properties that characterize the magnetite sample include magnetic susceptibilities at low and high magnetic fields, the saturation moment and the coercive force. An EG&G PARC model 155 vibrating magnetometer was used for the measurements. The measurements produced a hysteresis curve for the intensity of magnetization, M , versus the induced magnetic field, H . The magnetic properties can be determined from such a plot.

The magnetic susceptibility, X , is defined as the ratio of intensity of magnetization, M , to the induced magnetic field strength, H , (Equation 13.1).

$$X = \frac{M}{H} \quad (13.1)$$

For a ferromagnetic material, the susceptibility is not a constant and it depends on the magnetic field strength. The saturation moment, M_s , is the limiting value at which the intensity of magnetization levels off. The coercive force, H_c , is the magnitude of the induced magnetic field that is required to reduce the intensity of magnetization to zero.

13.3 Magnetite Sample

The magnetite used in the tests was obtained from the Craigmont mine which is the main source of magnetite for dense media separation in western Canadian coal operations. A description of the Craigmont deposit and its mineralogy were given in Section 5.2. Several other sources of magnetite from other deposits in British Columbia were also considered. A list of the deposits from which samples were obtained is given in Table 13.1.

13.3.1 Preparation of Magnetite Sample

A 125 kg sample of magnetite concentrate from the Craigmont stock piles was obtained for the planned test work. The sample contained some undesirable non-magnetic material that affects its quality. In particular, the sample density was 4690 kg m^{-3} , lower than the minimum recommended density of 4850 kg m^{-3} . Such a low sample density was attributed to the presence of low density non-magnetic minerals (silicates and calcite). The entire sample was therefore

Table 13.1 Magnetite samples considered for use in test work.

Company	Location
Cassiar Mining Corporation	Cassiar, B.C.
Craigmont Mine	Merritt, B.C.
Falcon Iron Property	MacKenzie, B.C.
Iron River Property	Campbell River, B.C.
Island Copper Mine	Port Hardy, B.C.
Brynor Mine	Kennedy Lake, B.C.

upgraded using several cleaning stages with a wet drum low intensity magnetic separator which increased the sample density to greater than 4850 kg m^{-3} .

The procedure used to upgrade the magnetite is presented in Figure 13.1. Since the magnetite was already milled no grinding was necessary. A rougher stage plus three cleaning stages were needed to increase the density to 4857 kg m^{-3} which meets the density specification. Based on microscopic examination of the non-magnetic particles, they appeared to be mostly non-liberated magnetite particles as well as liberated calcite and silicate particles. Standard splitting, riffing and sampling procedures were used to obtain suitable representative samples for analyses and test work.

13.3.2 Characterization of Upgraded Magnetite Sample

The properties of the magnetite sample (density, size distribution, magnetics content, electrophoretic mobility, chemical composition and magnetic properties) were determined using the procedures described in Section 13.2.

13.3.2.1 Magnetite Density

The results of the magnetite density determinations using three different methods are presented in Table 13.2. To ensure accuracy of measurements, the average of three volumetric flask determinations, the average of three air pycnometer determinations and the average of two wet pycnometer determinations are reported.

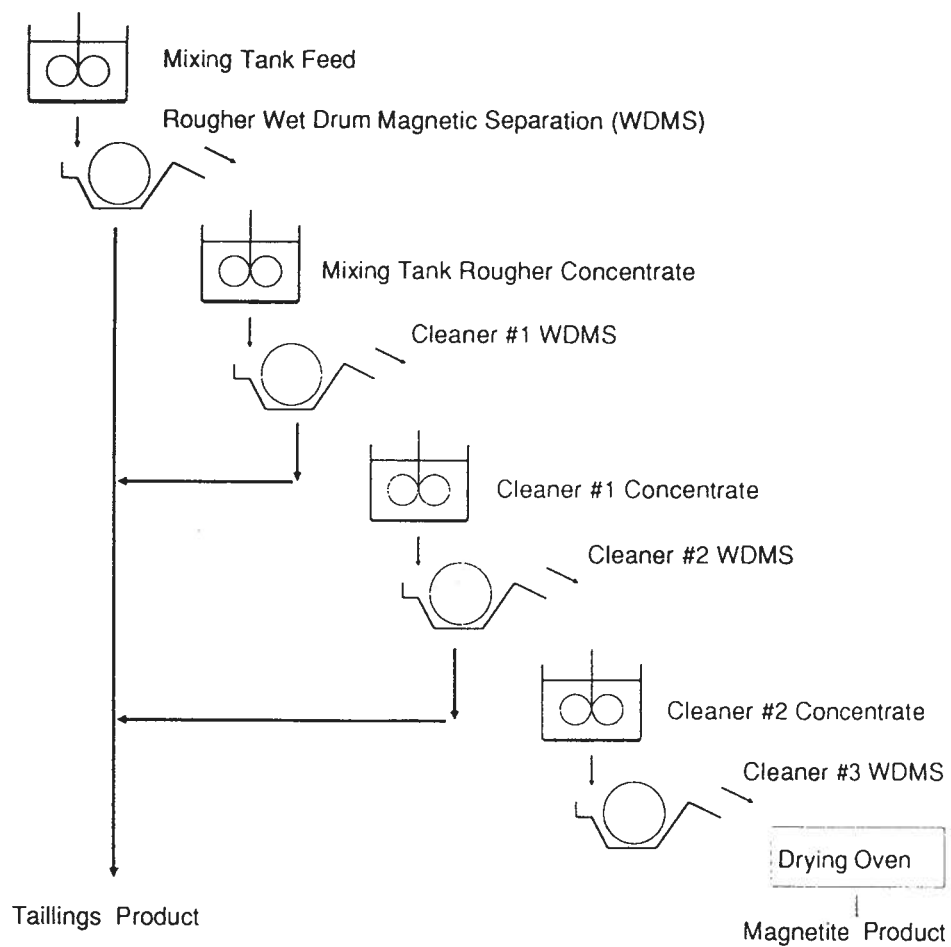


Figure 13.1 Process flow sheet showing the procedure that was used to upgrade the magnetite sample.

Table 13.2 Comparison of density measurement results for upgraded magnetite using wet pycnometer, air pycnometer and volumetric flask methods.

Method	Density (kg m ⁻³)		
	Measured	Mean	± 95% C.I.
Wet Pycnometer	4567		
	4564	4566	20
Air Pycnometer	4857		
	4867		
	4849	4857	22
Volumetric Flask	4880		
	4880		
	4872	4877	12

As seen, the volumetric flask results compare well to the air pycnometer results, but, the wet pycnometer produced lower density values. The lower densities determined by the wet pycnometer can be attributed to air trapped within the bed of solids which was difficult to remove. Higher and more accurate density values were obtained by heating the suspension in a volumetric flask which facilitated de-aeration. Good agreement between the air pycnometer and volumetric flask results indicated that the air pycnometer could be used to characterize the density of the solids accurately. It should be noted that while the air pycnometer provides a relatively quick and easy determination of the magnetite density, it was also found that the accuracy of the results depended on frequent calibration of the instrument. For the purposes of this dissertation, the air pycnometer densities were used since these measurements are relatively quick to perform.

13.3.2.2 Particle Size Distribution

The size distribution of the upgraded magnetite sample was determined using a Horiba PSA, an Elzone PSA and a Cyclosizer. The results of the three sets of measurements are presented in Table 13.3 and are plotted in Figure 13.2.

To ensure complete particle dispersion, the magnetite samples were demagnetized prior to measurements. The cyclosizer was run for 60 minutes with a water temperature of 11 degrees Celsius. For measurements with the Horiba PSA, a sucrose solution was used as the dispersing medium. The density of the solution was determined using a volumetric flask and was found to be 1270 kg m^{-3} . The solution viscosity, measured with a Haake RV20 viscometer at a

temperature of 25°C, was 40.0 mPa.s. The solids density was determined with an air pycnometer to be 4,857 kg m⁻³. The expected particle size range was estimated to be between 2 µm and 70 µm. To determine the size distribution, measurements were made over the 10 µm to 70 µm range and then over the 2 µm to 10 µm range. The Horiba software was then used to calculate the combined size distribution results. Three sets of data were generated in each size range which were averaged before combining the two measured size ranges together.

The results show that approximately 90% of the magnetite is finer than 45 µm (325 mesh) and that 30% is finer than 10 µm. Typical grades of magnetite used in dense media have a particle size distribution characterized by particle sizes that are approximately 95% finer than 40 µm and less than 10% finer than 10 µm (Osborne, 1988).

The size data was fit to the Rosin Rammler Bennett (RRB) distribution function (Equation 13.2) using non-linear regression (Newton's method). The RRB size and distribution moduli for each measurement technique are included in Table 13.3. Figure 13.2 shows that the size data plot as straight lines on RRB graph paper indicating that the RRB function is well suited to characterizing the size distributions of the sample.

$$F(d) = 100 \left(1 - \exp \left[- \left(\frac{d}{d_{63.2}} \right)^m \right] \right) \quad (13.2)$$

where, $F(d)$ is the cumulative percent passing on size d ,

m is the distribution modulus, and

$d_{63.2}$ is the size modulus (aperture through which 63.2% of material would pass).

Table 13.3 Size analysis results for upgraded magnetite, determined using Horiba PSA, Elzone PSA and Cyclosizer.

Size (µm)	% Passing		
	Elzone	Horiba	Cyclosizer
80	100	92.1	
70	100	89.7	
60	99.3	88.5	
50	96.6	86.8	
45	93.6	84.0	
40	88.2	81.9	
35	79.7	75.8	
30	69.3	68.2	88.2
25	58.9	60.5	
22			66.4
20	49.6	53.9	
15.6			49.0
15	40.1	49.2	
11.3			35.2
10	29.5	36.4	
8	24.7	29.1	26.6
6	19.1	24.9	
4	12.9	17.1	
$d_{63.2}$	24.4	24.5	19.4
m	1.26	0.96	1.44

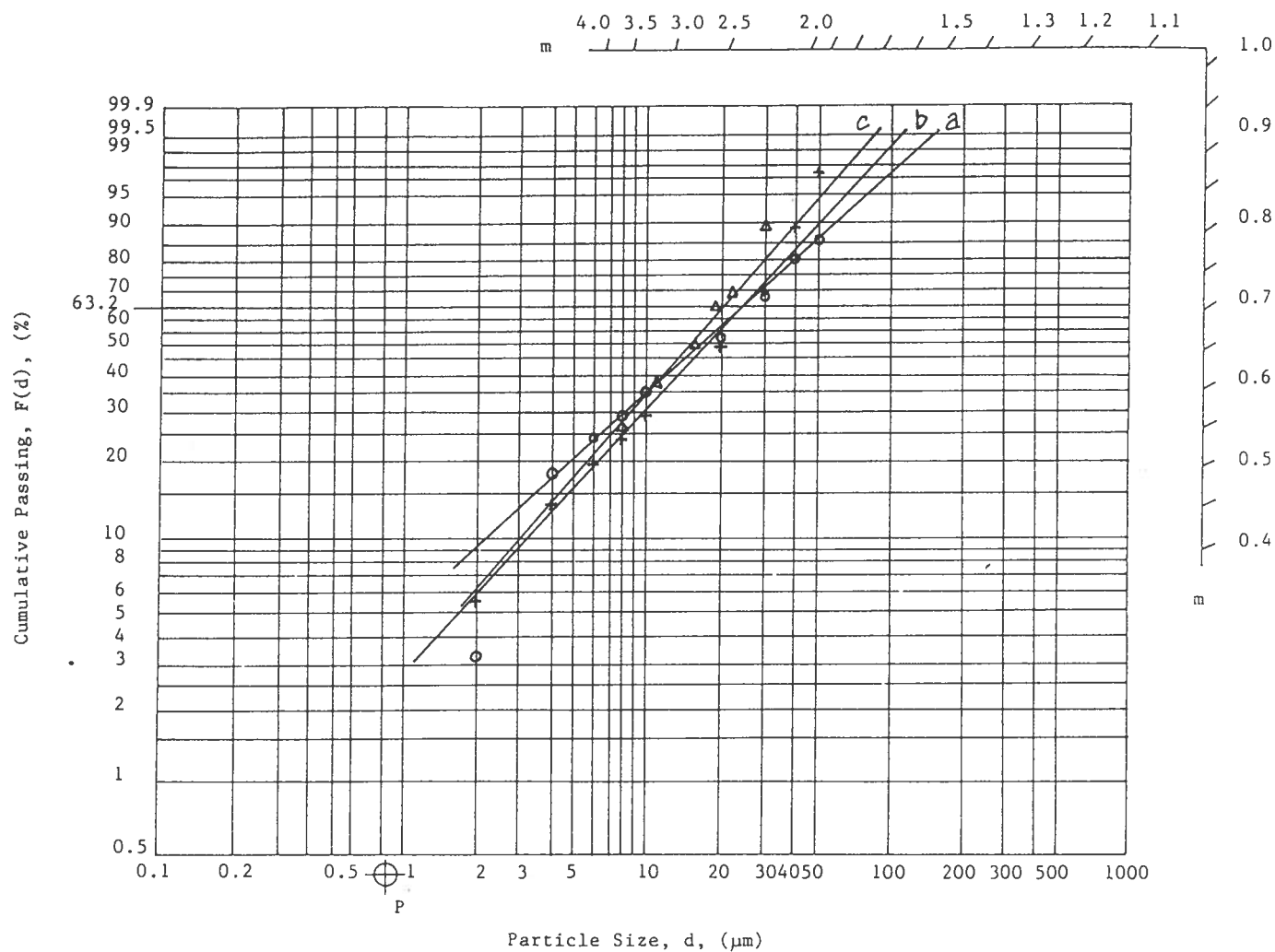


Figure 13.2 RRB particle size distribution of upgraded magnetite sample measured using a) Horiba PSA, b) Elzone PSA and c) Cyclosizer.

Examination of Table 13.3 and Figure 13.2 reveals that each measuring technique produced slightly different results. The differences in the results can be attributed to the different types of particle diameters that are measured. The Horiba PSA and cyclosizer measure Stokes diameters and the Elzone PSA measures spherical volume diameters. The difference between these types of diameters is primarily due to the non-spherical shapes of the particles (Allen, 1990). The data from the Elzone and the Horiba can be brought into coincidence with the cyclosizer data by multiplying their sizes by the (average) shape factors 1.18 and 1.05, respectively. The wider size distribution results obtained from the Horiba than from the Elzone indicates that the particle shape changes with particle size. In this case, the shape factor will be slightly different for particles of different sizes.

13.3.2.3 Electrophoretic Mobility

The electrophoretic mobility, EPM, was determined as a function of pH for the -10 μm size fraction separated from the upgraded magnetite sample using a Warman Cyclosizer. The measurements were carried out with a Zeta Meter and the pH of the suspension was controlled with HCl and NaOH. For measurements in the acidic pH range, the EPM was first determined at the natural suspension pH and then HCl was added to lower the pH for subsequent determinations. Similarly, for measurements in the basic pH range, the measurements were first carried out at the natural suspension pH which was subsequently increased by adding NaOH. Two batches had to be prepared for these experiments, one for the acid range and another for the basic range.

The electrophoretic mobility is plotted in Figure 13.3. It can be seen that the EPM was negative over almost the entire pH range and that an isoelectric point was situated around pH 2.3. According to the literature, pure iron oxide minerals have an isoelectric point (i.e.p.) in the pH range of 6.0 to 7.0. Possible explanations for this low i.e.p. value are:

- i. Surface contamination of the magnetite with surfactants,
- ii. Leaching and precipitation at particle surfaces due to leaching, and
- iii. Mineralogical impurities in magnetite particles.

It should be noted that the data presented in Figure 13.3 was produced from three independent sets of measurements. The -10 μm magnetite sample had a mean particle size of 3.3 μm , a density of 4970 kg m^{-3} , a total iron content of 68.0% and a SiO_2 assay of 2.8% indicating its high purity. It is therefore not likely that the EPM of quartz was being measured instead of for the magnetite. It is also noted that these specifications are very close to those of the bulk sample and other size fractions and therefore the -10 μm sample can be considered to be representative of these other samples.

The magnetite was produced as a secondary product from the Craigmont copper mine where the ore was subjected to flotation collectors, dispersing agents and flocculants. Trace amounts of any of these reagents can affect the EPM. In addition, the magnetite sample was obtained from a stock pile which was exposed to weathering. The weathering could have resulted in leaching and precipitation processes that altered the particle surfaces. It is also possible, however, that the magnetite contained fine inclusions of other minerals that affected the surface charge of the particles. Quartz, for example, has an i.e.p. situated around pH 2, which is very close to the measured i.e.p. values for magnetite. This supports the explanation that fine

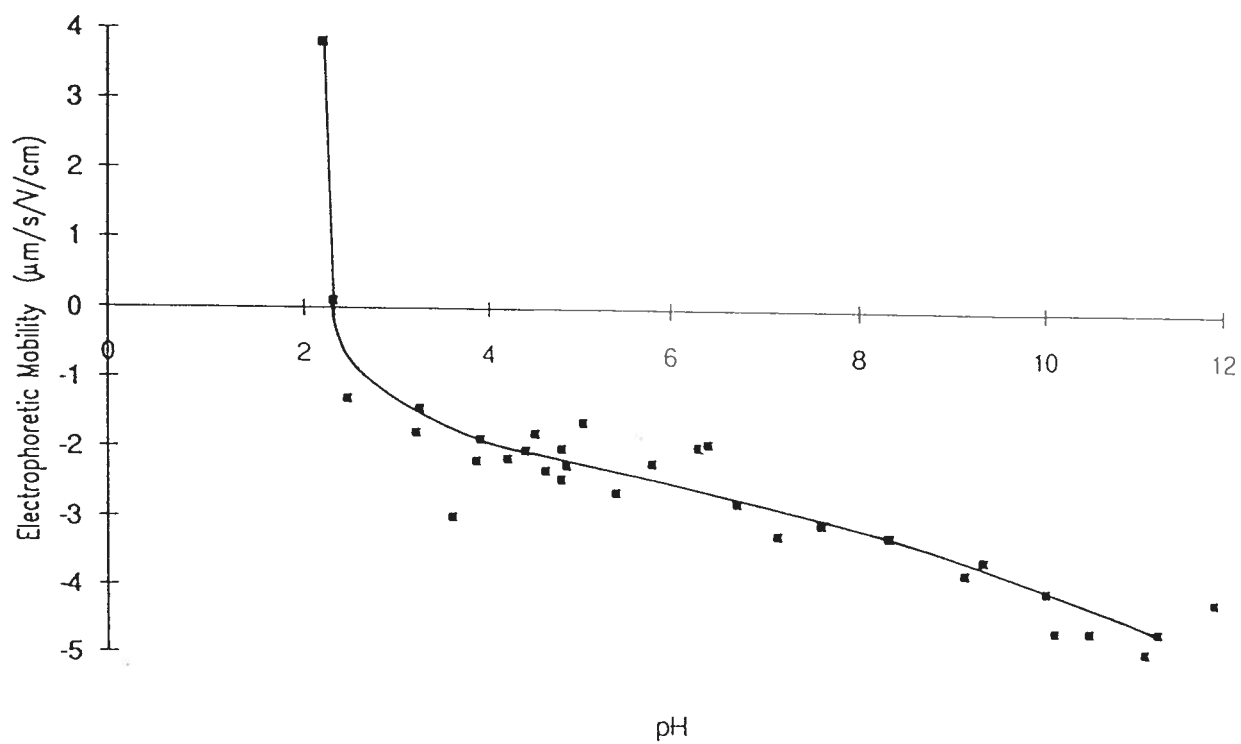


Figure 13.3 Electrophoretic mobility of -10 μm magnetite sample showing an iso-electric point in the pH range of 2.3.

quartz inclusions or contaminants determine the zeta potential of the magnetite particles.

To support this explanation, scanning electron micrographs were produced for the magnetite sample. Figure 13.4 a) shows the electron micrograph of the magnetite sample. Figure 13.4 b) shows an energy dispersive x-ray analyzer spectrum for the surface of the particles. The spectrum shows an iron peak but also a distinct silica peak. These results confirm that silica was present on the surface of the magnetite possibly as a contaminant or as very finely disseminated inclusions.

13.3.2.4 Magnetism Content

The magnetism content of the upgraded sample was determined with a Davis Tube to be 93%. This value is slightly lower than recommended limit of 95%. It should be noted, however, that such values are operator-dependent which explains why a magnetism content of 100% was not achieved despite prior upgrading of the sample with a wet drum magnetic separator.

13.3.2.5 Elemental Analyses

The assay levels of the elements found in the upgraded magnetite are presented in Table 13.4. The total iron and ferrous iron assays are 71.0% and 27.9%, respectively, which compare closely to the levels for pure magnetite of 72.4% and 24.1%, respectively. As indicated, the magnetite has a higher ferrous iron content than the pure magnetite which is based on its chemical formula. The difference cannot be explained by the presence of ferrous sulphide



Figure 13.4a Scanning electron micrograph of magnetite particles.

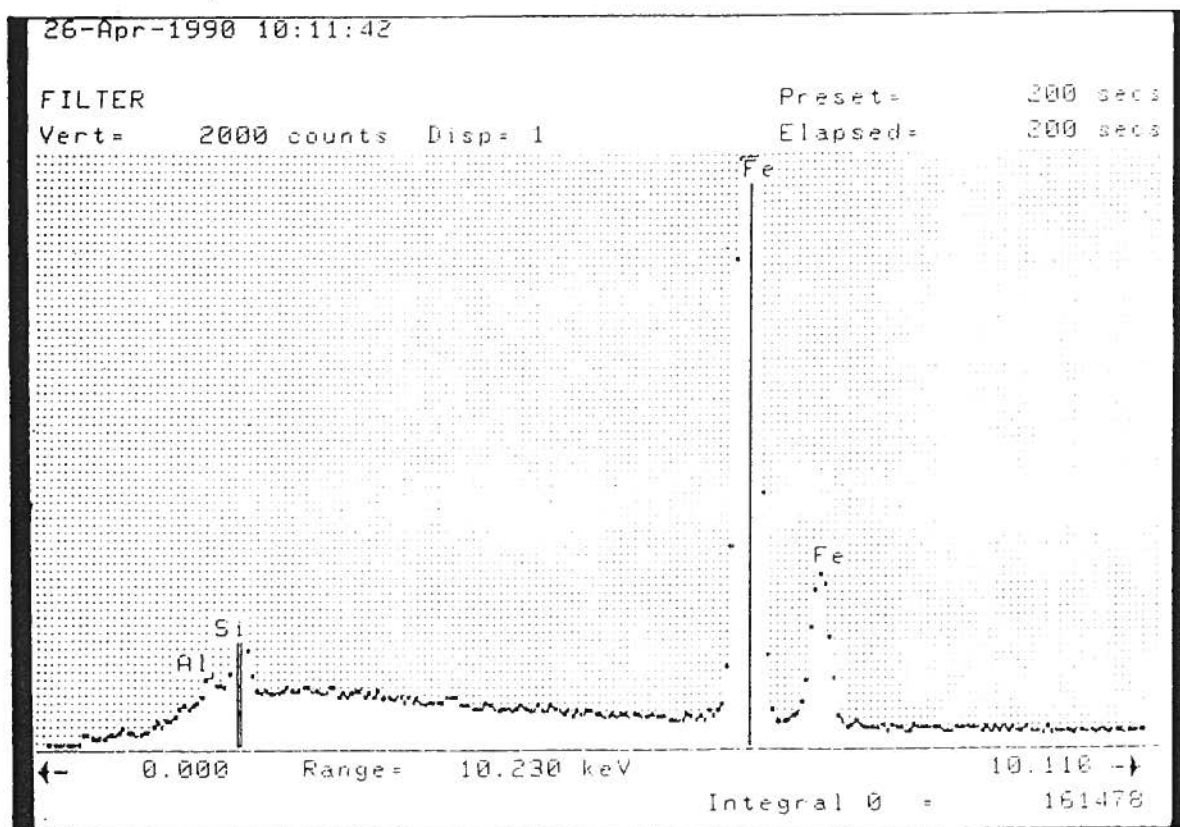


Figure 13.4b Energy dispersive x-ray analyzer spectrum for magnetite particles showing an iron peak and a distinct silica peak.

Table 13.4 Elemental analyses of upgraded magnetite sample.

Element	Assay (%)
Fe Total	71
Fe Ferrous	27.9
SiO ₂	4.1
Ca	0.34
Al	0.76
Mg	0.16
Mn	0.01
Ti	0.02
Cr	0.15
Cu	0.02
S Total	<0.01

minerals since the total sulphur content did not exceed 0.01%.

Many metal ions can replace iron ions in the magnetite lattice and have an adverse effect on the magnetic properties. Specifically, titanium can replace iron ions; this results in high remnant magnetism levels. The titanium assay was only 0.02%, and therefore, the magnetite could not be considered to be of the titaniferous form. The main impurity in the sample was silica which assayed 4.9%. Microscopic examination of the sample revealed that some silicate minerals were locked within coarse (+38 μm) particles. In addition, it was found that some of the silicate minerals were finely disseminated in the magnetite (see Section 13.3.2.3).

13.2.2.6 Magnetic Properties

The magnetic properties of the upgraded -45 μm magnetite were determined by using a vibrating magnetometer to produce an intensity of magnetization, M , versus induced magnetic field, H , hysteresis curve. From the hysteresis curve, the magnetic susceptibility at field strengths of 30 oersteds and 800 oersteds, the saturation moment and the coercive force were determined. The magnetic properties along with recommended levels (Osborne, 1986) are presented in Table 13.5.

Comparison of the results to the recommended levels indicates that the magnetite sample meets the recommended susceptibility and saturation moment levels; the coercive force was, however, high. The saturation moment and susceptibility values provide an indication of the magnitude of the force experienced by a particle in a magnetic field which in turn relates to its recoverability by magnetic separation. Since magnetic separation is used to recover and upgrade

Table 13.5 Magnetic properties of the -400 mesh upgraded magnetite sample.

Magnetic Property	Determined	Recommended
Initial Susceptibility - k_{30} (emu/g)	0.055	>0.050
Susceptibility - k_{800} (emu/g)	0.078	>0.053
Saturation Moment - M_{sat} (emu/g)	80.0	>80.0
Coercive Force - H_c (Oersteds)	86.5	<50.0

magnetite for re-use in a dense medium recovery circuit, it is desirable for these magnetic properties to be as high as possible.

The coercive force is a measure of the magnitude of the remnant magnetic attraction forces in a particle. If the coercive force is high, particles will attract to each other to form aggregates. The presence of such aggregates can have a deleterious effect on separation efficiency. Therefore, the coercive force should be as low as possible. The high coercive force indicates that the magnetite sample is susceptible to magnetic aggregation and should be demagnetized when used for dense media separation.

Figures 13.6 a) and b) are scanning electron micrographs of magnetized particles. The magnetized particles have a branched chain-like structure with small particles clinging to the surface of the large particles. From Figure 13.4 a) it can be seen that demagnetized particles do not aggregate to form chains. Due to the nature of the branched chain structure, magnetized particles would likely form voluminous aggregates and at a sufficiently high solids content would form a network structure.

13.3.3 Preparation of Size Fractions

To determine the effect of particle size on the properties of magnetite dense media, various size ranges of magnetite particles were prepared. Specifically, magnetite samples with size ranges finer than 45 μm , 30 μm and 15 μm were prepared. To prepare the -45 μm sample, upgraded magnetite was wet screened with a 270 mesh (45 μm) sieve. The -30 μm and -15 μm samples were prepared by using a Haultain Infrsizer.

a.



b.

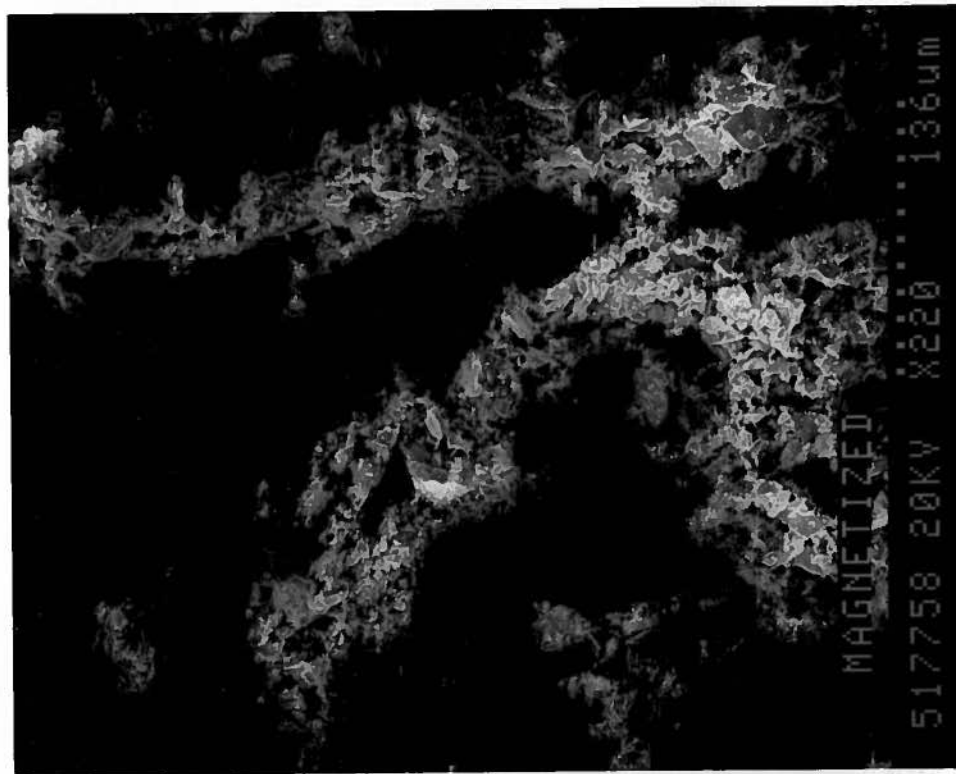


Figure 13.6 Scanning electron micrographs of a) magnetized (-75 μ m + 38 μ m) magnetite particles and b) magnetized -75 μ m magnetite particles.

The Haultain Infrasizer has a series of six air classifying cyclones that are designed to separate particles in the sub-sieve size ranges. The dimensions of the cyclones are designed to produce a root two size classification series. The finest particles were trapped in a filter at the end of the series of cyclones. The size separation was controlled by manipulating the air flow rate which was set at $20 \text{ dm}^3 \text{ min}^{-1}$.

To produce a sharp size separation in the Infrasizer, the particles must be dry and dispersed. To ensure that the standard grade magnetite samples were dry, they were placed in a drying oven for several hours. Since remnant magnetism could cause the particles to aggregate, the dried samples were passed through a demagnetizing coil immediately prior to classification. Samples were then fed to the Infrasizer, 0.5 kg at a time, which was run for twenty four hours before removing the cone products and another 0.5 kg sample was reloaded. During the classification, the cones were rapped periodically to remove particles that could have adhered to the walls of the cyclone which would have prevented them from being classified. The $-30 \mu\text{m}$ fraction was produced by combining the products from the second cyclone through to the filter. In a similar manner, $-15 \mu\text{m}$ size fraction was produced by combining the products from the fourth cyclone through to the filter.

13.3.4 Characterization of Size Ranges

The $-45 \mu\text{m}$, $-30 \mu\text{m}$ and $-15 \mu\text{m}$ size ranges were characterized with respect to particle size, density and chemical composition. The results of these analyses are summarized below.

13.3.4.1 Size Analysis of Size Fractions

The size distributions of the three size fractions were determined using the Horiba PSA. The size analyses results are presented in Table 13.6 and are plotted on RRB graph paper as shown in Figure 13.7. The RRB size and distribution moduli, presented in Table 13.6, indicate that the samples differ in size but have almost the same distribution. The samples meet the required size specifications of being finer than 45 μm , 30 μm and 15 μm respectively.

13.3.4.2 Density of Size Fractions

The densities of the size fractions were determined with the air pycnometer. The results are presented in Table 13.7 and reveal that density decreases with decreasing particle size. This trend can be explained by the density classification that also occurs in the air classifying cyclones. Normally, any non-magnetite low density particles report together with smaller high density particles. The reported density values were the average of three determinations. All densities were greater than 4900 kg m^{-3} which were greater than the density of the upgraded sample (4860 kg m^{-3}). It seems that the samples were upgraded by removing coarse low density particles such as non-liberated particles containing both magnetite and silicate minerals.

13.3.4.3 Elemental Composition of the Size Fractions

The elemental compositions of the three size fractions are presented in Table 13.8. It is

Table 13.6 Size analyses of -45 μm , -30 μm and -15 μm size fractions determined using the Horiba Particle Size Analyzer.

Size (μm)	% Passing		
	(-45 μm)	(-30 μm)	(-15 μm)
38	100.0	100.0	
32	95.7	99.1	
30		97.9	
26	76.7	95.1	
20	59.3	83.2	
18		76.8	99.1
17	51.1		97.8
16		69.1	96.0
14	41.5	62.0	90.6
12		54.3	82.3
11	32.4		76.6
10		46.3	69.9
8	21.7	37.6	55.8
6		27.2	40.9
5	10.5		31.9
4		16.3	22.9
2	1.7	4.8	6.8
$d_{63.2}$	19.9	13.6	8.8
m	1.79	1.54	1.78

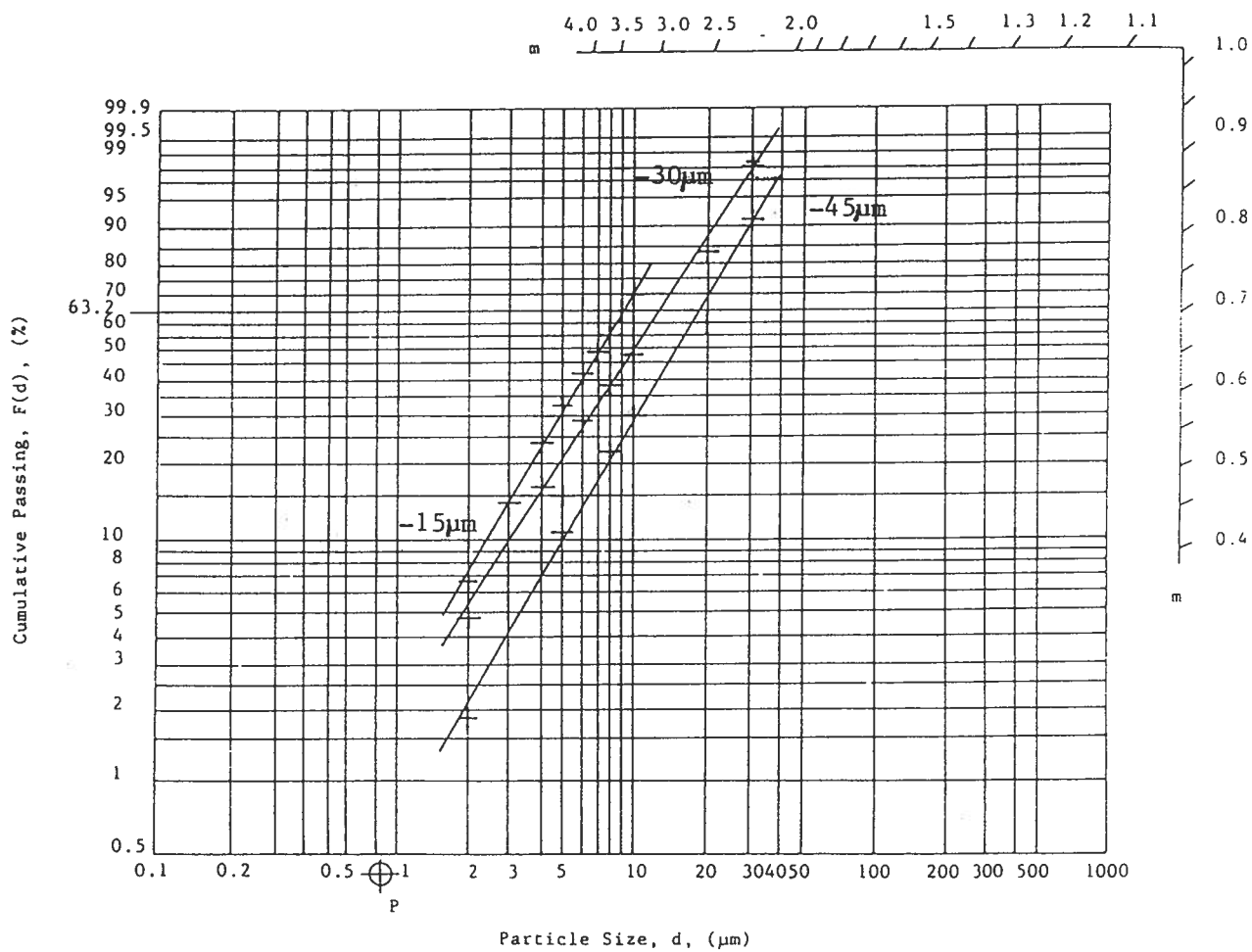


Figure 13.7 RRB particle size distributions of -45 μm , -30 μm and -15 μm magnetite samples determined using the Horiba PSA.

Table 13.7 Densities of the -45 μm , -30 μm and -15 μm size fractions determined using air pycnometer.

Sample	Density (kg m^{-3})		
	Measured	Mean	$\pm 95\%$ C.I.
Magnetite -45 μm	4970	4963	29
	4970		
	4950		
Magnetite -30 μm	4930	4943	38
	4960		
	4940		
Magnetite -15 μm	4930	4900	90
	4860		
	4910		

evident that there is little variance in the elemental compositions of the different size ranges. The ferrous iron assays ranging from 28.5% to 29.1% were higher than the levels indicated by the stoichiometric composition of magnetite. The low sulphur assay cannot account for the high ferrous iron assay which could be attributed to the presence of iron sulphide minerals. The main impurity in the samples is silica (SiO_2) which ranges from 2.3% to 2.4%.

13.3.5 Preparation of Narrow Size Fractions

In order to study the effect of particle size distribution on the properties of magnetite dense media, it was necessary to prepare samples of narrow size fractions which could be blended to create specific size distributions. The narrow size fractions were prepared using the Haultain Infrsizer (see Section 13.3.3). The Infrsizer was operated using an air flow rate of $20 \text{ dm}^3 \text{ min}^{-1}$. For each run, approximately 0.5 kg of sample was fed to the Infrsizer which was allowed to run for 24 hours before removing the products and feeding another sample. The cones were rapped periodically to detach particles that were stuck to the walls. A coarse fraction was prepared by screening at 270 mesh (53 μm) and 400 mesh (38 μm) using Tyler sieves.

13.3.6 Characterization of Narrow Size Fractions

The coarse fraction and Haultain Infrsizer cone products that were required for experiments were characterized with respect to density, magnetics content and elemental composition.

Table 13.8 Elemental analyses of the -45 µm, -30 µm and -15 µm size fractions.

Element	Sample		
	(-45 µm)	(-30 µm)	(-15 µm)
Fe Total	70.0	71.0	70.0
Fe Ferrous	29.1	29.1	28.1
SiO ₂	2.40	2.30	2.35
Al	0.02	0.025	0.025
Mg	0.07	0.09	0.10
Mn	0.015	0.02	0.015
Ti	0.0	0.0	0.0
S Total	<0.05	<0.05	<0.05

13.3.6.1 Size Analyses of the Narrow Size Fractions

The Elzone Particle Size Analyzer was used to perform the particle size analyses on the products. The results are presented in Table 13.9 and are plotted in Figure 13.8. The plot shows that the size fractions have narrow distributions. The geometric mean size and RRB size and distribution moduli for each of the products are also presented in Table 13.9.

13.3.6.2 Densities of Narrow Size Fractions

The density of each cone product was determined using an air pycnometer (see Section 13.2.1). The average of two determinations are presented in Table 13.10. The table shows that the density of the products from cone #3 through to the filter are higher than the sample from which they were separated (upgraded magnetite density was 4857 kg m^{-3}). This upgrading indicates that low density non-liberated particles must be in the coarser fractions. It is likely that the silica assays reported for the magnetite primarily result from the presence of these coarse middling particles. The coarse fraction density was very close to the upgraded magnetite density.

13.3.6.3 Elemental Composition of Size Fractions

The elemental compositions of each of the size fractions are presented in Table 13.11. The results indicated little variation in the chemical compositions of the size fractions.

Table 13.9 Size analyses of narrow size fractions determined using Elzone PSA and RRB size and distribution moduli.

Passing Size (μm)	% Passing					
	Coarse	Cone #3	Cone #4	Cone#5	Cone #6	Filter
70	99.7					
45	81.0					
40	54.6					
35	24.8					
33		93.1	100.0			
31		86.3	99.7			
30	10.0					
29		75.8	98.8	99.4		
27		61.2	97.2	99.2		
25	5.3	42.7	94.3	99.0		
23		25.4	89.4	98.6		
21		12.9	83.1	97.7		
19		6.0	74.9	96.0		
17		3.3	64.4	93.3		
15	1.6	2.0	50.8	89.2	99.3	
13		1.2	33.7	81.9	97.1	
11	0.0	0.4	19.0	66.7	93.8	99.8
9		0.0	10.1	45.6	88.6	98.5
7			4.4	28.3	77.8	95.2
5			1.6	14.4	43.8	85.1
4					23.1	71.4
3				4.5	8.2	46.6
2					1.7	15.3
1				0.2	0.0	0.3
Mean (μm)	38.1	25.4	14.7	8.5	5.1	3.3
$d_{63.2}$ (μm)	41.7	27.6	17.2	10.8	6.25	3.76
m	6.59	6.64	3.16	2.48	2.68	2.45

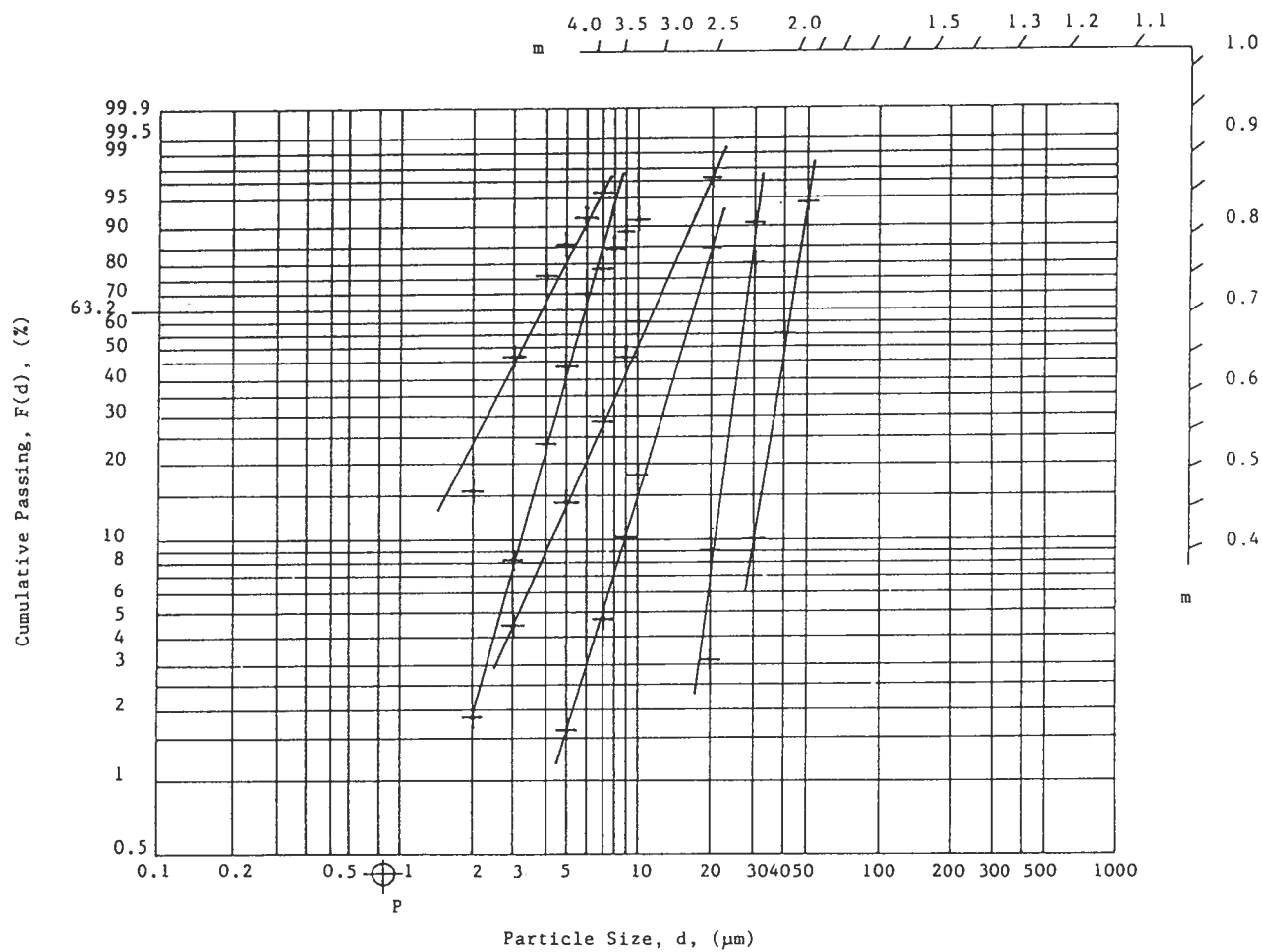


Figure 13.8 RRB particle size distributions for narrow size fractions of magnetite particles from Elzone PSA data.

Table 13.10 Densities of narrow size fractions determined using air pycnometer.

Sample	Density (kg m ₃)		
	Measured	Mean	± 95% C.I.
Coarse Fraction	4870	4860	127
	4850		
Cone #3	4940	4955	191
	4970		
Cone #4	5020	5020	0
	5020		
Cone #5	5040	5055	191
	5070		
Cone #6	5050	5040	127
	5030		
Filter	4990	4970	254
	4950		

Table 13.11 Elemental analyses of the narrow size fractions.

Element (%)	Sample					
	Coarse	Cone #3	Cone #4	Cone #5	Cone #6	Filter
Fe Total	69.0	70.0	68.0	71.0	74.0	68.0
Fe Ferrous	28.3	29.4	29.5	29.2	28.3	27.2
SiO ₂	4.4	3.6	2.6	2.2	2.25	2.8
Al	0.36	0.3	0.26	0.26	0.32	0.4
Mg	0.14	0.12	0.1	0.1	0.11	0.14
Mn	0.015	0.012	0.01	0.015	0.015	0.015
Ti	0.015	0.015	0.0	0.0	0.0	0.0
S Total	<0.05	<0.05	<0.05	<0.05	<0.05	<0.05

13.4 Chemical Reagents and Medium Contaminants

As part of the test program, the effects of various parameters on the properties of magnetite dense media were investigated. Specifically, the effects of pH, dispersing agents and various media contaminants were studied. The following describes the suspension additives used in the test work.

13.4.1 pH Modifiers

The dense medium pH levels were controlled by adding either hydrochloric acid or sodium hydroxide.

13.4.2 Organic Dispersants

Organic dispersing agents, including Dextran and Carboxyl Methyl Cellulose (C.M.C), were used in the test work. The Dextran used was the Polysciences Incorporated brand (Catalog Number 1341, Lot Number 84710). The molecular weight of the Dextran ranged from 15,000 to 20,000. The Dextran solutions were prepared by adding distilled water to produce a 10 g/l solution. To dissolve the Dextran, the solution was lightly agitated. Fresh solutions were prepared on a daily basis as required.

The C.M.C. used was from Polysciences Incorporated (Catalog Number 6140, Lot Number S-137-7). The molecular weight of the C.M.C. was 80,000. The 10 g/l aqueous solutions were

prepared by adding the C.M.C. to distilled water with slow agitation. Fresh samples were prepared on a daily basis as required.

13.4.3 Inorganic Dispersants

The inorganic dispersing agents used in experiments included BDH brands of sodium silicate and sodium hexametaphosphate. These dispersants were used to prepare 1 g/l aqueous solutions.

13.4.4 Medium Contaminants

When run-of-mine coal is fed to a dense medium separator, inefficient desliming allows fine coal and clays to enter the medium. In addition, since these types of particles are small, they are difficult to separate from the medium during the dense media recovery process. The presence of these particles can affect the properties of the medium. For these reasons the effects of such contaminants on the medium properties were also investigated.

Coal mined from the foothills of the Rocky Mountains in British Columbia and Alberta is very soft and, through normal handling, a large amount of fine particles are generated. The coal fines used in the test work were from the Bullmoose property in north east British Columbia. The coal was screened at 325 mesh to produce the fine fraction used in the experiments. The ash content of the -325 mesh fraction was determined to be 18.3%. To determine levels of contaminants in dense media, magnetite was also obtained from Luscar Sterco and Cardinal River

Coal in Alberta.

The most common clay minerals include kaolinite and bentonite. The Pioneer Washed Kaolin manufactured by the Georgia Kaolin Company was used in the tests. This sample is characterized by the following specifications: $\text{SiO}_2=45.68\%$, $\text{Al}_2\text{O}_3=38.51\%$, $\text{Fe}_2\text{O}_3=0.44\%$, $\text{TiO}_2=1.43\%$, $\text{CaO}=0.24\%$, $\text{MgO}=0.14\%$, $\text{L.O.I.}(1000^\circ\text{C})=31.51$ with average particle size= $1.1\text{ }\mu\text{m}$. The bentonite sample used in the experiments was a sodium based montmorillonite from Western Bentonite. The specifications for the sample are 85% montmorillonite with a chemical compositions of: $\text{SiO}_2=55.44\%$, $\text{Al}_2\text{O}_3=20.14\%$, $\text{Fe}_2\text{O}_3=3.67\%$, $\text{CaO}=0.49\%$, $\text{MgO}=2.49\%$ and $\text{Na}_2\text{O}=2.76\%$.

CHAPTER 14: SETTLING PROPERTIES OF MAGNETITE DENSE MEDIA

14.1 Introduction

In order to characterize the stability of magnetite suspensions, the mudline falling rate and the solids concentration profile as a function of time were determined for a magnetite suspension with 15% solids by volume (this corresponds to a medium density of 1579 kg m^{-3}).

14.2 Mudline Falling Rate

As described in Section 10.3, the settling of suspensions can be characterized by the falling rate of the supernatant-slurry interface (mudline). A high falling rate corresponds to a low medium stability and conversely, a low settling rate corresponds to a high medium stability. The interface settling rate therefore provides a relative indicator of the stability.

14.2.1 Procedure for Mudline Falling Rate Determinations

Suspensions of dense media were prepared by mixing the upgraded magnetite with distilled water to a volume solids content of 15%. This solids content is typical for dense media used in coal preparation and it corresponded to a medium density of 1579 kg m^{-3} . The suspensions were prepared in 250 ml graduated cylinders. To ensure that the suspensions were thoroughly dispersed, the graduated cylinders were inverted several times and placed in an

ultrasonic mixing bath. To eliminate remnant magnetism that could cause particle aggregation and thereby affect settling, the suspensions were passed through a demagnetizing coil three times.

The settling measurements involved determining the height of the position of the supernatant-slurry interface with time. The height was plotted against time and the initial slope of the line reported as the falling (settling) rate. Three sets of measurements were performed to evaluate the reproducibility of the results.

14.2.2 Results of Interface Settling Tests

Figure 14.1 is a photograph of a settling suspension of magnetite with 15% solids by volume. The suspension settled with a clear supernatant and a sharp mudline. The sharp interface indicates that the suspension settles as a bulk and that little differential settling occurred (hindered settling).

Figure 14.2 is a plot of the interface height versus time for the three sets of data. The figure shows all three sets of data produced the same settling curve indicating good reproducibility of results. The slope of the initial linear portion of the curve is taken to determine the settling rate of the suspension. The curve shows that the suspension settled with an almost constant rate for approximately eight minutes. After this time the settling rate decreased until the settling curve became horizontal as a result of the formation of a sediment. After 24 hours, the sediment height had decreased slightly as the result of subsidence. According to Cheng (1980a), this type of settling curve indicates that the particles in the suspension are aggregated. This aggregation can be explained by secondary minimum coagulation or by



Figure 14.1 Settling suspension of magnetite particles with a solids volume fraction of 15%. The photograph shows that the magnetite settles with a sharp supernatant/suspension interface.

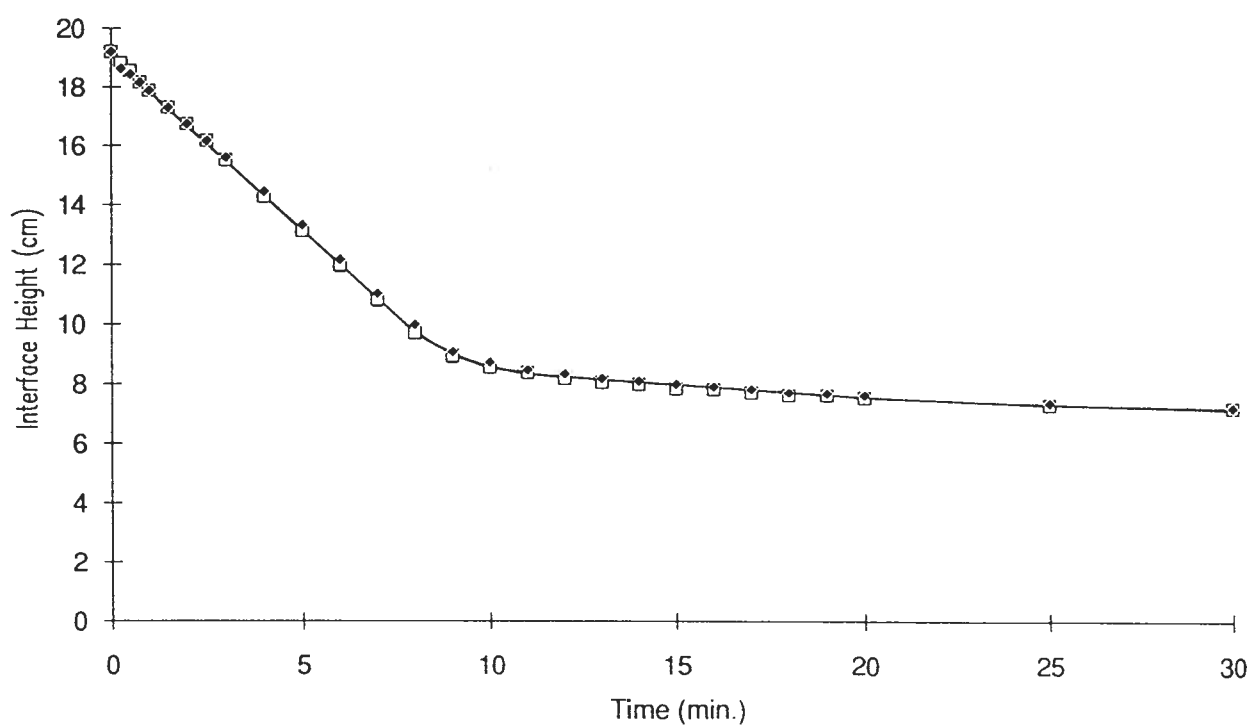


Figure 14.2 Magnetite suspension mudline interface height versus settling time showing three sets of data (solids volume fraction = 0.15, pH = 8.24, temperature = 25°C).

magnetic aggregation resulting from remnant magnetic forces. Although the magnetite was demagnetized, small particles can still exhibit remnant magnetism since they contain only a few magnetic domains which if randomized may not completely cancel the polarity of the particle.

Based on the average of the three tests, the initial falling rate was determined to be 1.42 cm min^{-1} . According to Osborne (1988), typical settling rates for dense media that behaves well in a plant are between 2.0 cm min^{-1} and 6.5 cm min^{-1} . The settling rates for these samples, therefore, represent a medium with a higher than average stability.

14.3 Solids Concentration Profile

The suspension settling rate is only an indicator of stability and does not fully describe the settling properties of magnetite dense media. For a more complete description of the settling properties, the solids concentration profile as a function of time was studied.

14.3.1 Procedure for Solids Concentration Profile Determinations

The solids concentration profile was determined by sampling a magnetite suspension from a graduated cylinder at several depths after allowing the suspension to settle for a pre-determined period of time. The solids contents of the samples were then determined and the solids concentration profiles were constructed.

The suspension used for the concentration profile determinations was a mixture of upgraded magnetite (see Section 13.3.1) and distilled water. Several suspensions were prepared

in 100 ml graduated cylinders to produce medium with a density of 1579 kg m^{-3} corresponding to a volume solids content of 15%. Prior to sampling, the suspension was demagnetized and the graduated cylinder was inverted several times to disperse the particles. A pipette was used to obtain the samples from different depths in the graduated cylinder. After mixing the suspension, the cylinder was placed upright and the pipette submerged to a predetermined depth. The suspension was then allowed to settle for a designated time period prior to drawing a sample. The pipette containing the sample was then weighed before being emptied into a dish in which it was dried. The solids content was then determined from the weight of the dried magnetite and the weight of the wet sample. The weight fraction was converted to a volume fraction based on the magnetite density of 4857 kg m^{-3} . The sampling heights ranged from 100 ml at the top of the graduated cylinder to 0 ml at the bottom of the cylinder. Samples were taken at heights corresponding to 10 ml intervals along the cylinder. The settling times at which the samples were taken ranged from 0 to 10 minutes. For each settling time, a fresh suspension was prepared and the entire set of experiments were repeated to ensure reproducibility of results.

14.3.2 Solids Concentration Profile Results

Solids concentration profiles for each settling time were plotted (Figure 14.3). The figure shows that magnetite dense media exhibit zone settling properties. As the suspension settled, a supernatant was formed at the top of the column. Below the supernatant, a small transition zone developed which had a lower solids content than the initial suspension. Below the transition zone, a constant density zone existed with approximately the same solids content as the initial

suspension. At the bottom, the solids built up to form a sediment with a high solids content.

Figure 14.4 is a contour plot showing the suspension solids concentration as a function of column height and settling time. The contour lines represent the borders between the zones and the slopes of the lines represent the interface falling rates. With time, the extent of the supernatant increased until after approximately 8 minutes it met the sediment. During this time, the constant density zone diminished in size from the entire column height to zero. The transition zone was quite small although its extent increased slightly with time. The small transition zone indicated that very little differential settling occurred; ie. most large and small particles settled at the same rate. This result supports Napier-Munn's (1984) conclusion that media segregation is controlled by bulk hindered settling rather than by classification in cyclones. However, at low solids concentrations Davis (1987) has shown that size classification does occur. The magnitude of the accelerating force likely influences the type of settling that occurs.

The supernatant-transition zone interface falling rate was determined to be 1.22 cm min^{-1} and the transition zone-constant density zone settling rate was 1.36 cm min^{-1} . These rates are similar to the rate determined from the settling test performed in Section 14.2.2 of 1.42 cm min^{-1} . The constant density zone-sediment interface falling rate was determined to be $-0.97 \text{ cm min}^{-1}$; the negative sign indicates that the sediment height increased with time.

If it can be assumed that the extent of the constant density in a dense medium separator represents the medium stability, then the transition zone-constant density zone interface settling rate provides is a good indicator of this stability. Since the extent of the transition zone is small and the falling rates of these two interfaces are similar, the supernatant-transition zone interface (mudline) falling rate can be considered a good indication of media stability.

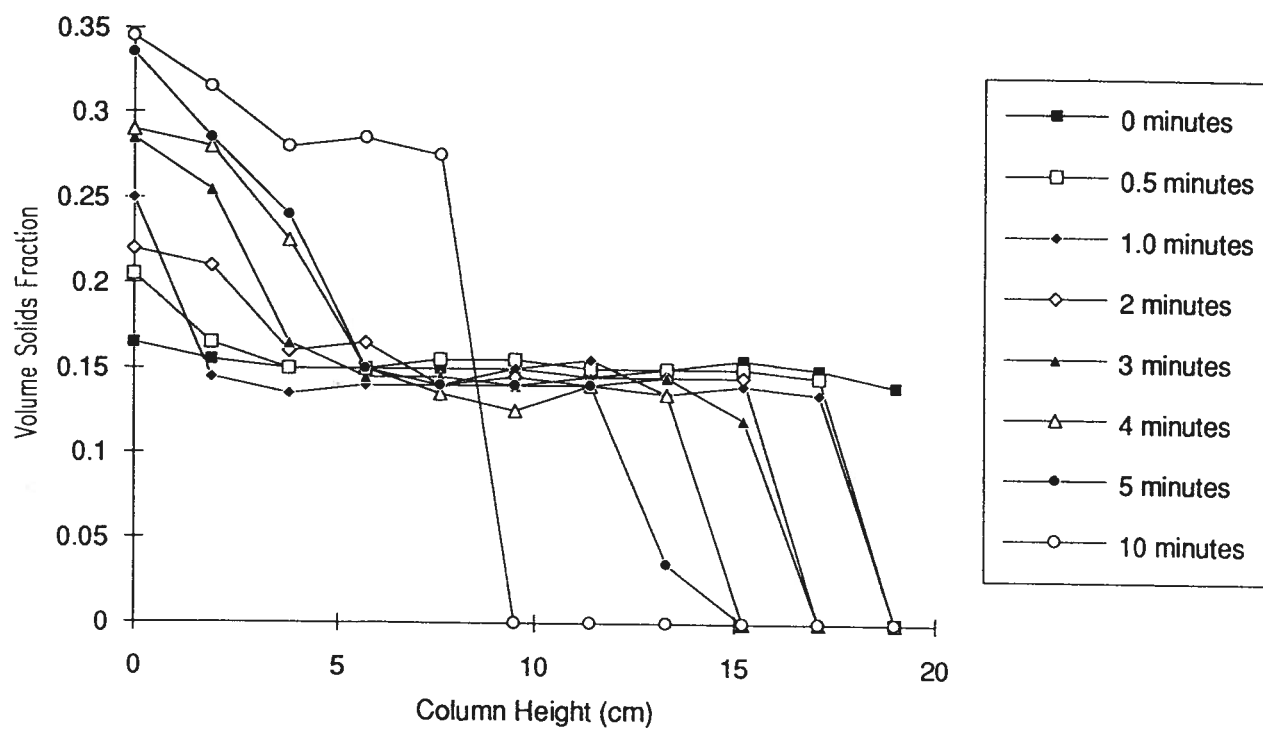


Figure 14.3 Volume solids fraction versus height in column of settling magnetite particles for settling times of zero minutes to ten minutes (solids volume fraction = 0.15, pH = 8.52, temperature = 25°C).

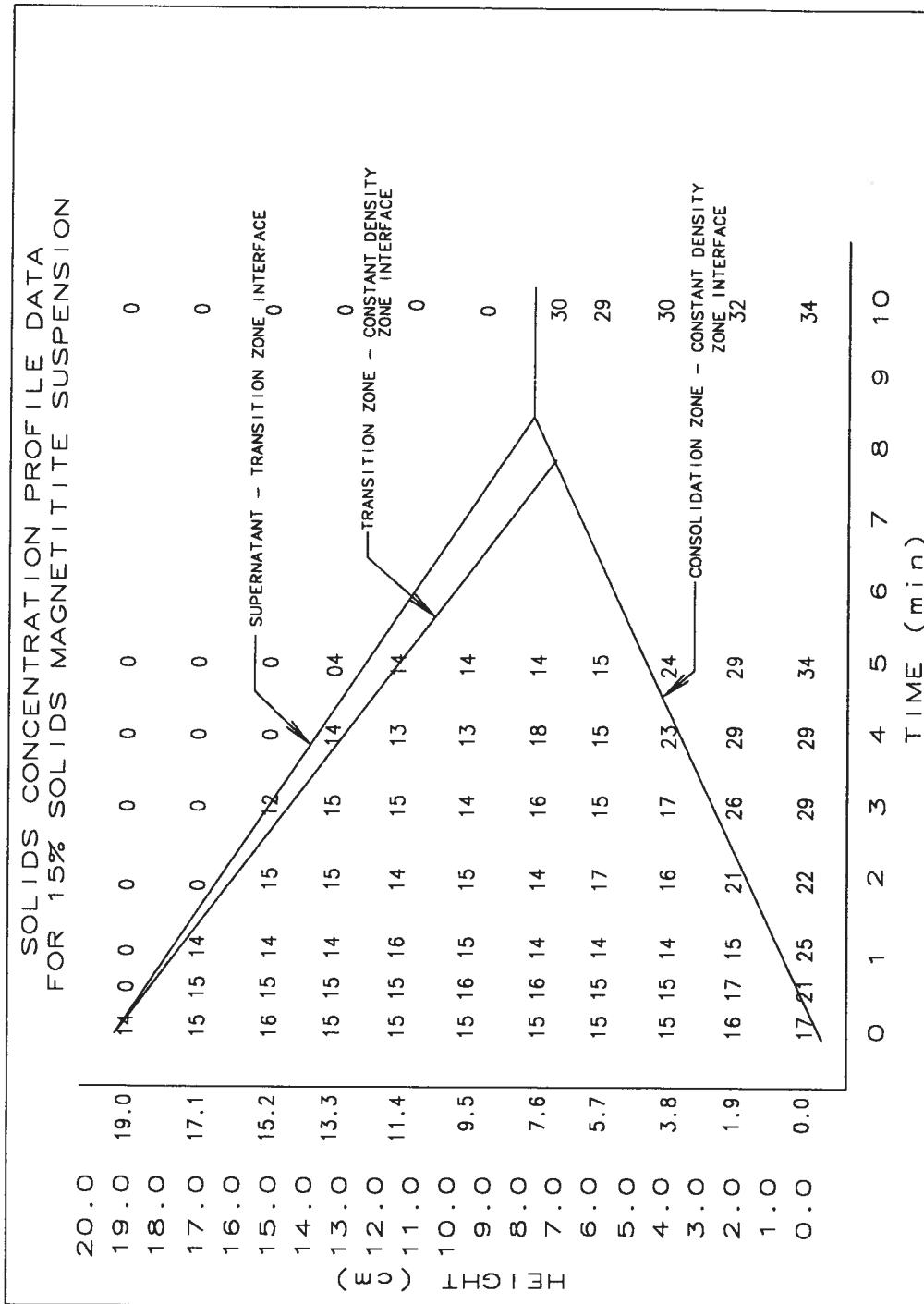


Figure 14.4 Magnetite volume solids content as a function of height and settling time showing settling zones (solids volume fraction - 0.15, pH = 8.52, temp. = 25°C).

As discussed in Section 10.2, particle interactions are responsible for bulk zone settling properties of suspensions. The shape of the settling curve indicates that the particles may be partially aggregated. This aggregation can explain the zone settling properties exhibited by the suspension. In particular, aggregates of similar size would settle at the same rate. Therefore a small transition zone would be expected with the bulk of the suspension settling together in a constant density zone.

14.4 Conclusions

It was found that a typical magnetite dense media suspension exhibits zone settling properties that are characterized by bulk settling rather than by differential settling. The suspension settling was characterized by the presence of four zones: a supernatant, a transition zone, a constant density zone and a sediment. The constant density zone had a solids content that was approximately equal to that of the initial suspension. The mudline falling rate was determined to be 1.42 cm min^{-1} which compared closely to the falling rate of the transition zone-constant density zone interface of 1.36 cm min^{-1} . Since these rates are similar and since the extent of the constant density zone should be directly related to dense media stability, the mudline settling rate should provide a good indication of the stability.

The settling characteristics of the suspension were explained by particle aggregation. Evidence of aggregation was based on the shape of the mudline settling curve and on the bulk settling properties determined from the solids concentration profile tests.

CHAPTER 15: RHEOMETER FIXTURE FOR SETTLING SUSPENSIONS

15.1 Introduction

The device constructed to measure the rheological properties of unstable mineral suspensions, consists of a specially designed cup and bob fixture that attaches to a concentric cylinder viscometer. This fixture was designed for suspensions that exhibit zone settling properties such as magnetite dense media (see Chapter 14) as well as many other mineral suspensions (see Section 10.2). In a column of suspension, settling particles form distinct zones including (from top to bottom) a supernatant, a transition zone, a constant density zone and a consolidation zone. With time, the extent of each of these zones changes until only a supernatant and a consolidation zone remain. The results presented in Chapter 14 indicated that magnetite suspensions exhibit this type of settling and that in a sufficiently long column, an extensive constant density zone would exist for a certain period of time. The measuring device was therefore designed so that the bob would be positioned within the constant density zone during rheological measurements.

The fixture was attached to a Haake viscometer (Searle type) in which the bob rotates and the shear stress is determined from the torque applied to the bob from the suspension. The viscometer used was a Haake RV20 with an M5 measuring head for low viscosity systems. The viscometer was interfaced to a PC which controlled the measurement and record the data. A photograph of the rheological laboratory equipment is presented in Figure 15.1.



Figure 15.1 Rheologic laboratory facility showing a) the Haake RV20 controller, b) the M5 viscometer, c) the PC and d) the temperature controller.

15.2 Details of the Fixture Design

A schematic diagram of the fixture is shown in Figure 15.2. It consists of an elongated cup and inner cylinder with a bob attached to an elongated shaft. It is arranged so that the bob is positioned in the constant density zone of the settling suspension. The extent of the constant density zone is proportional to the height of the settling column and it decreases at a rate that is proportional to the mudline settling rate. Therefore, to ensure a sufficient height of constant density zone, a rapidly settling suspension would require a tall settling column. These factors were taken into consideration when determining the height of the cup and the position of the bob.

Since the correct cup height and bob position is specific to the settling properties of the tested suspension, it was necessary to develop a concentration profile as a function of time for the system. The height of the column, H , was determined from the transition zone - constant density zone interface falling velocity, v_{ic} , the constant density zone - sediment rising rate, v_{cs} , the height of the bob, h_b , and measurement time, t . The column height was calculated from the following relationship (Equation 15.1).

$$H = v_{ic}t + v_{cs}t + h_b \quad (15.1)$$

Once the column height was established, the position of the bob was set so that it was maintained completely within the constant density zone during the time of measurement. The height from the bottom of the cup to the top of the bob, H_b , was calculated from Equation 15.2.

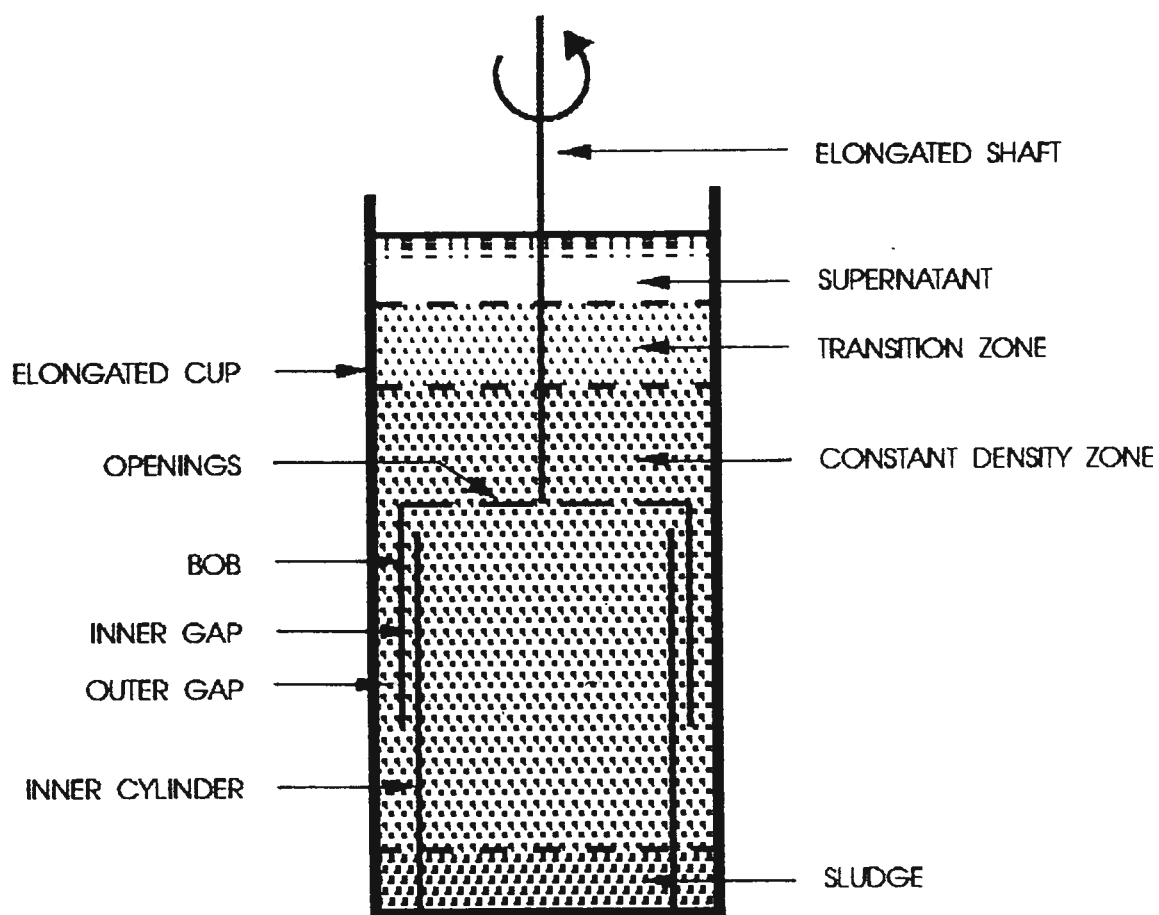


Figure 15.2 Rheometer fixture for settling suspensions showing the bob positioned in the constant density zone of a settling suspension.

$$H_b = H - v_{tc} t \quad (15.2)$$

There are several fixture geometries for concentric cylinder rheometers. Most have a single gap between the cup and the bob. With a single gap cup and bob arrangement, however, settling particles can build up on top of the submerged bob and result in the formation of a cone of particles. The particles would eventually slide into the annular gap and thereby alter the solids concentration in the measuring region. For this reason a double gap arrangement, modified to prevent the accumulation of solids, was used. The modification consisted of an open top on the bob with a hollow inner cylinder which allowed particles to settle through the top of the fixture. In order to define the shear stress at the inner side of the bob it was necessary to add the inner cylinder and thereby create the double gap arrangement. An advantage of the double gap arrangement was that it provides a greater fixture surface area than a single gap arrangement resulting in more accurate measurements.

The inner hollow cylinder was coaxially positioned within the cup and its height extended to just below the top of the bob. The radii were fixed so that the gaps between the bob and the outer cylinder and the bob and the inner cylinder provided an equal shear rate on the surfaces of the bob. In order to achieve equal shear rates, the radii had to satisfy the conditions given by Equation 15.3 (Moore and Davies, 1956).

$$\frac{r_1}{r_2} = \frac{r_3}{r_4} \quad (15.3)$$

where, r_1 is the radius to the outside of the inner cylinder,

r_2 is the radius to the inside of the bob,

r_3 is the radius to the outside of the bob, and

r_4 is the radius to the inside of the cup (see Figure 15.3).

The gap sizes between the concentric cylinders were set to be as small as possible to reduce the potential for non-Newtonian shear rate effects (see Section 6.2.2.2). Conversely, the gap size must be at least ten times the size of the diameter of the largest particle to prevent the particle from physically jamming (Sherman, 1970). If large particles bridge the gap and cause the rotating bob to jam, erratic shear stress values are obtained.

Other design features take end effects, wall slip effects and temperature effects into consideration. End effects were considered to be small because of the small surface area at the bottom of the double gap bob (Moore and Davies, 1956). The shaft and spoke arrangement supporting the bob, however, are immersed in the suspension and when rotating contribute to the measured torque.

Wall slip was minimized by using roughened cup and bob surfaces. The surfaces were roughened by cutting vertical grooves into them; the depths of these grooves were set to be at least as large as the largest particle in the suspension (Nguyen, 1983, Cheng, 1978 and Cheng 1984).

Rheological properties are very temperature sensitive. For this reason the entire cup and bob arrangement was surrounded by a temperature controlled water jacket.

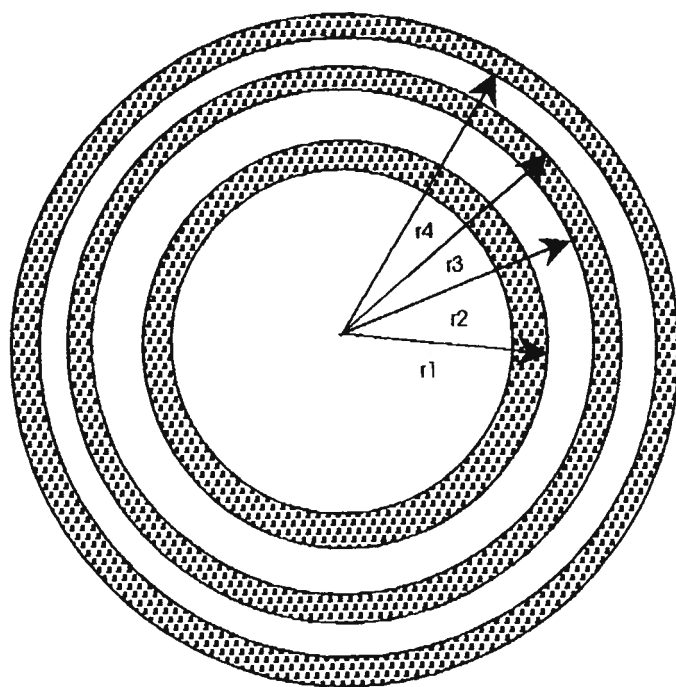


Figure 15.3 Plan view of a double concentric cylinder viscometer fixture.

15.3 Fixture Dimensions

The height of the elongated cup was determined based on the requirement to maintain the bob within the constant density zone for a measurement time period of six minutes. This measurement period was considered to be an adequate time to produce rheological flow curve data; Haake recommended a measurement time of at least two minutes for their viscometer. The interface velocities, determined by measuring the solids concentration profile in a column of suspension after various settling times (see Chapter 14), were needed to design the dimensions of the fixture (Equations 15.1 and 15.2).

The falling rate of the transition zone-constant density zone interface, v_{tc} , and rising rate of the constant density zone-sludge interface, v_{cs} , were determined to be 1.36 cm min^{-1} and 0.97 cm min^{-1} respectively for a typical magnetite suspension with 15% solids by volume. For a bob height of 6 cm and a measurement time period of six minutes, the height of the suspending column was determined to be 20.0 cm. To allow for variations in settling rates of different suspensions, a settling column 23 cm in height was selected. Equation 15.2 was then used to establish the position of the bob to ensure that it was placed in the constant density zone for the duration of the measurement. The height from the bottom of the cup to the top of the bob was calculated to be 11.8 cm.

The gap size was set to be only slightly larger than ten times the largest particle diameter in order to avoid particle bridging and reduce potential non-Newtonian shear rate effects. Since the size of magnetite particles used is generally much finer than $100 \text{ }\mu\text{m}$, the gap sizes were set at $1000 \text{ }\mu\text{m}$ and $1100 \text{ }\mu\text{m}$ for the inner and outer gaps, respectively.

The radii of the surfaces in the double gap geometry were selected to meet the requirements of Equation 15.3. The radii selected were 2.11 cm for the inside radius of the cup, r_4 , 2.00 cm for the outside radius of the bob, r_3 , 1.95 cm for the inside radius of the bob, r_2 , and 1.85 cm for the outside radius of the inner cylinder, r_1 (Figure 15.3).

To minimize the effects of wall slip, vertical grooves were cut into each of the shearing surfaces. The grooves were cut into the surface with a knurling tool and the depths were measured to be 250 μm which is approximately 2.5 times the size of the largest magnetite particles (100 μm).

Using the above dimensions, a prototype of the device was machined from brass. Photographs of each of the components of the fixture are presented in Figure 15.4. A sample size of 350 ml was needed for each rheological measurement.

15.4 Calibration of the Fixture

The Haake viscometer applies a rotational speed (ω) to the bob which is also attached to a strain gauge that measures a strain that is proportional to the torque (T) caused by the suspension. As indicated by Equations 15.4 and 15.5, to determine the shear rate and shear stress the rotational speed and torque values are multiplied by fixture constants.

$$\dot{\gamma} = M\omega \quad (15.4)$$

$$\tau = AT \quad (15.5)$$

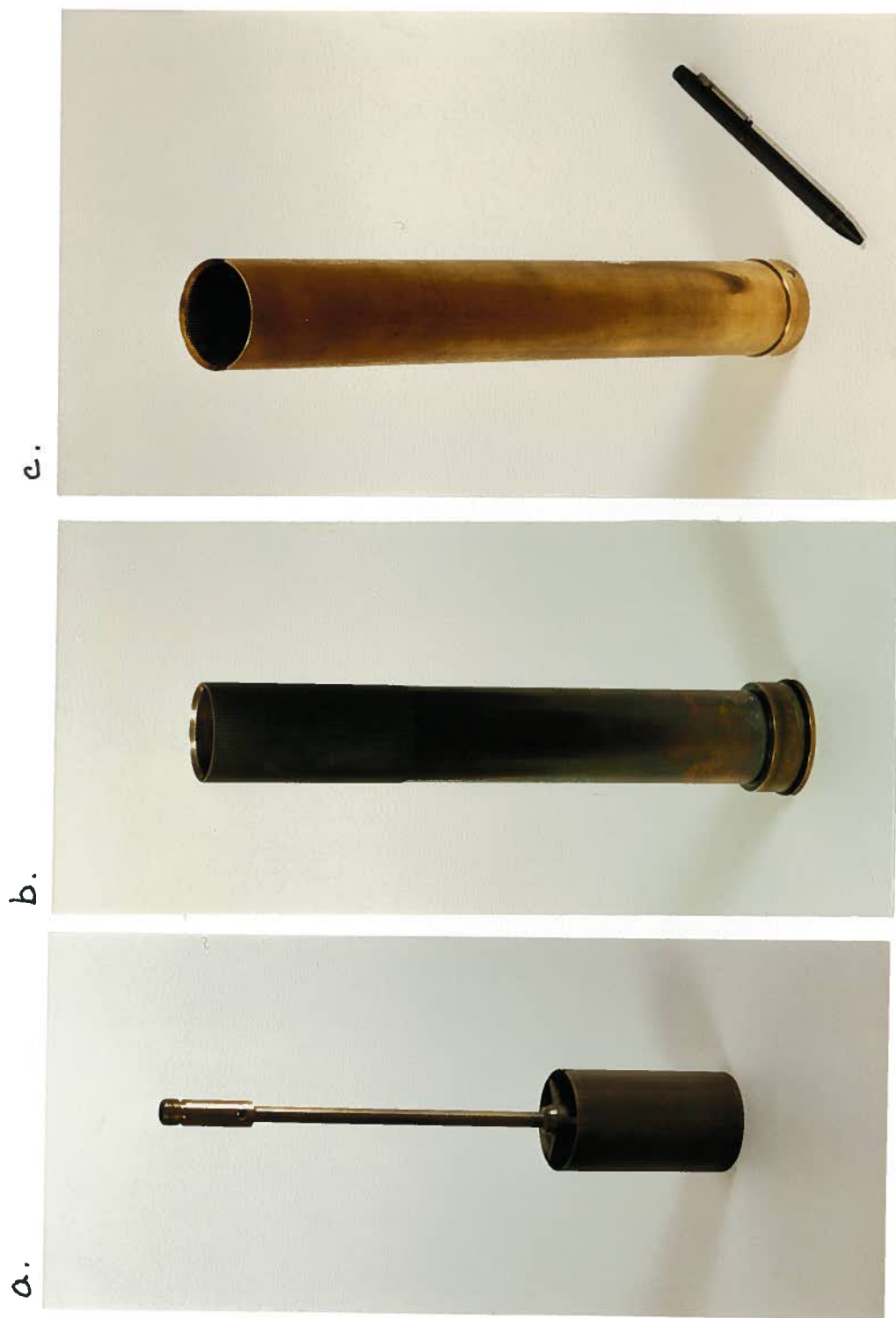


Figure 15.4 Rheometer fixture for measuring rheological properties of settling suspensions showing a) the bob, b) the inner cylinder, and c) the cup.

where, M can be determined from equation 15.6.

$$M = \frac{\pi}{6} \left(\frac{r_1^2}{(r_2^2 - r_1^2)} + \frac{r_4^2}{(r_4^2 - r_3^2)} \right) \quad (15.6)$$

The value of A was determined from measurements with standard viscosity oils (Brookfield Standard Viscosity Oils were used for calibrating the device). The procedure involved setting the value of A to 1.00 and measuring the viscosity of oils with known viscosities of 9.5 mPa.s and 50 mPa.s. Based on the measured viscosity, the value of A was adjusted so that the measured viscosity equalled the actual viscosity. The procedure was repeated until the determined level of A produced the correct viscosity results. The values of M and A for the fixture were determined to be 10.348 and 1.435 respectively. Figure 15.5 shows three sets of flow curves for each of the 9.5 mPa.s and 50 mPa.s oils. The data were fitted with a straight line, the slope of which is the fluid viscosity. The measured viscosities were 9.53 mPa.s and 49.45 mPa.s, respectively, which are sufficiently close to the actual values. The three sets of data for each oil agree very well indicating good reproducibility of the results.

15.5 Fixture Evaluation

Once the fixture was built and calibrated, the next step was to evaluate it with respect to measurement errors. Since the shaft and spokes that support the bob rotate in the suspension, a torque is applied to these components adding to the torque of the bob. Therefore, the contribution of the shaft and spokes to the measured stress had to be determined. In addition,

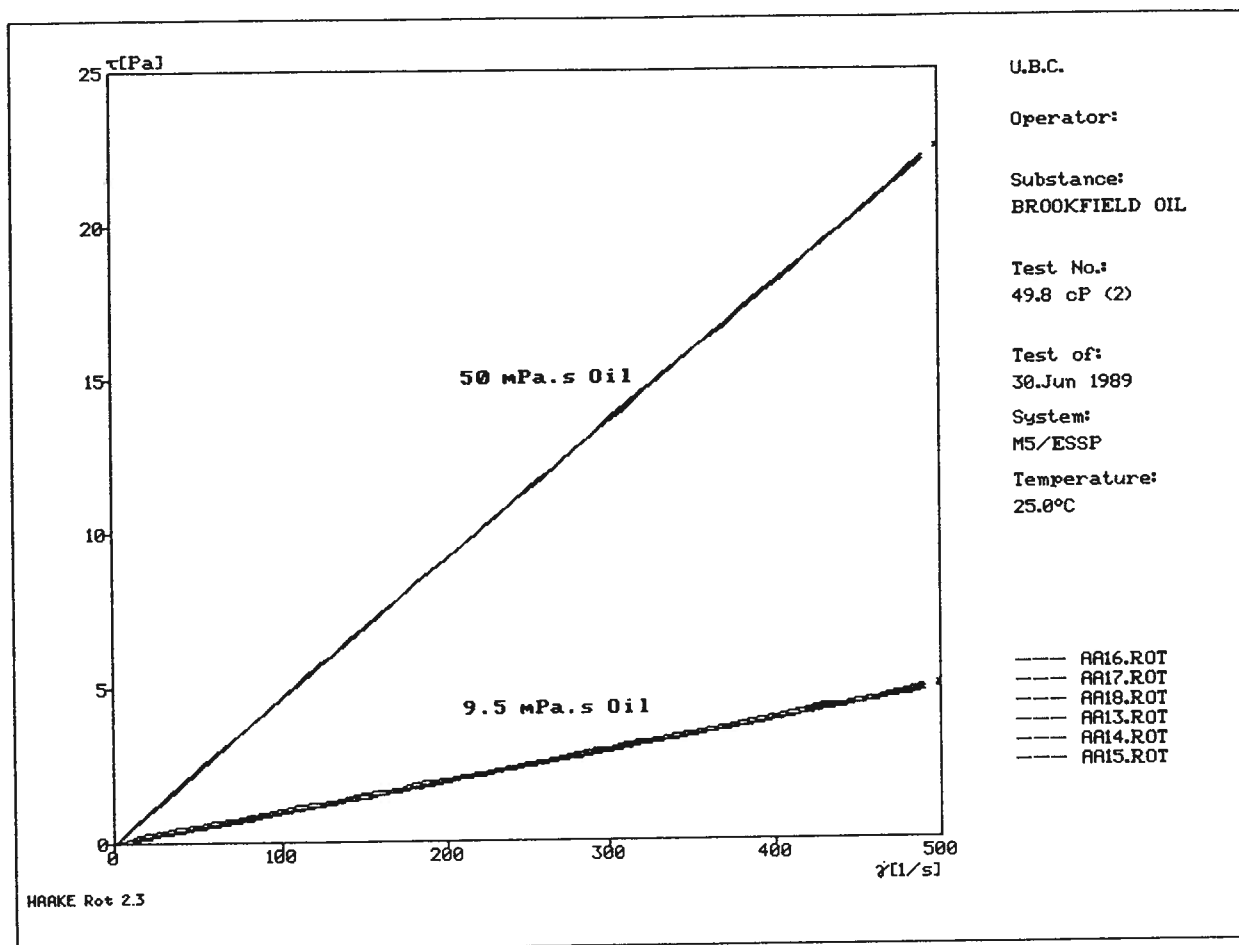


Figure 15.5 Flow curves produced with the developed rheometer fixture, for 9.5 mPa.s and 50 mPa.s standard viscosity oils. Three sets of data were plotted for each oil.

the shearing created by the rotating bob can affect particle settling. It was therefore necessary to check whether the bob remained positioned in a constant density zone during shearing.

As stated, the measurement errors associated with the end effects were considered to be negligible due to the small surface area of the bottom part of the bob (Moore and Davies, 1956, Sherman, 1965, Whorlow, 1980). The potential for wall slip was reduced by cutting grooves into the shearing surfaces of the fixture (see Section 15.3).

15.5.1 Effect of Shaft and Spokes on Measured Stresses

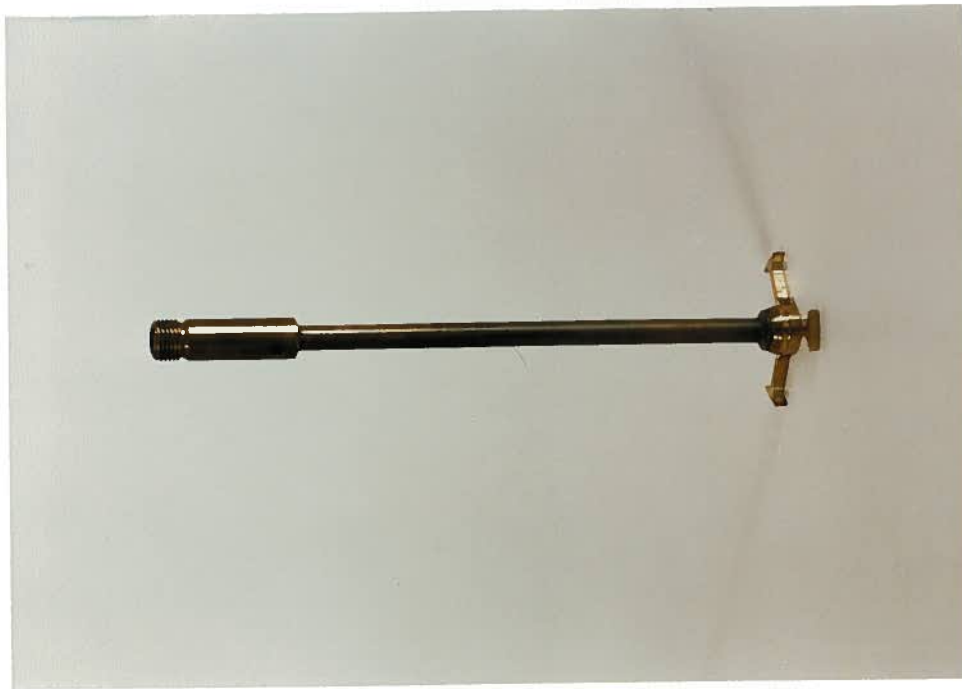
In order to quantify the error resulting from the additional torque produced by the shaft and spokes, each component was built and tested separately (Figure 15.6). Flow curves were then produced for a 49.8 mPa.s standard viscosity oil using:

- (a) the entire fixture,
- (b) the shaft, spokes and narrow cylinder,
- (c) the shaft and spokes, and
- (d) the shaft.

As can be seen from the flow curves in Figure 15.7, the contribution of each of the components to the measured stresses is small compared to the stress from the entire bob. The contribution of component (c), the shaft and spokes, best represents the magnitude of the measurement errors which were less than 5% of the measured stress. This effect could either be subtracted from the measured stress or it could be ignored since it is small and would not greatly affect the experimental results.



Figure 15.6a Photographs of the rheometer components: a) entire fixture, and b) shaft, spokes and cylindrical ring.



c.



d.

Figure 15.6b Photographs of the rheometer components: c) shaft and spokes, and d) shaft.

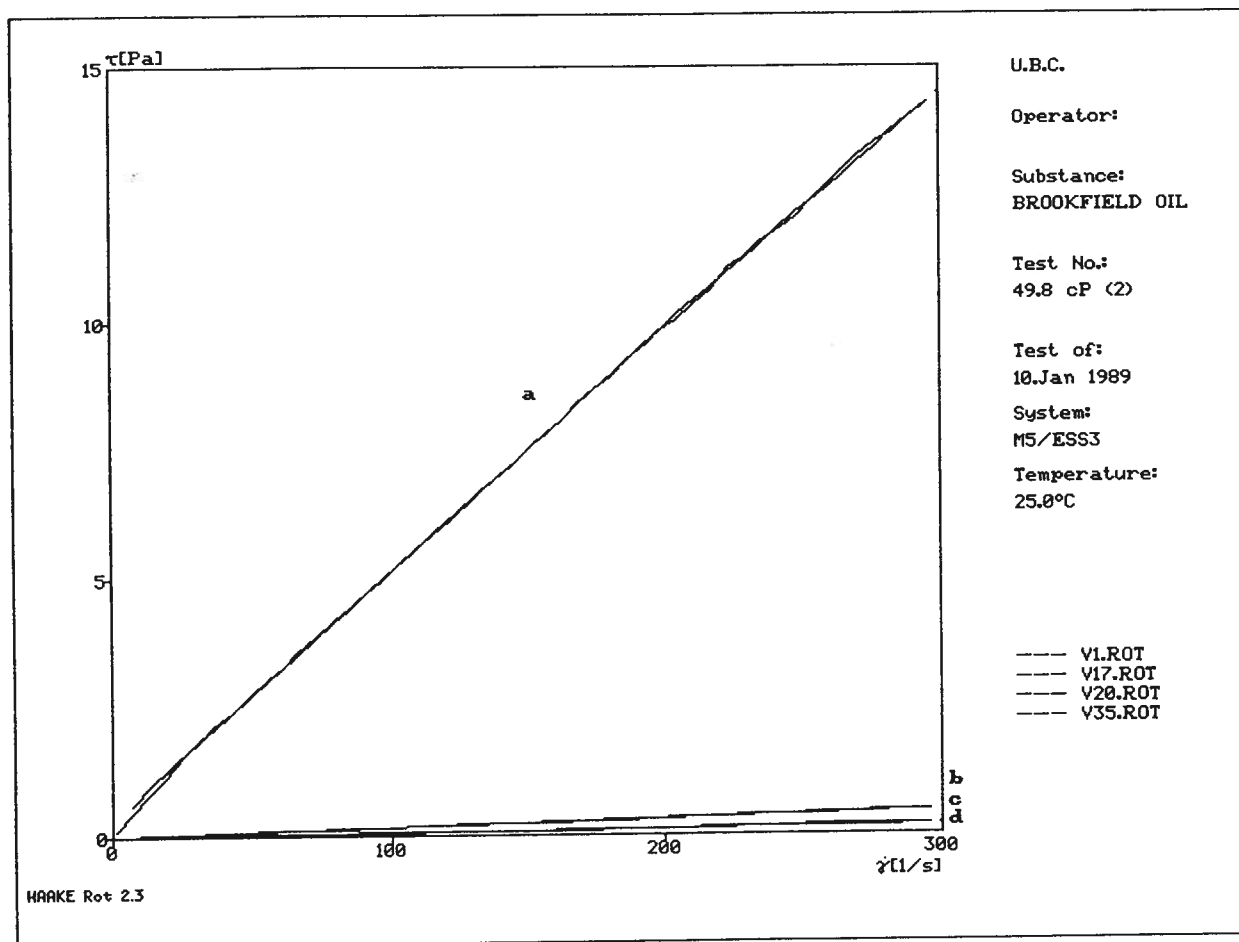


Figure 15.7 Flow curves produced for 10 mPa.s standard viscosity oil using a) the entire bob, b) the shaft, spokes and cylindrical ring, c) the shaft and spokes, and d) the shaft.

15.5.2 Particle Settling in the Elongated Fixture

Since the settling of particles in the elongated fixture occurs in a sheared environment during measurements, the settling properties may be different from those in an un-sheared column. To confirm that zone settling takes place in the elongated fixture and that measurements were made within the constant density zone, the solids concentration profile in the elongated fixture under sheared and un-sheared conditions was determined. Samples were taken at various positions in both of the annular gaps to determine if any variation in suspension composition occurred as a result of shearing. A duplicate fixture was machined with sampling points from which samples could be drawn using syringes so that the solids content of the suspension could be determined throughout the fixture. Figure 15.8 is a schematic diagram showing the sampling points and Figure 15.9 is a photograph of the fixture. This fixture had the same geometric dimensions as the device constructed for rheological measurements.

The solids concentration profile as a function of time was determined under un-sheared and sheared conditions. Samples were drawn from each position at specific times for subsequent solids content determinations. Between sampling periods, the suspension was inverted several times until the suspension was thoroughly mixed. Samples were then taken from top to bottom so that the compositions of successive samples were not greatly affected by changes in the suspension composition due to the removal of the previous samples.

The solids content for each sample position was used to construct the solids concentration profiles versus time for the suspension. The suspension was prepared by mixing upgraded magnetite and distilled water to a solids content of 15% by volume.

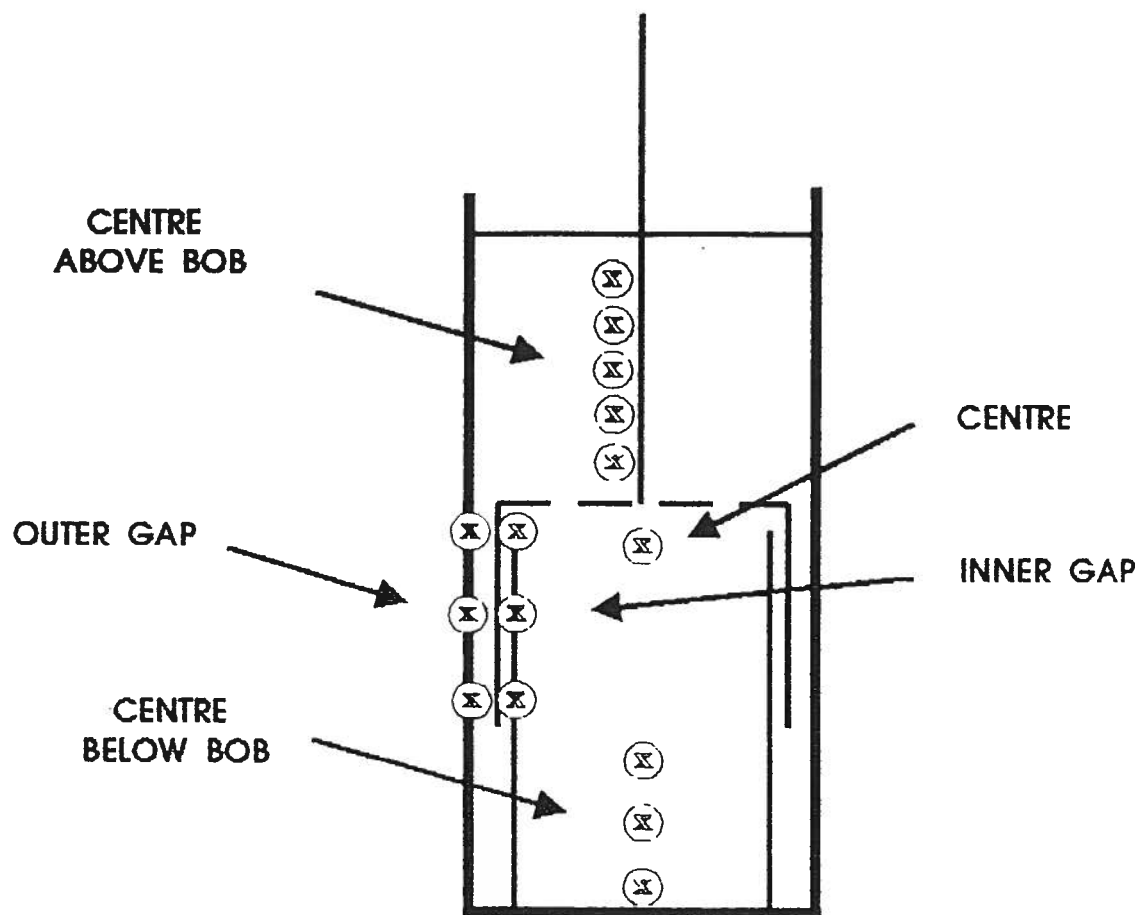


Figure 15.8 Rheometer fixture for settling suspensions showing sampling points for solids content determinations during rheological measurements.



Figure 15.9 Constructed rheometer fixture for solids content determinations during rheological measurements.

Figures 15.10a, b, c and d and 15.11a, b, c and d show the solids concentration profiles in the elongated fixture under un-sheared and sheared conditions, respectively. The suspension was sheared at a rate of 500 s^{-1} which represents an extreme high shear rate. The graphs show that zone settling conditions exist in the elongated fixture for both sheared and un-sheared conditions. Comparison of Figures 15.10a, b, c and d and 15.11a, b, c and d reveal that shearing had little effect on particle settling since solid concentration profiles are similar at any given time for the two systems.

The settling results showed that the bob was completely within the constant density zone for at least five minutes. At six minutes the top of the bob penetrated the supernatant zone. It is therefore expected that, for measurement times longer than six minutes, the stress would drop off as the solids content in the measuring region of the fixture declined.

To determine the acceptable measuring time period, the shear stress of the magnetite suspension, with a solids content of 15% by volume, was measured as a function of time at a shear rate of 500 s^{-1} . Figure 15.12 is a plot of the shear stress versus time showing that after approximately six minutes, the shear stress begins to decay. This measurement period coincided with the settling period required for the supernatant to reach the top of the bob and the period of time used to calculate the fixture dimensions. For the suspension with 15% solids by volume, the maximum measurement time was therefore determined to be approximately six minutes. For a faster settling suspension, a shorter measurement time would be appropriate while for a slower settling suspension a longer measurement time could be used.

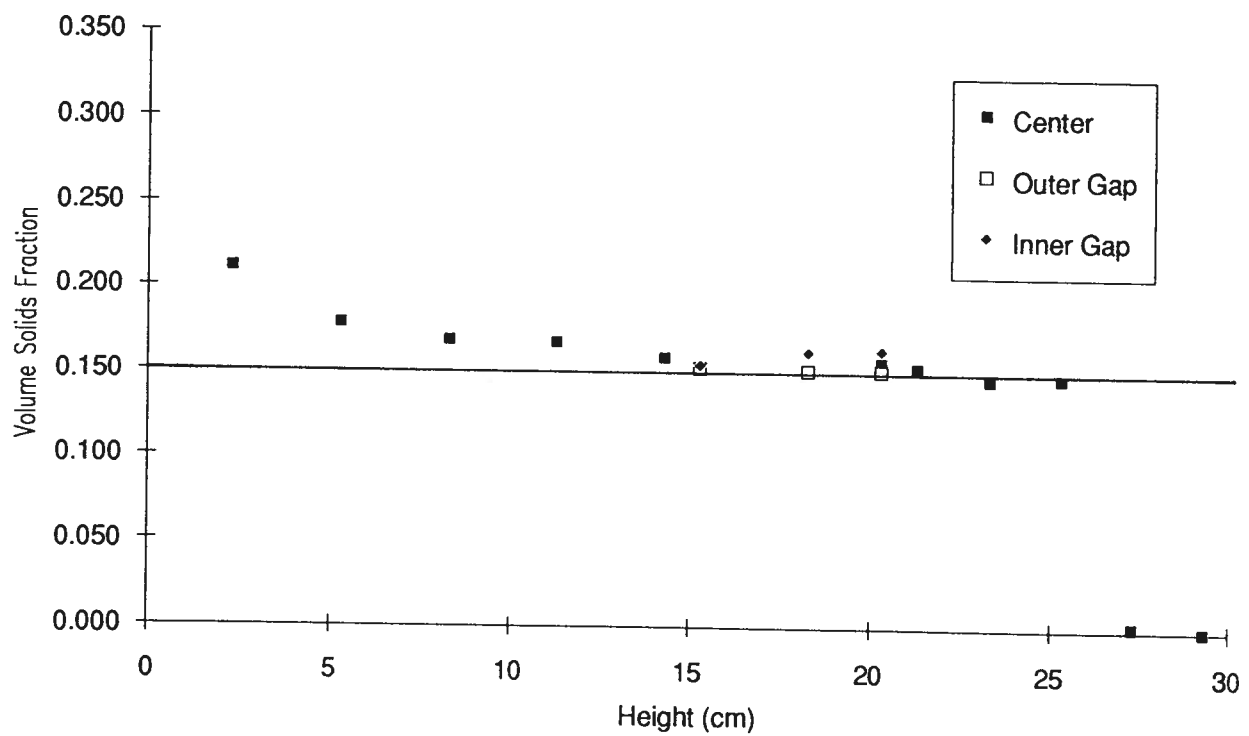


Figure 15.10a

Solids concentration profile in the rheometer fixture at a settling time of 2 minutes determined while the bob was not rotating.

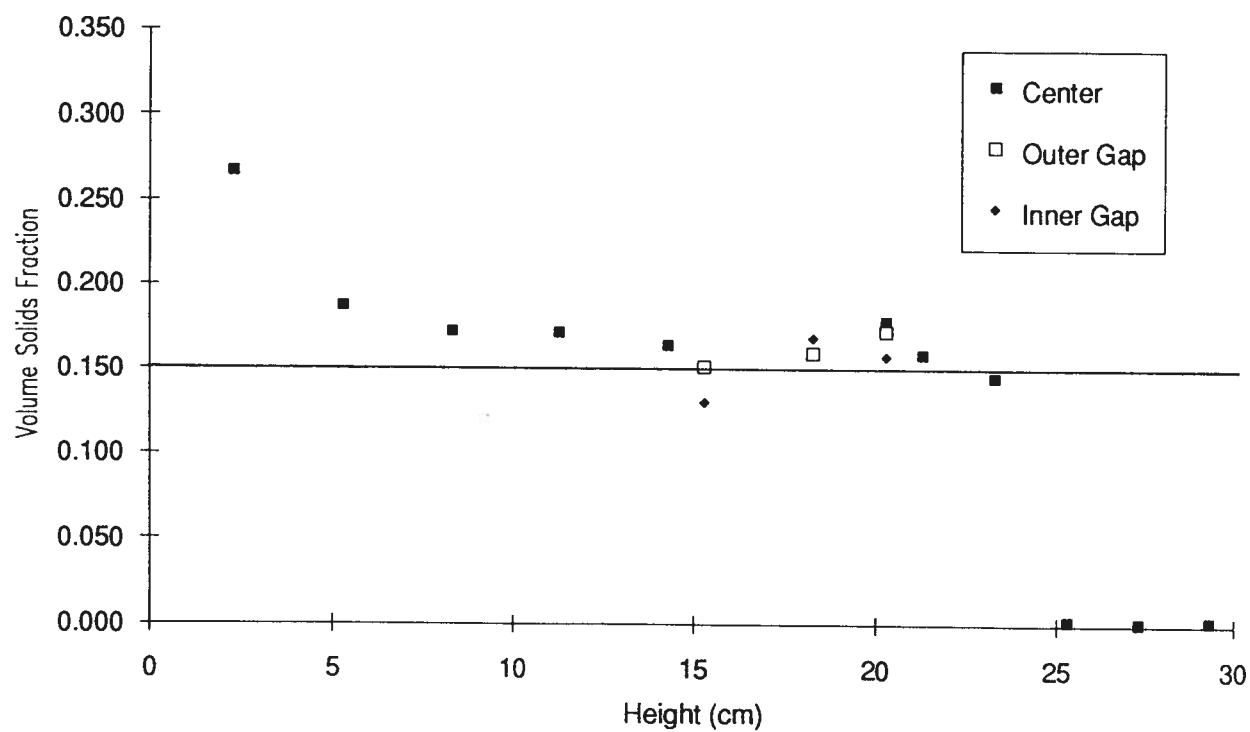


Figure 15.10b

Solids concentration profile in the rheometer fixture at a settling time of 4 minutes determined while the bob was not rotating.

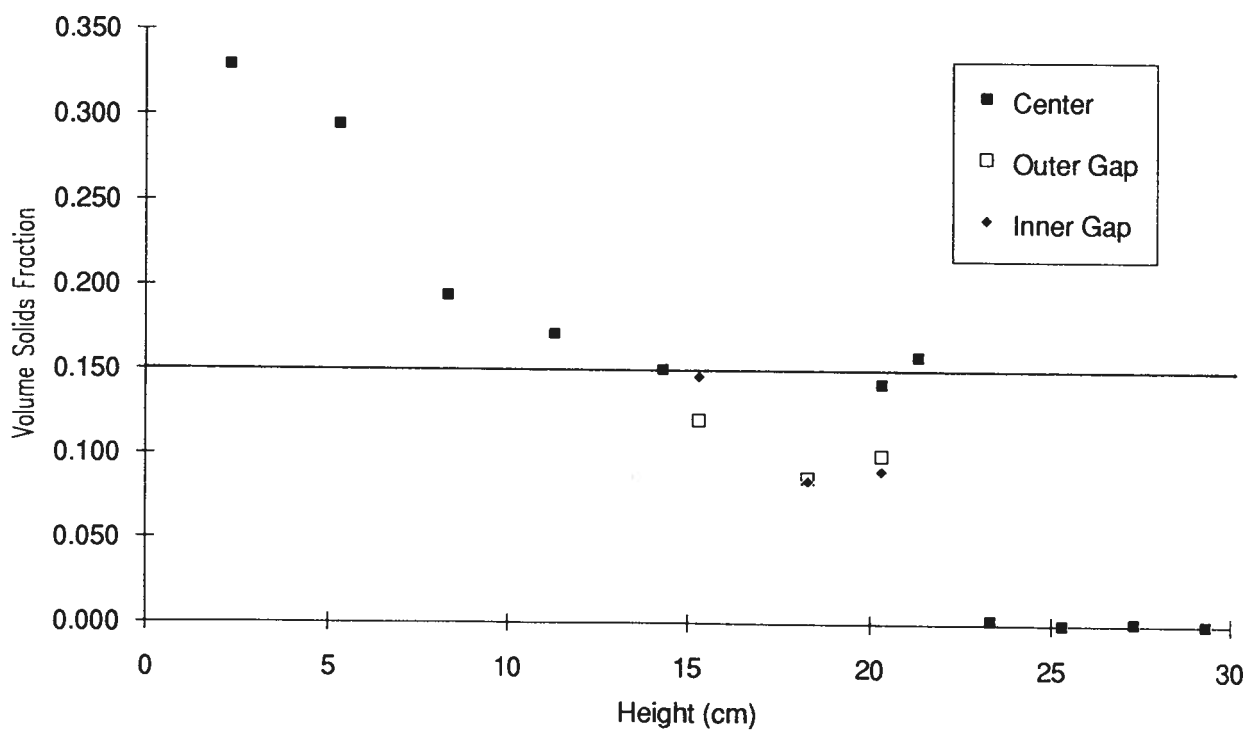


Figure 15.10c

Solids concentration profile in the rheometer fixture at a settling time of 6 minutes determined while the bob was not rotating.

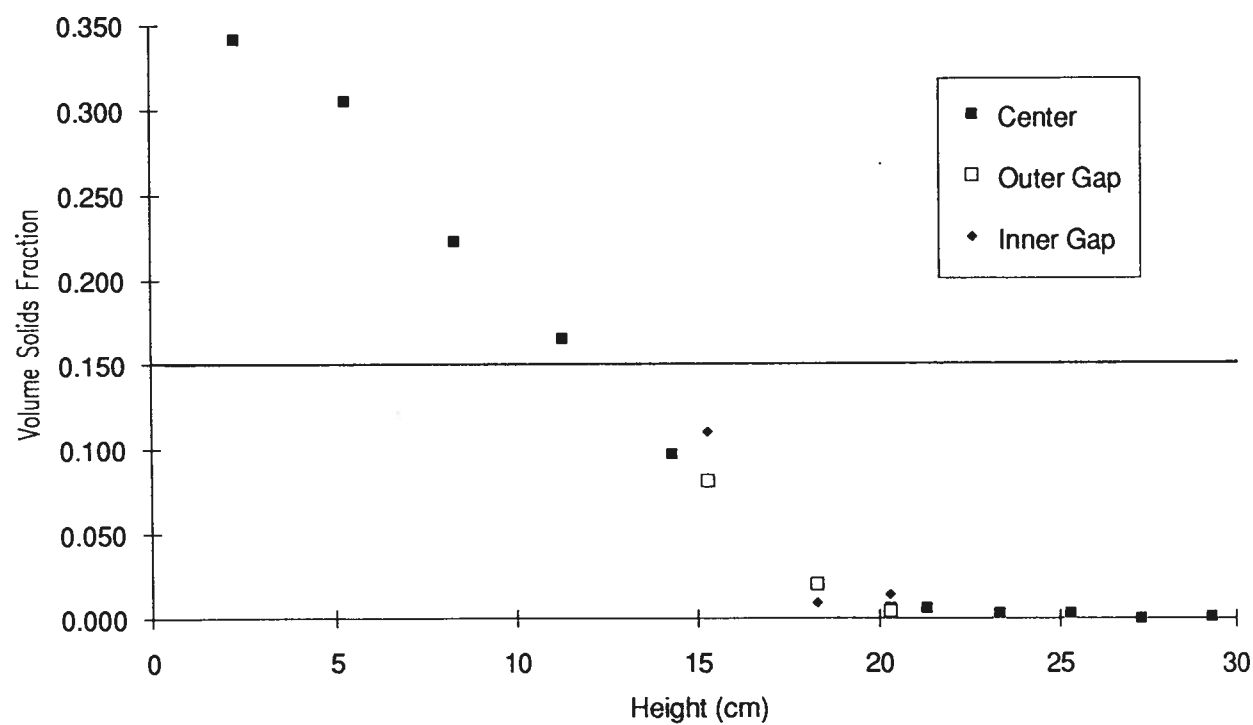


Figure 15.10d

Solids concentration profile in the rheometer fixture at a settling time of 8 minutes determined while the bob was not rotating.

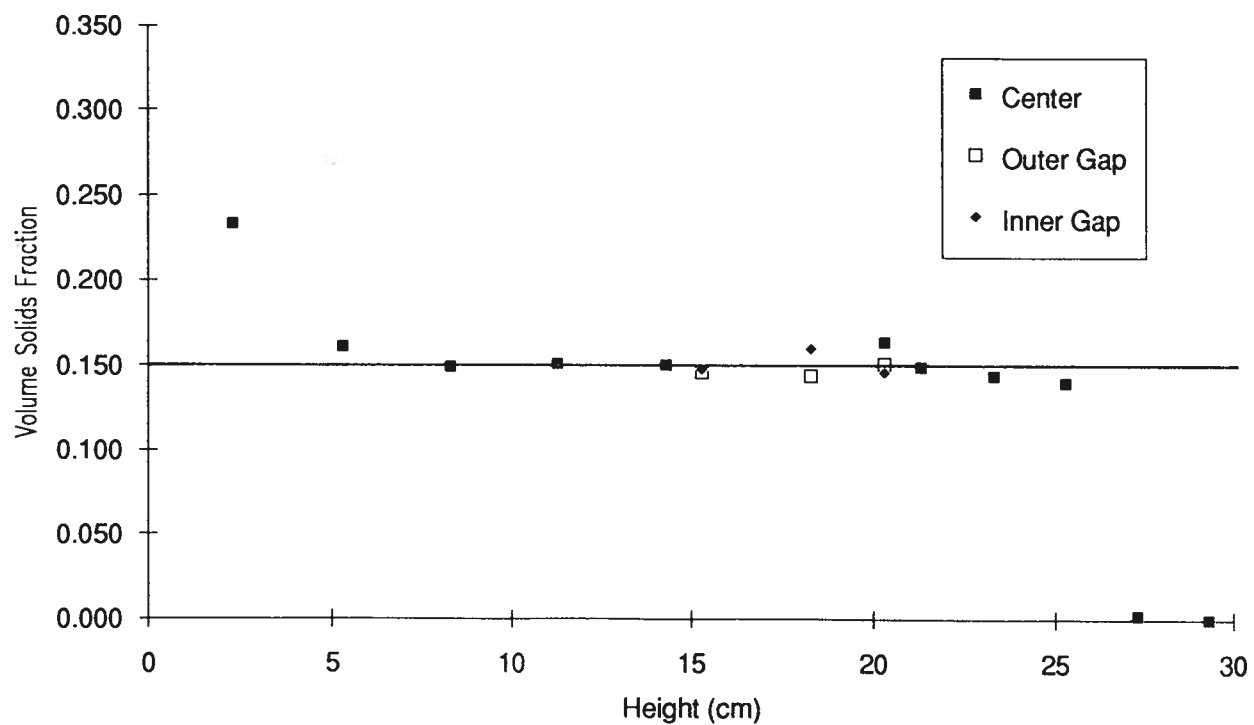


Figure 15.11a

Solids concentration profile in the rheometer fixture at a settling time of 2 minutes determined while the bob was rotating at a shear rate of 500 s^{-1} .

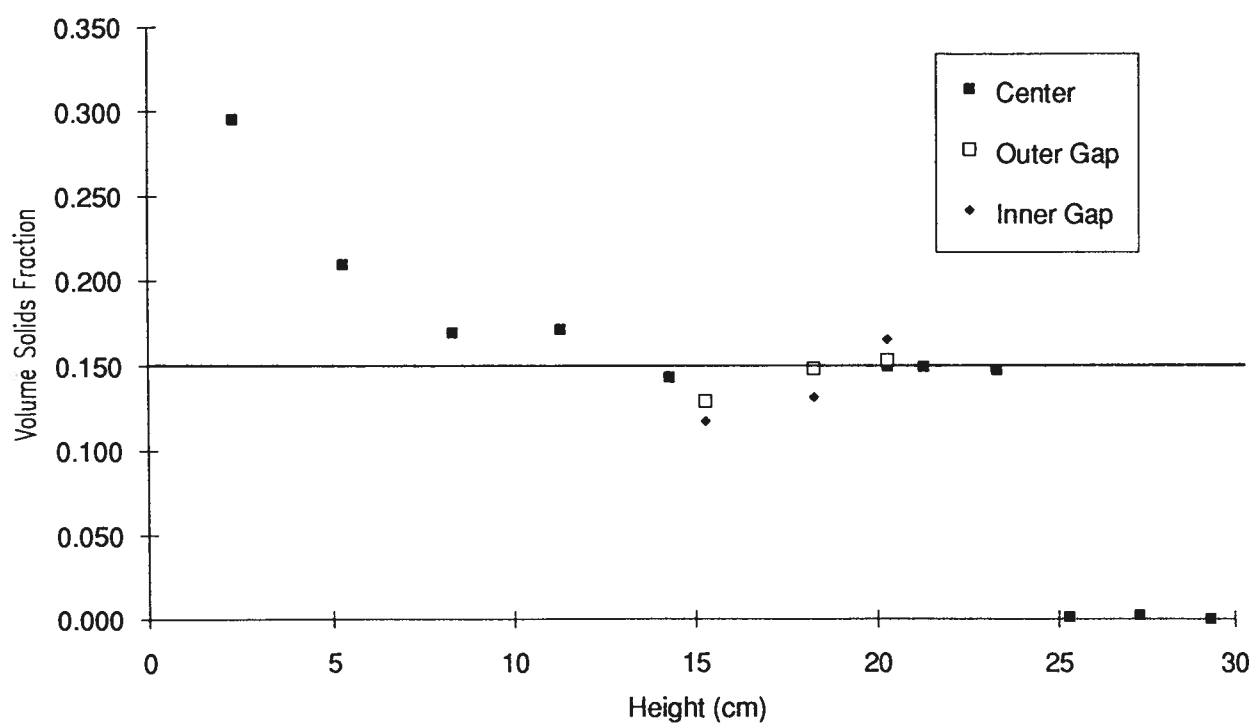


Figure 15.11b

Solids concentration profile in the rheometer fixture at a settling time of 4 minutes determined while the bob was rotating at a shear rate of 500 s^{-1} .

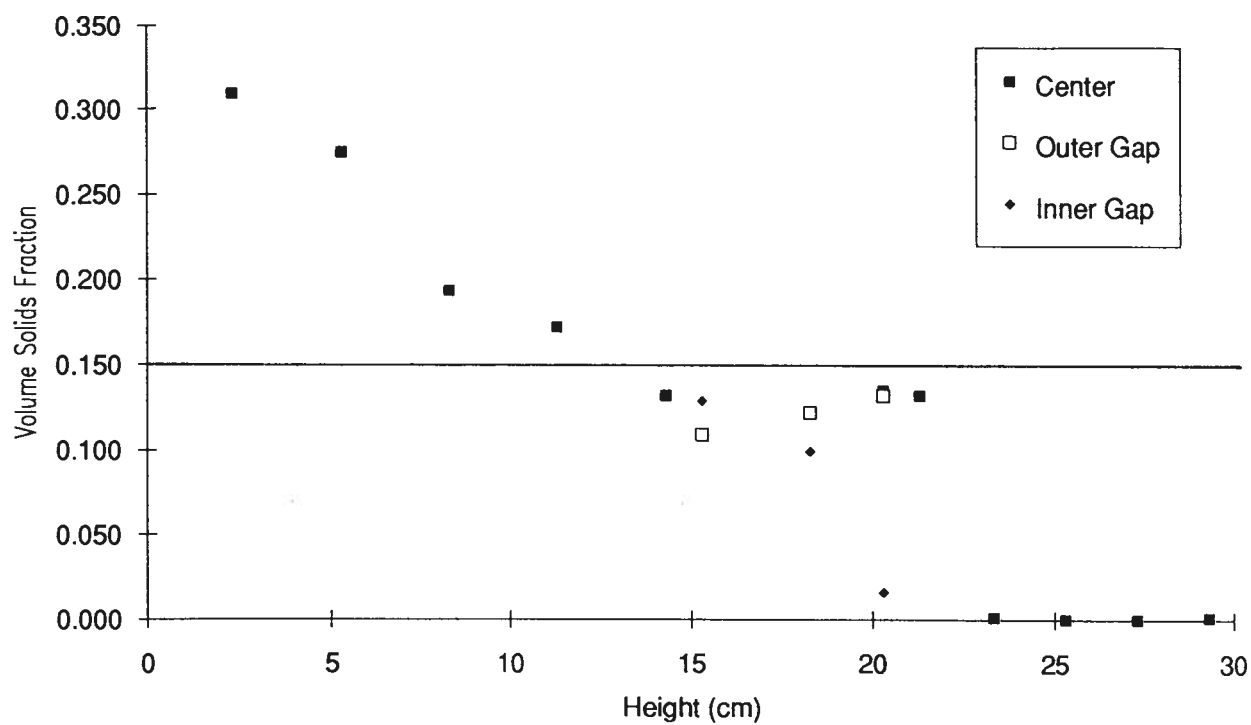


Figure 15.11c

Solids concentration profile in the rheometer fixture at a settling time of 6 minutes determined while the bob was rotating at a shear rate of 500 s^{-1} .

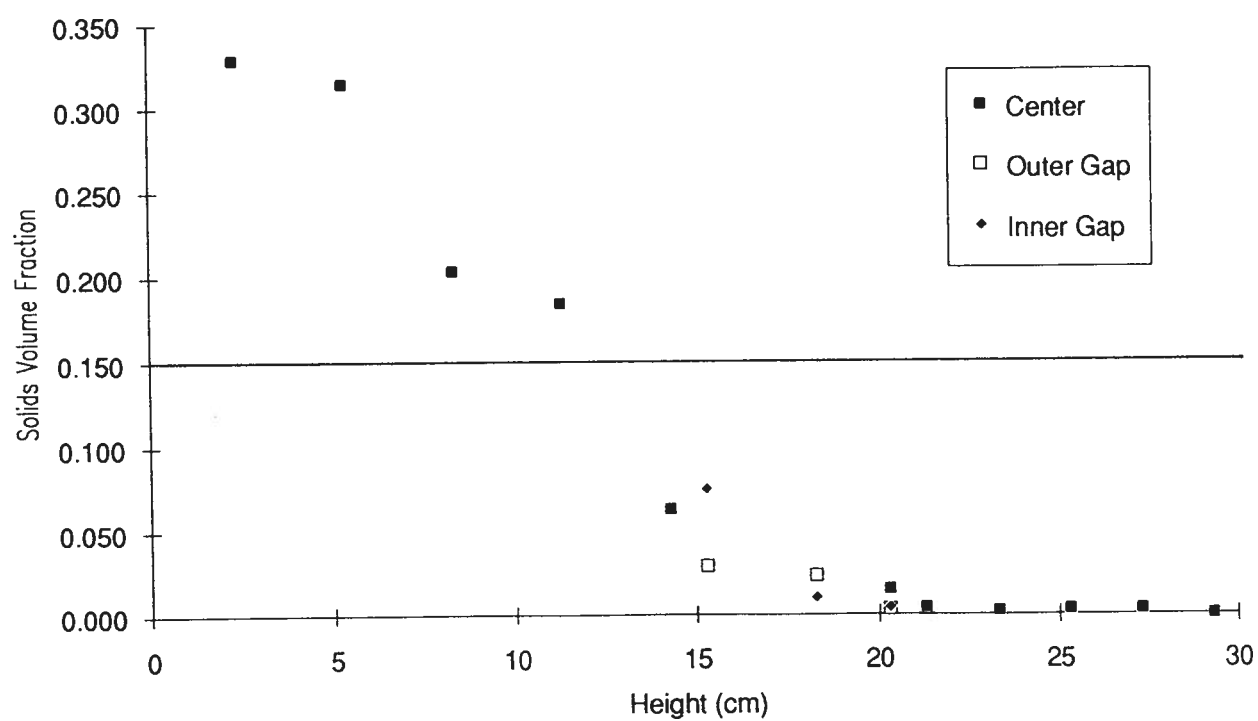


Figure 15.11d

Solids concentration profile in the rheometer fixture at a settling time of 8 minutes determined while the bob was rotating at a shear rate of 500 s^{-1} .

15.6 The Rheological Measurement Procedures

To determine the rheological properties of the magnetite suspensions, it was necessary to produce accurate rheological flow curves. Procedures were developed taking into consideration the possible errors associated with particle settling, turbulence and non-Newtonian flow. Measurements were carried out using the new elongated fixture attached to a Haake viscometer.

15.6.1 Measurement Time Periods

As previously discussed, the measurement period was constrained by the settling rate of the suspension. Conversely, for accurate rheological measurements, it was necessary to have a measuring period of sufficient length to minimize the effects of bob inertia on measured stresses. Since the bob has mass, if its rotational speed is abruptly changed, the inertia affects the measured stress values. Haake recommends periods of at least two minutes for a shear rate ramp measurement to avoid errors associated with the inertia. For example, when measuring shear stress over the shear rate from 0 s^{-1} to 300 s^{-1} , the ramped time should be at least two minutes. Based on the settling test results in the elongated fixture, measurement periods of at least two minutes could be used to eliminate inertia errors.

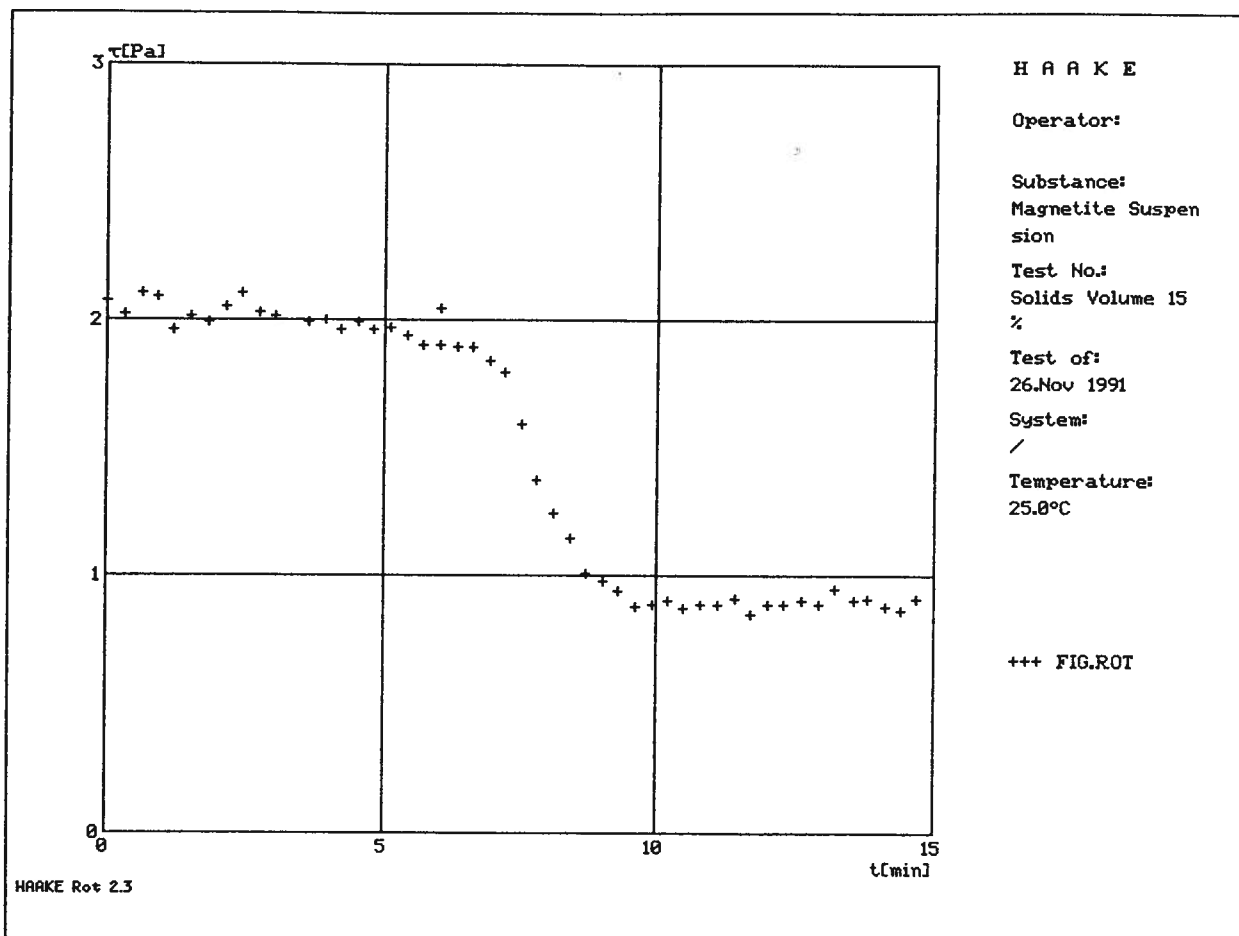


Figure 15.12 Measurement of shear stress at shear rate equal to 500 s^{-1} versus time for a magnetite suspension with a solids volume fraction of 0.15.

15.6.2 Shear Rate Measurement Range

The shear rate range over which the flow curves were measured was selected to cover shear conditions in dense media separators. In particular, the effective shear rates between coal particles and the dense medium should be used in any rheological measurements. In a dense media separator, the shear rates range from nearly zero to high shears where turbulence may prevail (see Section 4.2). The upper shear rate limit depends on the ability of the viscometer to make accurate measurements. At high shear rates, turbulence exists in the annular gap between the cup and the bob which would erroneously add to the measured viscous resistance (see Section 6.2.2.2). The onset of turbulence occurs with the formation of Taylor vortices in the annular gap (Schlichting, 1968). Taylor (1923) developed an empirical relation that provides an estimate of the shear rate at which this turbulence would form (see Equation 6.19). Using the dimensions for the outer gap and by making some assumptions regarding the properties of magnetite (suspension viscosity approximately equal to 5 mPa.s, suspension density of 1600 kg m⁻³), the critical shear rate was calculated to be approximately 548 s⁻¹. It should be noted that Equation 6.19 does not take into consideration the effects of particle size, particle density or suspension solids content on the critical shear rate. Each of these factors could affect the suspension inertia and thereby the critical shear rate for Taylor vortices formation. It is expected that with increasing particle size and density, a lower critical shear rate would apply.

Rheological tests were carried out with a transparent fixture in which horizontal bands were observed at shear rates greater than approximately 350 s⁻¹. Rheological measurements revealed that the flow curve turned upwards at shear rates greater than approximately 400 s⁻¹ (see

Figure 15.13). The visible horizontal bands and the erroneous dilatant properties can be explained by the onset of turbulence. To ensure that turbulence did not affect experimental results, the maximum shear rate used was 300 s^{-1} .

15.6.3 Non-Newtonian Shear Rate Corrections

Since dense media exhibit non-Newtonian flow properties, the shear rate across the annular gaps in the fixture will not decay in a linear manner. Shear rates must therefore be corrected to account for non-Newtonian properties. A program (Appendix II) was written using the method developed by Krieger (1968a, 1968b) to correct the shear rates (see Section 6.2.1). The basic functions of the program were to read the shear rate and shear stress data, the shear rates were then corrected using the calculation procedure outlined in Section 6.2.1. Preliminary tests with magnetite suspensions revealed that the corrected shear rate values were not very different from the original values. It is likely that the narrow gap size minimized the effects of the non-Newtonian flow. Therefore, the shear rate that is calculated based on the assumption that the velocity profile across the gap is linear provides a good approximation of the non-Newtonian velocity. Furthermore, it can be assumed that the narrower the gap, the smaller the error. Figure 15.14 shows a flow curve produced for a magnetite suspension with corrected and uncorrected shear rates. The two sets of data produce the same flow curve indicating that the corrected shear rate values are approximately the same as the uncorrected values. Since under extreme conditions, the magnetite suspensions could exhibit much more non-Newtonian flow properties than those found in the above tests, all of the rheological data were corrected.

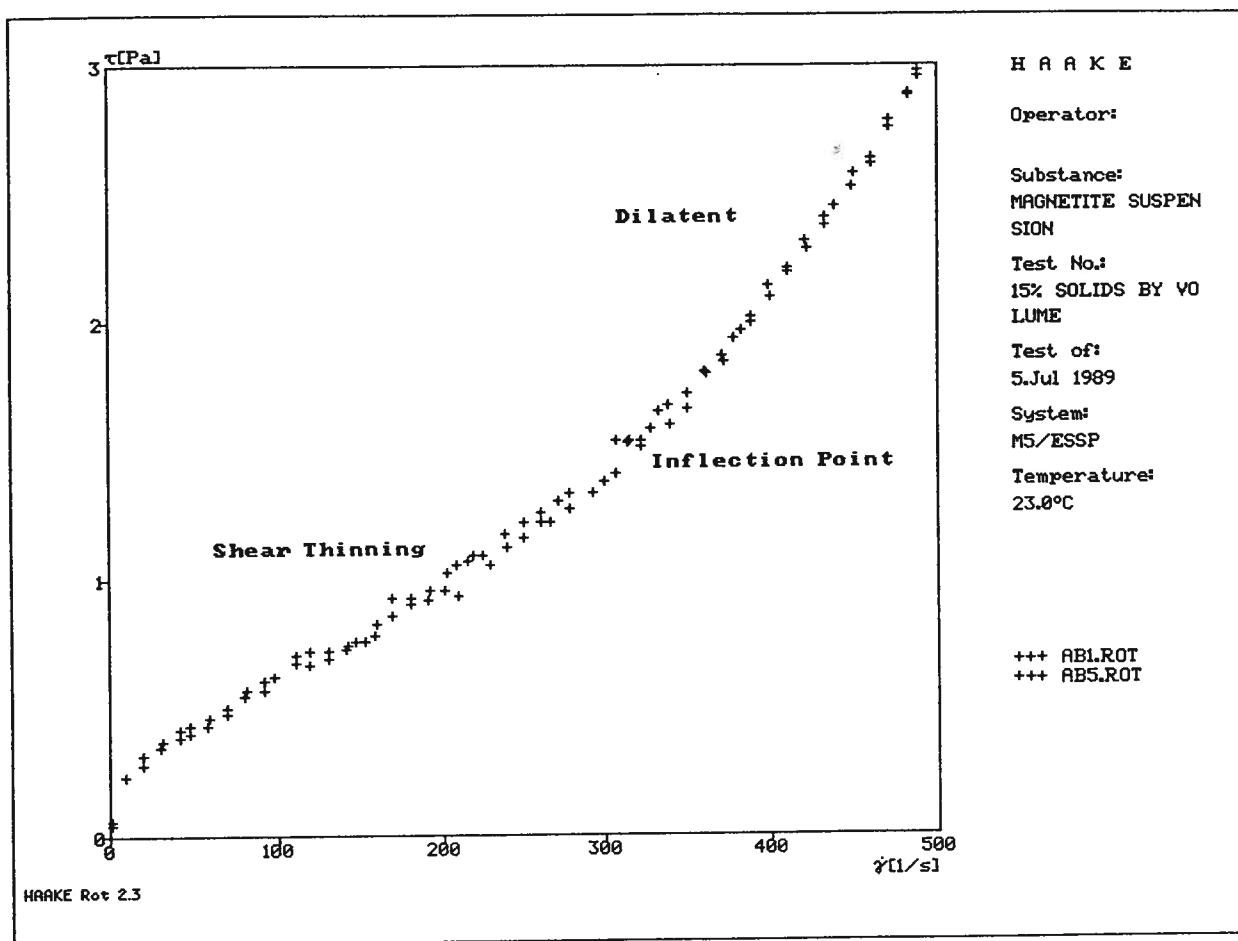


Figure 15.13 Rheological flow curve for a magnetite suspension with 15% solids by volume showing apparent dilatant flow behaviour at shear rates greater than approximately 40 s^{-1} .

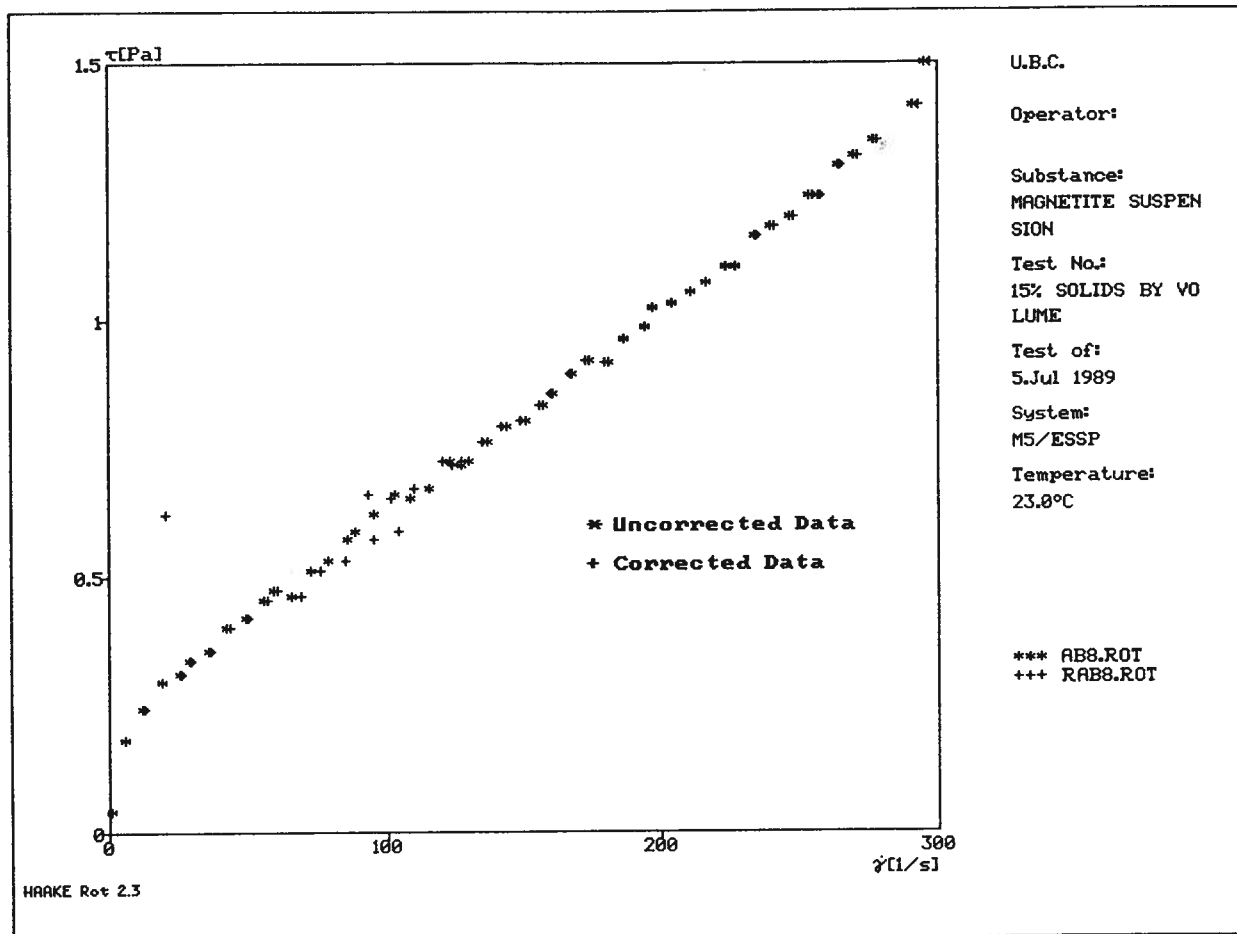


Figure 15.14 Flow curve for magnetite suspension (solids volume fraction = 0.15) with uncorrected shear rate data (AB8), and corrected shear rate data (RAB8).

15.7 Conclusions

A device to measure the rheological properties of settling suspensions was developed and evaluated. This device is an elongated double gap cup and bob arrangement (with some modifications) that can be attached to most rotational viscometers. The device was designed to measure the rheological properties of suspensions exhibiting zone settling properties characterized by the existence of a constant density zone. It was shown in Chapter 14 that magnetite dense media exhibits such zone settling properties.

The fixture was designed in such a way that the errors associated with measuring rheological properties of suspensions, such as wall slip and non-Newtonian shear rate effects are minimized. To minimize wall slip, vertical grooves were cut into the shearing surfaces of the cup and bob. Non-Newtonian shear rate effects were minimized by using narrow gaps and by correcting the shear rates using the method developed by Krieger (1968a, b).

The measurement procedures were developed to provide accurate results without errors associated with particle settling and turbulence. Measurement periods of at least two minutes could be used without concern of particle settling errors. To avoid turbulence, the maximum shear rate was determined to be 300 s^{-1} .

CHAPTER 16: RHEOLOGICAL PROPERTIES OF MAGNETITE DENSE MEDIA

16.1 Introduction

Rheological flow curves were obtained for magnetite suspensions using the developed fixture and following the procedures described in Chapter 15. The flow curves were then modelled with equations that fit the flow curve shape using the simplex optimization non-linear regression procedure. The fitted equations were compared to determine which model was best suited to describe the flow curve for the magnetite dense medium. Finally, the time dependent properties of the magnetite dense medium were characterized.

16.2 Flow Behaviour of Magnetite Dense Media

Flow curves were produced for a magnetite suspension with a solids content of 15% by volume corresponding to a medium density of 1579 kg m^{-3} . The flow curves were obtained for the shear rates ranging from 0 s^{-1} to 300 s^{-1} using a ramp time of two minutes while maintaining the suspension temperature at 25°C . Shear rates were calculated using Krieger's method (see Appendix II). Figure 16.1(a) is a plot of the shear stress versus shear rate showing three sets of data with each set consisting of fifty points. The plot shows a band of data points rather than a single line; such bands of data are typical for coarse particle suspensions and have been attributed to variations in suspension composition in the annular gap of concentric cylinder viscometers (Cheng, 1978, 1982).

The shape of the flow curve indicates that magnetite dense media exhibits shear thinning non-Newtonian flow properties. This result is supported by results obtained in Chapters 17 and 18. Figure 16.1 (b) is a plot of apparent viscosity versus shear rate for the same sets of data. As the plot indicates, the apparent viscosity decreases with increasing shear rate which is characteristic for shear thinning flow properties. From Figure 16.1 (a), it appears that the suspension has a yield stress, however, due to the sharp curvature of the data band towards the origin at low shear rates, the presence of a yield stress is not conclusive.

At high shear rates, the data of the shear stress versus shear rate is almost linear. Between the curved and linear segments of the curve, there is an inflection point (shear rate approximately 120 s^{-1}). The shape of the flow curve is believed to depend on the types and magnitude of inter-particle interactions that occur during shearing. The strong curvature over the low shear rate range and the possible existence of a yield stress indicate that a structure is present in the suspension. At high shear rates, shearing could break down this structure and viscous properties would likely result from other particle interactions such as hydrodynamic effects (see Section 8.2).

16.3 Flow Curve Modelling

In order to describe mathematically the flow behaviour of magnetite dense media, the flow curve equations were fitted to the rheological data. This was accomplished using the simplex optimization non-linear regression procedure developed by Nelder and Mead (1965). To select the best fitting model, a model discrimination procedure was used.

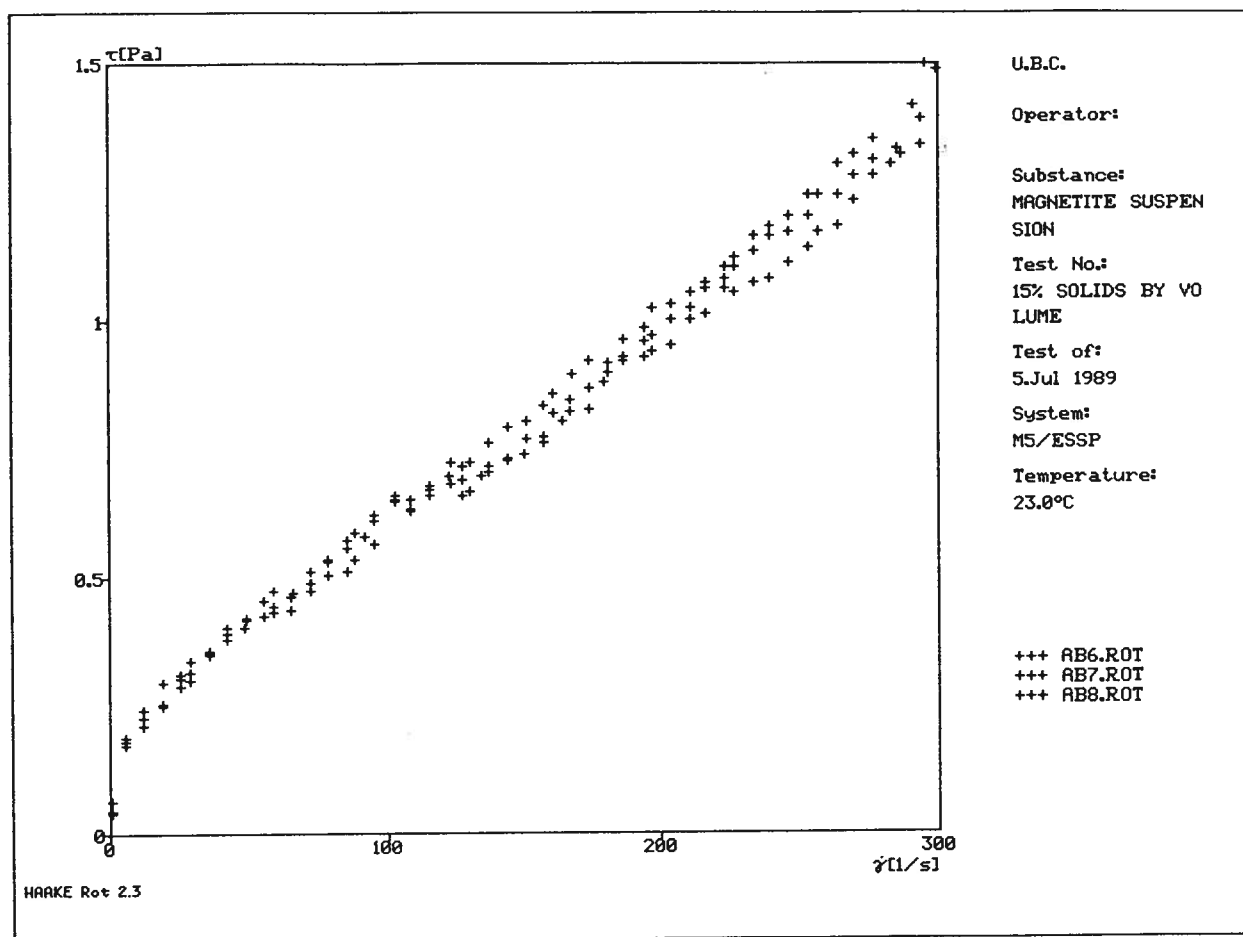


Figure 16.1a Flow curve for magnetite suspension with a solids volume fraction of 0.15 showing a band of data points produced from three consecutive measurements on the same suspension.

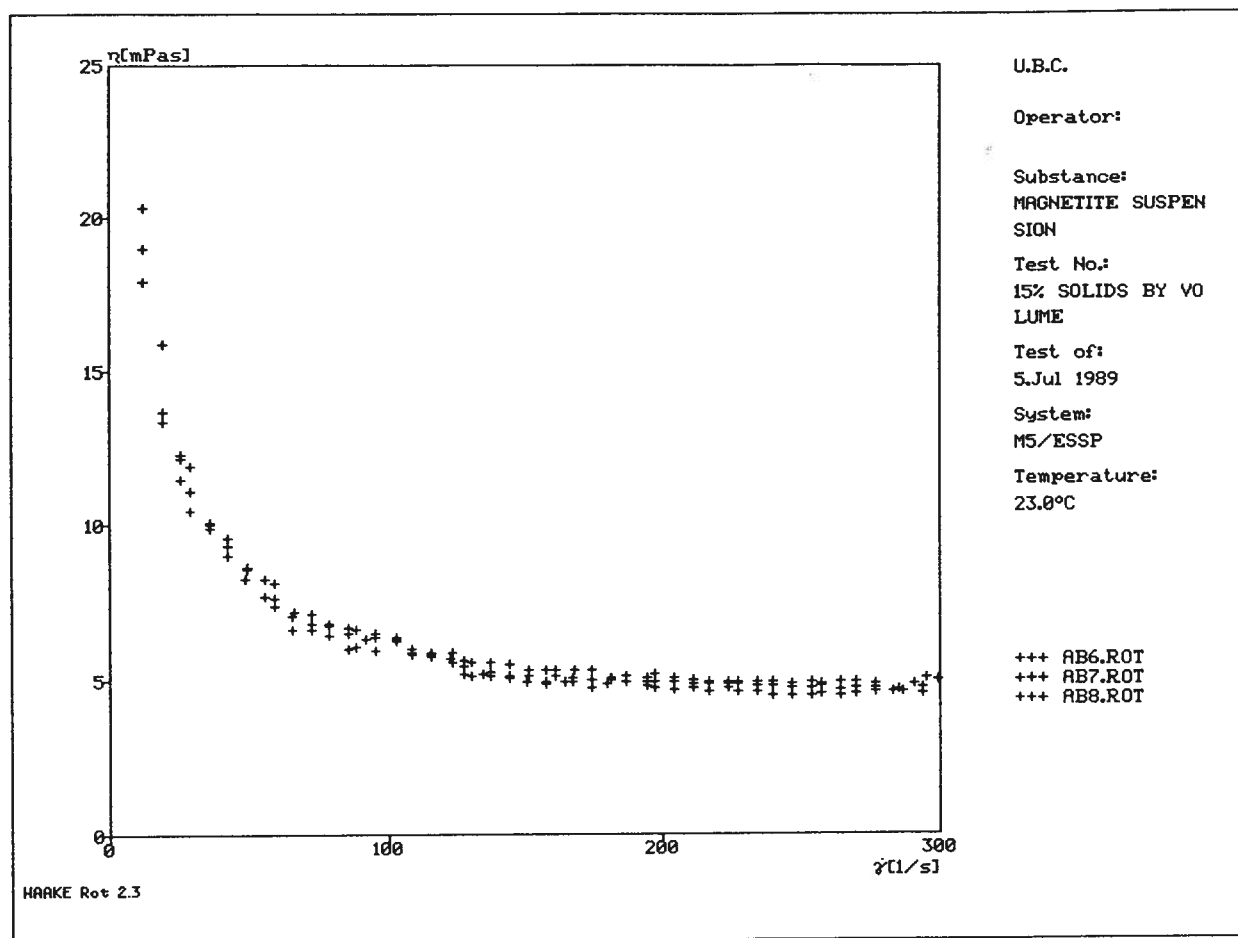


Figure 16.1b Apparent viscosity versus shear rate for a magnetite suspension with a solids volume fraction of 0.15 showing data points for three consecutive measurements on the same suspension.

16.3.1 Model Fitting

Four flow curve equations, including two equations with a yield stress term (the Casson and the Herschel Bulkley models), and two equations without a yield stress term (the Carreau and the Cross models) were fitted to the rheological data. All four equations can be applied to suspensions exhibiting shear thinning properties. The equations have been discussed in Section 7.2.2 and are presented in Table 16.1. The Bingham equation was not selected as it cannot model the curvature of the flow curves at low shear rates.

A simplex optimization regression program was written to fit the equations to the data. The program reads up to three sets of data (150 points) which is fitted to a selected equation. The simplex optimization method is a direct search method that can be used for non-linear equations (Nelder and Mead, 1965, Mular, 1972). This method moves a simplex towards a minimum weighted residual sum of squares. The simplex can expand, contract and reflect to locate the minimum. Once the objective function (weighted residual sum of squares) met a predetermined limiting value (1×10^{-8}), the program reached convergence and the equation coefficients were printed. If convergence was not achieved, the program was terminated after 1000 iterations. The weighting factor is defined as the inverse of the variance of the measured values. It was determined that the variance of the measured shear stress value was constant as a function of shear rate and therefore could be set to equal 1.0. The program was adapted from a program written by A.L. Mular (Appendix III). The coefficients for the four tested equations are presented in Table 16.2. Figures 16.2 a) to d) are plots of the fitted equations along with the flow curve data. All four equations appeared to fit the general flow curve shape.

Table 16.1 Rheological flow curve equations used to model flow curve data for magnetite suspensions.

Models	Equations
Equations with a yield stress coefficient	
Casson	$\tau = [\tau_{CY}^{1/2} + (\eta_C \dot{\gamma})^{1/2}]^2$
Herschel Bulkley	$\tau = \tau_{HB} + k\dot{\gamma}^n$
Equations without a yield stress coefficient	
Carreau	$\eta = \frac{\tau}{\dot{\gamma}} = \frac{\eta_o}{[1 + (t_1 \dot{\gamma})^2]^s}$
Cross	$\eta = \frac{\tau}{\dot{\gamma}} = \eta_{\infty} + \left(\frac{\eta_o - \eta_{\infty}}{1 + \alpha \dot{\gamma}^{2/3}} \right)$

Table 16.2 Coefficients of fitted rheological flow curve equations and R^2 values.

Model	Coefficients			R^2
Casson	$\tau_{CY} = 0.0657$	$\eta_c = 0.0028$		0.993
Herschel Bulkley	$\tau_{HB} = 0.0218$	$k = 0.0211$	$n = 0.725$	0.950
Carreau	$\eta_0 = 0.0405$	$t_1 = 5.49$	$s = 0.149$	0.940
Cross	$\eta_{\infty} = 0.029$	$\eta_0 = 2900$	$\alpha = 40700$	0.983

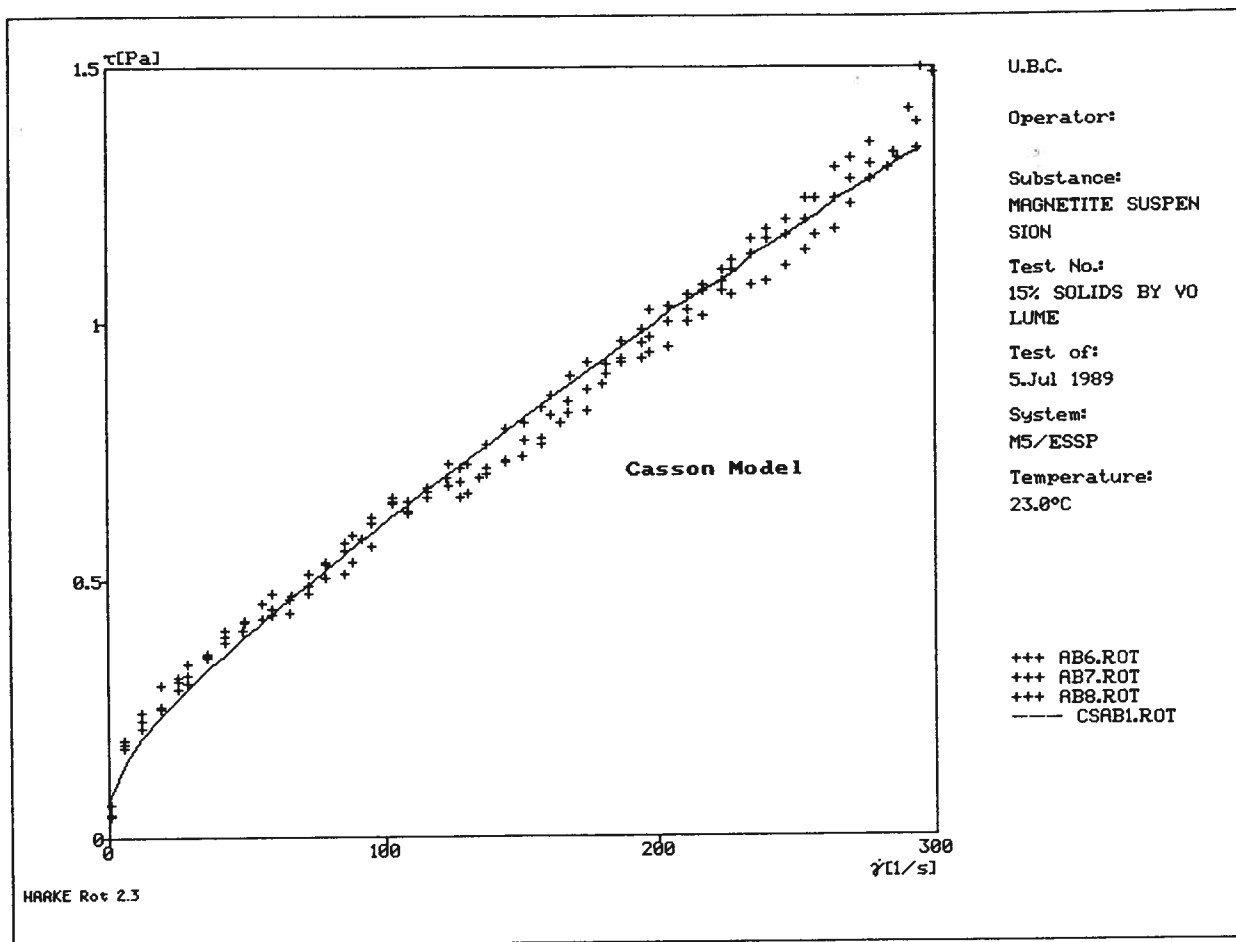


Figure 16.2a Rheological flow curve for a magnetite suspension with a solids volume fraction of 0.15 and fitted Casson model.

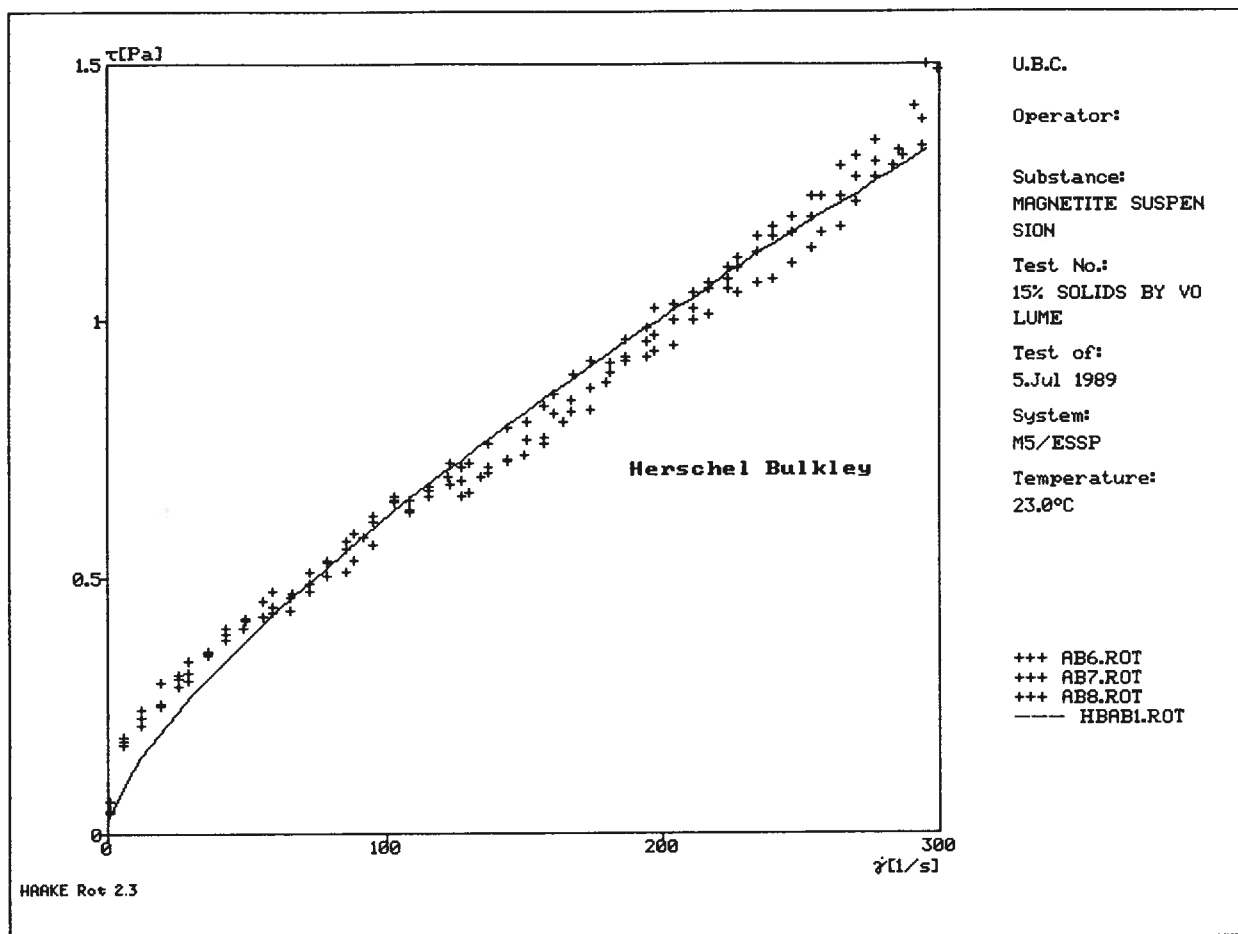


Figure 16.2b Rheological flow curve for a magnetite suspension with a solids volume fraction of 0.15 and fitted Herschel Bulkley model.

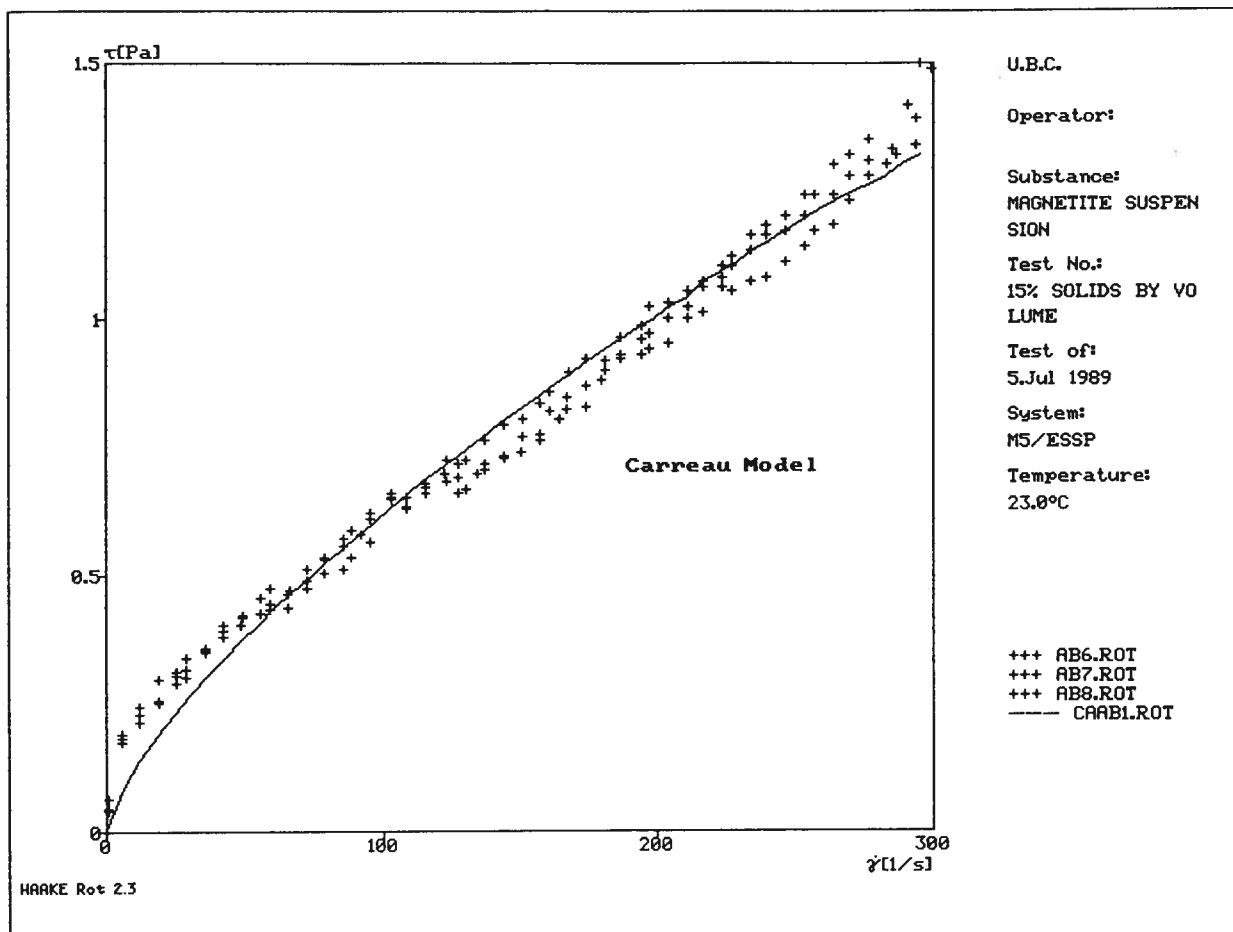


Figure 16.2c Rheological flow curve for a magnetite suspension with a solids volume fraction of 0.15 and fitted Carreau model.

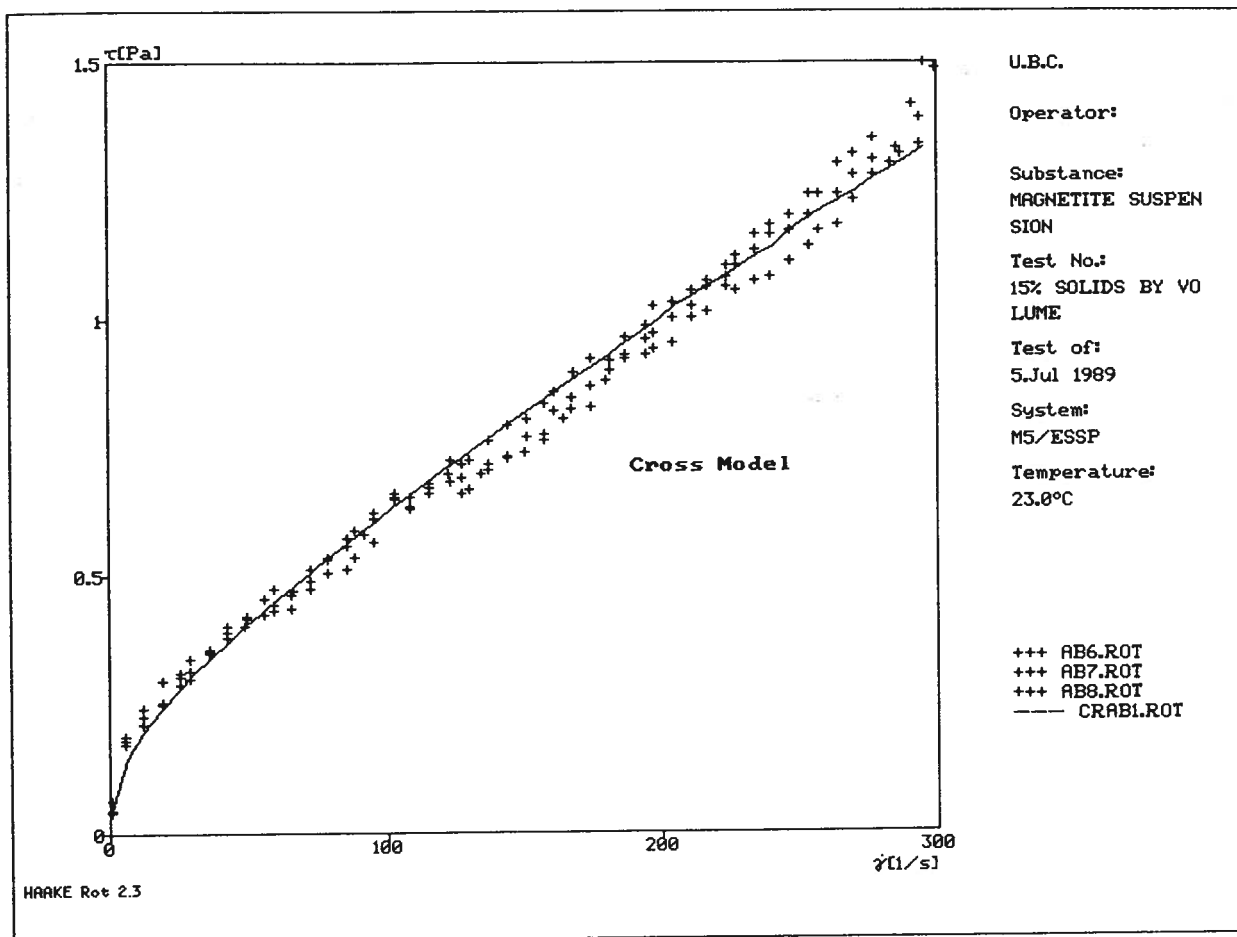


Figure 16.2d Rheological flow curve for a magnetite suspension with a solids volume fraction of 0.15 and fitted Cross model.

16.3.2 Model Discrimination

To determine which of the equations should be used to model the rheological properties of magnetite dense media, it was considered that:

- i. the model must fit the data over a wide range of shear rates;
- ii. the equation should be simple with a minimum number of coefficients; and
- iii. the coefficients should have physical significance.

Figures 16.2 a) to d) show that although each of the equations fit the shape of the flow curve, the equations with a yield stress term appear to fit the data better at the low shear rate range. To evaluate how well the four equations agree with the experimental data, Multiple Index of Determination values, R^2 , were calculated and are presented in Table 16.2. Based on these values, the Casson equation was found to fit the data best. However, since the models are non-linear, a better comparison of the equations could be obtained using a model discrimination procedure.

In order to compare the fitted equations, the model discrimination procedure developed by Williams and Klotz (1953) was applied. This method can be used to compare two models at a time. Assuming that model one correctly represents the data, a variable described by Equation 16.1 is defined and by substituting the predicted value from model one for the observed value, Equation 16.1 becomes Equation 16.2. If model one is better than model two, a plot of the variable calculated from Equation 16.1 versus $(Y_2 - Y_1)$ will produce a line with a negative slope. If model two is better, the slope will be positive.

$$Z = [Y - \frac{1}{2}(\hat{Y}_1 + \hat{Y}_2)] + \epsilon \quad (16.1)$$

$$Z = -\frac{1}{2}(\hat{Y}_2 - \hat{Y}_1) + \epsilon \quad (16.2)$$

where, Z is a defined variable,

Y is the observed value,

\hat{Y}_1 is the predicted value from model one, and

\hat{Y}_2 is the predicted value from model two.

A program was written to compare the models using the described model discrimination method (see Appendix IV). The results of the comparison of the fits of the four models are presented in Table 16.3. The results indicate that the Casson model fit the experimental results better than the other equations. It is also apparent from the results that models with a yield stress term are better than models with no yield stress term.

The Casson equation has only two coefficients, while the other equations have three. In addition, the Casson equation coefficients have physical significance in that they represent the yield stress and the high shear rate viscosity. It is worth noting that the coefficients have shear stress (Pa.) and viscosity (mPa.s) units respectively. Therefore, the Casson equation satisfies the conditions stated above: it is simple and easy to use, its coefficients have physical significance, and the equation fit the data better than other equations. It should be noted that the Casson yield stress is referred to as an apparent yield stress which means that it is determined using an indirect measurement method (see Section 6.3). Based on this evidence alone, it can not be concluded that dense media exhibits a true yield stress. However, studies have shown that Casson yield values compare well to values determined using direct measurement procedures (Nguyen, 1983).

Table 16.3 Results of model discrimination procedure to determine which flow curve equation best fit the rheological data.

Model #1	Model #2	Slope
Herschel Bulkley	Casson	0.985
Casson	Carreau	-0.926
Casson	Cross	-0.502
Herschel Bulkley	Carreau	-0.676
Herschel Bulkley	Cross	-0.500
Carreau	Cross	-0.500

16.4 Time Dependent Flow Properties

Suspensions exhibiting shear thinning flow properties can also exhibit time dependent properties (Van Wazer, 1963). Time dependent properties are related to the rates of structure formation and breakdown in a suspension. As shown in Section 16.2, magnetite dense media exhibits shear thinning flow properties which can be explained by the existence of a structure. To develop a better understanding of the structure in dense media suspensions, rheological hysteresis was measured for demagnetized and magnetized magnetite suspensions with a solids content of 15% by volume.

Time dependent properties were difficult to measure for the suspensions since before making a measurement, the suspension had to be mixed to re-suspend the particles. Mixing breaks down the structure and little time could be allowed for structure reformation prior to commencing the experiment. To provide time for structure formation, the suspension was placed in the viscometer one minute before commencing the test.

Figure 16.3 shows flow curve hysteresis for a demagnetized suspension that was produced by increasing the shear rate from 0 s^{-1} to 300 s^{-1} and subsequently decreasing it to 0 s^{-1} using two minute ramp times. Both the up ramp and down ramp curves exhibit shear thinning properties and an apparent yield stress. The down ramp curve lies below the up ramp curve indicating that after shearing the suspension exhibited a lower degree of structuring. This type of hysteresis is referred to as thixotropy. If the experiment was carried out immediately after re-suspending the magnetite, no hysteresis was observed. Since the medium is constantly moving in separators, the state of the suspension following mixing is likely representative of real conditions.

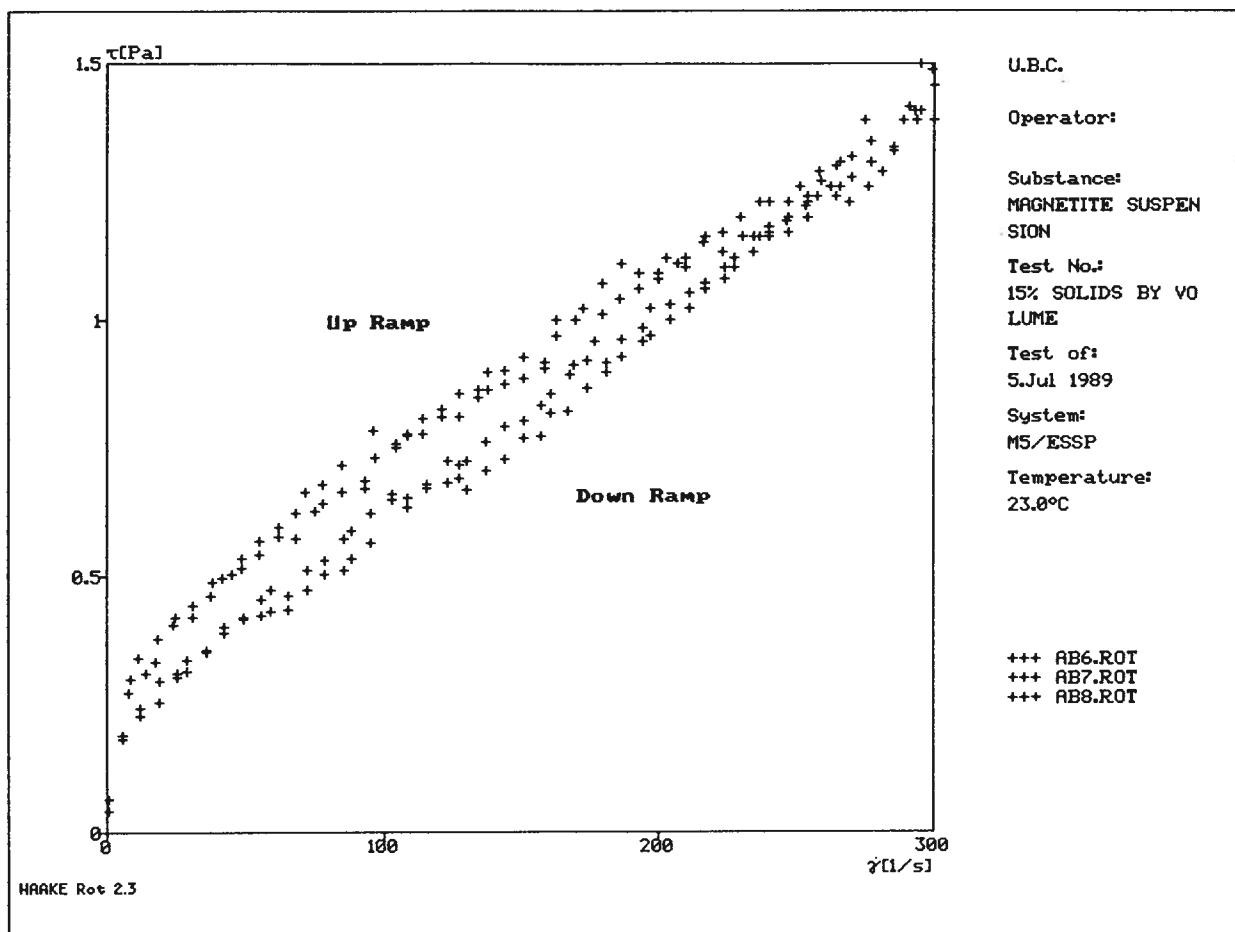


Figure 16.3 Flow curve hysteresis for demagnetized magnetite suspension with a solids volume fraction of 0.15.

Thixotropic properties can be explained by the time required to either align asymmetric particles during shearing (Pinder, 1964) or by the break up of aggregates to increase the particle dispersion to a state determined by the shear rate (Cheng, 1971). While magnetite particles are angular in shape, they do not have pronounced elongation. Therefore, the time dependent properties are better explained by the change in structure resulting from breakage of aggregates. Although the suspension was demagnetized, some remnant magnetism is believed to remain in the finest particles. The aggregation of these particles would explain the structure that is apparently present in the magnetite suspensions.

Figure 16.4 shows a hysteresis curve for a magnetized suspension. The flow curves show more pronounced non-Newtonian properties than the demagnetized suspension (see Figure 16.3). The hysteresis only occurred in the low shear rate range suggesting that at high shear rates the aggregates become dispersed. It was found that the structure in the magnetized suspension formed relatively quickly, since experiments performed immediately following mixing produced the same hysteresis. As shown in Section 13.2.2.6, magnetized particles form branched chain-like aggregates. In a suspension, these aggregates could attach to each other to form a continuous network structure. Shearing would break the attachments and with time breakdown the structure.

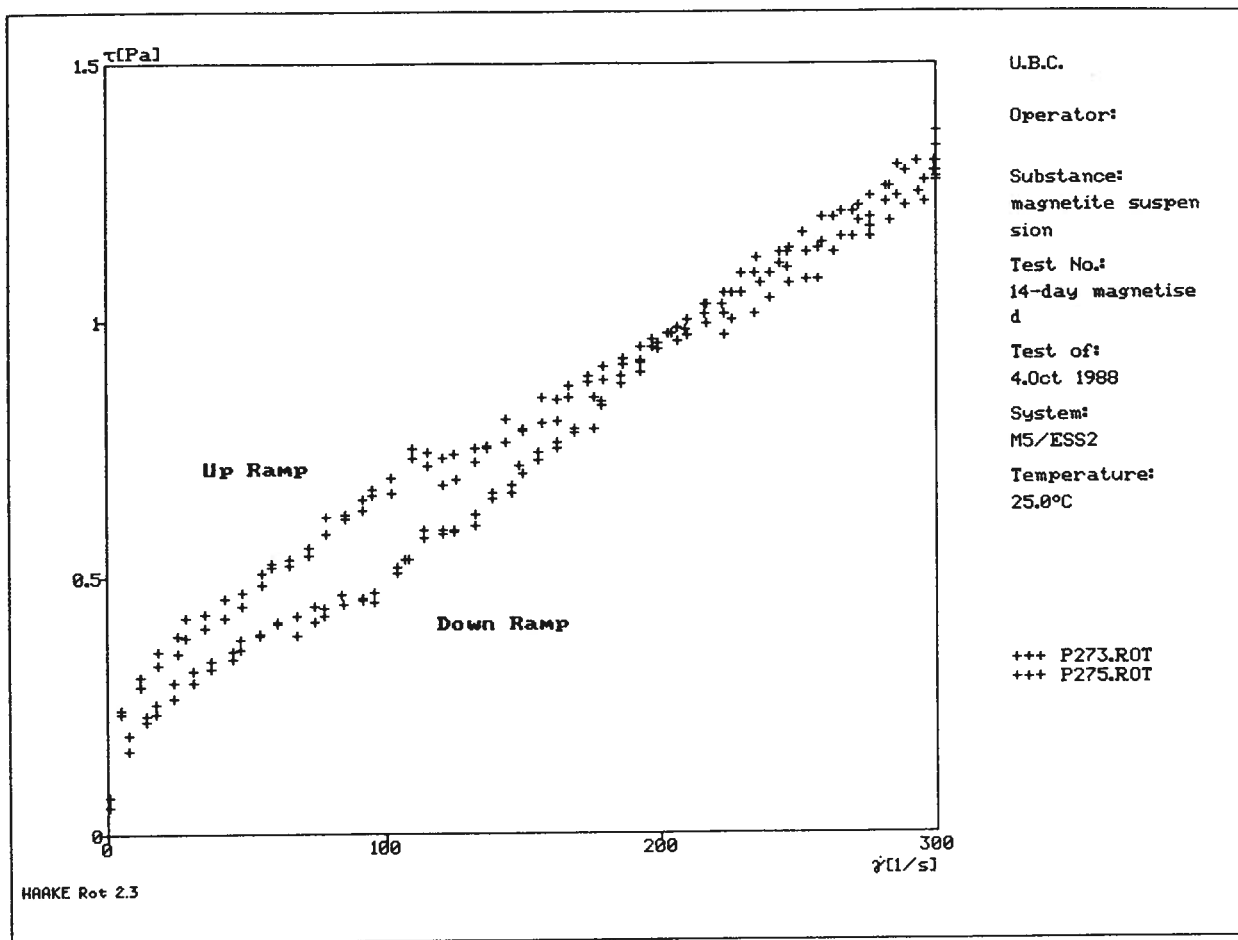


Figure 16.4 Flow curve hysteresis for a suspension of magnetized magnetite particles (volume solids fraction = 0.15).

16.5 Conclusions

The suspension of magnetite dense media used in the test work exhibited shear thinning rheological properties with an apparent yield stress. The flow behaviour was modelled using the Casson equation (see Table 16.1) which was found to fit the experimental results better than other rheological equations. The equation has a yield stress term which implies that the medium has a structure. As shown in Section 13.2.2.6, remnant particle magnetism results in the formation of a loose branched chain-like structure which may be responsible for the yield stress and shear thinning properties. The existence of a structure is supported by the thixotropic properties exhibited by the medium. The thixotropic properties were enhanced by magnetizing the particles, which indicates that remnant magnetism is at least partially responsible for the presence of a structure.

CHAPTER 17: EFFECT OF PHYSICO-MECHANICAL AND PHYSICO-CHEMICAL PARAMETERS ON MEDIUM PROPERTIES

17.1 Introduction

Various physico-mechanical and physico-chemical parameters are known to influence the properties of suspensions (see Chapter 8). Many of these parameters also affect the properties of magnetite dense media (see Chapter 9). Since the dense medium separation process is used in various applications under diverse conditions, media properties can vary extensively. The objective of this chapter is to characterize and model the rheological properties of magnetite dense media with diverse parameter conditions and to determine the relative significance of the parameters to the medium properties. The parameters investigated included: solids content, particle size, pH, magnetization, dispersing agents, coal fines, bentonite and kaolinite clays.

17.2 Determination of Parameter Levels

To investigate the effect of various parameters, suitable levels of the variables had to be chosen. The levels were determined from those found in industrial practice and, in the case of dispersing agents, the levels were determined from preliminary settling tests.

The suspension solids content is known to affect settling properties (see Section 10.2). Settling tests were performed on magnetite suspensions over the volume solids contents ranging from 5% to 25%. Figure 17.1 is a plot of settling rate versus solids content. The figure shows that at low solids content the suspension settles very quickly and, conversely, at high solids

content the settling rate is low. For coal preparation, media densities typically range from 1400 kg m⁻³ to 1800 kg m⁻³ which correspond to volume solid contents of approximately 10 % to 20 %. As seen from the plot, over this range of solids contents, the settling rate decreased significantly with increasing solids content. The results agree well with well known relationships between media stability and solids content; media stability is of greater concern at low solids contents.

The levels of particle sizes used in test work ranged from -45 µm to -15 µm (see Section 13.3.3). Figure 17.2 is a plot of settling rate versus particle size which shows that the settling rate decreased as the particle size decreased. The magnetite dense medium particle size is typically 90% finer than 45 µm. Since very fine magnetite has recently been tried in dense media separation tests on fine coal, there is a need to study the influence of much finer grades.

Many coal preparation plants use demagnetizing coils in their dense media recovery circuits to reduce the magnetic aggregation of the particles. Figure 17.3 shows settling curves for magnetized and demagnetized suspensions with a volume solids content of 15%. The demagnetized suspension settles much slower than the magnetized suspension indicating the importance of demagnetization to media stability. The settling rates for the demagnetized and magnetized magnetite were determined to be 1.58 cm min⁻¹ and 3.80 cm min⁻¹, respectively. From the sediment height at the end of the settling test, it is apparent that the volume of settled sediment was larger when particles were magnetized; this indicates that magnetized particles form a loose aggregated structure.

Settling tests were performed on magnetite suspensions with 15% solids by volume over the pH range of 2.0 to 12.0. The settling rates from these tests were plotted as a function of pH

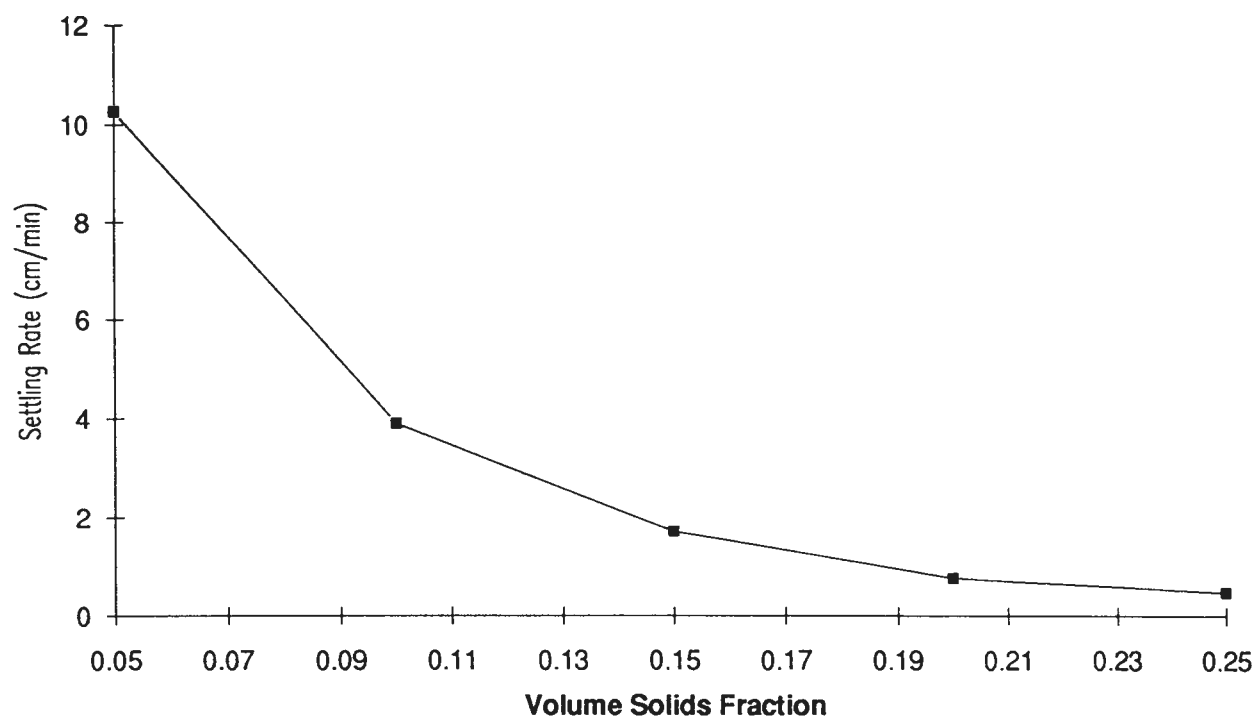


Figure 17.1 Effect of magnetite solids content on the settling rate.

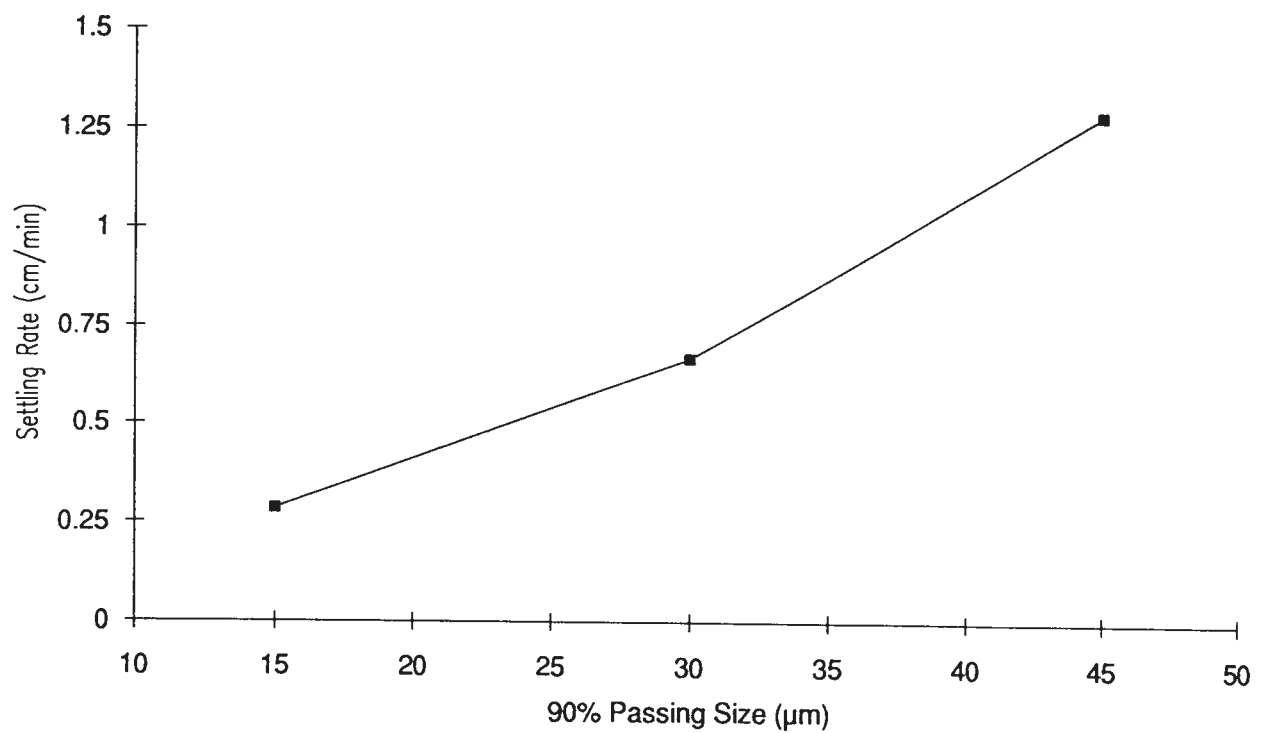


Figure 17.2 Effect of particle size on settling rate of magnetite suspensions (volume solids fraction = 0.15).

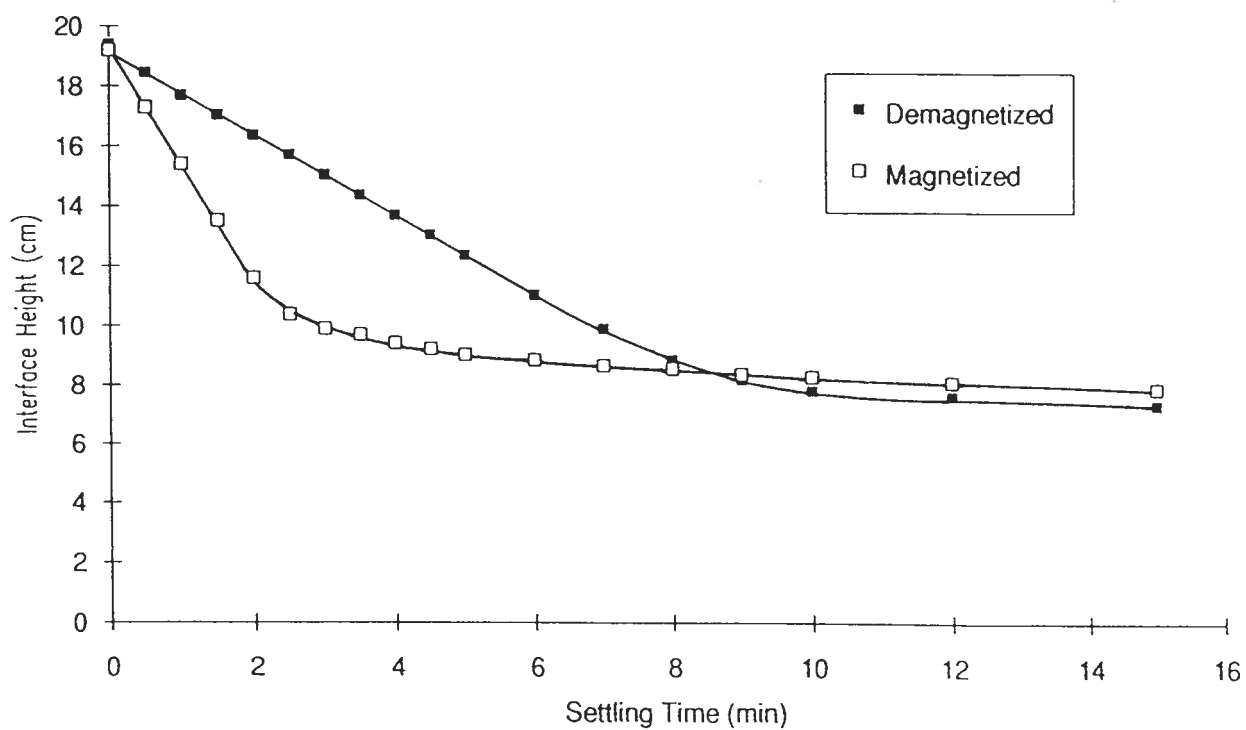


Figure 17.3 Supernatant/slurry interface height as a function of time for magnetized and demagnetized magnetite suspensions with a solids volume fraction of 0.15.

(Figure 17.4) which showed that the settling rate was not significantly influenced by the pH.

Electrophoretic mobility (EPM) measurements (see Section 13.3.2.3) indicated that the magnetite isoelectric point was approximately at pH 2.3 but that over the remaining pH range the EPM was negative and therefore particle dispersion should be maintained. The pH can, however, influence the dense medium behaviour through its influence on the coagulation of clays and on the mode of action of dispersing agents.

Dextran and carboxyl methyl cellulose have been tested for use in the processing of iron ore (see Section 8.4.2). To compare the effectiveness of these two reagents as dispersants and to establish suitable dosage levels, settling tests were performed using a magnetite suspension with 15% solids by volume. Figure 17.5 shows suspension settling rates as a function of dextran and C.M.C. dosage, respectively. For dosages up to 2.5 kg/T, dextran had only a small effect on the suspension settling rate. Over the same range of dosages, C.M.C. addition significantly reduced the settling rates of the suspension. The decreased settling rate indicated that particle interactions were affected by the adsorption of C.M.C..

Sodium silicate and sodium hexametaphosphate have been widely used as dispersing agents by the mineral industry. Therefore, settling tests were carried out with both of the dispersants so that their effectiveness could be compared. The settling rates were plotted as a function of dispersant dosages for the sodium silicate and sodium hexametaphosphate in Figure 17.6. The figure shows that for the range of levels tested, the settling rates were not significantly influenced. Since inorganic dispersants could have a significant effect on the properties of clays, and since the use of sodium silicate has been reported in iron ore processing (Yang, 1988), sodium silicate was selected as the inorganic dispersant for further testing.

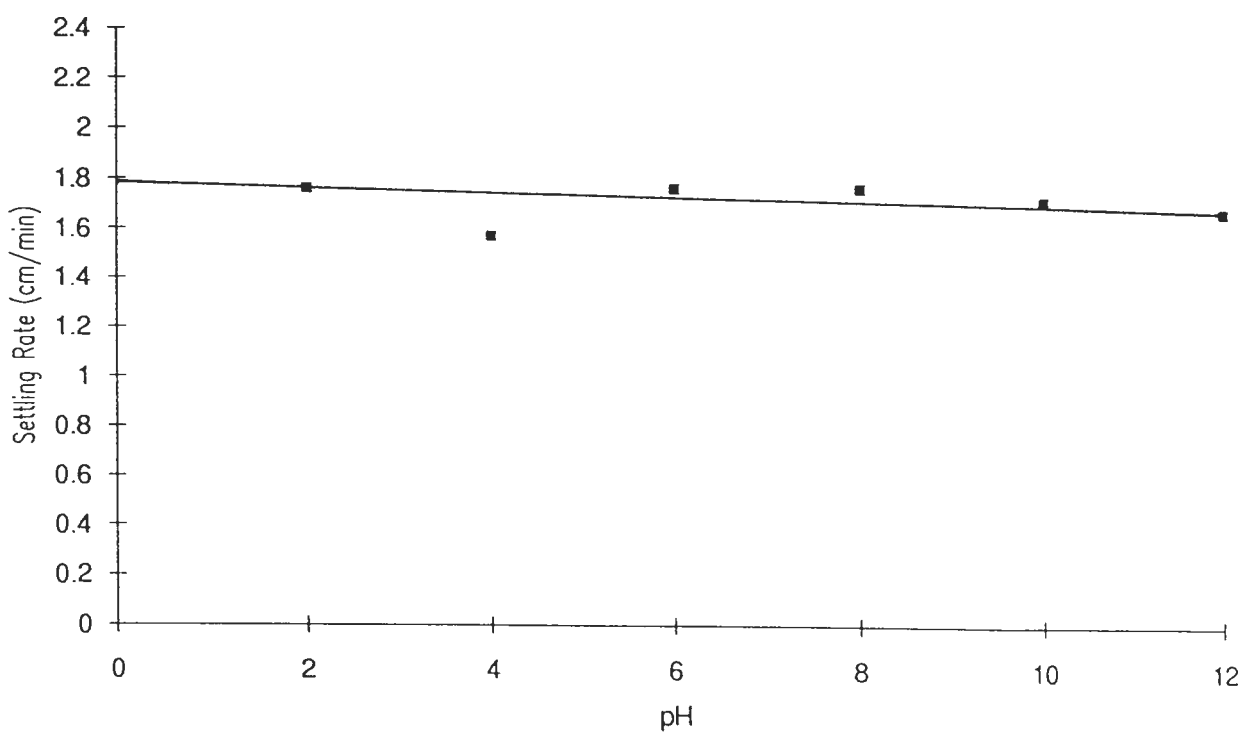


Figure 17.4 The effect of pH on the settling rates of magnetite suspensions (volume solids fraction = 0.15).

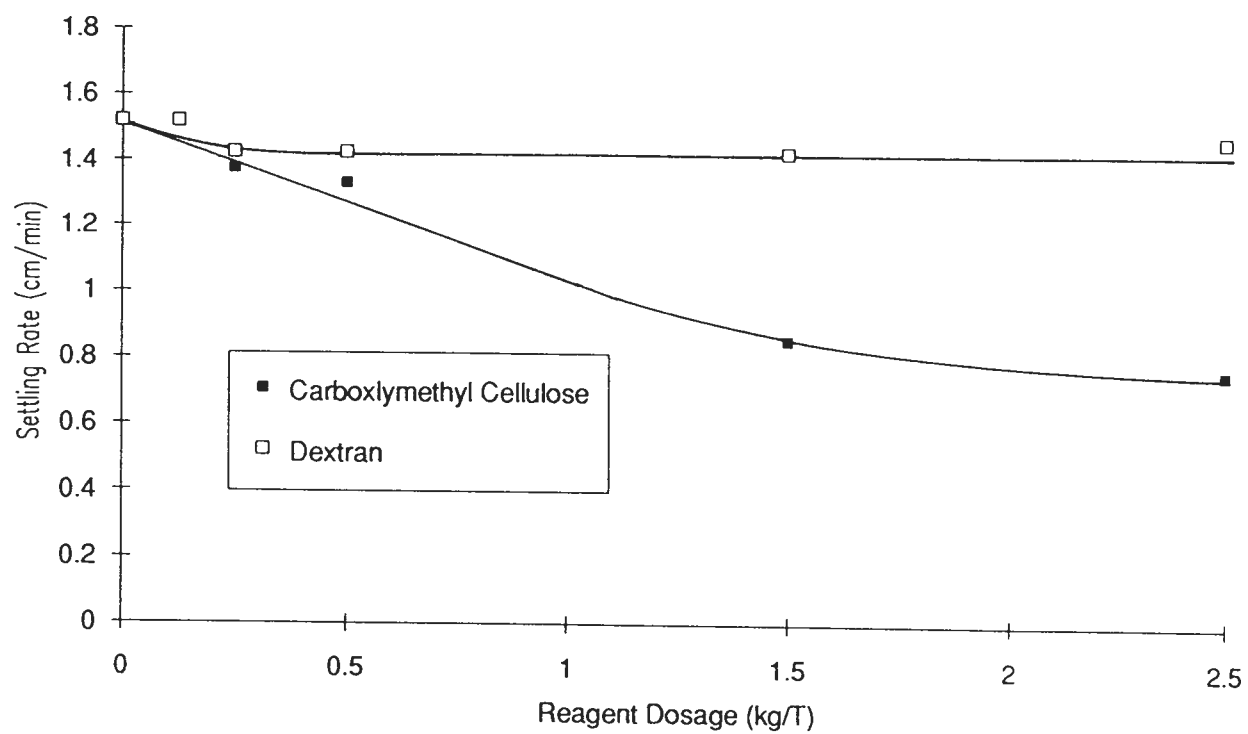


Figure 17.5 Effect of carboxymethyl cellulose and dextran on the settling rates of magnetite suspensions (volume solids fraction = 0.15).

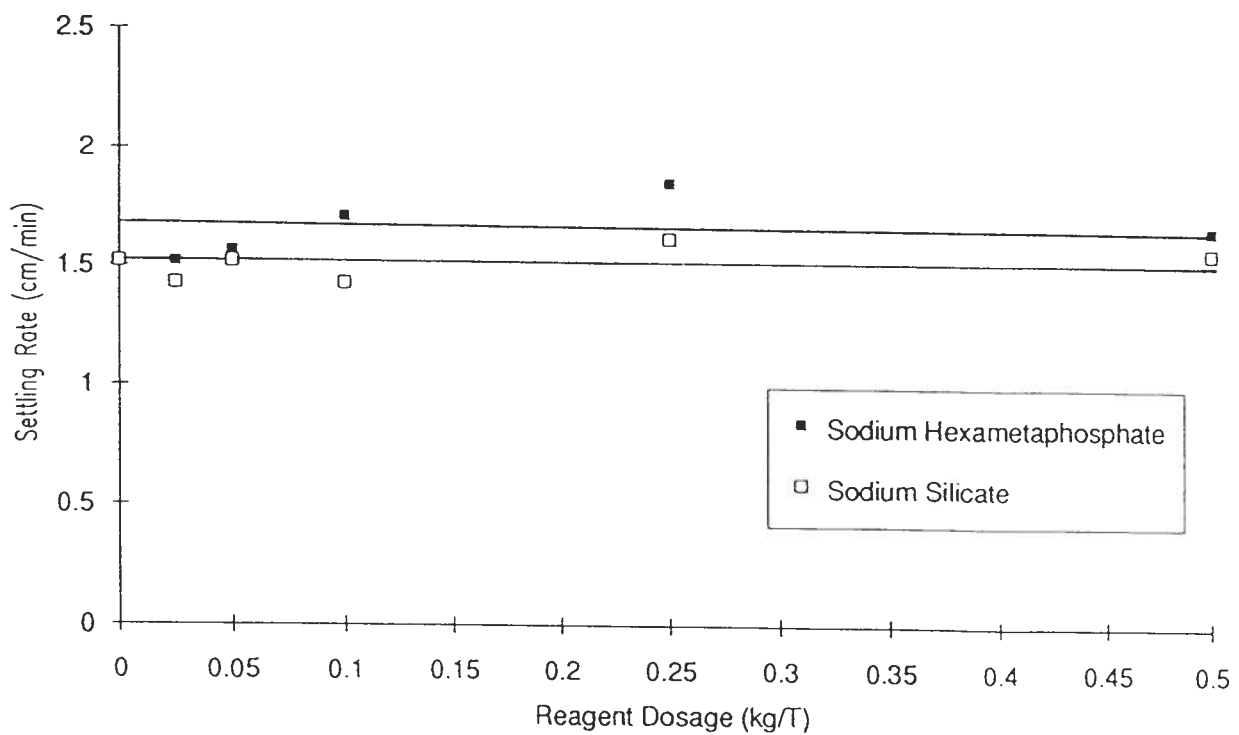


Figure 17.6 Effect of sodium hexametaphosphate and sodium silicate on the settling rates of magnetite suspensions (volume solids fraction = 0.15).

To determine the levels of contaminants in dense media, samples of media were taken from two western Canadian coal operations, Cardinal River Coal and Luscar Sterco. The samples were taken from the dense medium cyclone circuit at Cardinal River and from both the dense medium cyclone and Wemco drum circuits at Luscar Sterco. A Davis tube was used to separate the magnetics from the non-magnetics and the percent of -325 mesh (-45 μm) non-magnetics per unit volume of medium was determined. The results are presented in Table 17.1.

As seen from the table, the percent of fine non-magnetic particles in the medium ranged from 1.6% w/v to 13.9% w/v (contaminants levels were determined on a weight per volume of medium basis). Luscar Sterco is known to have kaolinite with some bentonite clays in their raw coal which are difficult to remove with deslime screens and separate from the dense medium. The high ash contents of the fine particles reported in Table 17.1 reveals that the fines are composed of clay rather than of coal. The levels of contaminants found in the medium from Cardinal River were believed to be more typical for raw coals that do not contain clay.

To determine the effect of coal fines on the settling properties of dense media, coal from the Bullmoose Operating Corporation in north eastern British Columbia was added to dense medium with a magnetite solids content of 15% by volume. The -325 mesh size fraction, with an ash content of 18.3%, was used in the settling tests. The suspension settling rates were plotted as a function of fine coal addition (Figure 17.7) which showed that even small amounts of fine coal significantly decreased the settling rate.

Table 17.1 Levels of -325 mesh (45 μm) contaminants in dense media.

Operation	Non-Magnetics -45 μm (% w/v)	Ash Content (%)
Cardinal River Coal D.M. Cyclone	1.58	24.7
Luscar Sterco Wemco Drum	7.57	96.1
Luscar Sterco D.M. Cyclone	13.9	88.5

Similarly, clays were added to dense media with a magnetite solids content of 15% by volume for settling tests. As indicated in Figure 17.7, kaolinite addition decreased the settling rate much more significantly than fine coal. When bentonite was added the settling rate dropped off very sharply and at an addition of 5% w/v the suspension was stable.

Comparing three curves in Figures 17.7 revealed that for the same levels of contaminant addition, the settling rates were reduced most by bentonite, second most by kaolinite and were least affected by fine coal. However, the addition of small amounts of each contaminant had a significant effect on settling rates.

17.3 Experimental Design

Experiments were performed to investigate the effects of physico-mechanical parameters, physico-chemical parameters and contaminants on the settling and rheological properties of magnetite dense media. The objective of these experiments was to determine the relative significance of each parameter to the medium properties and to characterize and model the rheological properties of the medium with diverse parameter conditions. The effects of nine parameters were investigated including solids content, particle size, magnetization, pH, inorganic dispersant (sodium silicate), organic dispersant (carboxymethyl cellulose), coal fines, kaolinite and bentonite.

In order to minimize the number of experiments performed and still provide the necessary information, a 2^{9-5}_{III} fractional factorial design was chosen. For this experimental design,

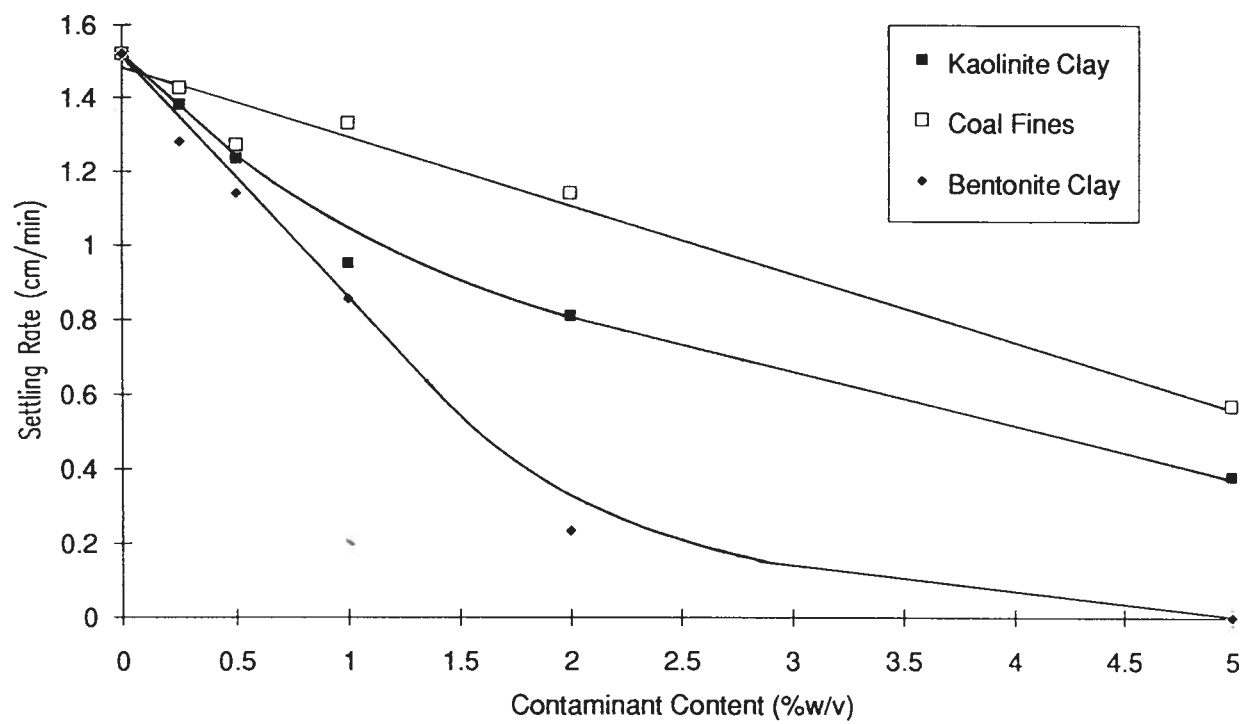


Figure 17.7 Effect of coal fines, kaolinite and bentonite content on the settling rate of magnetite suspensions with a volume solids fraction of 0.15.

sixteen sets of experiments plus four sets of centre point experiments were carried out. This design allowed for the determination of fifteen effects plus the mean effect. The principle generators for the design were:

$$X_0 = X_1X_2X_3X_5 = X_1X_3X_4X_7 = X_2X_3X_4X_6 = X_1X_2X_4X_8 = X_1X_2X_3X_4X_9 \quad (17.1)$$

The design is of resolution three, where main effects are confounded with two factor interactions and higher order interaction effects. A Plackett and Burman (1946) experimental design was considered; however the fractional factorial design was selected because it had a much less complicated alias structure.

The alias structure for the 2^{9-5}_{III} design is presented in Table 17.2; it shows the confounded main, two factor interaction and three factor interaction effects. Examination of the table reveals that all the main effects except for L_9 were confounded with only one two factor interaction involving L_9 . Therefore, parameter nine was selected as the parameter that would least likely interact with the remaining parameters. It was not expected that coal contamination would strongly interact with the other eight parameters and it was therefore selected as parameter nine. The remaining eight parameters were randomly assigned to variable numbers by drawing numbers from a dish. The order of performing the experimental runs was also determined by randomly selecting numbers from a dish.

In order to interpret the results, main effects were considered to be more significant than two factor interaction effects and two factor interactions were considered to be more significant than three factor interaction effects.

Table 17.2 Alias structure for fractional factorial design showing the confounded main effects, two factor interaction effects and three factor interaction effects.

$L_0 =$	$L_{169} =$	$L_{279} =$	$L_{389} =$	L_{459}				
$L_1 =$	$L_{69} =$	$L_{235} =$	$L_{248} =$	$L_{267} =$	$L_{347} =$	$L_{368} =$	$L_{456} =$	L_{578}
$L_2 =$	$L_{79} =$	$L_{135} =$	$L_{148} =$	$L_{167} =$	$L_{346} =$	$L_{378} =$	$L_{457} =$	L_{568}
$L_3 =$	$L_{89} =$	$L_{125} =$	$L_{147} =$	$L_{168} =$	$L_{246} =$	$L_{278} =$	$L_{458} =$	L_{567}
$L_4 =$	$L_{59} =$	$L_{137} =$	$L_{156} =$	$L_{236} =$	$L_{257} =$	$L_{358} =$	$L_{128} =$	L_{678}
$L_5 =$	$L_{49} =$	$L_{123} =$	$L_{146} =$	$L_{178} =$	$L_{247} =$	$L_{268} =$	$L_{348} =$	L_{367}
$L_6 =$	$L_{19} =$	$L_{127} =$	$L_{138} =$	$L_{145} =$	$L_{234} =$	$L_{258} =$	$L_{357} =$	L_{478}
$L_7 =$	$L_{29} =$	$L_{126} =$	$L_{134} =$	$L_{158} =$	$L_{238} =$	$L_{245} =$	$L_{356} =$	L_{468}
$L_8 =$	$L_{39} =$	$L_{124} =$	$L_{136} =$	$L_{157} =$	$L_{256} =$	$L_{237} =$	$L_{345} =$	L_{467}
$L_9 =$	$L_{16} =$	$L_{27} =$	$L_{38} =$	L_{45}				
$L_{12} =$	$L_{35} =$	$L_{48} =$	$L_{67} =$	$L_{269} =$	L_{179}			
$L_{13} =$	$L_{25} =$	$L_{47} =$	$L_{68} =$	$L_{189} =$	L_{369}			
$L_{14} =$	$L_{28} =$	$L_{37} =$	$L_{56} =$	$L_{159} =$	L_{469}			
$L_{15} =$	$L_{23} =$	$L_{46} =$	$L_{78} =$	$L_{149} =$	L_{569}			
$L_{17} =$	$L_{26} =$	$L_{34} =$	$L_{58} =$	$L_{129} =$	L_{679}			
$L_{18} =$	$L_{24} =$	$L_{36} =$	$L_{57} =$	$L_{139} =$	L_{689}			

The experimental design is presented in Table 17.3 showing the coded high (+1), low (-1) and centre point (0) levels used for each of the twenty sets of measurements. These high, low and centre point variable levels were chosen based on the results presented in Section 17.2. The variables and their respective levels corresponding to the coded levels are given in Table 17.4.

The measured responses (dependent variables) were the suspension settling rate, the sediment solids content and the coefficients of the fitted rheological models. Four different rheological models were fitted to flow curve data using the simplex optimization regression program described in Section 16.3.1. The best model was selected based on multiple index of determination values, R^2 , and the results of a model discrimination procedure (see Section 16.3.2). The coefficients of the best fitting model were then used as the dependent variables representing the rheological properties.

17.4 Sample Preparation

To reduce the potential for systematic errors associated with procedures used to prepare the suspension, all suspensions were prepared using exactly the same procedure.

The suspensions were prepared in cleaned 350 ml graduated cylinders. The glassware was cleaned by adding a few millilitres of concentrated nitric acid to the glass container. A few (three or four) drops of concentrated ethanol were then added to the nitric acid which produces a strongly oxidizing environment resulting in the breakdown of any organics that might be present. The glassware was then rinsed ten times with distilled water to remove any dissolved species. This cleaning procedure was used prior to preparing all of the suspensions.

Table 17.3 Coded levels for 2^{9-5}_{III} fractional factorial experimental design used to investigate the effects of suspension variables on rheology and stability.

Run #	Coded Experimental Variable Levels								
	X ₁	X ₂	X ₃	X ₄	X ₅	X ₆	X ₇	X ₈	X ₉
1	1	1	1	1	1	1	1	1	1
2	-1	1	1	1	-1	1	-1	-1	-1
3	1	-1	1	1	-1	-1	1	-1	-1
4	-1	-1	1	1	1	-1	-1	1	1
5	1	1	-1	1	-1	-1	-1	1	-1
6	-1	1	-1	1	1	-1	1	-1	1
7	1	-1	-1	1	1	1	-1	-1	1
8	-1	-1	-1	1	-1	1	1	1	-1
9	1	1	1	-1	1	-1	-1	-1	-1
10	-1	1	1	-1	-1	-1	1	1	1
11	1	-1	1	-1	-1	1	-1	1	1
12	-1	-1	1	-1	1	1	1	-1	-1
13	1	1	-1	-1	-1	1	1	-1	1
14	-1	1	-1	-1	1	1	-1	1	-1
15	1	-1	-1	-1	1	-1	1	1	-1
16	-1	-1	-1	-1	-1	-1	-1	-1	1
17	0	0	0	1	0	0	0	0	0
18	0	0	0	1	0	0	0	0	0
19	0	0	0	-1	0	0	0	0	0
20	0	0	0	-1	0	0	0	0	0

Table 17.4 Variable levels corresponding to coded levels.

Variable Description	Variable Levels		
Coded Levels	-1	0	1
X ₁ . Carboxymethyl Cellulose (kg/T)	0.5	1	1.5
X ₂ . Passing Size (µm)	45	30	15
X ₃ . Volume (%) Solids	10	15	20
X ₄ . Magnetization	Mag.		Demag.
X ₅ . Sodium Silicate (kg/T)	0.05	0.1	0.15
X ₆ . Kaolinite (% w/v)	0.25	0.5	0.75
X ₇ . pH	4.0	7.0	10
X ₈ . Bentonite (% w/v)	0.25	0.5	0.75
X ₉ . Coal Fines (% w/v)	0.25	0.5	0.75

The levels of the additives for each suspension are presented in Table 17.4. Since the bentonite was found to be difficult to disperse, it was added first to the graduated cylinder with 50 ml of distilled water and was thoroughly shaken and placed in an ultrasonic mixing bath. The bentonite suspension was allowed to wet overnight. Kaolinite, not as difficult to wet as the bentonite, was then added and once again the suspension was shaken and placed in an ultrasonic bath until the suspension was dispersed. The coal, sodium silicate and magnetite were then added in the presented order, with shaking and ultrasonic mixing between each addition. Distilled water was added as needed to disperse the particles. The suspension was then either magnetized by placing the cylinder in a demagnetizing coil and inducing a magnetic field for approximately five seconds or demagnetized by drawing the graduated cylinder through the demagnetizing coil three times. At this time the C.M.C. was added and the suspension was lightly shaken. The remaining water was then added before adjusting the pH using either sodium hydroxide or hydrochloric acid as required.

Once the suspensions were prepared, settling tests were performed. The same suspensions were then poured into the cup of the developed rheometer fixture (see Chapter 15) to carry out rheological measurements. Three flow curves were produced for each suspension to ensure reproducibility of results.

17.5 Characterization of Medium Properties

The settling curves for the twenty suspensions are presented in Appendix V. The mudline falling rates were used as the responses characterizing the stability of the suspensions. In

addition, the sediment volume was measured after twenty four hours from which the sediment volume solid content was determined. Since the sediment solids content provides an indication of the state of the aggregation, it was included as a response. The settling rates and sediment solids contents for each suspension are given in Table 17.5.

The rheological flow curves exhibited shear thinning properties as was shown in Chapter 16. With some suspension compositions, the non-Newtonian properties became very pronounced and the flow curve data intercepted the shear stress axis indicating the suspensions exhibited a yield stress. The rheological flow curves for all twenty sets of measurements are presented in Appendix V.

The coefficients of the best fitting flow curve model were used as the rheological responses (dependent variables) for the experimental program. The flow equations were fit to the data by using the simplex optimization non-linear regression program described in Section 16.3.1. The fitted models are graphically presented along with the flow curves in Appendix V.

Multiple index of determination values, R^2 , were determined for each model and a model discrimination procedure was used to determine which equation fit the data best. Table 17.6 shows the R^2 values calculated for each of the equations for the twenty suspensions. The equation fits each have 47 degrees of freedom except the Casson equation which has 48. Examination of the table reveals that the models with a yield stress term were better than models with no yield stress term. More importantly, in all twenty sets of experiments the Casson equation was found to fit the data best.

The validity of using the multiple index of determination values to compare the suitability of non-linear equations is questionable. Therefore, a model discrimination procedure developed

Table 17.5 Responses of rheological properties and settling properties for each of the experimental runs.

Run #	Casson Yield Stress (Pa.)	Casson Viscosity (mPa.s)	Settling Velocity (cm min ⁻¹)	Solids Packing Fraction
1	2.43	5.86	0.115	0.324
2	2.94	1.61	0.000	0.340
3	0.46	5.37	0.203	0.614
4	2.74	1.84	0.036	0.493
5	1.57	0.85	0.015	0.199
6	0.15	2.62	0.290	0.427
7	0.42	0.88	0.293	0.372
8	0.03	3.20	1.535	0.670
9	8.56	1.47	0.033	0.335
10	3.37	2.33	0.022	0.307
11	2.43	1.55	0.021	0.449
12	1.50	2.12	0.650	0.567
13	0.20	3.49	0.473	0.409
14	1.38	0.96	0.169	0.223
15	0.06	4.86	1.903	0.522
16	0.31	1.61	0.965	0.402
17	0.24	3.27	0.186	0.491
18	0.27	2.84	0.197	0.495
19	0.39	2.67	0.411	0.473
20	0.31	3.47	0.457	0.491

Table 17.6 Multiple index of determination values for each of the rheological equations fit to the measured flow curve data from the experimental program.

Run #	Coefficient of Multiple Determination, R^2			
	Herschel Bulkley	Casson	Carreau	Cross
1	0.978	0.999	0.967	0.941
2	0.911	0.998	0.904	0.664
3	0.984	0.997	0.980	0.979
4	0.841	0.975	0.839	0.643
5	0.720	0.912	0.662	0.029
6	0.970	0.986	0.964	0.966
7	0.940	0.983	0.924	0.858
8	0.992	0.995	0.991	0.993
9	0.959	0.978	0.943	0.220
10	0.988	0.998	0.941	0.701
11	0.631	0.871	0.582	0.125
12	0.913	0.971	0.895	0.776
13	0.979	0.992	0.976	0.987
14	0.850	0.969	0.818	0.771
15	0.989	0.993	0.988	0.993
16	0.932	0.971	0.922	0.947
17	0.973	0.991	0.969	0.984
18	0.964	0.988	0.958	0.976
19	0.937	0.974	0.928	0.954
20	0.957	0.982	0.951	0.967

by Williams and Kloot (1953) was used to determine the best fitting model. Details of the method have been discussed in Section 16.3.2 and the program is presented in Appendix IV. The results of this exercise confirmed that the Casson equation describes the rheological data better than the other rheological equations. The coefficients of this equation, including the Casson yield stress and the Casson viscosity, became the dependent variables for the experimental program. Hereafter, the terms yield stress and viscosity refer to the respective Casson equation coefficients unless otherwise stated. The yield stress and viscosity responses for each suspension are presented in Table 17.5 along with the settling rates and sediment solids contents.

17.6 Evaluation of the Effects on Medium Properties

The variable effects for each of the responses and their confidence intervals were calculated. The estimates of the effects were calculated as follows:

$$L_i = \hat{l}_i \pm t_{v,1-\alpha} V(\hat{l}_i)^{.5} \quad (17.2)$$

in which,

$$\hat{l}_i = \hat{l}_0 + \sum \frac{Y_i X_i}{n/2} \quad (17.3)$$

and,

$$\hat{l}_0 = \sum \frac{Y_i}{n} \quad (17.4)$$

where,

L_i is the value of the effect,

\hat{l}_i is the estimated values of the effect,

\hat{l}_0 is the mean effect,

$t_{v,1-\alpha}$ is the t-statistic probability,

$V(\hat{l}_i)$ is the variance of the estimated effects based on the repeat runs,

Y_i is the measured value of the response,

X_i is the level of the variable, and

n is the number of experimental runs.

The 95% confidence intervals were calculated from the repeat runs. The effects for each of the responses as well as their respective confidence intervals are presented in Table 17.7. Based on the calculated confidence intervals, effects that were determined to be insignificant have been highlighted in the table.

17.7 Results of Experimental Program

The relative significance of the variables to media properties was determined from the results of the experimental program. Table 17.8 presents the variable effects in order of magnitude. The table reveals that:

- i. Several parameters affected the Casson yield stress while only a few parameters influenced the Casson viscosity;
- ii. The four most significant variable effects for the Casson yield stress and for the settling rate are the same;
- iii. Both main effects and interaction effects are important;

Table 17.7 Estimated effects of each variable for each of the determined responses.

Variable	Casson Yield Stress	Casson Viscosity	Settling Velocity	Solids Packing Fraction
L ₀	1.49	2.64	0.399	0.473
L ₁	0.46	1.01	-0.076	-0.027
L ₂	1.58	-0.28	-0.561	-0.192
L ₃	2.54	0.46	-0.570	0.027
L ₄	-0.88	0.48	-0.219	0.027
L ₅	0.74	0.07	0.032	-0.014
L ₆	-0.74	-0.16	-0.026	0.008
L ₇	-1.52	2.38	0.457	0.130
L ₈	-0.07	0.28	0.114	-0.036
L ₉	-0.56	-0.03	-0.287	-0.037
L ₁₂	0.77	0.03	0.115	0.020
L ₁₃	0.37	0.58	-0.008	0.028
L ₁₄	-0.71	-0.08	-0.232	-0.078
L ₁₅	0.96	0.38	0.376	-0.015
L ₁₇	-0.94	1.32	0.126	-0.001
L ₁₈	-0.72	0.19	0.149	-0.023
95% Confidence Interval	0.08	0.98	0.050	0.020

- iv. The most significant main effects are due to changes in solids content, particle size and pH; and
- v. The most significant interaction effects are L_{15} and L_{17} (see Tables 17.2 and 17.4).

17.7.1 Analyses of Measured Responses

Table 17.8 reveals that most parameters had a significant effect on the yield stress and that only a few parameters influenced the Casson viscosity. Therefore the results indicate that the Casson yield stress is the primary controllable rheological property. Since the existence of a yield stress has been associated with the presence of a structure resulting from particle aggregation (Papenhuijzen, 1972, Hunter and Firth, 1976), it is apparent that changes in the parameter levels affected the magnitude of aggregation. It should be noted that the Casson equation was developed for aggregating suspensions (Casson, 1959).

For all suspensions, the yield stress dominated the rheological properties. This result can be demonstrated by calculating the contributions of the yield stress and Casson viscosity to the apparent viscosity. For example, the apparent viscosity can be calculated from Equation 17.5. The first term on the right side of Equation 17.5 represents the apparent viscosity resulting from the yield stress, the second term represents the Casson viscosity contribution and the third term represents the interaction between the two coefficients that account for curvature of the flow curve.

$$\eta_{ap} = \frac{\tau}{\dot{\gamma}} = \frac{\tau_{CY}}{\dot{\gamma}} + \eta_C + \left(\frac{\tau_{CY}\eta_C}{\dot{\gamma}}\right)^{0.5} \quad (17.5)$$

Table 17.8 Statistically significant estimates of the effects in order of magnitude.

Casson Yield Stress	Casson Viscosity	Settling Velocity	Solids Packing Fraction
$L_0=1.49$	$L_0=2.64$	$L_0=0.399$	$L_0=0.473$
$L_3=2.54$	$L_7=2.38$	$L_3=-0.570$	$L_2=-0.192$
$L_2=1.58$	$L_{17}=1.32$	$L_2=-0.561$	$L_7=0.130$
$L_7=-1.52$	$L_1=1.01$	$L_7=0.457$	$L_{14}=-0.078$
$L_{15}=0.96$		$L_{15}=0.376$	$L_9=-0.037$
$L_{17}=-0.94$		$L_9=-0.287$	$L_8=-0.036$
$L_4=-0.88$		$L_{14}=-0.232$	$L_{13}=0.028$
$L_{12}=0.77$		$L_4=-0.219$	$L_1=-0.027$
$L_5=0.74$		$L_{18}=0.149$	$L_3=0.027$
$L_6=-0.74$		$L_{17}=0.126$	$L_4=0.027$
$L_{18}=-0.72$		$L_{12}=0.115$	$L_{18}=-0.023$
$L_{14}=-0.71$		$L_8=0.114$	$L_{12}=0.020$
$L_9=-0.56$		$L_1=-0.076$	
$L_1=0.46$			
$L_{13}=0.36$			

Based on the mean values of the responses (mean Casson yield stress = 1.49 Pa, mean Casson viscosity = 2.64×10^{-3} mPa.s) at a shear rate of 100 s^{-1} , the apparent viscosity is 23.8 mPa.s. The contribution of the yield stress, viscosity and third term to this apparent viscosity are 14.9 mPa.s, 2.64 mPa.s and 6.27 mPa.s, respectively. The yield stress clearly contributes more to the apparent viscosity than the other terms.

As can be seen from the flow curves presented in Appendix V, the apparent viscosity decreased with increasing shear rate and the flow curves became linear. These results can be explained by changes in the structure resulting from shearing of the suspension (Cheng, 1980b). By increasing shear rate, the rate of aggregate breakages exceeds the rate of aggregate formation leading to shear induced dispersion and the break down of the structure. Therefore, as the structure breaks down, the apparent viscosity decreases (Sherman, 1965, Laapas, 1982, 1985, Sherman, 1965). Once the particles are dispersed, hydrodynamic effects determine the viscosity resulting in a linear shear stress to shear rate relationship.

Since the four most significant variables that influence both the Casson yield stress and the settling rate are the same, the yield stress and the settling rate are apparently interrelated. Specifically, if the variables affect the yield stress through their influence on the suspension structure, the same structure may determine the settling properties of the suspensions.

In this case, a clear relationship should exist between the suspension settling rate and the yield stress. Figure 17.8 is a plot of the Casson yield stress versus the settling rates for the twenty sets of experiments. The figure shows that when settling rates are low the yield stress is high and vice versa. These results support the explanation that the structure that determines the yield stress also determines the settling rate. The non-linear relationship between the yield

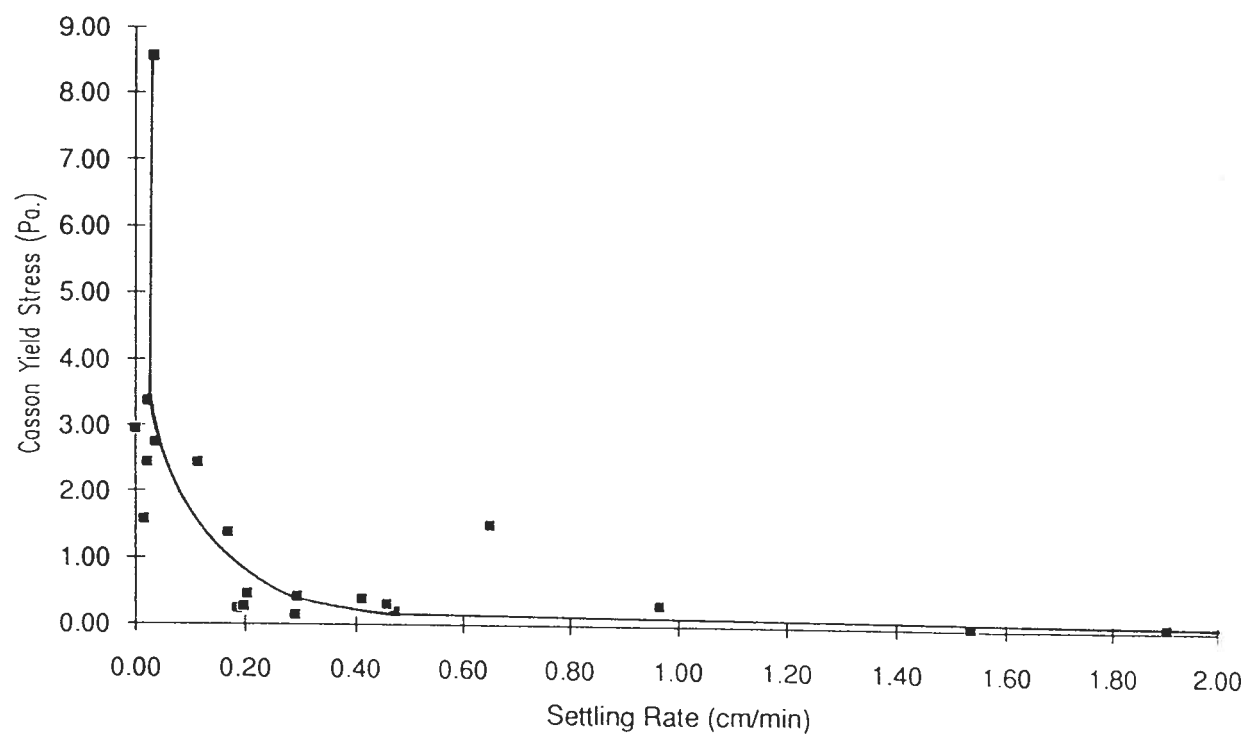


Figure 17.8 Relationship between the Casson yield stress and the settling rate.

stress and settling rate indicates that it is possible to optimize the medium properties by reducing the yield stress while maintaining relatively low settling rates.

Cheng (1980a) stated that the zone settling properties of suspensions could be explained by the existence of a structure resulting from particle aggregation. It was shown in Chapter 14, that magnetite suspensions exhibit such settling properties. The apparent relationship between the yield stress and the settling rate also support the explanation that the suspension has a structure that determine its physical properties.

The sediment volume solids contents in the experiments ranged from 19.9% to 67.0% (Table 17.5). Sediment solids contents less than approximately 50% indicate that some type of loose aggregated structure exists. Such a structure has been associated with coagulated clay particles (Street, 1956, Kitchener, 1969). In addition, it was shown in Section 13.2.2.6 that magnetically aggregated particles form a loose structure. Both types of structure likely contribute to the physical properties of the suspensions.

17.7.2 Effects of Suspension Parameters on Medium Properties

Changes in the particle size, suspension pH and suspension solids content had the greatest effect on the medium properties. Other main effects that significantly influenced the medium properties were due to demagnetization and the additions of coal fines and carboxylmethyl cellulose. Over the range of levels tested, changes in bentonite, kaolinite, and sodium silicate additions had only small effects on the medium properties. It should be noted that these variables may have had a large effect on the medium properties; however, the changes in the responses

over the ranges of variable levels may have been small.

The most important interaction effects were, L_{15} and L_{17} , although, L_{14} , L_{12} , L_{18} and L_{16} were also important. To determine which interactions were responsible for these effects, the alias structure was examined to identify which could physically account for the effects. To interpret the results, main effects were considered to be more significant than two factor interaction effects and two factor interaction effects were considered to be more significant than three factor interaction effects. While it is not possible to determine the importance of algebraically confounded effects independently of each other without further experimentation, a physical understanding of their influences allows for some interpretation. These results highlight the relationship between the medium properties that are important to separation performance and the parameters and their interactions that influence these properties.

17.7.2.1 Effect of Solids Concentration

The signs (+/-) of the effects indicate that with increasing solids content, the settling rate decreased and the Casson yield stress increased; however the Casson viscosity was not affected. Several investigators have shown that above a critical solids content, the relative viscosity increases in an exponential manner with increasing solids concentrations (Rutgers, 1962a, 1962b). For suspensions exhibiting non-Newtonian flow properties, the relative viscosity is equivalent to an apparent viscosity divided by the viscosity of the suspending fluid. The results indicate that for magnetite dense media, the increase in apparent viscosity with increasing solids concentration is primarily due to the increase in the Casson yield stress.

Papenhuijzen (1972) attributed the existence of a yield stress to the presence of a network structure that is formed by aggregating particles. Furthermore, with increasing solids concentration, particle aggregation increases which in turn increases the suspension yield stress.

The decrease in settling rates with increasing solids content of suspensions has been attributed to an increase in hindered settling effects (Richardson and Zaki, 1954, Garside and Al-Dibouni, 1977, Zimmel, 1985). However, the presence of the structure described above could effect the settling rate by physically supporting the particles (Cheng, 1980a). As was shown, the yield stress and the settling rate are inter-related. Therefore, the same structure that is responsible for the increase in yield stress due to increasing solids content is likely responsible for the corresponding decrease in settling rate with increasing solids content.

17.7.2.2 Effect of Particle Size

By decreasing the particle size, the signs (+/-) of the effects indicate that the suspension settling rate decreased, the Casson yield stress increased and the Casson viscosity was not affected. Since particle size influenced the yield stress and not the viscosity, the contribution of particle size to medium rheological properties can be attributed to the effect of particle size on the suspension structure. For small particles, inter-particle forces of attraction and repulsion dominate over particle inertial forces. Therefore, small particles are more susceptible to aggregation effects than coarse ones (Williams, 1951, Saunders, 1967, Parkinson et al, 1970). Enhancing the magnitude of aggregation effects by decreasing the particle size facilitates the formation of a structure.

The decrease in settling rate with decreasing particle size can be explained by the Stokes (1891) relationship between particle settling rate and particle size as well as by the enhanced structure formed by small particles (Cheng, 1980a). A network structure would physically support the particles and thereby prevent them from settling. Such a structure also helps to explain the zone settling properties exhibited by magnetite suspensions. In Chapter 14, experimental results indicated the particles settled as a bulk (hindered settling) rather than differentially based on size. The presence of aggregates and a particle network structure inhibits differential settling.

The interaction effect, L_{23} , for particle size and solids content (confounded with L_{15}) had a significant influence on both the settling velocity and the yield stress. The interaction effect indicates that the dependency on solids content is different for particles of different size. Sherman (1965) and Laapas (1982, 1985) explained the relationship between the suspension yield stress and the interaction effect of solids concentration and particle size as follows. Below a critical concentration, the structure may not be continuous, resulting in a low or non-existent yield stress. This critical concentration is a function of particle size and it decreases as the particle size decreases. Therefore, to reduce the yield stress (apparent viscosity) at high solids concentrations (medium densities), a coarse grade of magnetite should be used. Conversely, to improve media stability, at low solids concentrations (media densities), fine grades of magnetite should be used.

17.7.2.3 Effect of Suspension pH

The suspension pH was found to be the third most important variable. Although pH was shown to have no significant effect on settling rates of pure magnetite suspensions (see Section 17.2), the effects on settling rates, yield stress and viscosity were very significant for the present set of experiments. It is therefore likely that pH influenced the medium properties through its effect on clays and interactions with dispersing agents.

By increasing the pH from 4.0 to 10.0, the yield stress decreased, the viscosity increased and the settling rate increased. At a low pH, clay particles coagulate to form a "house of cards" structure as a result of positively charged edges and negatively charged surfaces (Street, 1956, Kitchener, 1969). Even with small amounts of bentonite, this structure may be quite profound. The structure is responsible for a high suspension yield stress (Nicol and Hunter, 1970) and it supports the magnetite particles and thereby prevents them from settling. At a high pH, the clay particles become dispersed and the structure breaks down resulting in a lower yield stress (Nicol and Hunter, 1970). In addition, the magnetite particles, which are no longer supported by the structure of the clay, can settle faster, thereby increasing the settling rate of the suspension.

Although the yield stress decreased with increasing pH, the Casson viscosity increased. At a high pH, the particles disperse due to higher electrostatic repulsive forces. Leong and Boger (1989) observed that with increasing electrostatic repulsion between particles, the suspension viscosity increased while the yield stress remained small. They attributed the increase in viscosity to an increase in the magnitude of electroviscous effects. Electroviscous effects could therefore explain the increase in the Casson viscosity with increasing pH.

While changes in the levels of bentonite and kaolinite additions had only small effects on the suspension properties, the explanation of the effects of pH on clays suggests that their presence had a large effect on the properties of the medium.

The pH also jointly interacts with dispersing agents to influence the responses (Laskowski, 1988). From examination of the alias structure (Table 17.2) and the list of significant effects (Table 17.8), it can be seen that the interaction effects between pH and C.M.C.(L₁₇) and sodium silicate (L₅₇ confounded with L₁₈) influence the properties of the suspension. By increasing both the C.M.C. dosage and the pH, the yield stress decreased, the viscosity increased and the settling rate increased. Similarly, increasing the sodium silicate dosage and the pH, resulted in a decreased yield stress and increased settling rate.

The effects of C.M.C. and sodium silicate can be explained by their effectiveness in dispersing particles. At low pH, C.M.C. can precipitate to form fine colloidal particles rendering it less effective. At high pH, C.M.C. is ionized and disperses the magnetite and clay particles. It is also possible that at low pH, polysilicic acid precipitates from the sodium silicate rendering it less effective as a dispersing agent, and at high pH, ionic species electrostatically stabilize the suspension.

The dispersion of the particles resulting from greater repulsive forces decreases the structure of the suspension and therefore also decreases the yield stress. In addition, more negative values of the zeta potential enhance electroviscous effects which can increase the viscosity. The lack of a structure to support and thereby prevent particles from settling results in an increased settling rate.

17.7.2.4 Effect of Magnetization

The signs (+/-) of the effects of magnetization (Table 17.8), reveal that settling rate and yield stress decreased by demagnetizing the magnetite. Demagnetizing results in better dispersion of particles which decreases the size of the settling units and, therefore, also decreases their settling rates. The yield stress decreases as a result of the decrease in the inter-particle interactions that are responsible for the formation of a structure. Clearly, demagnetization results in improved media stability and rheology.

17.8 Conclusions

Suspensions were prepared with a diverse set of parameter conditions to determine the influence of the parameters on the properties of dense media. Based on the experimental results, the following conclusions can be drawn.

The suspensions exhibit shear thinning rheological properties and have an apparent yield stress. These rheological properties were successfully modelled using the Casson equation which fit the flow curves better than the Herschel Bulkley, Carreau and Cross equations.

The Casson yield stress term was found to be the most controllable rheological parameter since it was influenced by most of the suspension variables. The Casson viscosity was only affected by a few of the parameters. In addition, it was determined that the Casson yield stress contributed more to the apparent viscosity of the suspensions than the Casson viscosity term.

The settling rates of the suspensions were affected by many of the same parameters as

the yield stress. It was revealed that the settling rate and the yield stress are inter-related in a non-linear manner. The settling properties and yield stress could be explained by the presence of a structure resulting from particle aggregation.

Although all parameters influenced the medium properties, for the ranges of variables that were tested, the solids content, particle size and pH were determined to be the most significant. Increasing the solids content and decreasing the particle size resulted in higher yield stress values and lower settling rates. An interaction effect between solids content and particle size indicated that the critical medium solids content, above which the medium becomes excessively viscous, is different for media particles of different size. The effect of pH was explained by its influence on clays and dispersing agents. Most notable was that increasing the pH resulted in a lower Casson yield stress, a higher Casson viscosity and a higher settling rate.

Demagnetization improved both the medium rheology and the medium stability by decreasing the yield stress, and by decreasing the settling rate, respectively. This result emphasizes the importance of demagnetization to the properties of magnetite dense media.

CHAPTER 18: EFFECT OF PARTICLE SIZE DISTRIBUTION ON MEDIUM PROPERTIES

18.1 Introduction

As discussed in Section 8.3.5, the viscosity of dispersed particle suspensions can be reduced by controlling the particle size distribution. Specifically, viscosities can be reduced by using a bimodal particle size distribution characterized by a low small particle to large particle diameter ratio and a fine particle fraction of between 0.25 and 0.50 of the total solids content. The objective of this chapter is to investigate the effects of particle size distribution on the rheology and stability of magnetite suspensions by:

- i. Developing a model to predict the rheological and settling properties of magnetite dense media as a function of particle size distribution and solid contents, and
- ii. Identifying how particle size distribution variables affect the rheological and settling properties of magnetite suspensions.

18.2 Experimental Design

Based on the reviewed literature, important size distribution variables for bimodal suspensions include the ratio of small to large particle diameters (Equation 18.1) and the small particle fraction of the total solids content (Equation 18.2). Since the effect of particle size distribution is more pronounced at high solids contents than at low ones (Ferrini et al, 1988), solids content was also included as a variable.

$$Size\ Ratio = \frac{d_s}{d_l} \quad (18.1)$$

where, d_s is the mean particle size of small particles, and

d_l is the mean particle size of large particles,

$$\phi_f = Fine\ Fraction = 1.00 - Coarse\ Fraction \quad (18.2)$$

The variable levels were selected based on the levels reported in the literature (see Section 8.3.5). The optimum fraction of fine particles has been reported to range from 0.25 to 0.45 (Chong et al, 1968, Parkinson et al, 1970, Round et al, 1984, and Ferrini et al, 1988).

Fidleris and Whitmore (1961) found that for bimodal suspensions with fine particle to coarse particle diameter ratios of less than approximately 0.1, the fine particles flowed between coarse particles together with the suspending liquid and did not physically interact with the large particles. As the particle diameter ratio increased, the small particles began to interact with the large ones resulting in an increase in the suspension viscosity. The size fractions that were prepared for the test work had geometric mean particle sizes ranging from 3.3 μm to 25.5 μm for the small particles and 38.1 μm for the large particles. The small particles were mixed with the large particles to produce suspensions with mean particle size ratios ranging from 0.086 to 0.669.

The suspension solids contents ranged from 11.6% to 28.4% solids by volume, which corresponded to media densities of approximately 1450 kg m^{-3} to 2100 kg m^{-3} . The size fractions and the preparation procedures are described in Section 13.3.5..

The experiments were carried out using a central composite experimental design. Table

18.1 shows the coded levels of variables for the sixteen sets of experiments. The design includes a 2^3 full factorial design portion, involving eight runs, six star point runs and two centre point runs. Table 18.2 shows the variable levels corresponding to the coded levels. This experimental design provided sufficient information to fit the responses to second order equations involving the variables. The experimental runs were carried out in random order determined by selecting numbers from a dish.

The dependent variables included settling rates and the coefficients of the Casson equation which was fit to flow curve data for each suspension. The Casson equation was fit to the data by using a simplex non-linear regression program (see Section 16.3.1). All the rheological measurements were made using the developed rheometer fixture for settling suspensions and the procedures described in Chapter 15.

Once the measurements were completed, statistical models were developed for each response as a function of the investigated variables. Linear regression was used to fit the equations to the responses using SYSTAT which is a statistical program system. From the regression, the values of the coefficients were determined. By using a step-wise regression procedure, insignificant coefficients were removed from the model based on a t-statistic probability. The fit of the equation was then evaluated based the coefficient of multiple determination, R^2 (48 degrees of freedom). From the fitted second order equation, response surfaces were produced to illustrate how the parameters affected the medium properties.

Table 18.1 Coded variable levels for central composite experimental design.

Run #	Experimental Variable		
	Size Ratio, X_1	Fine Fraction, X_2	Volume Fraction, X_3
1	1	1	1
2	-1	1	1
3	1	-1	1
4	-1	-1	1
5	1	1	-1
6	-1	1	-1
7	1	-1	-1
8	-1	-1	-1
9	*	0	0
10	-*	0	0
11	0	*	0
12	0	-*	0
13	0	0	*
14	0	0	-*
15	0	0	0
16	0	0	0

Table 18.2 Variable levels corresponding to coded levels.

Variable Description	Variable Levels				
Coded Levels	-*	-1	0	1	*
X_1 Size Ratio	0.09	0.13	0.22	0.39	0.67
X_2 Fine Fraction	0.199	0.25	0.325	0.40	0.451
X_3 Volume Fraction	0.116	0.15	0.20	0.25	0.284

18.3 Experimental Procedure

In order to reduce the possibility of systematic errors, each suspension was prepared using the following procedure:

- i. The appropriate weight of fine magnetite particles was added to a cleaned 350 ml graduated cylinder with 50 ml of distilled water. The suspension was shaken and placed in an ultrasonic bath to disperse the particles.
- ii. The weighed coarse particles were then added to the fine particle suspension and the mixture was again shaken and placed into an ultrasonic bath.
- iii. The remaining weight of distilled water was then added to the graduated cylinder which was shaken and placed in an ultrasonics bath to ensure particle dispersion.
- iv. Prior to proceeding with any measurements, the suspension was demagnetized by passing the graduated cylinder through a demagnetizing coil three times and the suspension pH was measured.
- v. Once the suspension was prepared, a settling test was performed which involved recording the supernatant-slurry interface height for a period of an hour and then taking a sludge depth reading.
- vi. Following the settling test, the suspension was demagnetized again and then poured into the cup of the rheometer fixture. Three sets of flow curve data were produced for each suspension. The temperatures of the suspensions were maintained at 25°C for all rheological measurements. Between each set of measurements, the cup was removed from the rheometer and inverted several times to re-suspended the suspension.

Once the measurements were completed, settling rates were determined and the Casson equation was fit to the flow curve data to determine the flow curve model coefficients. The Casson equation coefficients and settling rates for each of the experimental runs are presented in Table 18.3. The settling curves and fitted flow curves for the sixteen sets of experiments are presented in Appendix VI.

18.4 Modelling the Effects of Particle Size Distribution

The Casson yield stress, Casson viscosity and settling rate of the suspensions were fit to a second order polynomial equation using linear regression. The general form of the polynomial equation that was fit to each set of responses is presented in Equation 18.3.

$$Y = A_0 + A_1X_1 + A_2X_2 + A_3X_3 + A_{12}X_1X_2 + A_{13}X_1X_3 + A_{23}X_2X_3 + A_{11}X_1^2 + A_{22}X_2^2 + A_{33}X_3^2 + A_{123}X_1X_2X_3 \quad (18.3)$$

where, A_i represent the model coefficients, and

X_i represent the un-coded variable levels.

Significant coefficients along with multiple index of determination values for each of the fitted equations are presented in Table 18.4. The t-test results along with an analyses of variance for each fitted equation are presented in Appendix VII.

Table 18.3 Settling rate, Casson yield stress and Casson viscosity responses for experimental program.

Run #	Response		
	Casson Yield Stress (Pa)	Casson Viscosity (mPa.s)	Settling Rate (cm min ⁻¹)
1	0.125	7.2	1.23
2	1.587	1.2	0.46
3	0.060	7.3	1.47
4	0.725	2.6	0.80
5	0.050	2.4	4.67
6	0.130	3.1	1.11
7	0.070	1.4	5.08
8	0.024	3.8	1.87
9	0.000	7.1	3.22
10	0.910	2.1	0.52
11	0.125	4.8	1.18
12	0.019	5.9	2.03
13	0.721	4.5	0.62
14	0.049	1.5	5.32
15	0.015	6.4	1.51
16	0.076	4.8	1.49
Standard Error	0.043	1.1	0.01

Table 18.4 Casson yield stress, Casson viscosity and settling rate coefficients for fitted second order models.

Coefficient	Casson Yield Stress	Casson Viscosity	Settling Rate
A_0			7.84
A_1		-45.6	32.5
A_2			-3.11
A_3	-9.53	75.6	-76.1
A_{12}			
A_{13}		261	-97.1
A_{23}	28.2		
A_{11}	6.12		-10.0
A_{22}			
A_{33}	31.0	-303	189
A_{123}	-87.7		
R^2	0.89	0.96	0.97

The coefficient of multiple determination, R^2 , values (see Table 18.4) indicate that the equations for the settling rate and Casson viscosity provide good fits to the data. The expression for the yield stress has a slightly lower index ($R^2 = 0.894$). The fit was, however, considered to be adequate to indicate trends in the yield stress as a function of the variables. Predicted versus estimated responses are plotted in Figures 18.1, 18.2 and 18.3 for the yield stress, viscosity and settling rate respectively. These figures also indicate that while the models for the settling rate and viscosity provide good fits, the yield stress model fit is also adequate. The analyses of variance and degrees of freedom for each model along with the t-statistic probability for each coefficient are presented in Appendix VII.

18.5 Analyses of Regression Models

From the fitted second order models for each of the responses, the response surfaces were plotted. These response surfaces reveal: the variable levels that correspond to maximum and minimum response levels; and the relationships between the variable levels and trends in the responses. The results can be explained in terms of the effects of solids content, particle size and particle size distribution, on the rheological and stability properties of suspensions. In the discussion of the results, the terms yield stress and viscosity refer to the Casson yield stress and Casson viscosity, respectively.

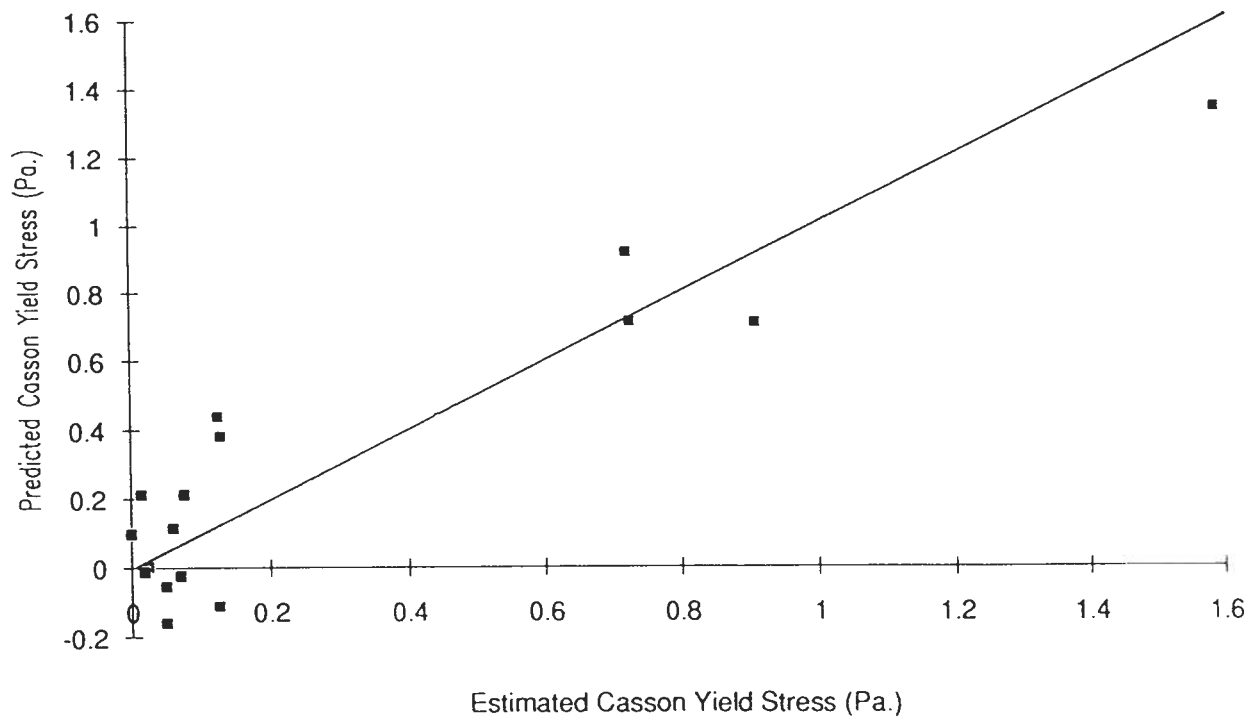


Figure 18.1 Predicted versus estimated Casson yield stress responses.

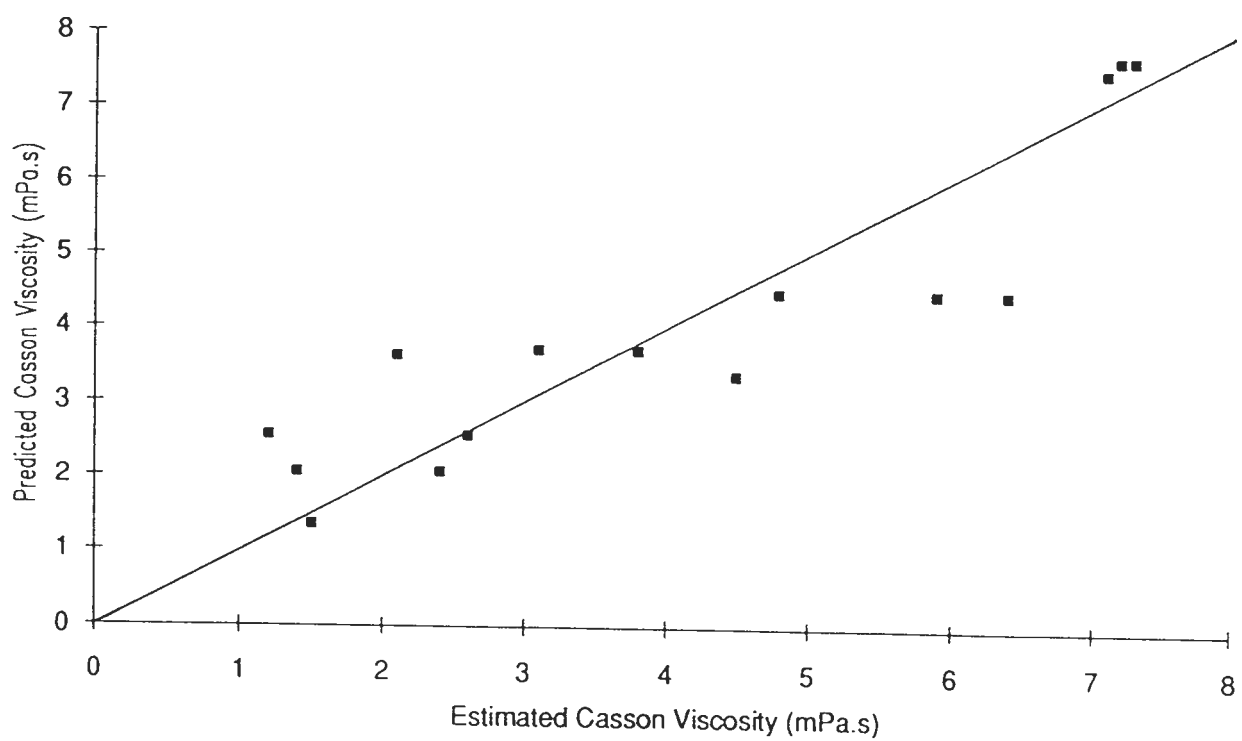


Figure 18.2 Predicted versus estimated Casson viscosity responses.

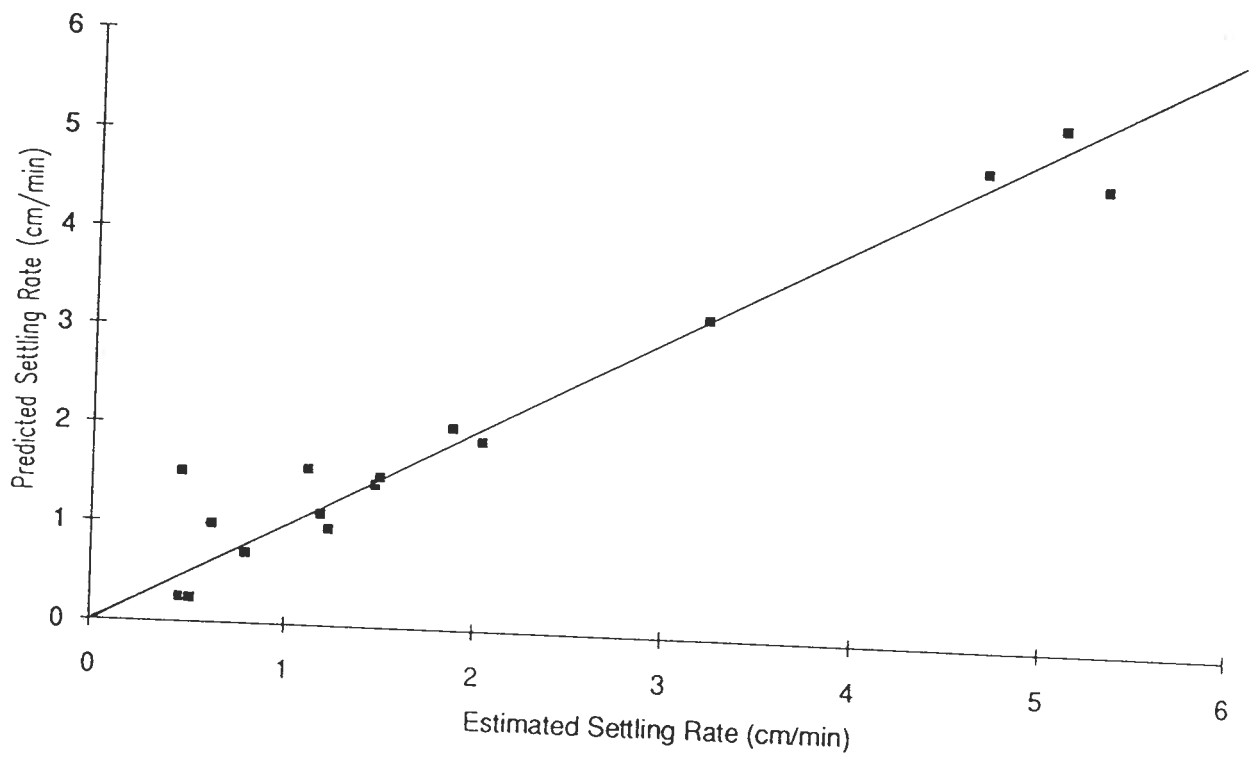


Figure 18.3 Predicted versus estimated settling rate responses.

18.5.1 Effect of Particle Size Distribution on the Casson Yield Stress

As indicated in Table 18.4, the Casson yield stress was affected by each of the variables; mean size ratio, fine fraction and suspension solids content. The table shows that interactions terms and second order terms were required to fit the yield stress to the data.

Figures 18.4 and 18.5 are contour plots of the yield stress determined with the solids content set at 15% and 25%, respectively. Both plots show that a minimum yield stress valley exists that is a function of both the size ratio and the fine fraction. This minimum yield stress valley has a trend along a diagonal line that corresponds to increasing size ratios and fine fractions. From the contour intervals it can be seen that the yield stress increases in a non-linear manner above and below this diagonal line.

By comparing Figures 18.4 and 18.5, it can be seen that the effect of particle size distribution is more pronounced at a high solids content. At 15% solids content, the minimum yield stress valley is quite broad and the increase in the yield stress perpendicular to the trend of the valley is gradual. At 25% solids, the valley is defined better showing more pronounced increases in the yield stress perpendicular to the trend of the valley. The plot indicates that the yield stress valley dips with increasing fine fraction and size ratio.

The figure indicates that at low particle size ratios (less than approximately 0.20), the yield stress increases with increasing fine fraction. This increase can be explained by the effect of larger amounts of fine particles on the yield stress. In Chapter 17 it was shown that as the particle size decreased, the yield stress increased. The result was attributed to the greater susceptibility of small particles to aggregation which leads to the structure formation. The

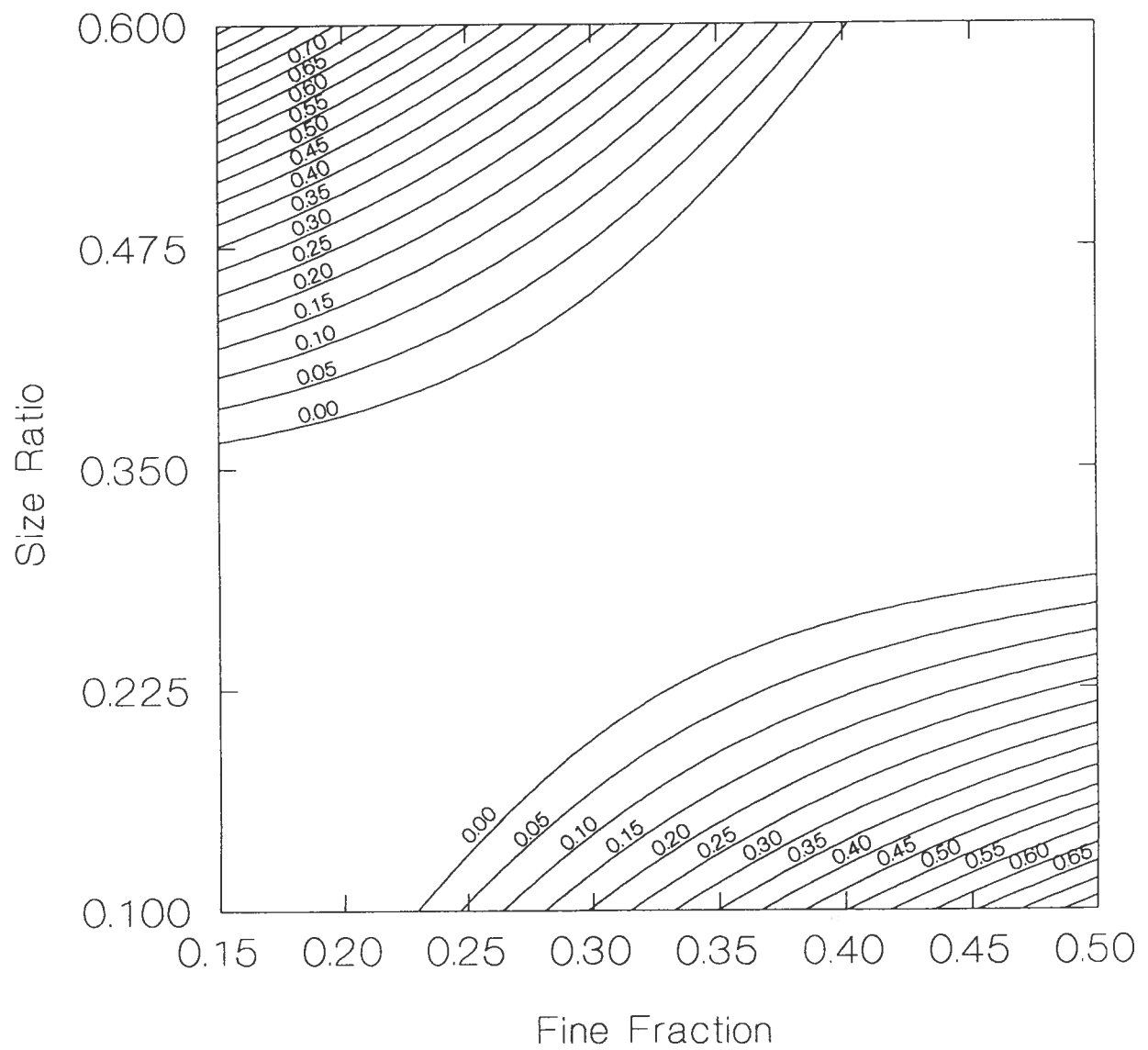


Figure 18.4 Response contours of the Casson yield stress (Pa.) as a function of size ratio and fine fraction (magnetite volume solids content = 0.15).

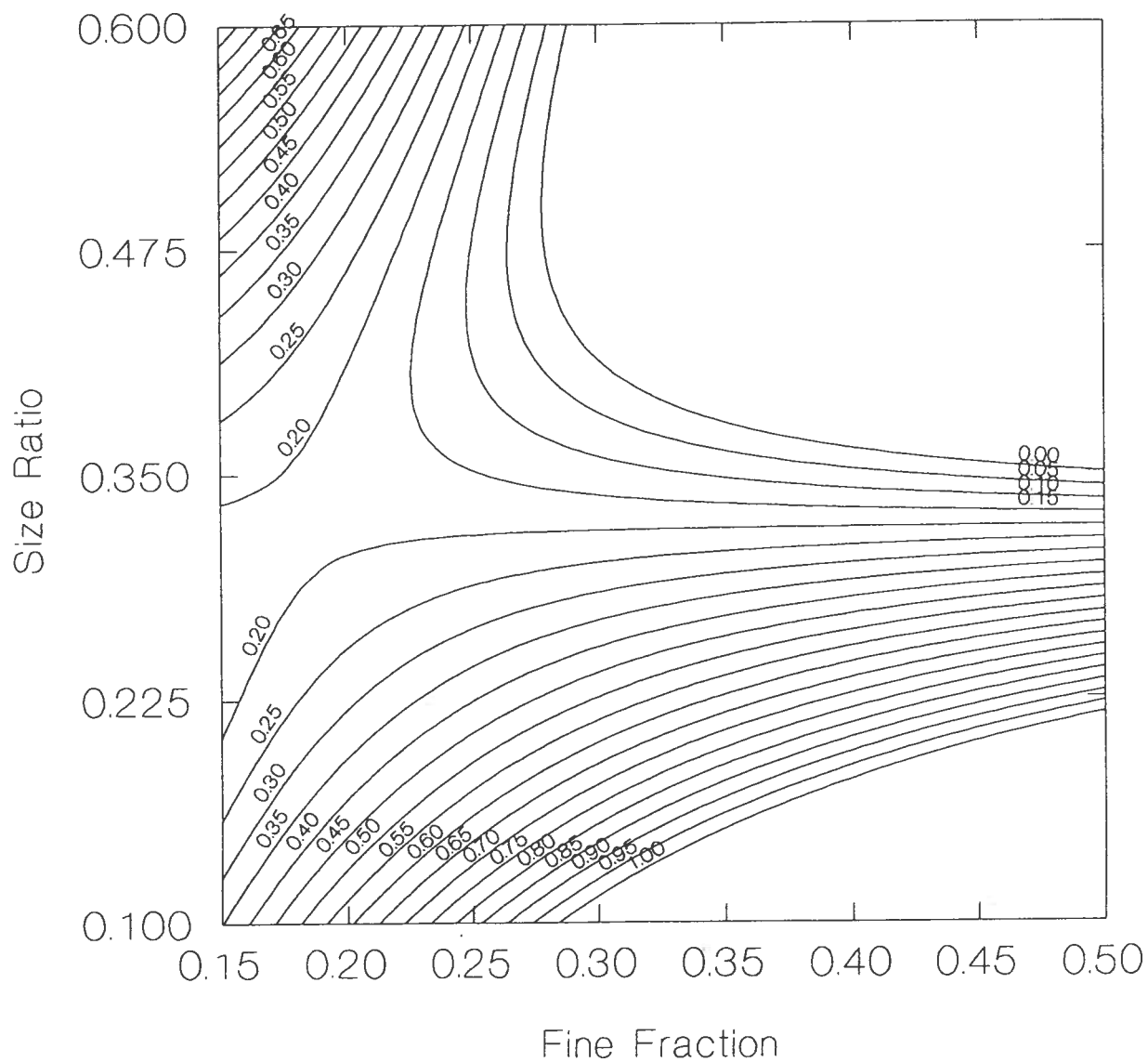


Figure 18.5 Response contours of the Casson yield stress (Pa.) as a function of size ratio on fine fraction (magnetite volume solids content = 0.25).

magnetite particle aggregation is believed to result from remnant magnetism. Although the particles were demagnetized, it is difficult to demagnetize very small particles ($\sim 10 \mu\text{m}$) since such particles may contain only a few magnetic domains in which case the polarity of the particle may not be completely cancelled (Graham and Lamb, 1982).

At high particle size ratios (greater than approximately 0.30), the yield stress decreased with increasing fine fraction. In this case the particles comprising the fine fraction are relatively large ($\sim 10 \mu\text{m}$), and can therefore be demagnetized more effectively. Therefore, particle aggregation should not be as pronounced. Despite the reduction in magnetic aggregation with increasing size ratio, the suspensions still exhibit an apparent yield stress.

At high size ratio and low fine fraction levels, the suspensions are nearly mono-disperse with large particles. Since the density differential between magnetite and water is high (almost 4000 kg m^{-3}), the large magnetite particles experience large inertial forces allowing them to physically collide and dissipate energy through friction and the loss of translational and rotational momentum (Thomas, 1965, Clarke, 1967, Brenner, 1972). Laapas (1985) found that for suspensions of large particles, the suspension yield stress increased as the density difference between the particles and the suspending fluid increased as a result of these physical interactions. The apparent yield stress at high size ratios can therefore be explained by physical interactions rather than by particle aggregation.

As the fine fraction of non-aggregated small particles is increased, there is corresponding reduction in the fraction of large particles (see Equation 18.2). Therefore, the amount of energy dissipated from the large particle interactions is decreased and the yield stress decreases.

Based on the above explanations, the yield stress valley from the contour plot corresponds

to conditions for low aggregation effects and low particle inertia effects. Along a line of constant fine fraction, the yield stress is high at low size ratios due to aggregation effects. As the size ratio is increased, the yield stress decreases until it reaches the bottom of the yield stress valley after which it begins to increase due to particle inertia effects. At small particle size ratios, the particle inertia effects must therefore be quite small even if the suspension is composed of mostly large particles. It has been suggested that small particles act like ball bearings between coarse particles (Eveson, 1953, Chong et al, 1971 and Round et al, 1984), which would reduce the frictional energy dissipation. As the size ratio is increased above 0.1, the small particles begin to interact with the coarse particles (Fidleris and Whitmore, 1961) and therefore the ball bearing effect is reduced. In addition, bimodal suspensions have been described as a suspension of large particles in a liquid with the viscosity and density of the fine particle suspension (Fidleris and Whitmore, 1961). In this case, the effective density differential between the large magnetite particles and fine particle suspension would decrease. As found by Laapas (1985), a decrease in density differential would result in a lower yield stress.

For dense media separation it is desirable to minimize the yield stress of a suspension, since the yield stress contributes to its apparent viscosity. From the results, at low solids contents the yield stress is low and is not greatly affected by the size distribution. At high solids contents, particle size ratios and fractions of fine particles can be set to reduce the yield stress. For the tested particle size distributions, the results indicate that particle size ratios between approximately 0.2 and 0.3 correspond to a low yield stress.

18.5.2 Effect of Particle Size Distribution on the Casson Viscosity

Over the tested ranges of the variables, the Casson viscosity was found to depend on the ratio of mean particle sizes and solids content but was not dependent on the fine fraction (Table 18.4). A contour plot of the Casson viscosity against solids content and size ratio shows that a maximum viscosity exists along a ridge that rises along a diagonal line with increasing solids content and size ratio (Figure 18.6).

The Casson viscosity represents the suspension viscosity at high shear rates. At such high shear rates, the magnetite particles are expected to be dispersed due to the shear conditions. Therefore particle aggregation is not considered to be significant. Hydrodynamic effects, electroviscous effects and inertial effects can, however, be important.

The plot indicates that for a low suspension solids content (less than approximately 15%), decreasing the size ratio increases the Casson viscosity. Since the coarse fraction size is fixed, decreasing the size ratio corresponds to a decrease in the particle size of the fine fraction. As the size of fine particles is decreased, the specific particle surface area of the suspension increases. Since the magnitudes of hydrodynamic effects (Yen, 1968, Yucel and Hughes, 1984) and electroviscous effects (Goodwin, 1981) are proportional to the specific surface area, the viscosity increases with decreasing particle size ratio.

Conversely, at a high suspension solids content (greater than approximately 20%), increasing the particle size ratio results in an increase in the Casson viscosity. Since the magnetite is much denser than the water, at the high shear rates, solids contents and size ratios, particles can collide and dissipate energy as a result of friction and losses of translational and

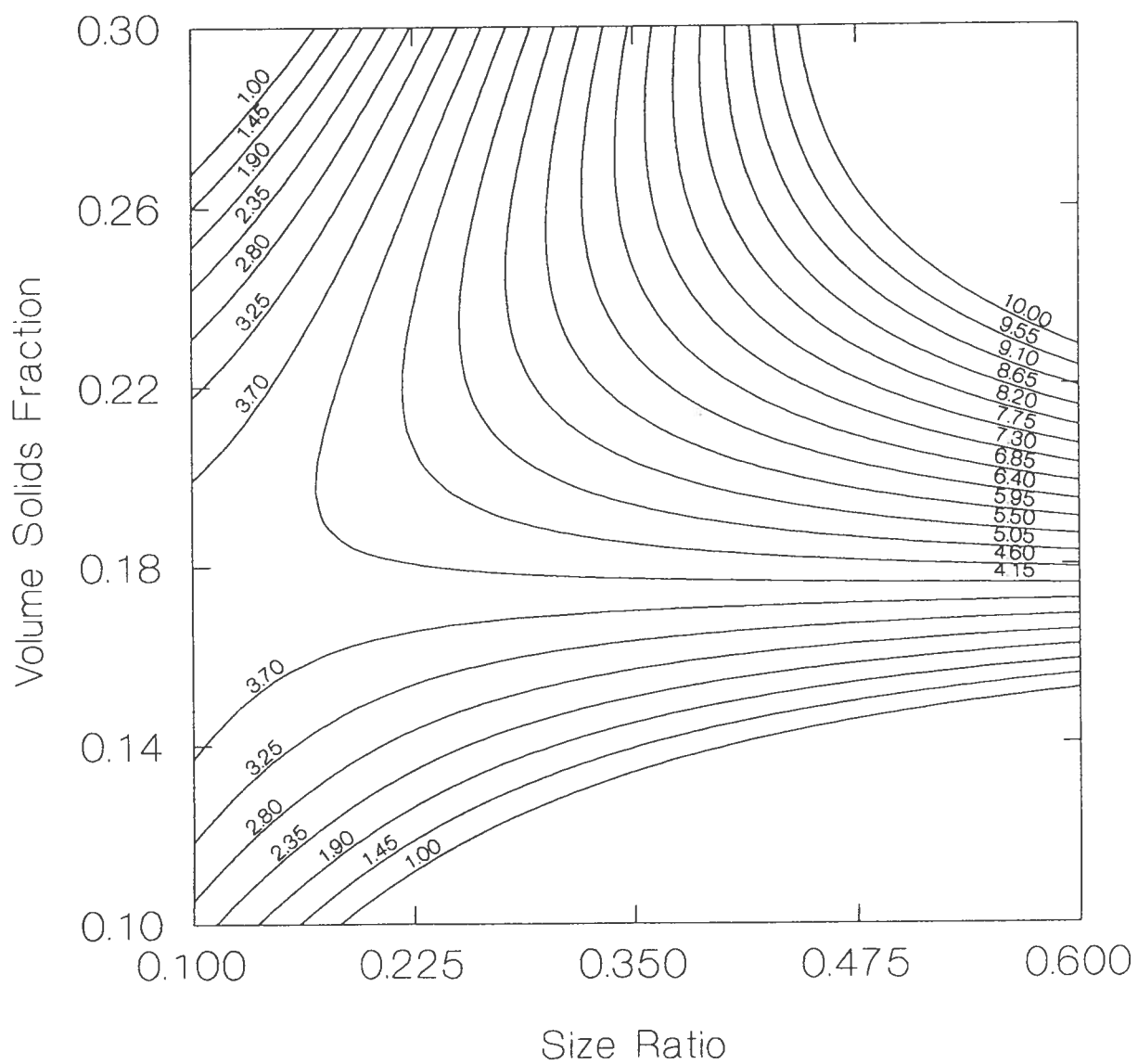


Figure 18.6 Response contours of the Casson viscosity (mPa.s) as a function of size ratio and volume solids fraction.

rotational momentum (Clarke, 1967, Brenner, 1972). It has been shown that physical interactions between the small particles and large particles become more significant as the size ratio is increased (Fidleris and Whitmore, 1961), resulting in an increased viscosity.

Based on the above explanations, the maximum Casson viscosity along the rising ridge corresponds to conditions of high inertial, hydrodynamic and electroviscous effects. To reduce the high shear rate viscosity of magnetite dense media at low solids contents (less than approximately 15%), the particle size ratio should be as large as possible to minimize hydrodynamic effects and electroviscous effects. To reduce the viscosity at high media densities (greater than approximately 20%), the particle size ratio should be as small as possible to minimize the contribution of the small particles to the inertial effects.

From previous investigations with bimodal suspensions, Klein et al (1988) showed that the plastic viscosity (Bingham plastic equation) was a minimum at a fine fraction of approximately 0.30. No such minimum was observed for the Bingham yield stress which gradually increased with increasing fine fraction. From the experiments carried out in this study, a minimum Casson yield stress occurred along a line of increasing fine fraction and size ratio and it was found that over the tested levels of variables, the Casson viscosity was not dependent on the fine fraction. The apparent discrepancy can be explained by the different fits of the two equations to the flow curves. It should be noted that the Casson equation fits the rheological curves better than the Bingham equation. In particular, the minimum obtained for the plastic viscosity corresponds to the minimum in the Casson yield stress rather than to a minimum in the Casson viscosity.

18.5.3 Effect of Particle Size Distribution on the Settling Rate

Table 18.4 indicates that each of the variables, size ratio, fine fraction and solids content, affected the settling rate of the suspensions. The table shows that second order terms and interactions between the variables influenced the settling rate. To illustrate how the settling rate is affected by the variables, contour plots of settling rate as a function of fine fraction and size ratio at solids contents of 12.5% and 17.5% are presented in Figures 18.7 and 18.8, respectively.

The plots show that the suspension settling rate is lowest when the size ratio is small and the fine fraction is large. The effect of small particles on the settling rates of poly-disperse suspensions has been explained in terms of the "carrier" properties provided by small particles to large particles (Selim, 1983, Williams and Amarasinghe, 1989). Specifically, the fine particles and water behave like a dense viscous liquid to the large particles and thereby decrease the settling rate.

As discussed in previous sections, the fine magnetite particles can form a loose aggregated structure as a result of remnant magnetism. The existence of a continuous structure depends on the size and solids fraction of fine particles. At sufficiently high fraction of small particles, this structure can support the larger particles and thereby reduce their settling rate. The existence of a structure is supported by the relationship between the yield stress and the settling rate (Figure 18.9). The figure shows the same type of relationship that was observed in Chapter 17. Specifically, a non-linear relationship exists between the settling rate and the yield stress in which a low yield value corresponds to a high settling rate and vice versa. This relationship indicates that the settling rate is affected by the same structure that is responsible for the yield stress.

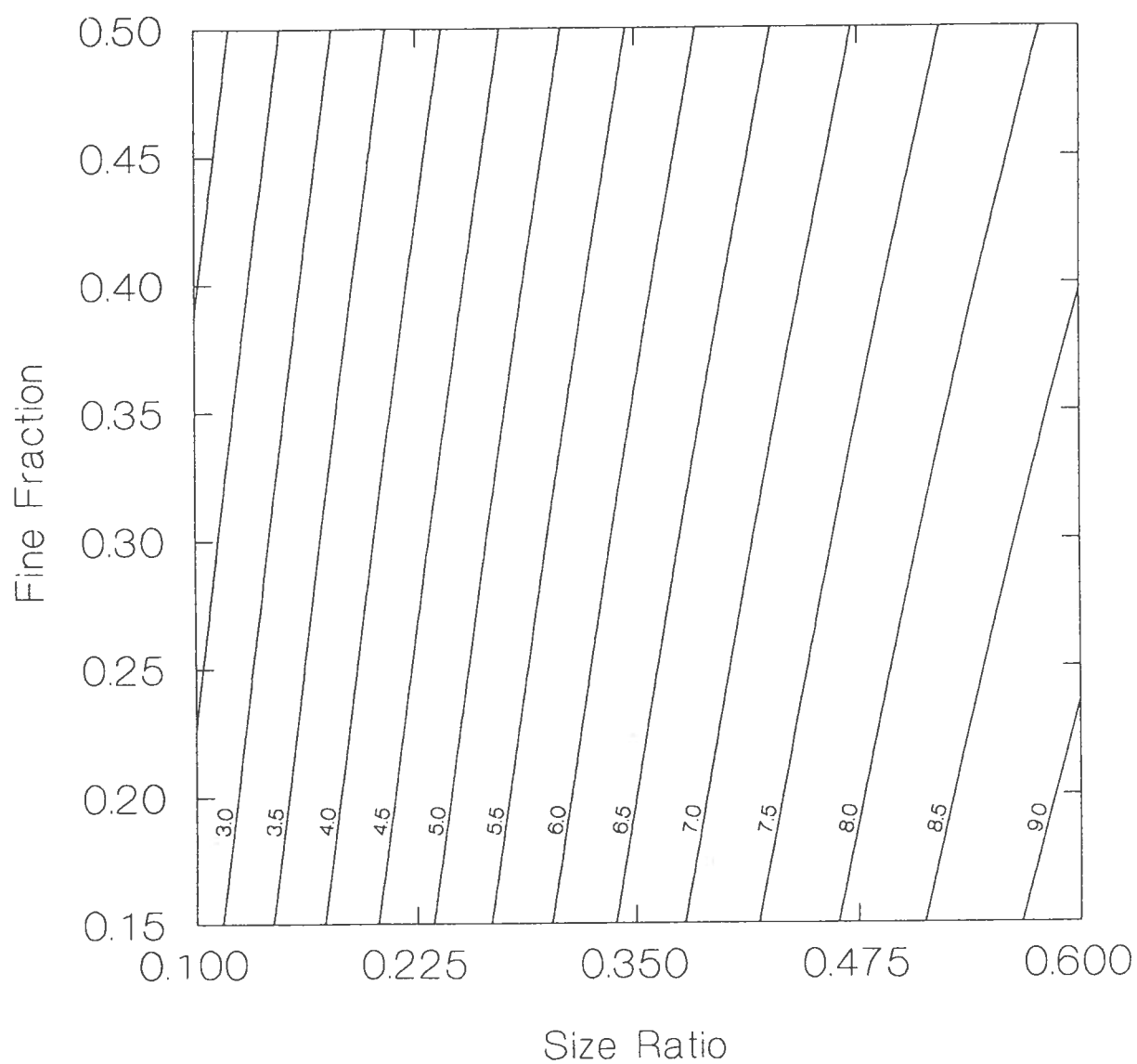


Figure 18.7 Response contours of the settling rate (cm min^{-1}) as a function of size ratio and fine fraction (magnetite volume solids fraction = 0.125).

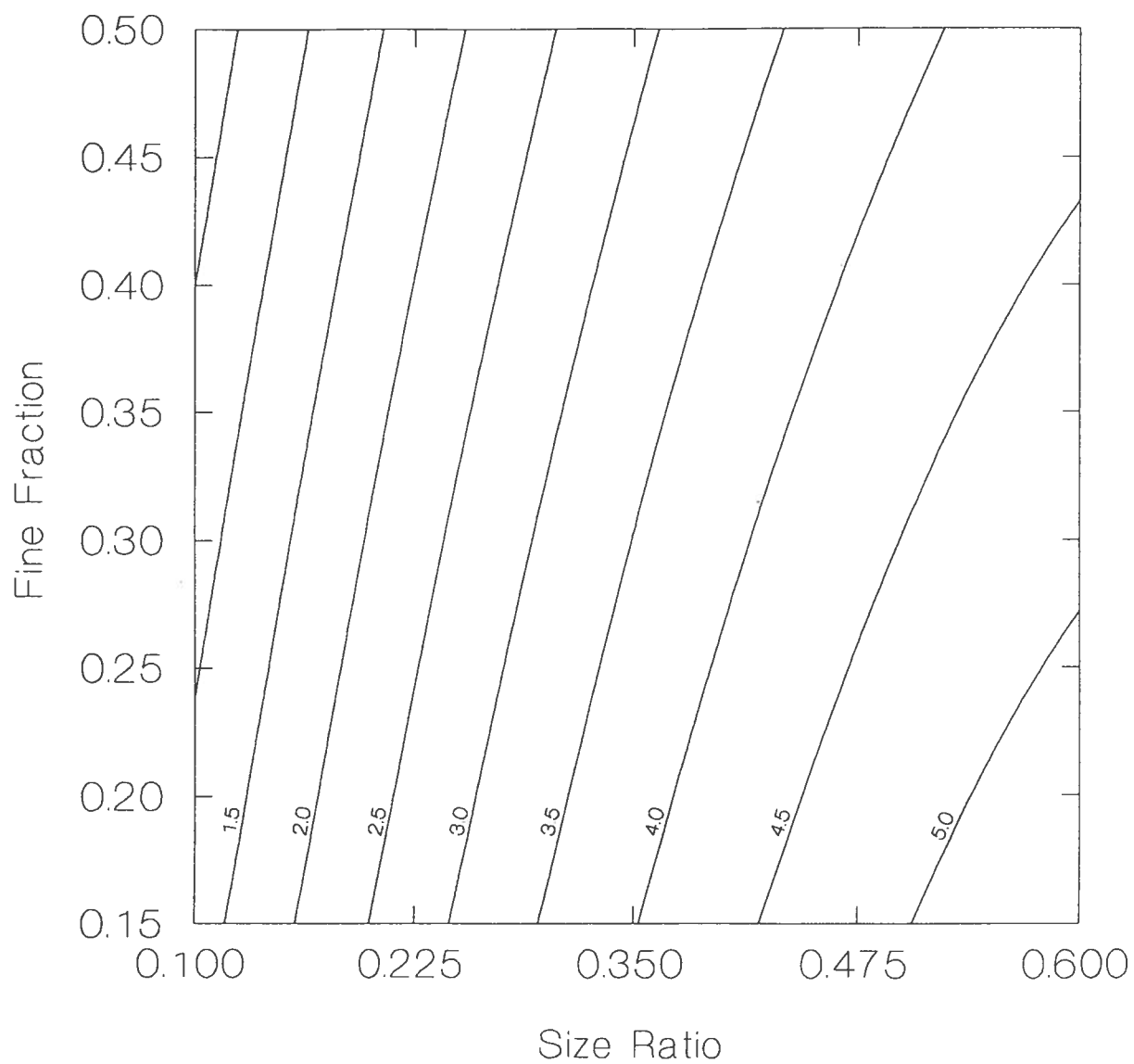


Figure 18.8 Response contours of the settling rate (cm min^{-1}) as a function of size ratio and fine fraction (magnetite volume solids fraction = 0.175).

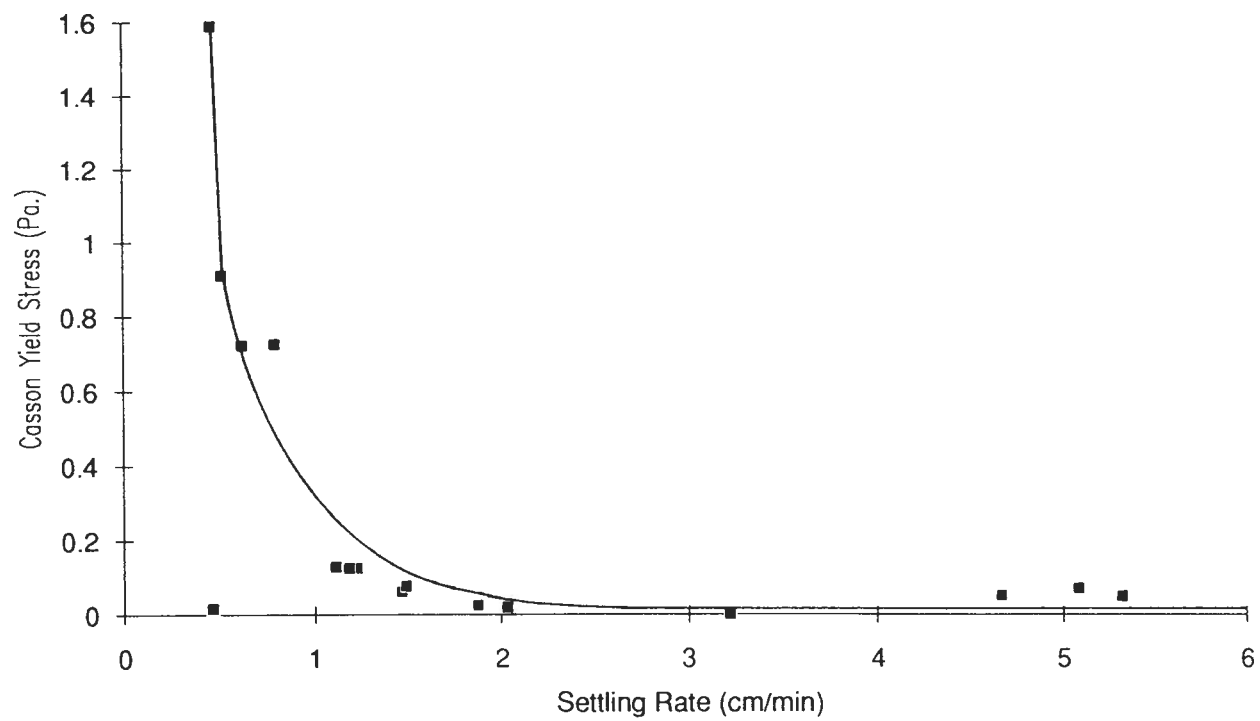


Figure 18.9 Relationship between the Casson yield stress and the settling rate.

It is worth noting that no relationship was found between the viscosity term and the settling rate. It is therefore apparent that the relationship between the apparent viscosity and the stability of magnetite dense media that is referred to in the literature (Davis, 1987, Napier-Munn, 1990) can be attributed to the contribution of the yield stress to the apparent viscosity.

Examination of the contour lines in Figures 18.7 and 18.8 indicates that the size ratio has a more significant effect than the fraction of small particles. This result suggests that to achieve a good media stability, either a small amount of very fine particles, or significantly larger amount of slightly larger particles, can be added to the medium. Therefore, to improve media stability it may be possible to add small amounts of very fine magnetite to the dense medium circuit periodically.

18.5.4 Optimization of Medium Properties

As discussed in the previous sections, particle size distribution can be manipulated to control the properties of magnetite dense media. Optimum media properties refer to a medium with a low settling rate, a low Casson yield stress and a low Casson viscosity. For coal preparation, medium solid contents range from 10% to 20% over which range rheological properties must be compromised to ensure adequate stability. At higher medium densities used for the separation of minerals, the medium can be excessively viscous while the stability is of lesser concern. The results indicate that the medium properties can be improved by manipulating the particle size distribution of the dense medium.

The results imply that the medium stability can be improved at low medium densities by

the addition of a small amount of very fine magnetite particles. Alternatively, the same stability can be produced by adding significantly larger amounts of slightly larger particles (15 μm). The results showed that adding a small amount of very small magnetite particles ($\sim 10 \mu\text{m}$) did not greatly increase the Casson yield stress. However, adding larger amounts of slightly larger particles (15 μm) increased the yield stress substantially. Therefore to improve the medium stability without adversely affecting the yield stress, it is recommended to add a relatively small amount of very fine magnetite to the medium.

At high medium densities (2000 kg m^{-3}), the suspension yield stress is lowest for the size ratio range of 0.20 to 0.35. However, over this range of size ratios, the Casson viscosity is quite high. To reduce the viscosity, lower size ratios should be used (Figure 18.6) which increases the yield stress (Figure 18.5). Therefore, at high medium densities there must be a compromise between the Casson yield stress and the Casson viscosity.

18.6 Conclusions

Experiments were performed to investigate the effect of particle size distribution on the properties of magnetite dense media. The suspensions exhibited shear thinning rheological properties that were modelled with the Casson equation.

Models were developed for the suspension settling rate, the Casson yield stress and the Casson viscosity as a function of the solids content and the bimodal size distribution parameters, mean size ratio and fine fraction. It was found that second order models with interaction terms were required to fit the responses to the variables.

The Casson yield stress was found to depend on each of the variables; size ratio, fine fraction and solids content. At a given solids content, it was found that a minimum yield stress existed that is a function of the size ratio and the fine fraction. Contour plots of yield stress as a function of size ratio and fine fraction showed that the minimum yield stress occurred along a valley with a trend corresponding to increasing size ratio and fine fraction. At size ratios of approximately 0.2 to 0.3, the fine fraction had only a small effect on the yield stress. Increasing the solids concentration enhanced the effect of size distribution on the yield stress.

The Casson viscosity was found to depend on the size ratio and solids content; however, for the investigated levels of the variables, the viscosity did not depend on the fine fraction. A contour plot of viscosity as a function of the size ratio and solids content, showed that a viscosity maximum exists along a ridge. The trend of the ridge corresponded to increasing size ratios and solids contents.

The settling rate was found to depend on each of the variables; size ratio, fine fraction and solids content. Contour plots at given solids contents revealed that the settling rate decreased (stability improved) with decreasing size ratio and increasing fine fraction. The results indicated that the size ratio affected the settling rate more than the fine fraction. At low solids contents the effect of size ratio was very pronounced indicating that media stability could be easily improved by adding a small amount of very fine magnetite particles.

It was found that the settling rate and the Casson yield stress are interrelated in a non-linear manner. A suspension with a high yield stress has a low settling rate and vice versa. The relationship can be explained by the existence of a structure in the suspension.

CHAPTER 19: CONCLUSIONS AND RECOMMENDATIONS FOR FURTHER WORK

19.1 Conclusions

The conclusions drawn from the experimental programs carried out in the thesis are as follows.

1. Settling tests on suspensions of magnetite particles with solids contents typically found in dense media indicated that:

i. Magnetite suspensions exhibit bulk (hindered) rather than differential settling properties.

ii. The bulk settling properties were characterized by the presence of four zones (from top to bottom): a supernatant, a transition zone, a constant density zone and a sediment. The constant density zone has a solids content that is approximately equal to that of the initial suspension.

iii. The mudline settling rate of a magnetite suspension is very close to the settling rate of the transition zone - constant density zone interface. Since the extent of the constant density zone and the rate at which it diminishes in size characterizes the medium stability, the mudline settling rate provides a good indication of the settling stability.

2. A rheometer fixture was developed to measure the rheological properties of settling suspensions. The fixture is a modified double gap concentric cylinder cup and bob arrangement that attaches to rotational viscometers. It was designed for suspensions exhibiting zone settling properties by positioning the bob in the constant density zone during the rheological

measurements. The design also accounts for typical measurement errors associated with wall slip and end effects and it is surrounded by a temperature controlled water jacket so that the suspension temperature can be controlled. The fixture is an improvement over existing devices since no undefined shearing is required to maintain a homogeneous suspension composition during rheological measurements.

Measurement procedures were developed to account for non-Newtonian shear rate effects, bob inertia effects and high shear rate limitations due to turbulence. The new device was used to characterize the rheological properties of magnetite suspensions and to study the effects of suspension variables on these rheological properties. More recently it has been used to measure the rheological properties of quartz suspensions and of various sulphide mineral suspensions.

3. Rheological measurements on magnetite suspensions with compositions found in dense media indicated that:

i. Magnetite dense media exhibits shear thinning flow properties with an apparent yield stress.

ii. The Casson flow curve model, which is a simple two parameter equation, can be used to characterize the flow behaviour of magnetite suspensions. The model was found to fit the flow curves better than other well known models including the Herschel Bulkley, Carreau and Cross models.

iii. Magnetite suspensions exhibit thixotropic properties that are enhanced by magnetizing the suspension particles.

iv. The apparent yield stress, the thixotropic properties and zone settling properties exhibited by magnetite suspensions suggest that a structure exists in these suspensions. The

structure is believed to result from particle aggregation that can be attributed to remnant particle magnetism.

v. The Bingham plastic equation could not fit the curvature of the flow curve data at low shear rates and was therefore not considered to be a suitable model. The review of the literature indicated that, because the Bingham equation cannot fit the curvature, exhibited by many suspensions, at low shear rates the model over estimates the yield value. However, yield values determined from the Casson equation compared well to those determined using direct measurement procedures.

4. From a statistically designed experimental program, the effects of physico-mechanical parameters (magnetite solids content and particle size), physico-chemical parameters (pH, sodium silicate, carboxymethyl cellulose and demagnetization) and contaminants (coal fines, kaolinite and bentonite) on measured settling and rheological properties were investigated. For a diverse set of parameter conditions, the results of the experimental program revealed that:

- i. The suspensions exhibit thinning flow behaviours and have an apparent yield stress.
- ii. The flow behaviours can be accurately modelled using the Casson equation which was found to provide a better fit to all twenty sets of flow curves than the Herschel Bulkley, Carreau and Cross models.
- iii. The Casson yield stress was influenced significantly by most of the suspension variables while the Casson viscosity was affected by only a few of the parameters indicating that the yield stress term is the most controllable rheological property.
- iv. The Casson yield stress dominated the viscous properties of the suspension. In

particular, the contribution of the Casson yield stress to the apparent viscosity is significantly greater than the contribution from the Casson viscosity term.

v. The suspension parameters that influenced the yield stress term most, also had the greatest effect on the mudline settling rate. It was revealed that the yield stress and the settling rate are inversely related such that when the yield stress is high the setting rate is low and vice versa.

vi. Based on the magnitudes of the effects on the measured responses, the magnetite solids content, particle size and pH are the most significant parameters.

vii. Increasing the solids content resulted in an increased Casson yield stress and a decreased settling rate while the Casson viscosity was not significantly affected. Increasing the particle size decreased the Casson yield stress, increased the settling rate and had no effect on the Casson viscosity. An interaction effect between solids content and particle size also influenced the yield stress and settling rate responses.

viii. Since changes in pH did not alter the settling rates of pure magnetite suspensions, its effect on the suspensions in the experimental program was attributed to its influence on clay particle coagulation and its interactions with sodium silicate and carboxymethyl cellulose.

ix. Increasing the pH decreased the Casson yield stress and increased both the settling rate and Casson viscosity. The results can be explained as follows. In the acidic and neutral pH range clay particles coagulate to form a structure that contributes to the yield stress and prevents particle settling. In the basic pH range, the clay particles disperse resulting in a lower structural state which corresponds to a lower yield stress and allows particles to settle. In addition, with increasing pH electrostatic repulsive forces between particles may enhance the contributions of

electroviscous effects to the Casson viscosity.

x. At high pH, the dispersants, sodium silicate and carboxymethyl cellulose, became more effective. The interaction effect between pH and the dispersing agents revealed that by jointly increasing the pH and dispersant dosages the Casson yield stress decreased and the settling rate and Casson viscosity increased. The carboxymethyl cellulose influenced the suspension properties more than the sodium silicate.

xi. Demagnetization improves media properties by decreasing the Casson yield stress and increasing the settling rate but does not significantly influence the Casson viscosity.

5. The effects of bimodal particle size distribution on the rheological and settling properties of magnetite suspensions were investigated using a statistically designed experimental program. The findings are as follows:

i. The determined responses, Casson yield stress and settling rate are affected by the particle size distribution parameters which include the ratio of mean particle sizes of the two size fractions and the fraction of the solids that are fine particles. For the levels of the size distribution variables investigated, the Casson viscosity was influenced by the particle size ratio but not by the fine fraction. The effects of size distribution on the rheological properties was more pronounced at a high solids content.

ii. The Casson yield stress was modelled using a second order equation as a function of the size ratio, the fine fraction and the solids content. The model revealed that a minimum apparent yield stress exists along a line of compositions corresponding to increasing size ratios and fine fractions. The minimum is most pronounced over the size ratio range of 0.2 to 0.35. At a high suspension solids content, the effects of size distribution on the yield value are much

more pronounced.

iii. The Casson viscosity was found to be affected by the size ratio and solids content in a non-linear manner that was modelled using a second order equation. The model indicated that the viscosity term was a maximum along a line of composition corresponding to increasing size ratio and solids content.

iv. The mudline settling rate was modelled as a function of size ratio, fine fraction and solids content using a second order equation. The model revealed that the settling rate decreased in a non-linear manner with increasing size ratio and fine fraction. The size ratio was shown to be more significant than the fine fraction. In particular, the results indicated that stability of bimodal suspensions can be improved by using a small fine fraction of particles with a very small size ratio or by using a much greater fine fraction of particles with slightly larger size ratio.

v. From the results of the experimental program it was found that the Casson yield stress and the settling rate are inversely in the same manner as was indicated from investigations into the effects of various parameters on the medium properties. Specifically, when the suspension yield value is high the settling rate is low and vice versa. This result suggests that the relationship between media viscosity and stability that is referred to in the literature can be more accurately attributed to the yield stress - settling rate relationship.

19.2 Recommendations For Further Work

1. The test work carried out for this thesis is part of ongoing research in the Department of Mining and Mineral Process Engineering to study the dense media separation process. The results of this thesis should be applied to this research. Specifically, the results should be used to develop models that relate separation performance to accurately characterized rheological and settling properties. From models of this type, the medium properties that are important to the separation performance could be assessed using bench scale test work. Once such relationships exist, the effects of various parameters (magnetite particle size, pH, etc.) on separation performance can be assessed.
2. From electrophoretic mobility (EPM) measurements, it was found that the magnetite sample exhibited an anomalous iso-electric point. Since surface chemical interactions with other particles and with various surfactants may be important to the medium rheology and stability, this anomalous result should be investigated. Specifically, measurements were made using unground material which may have been coated with precipitates produced from weathering. Therefore, EPM measurements should be made using a sample with freshly ground surfaces.
3. It was found that magnetite suspensions exhibit zone settling properties characterized by the existence of a constant density zone. While the solids content of this zone was constant through its vertical extent, tests were not performed to determine the size distribution at different levels. To confirm that differential settling does not occur, such a study should be carried out.
4. To investigate the implications of the shear thinning flow properties and the apparent yield stress to the dense medium separation process, there is a need to know how these properties

influence particle settling. Specifically, tests should be performed to determine if the apparent yield value affects particle settling through its contribution to the apparent viscosity or if it is a measure of an additional stress that must be overcome before a particle can settle. Test that relates drag coefficients to the Casson model coefficients would be useful. Investigations should also be carried out to provide better estimates of the effective shear rates experienced by coal particles in the separator.

5. Due to the potential implications of a yield stress on separation performance, test work should be carried out to determine if magnetite dense media exhibits a true yield value. This could be tested by using direct yield stress measurement procedures such as the vane method (see Section 6.3).

6. The inverse relationship between the Casson yield stress and the settling rate was explained by the presence of a structure that influence both medium properties. Test work should be performed to provide more evidence of the structure. Direct measurements of the yield stress as recommended above would provide additional evidence.

7. Results of the experimental test work indicated that the properties of magnetite dense media can be controlled by manipulating various parameters. Further investigations into the effects of many of these parameters (particle size, magnetization and the additions of dispersants) is warranted. Specifically:

i. The addition of C.M.C. was found to decrease the settling rate of pure magnetite suspensions; however, no experiments were performed to determine the effect of C.M.C. on the rheological properties of pure magnetite suspensions.

ii. The rheological and settling test results could be explained by the presence of a

structure resulting from magnetic aggregation of particles. Despite demagnetization, the suspensions still exhibited an apparent yield stress, thixotropic properties and zone settling properties. The results indicated that demagnetization was not complete which was attributed to the difficulties associated with demagnetizing fine magnetite particles. To confirm this explanation, it is recommended to investigate the effect of demagnetization on fine magnetite particles.

iii. To achieve good stability and rheological properties in dense media, it has been recommended to use fine magnetite particles for low media densities and large particles for high media densities. This practice is supported by the experimental results which showed that media properties are influenced by an interaction effect between solids content and particle size. More detailed information concerning this interaction effect may assist in determining optimum particle sizes for specific media densities.

8. Experiments carried out to investigate the effect of particle size distribution on media properties indicated that the size distribution can be manipulated to optimize media properties. Further experiments are required to more accurately define particle size distributions corresponding to optimum media properties.

9. This work emphasizes the importance of accurately characterizing the rheological properties of magnetite suspensions so that the effects of media parameters can be understood. The rheometer fixture developed to measure the rheological properties of settling suspensions could also be used to characterize the rheological properties of other industrially important unstable suspensions.

REFERENCES

- Aarnio, A.A., Laapas, H.R., 1988, "Rheological Properties of Finely Ground Quartz and Feldspar Slurries", Proc. 10th Int. Congr. on Rheol., 1, P.H. Uhlher, ed, Australian Society of Rheology, Sydney, 119-121.
- Ahuja, S.K., Isganitis, L., 1988, "Viscoelasticity of Non-aqueous Suspensions", Proc. 10th Int. Congr. on Rheol., 1, P.H. Uhlher, ed, Australian Society of Rheology, Sydney, 131-3.
- Al-Fariss, T., Pinder, K.L., 1987, "Flow Through Porous Media of a Shear-Thinning Liquid with Yield Stress", Can. J. Chem. Eng., 65, 391-406.
- Alderman, N.J., Ram Babu, D., Hughes, T.L., Maitland, G.C., 1988, "The Rheological Properties of Water-Based Drilling Fluids", Proc. 10th Int. Congr. on Rheol., 1, P.H. Uhlher, ed, Australian Society of Rheology, Sydney, 140-2.
- Allen, T., 1990, Particle Size Measurement, 4th ed., Chapman and Hall, New York, 806.
- Alessandrini, A., Kikic, I., Lapasin, R., 1983, "Rheology of coal suspensions", Rheol. Acta, 22, 500-4.
- Anon, 1985, "The Testing of Magnetite for Use in Coal Preparation", Draft Proposal ISO/DP 8833, 22pp.
- Aplan, F.F., Spedden, H.R., 1964, "Viscosity Control in Heavy-Media Suspensions", Proc. 7th Int. Min. Proc. Congr., N. Arbiter, ed, Gordon & Breach, New York, 103-113.
- Atlas, H., Casassa, E.Z., Parfitt, G.D., Rao, A.S., Toor, E.W., 1985, "The Stability and Rheology of Coal/Water Slurries", 10th Ann. Powder & Bulk Solids Conf. Proc., Rosemont, Ill., University of Microfilm International, Ann Arbor, Michigan, 771-8.
- Berg, R.H., 1958, "Electronic Size Analysis of Subsieve Particles by Flowing Through a Small Liquid Resister", Special Technical Publication, 234, Am. Soc. for Testing Materials.
- Berghofer, W., 1959, "Konsistenz und Schwertrubeaufbereitung", Bergbauwissenschaften, 6(20), 493-504, 533-541.
- Boger, D.V., Sarmiento, G., Tiu, C., Uhlherr, P.H.T., 1978, "Flow of Mineral Slurries", The Aus. IMM Conference, North Queensland, 291-8.
- Bradley, D., The Hydrocyclone, Pergamon Press, New York
- Brenner, H., 1972, "Suspension Rheology", Progress in Heat and Mass Transfer, W. Schowalter, ed, Pergamon Press, New York, 89-129.

- Brown, J.P., Pinder, K.L., 1971, "Time Dependent Rheology of Artificial Slurries", Can. J. Chem. Eng., 49, 38-43.
- Burch, E, Stone, C, 1985, "Feeding to Zero: Island Creek's Experience in Kentucky", Coal Age, 1, 66-70.
- Burt, R.O., 1984, Gravity Concentration Technology, Elsevier, Amsterdam, p. 567.
- Cann, R.M., 1979, Geochemistry of Magnetite and the Genesis of Magnetite-Apatite Lodes in the Iron Mask Batholith, British Columbia, M.Sc Thesis, University of British Columbia.
- Carreau, P.J., 1972, "Rheological Equations from Molecular Network Theories", Trans. Soc. Rheology, 16(1), 99-127.
- Carreau, P.J., De Kee, D., 1979a, "Review of Some Useful Rheological Equations", Can. J. Chem. Eng., 57, 3-15.
- Carreau, P.J., De Kee, D., 1979b, "An Analysis of the Viscous Behaviour of Polymeric Solutions", Can. J. Chem. Eng., 57, 135-140.
- Castillo, C., Williams, M.C., 1979, "Rheology of Very Concentrated Coal Suspensions", Chem. Eng. Commun., 3, 529-547.
- Casassa, E.Z., Parfitt, G.D., Rao, A.S., Toor, E.W., 1984, "The Effect of Surface Active Additives on Coal/Water Slurry Rheology", ASME Spec. Publ. 84-WA/HT-96, 10pp.
- Casson, N., 1959, "A Flow Equation for Pigment-oil Suspensions of the Printing Ink Type", Rheology of Disperse Systems, C.C. Mill, ed, Pergamon Press, New York, 84-104.
- Chakravarti, A.K., Chattopadhyay, J., Sarkar, G.G., Lahiri, A., 1958, "A Study of the Properties of Some Suspensions Suitable for Use in Dense Media Coal Washing", Ind. Min. J., 6, 1-11.
- Chance, T.M., 1924, "A New Method of Separating Materials of Different Specific Gravities", Trans. AIME, 70, 740-749.
- Chaston, R.R.M., Napier-Munn, T.J., 1974, "Design and Operation of Dense-medium Cyclone Plants for the Recovery of Diamonds in Africa", J. S. Afr. Inst. Min. Met., 75(1), 120-133.
- Chen, Z.Q., Xin, Y.Ch., Lu, Ch.X., 1988, "Negative thixotropic behaviour of montmorillonite and hydrolyzed polyacrylamide system", Progress and Trends in Rheology II, Prague, H. Giesekus, ed, Springer-Verlag, New York, 328-9.

- Cheng, D.C-H., 1971, "The Characterization of Thixotropic Behaviour", Warren Spring Laboratory, LR 157(MH), 29pp.
- Cheng, D.C-H., Richmond, R.A., 1978, "Some observations on the rheological behaviour of dense suspensions", Rheol. Acta., 17, 446-453.
- Cheng, D.C-H., 1980a, "Sedimentation of suspensions and storage stability", Chem. and Ind., 5, 407-414.
- Cheng, D.C-H., 1980b, "Viscosity-concentration equations and flow curves for suspensions", Chem. and Ind., 5, 403-6.
- Cheng, D.C-H., 1984, "Further Observations of the Rheological Behaviour of Dense Suspensions", Powder Tech., 37, 255-273.
- Cheng, D.C-H., 1985, "Yield Stress: A Time-dependent Property and How to Measure It", New Techniques in Experimental Rheology, Reading, England, Brit. Soc. of Rheol. Conf., 14pp.
- Cheng, D.C-H., 1988, "High Shear Limitations in Viscometers", Proc. 10th Int. Congr. on Rheol., 1, Sydney, P.H. Uhlherr, ed, Australian Society of Rheology, 250-3.
- Chong, J.S., Christiansen, E.B., Baer, A.D., 1971, "Rheology of Concentrated Suspensions", J. Appl. Polymer Sci., 15, 2007-2021.
- Clarke, B., 1967, "Rheology of Coarse Settling Suspensions", Trans. Inst. Chem. Eng., 45, T251-6.
- Collins, B., Napier-Munn, T.J., Sciarone, M., 1974, "The production, properties, and selection of Ferrosilicon powders for heavy-medium separation", J. S. Afr. Inst. Min. and Met., 12, 103-119.
- Collins, D.N., Turnbull, P., Wright, R., Ngan, W., 1983 "Separation efficiency in dense media cyclones", Trans IMM, 92, C38-C51.
- Cormode, D.A., White, G.A., 1988, "Heavy media separation studies at Cominco potash", Proc. 90th An. Meet. of the CIM, Edmonton, CIM, Montreal, 25pp.
- Cross, M.M., 1964, "Rheology of Non-Newtonian Fluids: A New Flow Equation for Pseudoplastic Systems", J. Coll. Sci., 90, 417-437.
- Cross, M.M., 1969, "Kinetic Interpretation of Non-Newtonian Flow", J. Coll. Interf. Sci., 33(1), 30-5.
- Czaban, S., Parzonka, W., Havlik, V., 1988, "Non-Newtonian behaviour of kaolin suspensions",

- Progress and Trends in Rheology II, Prague, H. Giesekus, ed, Springer-Verlag, New York, 325-8.
- Davis, J.J., Lyman, G.J., 1983, "Magnetite Recovery Using a Wet Drum Separator", Proc. Australas. Inst. Min. Met., 287, 51-60.
- Davis, J.J., 1987, "A Study of Coal Washing Dense Medium Cyclones", PhD. Thesis, University of Queensland, Brisbane, 113pp.
- Davis, J.J., Wood, C.J., Lyman, G.J., 1985, "The Use of Density Tracers for the Determination of Dense Medium Cyclone Partition Characteristics", Coal Prep., 2, 107-125.
- Davis, J.J., Napier-Munn, T.J., 1987, "The Influence of Medium Viscosity on the Performance of Dense Medium Cyclones in Coal Preparation", Proc. 3rd Int. Conf. on Hydrocyclones, Oxford, P. Wood, ed, Elsevier, New York, 155-165.
- Davies, R.J., 1986, "Report on Survey of Magnetite-Medium Usage in Heavy Media Coal Cleaning", EMR Canmet.
- Davies, R.J., 1986, "Report on Plant Procedures and Magnetite Testing and Analysis", EMR Canmet.
- Dedegil, M.Y., 1986, "Drag Coefficient and Settling Velocity of Particles in Non-Newtonian Suspensions", ASME Fluids Engineering Division, 38, 9-15.
- Derjaguin, D.V., Landua, L.D., 1941, "Theory of the Stability of Strongly Charged Lyophobic Sols and of the Adhesion of Strongly Charged Particles in Solutions of Electrolytes:", Acta Physiochim, 14, USSR, p. 633-622.
- Derjaguin, D.V., 1989, "Theory of stability of colloids and thin films", Consultants Bureau, New York.
- Deurbrouck, A.W., Hudy, Jr., J., 1972, "Performance Characteristics of Coal-Washing Equipment: Dense-Medium Cyclones", USBM RI-7673, 34pp.
- DeVaney, F.D., Shelton, S.M., 1940, "Properties of Suspension Mediums for Float-and-Sink Concentration", USBM RI-3469R, 66pp.
- Doraiswamy, D., Tsao, I.L., Danforth, S.C., Beris, A.N., Metzner, A.B., 1988, "The Rheology of Ceramic Suspensions", Proc. 10th Int. Congr. on Rheol., 1, Sydney, P.H. Uhlherr, ed, Australian Society of Rheology, 300-2.
- Dreissen, H., Jennekens, H., 1982, "History of Coal Washing in Holland and Its Impact Abroad", Proc. 9th Int. Coal Prep. Congr., New Delhi, S.R.R. Rao, ed, Indian Organizing

Committee for 9th Int. coal Prep. Congr., Calcutta, 73-8.

Du Plessis, M.P., Ansley, R.W., 1967, "Settling Parameters in Solid Pipe Lining", Proc. Am. Soc. Civ. Eng. J., 93, 1-17.

Duty, R.L., Reid, W.H., 1964, "On the stability of viscous flow between rotating cylinders" J. of Fluid Mech., 20(1), 81-94.

Eilers, H., 1941, Kolloid Z.Z. Polymer, 97, p. 313.

Einstein, A., 1905, Ann. Phys., 17, p. 459.

Erten, M.H., 1964, "Investigations of the Effects of Magnetization and Demagnetization on the Settling Rate and Viscosity of Magnetite Dense Media used in Dense-Medium Coal Washeries", Habilitation Thesis, Orta Dugo Teknik Universitesi, pp. 165.

Everett, D.H., 1988, The Basic Principles of Colloid Science, The Royal Society of Chemistry, 221pp.

Eveson, G.F., 1953, "Properties of Suspensions Used in Coal Cleaning", J. Inst. Fuel, 26(152), 139-145.

Eveson, G.F., 1957, "The Viscosity of Stable Suspensions of Spheres at Low Rates of Shear", Rheology of Disperse Systems, C.C.Mill, ed, Pergamon Press, New York, 61-9.

Eveson, G.F., 1959, "A Rheological Approach to Certain Features of Dense-Medium Coal-Cleaning Plant Operation", J. Oil Colour Chem., 42, 146-179.

Farris, R.J., 1968, "Prediction of the Viscosity of Multimodal Suspensions from Unimodal Viscosity Data", Trans. Soc. Rheol., 12(2), 281-301.

Fedors, R.F., 1973, "Relationships Between Viscosity and Concentration for Newtonian Suspensions", J. Coll. Interf. Sci., 46(3), 545-7.

Fedors, R.F., 1975, "Viscosity of Newtonian Suspensions", Polymer, 16, 305-6.

Fedors, R.F., 1979a, "A Relationship between Maximum Packing of Particles and Particle Size", Powder Tech., 23, 71-6.

Fedors, R.F., Landel, R.F., 1979b, "Effect of Surface Adsorption and Agglomeration on the Packing of Particles", Powder Tech., 23, 219-223.

Fedors, R.F., Landel, R.F., 1979c, "An Empirical Method of Estimating the Void Fraction in Mixtures of Uniform Particles of Different Size", Powder Tech., 23, 225-231.

- Fern, K.A., 1952, "The Cyclone as a Separating Tool in Mineral Dressing", Trans Instn Chem Engrs, 30, 82-86.
- Ferrara R.F., 1973, "Relationships Between Viscosity and Concentration for Newtonian Suspensions", J. Coll. Interf. Sci., 46(3), 545-7.
- Ferrara, G., Schena, G.D., 1986, "Influence of contamination and type of ferrosilicon on viscosity and stability of dense media", Trans IMM, 95, C211-5.
- Ferrara, G., Schena, G.D., 1987, "Cycloning in Dense Media Separation", Proc. 3rd Int. Conf. on Hydrocyclones, Oxford, P. Wood, ed, Elsevier, New York, 101-110.
- Ferrara, G., Schena, G.D., 1988, "Design Criteria and Control Strategies for Dynamic Dense Media Separation Processes Treating Fine Ores", Proc. 16th Int. Min. Proc. Congr., E. Forsberg, ed, Elsevier, Amsterdam, 885-904.
- Ferrini, F., Ercolani, D., de Cindio, B., Nicodemo, L., Nicolais, L., Ranaudo, S., 1979, "Shear viscosity of settling suspensions", Rheol. Acta, 18(2), 289-296.
- Ferrini, F., Battarra, V., Donati, E., Piccinini, C., 1984, "Organization of Particle Grading for High Concentration Coal Slurry", Hydrotransport 9, Rome, BHRA Fluid Engineering, 75pp.
- Fidleris, V., Whitmore, R.N., 1961, Rheol. Acta., 1, 4-6.
- Firth, B.A., Hunter, R.J., 1976, "Flow Properties of Coagulated Colloidal Suspensions. III. The Elastic Floc Model", J. Coll. Interf. Sci., 57, 266-275.
- Fourie, P.J.F., Van Der Walt, P.J., Falcon, L.M., 1980, "The beneficiation of fine coal by dense-medium cyclone", J. S. Afr. IMM, 80, 357-361.
- Frankel, N.A., Acrivos, A., 1967, "On the viscosity of a concentrated suspension of solid spheres", Chem. Eng. Sci., 22, 847-853.
- Friend, J.P., Kitchener, J.A., 1973, "Some Physico-chemical Aspects of the Separation of Finely Divided Minerals by Selective Flocculation", Chem. Eng. Sci., 28, 1071-1080.
- Furnas, C.C., 1931, "Grading Aggregates. I. Mathematical Relations for Beds of Broken Solids of Maximum Density", Ind. and Eng. Chem., 23(9), 1052-1064.
- Geer, M.R., Sokaski, M., West, J.M., Yancey, H.F., 1957, "The Role of Viscosity in Dense-Medium Coal Cleaning", USBM RI-5354, 25pp.
- Gillespie, T., 1963, "The Effect of Size Distribution on the Rate Constants for Collisions in

- Disperse Systems", J. Coll. Sci., 18, 562-7.
- Goldsmith, H.L., Mason, S.G., 1967, "The Microrheology of Dispersions", Proc. 4th Int. Congr. on Rheology, Providence, Rhode Island, F.R. Eirich, ed, John Wiley & Son, New York, 85-250.
- Goodwin, J.W., 1981, "Some Uses of Rheology in Colloid Science", Colloidal Dispersions, J.W. Goodwin (ed), Royal Society of Chemistry, London, 165-195.
- Govier, G.W., Shook, C.A., Lilge, E.O., 1957, "The Rheological Properties of Water Suspensions of Finely Subdivided Magnetite, Galena and Ferrosilicon", CIM Trans., LX, CIM publ., 147-154.
- Graebel, W.P., 1964, "The Hydrodynamic Stability of a Bingham Fluid in Couette Flow", Second-order Effects in Elasticity, Plasticity and Fluid Dynamics., M. Reiner, D. Abir, ed, Pergamon Press, Oxford, 636-649.
- Graham, C.C., Lamb, R., 1982, "Coal Preparation - Dense Media Rheology A Review of Measurement and Control", ACIRL P.R.-82-3, 52pp.
- Graham, C.C., Lamp, R., 1983, "A Study of Dense Media Rheology", Proc. 2nd Austr. Coal Prep. Conf., Rockhampton, 107-128.
- Greenspan, H.P., Ungarish, M., 1982, "On Hindered Settling of Particles of Different Sizes", Int. J. Multiphase Flow, 8(6), 587-604.
- Griskey, R.G., 1989, "How to Tame, Handle and Process Shear-Thickening Fluids; A Very Important but Poorly Understood Class of Non-newtonian Fluids", ViscTech, Chicago, Omni Press 329-353.
- Hancock, K.D., 1988, Magnetite Occurrences in British Columbia, Prov. of B.C., Min. of Energy Mines & Petrol Resources, pp.28.
- Hanks, R.W., 1981, "Hydraulic Design for Flow of Complex Fluids", Course Notes, Society of Rheology, New York, 329pp.
- Harris, D.L., Reid, W.H., 1964, "On the stability of viscous flow between rotating cylinders. Part 2. Numerical analysis", J. Fluid Mech., 20(1), 95-101.
- Harris, J., 1977, Rheology and non-Newtonian Flow, Longman, New York.
- Hartig, H.E., Onstad, N.I., Foot, N.J., 1951, "Demagnetization of Magnetite", Univ. of Minnesota IC-No. 7, 22pp.

- Helfricht, R., Schatz, J., 1989, "The Use of Dispersants in Kaolin Processing", Proc. 2nd World Congress on Non-Metallic Minerals, Beijing, 735-740.
- Himmelblau, D.M., 1970, "Identification of the Best Models", Process Analysis by Statistical Methods, Wiley, New York, 208-283.
- Hocquart, R., Decruppe, J.P., Cressely, R., 1988, "Flow Birefringence of Solutions of Rigid Particles Near the First Transition from Laminar Flow to Taylor Vortex Flow", Proc. 10th Int. Congr. on Rheol., 1, P.H. Uhlher, ed, Australian Society of Rheology, Sydney, 410-2.
- Horie, M., Pinder, K.L., 1979, "Time-Dependent Shear Flow of Artificial Slurries in Coaxial Cylinder Viscometer with a Wide Gap", Can. J. Chem. Eng., 57, 125-134.
- Horsley, R.R., Snow, R.J., 1988, "The rheology of some Australian mine tailings", Progress and Trends in Rheology II, Prague, H. Geisekus, ed, Springer-Verlag, New York, 344-6.
- Horsley, R.R., Allen, D.W., 1987, "The Effect of Yield Stress on Hydrocyclone Performance in the Mining Industry", Proc. 3rd Int. Conf. on Hydrocyclones, Oxford, P. Wood, ed, Elsevier, New York, 269-275.
- Hudy, J., 1968, "Performance Characteristics of Coal-Washing Equipment Dense-Medium Coarse-Coal Vessels", USBM RI-7154, 29pp.
- Hunter, R.J., Firth, B.A., 1976, "Electrochemical Control of the Flow Behaviour of Coagulated Colloidal Sols", Trends in Electrochemistry, J.O'M. Bockris, D.A.J. Rand, B.J. Welch, eds, Plenum Press, New York, 193-202.
- Hunter, R.J., 1985a, "Rheological and Sedimentation Behaviour of Strongly Interacting Colloidal Systems", Modern Trends of Colloid Science in Chemistry and Biology, H.F. Eike, ed, Basel, Birkhauser Verlag, 184-202.
- Hunter, R.J., Everett, D.W., 1988, "The Elastic Behaviour of Coagulated Colloidal Dispersions", Proc. 10th Int. Congr. on Rheology, 1, P.H. Uhlherr, Sydney, Australian Society of Rheology, 428-430.
- Iwasaki, I., Carlson, W.J., Parmerter, S.M., 1969, "The Use of Starches and Starch Derivatives as Depressants and Flocculants in Iron Ore Beneficiation", Trans. AIME, 244, 88-98.
- Jones, R.L., Chandler, H.D., 1989, "The effect of drag-reducing additives on the rheological properties of silica-water suspensions containing iron(III) oxide and of a typical gold-mine slurry", J. S. Afr. Inst. Min. and Met., 89(6), 187-191.
- Jonker, L., 1984, "The Development of Standard Procedures for the Evaluation of Magnetite for Use in Heavy-Medium Separation", MINTEK Report No. M144, 21pp.

- Kamiyama, S., Satoh, A., 1989, "Rheological Properties of Magnetic Fluids with the Formation of Clusters: Analysis of Simple Shear Flow in a Strong Magnetic Field", J. Coll. Interf. Sci., 127(1), 173-188.
- Kelsall, D.F., 1952, "A Study of the Motion of Solid Particles in a Hydraulic Cyclone", Trans. Inst. Chem. Eng., 30, 87-108.
- Kikkawa, H., Okiura, K., Arikawa, Y., 1984, "Development of Highly Loaded CWM Preparation System", 921-932.
- Killmeyer, R.P., 1982, "Dense-Medium Cycloning of Fine Coal at Low Specific Gravities", US DOE/PETC/TR-83/2, 13pp.
- King, R.P., Juckes, A.H., 1984, "Cleaning of Fine Coals by Dense-Medium Hydrocyclone", Powder Tech., 40, 147-160.
- King, R.P., Juckes, A.H., 1988, "Performance of a Dense-Medium Cyclone When Beneficiating Fine Coal", Coal Prep., 5, 185-210.
- Kirchberg, H., Topfer, E., Scheibe, W., 1975, "The effect of suspension properties on separating efficiency of mechanical classifiers", Proc. 11th Int. Min. Proc. Cong., University of Cagliari, Italy, 219-244.
- Kitchener, J.A., 1969, "Colloidal Minerals: Chemical Aspects of their Dispersion, Flocculation and Filtration", Filtr. and Sep., 6(5), 1-6.
- Klassen, V.I., Litovko, V.I., Myasnikov, N.F., 1964, "Improvement of Physical and Mechanical Properties of Ferrosilicon Suspensions with Help of Reagents", Proc. 7th Int. Min. Proc. Cong., 1, N. Arbiter, Gordon and Breach, New York, 95-101.
- Klassen, V.I., Krasnov, G.D., Litovko, V.I., Blagova, Z.S., 1966, "New Methods of Preparation. Part I: Methods of Improving the Physical and Mechanical Properties of Magnetite Suspensions", 5th Int. Coal Prep. Conf., Pittsburgh, D.O.E., D5.
- Klein, B., Partridge, S.J., Laskowski, 1988, "Influence of Physicomechanical Properties on the Rheology and Stability of Magnetite Dense Media", Int. Symp. on the Prod. and Proc. of Fine Particles, Montreal, A.J. Plumptre, ed, Pergamon Press, Toronto, 397-407.
- Klein, B., Laskowski, J.S., Mular, A.L., 1990, "Rheology of Magnetite Dense Media: Modelling and Control", Proc. 11th Int. Coal Prep. Congr., Tokyo, 51-56.
- Klembowski, 1986, "Continuous Measurements of Viscous Properties of Suspensions with Settling Particles", Progress and Trends in Rheology II, Prague, H. Giesekus et. al., ed, Springer-Verlag, New York, 177-9.

- Klima, M.S., Killmeyer, R.P., 1990, "Effect of Operating Conditions on Micronized-Magnetite Cycloning Performance", Coal Prep'90, Cincinnati, 15pp.
- Krieger, I.M., Elrod, H., 1951, "Direct Determination of the Flow Curves of Non-Newtonian Fluids. II. Shearing Rate in the Concentric Cylinder Viscometer", J. Appl. Phys., 24(2), 134-6.
- Krieger, I.M., Elrod, H., 1952, "Direct Determination of the Flow Curves of Non-Newtonian Fluids. III. Standardized Treatment of Viscometric Data", J. Appl. Phys., 25(1), 72-5.
- Krieger, I.M., Dougherty, T.J., 1959, "A Mechanism for Non-Newtonian Flow in Suspensions of Rigid Spheres", Trans. Soc. Rheol., III, 137-152.
- Krieger, I.M., 1968a, "Shear Rate in the Couette Viscometer", Trans. Soc. Rheol., 12(1), 5-11.
- Krieger, I.M., 1968b, "Computation of Shear Rate in the Couette Viscometer", Proc. 5th Int. Congr. on Rheol., Kyoto, S. Onogi, ed, University of Tokyo Press, Tokyo, 511-6.
- Krieger, I.M., 1971, "Rheology of Monodisperse Latices", Advan. Coll. Interf. Sci., 3, 111-136.
- Krueger, E.R., Gross, A., Di Prima, R.C., 1966, "On the relative importance of Taylor-vortex and non-axisymmetric modes in flow between rotating cylinders", J. Fluid Mech., 24(3), 521-538.
- Laapas, H., 1982, "Viscosity Measurement of Fast Settling Mineral Suspensions with a Modified Capillary Tube Viscometer", Proc. 5th Int. Symp. on Powder Tech., Kyoto, Hemisphere Publications, 216-223.
- Laapas, H.R., 1985, "Rheology of Fast Settling Mineral Slurries", Proc. 15th Int. Min. Proc. Cong., Cannes, Société de l'industrie minière, Paris, 28-40.
- Lang, E.R., Rha, C-K., 1984, "Analysis and Estimation of the Yield Stress of Dispersions", 659-665.
- Lapasin, R., Ferrara, G., Ruscio, E., Schena, G.D., 1988, Rheological Characterization of Magnetite Dense Media", Coal Prep., 5, 167-183.
- Laskowski, J.S., Walters, A.D., 1987, "Coal Preparation", Encycl. of Phys. Sci. & Tech., 3, Academic Press, 37-61.
- Laskowski, J.S., 1988, "Dispersing Agents in Mineral Processing", Froth Flotation, S.H. Castro, J.A. Moisan, eds, Elsevier, 1-16.
- Laskowski, J.S., Pugh, R.J., 1992, "Dispersions Stability and Dispersing Agents", Colloid

- Chemistry in Mineral Processing, Chapter 4, J.S.Laskowski, J.Ralston (ed) Elsevier, 115-172.
- Lathioor, R.A., Osborne, D.G., 1984, "Dense Medium Cyclone Cleaning of Fine Coal", Proc. 2nd Int. Conf. on Hydrocyclones, Paper G1, Bath, England, Elsevier, New York, 233-252.
- Lee, D.I., 1970, "Packing of Spheres and Its Effect on the Viscosity of Suspensions", J. Paint Tech., 42(550), 579-587.
- Leighton, D., Acrivos, A., 1987, "The shear-induced migration of particles in concentrated suspensions", J. Fluid Mech., 181, 415-439.
- Leja, J., 1983, Surface Chemistry of Froth Flotation, Plenum Press, New York, pp 758.
- Leong, Y.K., Boger D.V., 1988, "Importance of Surface Chemistry in Concentrated Suspension Rheology", Proc. 10th Int. Congr. on Rheol., 2, P.H. Uhlherr, ed, Australian Society of Rheology, Sydney, 85-87.
- Leong, Y.K., Boger, D.V., 1990, "Surface Chemistry Effects on Concentrated Suspension Rheology", J. Coll. Interf. Sci., 136(1), 249-258.
- Lewis, T.B., Nielsen, L.E., 1968, "Viscosity of Dispersed and Aggregated Suspensions of Spheres", Trans. Soc. Rheol., 12(3), 421-443.
- Lilge, E.O., Fregren, T.E., Purdy, G.R., 1957, "Apparent Viscosities of Heavy Media and the Driessen Cone", Trans. IMM, 67, 229-249.
- Lin, K.F., Burdick, C.L., 1988, "Polymeric Depressants", Surfactant Science Series, 27, 471-483.
- Lockyer, M.A., Davies, J.M., Jones, T.E.R., 1980, "The importance of rheology in the determination of the carrying capacity of oil-drilling fluids", Proc. 8th Int. Congr. on Rheol., Naples, Italy, G. Astarita et al, eds, Plenum Press, New York.
- Mannheimer, R.J., 1982, "Rheological Evaluation of Cement Slurries", Southwest Research Institute Final Report No. SwR-6836, Dallas, 45pp.
- Mannheimer, R.J., 1985, "Flow Characteristics of Slurries at Shear Stresses Near the Yield Value", Proc. 10th Int. Conf. on Slurry Tech., G.H. Eatman, ed, Hydro Transport 10, BHRA Fluid Engineering, Lake Tahoe, Nevada, 123-133.
- McGeary, R.K., 1961, "Mechanical Packing of Spherical Particles", J. Am. Cer. Soc., 44(10), 513-522.
- Meagher, L., Farrow, J.B., Horsley, R.R., Warren, L.J., 1988, "The Effect of Dissolved Ions on

- the Rheology of Concentrated Quartz Suspensions", Proc. 10th Int. Congr. on Rheol., 2, P.H. Uhlherr, ed, Sydney, Australian Society of Rheology, 118-120.
- Meerman, P.G., 1958, "Geomagnetic Flocculation: An Explanation of the Rheological Behaviour of Suspended Magnetite", Rheol. Acta, 1(2-3), 106-110.
- Mehta, R.V., Prabhakaran, P., Patel, H.I., 1983, "Thixotropy of Certain Diester Based Magnetic Fluids in a Magnetic Field", J. Magnetism and Magnetic Mat., 39, 35-8.
- Mewis, J., Spaul, A.J.B., 1976, "Rheology of Concentrated Dispersions", Adv. Coll. Interf. Sci., 6, 173-200.
- Michaels, A.S., Bolger, J.C., 1962, "Settling Rates and Sediment Volumes of Flocculated Kaolin Suspensions", I&EC Fundamentals, 1(1), 24-33.
- Mills, P., Snabre, P., 1988, "The fractal concept in the rheology of concentrated suspensions", Progress and Trends in Rheology II, Prague, H. Giesekus, ed, Springer-Verlag, New York, 105-8.
- Mooney, M., 1951, "The Viscosity of a Concentrated Suspension of Spherical Particles", J. Coll. Sci., 6, 162-170.
- Moore, F., Davies, L.J., 1956, "A New Rotational Viscometer and Some Preliminary Results", Trans. Brit. Cer. Soc., 55, 313-338.
- Mular, A.L., 1972, "Empirical Modelling and Optimization of Mineral Processes", Minerals Sci. Engng., 4(3), 30-42.
- Mun, R.P., Boger, D.V., 1988, "Turbulent Pipe Flow of Yield Stress Fluids", Proc. 10th Int. Congr. on Rheology, 2, P.H. Uhlher, ed, Australian Society of Rheology, Sydney, 145-7.
- Murray, W., 1990, private correspondence.
- Napier-Munn, T.J., 1980, "Influence of Medium Viscosity on the Density Separation of Minerals in Cyclones", Int. Conf. on Hydrocyclones, Paper 6, Cambridge, Elsevier, New York, 63-82.
- Napier-Munn, T.J., 1983, "The Mechanism of Separation in Dense Medium Cyclones", Ph.D. Thesis, University of London, London.
- Napier-Munn, T.J., 1984, "The Mechanism of Separation in Dense Medium Cyclones", 2nd Int. Conf. on Hydrocyclones, Paper G2 Bath, England, Elsevier, New York, 253-280.
- Napier-Munn, T.J., Reeves, T.J., Hansen, J.Y., 1989, "The Monitoring of Medium Rheology in

- Dense Medium Cyclone Plants", Aus IMM Bull. and Proc., 294(3), 85-93.
- Napier-Munn, T.J., 1990, "The Effect of Dense Medium Viscosity on Separation Efficiency", Coal Prep., 8, 145-165.
- Napier-Munn, T.J., Scott, I.A., 1990, "The Effect of Demagnetisation and Ore Contamination on the Viscosity of the Medium in a Dense Medium Cyclone Plant", Minerals Eng., 3(6), 607-613.
- Nelder, J.A., Mead, R., 1965, "A Simplex Method for Function Minimization", Comput. J., 7, 308-313.
- Nguyen Q.D., 1983, "Rheology of Concentrated Bauxite Residue Suspensions", PhD. Thesis, Monash University, 386pp.
- Nguyen, Q.D., Boger, D.V., 1983, "Yield Stress Measurement for Concentrated Suspensions", J. Rheol., 27(4), 321-349.
- Nguyen, Q.D., Boger, D.V., 1984, "Exploiting the Rheology of Highly Concentrated Suspensions", Proc. 9th Int. Congr. on Rheol., 1, Mexico City, B. Mena, ed, Universidad Nacional Autonoma De Mexico, Mexico City, 153-171.
- Nguyen, Q.D., Boger, D.V., 1985, "Direct Yield Stress Measurement with the Vane Method", J. Rheol., 29(3), 335-347.
- Nguyen, Q.D., 1989, "Time-dependent Flow Behaviour of Concentrated Industrial Suspensions", ViscTech, Chicago, Omni Press, 65-76.
- Nicol, S.K., Hunter, R.J., 1970, "Some Rheological and Electrokinetic Properties of Kaolinite Suspensions", Austr. J. Chem., 2177-2186.
- Ogden, I.K., Rutter, P.R., 1984, "The Sedimentation Stability and Viscosity of Coal Oil Dispersions", Colloids and Surf., 8, 249-259.
- Ohl, N., Gleissle, W., 1988, "Shear Flow Behaviour of Viscoelastic Suspensions: Prediction and Measurement of Shear and Normal Stress", Proc. 10th Int. Congr. on Rheol., 2, P.H. Uhlherr, ed, Australian Society of Rheology, Sydney, 154-6.
- Oldroyd, J.G., 1956, "Non-Newtonian Flow of Liquids and Solids", Rheology: Theory and Applications, 1, F.R. Eirich, Academic Press, New York, 653-682.
- Onstad, N.I. et al, "1954, "Method and Apparatus for Demagnetizing Magnetic Ores Having High Coercive Force", US Patent No. 2,678,130, 8pp.

- Osborne, D.G., 1988, "Dense-Medium Separation", Coal Preparation Technology, 1, Graham & Trotman, London, 199-287.
- Overbeek, J.Th.G., 1952, "The interaction between colloidal particles", Coll. Sci., 1, 245-277.
- Overend, I.J., Horsley, R.R., Jones, R.L., Vinycomb, R.K., 1984, "A New Method for the Measurement of Rheological Properties of Settling Slurries", Proc. 9th Int. Congr. on Rheology, 2, Mexico City, B. Mena et al, eds, Universidad Nacional Autonoma De Mexico, Mexico City, 583-590.
- Papenhuijzen, J.M.P., 1972, "The role of particle interactions in the rheology of dispersed systems", Rheol. Acta, 11, 73-88.
- Parkinson, C., Matsumoto, S., Sherman, P., 1970, "The Influence of Particle-Size Distribution on the Apparent Viscosity of Non-Newtonian Dispersed Systems", J. Coll. Interf. Sci., 33(1), 150-160.
- Pinder, K.L., 1964, "Time Dependent Rheology of the Tetrahydrofuran Hydrogen Sulphide Gas Hydrate Slurry", Can. J. Chem. Eng., 132-8.
- Plackett, R.L., Burman, J.P., 1946a, "The Design of Optimum Multifactorial Experiments", Biometrika, 33, 305-325.
- Plackett, R.L., 1946b, "Some Generalizations in the Multifactorial Design", Biometrika, 33, 328-332.
- Purohit, N.K., Roy, A.N., 1965, "Studies on the Rheological Properties of Rapidly Settling Suspensions Including Minerals", Proc. 8th Commonwealth Min. & Met. Congr. AIMM, 6 (Paper 39), Aus. I.M.M. 455-466.
- Purohit, N.K., Roy, A.N., 1968, "Studies on the Rheological Properties of Rapidly Settling Suspensions Including Minerals", Trans. IMM, C201-C208.
- Reeves, T.J., 1990, "On-Line Viscosity Measurement Under Industrial Conditions", Coal Prep., 8, 1-9.
- Renahan, M.J., Pullum, L., Lambrianidis, J., Bhattacharya, S.N., 1988a, "Effects of Coarse Particle Size Fractions on Rheology of Coal Suspensions Containing Fine Particles", Proc. 10th Int. Congr. on Rheol., 2, P.H. Uhlherr, ed, Australian Society of Rheology, Sydney, 207-10.
- Renahan, M.J., Snow, R.J., Bhattacharya, S.N., 1988b, "Factors Affecting the Maximum Allowable Volumetric Fraction of Mineral Slurry Systems", Proc. 10th Int. Congr. on Rheol., 2, Sydney, Australian Society of Rheology, 211-4.

- Reynolds, P.A., Jones, T.E.R., 1989, "An Experimental Study of the Settling Velocities of Single Particles in Non-Newtonian Fluids", Int. J. Min. Proc., 25, 47-77.
- Richardson, J.F., Zaki, W.N., 1954, Trans. Inst. Chem. Eng., 32, 35.
- Roscoe, R., 1952, "The viscosity of suspensions of rigid spheres", Brit. J. Appl. Phys., 3, 267-9.
- Round, G.F., Hessari, A.R., 1984, "The Effect of Size Distribution and pH on the Rheology of Coal Slurries", Hydrotransport 9, BHRA Fluid Engineering, 151-5.
- Rukin, E.I., Slivinskaya, I.I., Delyagin, G.N., Isaev, V.V., 1977, "Influence of the Grain-size Composition of Coal on the Properties of Aqueous Coal Suspensions", Solid Fuel Chem., 11, 54-9.
- Russel, W.B., 1980, "Review of the Role of Colloidal Forces in the Rheology of Suspensions", J. Rheol., 24(3), 287-317.
- Rutgers, I.R., 1962a, "Relative Viscosity of Suspensions of Rigid Spheres in Newtonian Liquids", Rheol. Acta, 2(3), 202-10.
- Rutgers, I.R., 1962b, "Relative Viscosity and Concentration", Rheol. Acta, 2(3), 305-348.
- Sadowski, Z., Mager, J., and Laskowski, J., 1978, "Hindered Settling of Coagulating Suspensions", Powder Tech., 21, 73-9.
- Sadowski, Z., and Laskowski, J., 1980, "Hindered Settling - A New Method of the i.e.p. Determination of Minerals", Colloids and Surf., 1, 151-9.
- Saraf, D.N., Khullar, S.D., 1975, "Some Studies on the Viscosity of Settling Suspensions", Can. J. Chem. Eng., 53, 449-452.
- Saunders, F.L., 1967, "Rheological Properties of Monodisperse Latex Systems: Flow Curves of Thickened Latexes", J. Coll. Interf. Sci., 23, 230-6.
- Schlegel, D., 1988a, "A new method for determining the wall effects with a Couette viscometer", Progress and Trends in Rheology II, Prague, H. Giesekus et al, ed, Springer-Verlag, New York, 172-4.
- Schlegel, D., 1988b, "Test of a New Two-gap Method for the Couette Viscometer with Suspensions of Glass Spheres in Oil", Proc. 10th Int. Congr. on Rheol., 2, P.H. Uhlherr, ed, Australian Society of Rheology, Sydney, 248-250.
- Schlichting, H., 1979, Boundary Layer Theory, 7th Edition, New York, trans J. Kestin, McGraw-Hill, New York, 510-542.

- Schranz, H., 1954, "The Use of Heavy Media of high Density and reduced Consistency in Dense-Medium Washing", Proc. 2nd Int. Coal Prep. Congr., Essen, 6pp.
- Schreuder, F.W.A.M., Stein, H.N., 1986, "Rheology of non-coagulating suspensions", Progress and Trends in Rheology II, Prague, H. Giesekuse et al, ed, Springer-Verlag, New York, 320-3.
- Scott, I.A., Davis, J.J., Manlapig, E.V., 1986, "A Methodology for Modelling Dense Medium Cyclones", Proc. 13th Cong. Council Min. Met. Insts., Singapore, Aus. I.M.M., 67-76.
- Scott, I.A., Baguley, P.J., Napier-Munn, T.J., 1987, "The Influence of Medium Rheology on the Separation of Minerals in Dense Medium Drums and Cyclones", Dense Medium Operators' Conference, Aus. I.M.M., Parkville, Victoria, Brisbane, 205-215.
- Scott, I.A., 1988, "A Dense Medium Cyclone Model Based on the Pivot Phenomenon", PhD Thesis, University of Queensland, Brisbane.
- Selim, M.S., Kothari, A.C., Turian, R.M., 1983, "Sedimentation of Multisized Particles in Concentrated Suspensions", AIChE J., 29(6), 1029-1039.
- Seshadri, V., Sutura, S.P., 1970, "Apparent Viscosity of Coarse, Concentrated Suspensions in Tube Flow", Trans. Soc. Rheol., 14(3), 351-373.
- Sherman, P., 1965, "An Equation for the Newtonian Contribution to Pseudoplastic Flow in Concentrated Dispersions", 4th Int. Congr. on Rheol., 4(3), E.H. Lee, John Wiley & Sons, New York, Providence, Rhode Island, 605-620.
- Shewchuk, M., 1983, The Craigmont Story, Hancock House, Surrey, B.C.
- Simha, R., 1952, "A Treatment of the Viscosity of Concentrated Suspensions", J. App. Phys., 23(9), 1020-5.
- Smoluchowski, M. von, 1916, Physik Zeitschrift, 17, 557-583.
- Speers, R.A., Holme, K.R., Tung, M.A., Williamson, W.T., 1987, "Drilling fluid shear stress overshoot behaviour", Rheol. Acta, 26, 447-452.
- Speers, R.A., Durance, T.D., Tung, M.A., 1989, "Flow Behaviour of Commercial Brewing Yeast Suspensions", Rheology of Food, Pharmaceutical and Biological Materials, R.E. Carter, ed, Elsevier, Essex, England, 27pp.
- Steinour, H.H., "Rate of sedimentation: nonflocculated suspensions of uniform spheres," Ind. Engng Chem., 36, 618-624.

- Stoessner, R.D., 1987, "Selection of Dense Medium Cyclones for Low Gravity Fine Coal Cleaning", Proc. 3rd Int. Conf. on Hydrocyclones, Oxford, England, Elsevier, New York, 111-9.
- Stokes, G.C., 1891, Mathematical and Physical Paper III, Cambridge.
- Street, N., 1956, Austr. J. Chem., 9, 467.
- Sun, Z-S., Denn, M.M., 1972, "Stability of Rotational Couette Flow of Polymer Solutions", AIChE J., 18(5), 1010-5.
- Sweeny, K.H., Geckler, R.D., 1954, "The Rheology of Suspensions", J. App. Phys., 25(9), 1135-1144.
- Tadros, Th.F., 1980, "Physical Stability of Suspension Concentrates", Adv. Coll. and Interf. Sci., 12, 141-261.
- Tadros, Th.F., 1985, "Rheology of concentrated suspensions", Chem. and Ind., 1, 210-8.
- Tadros, Th.F., 1988, "Rheology of Concentrated Stable and Flocculated Suspensions", Proc. of the Eng. Found. Conf., Palm Coast, Florida, Minerals, Metals & Materials Society, 43-87.
- Tadros, Th.F., Zsedanai, A., 1990, "Viscoelastic Properties of Aqueous Concentrated Pesticidal Suspension Concentrates", Colloids and Surf., 43, 95-103.
- Tam, K.C., Moussa, T., Tiu, C., 1988, "Comparison of Rheological Properties of Organic and Aqueous Drag Reducing Solutions", Proc. 10th Int. Congr. on Rheol., 2, P.H. Uhlherr, ed, Australian Society of Rheology, Sydney, 298-300.
- Taylor, G.I., 1923, "Stability of a viscous liquid contained between two rotating cylinders", Phil. Trans. A223, 289-343.
- Thomas, D.G., 1965, "Transport Characteristics of Suspension: VII. A Note on the Viscosity of Newtonian Suspensions of Uniform Spherical Particles", J. Coll. Sci., 20, 267-277.
- Ting, A.P., Luebbbers, R.H., 1957, "Viscosity of Suspensions of Spherical and Other Isodimensional Particles in Liquids", A.I.Ch.E., J., 3(1), 111-7.
- Tipler, P.A., 1976, Physics, Worth Publishers, New York, 953pp.
- Tsai, S.C., Knell, E.W., 1986, "Viscometry and rheology of coal water slurry", Fuel, 66, 2-7.
- Tung, M.A., Speers, R.A., 1985, "Development of Yield Stress Measurement Methodology", Literature Review, 11pp.

- Tung, M.A., Speers, R.A., Britt, I.J., Wilson, L.L., 1986a, "Development of Yield Stress Measurement Methodology", Second Quarter Report, 14pp.
- Tung, M.A., Speers, R.A., 1986b, "Development of Yield Stress Measurement Methodology", Final Progress Report, 43pp.
- Tung, M.A., Speers, R.A., Britt, I.J., Owen, S.R., Wilson, L.L., 1989, "Yield Stress Characterization of Structured Foods", Proc. 5th Int. Cong. Eng. and Food, Cologne, Elsevier, Amsterdam, 10pp.
- Valentik, L., Whitmore, R.L., 1964, "Controlling the Performance of Dense-Medium Baths" Proc. 7th Int. Min. Proc. Cong., N. Arbiter, ed, Gordon and Breach, New York. 87-93.
- Valentik, L., Whitmore, R.L., 1965, "The terminal velocity of spheres in Bingham plastics", Brit. J. Appl. Phys., 16, 1197-1203.
- Valentyik, L., 1971, "Instrumentation and Control of the Specific Gravity and the Rheology of Heavy-Media Suspensions", Min. Sci. Eng., 38-44.
- Valentik, L., 1972, "Rheological Properties of Heavy Media Suspensions Stabilized by Polymers", Trans. Soc. Min. Eng., 252, 99-105.
- Valentik, L., Patton, J.T., 1976, "Rheological Properties of Heavy-Media Suspensions Stabilized by Polymers and Bentonites", Trans. Soc. Min. Eng., 260, 113-8.
- Van Der Walt, P.J., Fourie, A.M., 1957, "Determination of the Viscosity of Unstable Industrial Suspensions with the Aid of a Stormer Viscometer", J. S. Afr. Inst. Min. and Met., 709-723.
- Van Der Walt, P.J., Falcon, L.M., Fourie, P.J.F., 1981, "Dense Medium Separation of Minus 0.5mm Coal Fines", Proc. 1st Austr. Coal Prep. Conf., Paper E1, Newcastle, Coal Preparation Societies of New South Wales and Queensland, 208-219.
- van de Ven, T.G.M., Hunter, R.J., 1977, "The energy dissipation in sheared coagulated sols", Rheol. Acta, 16, 391-543.
- Van Wazer, J.R., Lyons, J.W., Kim, K.Y., Colwell, R.E., 1963, Viscosity and Flow Measurement, John Wiley & Sons, New York, 389pp.
- Verwey, E.J.W., Overbeek, J.Th.G., 1948, Theory of Stability of Lyophobic Colloids, The Interaction of Sol Particles Having an Electric Double Layer, Elsevier, Amsterdam, 199pp.
- Voet, A., Suriani, L.R., 1950, "Dielectrics and Rheology of Dispersed Magnetized Particles", Trans. Soc. Rheol., 155-161.

- Wein, O., Tovchigrechko, V.V., Pokryvaylo, N.A., 1988, "Wall effects in Non-Newtonian fluids", Progress and Trends in Rheology II, Prague, H. Giesekus et al, ed, Springer-Verlag, New York, 332-3.
- Westman, A.E.R., Hugill, H.R., 1930, "The Packing of Particles", J. Am. Cer. Soc., 13(10), 767-779.
- White, G.A., Littman, C., Cormode, D.A., 1987, "Dense Media Separation of Potash Ore Using Tri-flo Dense Media Separation" Cominco Fertilizer, File 14SQ.23440-6-9123.
- White, H.E., Walton, S.F., 1937, "Particle Packing and Particle Shape", J. Am. Cer. Soc., 20(5), 155-166.
- Whitmore, R.L., 1957a, "The Relationship of the Viscosity to the Settling Rate of Slurries", J. Inst. of Fuel, 238-242.
- Whitmore, R.L., 1958, "Coal Preparation: The Separation Efficiency of Dense Medium Baths" J. Inst. of Fuel, 422-8.
- Whitmore, R.L., 1959, "The Viscous Flow of Disperse Suspensions in Tubes", Rheology of Disperse Systems, C.C. Mill, ed, Pergamon Press, New York, 49-60.
- Whitmore, R.L., 1968, "Drag Forces in Bingham Plastics", Proc. 5th Int. Congr. on Rheol., 1, Kyoto, S. Onogi, ed, University of Tokyo Press, Tokyo, 353-360.
- Whorlow, R.W., 1980, Rheological Techniques, Ch-2, 60-111, Ch-3, Halsted Press, New York, 131-191.
- Wildemuth, C.R., Williams, M.C., 1985, "A new interpretation of viscosity and yield stress in dense slurries: coal and other irregular particles", Rheol. Acta, 24, 75-91.
- Williams, E.J., Kloot, N.H., 1953, "Interpolation in a Series of Correlated Observations", Austr. J. App. Sci., 4, 1-17.
- Williams, P.S., 1951, "Some Effects on the Flow of Concentrated Suspensions of Variations in Particle Size and Shape", Faraday Soc. Disc., No. 11, 47-55.
- Williams, R.A., Amarasinghe, W.P.K., 1989, "Measurement and simulation of sedimentation behaviour of concentrated polydisperse suspensions", Trans IMM, C68-C82.
- Williams, R.A., Xie, C.G., Bragg, R., Amarasinghe, W.P.K., 1990, "Experimental Techniques for Monitoring Sedimentation in Optically Opaque Suspensions", Colloids and Surf., 43, 1-32.
- Windhab, E., 1986, "A new method for describing the time-dependent rheological behaviour of

- concentrated suspensions", Progress and Trends in Rheology II, Prague, H. Giesekus, ed, Springer-Verlag, New York, 317-320.
- Yancey, H.F., Geer, M.R., Sokaski, M., 1958, "Viscosity - Its Measurement and Importance in Dense-Medium Cleaning of the Fine Sizes of Coal", Proc. 3rd Int. Coal Prep. Conf., Brussels 583-591.
- Yang, D.C., 1988, "Reagents in Iron Ore Processing", Surfactant Sci. Ser., 27, 579-644.
- Yen, W.-T., 1968, "Surface Area and Viscosity Relationship for Minerals", M.Sc. Thesis, McGill University, Montreal, 110pp.
- Yopps, S.W., Spottiswood, D.J., Bull, W.R., Pillai, K.J., 1987, "A Study of the Effect of Slurry Rheology on Hydrocyclone Performance", Proc. 3rd Int. Conf. on Hydrocyclones, P. Wood, Oxford, England, Elsevier, New York, 59-63.
- Yoshimura, A., Prud'homme, R.K., 1988, "Wall Slip Corrections for Couette and Parallel Disk Viscometers", J. Rheol., 32(1), 53-67.
- Yucel, O., Hughes, M.R., 1984, "Sensitivity of Pressure Drop to Particle Size Distribution and Related Rheologic Characteristics of Hetero-Homogeneous Slurries", Hydrotransport 9, Lake Tahoe, BHRA Fluid Engineering, 251-7.
- Zheng, R-z., Zeng, F., Hu, K-M., 1984, "Research on CWM Preparation Technique with Chinese Coals", China Institute of Mining, 234-250.
- Zimmels, Y., 1985, "Accelerated and Steady Particle Flows in Newtonian Fluids", Encyl. of Fluid Mech., 5, Cheremisinoff, N.P. (Ed), Gulf Publ. Col, Houston, 94-153.

APPENDIX I

Publications Related to this Thesis

The following papers have been presented or published in support of this work:

Klein, B., Partridge, S.J., Laskowski, J.S., 1988, "Physicomechanical and Physicochemical Aspects of Magnetite Dense Medium Rheology", 4th Austr. Coal Prep. Conf., Gladstone Austr., P. Holtman, ed, Coal Preparation Societies of New South Wales and Queensland, 340-360.

Klein, B., Partridge, S.J., Laskowski, 1988, "Influence of Physicomechanical Properties on the Rheology and Stability of Magnetite Dense Media", Int. Symp. on the Prod. and Proc. of Fine Particles, Montreal, A.J. Plumpton, ed, Pergamon Press, Toronto, 397-407.

Laskowski, J.S., Klein, B., Partridge, S.J., 1988, "Apparatus for the Determination of the Rheological Properties of Settling Suspensions", Canadian Letters Patent, Serial No. 575,872.

Laskowski, J.S., Klein, B., Partridge, S.J., 1991, "Apparatus for the Determination of the Rheological Properties of Settling Suspensions", United States Patent, No. 5,056,358.

Klein, B., Laskowski, J.S., Mular, A.L., 1990, "Rheology of Magnetite Dense Media: Modelling and Control", Proc. 11th Int. Coal Prep. Congr., Tokyo, 51-56.

Klein, B., Partridge, S.J., Laskowski, J.S., 1990, "Rheology of Unstable Mineral Suspensions", Coal Preparation, 8, 123-124.

APPENDIX II

Program For Shear Rate Corrections

This program uses the method developed by Krieger (1968a, 1968b) to calculate the shear rates for non-Newtonian fluids in the annular gap of a concentric cylinder viscometer. The program was written to read flow curve data from a file produced with the Haake viscometer software. Each shear rate is recalculated and restored along with the corresponding shear stress values. The mathematical formulae to calculate the corrected shear rates are presented in Chapter 6. The program was written in the language Basic.

```

10  '*****
20  '
30  ' THIS PROGRAM READS IN A HAAKE DATA FILE AND CORRECTS THE SHEAR
40  ' RATES FOR NON-NEWTONIAN FLUID FLOW BEHAVIOUR. THE HAAKE DATA FILE
50  ' IS STORED UNDER A NEW FILE NAME WITH THE SHEAR RATES BEING REPLACED
60  ' WITH THE CORRECTED VALUES.
70  '
80  ' APRIL 15, 1989    B. KLEIN
90  '
100 '
110 '*****
120 GOSUB 230 'DEFINE VARIABLES AND INITIALIZE VALUES
130 GOSUB 800 'READ IN HAAKE DATA FILE
140 GOSUB 1030 'CALCULATE ANGULAR VELOCITY OF SHEAR RATES
150 GOSUB 1190 'CALCULATE SLOPES OF LOG(OMEGA) VS LOG(TAU)
160 GOSUB 1350 ' CALCULATE  $D^2(\text{LOG}(\text{TAU}))/D(\text{LOG}(\text{OMEGA}))^2$ 
170 GOSUB 1510 ' CALCULATE T - TERMS WHERE  $T=2*N*\text{LOG}(S)$ 
180 GOSUB 1700 ' CALCULATE  $F(T)=F(2*N*\text{LOG}(S))$ 
190 GOSUB 1890 ' CALCULATE CORRECTION TERM
200 GOSUB 2080 'CALCULATE CORRECTED SHEAR RATES
210 GOSUB 2310 'SAVE DATA FILE WITH CORRECTED SHEAR RATES
220 END
230 '
240 ' DEFINE VARIABLES AND INITIALIZE VALUES
250 '
260 ' A$ - INPUT FILENAME STRING
270 ' B1 - B9 - STRING AND NUMERIC INPUT FROM LINE 1 OF DATA FILE
280 ' C1 - C6 - NUMERIC INPUT FROM LINE 2 OF DATA FILE
290 ' D(I,J) - DATA FILE APPARENT VISCOSITY
300 ' TAU(I,J) - DATA FILE SHEAR STRESS
310 ' GAMMA(I,J) - DATA FILE SHEAR RATE
320 ' E(I,J) - DATA FILE TIME
330 ' F(I,J) - DATA FILE TEMPERTATURE
340 ' G$ - NUMERIC INPUT FROM LINE AFTER FIRST RAMP
350 ' H1 - H6 - NUMERIC INPUT FROM LINE AFTER HOLD PERIOD
360 ' L$ - FINAL LINE OF DATA FILE STRING
370 ' OMEGA(I,J) - ROTATIONAL SPEED
380 ' K1 - CONVERSION FACTOR FOR NEWTONIAN SHEAR STRESS TO ROTATIONAL SPEED
390 ' N(I,J) - SLOPE OF LOG(OMEGA) VS LOG(TAU)
400 ' NP(I,J) - SLOPE OF LOG(OMEGA) VS N
410 ' T1(I,J) - T - TERM FOR INNER GAP
420 ' T2(I,J) - T - TERM FOR OUTER GAP
430 ' FT1(I,J) - EVALUATED FUNCTION OF T1 TERM
440 ' FT2(I,J) - EVALUATED FUNCTION OF T2 TERM
450 ' CT1(I,J) - CORRECTION TERM FOR INNER GAP
460 ' CT2(I,J) - CORRECTION TERM FOR OUTER GAP
470 ' CGAM1(I,J) - CORRECTED SHEAR RATE FOR INNER GAP
480 ' CGAM2(I,J) - CORRECTED SHEAR RATE FOR OUTER GAP
490 ' CGAM(I,J) - CORRECTED TOTAL SHEAR RATE
500 ' S - RADIUS RATIO

```

```

510 ' P$ - NAME OF CORRECTED DATA FILE
520 DIM D(50,3), TAU(50,3), GAMMA(50,3), E(50,3), F(50,3), OMEGA(50,3)
530 DIM N(50,3), NP(50,3), T1(50,3), T2(50,3), FT1(50,3), FT2(50,3)
540 DIM CT1(50,3), CT2(50,3), CGAM1(50,3), CGAM2(50,3), CGAM(50,3)
550 FOR J=1 TO 3
560 FOR I=1 TO 50
570 D(I,J)=0
580 TAU(I,J)=0
590 GAMMA(I,J)=0
600 E(I,J)=0
610 F(I,J)=0
620 N(I,J)=0
630 NP(I,J)=0
640 T1(I,J)=0
650 T2(I,J)=0
660 FT1(I,J)=0
670 FT2(I,J)=0
680 CT1(I,J)=0
690 CT2(I,J)=0
700 CGAM1(I,J)=0
710 CGAM2(I,J)=0
720 CGAM(I,J)=0
730 OMEGA(I,J)=0
740 NEXT I
750 NEXT J
760 K1=.010678
770 S1=1.0252
780 S2=1.0189
790 RETURN
800 '
810 ' READ IN HAAKE DATA FILE
820 '
830 LINE INPUT "FILE NAME ? ":A$
840 OPEN A$ FOR INPUT AS #1
850 INPUT #1, B1$, B2$, B3$, B4$, B5, B6, B7$, B8, B9
860 INPUT #1, C1, C2, C3, C4, C5, C6
870 FOR I=1 TO 50
880 J=1
890 INPUT #1, D(I,J), TAU(I,J), GAMMA(I,J), E(I,J), F(I,J)
900 NEXT I
910 INPUT #1, G1, G2, G3, G4, G5, G6
920 FOR I=1 TO 6
930 J=2
940 INPUT #1, D(I,J), TAU(I,J), GAMMA(I,J), E(I,J), F(I,J)
950 NEXT I
960 INPUT #1, H1, H2, H3, H4, H5, H6
970 FOR I=1 TO 50
980 J=3
990 INPUT #1, D(I,J), TAU(I,J), GAMMA(I,J), E(I,J), F(I,J)
1000 NEXT I

```



```

1010 INPUT #1, L$
1020 RETURN
1030 '
1040 ' CALCULATE ANGULAR VELOCITIES FROM SHEAR RATE DATA
1050 '
1060 FOR I=1 TO 50
1070 J=1
1080 OMEGA(I,J)=GAMMA(I,J)*K1
1090 NEXT J
1100 FOR I=1 TO 6
1110 J=2
1120 OMEGA(I,J)=GAMMA(I,J)*K1
1130 NEXT J
1140 FOR I=1 TO 50
1150 J=3
1160 OMEGA(I,J)=GAMMA(I,J)*K1
1170 NEXT J
1180 RETURN
1190 '
1200 ' CALCULATE SLOPES OF LOG(OMEGA) VS LOG(TAU)
1210 '
1220 FOR I=1 TO 50
1230 J=1
1240 N(I,J)=LOG(TAU(I,J))/LOG(OMEGA(I,J))
1250 NEXT J
1260 FOR I=1 TO 6
1270 J=2
1280 N(I,J)=LOG(TAU(I,J))/LOG(OMEGA(I,J))
1290 NEXT J
1300 FOR I=1 TO 50
1310 J=3
1320 N(I,J)=LOG(TAU(I,J))/LOG(OMEGA(I,J))
1330 NEXT J
1340 RETURN
1350 '
1360 ' CALCULATE N-PRIME
1370 '
1380 FOR I=1 TO 50
1390 J=1
1400 NP(I,J)=N(I,J)/LOG(OMEGA(I,J))
1410 NEXT J
1420 FOR I=1 TO 6
1430 J=2
1440 NP(I,J)=N(I,J)/LOG(OMEGA(I,J))
1450 NEXT J
1460 FOR I=1 TO 50
1470 J=3
1480 NP(I,J)=N(I,J)/LOG(OMEGA(I,J))
1490 NEXT J
1500 RETURN

```

```

1510 '
1520 ' CALCULATE T - TERM
1530 '
1540 FOR I=1 TO 50
1550 J=1
1560 T1(I,J)=2*N(I,J)*LOG(S1)
1570 T2(I,J)=2*N(I,J)*LOG(S2)
1580 NEXT I
1590 FOR I=1 TO 6
1600 J=2
1610 T1(I,J)=2*N(I,J)*LOG(S1)
1620 T2(I,J)=2*N(I,J)*LOG(S2)
1630 NEXT I
1640 FOR I=1 TO 50
1650 J=3
1660 T1(I,J)=2*N(I,J)*LOG(S1)
1670 T2(I,J)=2*N(I,J)*LOG(S2)
1680 NEXT I
1690 RETURN
1700 '
1710 ' CALCULATE F(T) TERMS
1720 '
1730 FOR I=1 TO 50
1740 J=1
1750 FT1(I,J)=((T1(I,J)^2)/12)*(1-(T1(I,J)/2)+((T1(I,J)^2)/15))
1760 FT2(I,J)=((T2(I,J)^2)/12)*(1-(T2(I,J)/2)+((T2(I,J)^2)/15))
1770 NEXT I
1780 FOR I=1 TO 6
1790 J=2
1800 FT1(I,J)=((T1(I,J)^2)/12)*(1-(T1(I,J)/2)+((T1(I,J)^2)/15))
1810 FT2(I,J)=((T2(I,J)^2)/12)*(1-(T2(I,J)/2)+((T2(I,J)^2)/15))
1820 NEXT I
1830 FOR I=1 TO 50
1840 J=3
1850 FT1(I,J)=((T1(I,J)^2)/12)*(1-(T1(I,J)/2)+((T1(I,J)^2)/15))
1860 FT2(I,J)=((T2(I,J)^2)/12)*(1-(T2(I,J)/2)+((T2(I,J)^2)/15))
1870 NEXT I
1880 RETURN
1890 '
1900 ' CALCULATE CORRECTION TERMS
1910 '
1920 FOR I=1 TO 50
1930 J=1
1940 CT1(I,J)=(1+(NP(I,J)*FT1(I,J))/(N(I,J)^2))
1950 CT2(I,J)=(1+(NP(I,J)*FT2(I,J))/(N(I,J)^2))
1960 NEXT I
1970 FOR I=1 TO 6
1980 J=2
1990 CT1(I,J)=(1+(NP(I,J)*FT1(I,J))/(N(I,J)^2))
2000 CT2(I,J)=(1+(NP(I,J)*FT2(I,J))/(N(I,J)^2))

```

```

2010 NEXT I
2020 FOR I=1 TO 50
2030 J=3
2040 CT1(I,J)=(1+(NP(I,J)*FT1(I,J))/(N(I,J)^2))
2050 CT2(I,J)=(1+(NP(I,J)*FT2(I,J))/(N(I,J)^2))
2060 NEXT I
2070 RETURN
2080 '
2090 '
2100 ' CALCULATE CORRECTED SHEAR RATES
2110 '
2120 FOR I=1 TO 50
2130 J=1
2140 CGAM1(I,J)=2*N(I,J)*OMEGA(I,J)*CT1(I,J)/(1-S1^(-2*N(I,J)))
2150 CGAM2(I,J)=2*N(I,J)*OMEGA(I,J)*CT2(I,J)/(1-S2^(-2*N(I,J)))
2160 CGAM(I,J)= CGAM1(I,J)+CGAM2(I,J)
2170 NEXT I
2180 FOR I=1 TO 6
2190 J=2
2200 CGAM1(I,J)=2*N(I,J)*OMEGA(I,J)*CT1(I,J)/(1-S1^(-2*N(I,J)))
2210 CGAM2(I,J)=2*N(I,J)*OMEGA(I,J)*CT2(I,J)/(1-S2^(-2*N(I,J)))
2220 CGAM(I,J)= CGAM1(I,J)+CGAM2(I,J)
2230 NEXT I
2240 FOR I=1 TO 50
2250 J=3
2260 CGAM1(I,J)=2*N(I,J)*OMEGA(I,J)*CT1(I,J)/(1-S1^(-2*N(I,J)))
2270 CGAM2(I,J)=2*N(I,J)*OMEGA(I,J)*CT2(I,J)/(1-S2^(-2*N(I,J)))
2280 CGAM(I,J)= CGAM1(I,J)+CGAM2(I,J)
2290 NEXT I
2300 RETURN
2310 '
2320 ' SAVE DATA FILE WITH THE CORRECTED SHEAR RATES
2330 '
2340 LINE INPUT "SAVE FILE AS: ";P$
2350 OPEN P$ FOR OUTPUT AS #2
2360 WRITE #2, B1$, B2$, B3$, B4$, B5, B6, B7$, B8, B9
2370 WRITE #2, C1, C2, C3, C4, C5, C6
2380 FOR I=1 TO 50
2390 J=1
2400 PRINT #2,USING"####^ ^ ^ ^"; D(I,J), TAU(I,J), CGAM(I,J), E(I,J), F(I,J)
2410 NEXT I
2420 WRITE #2, G1, G2, G3, G4, G5, G6
2430 FOR I=1 TO 6
2440 J=2
2450 PRINT #2,USING"####^ ^ ^ ^"; D(I,J), TAU(I,J), CGAM(I,J), E(I,J), F(I,J)
2460 NEXT I
2470 WRITE #2, H1, H2, H3, H4, H5, H6
2480 FOR I=1 TO 50
2490 J=3
2500 PRINT #2,USING"####^ ^ ^ ^"; D(I,J), TAU(I,J), CGAM(I,J), E(I,J), F(I,J)

```

```
2510 NEXT I
2520 WRITE #2, L$
2530 RETURN
```

APPENDIX III
Simplex Optimization Program for Modelling
Rheological Flow Curve Data

This program uses the simplex optimization regression method (Nelder and Mead, 1954) to fit rheological flow curve models to flow curve data. A brief description of the method can be found in Chapter 15. The program reads up to three sets of rheological data with fifty points each. It then asks the user which model should be fit to the data and the regression begins. The program ends when the objective function, residual sum of squares, reaches a limit which was set at 10^{-8} or after 1000 iterations. The program then prints the residual sum of squares, the multiple index of determination and the flow curve model coefficients. The program was written in the computer language BASIC.

```

10 '
20 '
30 '*****
40 '
50 ' SIMPOP2.BAS
60 '
70 ' THIS PROGRAM USES THE SIMPLEX OPTIMIZATION METHOD FOR MAXIMIZING
80 ' OR MINIMIZING AN OBJECTIVE FUNCTION
90 ' IT CAN FIT FIVE DIFFERENT MODELS TO RHEOLOGICAL DATA PRODUCED BY THE
100 ' HAAKE VISCOMETER. IT WILL READ IN UP TO THREE DATA SETS AND FIT THE
110 ' EQUATIONS TO THEIR MEANS. THE EQUATIONS ARE THE HERSCHEL-BULKLEY, CASSON
120 ' LOGARITHMIC, CARREAU AND CROSS MODELS. THE OUTPUT PROVIDES THE EQUATION
130 ' COEFFICIENTS AND FIT CRITERION.
140 '
150 ' AUGUST 3, 1989 B. KLEIN
160 '
170 '
180 '*****
190 '
200 ' DEFINE VARIABLES -
210 '
220 ' N - NUMBER OF CONSTANTS IN EQUATION
230 ' A - REFLECTION COEFFICIENT
240 ' V - EXPANSION COEFFICIENT
250 ' B - CONTRACTION COEFFICIENT
260 ' C(1,J) - STARTING CONSTANT VALUES A,B,C
270 ' D(1,J) - STEP SIZES FOR CONSTANTS A,B,C
280 ' M - NUMBER OF DATA POINTS TO BE READ
290 ' F(I) - SHEAR STRESS DATA
300 ' G(I) - SHEAR RATE DATA
310 ' W(I) -WEIGHTING FACTOR
320 '
330 ' SET DIMENSIONS OF MATRICES
340 '
345 DEFDBL X
350 DIM D(1,10), C(1,10), X(11,10), Z(1,10), Y(11,1), Q(11,10)
360 DIM F(50),G(50),W(50),FI(50,4), DUM1(50), DUM2(50), DUM3(50)
370 GOTO 520
380 '
390 ' ASSIGN ZERO VALUES TO ALL MATRICES AND ARRAYS
400 '
410 FOR I=1 TO 4
420 FOR J=1 TO 3
430 X(I,J)=0
440 Y(I,1)=0
450 Q(I,J)=0
460 Z(1,J)=0
470 C(1,J)=0
480 D(1,J)=0
490 NEXT J
500 NEXT I

```

```

510 RETURN
520 '
530 ' ASSIGN NUMBER OF DATA POINTS TO BE READ TO - M -
540 ' READ DATA FILE INTO G(I)-SHEAR RATE AND F(I)-SHEAR STRESS
550 '
560 INPUT "NUMBER OF DATA SETS";DS
570 INPUT "NUMBER OF DATA POINTS TO BE READ ";M
580 FOR J=1 TO DS
590 LINE INPUT "FILE NAME ? ";F$
600 OPEN F$ FOR INPUT AS #J
610 INPUT #J, A1$, A2$, A3$, A4$, A5, A6, A7$, A8, A9
620 INPUT #J, A10, A11, A12, A13, A14, A15
630 FOR I=1 TO M
640 INPUT #J, DUM1(I), FI(I,J), G(I), DUM2(I), DUM3(I)
650 NEXT I
660 NEXT J
670 ' INPUT TEST DESCRIPTION
680 LPRINT CHR$(14);"FITTED EQUATIONS USING SIMPLEX OPTIMIZATION"
690 LPRINT CHR$(14);"DATA SHEET"
700 LPRINT
710 'LINE INPUT "MODEL FILE NAME ?";AA$
720 LINE INPUT "TIME ?";AQ$
730 LINE INPUT "SOURCE FILES ?";SF$
740 LINE INPUT "MODEL ? ";MN$
750 '
760 '
770 ' CALCULATE MEAN STRESS VALUES FROM DATA FILES
780 '
790 FOR I=1 TO M
800 F(I)=0
810 FOR J=1 TO DS
820 F(I)=F(I)+FI(I,J)
830 NEXT J
840 F(I)=F(I)/DS
850 NEXT I
860 '
870 ' CALCULATE WEIGHTING FACTORS
880 '
890 IF DS=1 GOTO 990
900 FOR I=1 TO M
910 TP=0
920 FOR J=1 TO DS
930 TP=TP+(ABS(F(I)-FI(I,J)))^2
940 NEXT J
950 TP=TP/(DS-1)
960 W(I)=1/TP
970 NEXT I
980 GOTO 990 '540
990 FOR I=1 TO M
1000 W(I)=1

```



```

1010 NEXT I
1020 U=5
1030 FOR I=1 TO M 'TEMPORARY PRINT STATEMENTS- STRESS VALUES, MEAN STRESS, W.F
1040 FOR J=1 TO DS
1050 'PRINT FI(I,J),
1060 NEXT J
1070 'PRINT F(I), W(I)
1080 NEXT I
1090 '
1100 ' SELECT MODELS FOR FITTING DATA
1110 '
1120 PRINT
1130 PRINT "SELECT MODEL(S)"
1140 PRINT " 0 - ALL MODELS"
1150 PRINT " 1 - Y = A + BX^C"
1160 PRINT " 2 - Y = (A^1/2 + (BX)^1/2)^2 "
1170 PRINT " 3 - Y = A + BLOG(X)"
1180 PRINT " 4 - Y = AX/(1 + (BX)^2)^C"
1190 PRINT " 5 - Y = X(A + (B-A)/(1+CX^2/3))"
1200 PRINT
1210 GOTO 1230
1220 PRINT "TRY AGAIN"
1230 INPUT "MODEL ";E
1240 IF E=0 THEN 1310
1250 IF E=1 THEN 1380
1260 IF E=2 THEN 1500
1270 IF E=3 THEN 1610
1280 IF E=4 THEN 1710
1290 IF E=5 THEN 1840
1300 GOTO 1220
1310 FOR U=1 TO 5
1320 PRINT "U= ";U
1330 E=U
1340 GOTO 1240
1350 '
1360 '
1370 '
1380 ' HERSCHEL-BULKLEY EQUATION
1390 '
1400 N=3
1410 GOSUB 390
1420 C(1,1)=.001
1430 C(1,2)=.001
1440 C(1,3)=.08
1450 FOR J=1 TO N
1460 D(1,J)=.1*C(1,J)
1470 NEXT J
1480 GOTO 1960
1490 '
1500 ' CASSON MODEL

```

```

1510 '
1520 N=2
1530 GOSUB 390
1540 C(1,1)=.01
1550 C(1,2)=.01
1560 FOR J=1 TO N
1570 D(1,J)=.1*C(1,J)
1580 NEXT J
1590 GOTO 1960
1600 '
1610 ' LOGARITHMIC MODEL
1620 '
1630 N=2
1640 GOSUB 390
1650 C(1,1)=.01
1660 C(1,2)=.5
1670 FOR J=1 TO N
1680 D(1,J)=.1*C(1,J)
1690 NEXT J
1700 GOTO 1960
1710 '
1720 ' CARREAU MODEL
1730 '
1740 N=3
1750 GOSUB 390
1760 C(1,1)=1
1770 C(1,2)=.1
1780 C(1,3)=.1
1790 FOR J=1 TO N
1800 D(1,J)=.1*C(1,J)
1810 NEXT J
1820 GOTO 1960
1830 '
1840 ' CROSS MODEL
1850 '
1860 N=3
1870 GOSUB 390
1880 C(1,1)=1
1890 C(1,2)=.1
1900 C(1,3)=.1
1910 FOR J=1 TO N
1920 D(1,J)=.1*C(1,J)
1930 NEXT J
1940 GOTO 1960
1950 '
1960 A=1
1970 V=2
1980 B=.5
1990 '
2000 ' SET UP INITIAL SIMPLEX WITH VERTICES STORED IN X(I,J)

```

```

2010 '
2020 FOR J=1 TO N
2030 FOR I=1 TO N+1
2040 X(I,J)=C(1,J)-(2/(J+1))*D(1,J)
2050 IF I=J+1 THEN 2070
2060 NEXT I
2070 X(I,J)=C(1,J)+((2/(J+1))*D(1,J))*J
2080 FOR I=J+2 TO N+1
2090 X(I,J)=C(1,J)
2100 NEXT I
2110 NEXT J
2120 '
2130 '
2140 Z7=0
2150 Z8=0
2160 Z9=0
2170 T3=9.999999E+35
2180 '
2190 ' DETERMINE VALUES OF OBJECTIVE FUNCTION AT EACH VERTICE OF SIMPLEX
2200 '
2210 FOR I=1 TO N+1
2220 H=I
2230 GOSUB 3440
2240 Y(I,1)=Y1
2250 NEXT I
2260 GOSUB 3620 ' SORT VALUES SUBROUTINE
2270 '
2280 ' DETERMINE STANDARD DEVIATION OF OBJECTIVE FUNCTION VALUES AT VERTICES
2290 '
2300 T1=0
2310 T2=0
2320 T4=0
2330 FOR I=1 TO N+1
2340 T2=T2+Y(I,1)
2350 NEXT I
2360 T1=T2/(N+1)
2370 FOR I=1 TO N+1
2380 T4=T4+(Y(I,1)-T1)^2
2390 NEXT I
2400 T=SQR(T4/N)
2410 '
2420 ' PROGRAM LIMITS AND OUTPUT
2430 '
2440 IF T>1E-08 THEN 2580
2450 GOTO 2480
2460 PRINT "CYCLE LIMIT = " Z9
2470 PRINT "CONVERGENCE FUNCTION = " T
2480 GOSUB 3890 'PRINT FITS AND RESIDUALS SUBROUTINE
2490 GOSUB 4050 'PRINT TEST DESCRIPTION
2500 GOSUB 4190 'PRINT COEFFICIENTS SUBROUTINE

```

```

2510 GOSUB 4340 'CALCULATE AND PRINT INDEX OF DETERMINATION SUBROUTINE
2520 GOSUB 4690 'CREATE DATA FILE WITH FITTED POINTS SUBROUTINE
2530 IF U=5 THEN 2550
2540 NEXT U
2550 STOP
2560 '
2570 '
2580 IF Z9>1000 THEN 2460
2590 IF T>T3 THEN 2680
2600 T3=T
2610 PRINT "ITERATION","STD. DEV.," "LOW VERTEX","HIGH VERTEX"
2620 PRINT Z9,INT(T*10000+.5)/10000,INT(Y(L,1)*10000+.5)/10000,
2630 PRINT INT(Y(H,1)*10000+.5)/10000
2640 '
2650 ' REFLECTION
2660 ' DETERMINE CENTROID AND COORDINATES OF NEW VERTICE
2670 '
2680 FOR I=1 TO N+1
2690 FOR J=1 TO N
2700 Q(I,J)=X(I,J)
2710 NEXT J
2720 NEXT I
2730 FOR J=1 TO N
2740 P=0
2750 FOR I=1 TO N+1
2760 IF I=H THEN 2780
2770 P=P+X(I,J)/N
2780 NEXT I
2790 Z(1,J)=(1+A)*P-A*X(H,J)
2800 X(H,J)=Z(1,J)
2810 D(1,J)=P
2820 NEXT J
2830 '
2840 '
2850 GOSUB 3440
2860 FOR I=1 TO N+1
2870 FOR J=1 TO N
2880 X(I,J)=Q(I,J)
2890 NEXT J
2900 NEXT I
2910 Y=Y1
2920 IF Y>=Y(L,1) THEN 3050
2930 '
2940 ' EXPANSION
2950 ' EXPAND COORDINATES OF REFLECTED VERTICE AND DETERMINE THE VALUE
2960 ' OF THE OBJECTIVE FUNCTION AT THIS POINT
2970 '
2980 FOR J=1 TO N
2990 X(H,J)=(1+V)*Z(1,J)-V*D(1,J)
3000 NEXT J

```

```

3010 GOSUB 3440
3020 IF Y1>Y THEN 3060
3030 Y(H,1)=Y1
3040 GOTO 2260
3050 IF Y>Y(S,1) THEN 3110
3060 Y(H,1)=Y
3070 FOR J=1 TO N
3080 X(H,J)=Z(1,J)
3090 NEXT J
3100 GOTO 2260
3110 IF Y>Y(H,1) THEN 3190
3120 FOR J=1 TO N
3130 X(H,J)=Z(1,J)
3140 NEXT J
3150 Y(H,1)=Y
3160 '
3170 ' CONTRACTION
3180 '
3190 FOR J=1 TO N
3200 X(H,J)=B*X(H,J)+(1-B)*D(1,J)
3210 NEXT J
3220 GOSUB 3440
3230 IF Y1>Y(H,1) THEN 3290
3240 Y(H,1)=Y1
3250 GOTO 2260
3260 '
3270 ' SHRINK
3280 '
3290 FOR J=1 TO N
3300 FOR I=1 TO N+1
3310 X(I,J)=(Q(I,J)+Q(L,J))/2
3320 NEXT I
3330 NEXT J
3340 Z8=Z8+1
3350 '
3360 '
3370 PRINT
3380 PRINT "STEP CHANGE":Z8
3390 PRINT
3400 GOTO 2210
3410 '
3420 ' CALCULATE VALUE OF OBJECTIVE FUNCTION AT VERTICE
3430 '
3440 S1=0
3450 S2=0
3460 FOR K=1 TO M
3470 IF E=1 THEN 3520
3480 IF E=2 THEN 3530
3490 IF E=3 THEN 3540
3500 IF E=4 THEN 3550

```

```

3510 S2=G(K)*(X(H,1)+(X(H,2)-X(H,1))/(1+X(H,3)*G(K)^(2/3))):GOTO 3560
3520 S2=X(H,1)+X(H,2)*G(K)^X(H,3):GOTO 3560
3530 S2=(SQR(ABS(X(H,1)))+SQR(ABS(X(H,2))*G(K)))^2:GOTO 3560
3540 S2=ABS(X(H,1))+ABS(X(H,2))*LOG(G(K)):GOTO 3560
3550 S2=ABS(X(H,1))*G(K)/(1+(ABS(X(H,2))*G(K))^2)^ABS(X(H,3)):GOTO 3560
3560 S1=S1+W(K)*(F(K)-S2)^2
3570 NEXT K
3580 Y1=S1
3590 Z9=Z9+1
3600 RETURN
3610 '
3620 ' SORT VALUES AT VERTICES AND RETURN THE COORDINATES OF THE
3630 ' HIGHEST, SECOND HIGHEST AND LOWEST W.R.T. OBJECTIVE FUNCTION
3640 ' VALUES
3650 '
3660 L=1
3670 H=1
3680 S=1
3690 FOR I=2 TO N+1
3700 IF Y(I,1)>Y(H,1) THEN 3740
3710 IF Y(I,1)<Y(L,1) THEN 3760
3720 NEXT I
3730 GOTO 3780
3740 H=I
3750 GOTO 3710
3760 L=I
3770 GOTO 3720
3780 R=Y(H,1)
3790 Y(H,1)=0
3800 FOR I=2 TO N+1
3810 IF Y(I,1)>Y(S,1) THEN 3840
3820 NEXT I
3830 GOTO 3860
3840 S=I
3850 GOTO 3820
3860 Y(H,1)=R
3870 RETURN
3880 END
3890 'PROGRAM OUTPUT
3900 PRINT "CONVERGENCE"
3910 ' PRINT FITS AND RESIDUALS
3920 H=L
3930 PRINT "MEAS. Y","PRED. Y","RESIDUALS","% DIFF"
3940 FOR I=1 TO M
3950 GAM=G(I)
3960 IF E=1 THEN GOSUB 5010: GOTO 4010
3970 IF E=2 THEN GOSUB 5030: GOTO 4010
3980 IF E=3 THEN GOSUB 5050: GOTO 4010
3990 IF E=4 THEN GOSUB 5070: GOTO 4010
4000 GOSUB 5090

```

```

4010 PRINT F(I),INT(G2*1000+.5)/1000,INT((F(I)-G2)*1000+.5)/1000,
4020 PRINT INT(((F(I)-G2)/F(I))*1000+.5)/1000
4030 NEXT I
4040 RETURN
4050 'PRINT TEST DESCRIPTION
4060 LINE INPUT "FILE NAME ? ";AA$
4070 LPRINT "FILE NAME:",AA$.
4080 LPRINT "DATE:",A7$
4090 LPRINT
4100 LPRINT "MEASURING SYSTEM: ";A4$.
4110 LPRINT "SENSOR:",A3$
4120 LPRINT
4130 LPRINT "SOURCE FILES:".SF$
4140 LPRINT "SAMPLE:",A1$,
4150 LPRINT "DESCRIPTION:".A2$
4160 LPRINT
4170 RETURN
4180 '
4190 'PRINT EQUATIONS AND COEFFICIENTS
4200 LPRINT "MODEL:",MN$
4210 LPRINT
4220 IF E=1 THEN LPRINT "Y=A+B*X^C": GOTO 4270
4230 IF E=2 THEN LPRINT "Y=(A^.5+(B*X)^.5)^2": GOTO 4270
4240 IF E=3 THEN LPRINT "Y=A+B*LOG(X)": GOTO 4270
4250 IF E=4 THEN LPRINT "Y=A*X/(1+(B*X)^2)^C": GOTO 4270
4260 LPRINT "Y=X(A+(B-A)/(1+CX^2/3))"
4270 LPRINT
4280 LPRINT "A=";INT(ABS(X(H,1)*10000+.5))/10000
4285 LPRINT "B=": USING "#.#####";ABS(X(H,2))
4290 'LPRINT "B=";INT(ABS(X(H,2)*10000+.5))/10000
4300 IF X(H,3)>0 THEN LPRINT "C=";INT(ABS(X(H,3)*10000+.5))/10000
4310 LPRINT
4320 RETURN
4330 '
4340 'CALCULATE AND PRINT INDEX OF DETERMINATION
4350 YBAR=0
4360 R1=0
4370 R2=0
4380 R3=0
4390 CO1=0
4400 CO3=0
4410 ' CALCULATE MEAN STRESS YBAR
4420 FOR I=1 TO M
4430 YBAR=YBAR+F(I)
4440 NEXT I
4450 YBAR=YBAR/M
4460 FOR I=1 TO M
4470 GAM=G(I)
4480 IF E=1 THEN GOSUB 5010: GOTO 4530
4490 IF E=2 THEN GOSUB 5030: GOTO 4530
4500 IF E=3 THEN GOSUB 5050: GOTO 4530

```

```

4510 IF E=4 THEN GOSUB 5070: GOTO 4530
4520 GOSUB 5090
4530 R1=R1+(G2-YBAR)^2
4540 R2=R2+(F(I)-YBAR)^2
4550 CO1=CO1+(F(I)-G2)^2
4560 NEXT I
4570 R3=R2/R1
4580 CO3=1-(CO1/R1)
4590 LPRINT "INDEX OF DETERMINATION, R^2 = ";R3
4600 LPRINT "COEFFICIENT OF DETERMINATION, r^2 = ";CO3
4610 LPRINT "RESIDUAL SUM OF SQUARES, SS = ";S1
4620 IF E=2 THEN DV=48: GOTO 4640
4630 DV=47
4640 LPRINT "VARIANCE OF FITTED EQUATION, VAR. = ";S1/DV
4650 LPRINT "NUMBER OF ITERATIONS, N = ";Z9
4660 RETURN
4670 '
4680 '
4690 CT=E+2
4700 CT=CT+1
4710 GAM=.1
4720 C5=25
4730 A5=100
4740 C9=3/50
4750 C4=0
4760 OPEN AA$ FOR OUTPUT AS #CT
4770 WRITE #CT,A1$,A2$,A3$,A4$,A5,A6,A7$,A8,A9
4780 WRITE #CT,A10,A11,A12,A13,A14,A15
4790 IF GAM>=G(50) GOTO 4820
4800 GOSUB 4910
4810 GOTO 4790
4820 A11=0
4830 A14=3
4840 A15=0
4850 WRITE #CT,A10,A11,A12,A13,A14,A15
4860 A10=0
4870 A14=1
4880 WRITE #CT,A10,A11,A12,A13,A14,A15
4890 WRITE #CT,AQ$
4900 RETURN
4910 IF E=1 THEN GOSUB 5010: GOTO 4960
4920 IF E=2 THEN GOSUB 5030: GOTO 4960
4930 IF E=3 THEN GOSUB 5050: GOTO 4960
4940 IF E=4 THEN GOSUB 5070: GOTO 4960
4950 GOSUB 5090
4960 C1=G2/GAM
4970 C4=C4+C9
4980 PRINT #CT,USING"####^ ^ ^ ^";C1,G2,GAM,C4,C5
4990 GAM=GAM+(G(50)/50)
5000 RETURN

```



```

5010 G2=X(H,1)+X(H,2)*GAM^X(H,3)
5020 GOTO 5100
5030 G2=(SQR(ABS(X(H,1)))+SQR(ABS(X(H,2))*GAM))^2
5040 GOTO 5100
5050 G2=ABS(X(H,1))+ABS(X(H,2))*LOG(GAM)
5060 GOTO 5100
5070 G2=ABS(X(H,1))*GAM/(1+(ABS(X(H,2))*GAM)^2)^ABS(X(H,3))
5080 GOTO 5100
5090 G2=GAM*(X(H,1)+(X(H,2)-X(H,1))/(1+X(H,3)*GAM^(2/3)))
5100 RETURN

```

APPENDIX IV

Model Discrimination Program to Compare Fits of Rheological Flow Curve Models

This program was written to compare the fits of two flow curve models to the flow curve data. The model discrimination procedure developed by Williams and Klotz was used. The program reads in information about the two models to be compared and the flow curve data. A slope is calculated which if negative means that model one fits the data better and if positive it means that model two fits the data better. Details of the procedure have been presented in Chapter 15. The program was written in the computer language Basic.

```

10 '
20 '
30 '*****
40 '
50 '
60 ' THIS PROGRAM USES THE WILLIAMS AND KLOOT METHOD OF MODEL
70 ' DISCRIMINATION TO DISTINGUISH WHICH IS THE BETTER OF TWO MODELS.
80 ' THE MODELS HAVE BEEN FITTED TO RHEOLOGICAL FLOW CURVE DATA.
90 '
100 '          AUGUST 11, 1989 B. KLEIN
110 '
120 '
130 '*****
140 '
150 GOSUB 460 'DEFINE AND INITIALIZE VARIABLES
160 GOSUB 630 'READ IN DATA FILES
170 GOSUB 800 ' CALCULATE MEAN STRESS VALUES
180 GOSUB 910 'SELECT MODELS TO COMPARE
190 MN=M1
200 PRINT 'ENTER COEFFICIENTS FOR MODEL 1
210 GOSUB 1020 'ENTER VALUES OF COEFFICIENTS FOR MODEL 1
220 MN=M2
230 PRINT 'ENTER COEFFICIENTS FOR MODEL 2
240 GOSUB 1020 'ENTER VALUES OF COEFFICIENTS FOR MODEL 2
250 MN=M1
260 GOSUB 1260 'CALCULATE STRESS VALUES FOR MODEL 1
270 MN=M2
280 GOSUB 1260 'CALCULATE STRESS VALUES FOR MODEL 2
290 PRINT "MEAN STRESS","MOD1 STRESS","MOD2 STRESS"
300 PRINT '
305 FOR I= 1 TO M
310 PRINT F(I),YF(M1,I),YF(M2,I)
320 NEXT I
330 LPRINT '
340 PRINT '
350 GOSUB 1350 ' CALCULATE Z VALUES
360 GOSUB 1390 ' CALCULATE STRESS DIFFERENCE
370 PRINT "Z-VALUE","X-VALUE"
380 FOR I=1 TO M
390 PRINT USING "      ###.###";Z(I),X(I)
400 NEXT I
410 PRINT '
420 PRINT '
430 GOSUB 1440 ' CALCULATE LEAST SQUARES COEFFICIENT
440 GOSUB 1510 ' PROGRAM OUTPUT
450 STOP
460 '
470 ' M - NUMBER OF DATA POINTS TO BE READ
480 ' FI(I,J) - SHEAR STRESS DATA
490 ' G(I) - SHEAR RATE DATA
500 ' F(I) - MEAN SHEAR STRESS VALUE

```

```

510 ' YM(I) - SHEAR STRESS CALCULATED FROM MODEL
520 ' YF(MN,I) - MODEL 1 AND MODEL 2 SHEAR STRESS VALUES
530 '
540 ' SET DIMENSIONS OF MATRICES
550 '
560 DIM F(50), G(50), FI(50,3), D1(50), D2(50), D3(50)
570 DIM YM(50), YF(4,50), Z(50), X(50)
580 AA=0
590 BB=0
600 CC=0
610 RETURN
620 '
630 ' READ IN DATA FILES
640 ' ASSIGN NUMBER OF DATA POINTS TO BE READ TO - M -
650 ' READ DATA FILE INTO G(I)-SHEAR RATE AND F(I)-SHEAR STRESS
660 '
670 INPUT "NUMBER OF DATA SETS";DS
680 INPUT "NUMBER OF DATA POINTS TO BE READ ";M
690 FOR J=1 TO DS
700 LINE INPUT "FILE NAME ? ";FS$
710 OPEN FS$ FOR INPUT AS #J
720 INPUT #J, A1$, A2$, A3$, A4$, A5, A6, A7$, A8, A9
730 INPUT #J, A10, A11, A12, A13, A14, A15
740 FOR I=1 TO M
750 INPUT #J, D1(I), FI(I,J), G(I), D2(I), D3(I)
760 NEXT I
770 NEXT J
780 RETURN
790 '
800 ' CALCULATE MEAN STRESS VALUES FROM DATA FILES
810 '
820 FOR I=1 TO M
830 F(I)=0
840 FOR J=1 TO DS
850 F(I)=F(I)+FI(I,J)
860 NEXT J
870 F(I)=F(I)/DS
880 NEXT I
890 RETURN
900 '
910 'SELECT MODELS TO COMPARE
920 '
925 INPUT "RUN NUMBER IS: ";NUM
930 PRINT " 1 - HERSCHEL BULKLEY EQUATION "
940 PRINT " 2 - CASSON EQUATION "
950 PRINT " 3 - CARREAU MODEL "
960 PRINT " 4 - CROSS MODEL "
970 INPUT "SELECT FIRST MODEL";M1
980 INPUT "FIRST MODEL NAME IS: ";MOD1$
990 INPUT "SELECT SECOND MODEL";M2
1000 INPUT "SECOND MODEL NAME IS: ";MOD2$

```

```

1010 RETURN
1020 ' ENTER VALUES OF COEFFICIENTS
1030 IF MN=1 THEN GOTO 1070
1040 IF MN=2 THEN GOTO 1120
1050 IF MN=3 THEN GOTO 1160
1060 IF MN=4 THEN GOTO 1210
1070 PRINT " Y = A + Bx^C "
1080 INPUT "ENTER VALUE OF COEFFICIENT A: ";C1
1090 INPUT "ENTER VALUE OF COEFFICIENT B: ";C2
1100 INPUT "ENTER VALUE OF COEFFICIENT C: ";C3
1110 GOTO 1250
1120 PRINT " Y = (A^1/2 + BX^1/2)^2 "
1130 INPUT "ENTER VALUE OF COEFFICIENT A: ";C4
1140 INPUT "ENTER VALUE OF COEFFICIENT B: ";C5
1150 GOTO 1250
1160 PRINT " Y = AX/(1+(BX)^2)^C "
1170 INPUT "ENTER VALUE OF COEFFICIENT A: ";C6
1180 INPUT "ENTER VALUE OF COEFFICIENT B: ";C7
1190 INPUT "ENTER VALUE OF COEFFICIENT C: ";C8
1200 GOTO 1250
1210 PRINT " Y = X(A+(B-A)/(1+CX^2/3)) "
1220 INPUT "ENTER VALUE OF COEFFICIENT A: ";C9
1230 INPUT "ENTER VALUE OF COEFFICIENT B: ";C10
1240 INPUT "ENTER VALUE OF COEFFICIENT B: ";C11
1250 RETURN
1260 ' CALCULATE STRESS VALUES FOR MODELS
1270 FOR I=1 TO M
1280 IF MN=1 THEN GOSUB 1560
1290 IF MN=2 THEN GOSUB 1590
1300 IF MN=3 THEN GOSUB 1620
1310 IF MN=4 THEN GOSUB 1650
1320 YF(MN,I)=YM(I)
1330 NEXT I
1340 RETURN
1350 'CALCULATE Z VALUES
1360 FOR I=1 TO M
1370 Z(I)=F(I)-.5*(YF(M1,I)+YF(M2,I))
1380 NEXT I
1390 ' CALCULATE STRESS DIFFERENCE
1400 FOR I= 1 TO M
1410 X(I)=YF(M2,I)-YF(M1,I)
1420 NEXT I
1430 RETURN
1440 'CALCULATE LEAST SQUARES COEFFICIENT
1450 FOR I=1 TO M
1460 AA=AA+X(I)*Z(I)
1470 BB=BB+(X(I))^2
1480 NEXT I
1490 CC=AA/BB
1500 RETURN

```

```

1510 ' PROGRAM OUTPUT
1520 LPRINT "RUN #":NUM,"MOD1 = ";MOD1$,"MOD2 = ";MOD2$,"LAMDA";CC
1530 LPRINT '
1540 RETURN
1550 '
1560 ' HERSCHEL BULKLEY EQUATION
1570 YM(I)=C1+C2*G(I)^C3
1580 RETURN
1590 ' CASSON EQUATION
1600 YM(I)=(SQR(C4)+SQR(C5*G(I)))^2
1610 RETURN
1620 ' CARREAU MODEL
1630 YM(I)=(C6*G(I))/((1+(C7*G(I))^2)^C8)
1640 RETURN
1650 ' CROSS MODEL
1660 YM(I)=G(I)*(C9+(C10-C9)/(1+C11*(G(I)^2/3)))
1670 RETURN

```

APPENDIX V

Settling Curves and Modelled Rheological

Flow Curves for Investigations into the

Effects of Various Parameters on Media Properties

Run #1: Suspension Composition

Carboxymethyl Cellulose (kg T ⁻¹):	1.50
Particle Passing Size (μm):	15.0
Solids Volume Fraction:	0.20
Magnetization:	Demagnetized
Sodium Silicate (kg T ⁻¹):	0.15
Kaolinite (% w/v):	0.75
pH:	10.0
Bentonite (% w/v):	0.75
Fine Coal (% w/v):	0.75

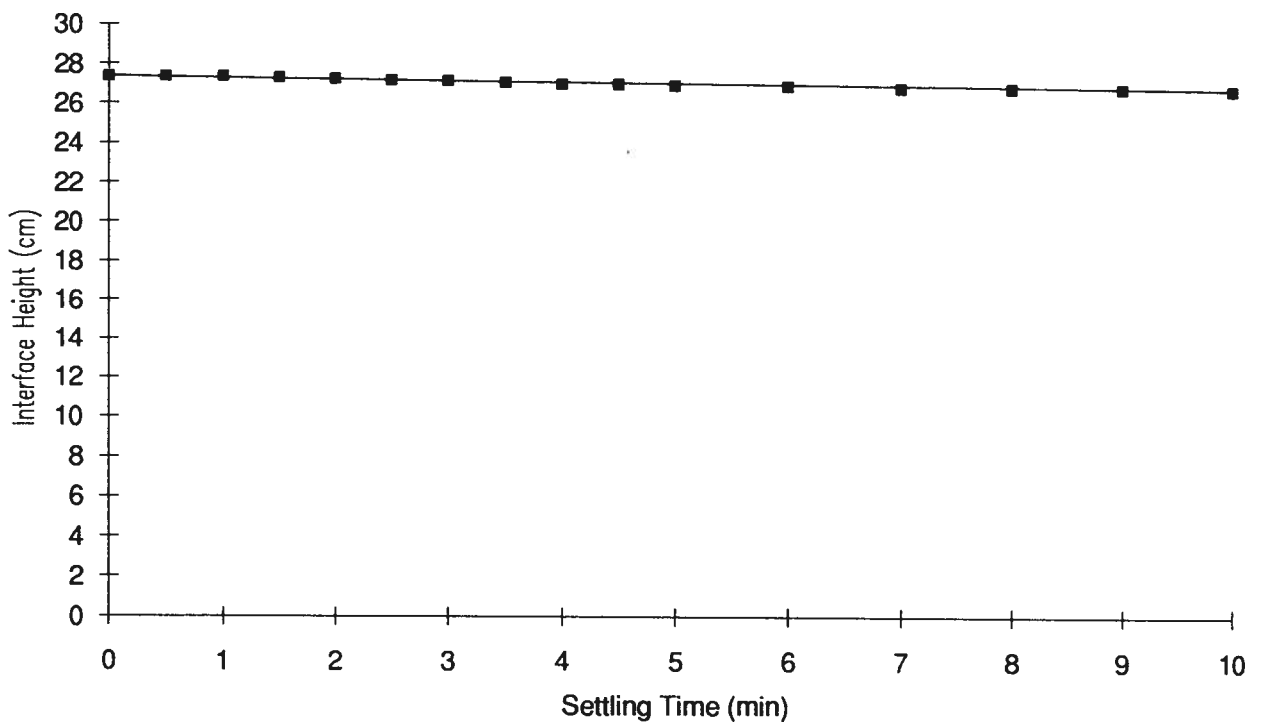


Figure AV.1 Settling curve interface height as a function of time for experimental Run #1.

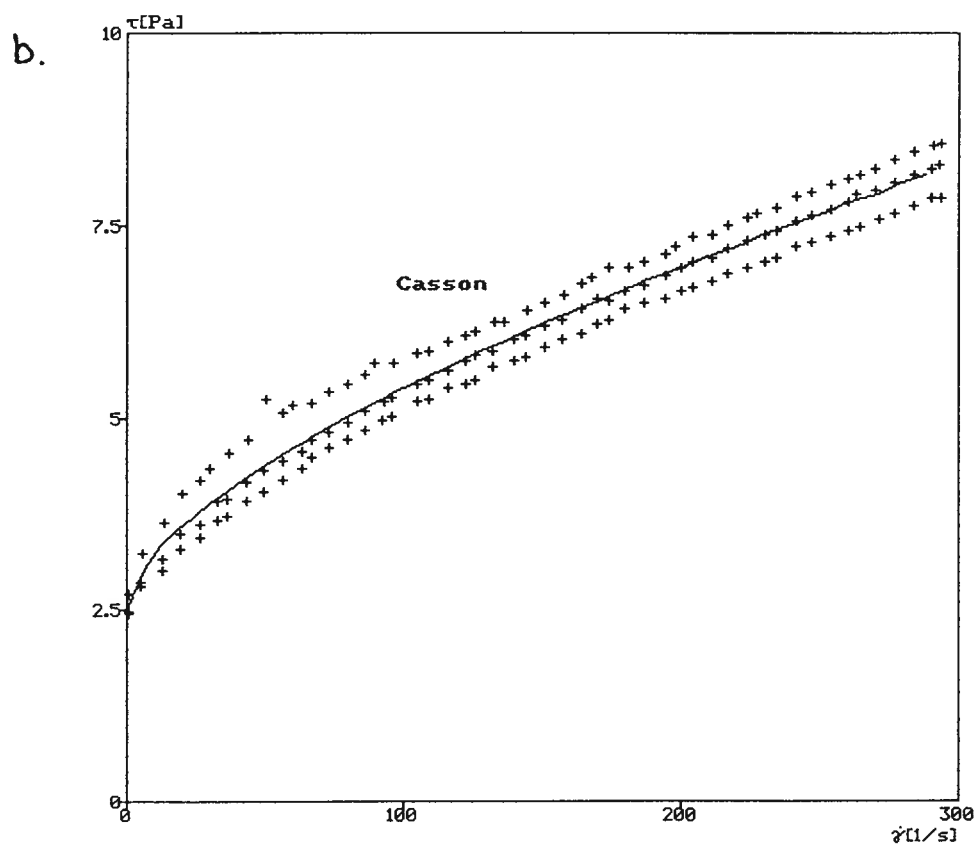
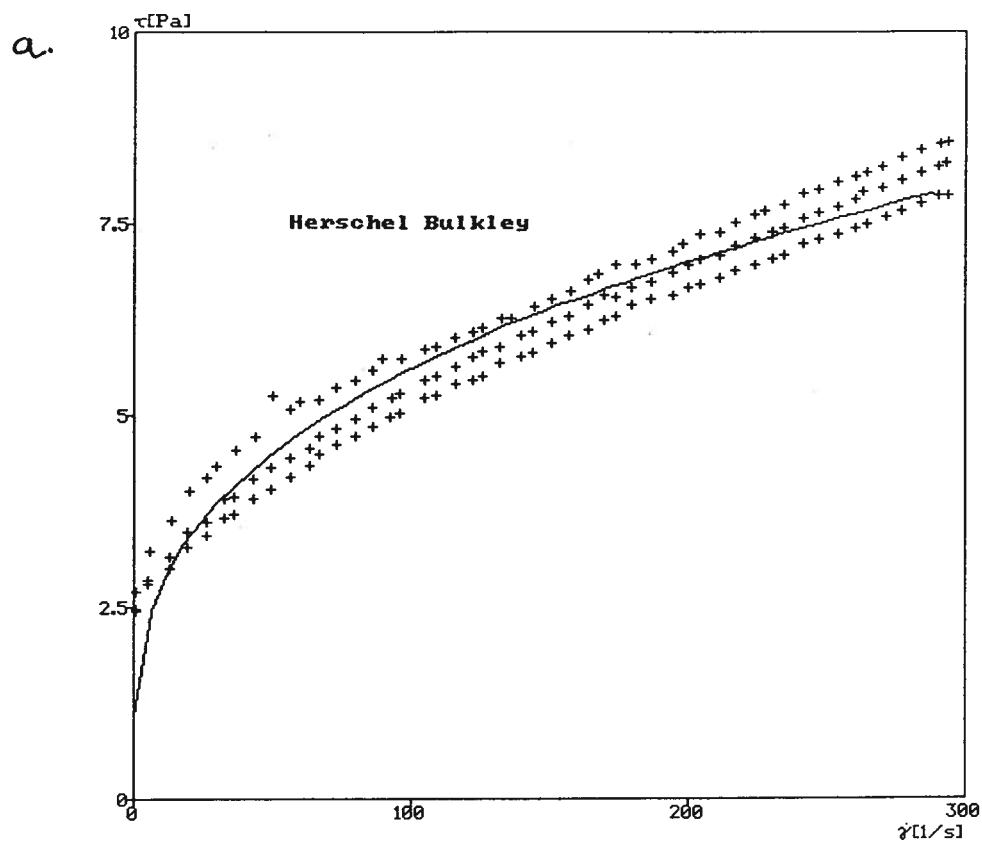


Figure AV.2 Rheological flow curve with fitted a) Herschel Bulkley and b) Casson models for experimental Run #1.

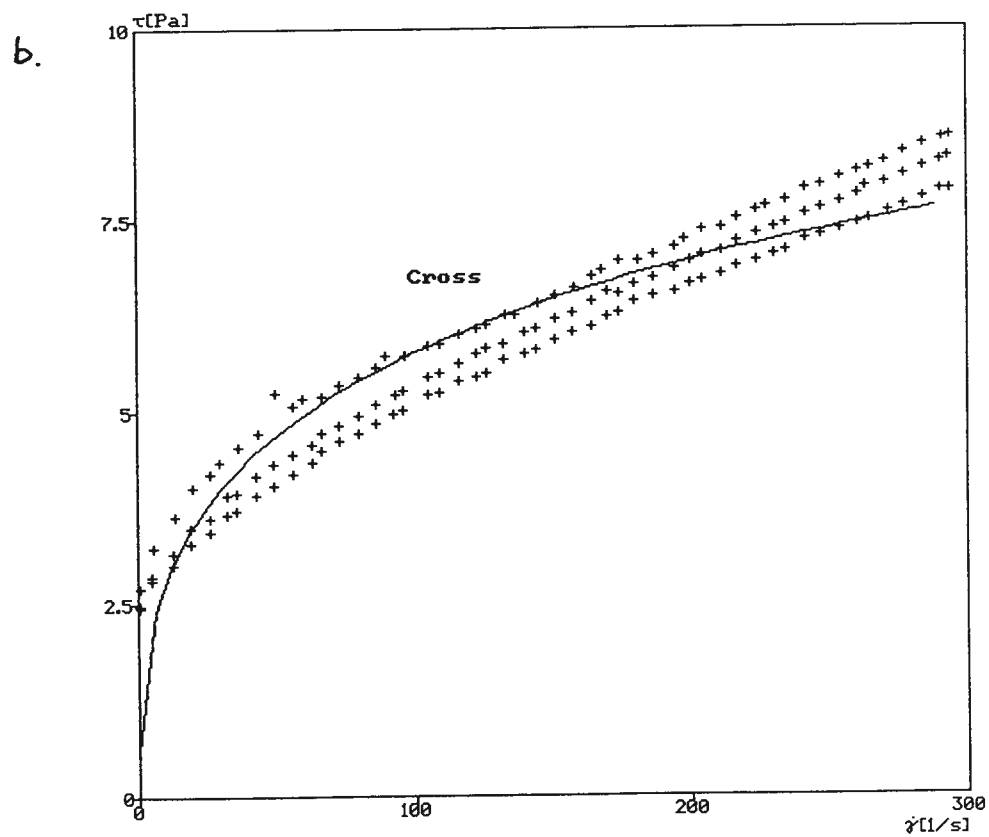
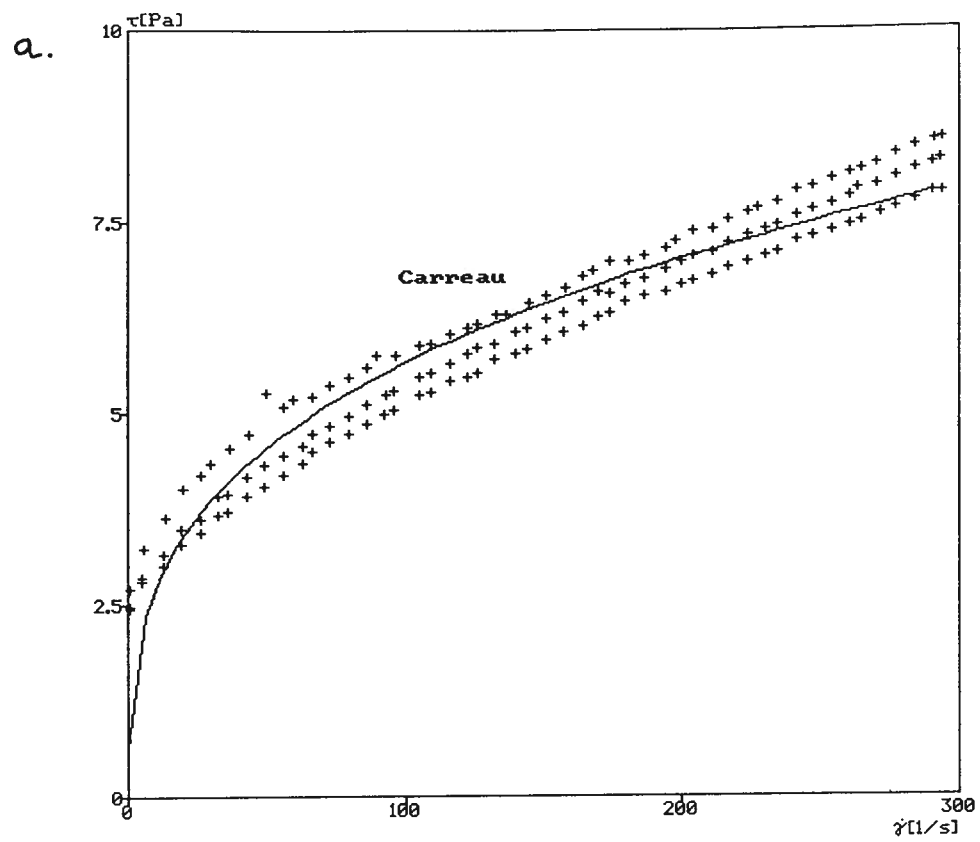


Figure AV.3 Rheological flow curve with fitted a) Carreau and b) Cross models for experimental Run #1.

Run #2: Suspension Composition

Carboxymethyl Cellulose (kg T ⁻¹):	0.50
Particle Passing Size (μm):	15.0
Solids Volume Fraction:	0.20
Magnetization:	Demagnetized
Sodium Silicate (kg T ⁻¹):	0.05
Kaolinite (% w/v):	0.75
pH:	4.0
Bentonite (% w/v):	0.25
Fine Coal (% w/v):	0.25

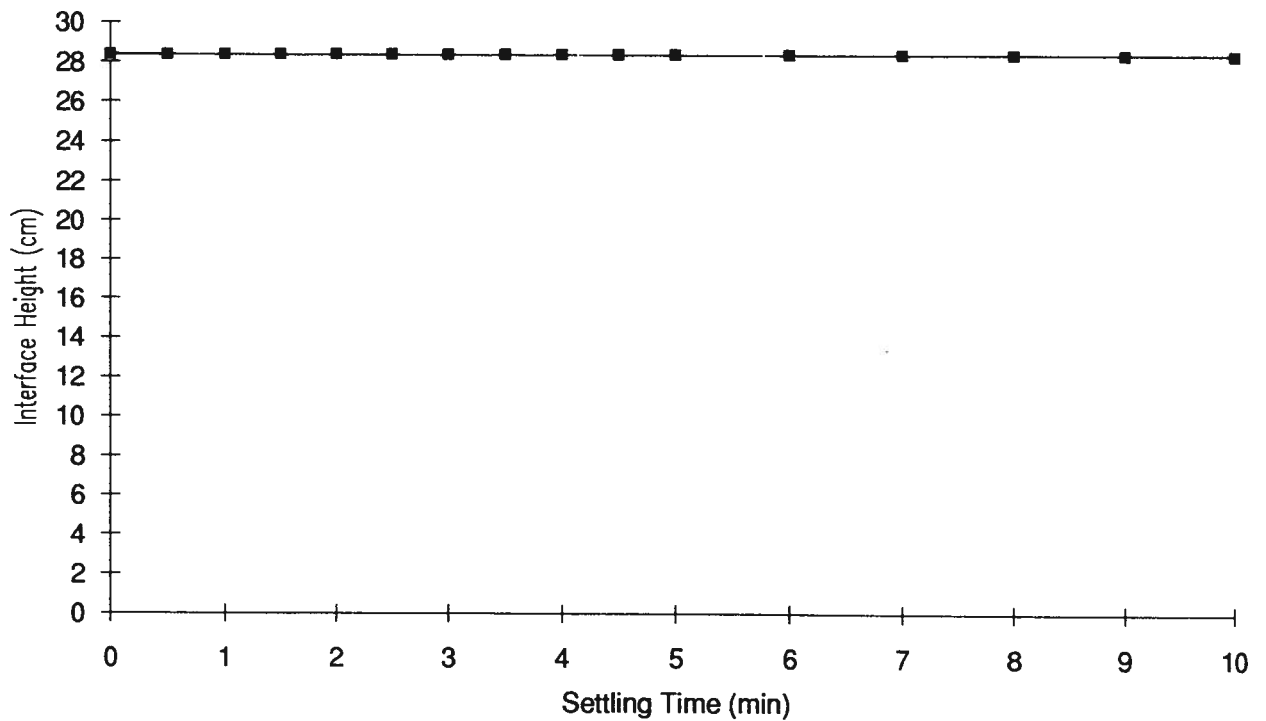


Figure AV.4 Settling curve interface height as a function of time for experimental Run #2.

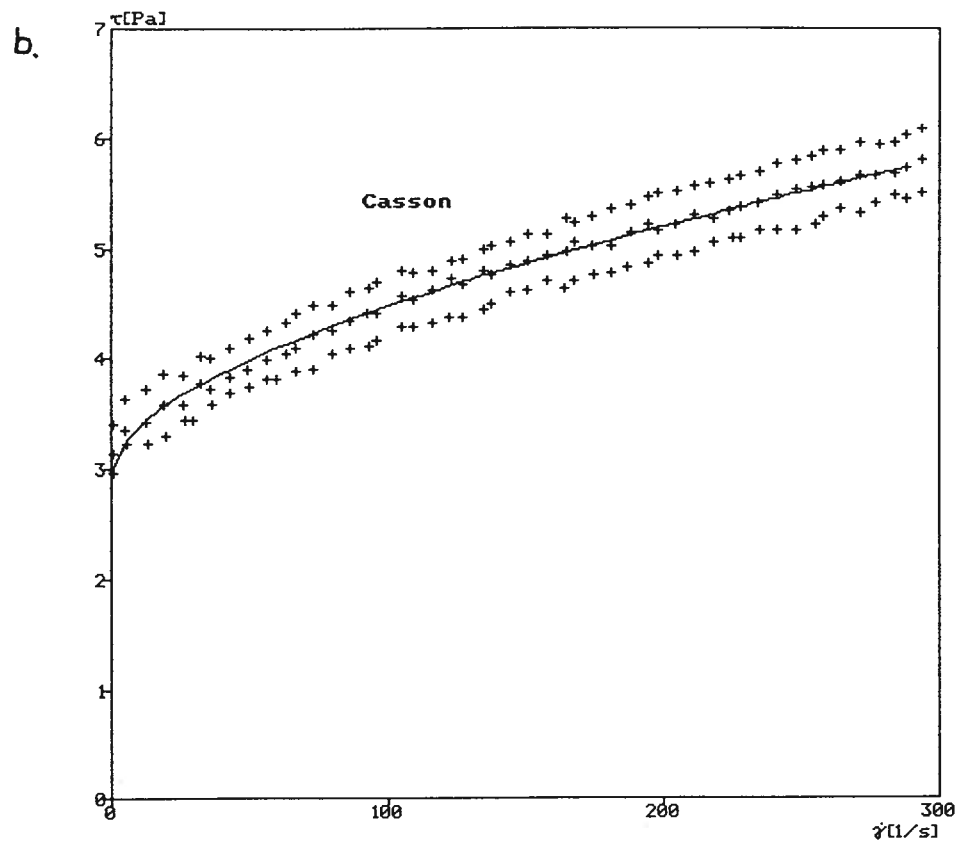
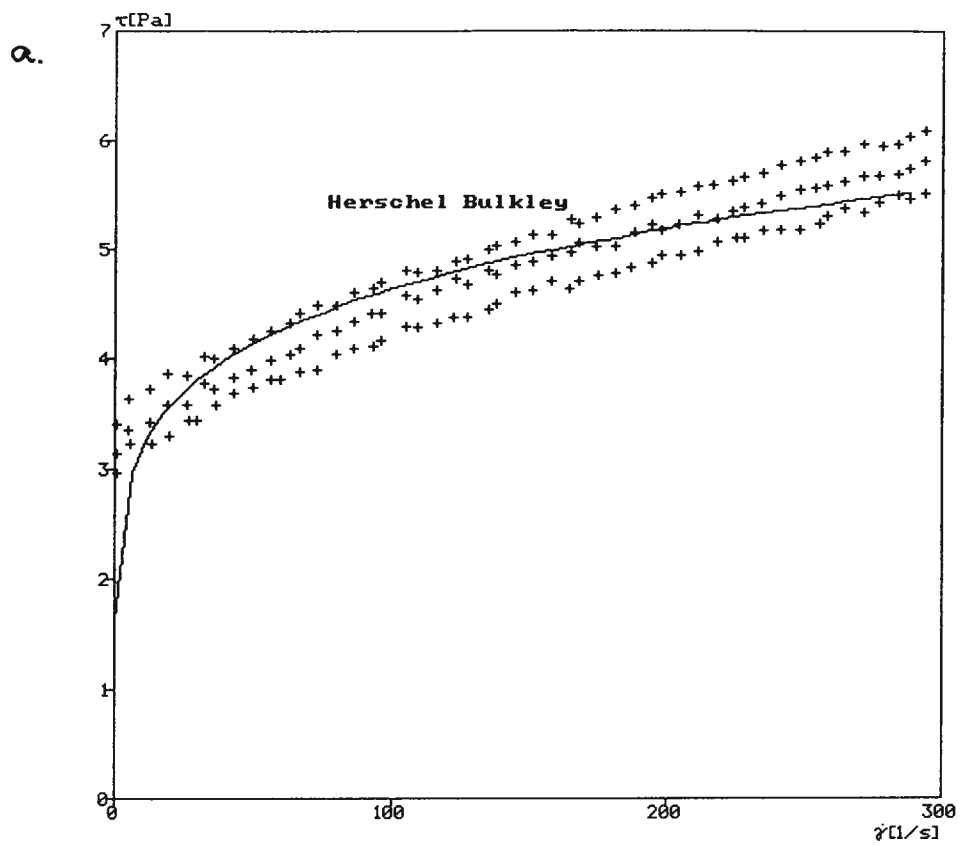


Figure AV.5 Rheological flow curve with fitted a) Herschel Bulkley and b) Casson models for experimental Run #2.

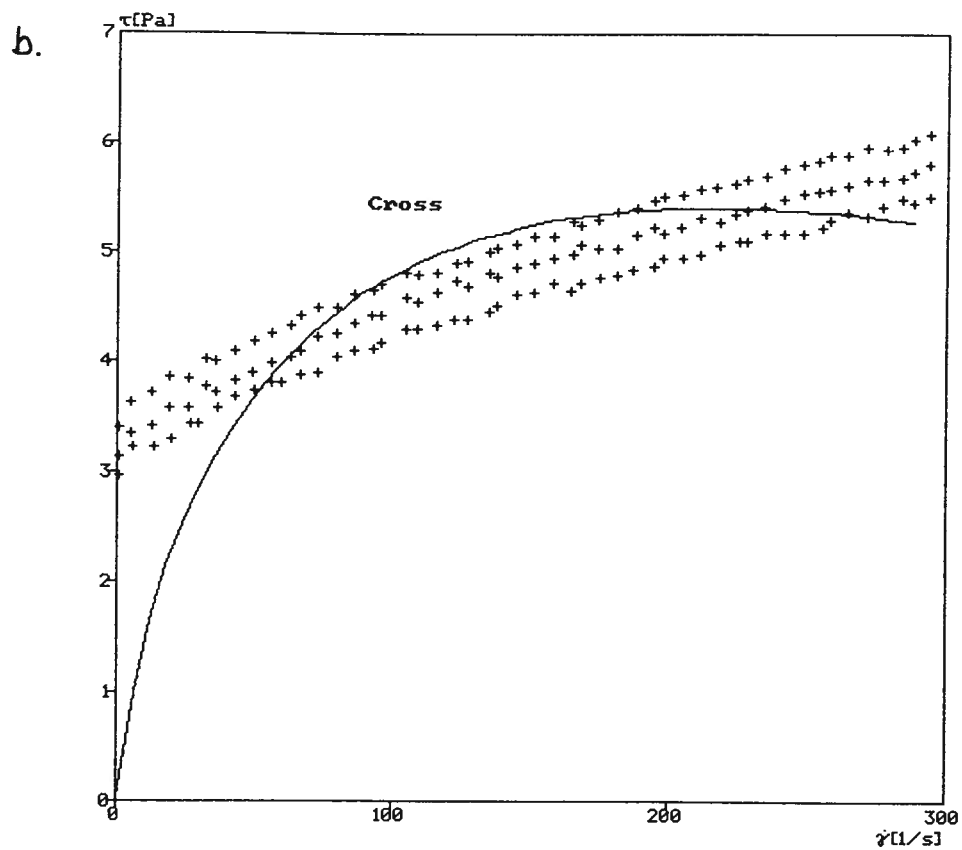
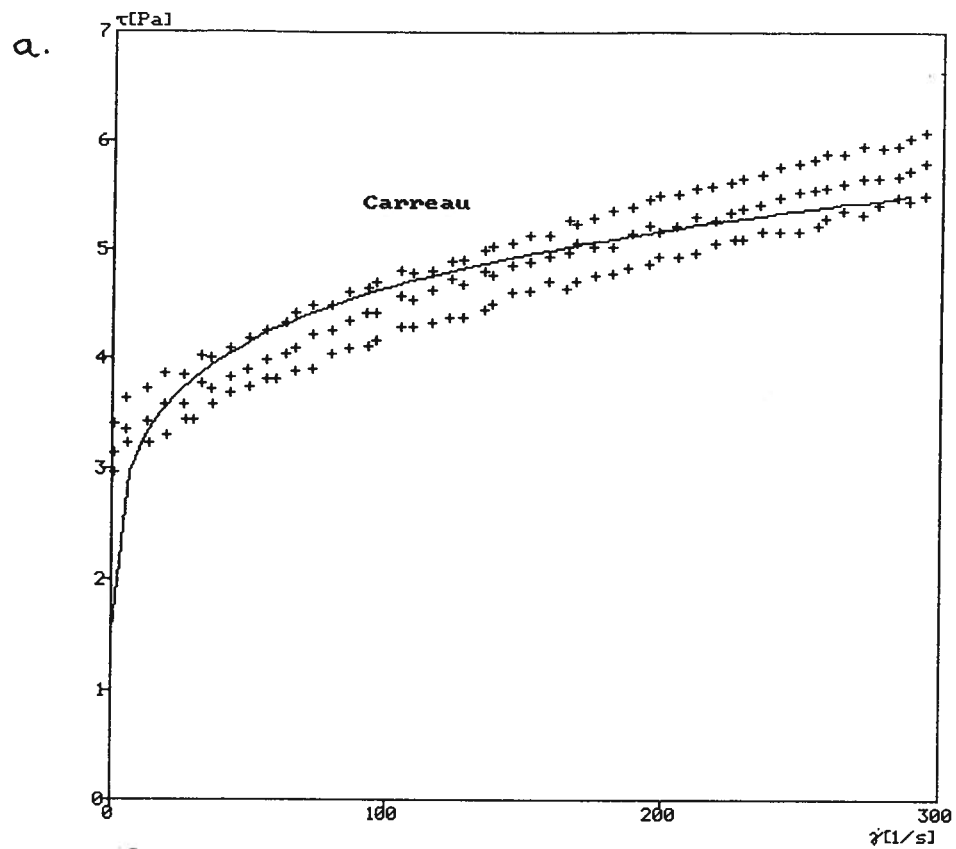


Figure AV.6 Rheological flow curve with fitted a) Carreau and b) Cross models for experimental Run #2.

Run #3: Suspension Composition

Carboxymethyl Cellulose (kg T^{-1}):	1.50
Particle Passing Size (μm):	45.0
Solids Volume Fraction:	0.20
Magnetization:	Demagnetized
Sodium Silicate (kg T^{-1}):	0.05
Kaolinite (% w/v):	0.25
pH:	10.0
Bentonite (% w/v):	0.25
Fine Coal (% w/v):	0.25

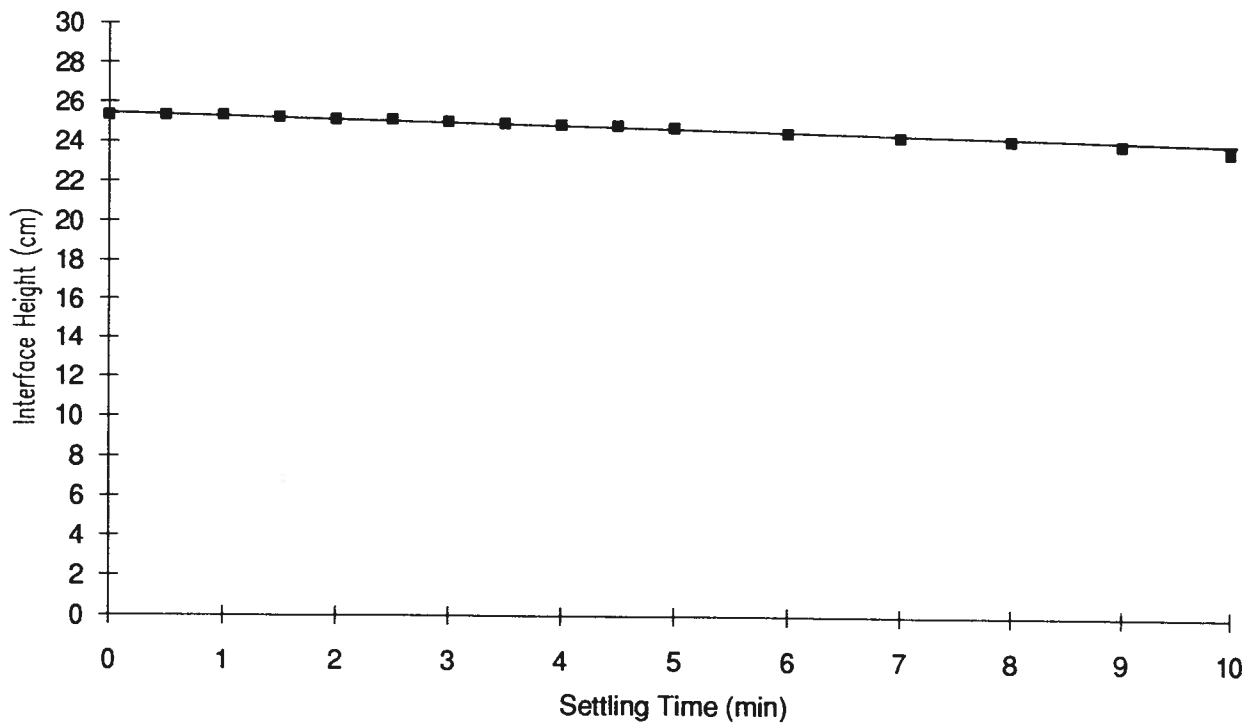


Figure AV.7 Settling curve interface height as a function of time for experimental Run #3.

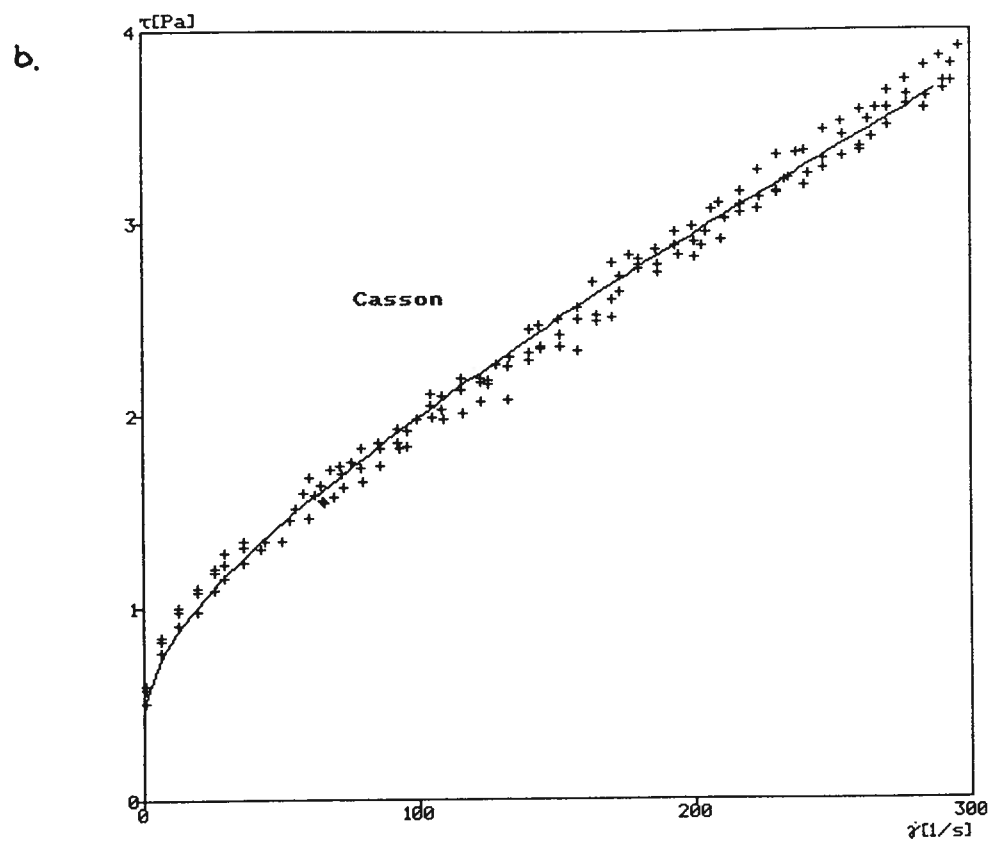
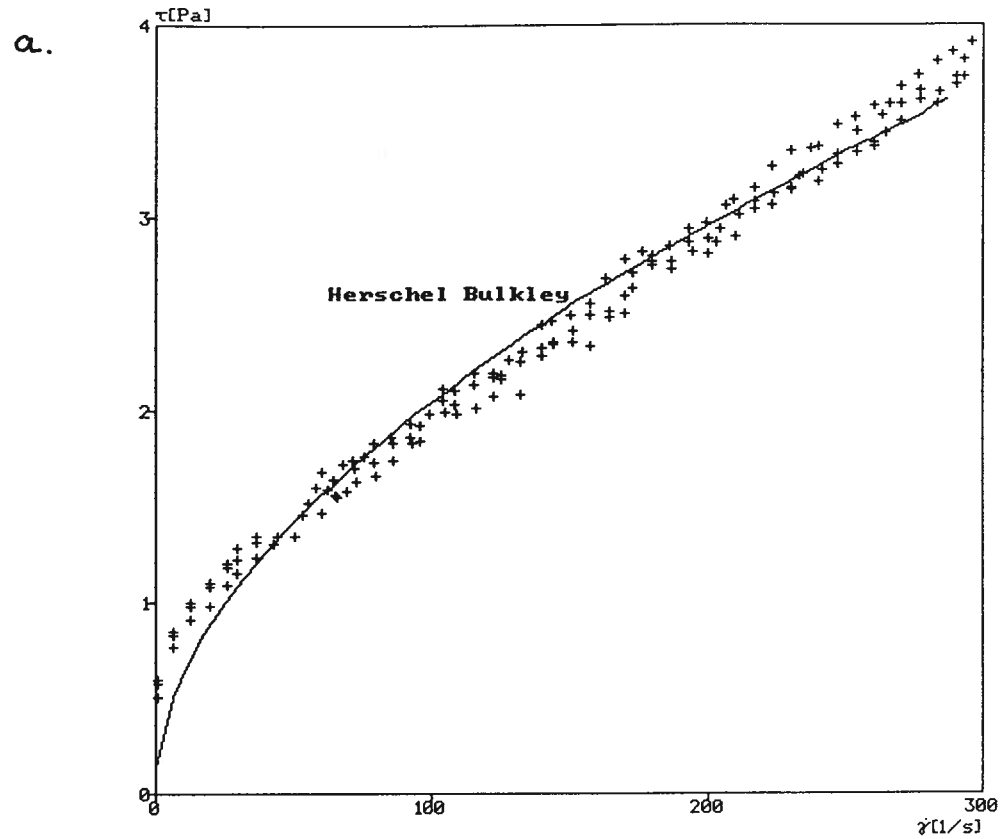


Figure AV.8 Rheological flow curve with fitted a) Herschel Bulkley and b) Casson models for experimental Run #3.

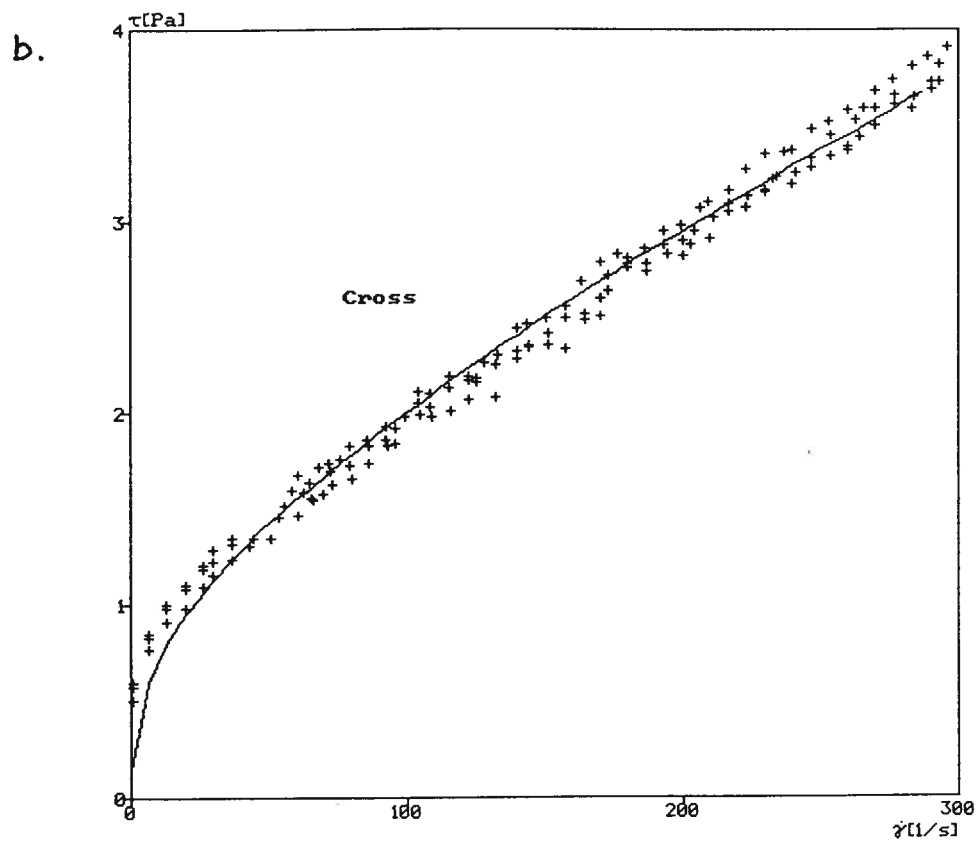
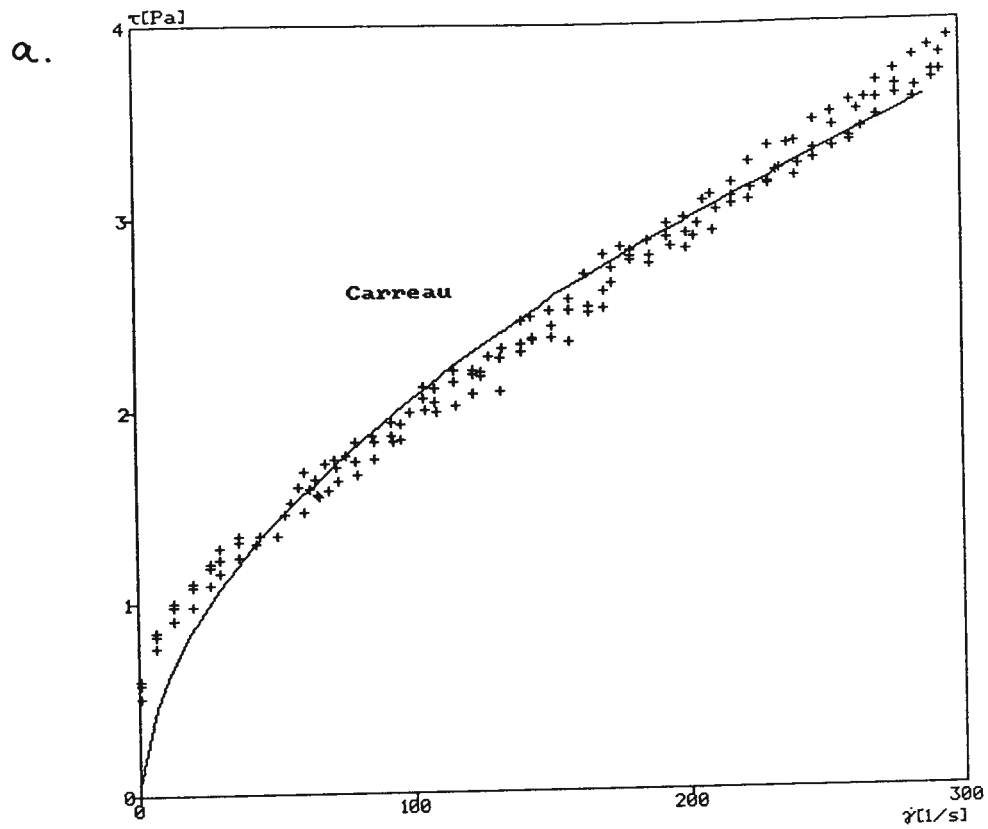


Figure AV.9 Rheological flow curve with fitted a) Carreau and b) Cross models for experimental Run #3.

Run #4: Suspension Composition

Carboxymethyl Cellulose (kg T ⁻¹):	0.50
Particle Passing Size (μm):	45.0
Solids Volume Fraction:	0.20
Magnetization:	Demagnetized
Sodium Silicate (kg T ⁻¹):	0.15
Kaolinite (% w/v):	0.25
pH:	4.0
Bentonite (% w/v):	0.75
Fine Coal (% w/v):	0.75

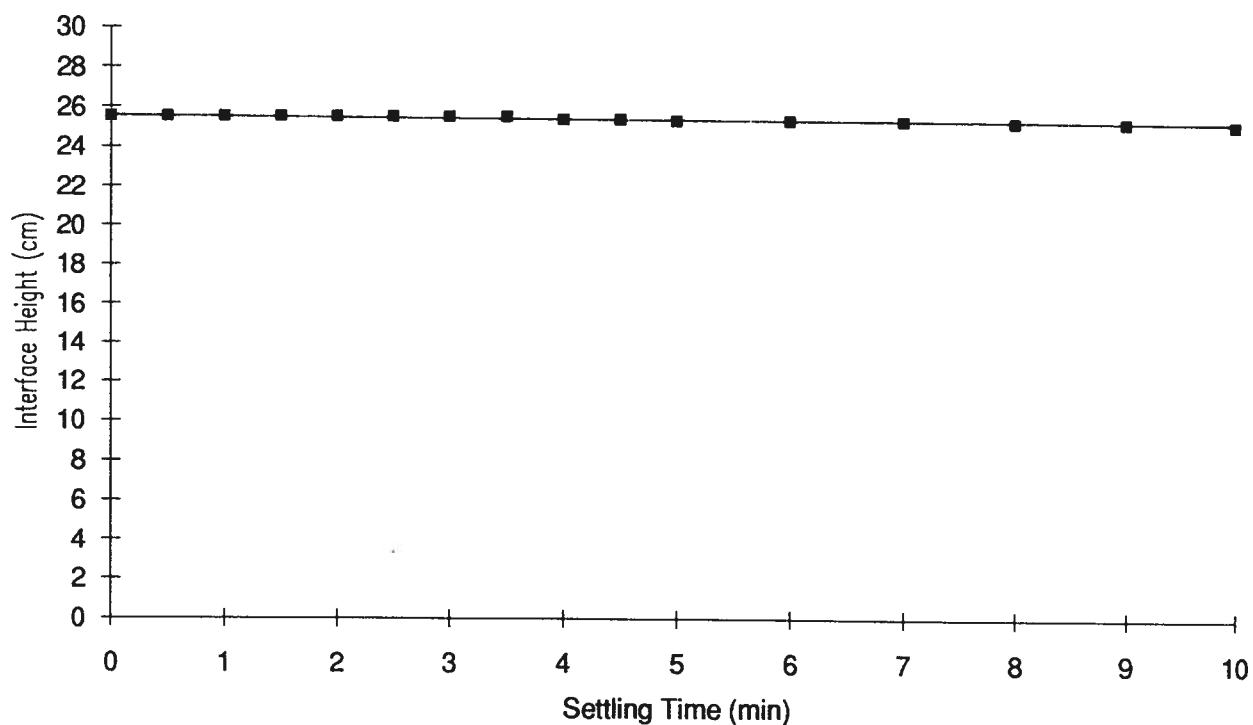


Figure AV.10 Settling curve interface height as a function of time for experimental Run #4.

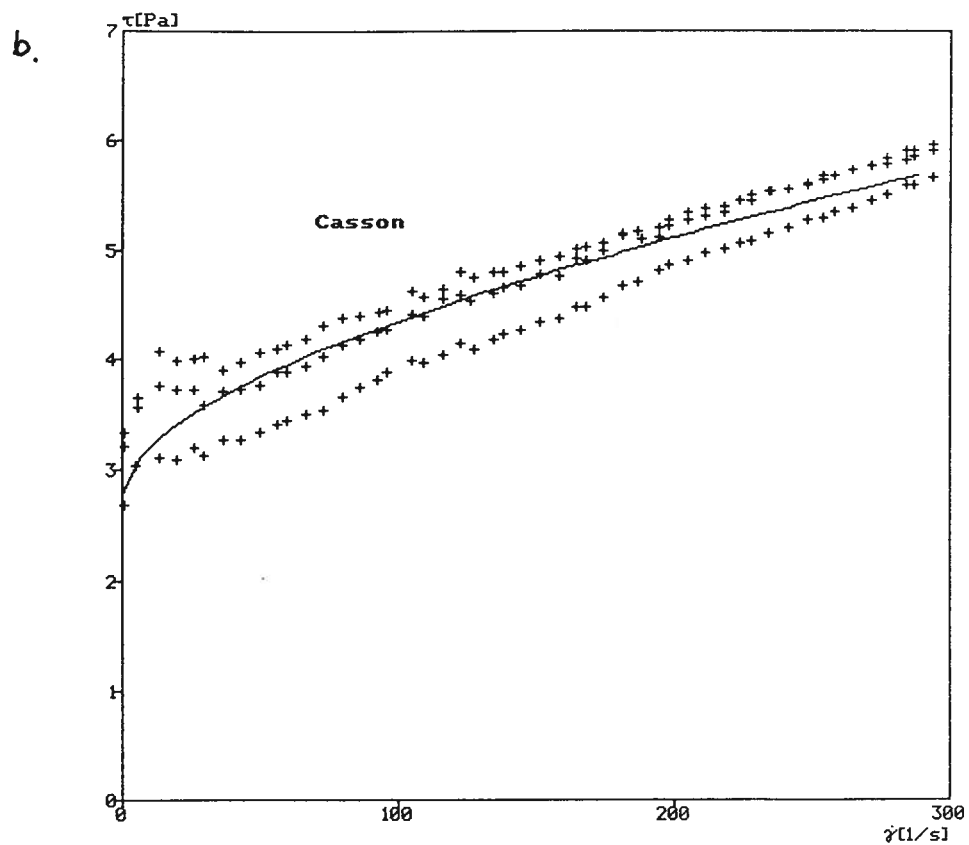
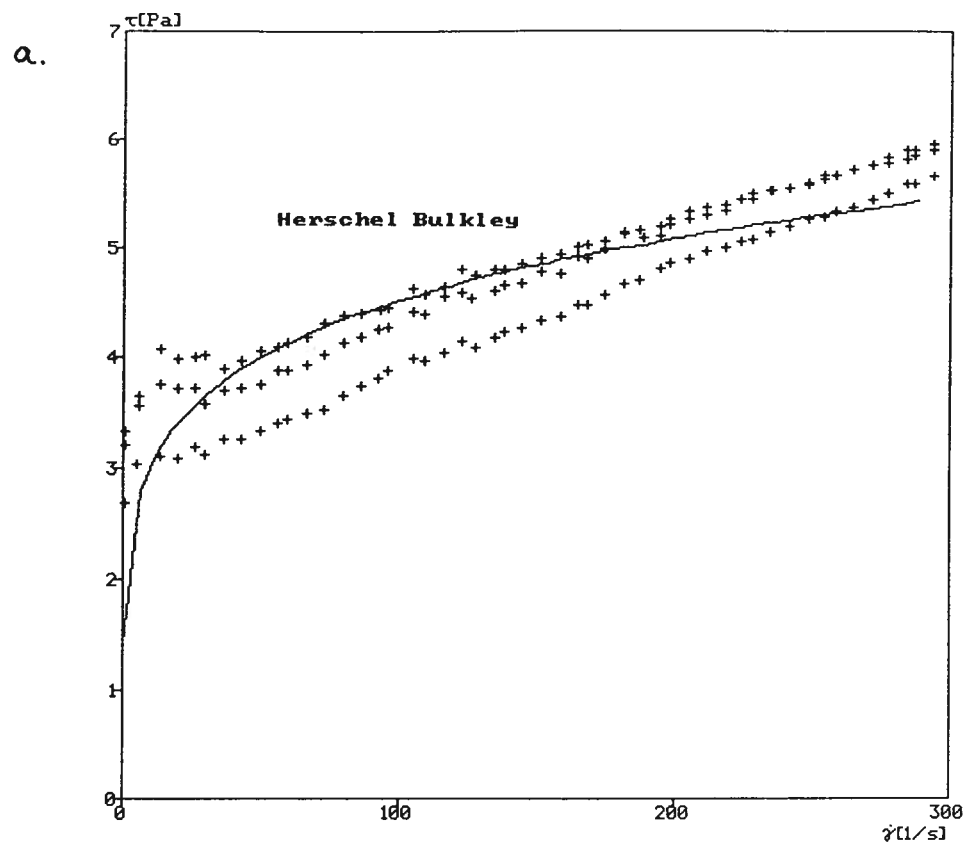


Figure AV.11 Rheological flow curve with fitted a) Herschel Bulkley and b) Casson models for experimental Run #4.

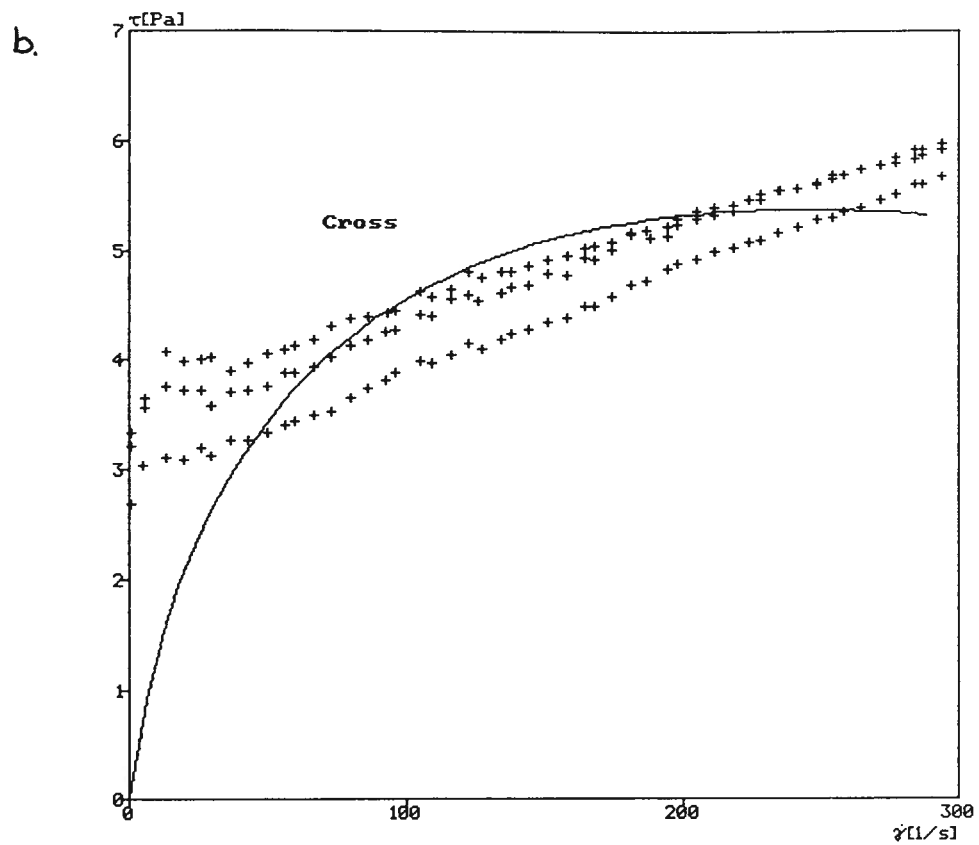
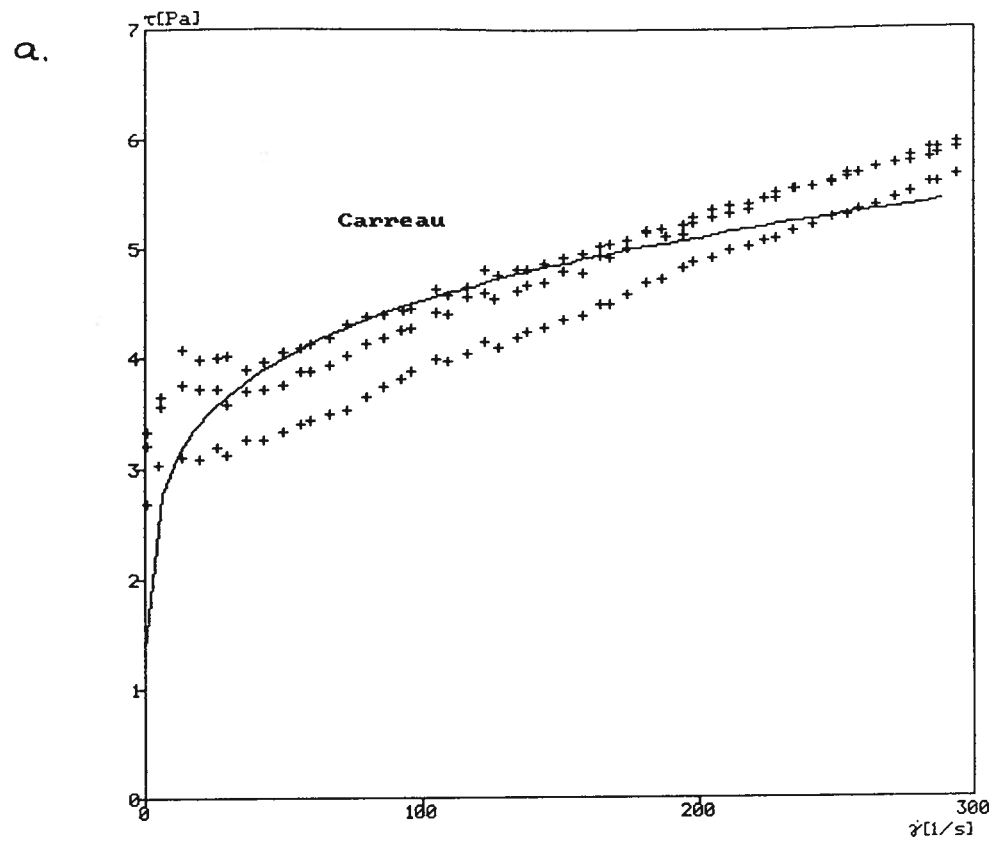


Figure AV.12 Rheological flow curve with fitted a) Carreau and b) Cross models for experimental Run #4.

Run #5: Suspension Composition

Carboxymethyl Cellulose (kg T ⁻¹):	1.50
Particle Passing Size (μm):	15.0
Solids Volume Fraction:	0.10
Magnetization:	Demagnetized
Sodium Silicate (kg T ⁻¹):	0.05
Kaolinite (% w/v):	0.25
pH:	4.0
Bentonite (% w/v):	0.75
Fine Coal (% w/v):	0.25

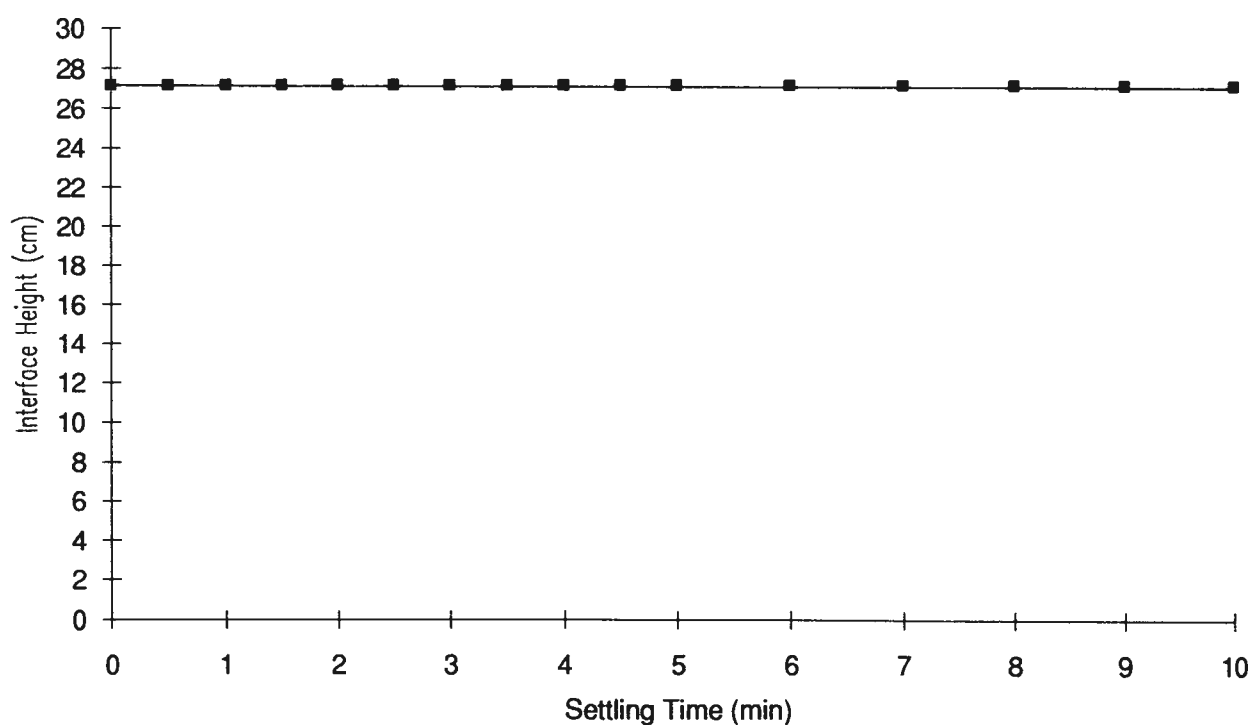
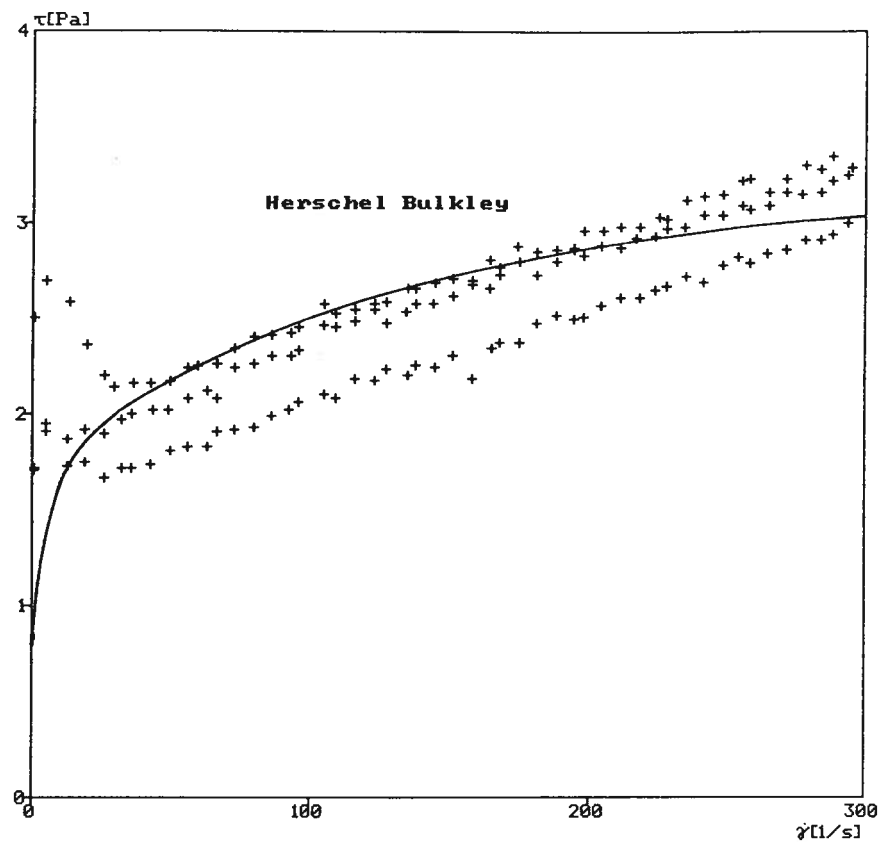


Figure AV.13 Settling curve interface height as a function of time for experimental Run #5.

a



b.

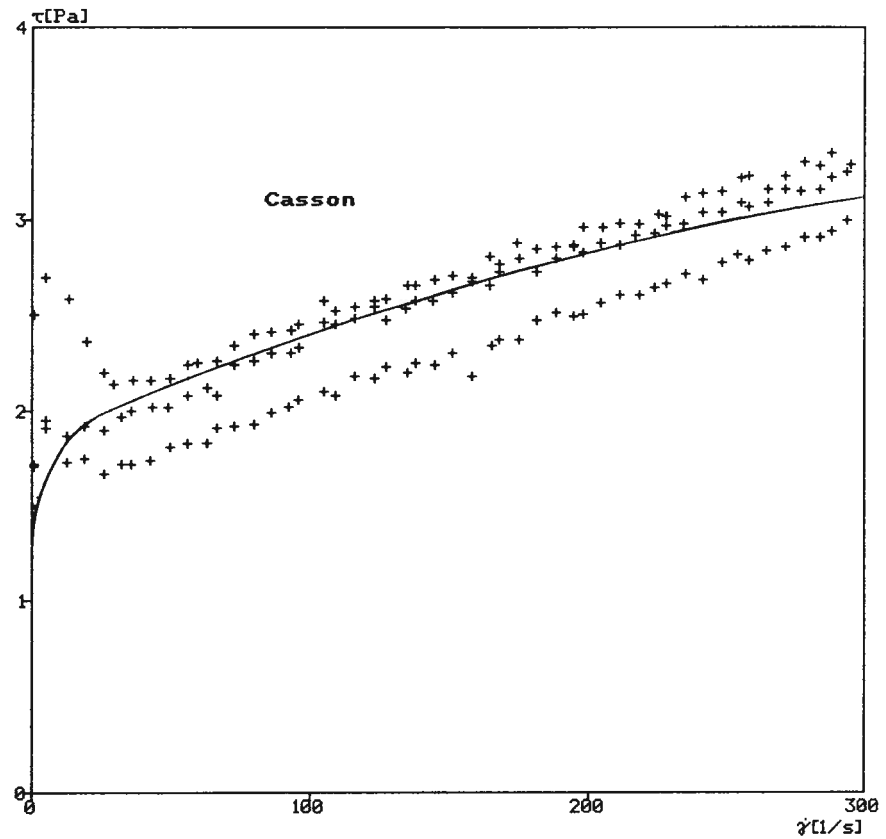
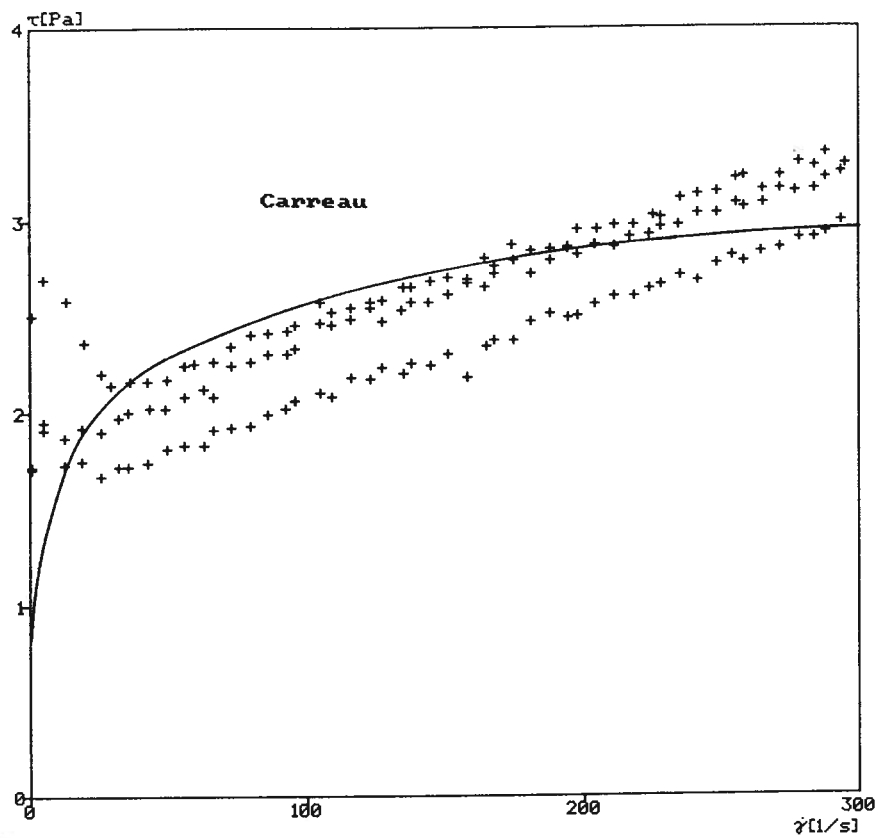


Figure AV.14 Rheological flow curve with fitted a) Herschel Bulkley and b) Casson models for experimental Run #5.

a.



b.

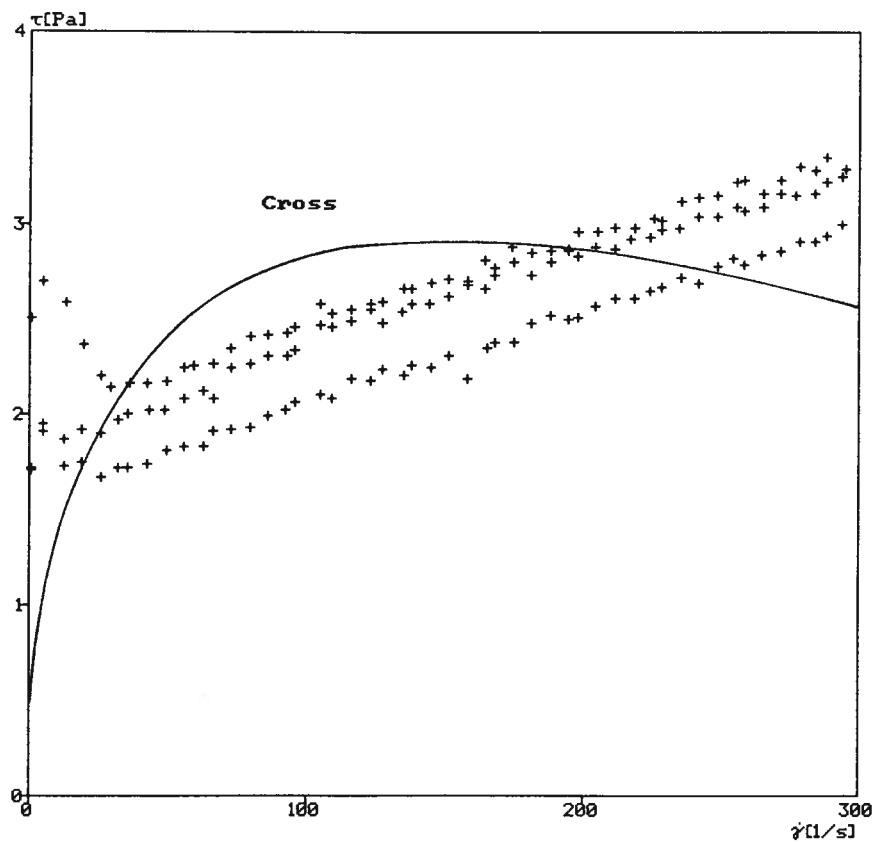


Figure AV.15 Rheological flow curve with fitted a) Carreau and b) Cross models for experimental Run #5.

Run #6: Suspension Composition

Carboxymethyl Cellulose (kg T^{-1}):	0.50
Particle Passing Size (μm):	15.0
Solids Volume Fraction:	0.10
Magnetization:	Demagnetized
Sodium Silicate (kg T^{-1}):	0.15
Kaolinite (% w/v):	0.25
pH:	10.0
Bentonite (% w/v):	0.25
Fine Coal (% w/v):	0.75

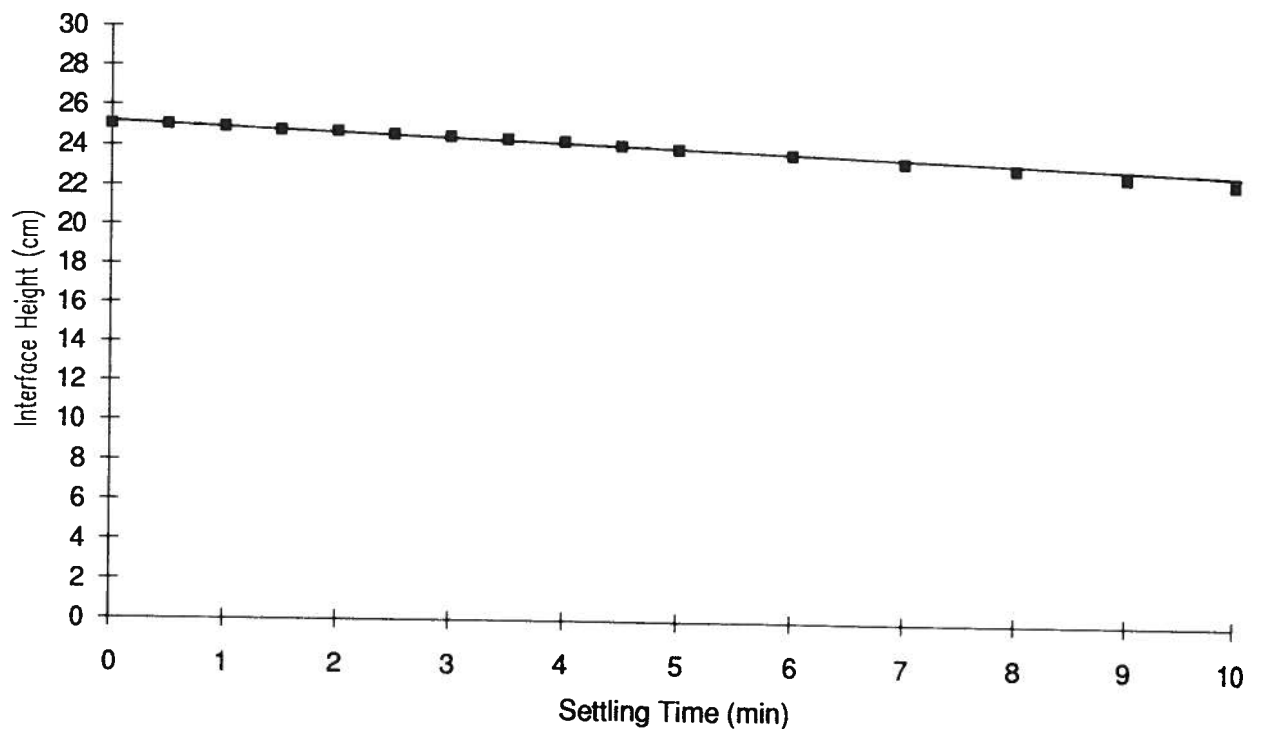


Figure AV.16 Settling curve interface height as a function of time for experimental Run #6.

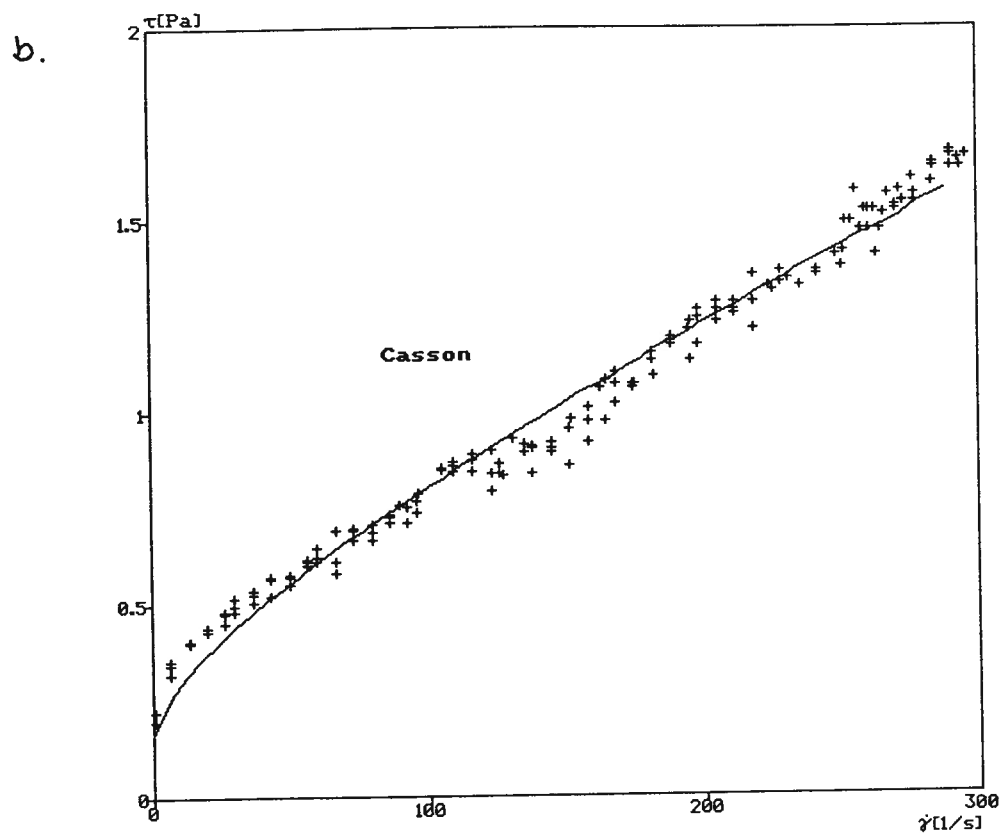
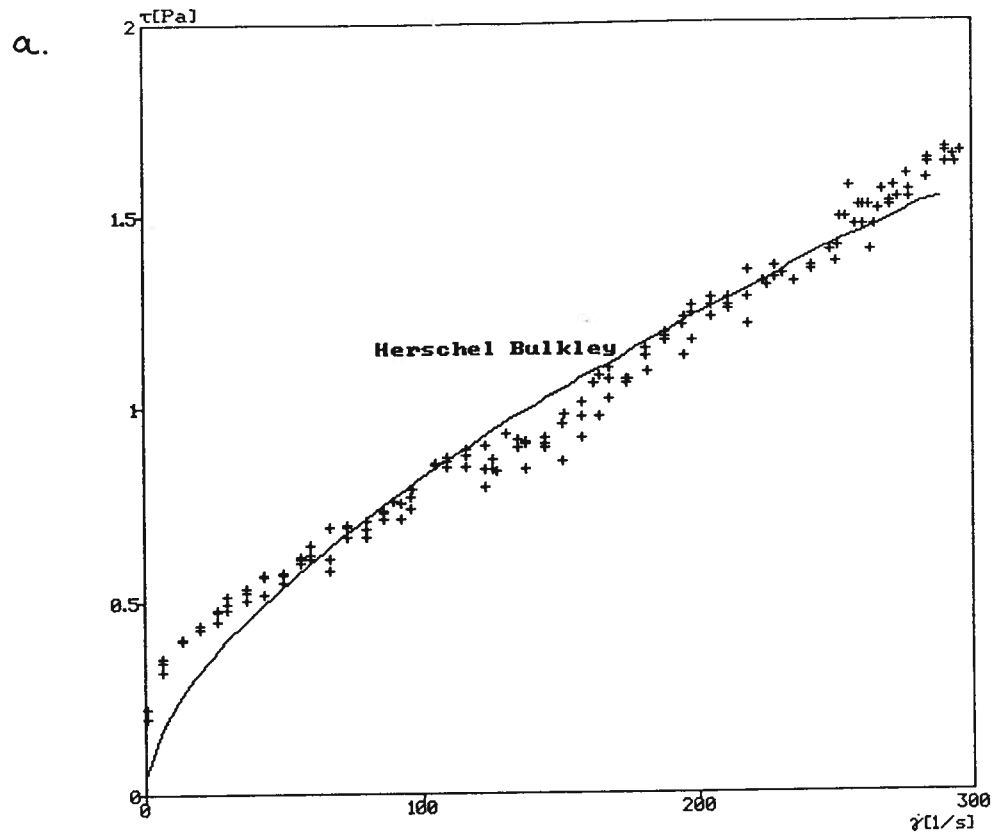


Figure AV.17 Rheological flow curve with fitted a) Herschel Bulkley and b) Casson models for experimental Run #6.

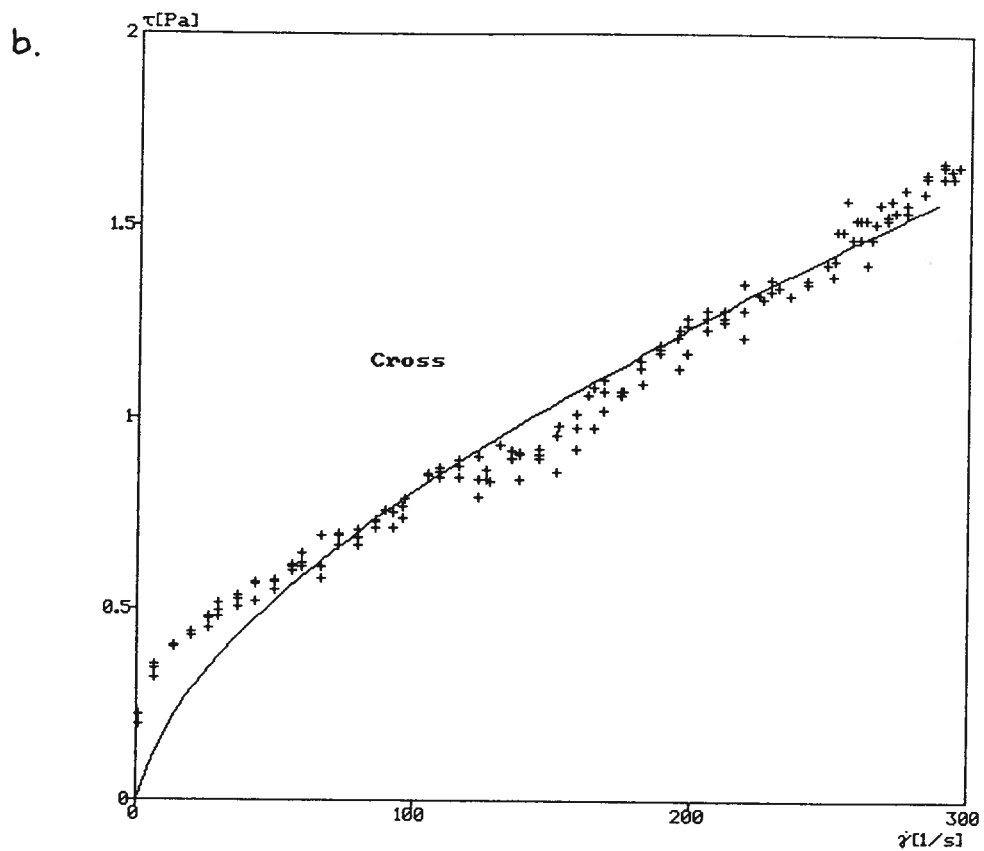
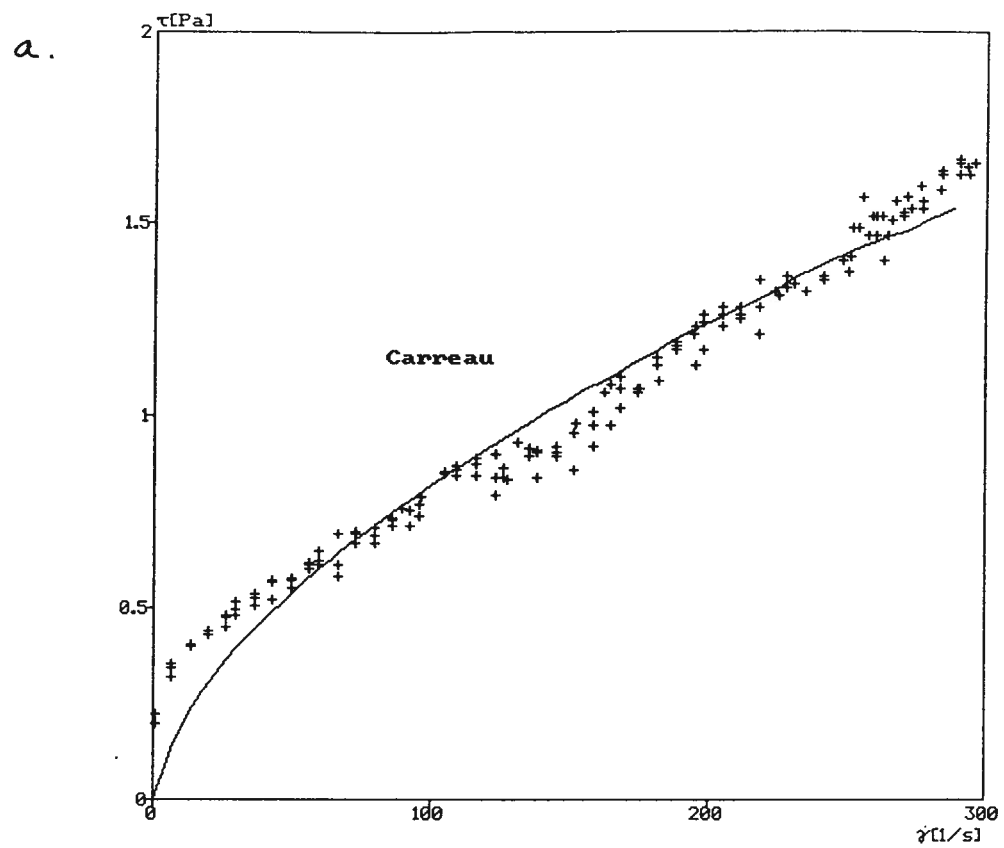


Figure AV.18 Rheological flow curve with fitted a) Carreau and b) Cross models for experimental Run #6.

Run #7: Suspension Composition

Carboxymethyl Cellulose (kg T ⁻¹):	1.50
Particle Passing Size (μm):	45.0
Solids Volume Fraction:	0.10
Magnetization:	Demagnetized
Sodium Silicate (kg T ⁻¹):	0.15
Kaolinite (% w/v):	0.75
pH:	4.0
Bentonite (% w/v):	0.25
Fine Coal (% w/v):	0.75

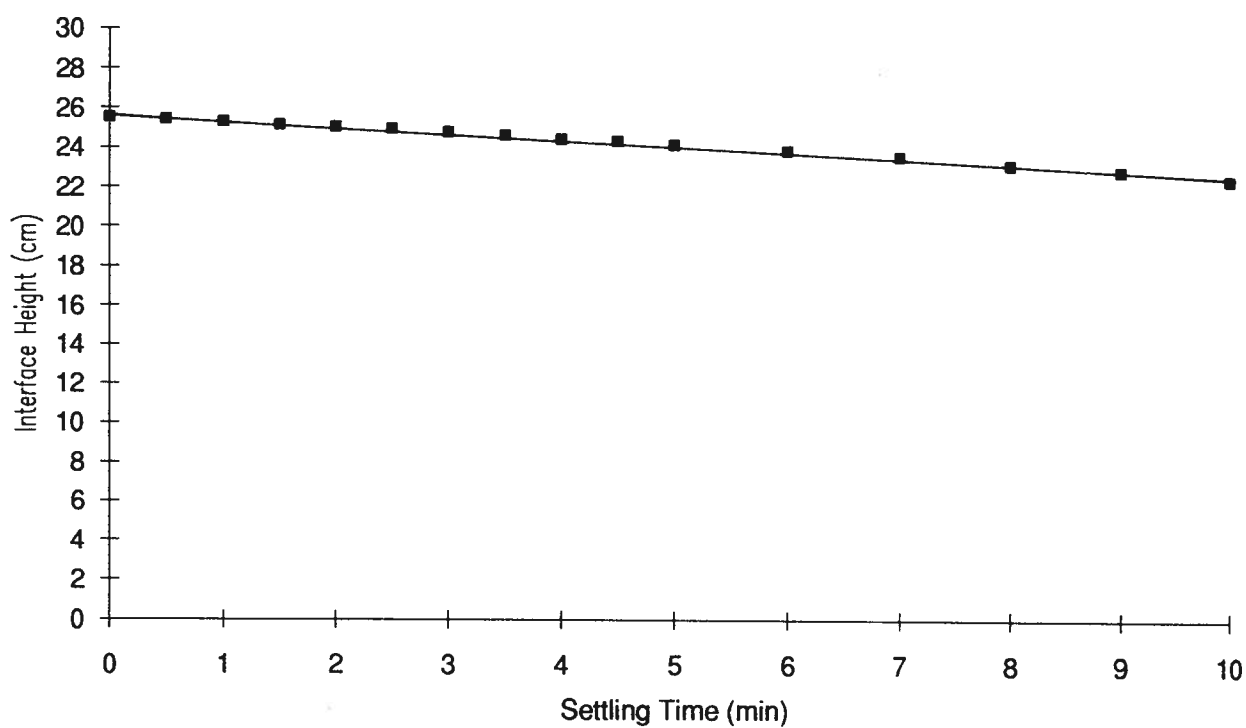


Figure AV.19 Settling curve interface height as a function of time for experimental Run #7.

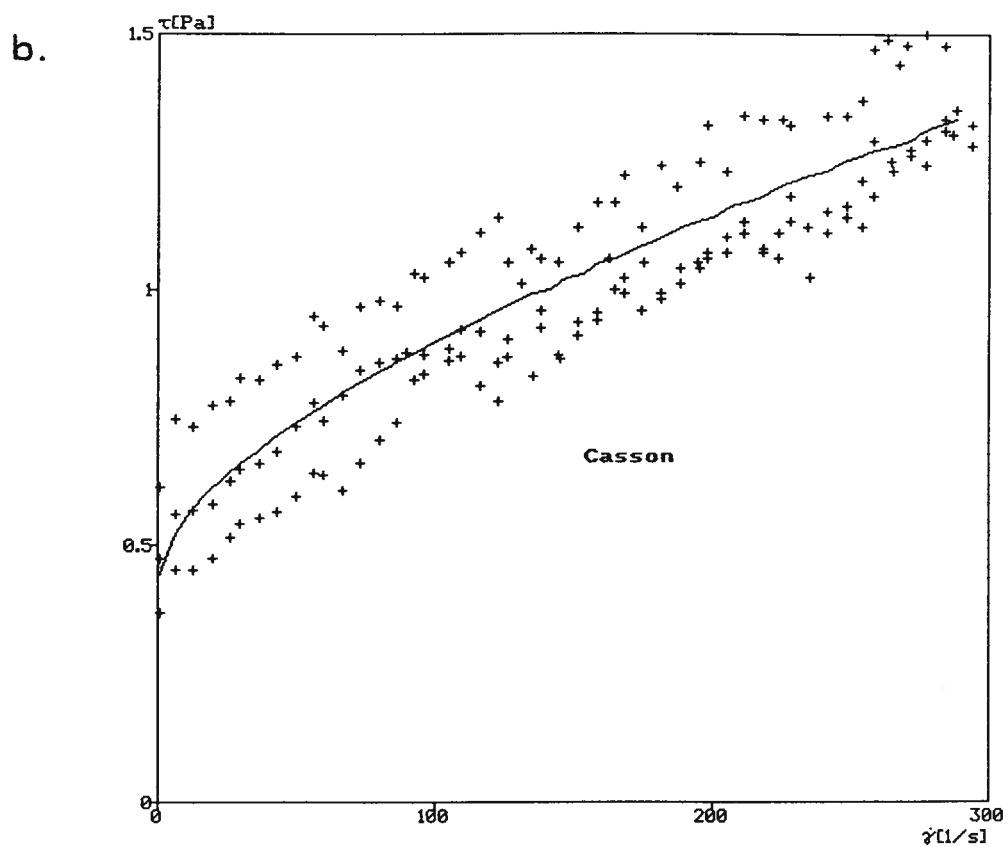
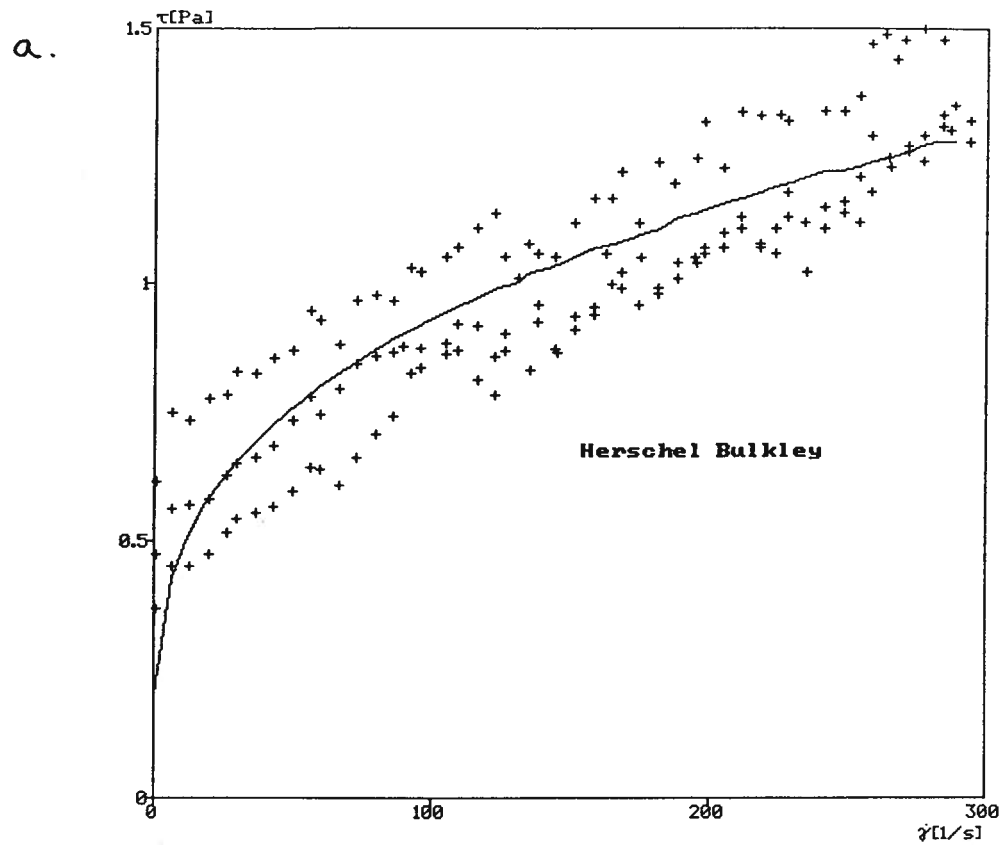


Figure AV.20 Rheological flow curve with fitted a) Herschel Bulkley and b) Casson models for experimental Run #7.

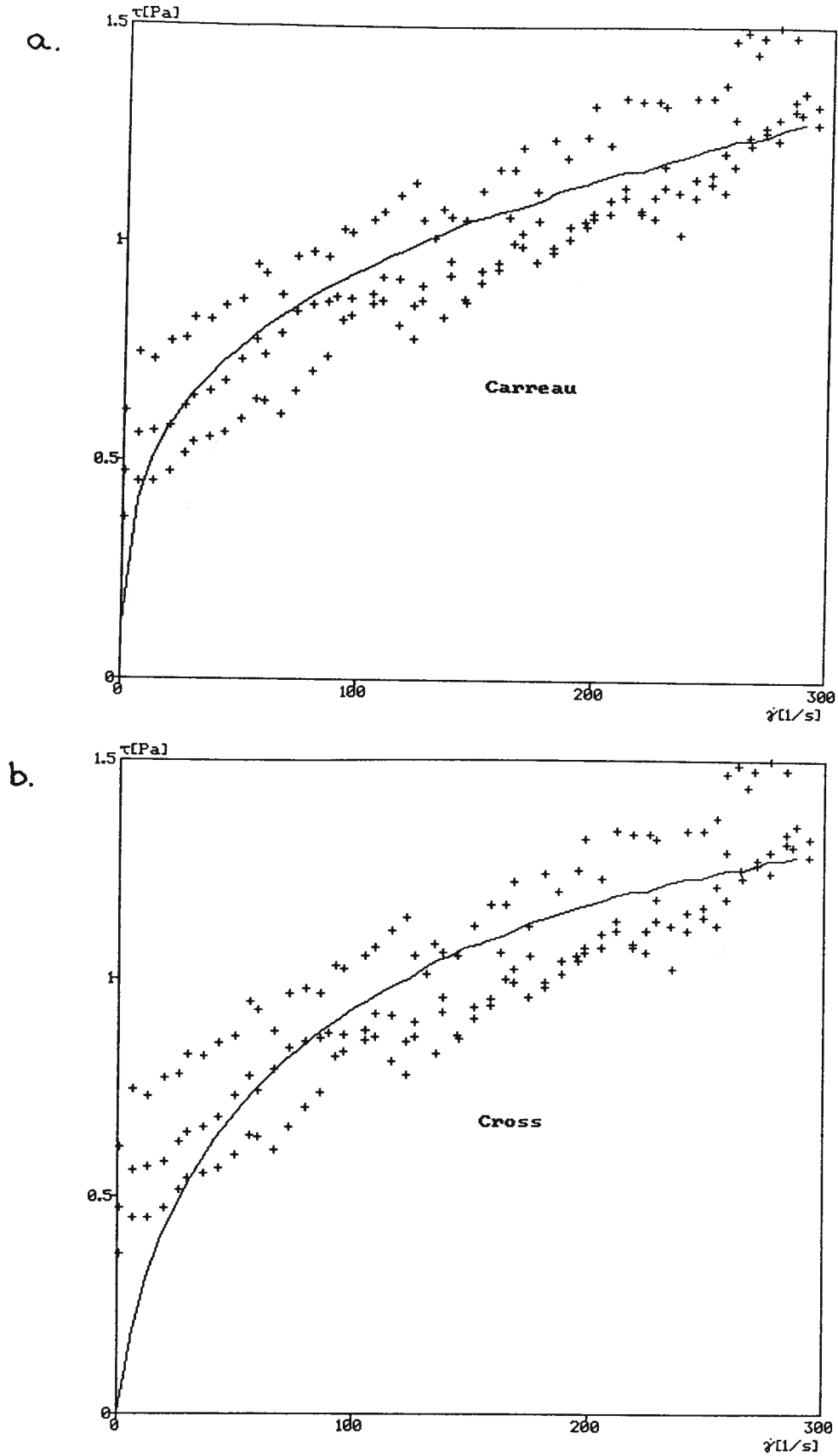


Figure AV.21 Rheological flow curve with fitted a) Carreau and b) Cross models for experimental Run #7.

Run #8: Suspension Composition

Carboxymethyl Cellulose (kg T ⁻¹):	0.50
Particle Passing Size (μm):	45.0
Solids Volume Fraction:	0.10
Magnetization:	Demagnetized
Sodium Silicate (kg T ⁻¹):	0.05
Kaolinite (% w/v):	0.75
pH:	10.0
Bentonite (% w/v):	0.75
Fine Coal (% w/v):	0.25

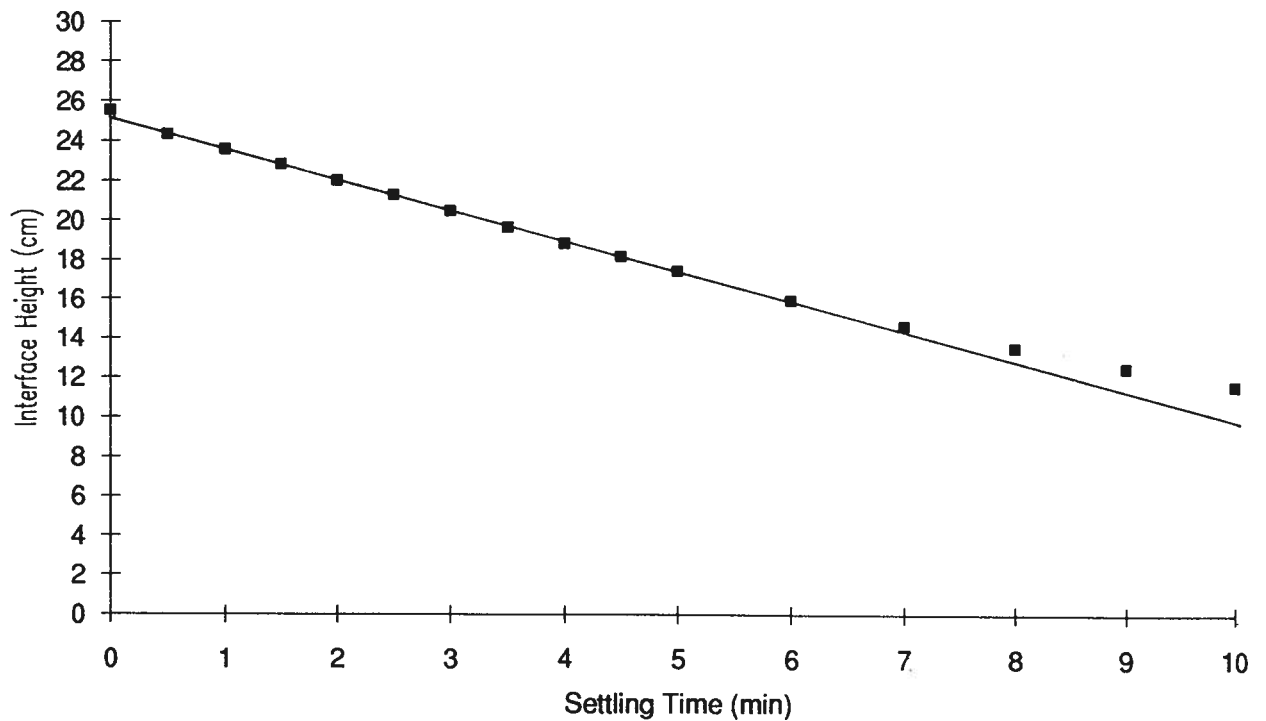


Figure AV.22 Settling curve interface height as a function of time for experimental Run #8.

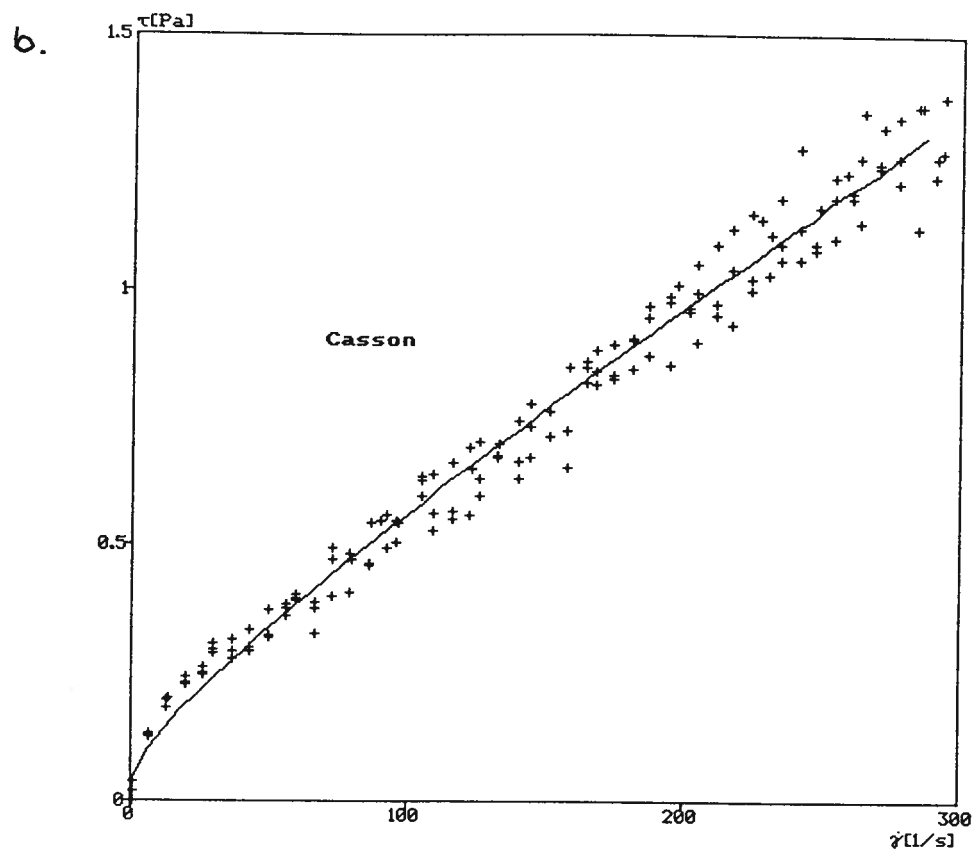
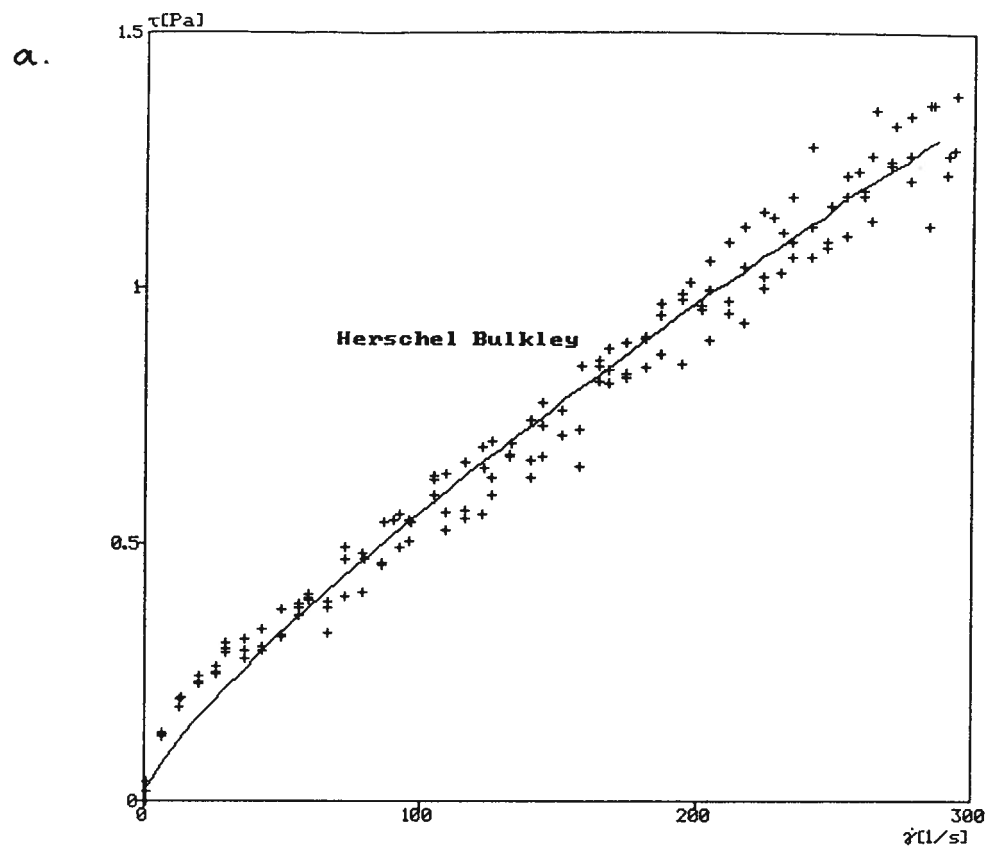


Figure AV.23 Rheological flow curve with fitted a) Herschel Bulkley and b) Casson models for experimental Run #8.

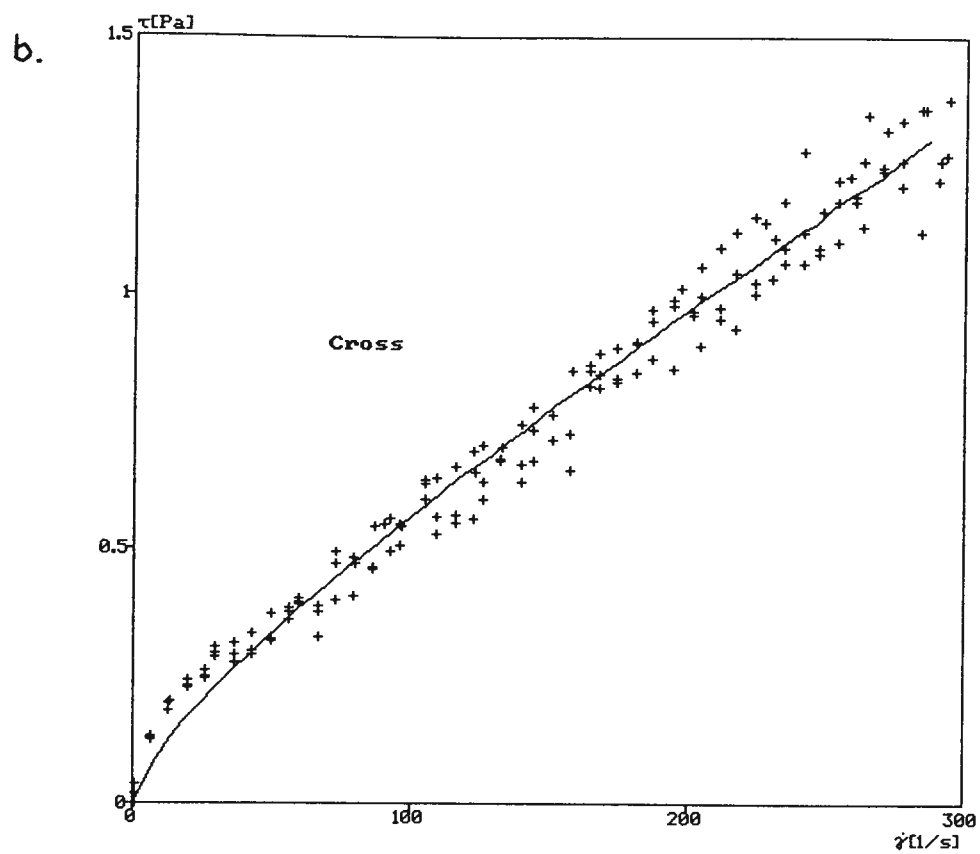
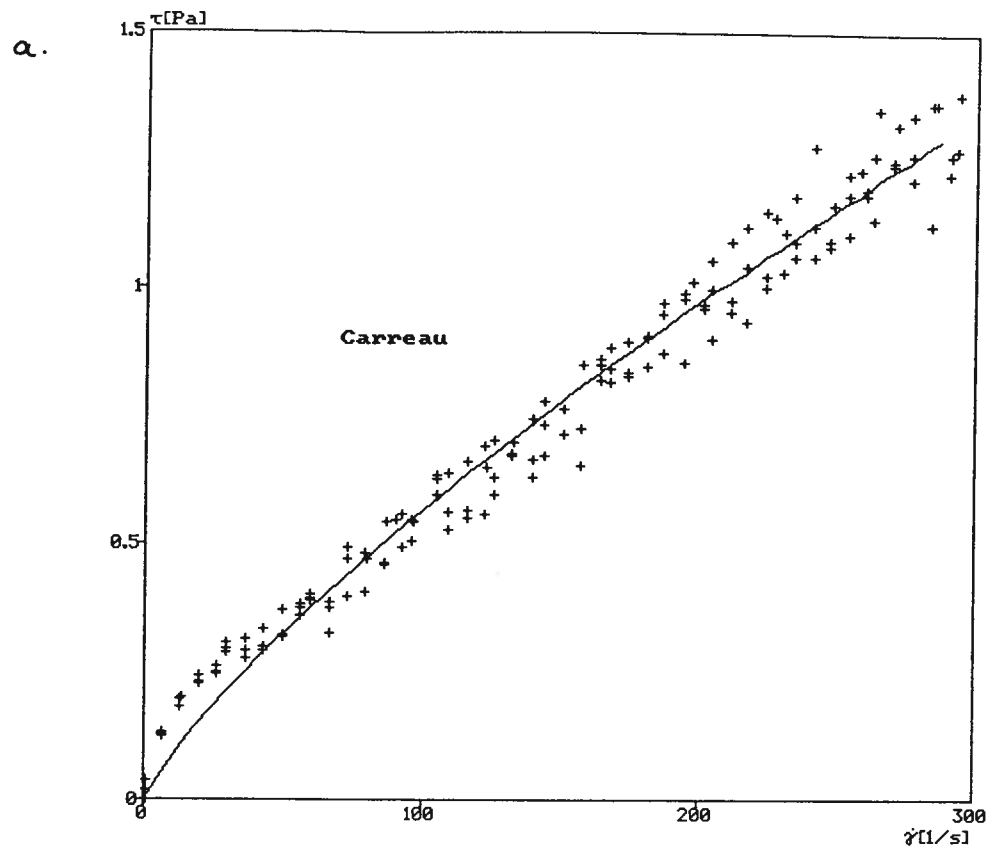


Figure AV.24 Rheological flow curve with fitted a) Carreau and b) Cross models for experimental Run #8.

Run #9: Suspension Composition

Carboxymethyl Cellulose (kg T ⁻¹):	1.50
Particle Passing Size (μm):	15.0
Solids Volume Fraction:	0.20
Magnetization:	Magnetized
Sodium Silicate (kg T ⁻¹):	0.15
Kaolinite (% w/v):	0.25
pH:	4.0
Bentonite (% w/v):	0.25
Fine Coal (% w/v):	0.25

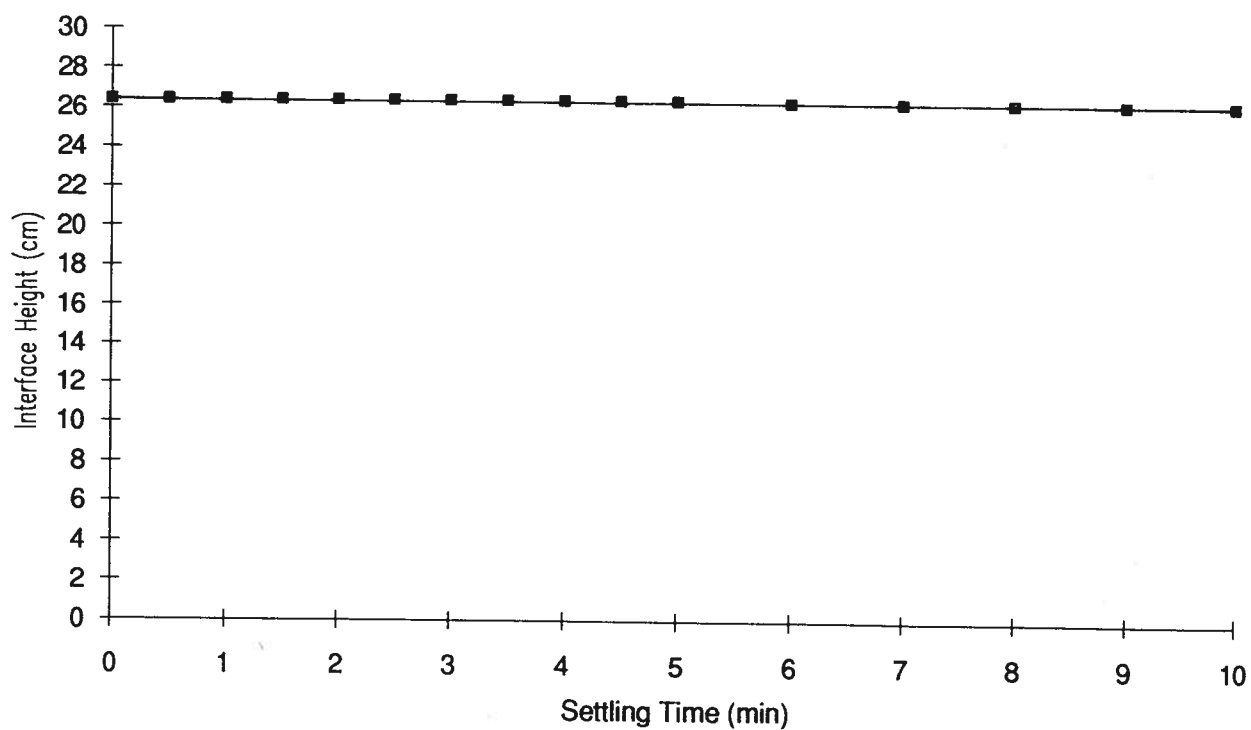


Figure AV.25 Settling curve interface height as a function of time for experimental Run #9.

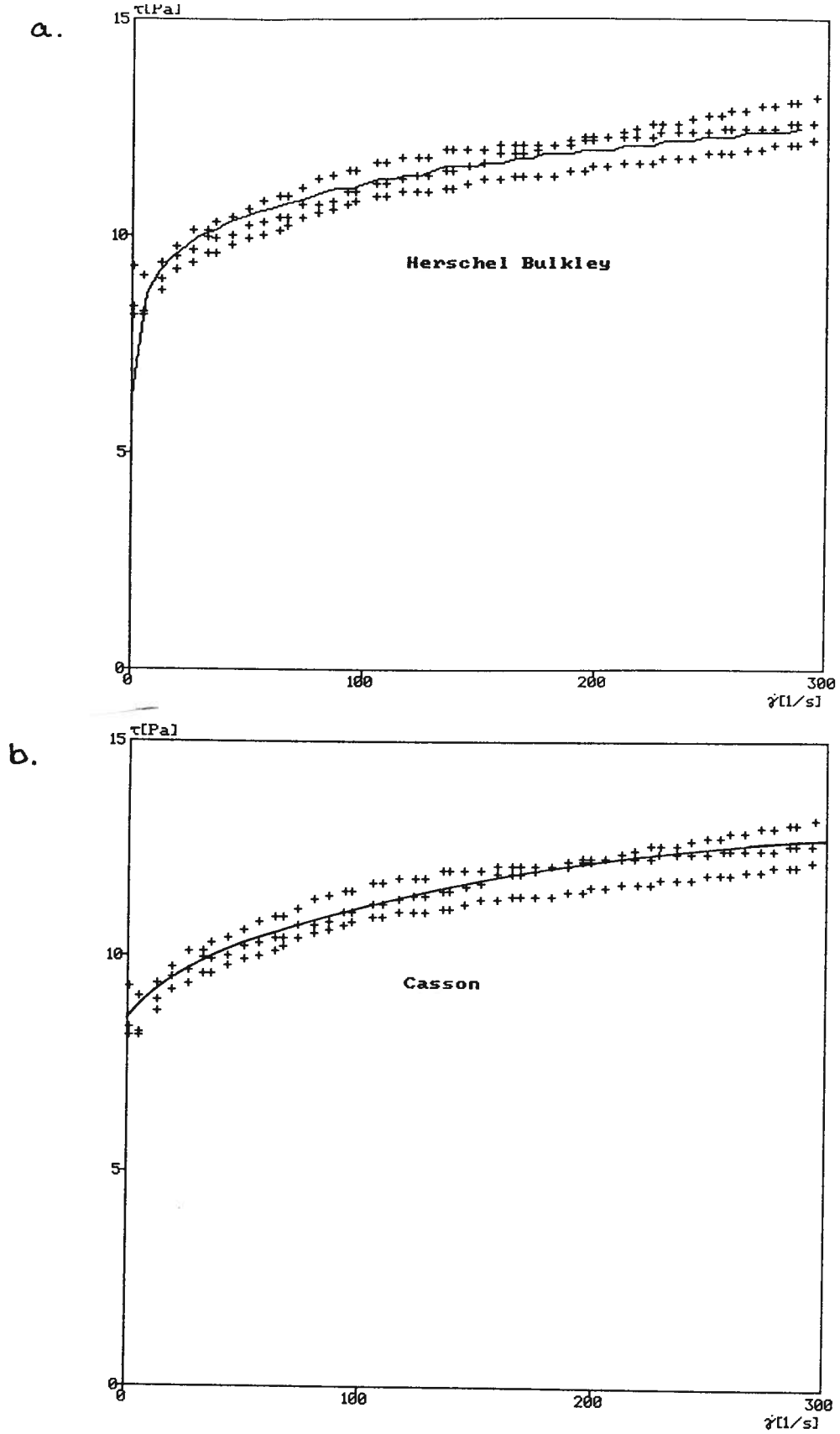


Figure AV.26 Rheological flow curve with fitted a) Herschel Bulkley and b) Casson models for experimental Run #9.

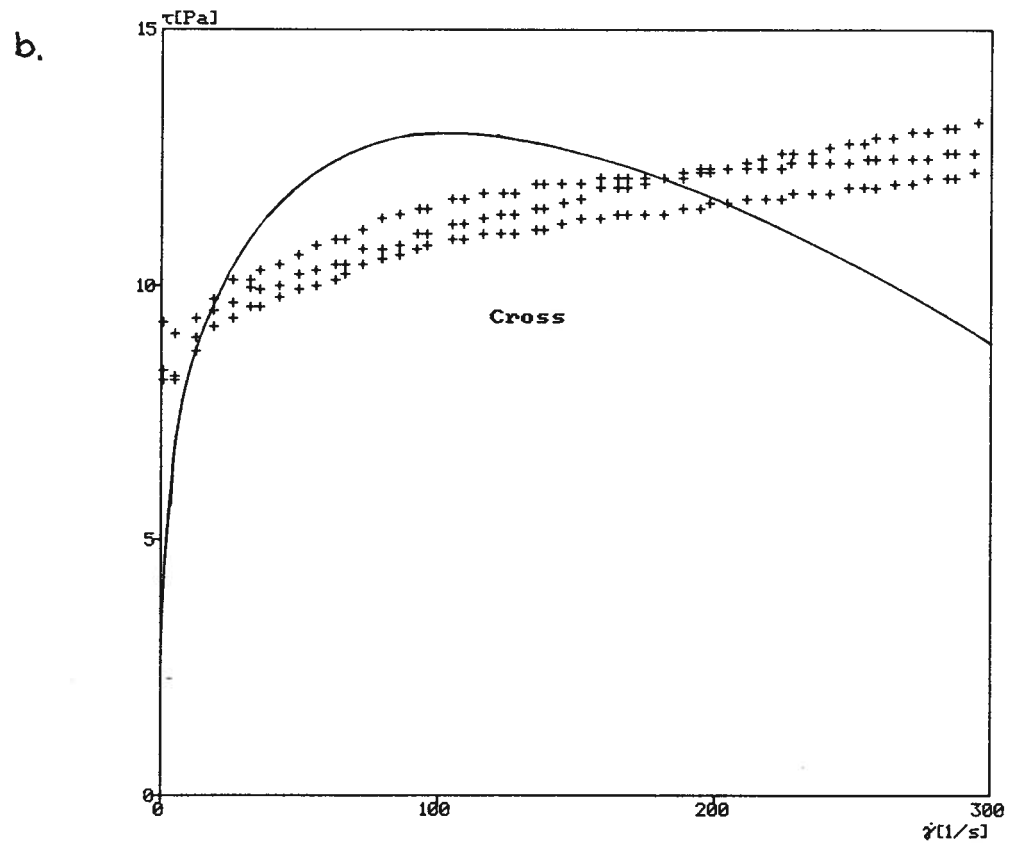
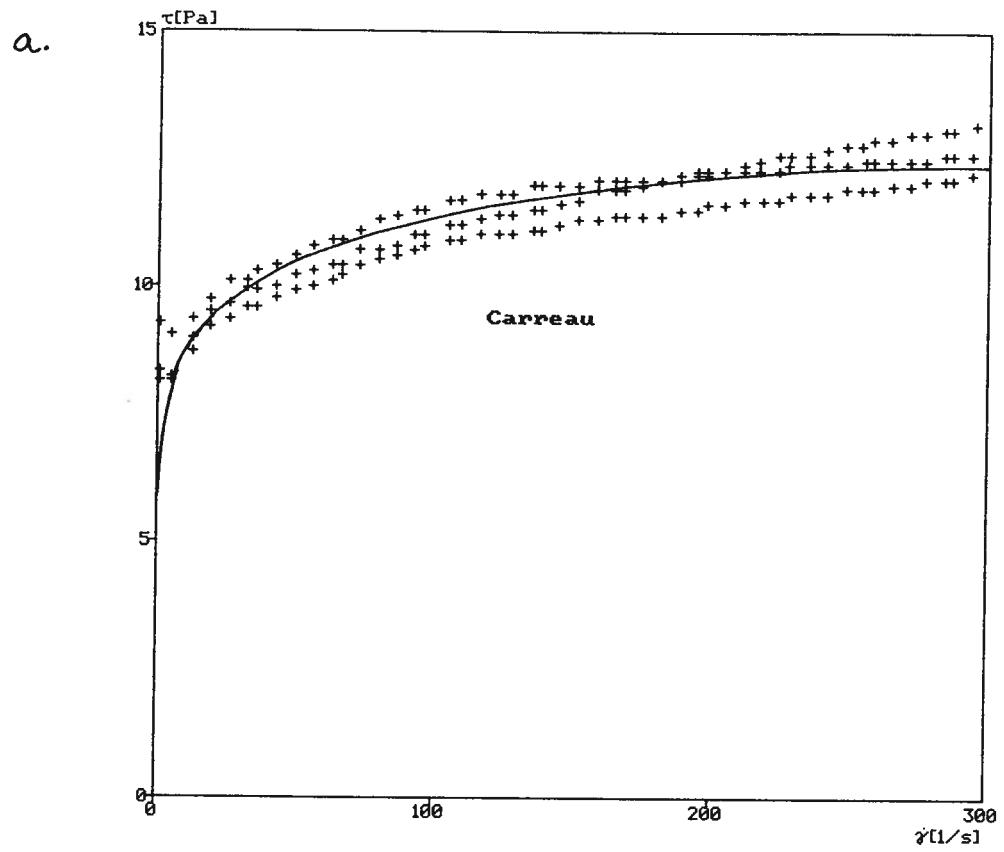


Figure AV.27 Rheological flow curve with fitted a) Carreau and b) Cross models for experimental Run #9.

Run #10: Suspension Composition

Carboxymethyl Cellulose (kg T^{-1}):	0.50
Particle Passing Size (μm):	15.0
Solids Volume Fraction:	0.20
Magnetization:	Magnetized
Sodium Silicate (kg T^{-1}):	0.05
Kaolinite (% w/v):	0.25
pH:	10.0
Bentonite (% w/v):	0.75
Fine Coal (% w/v):	0.75

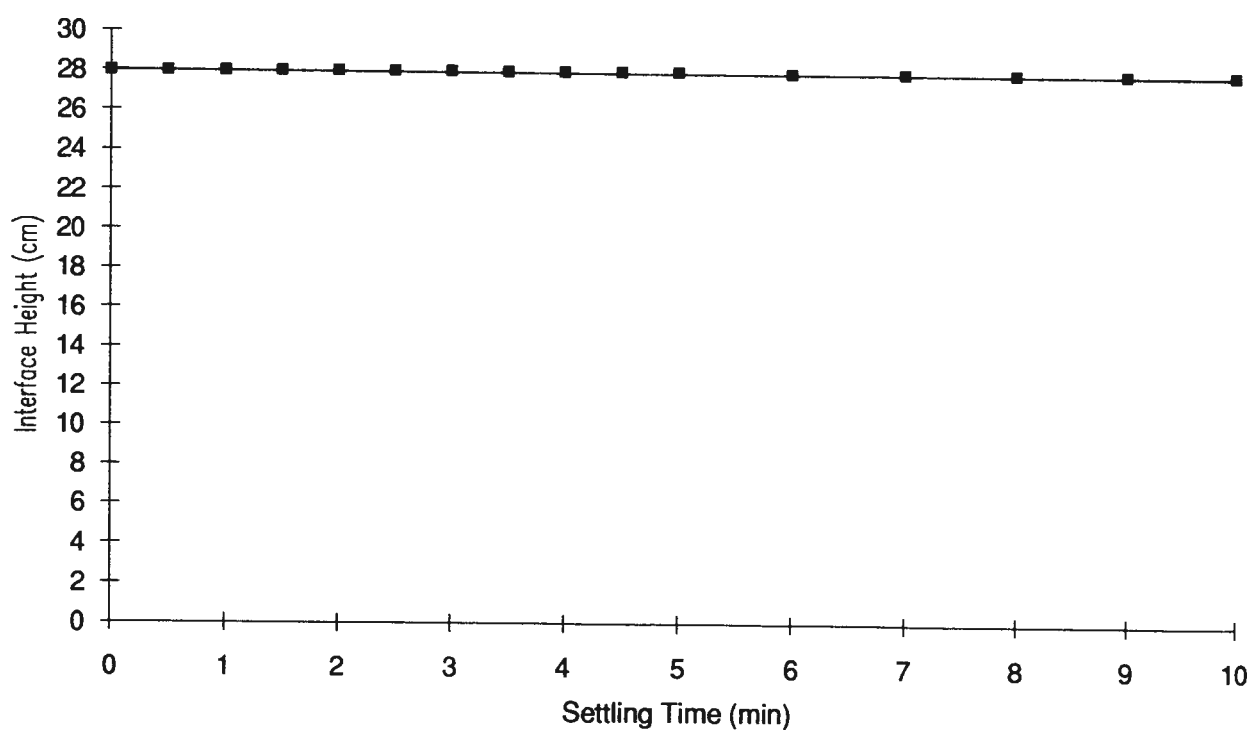


Figure AV.28 Settling curve interface height as a function of time for experimental Run #10.

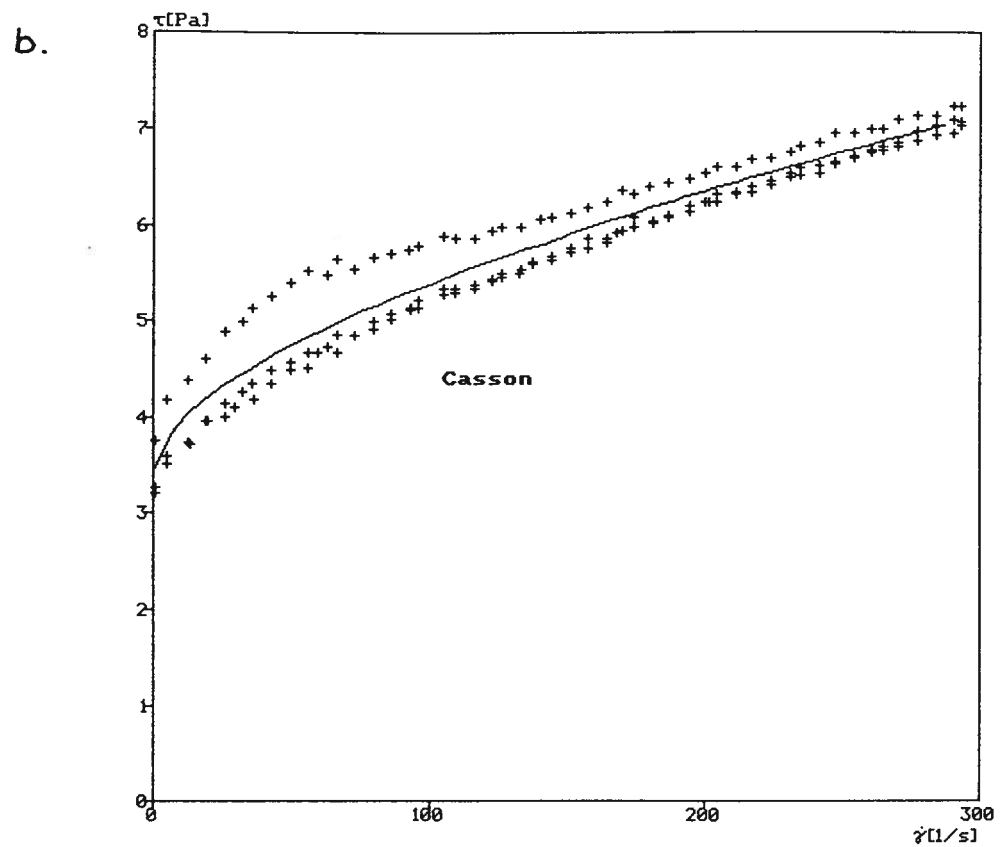
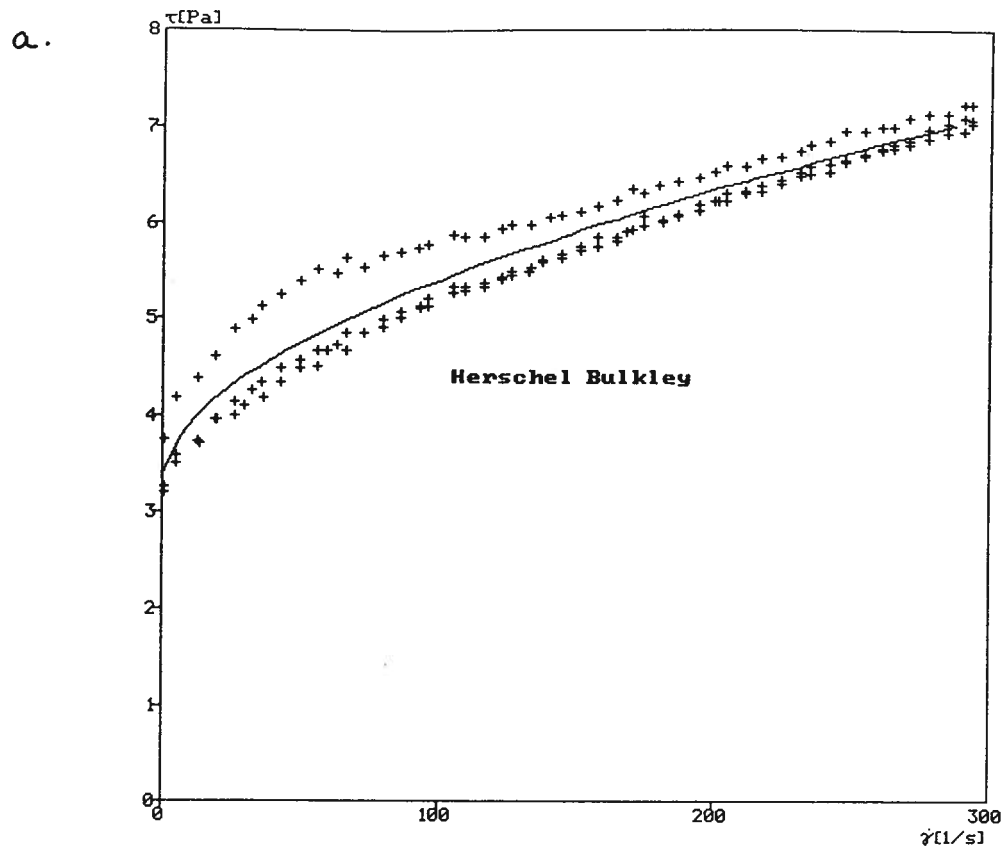


Figure AV.29 Rheological flow curve with fitted a) Herschel Bulkley and b) Casson models for experimental Run #10.

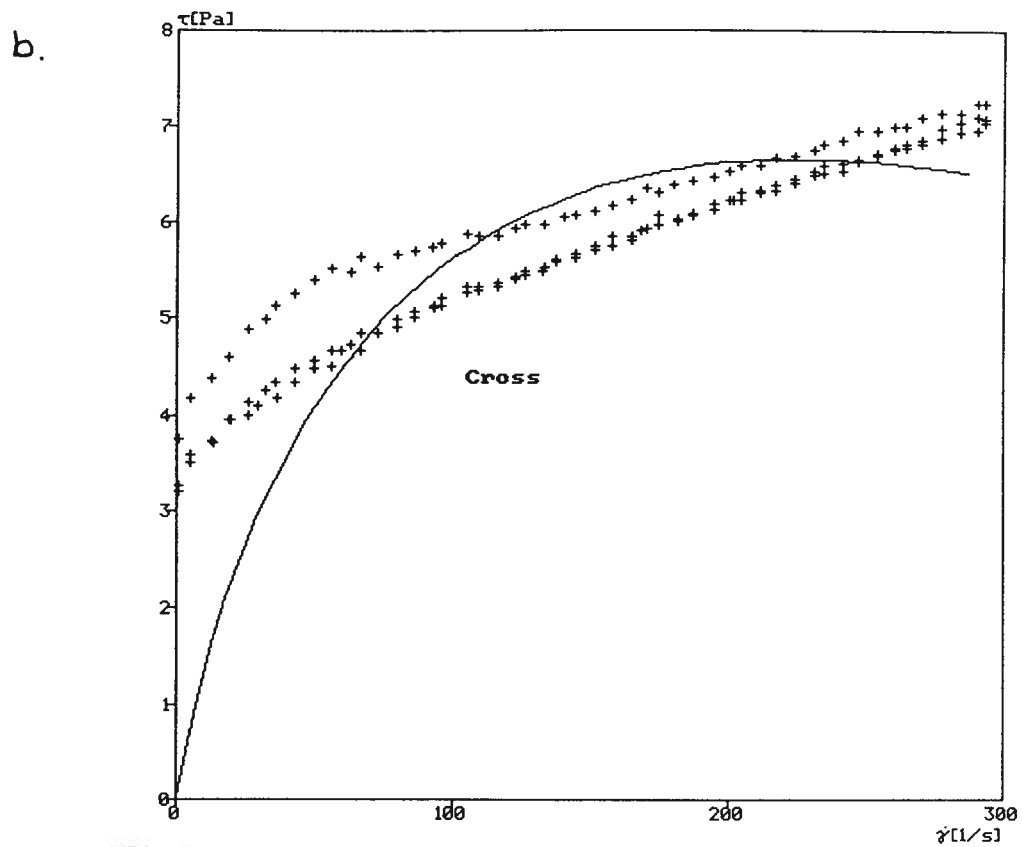
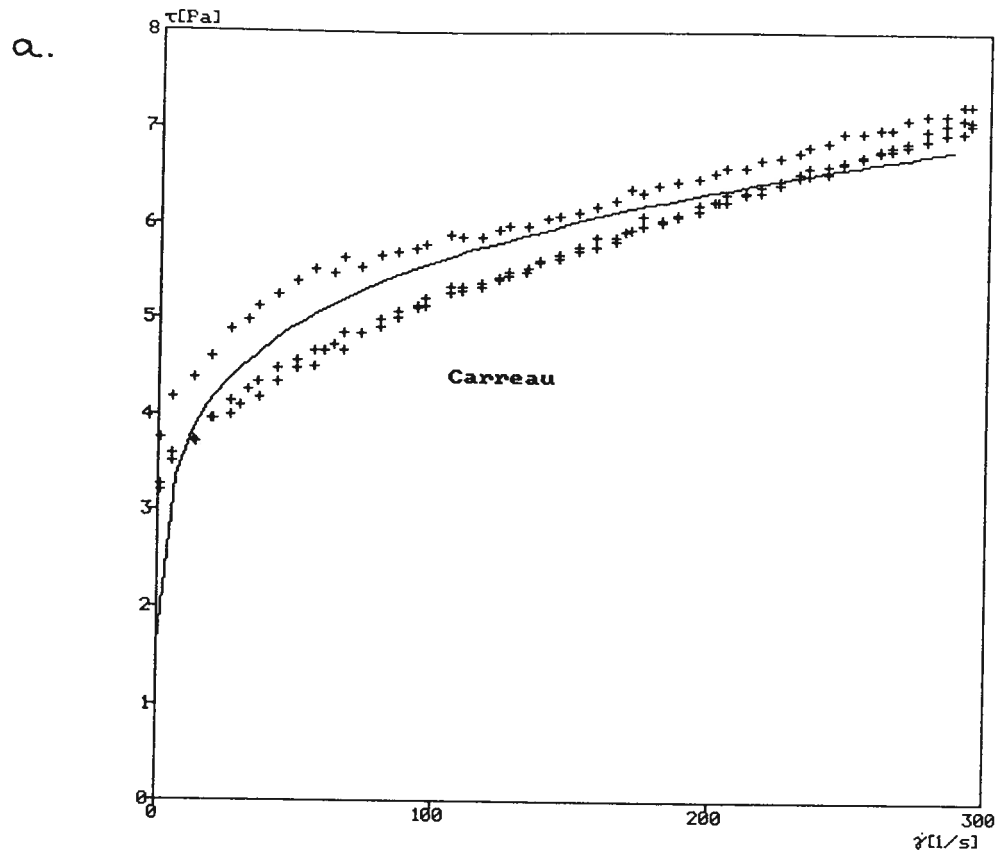


Figure AV.30 Rheological flow curve with fitted a) Carreau and b) Cross models for experimental Run #10.

Run #11: Suspension Composition

Carboxymethyl Cellulose (kg T^{-1}):	1.50
Particle Passing Size (μm):	45.0
Solids Volume Fraction:	0.20
Magnetization:	Magnetized
Sodium Silicate (kg T^{-1}):	0.05
Kaolinite (% w/v):	0.75
pH:	4.0
Bentonite (% w/v):	0.75
Fine Coal (% w/v):	0.75

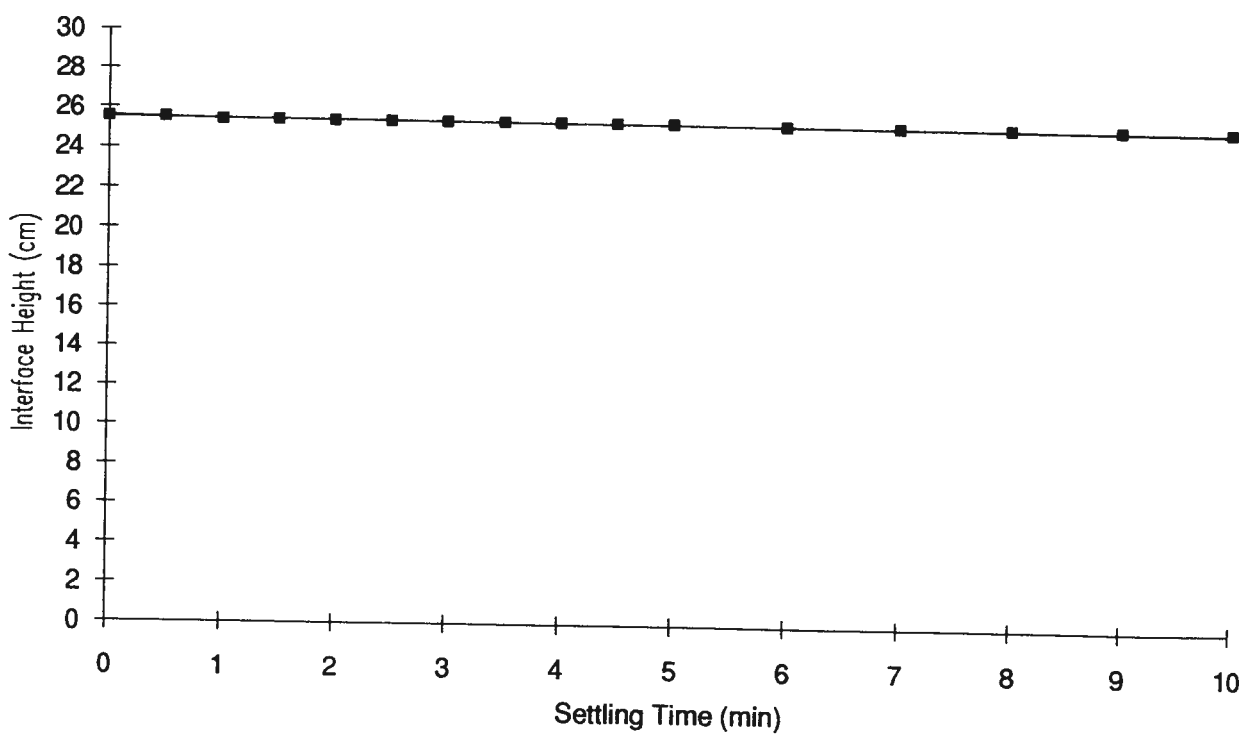


Figure AV.31 Settling curve interface height as a function of time for experimental Run #11.

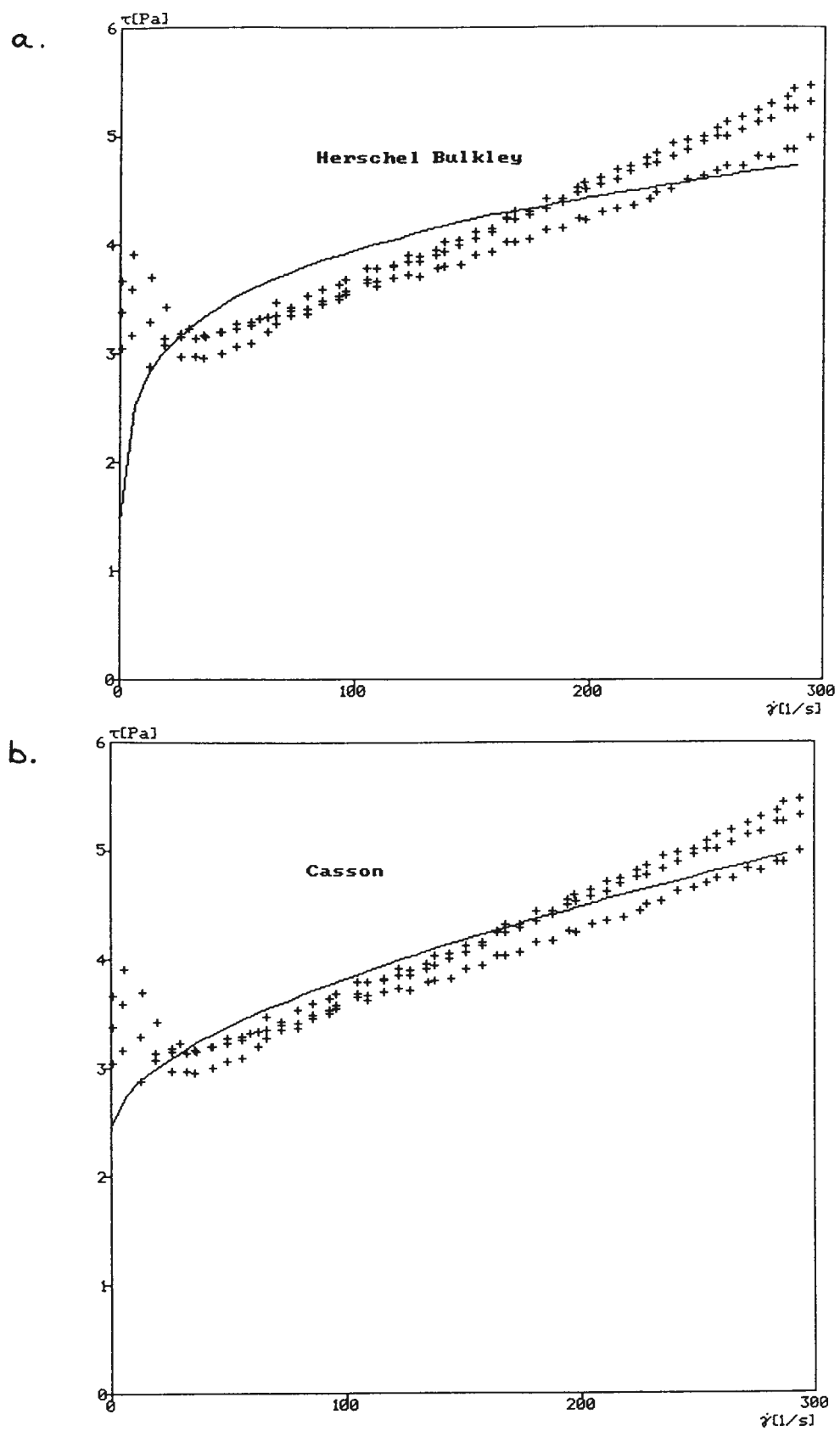


Figure AV.32 Rheological flow curve with fitted a) Herschel Bulkley and b) Casson models for experimental Run #11.

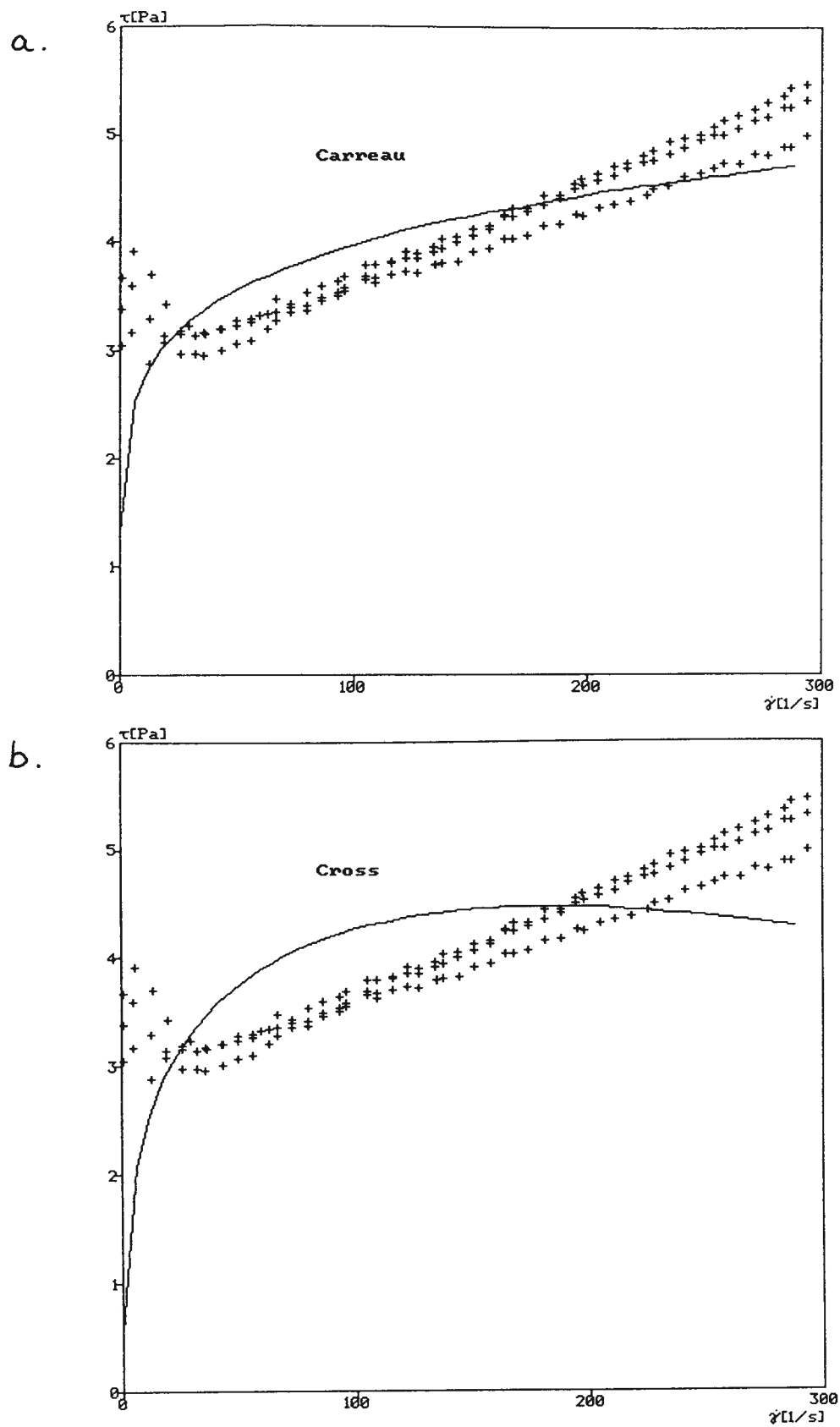


Figure AV.33 Rheological flow curve with fitted a) Carreau and b) Cross models for experimental Run #11.

Run #12: Suspension Composition

Carboxymethyl Cellulose (kg T ⁻¹):	0.50
Particle Passing Size (μm):	45.0
Solids Volume Fraction:	0.20
Magnetization:	Magnetized
Sodium Silicate (kg T ⁻¹):	0.15
Kaolinite (% w/v):	0.75
pH:	10.0
Bentonite (% w/v):	0.25
Fine Coal (% w/v):	0.25

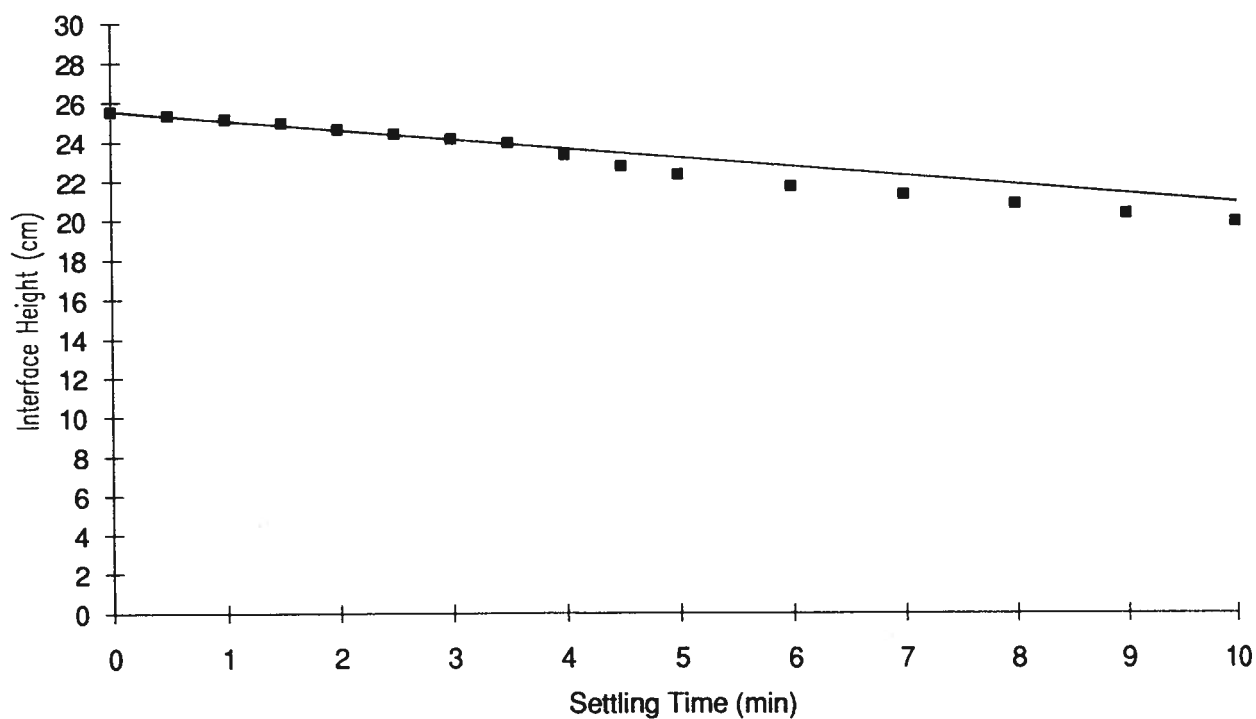


Figure AV.34 Settling curve interface height as a function of time for experimental Run #12.

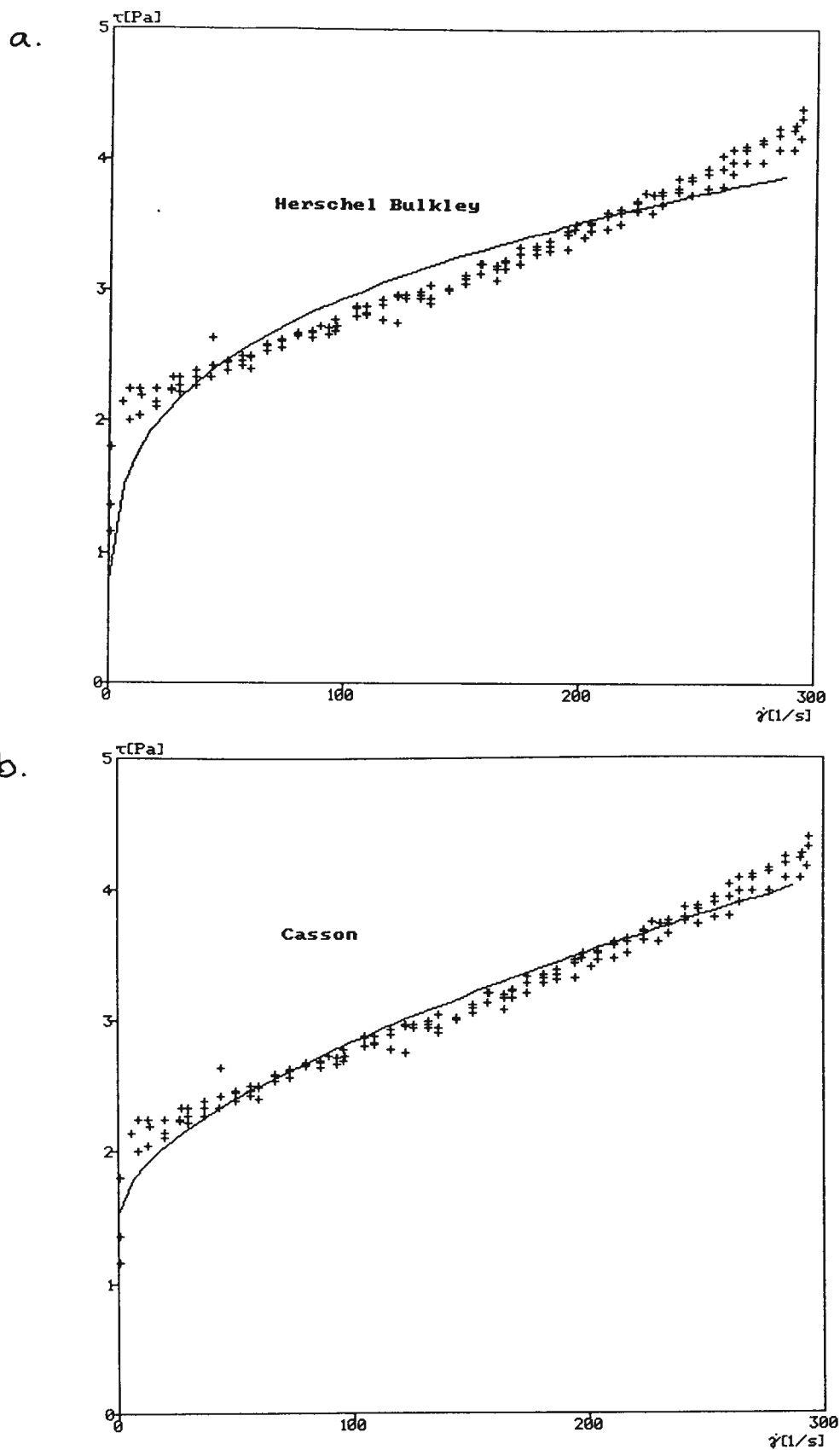


Figure AV.34 Rheological flow curve with fitted a) Herschel Bulkley and b) Casson models for experimental Run #12.

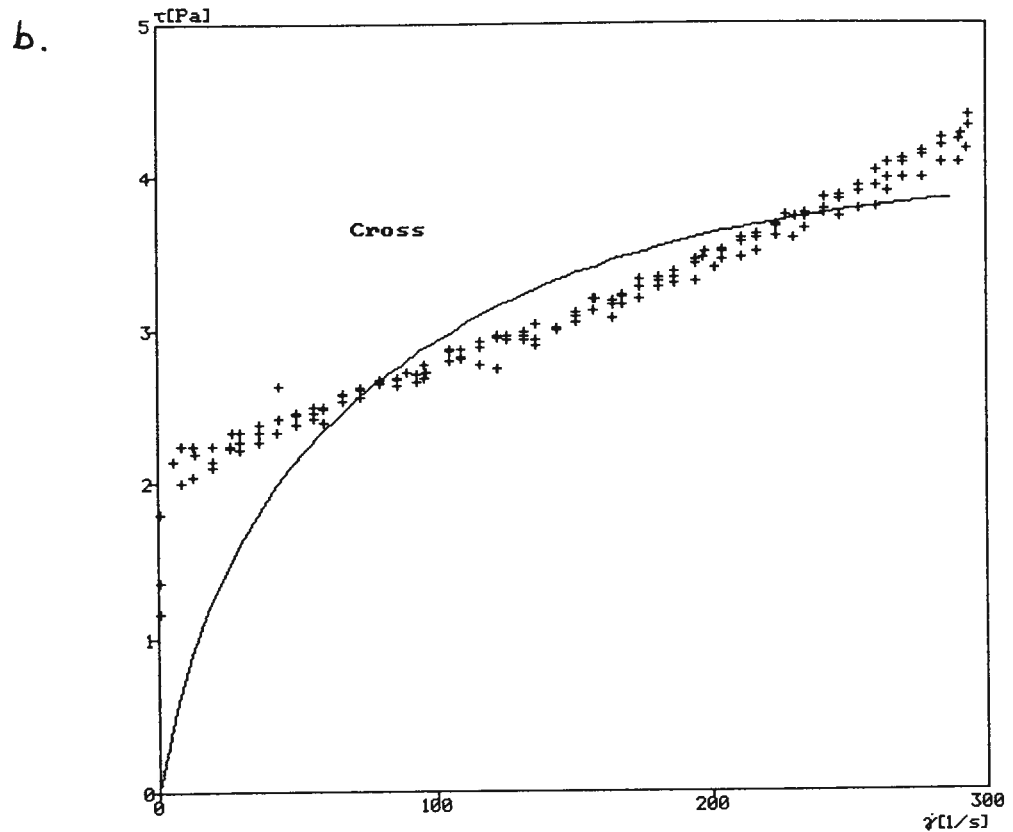
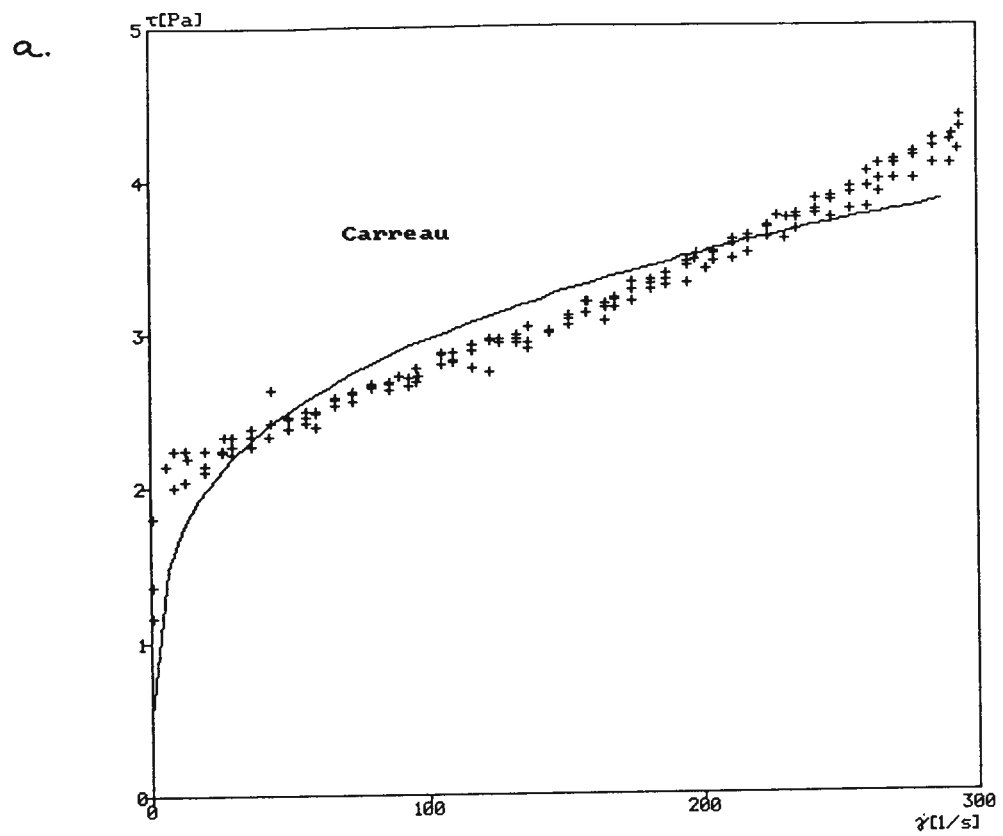


Figure AV.36 Rheological flow curve with fitted a) Carreau and b) Cross models for experimental Run #12.

Run #13: Suspension Composition

Carboxymethyl Cellulose (kg T ⁻¹):	1.50
Particle Passing Size (μm):	15.0
Solids Volume Fraction:	0.10
Magnetization:	Magnetized
Sodium Silicate (kg T ⁻¹):	0.05
Kaolinite (% w/v):	0.75
pH:	10.0
Bentonite (% w/v):	0.25
Fine Coal (% w/v):	0.75

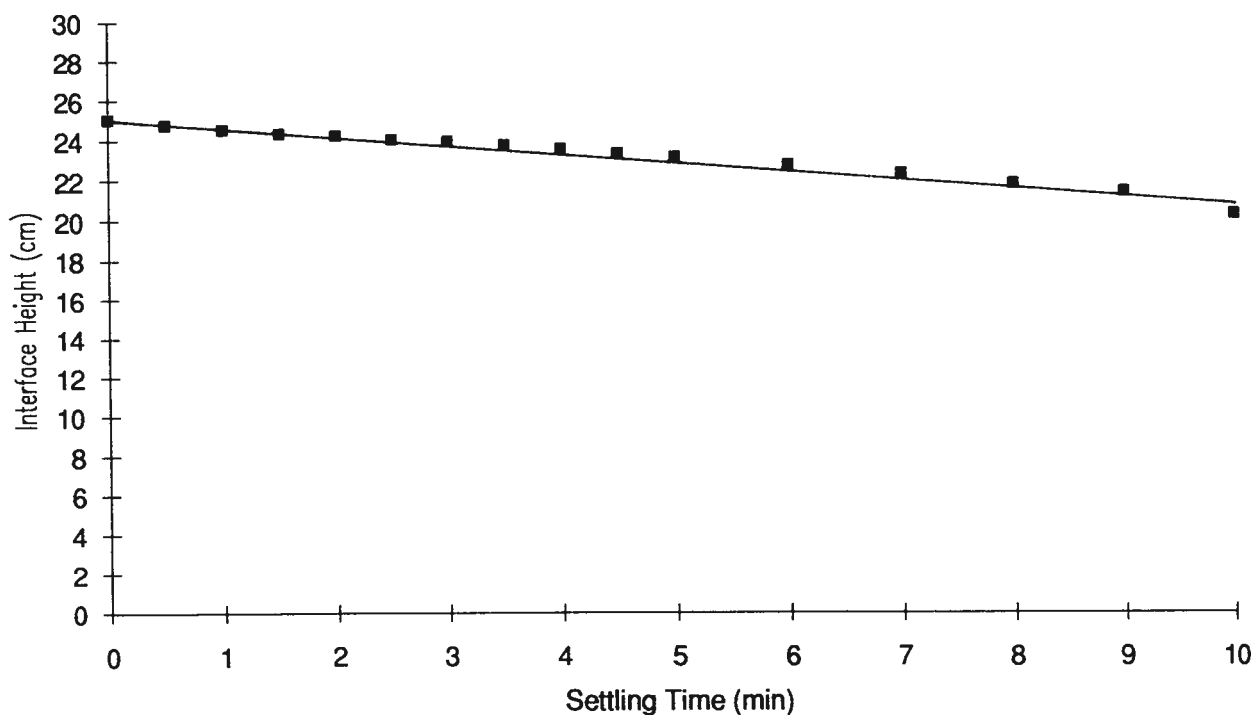


Figure AV.37 Settling curve interface height as a function of time for experimental Run #13.

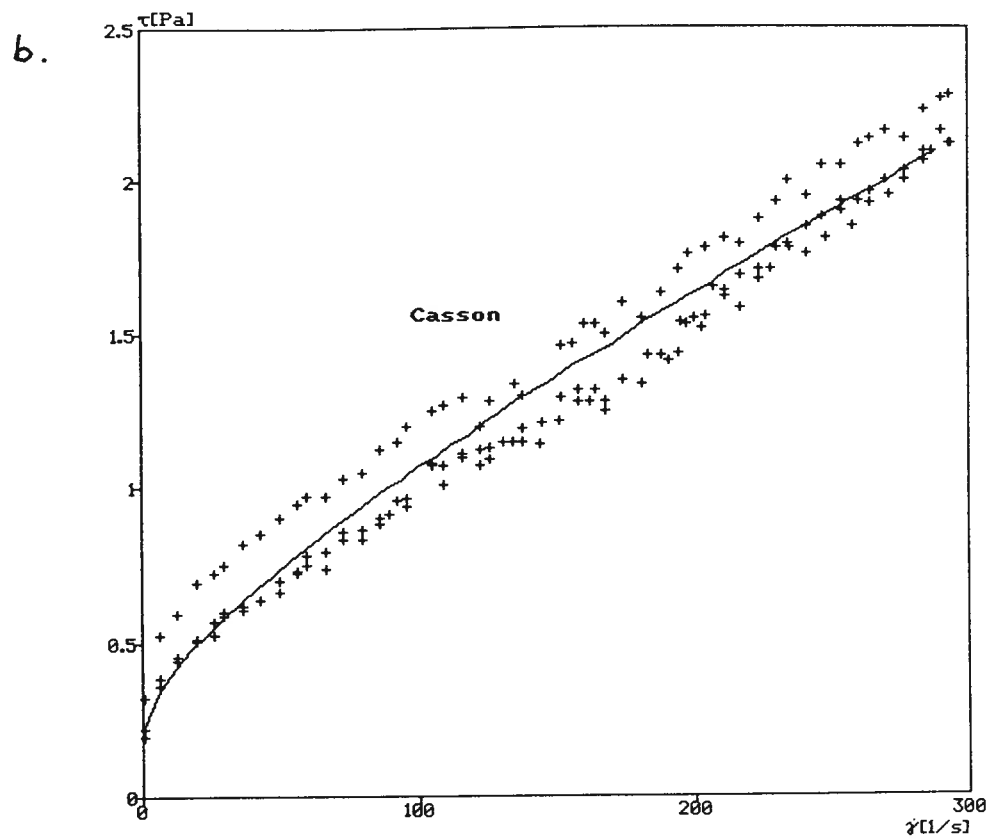
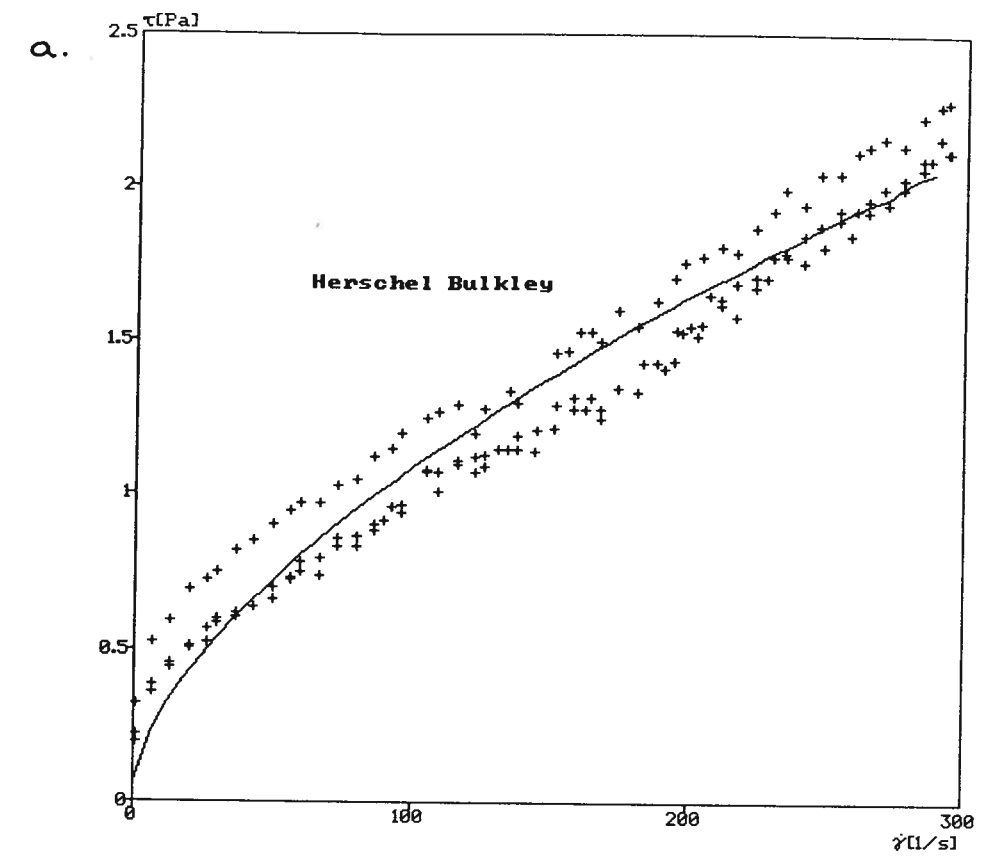


Figure AV.38 Rheological flow curve with fitted a) Herschel Bulkley and b) Casson models for experimental Run #13.

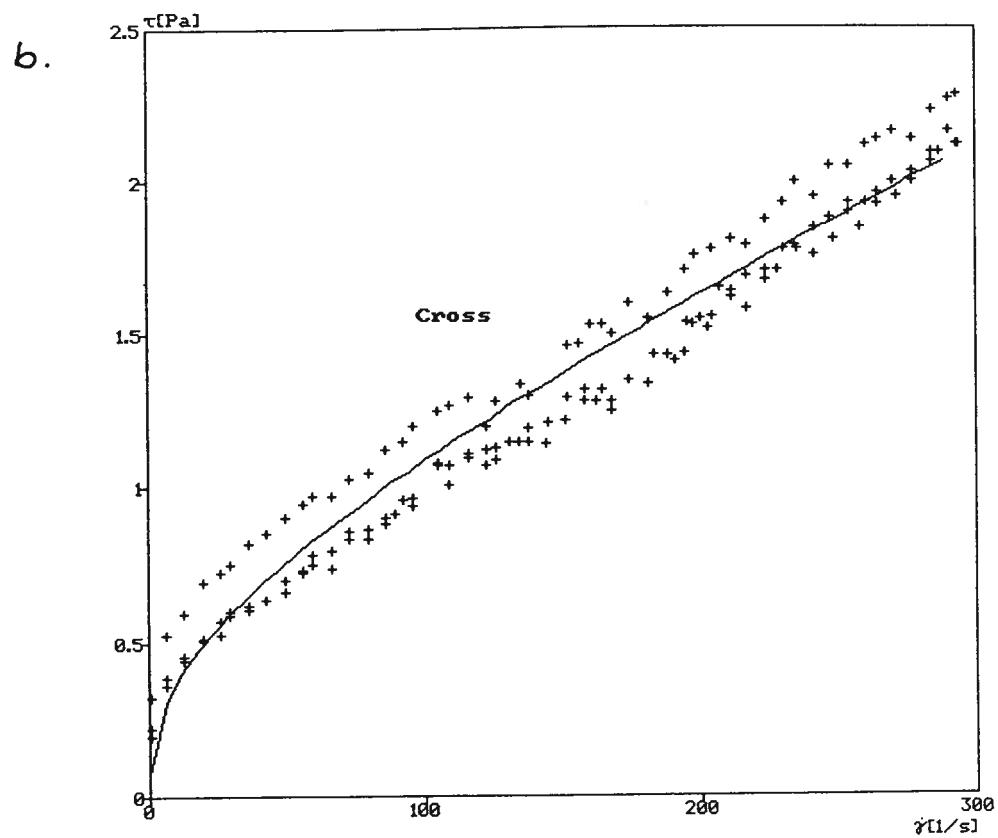
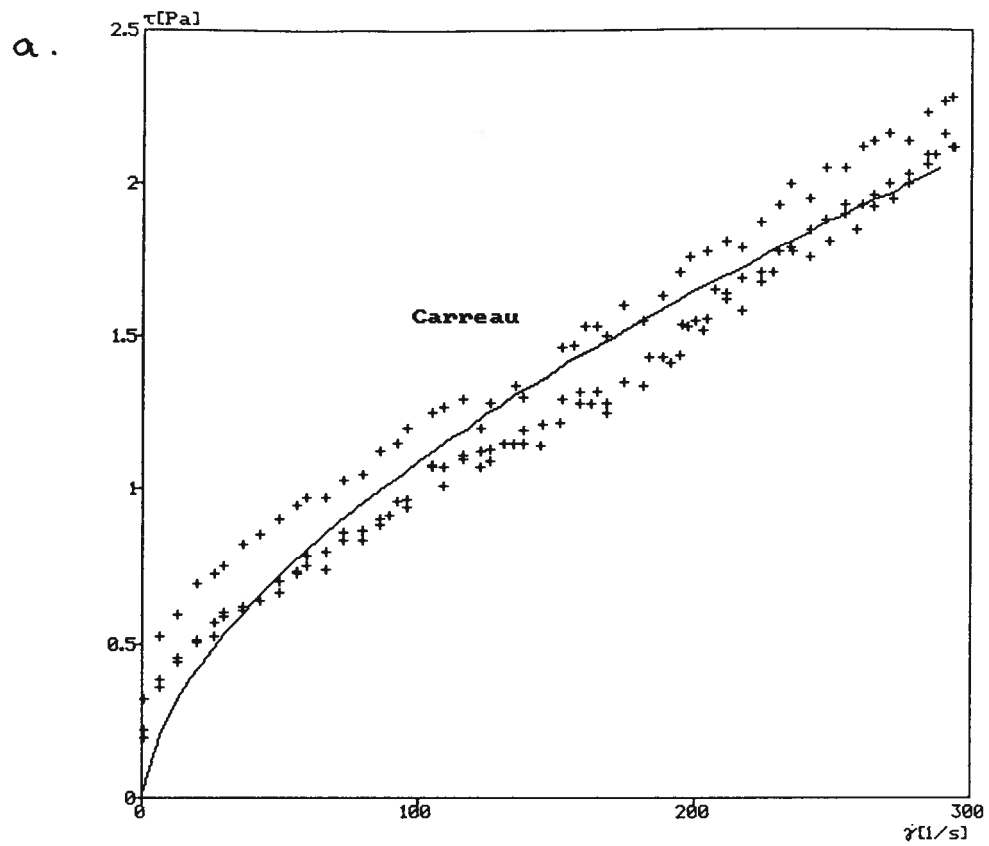


Figure AV.39 Rheological flow curve with fitted a) Carreau and b) Cross models for experimental Run #13.

Run #14: Suspension Composition

Carboxymethyl Cellulose (kg T^{-1}):	0.50
Particle Passing Size (μm):	15.0
Solids Volume Fraction:	0.10
Magnetization:	Magnetized
Sodium Silicate (kg T^{-1}):	0.15
Kaolinite (% w/v):	0.75
pH:	4.0
Bentonite (% w/v):	0.75
Fine Coal (% w/v):	0.25

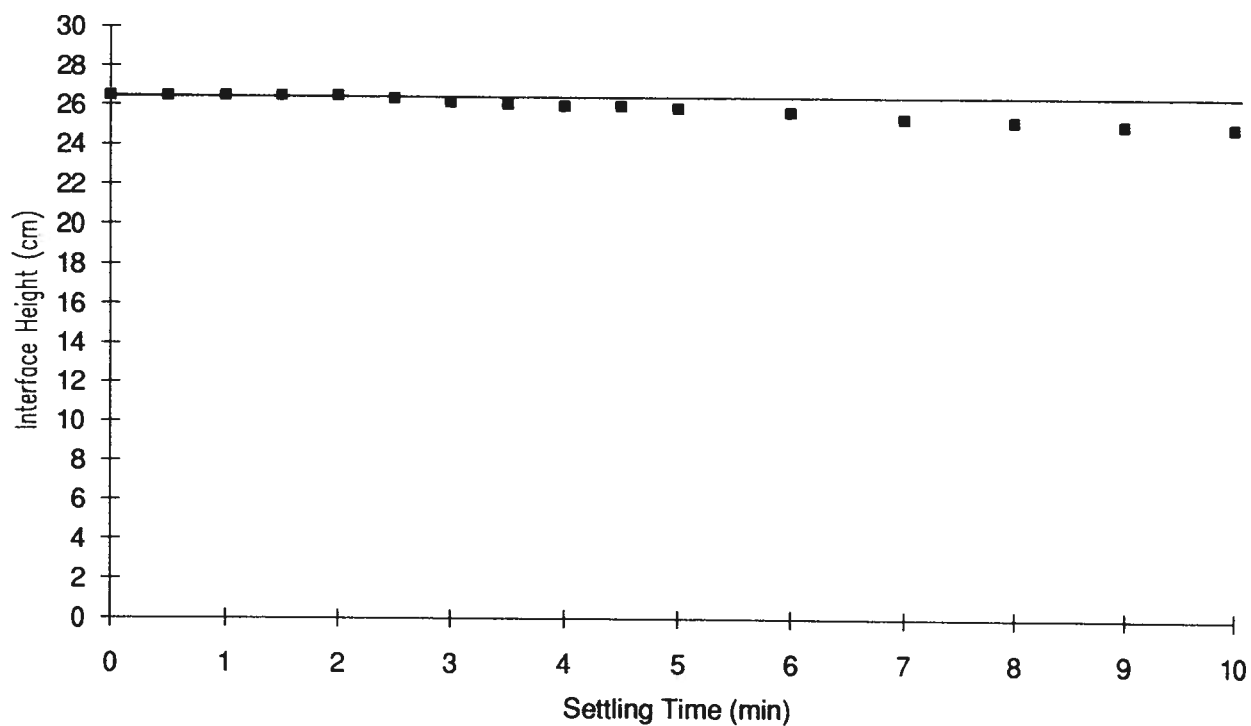


Figure AV.40 Settling curve interface height as a function of time for experimental Run #14.

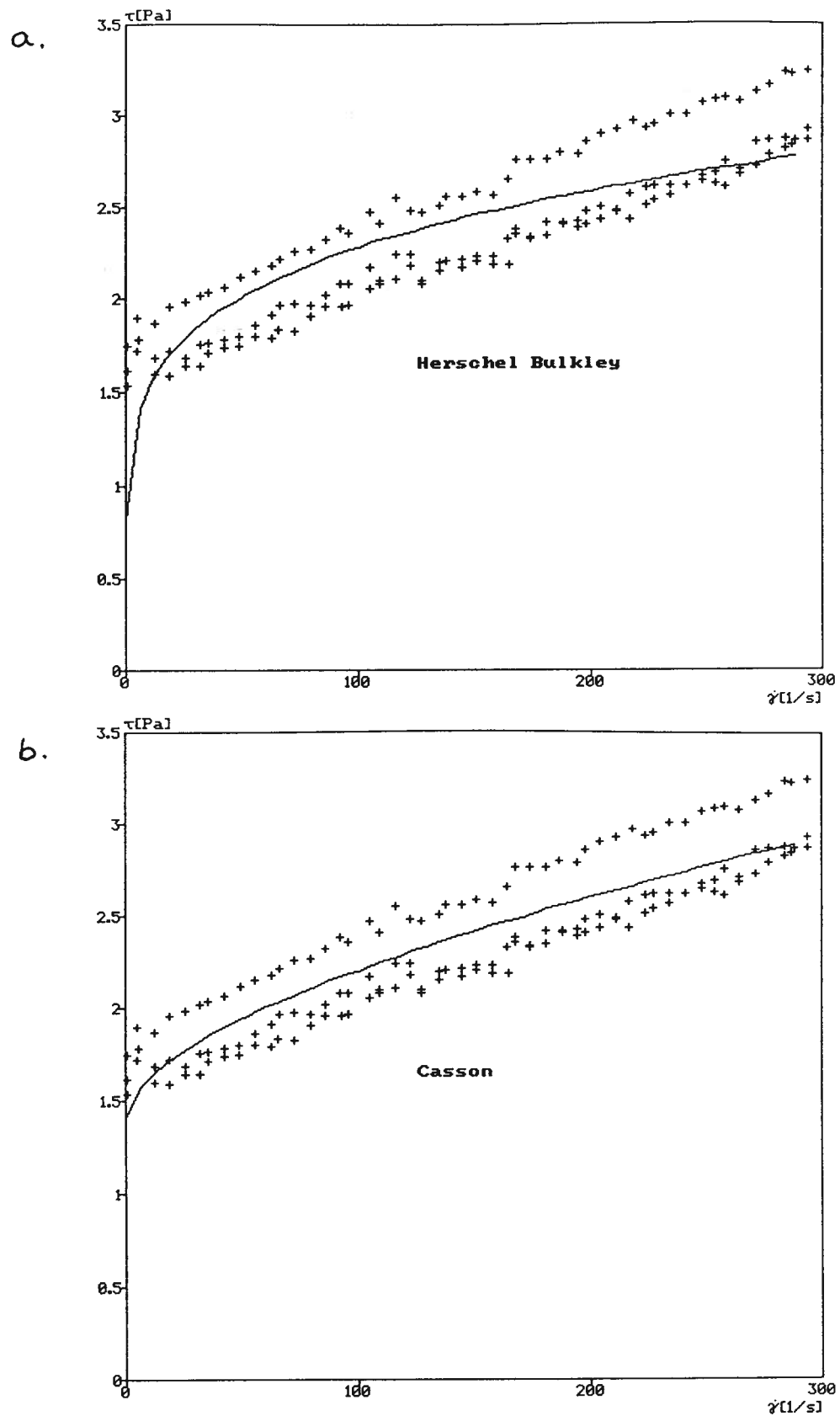


Figure AV.41 Rheological flow curve with fitted a) Herschel Bulkley and b) Casson models for experimental Run #14.

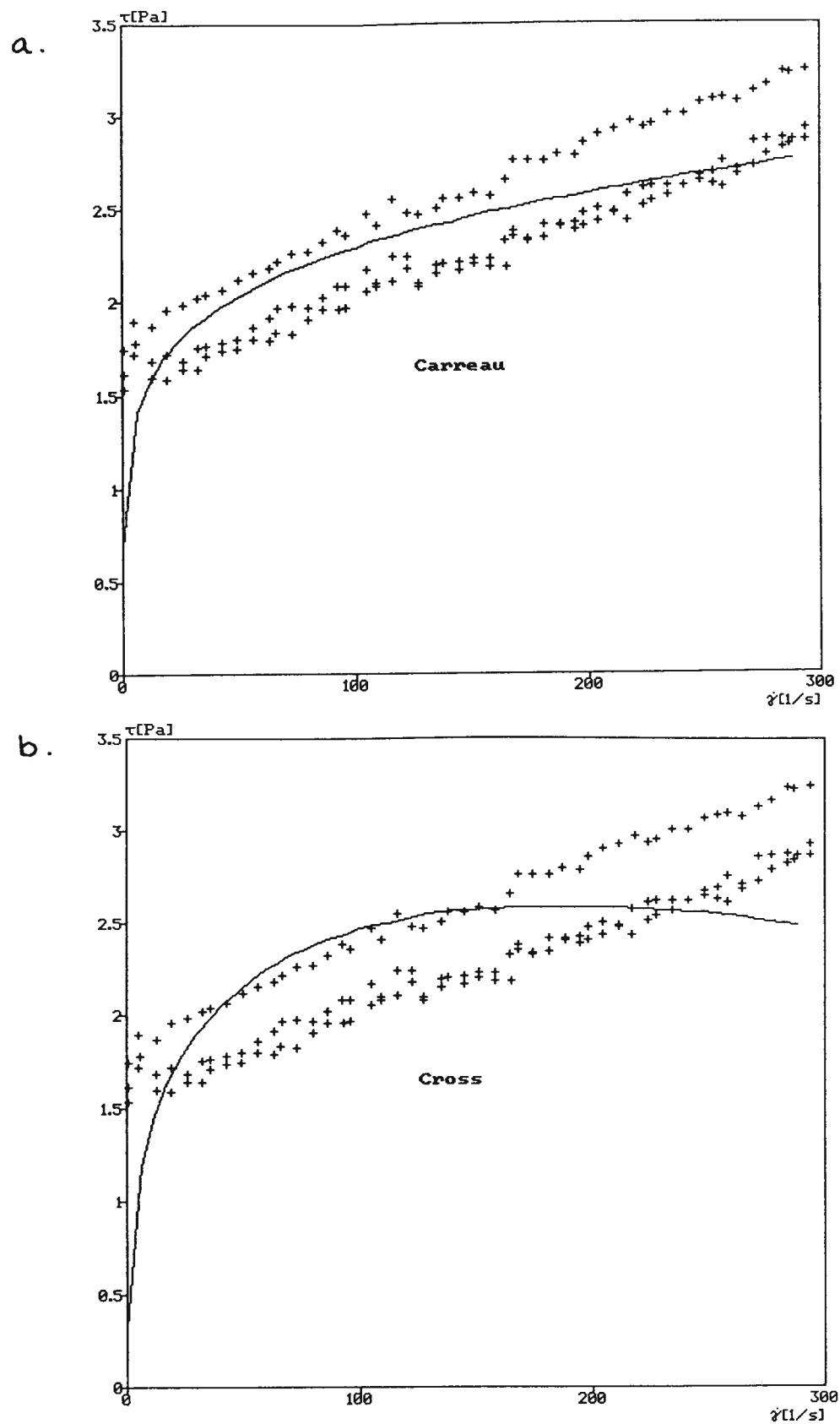


Figure AV.42 Rheological flow curve with fitted a) Carreau and b) Cross models for experimental Run #14.

Run #15: Suspension Composition

Carboxymethyl Cellulose (kg T ⁻¹):	1.50
Particle Passing Size (μm):	45.0
Solids Volume Fraction:	0.10
Magnetization:	Magnetized
Sodium Silicate (kg T ⁻¹):	0.15
Kaolinite (% w/v):	0.25
pH:	10.0
Bentonite (% w/v):	0.75
Fine Coal (% w/v):	0.25

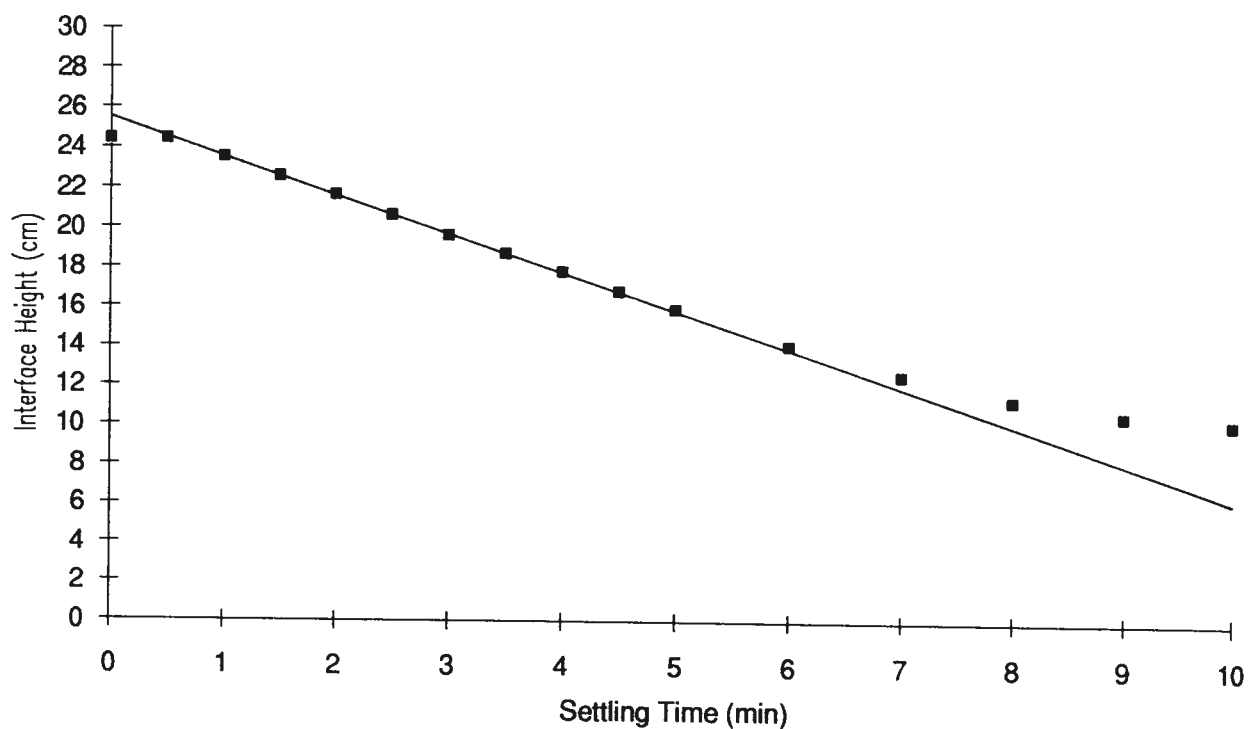


Figure AV.43 Settling curve interface height as a function of time for experimental Run #15.

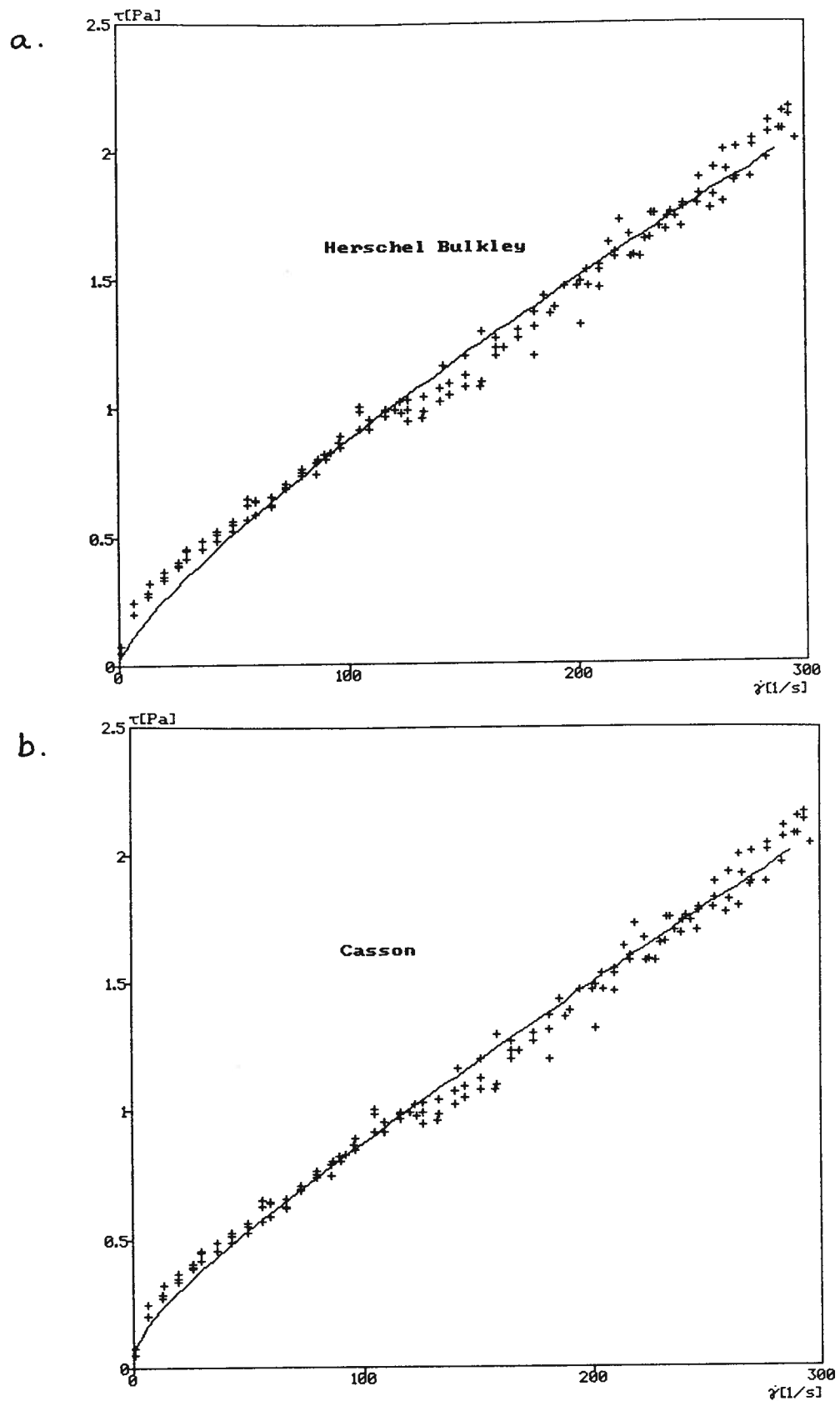


Figure AV.44 Rheological flow curve with fitted a) Herschel Bulkley and b) Casson models for experimental Run #15.

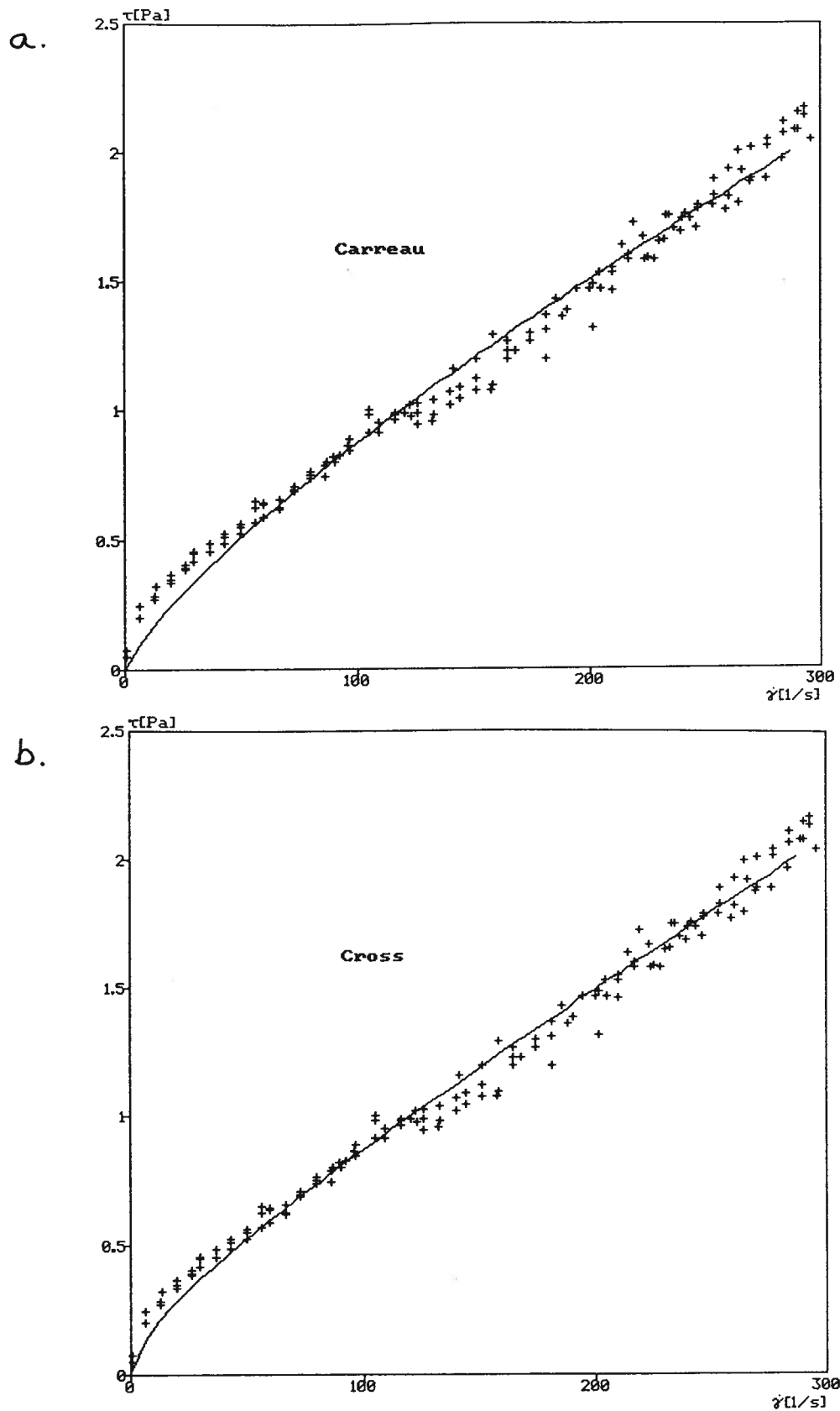


Figure AV.45 Rheological flow curve with fitted a) Carreau and b) Cross models for experimental Run #15.

Run #16: Suspension Composition

Carboxymethyl Cellulose (kg T ⁻¹):	0.50
Particle Passing Size (μm):	45.0
Solids Volume Fraction:	0.10
Magnetization:	Magnetized
Sodium Silicate (kg T ⁻¹):	0.05
Kaolinite (% w/v):	0.25
pH:	4.0
Bentonite (% w/v):	0.25
Fine Coal (% w/v):	0.75

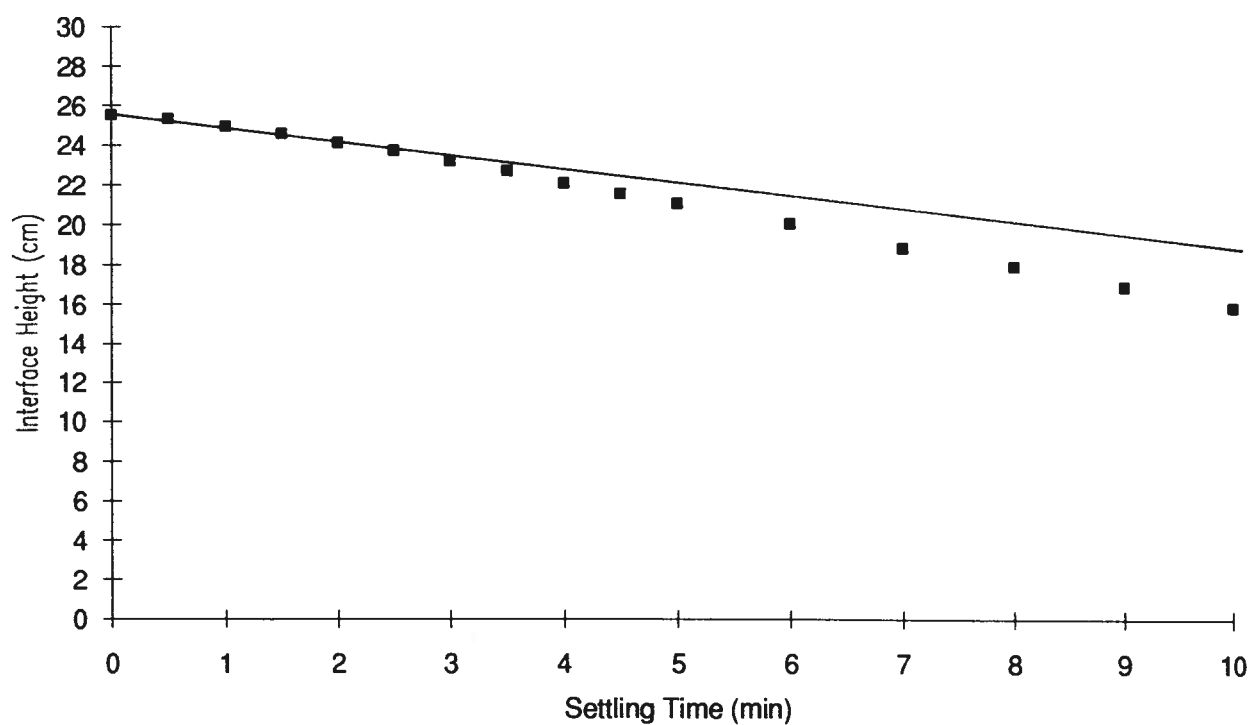


Figure AV.46 Settling curve interface height as a function of time for experimental Run #16.

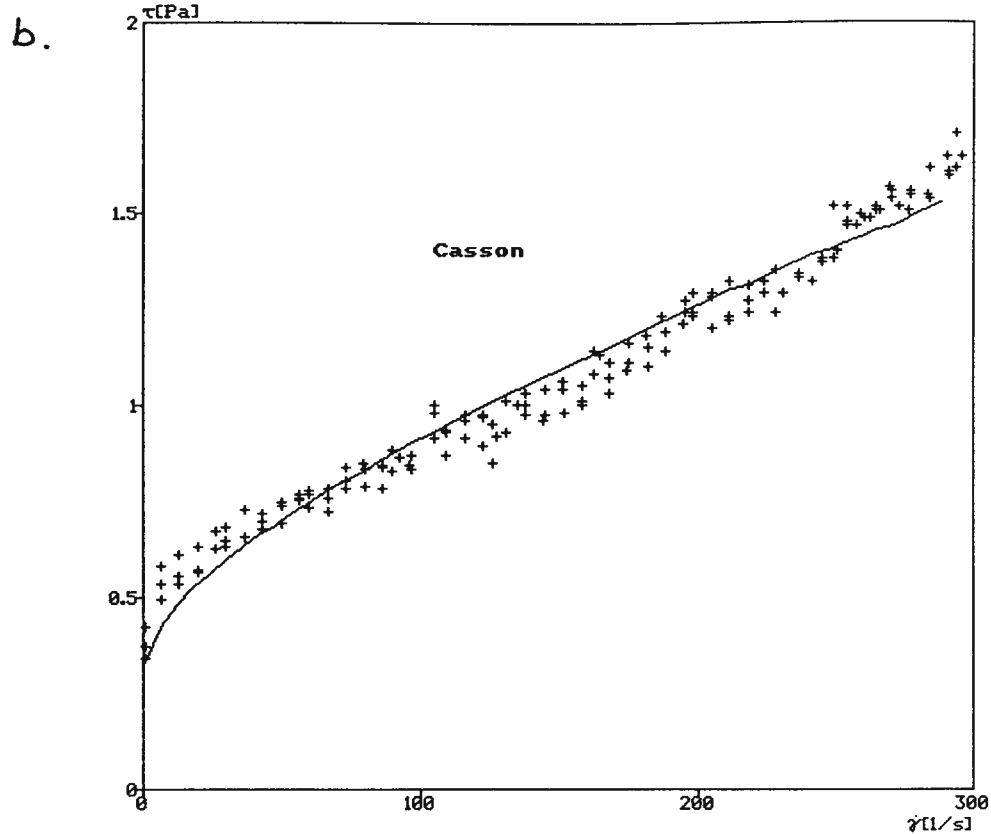
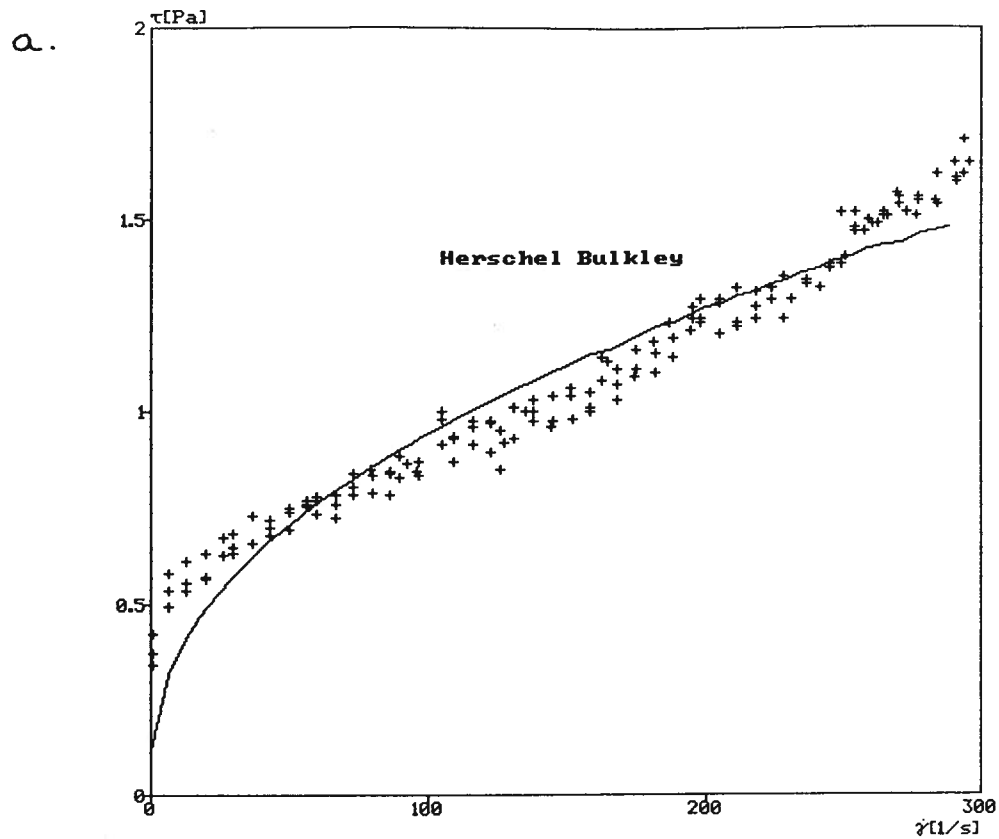


Figure AV.47 Rheological flow curve with fitted a) Herschel Bulkley and b) Casson models for experimental Run #16.

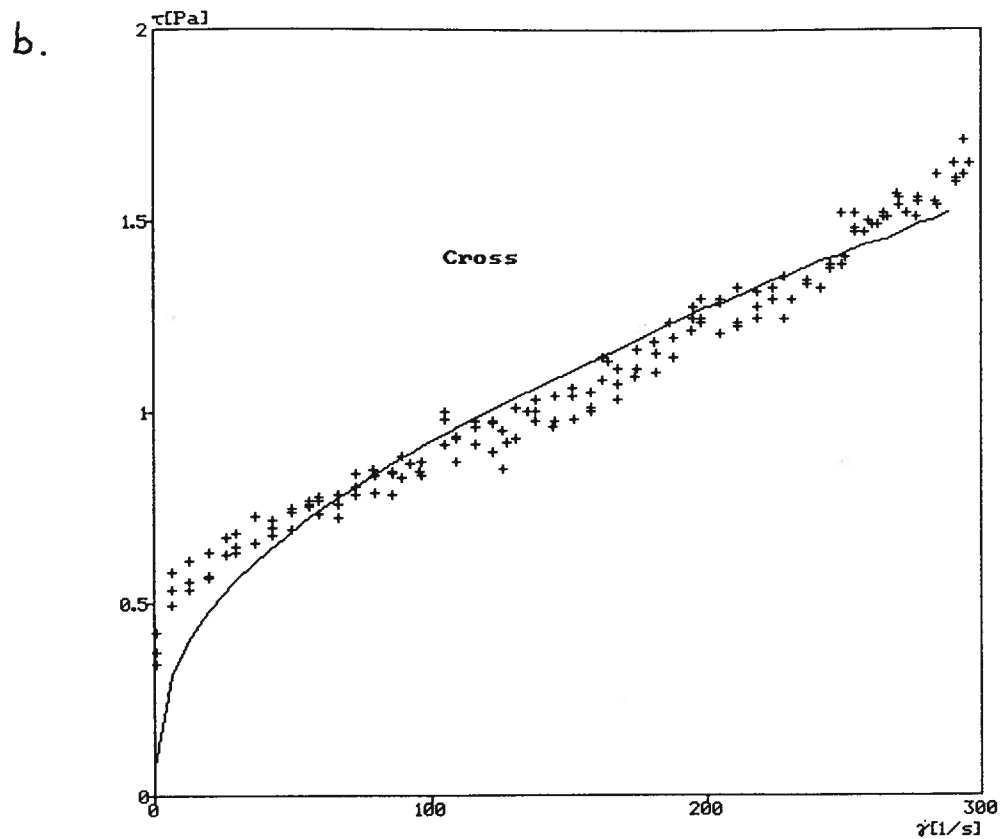
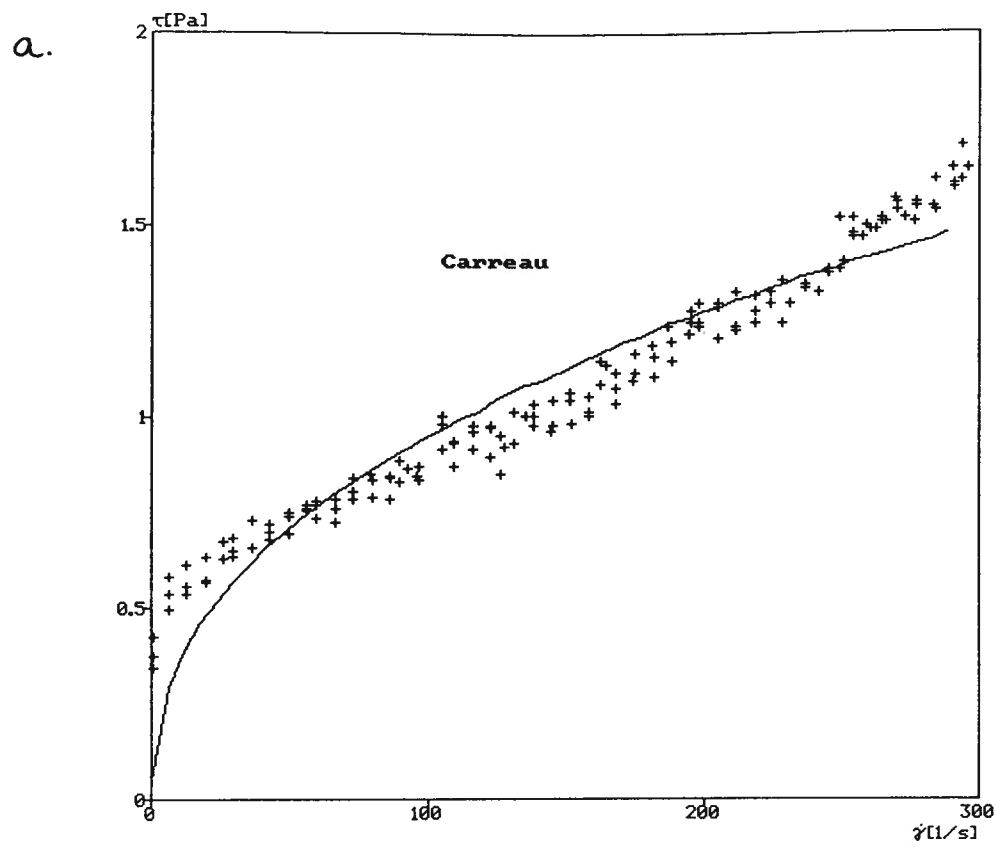


Figure AV.48 Rheological flow curve with fitted a) Carreau and b) Cross models for experimental Run #16.

Run #17: Suspension Composition

Carboxymethyl Cellulose (kg T ⁻¹):	1.00
Particle Passing Size (μm):	30.0
Solids Volume Fraction:	0.15
Magnetization:	Demagnetized
Sodium Silicate (kg T ⁻¹):	0.10
Kaolinite (% w/v):	0.50
pH:	7.0
Bentonite (% w/v):	0.50
Fine Coal (% w/v):	0.50

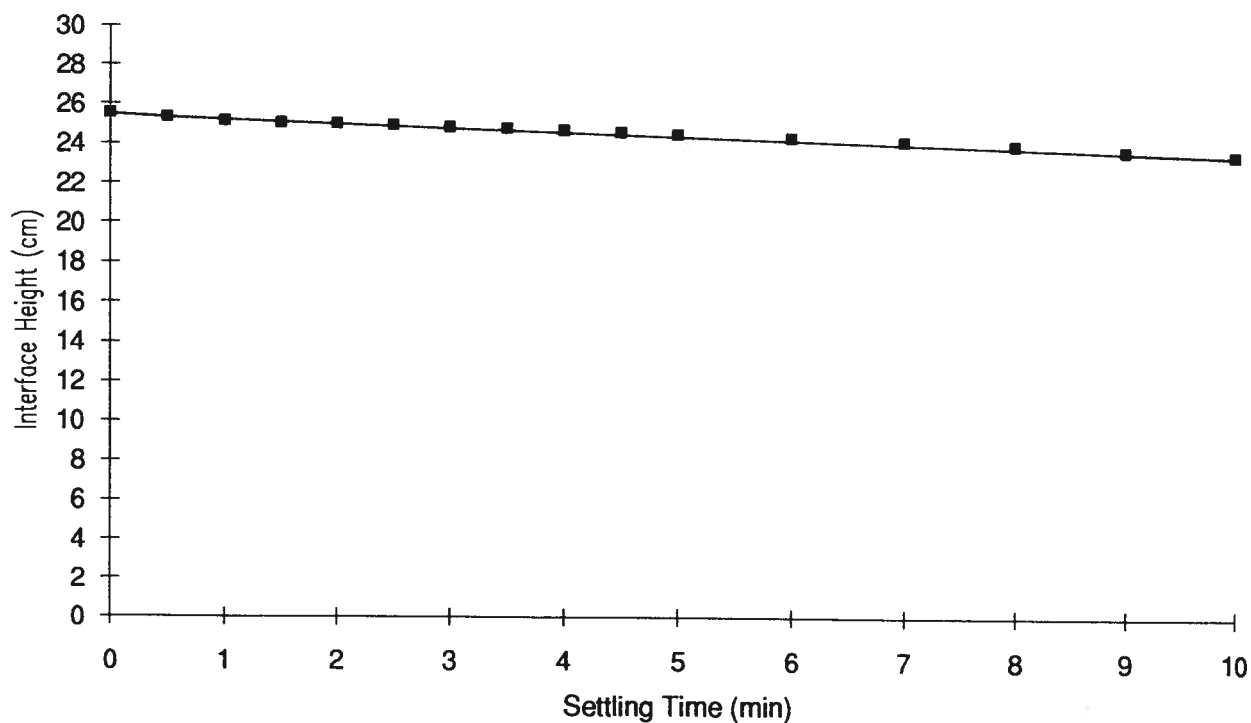


Figure AV.49 Settling curve interface height as a function of time for experimental Run #17.

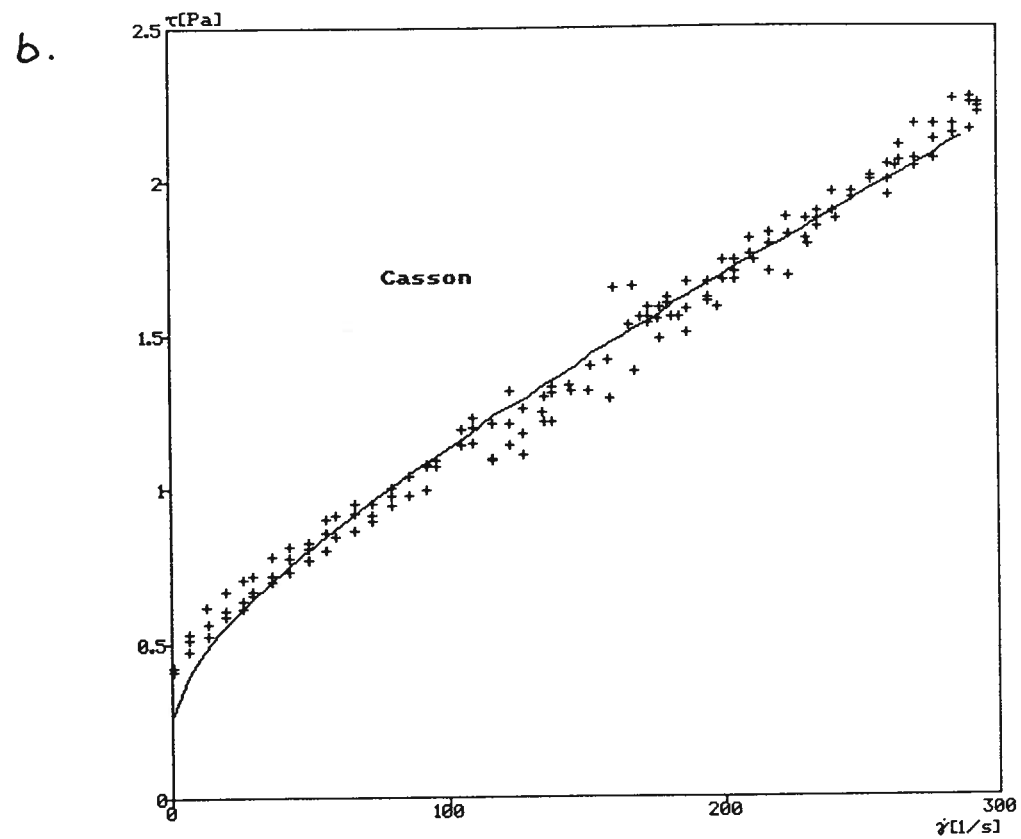
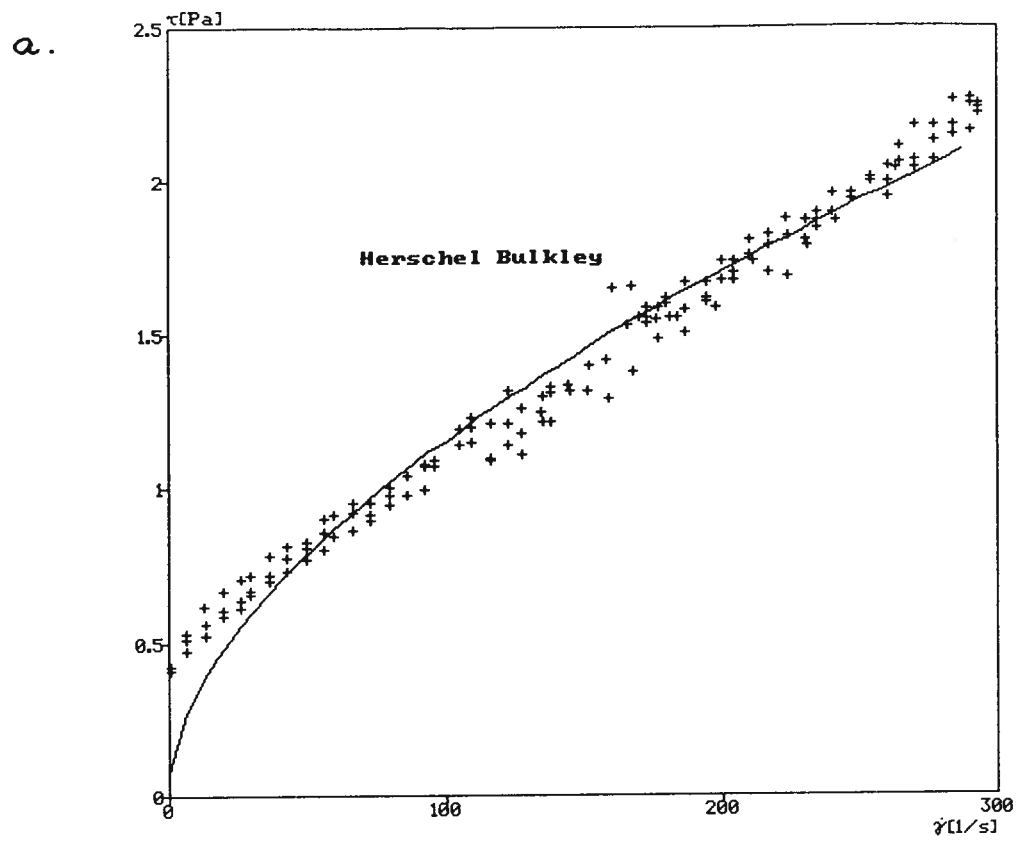


Figure AV.50 Rheological flow curve with fitted a) Herschel Bulkley and b) Casson models for experimental Run #18.

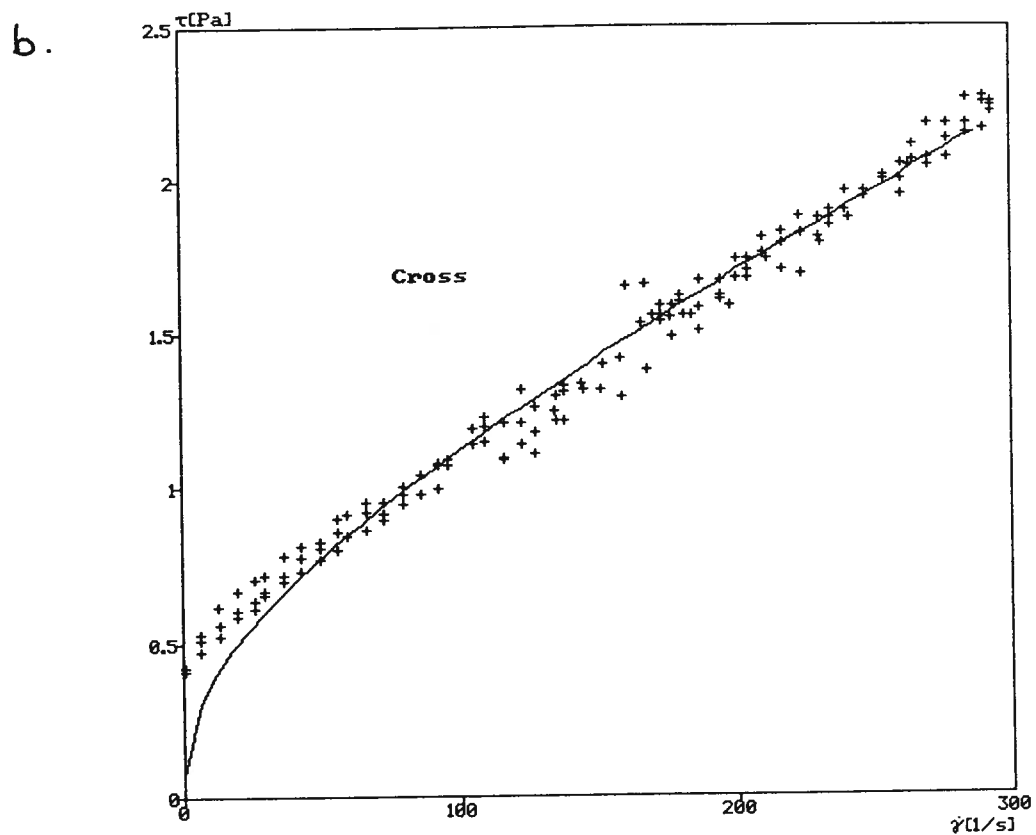
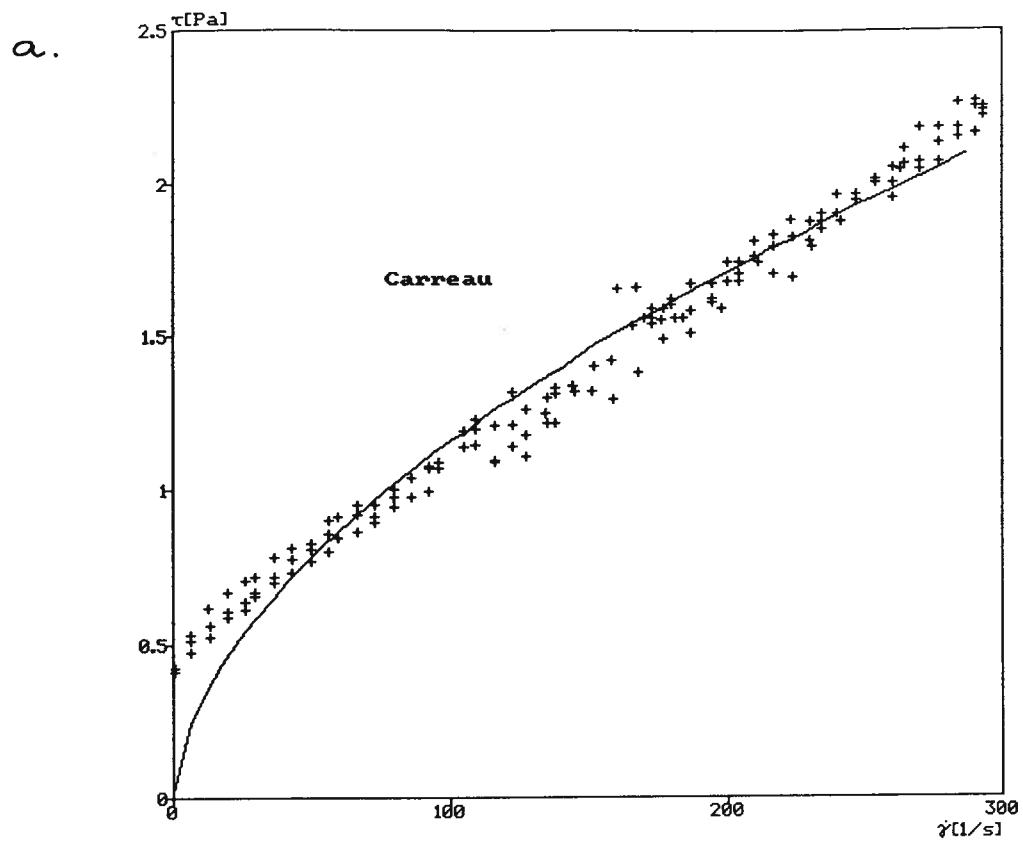


Figure AV.51 Rheological flow curve with fitted a) Carreau and b) Cross models for experimental Run #17.

Run #18: Suspension Composition

Carboxymethyl Cellulose (kg T ⁻¹):	1.00
Particle Passing Size (μm):	30.0
Solids Volume Fraction:	0.15
Magnetization:	Demagnetized
Sodium Silicate (kg T ⁻¹):	0.10
Kaolinite (% w/v):	0.50
pH:	7.0
Bentonite (% w/v):	0.50
Fine Coal (% w/v):	0.50

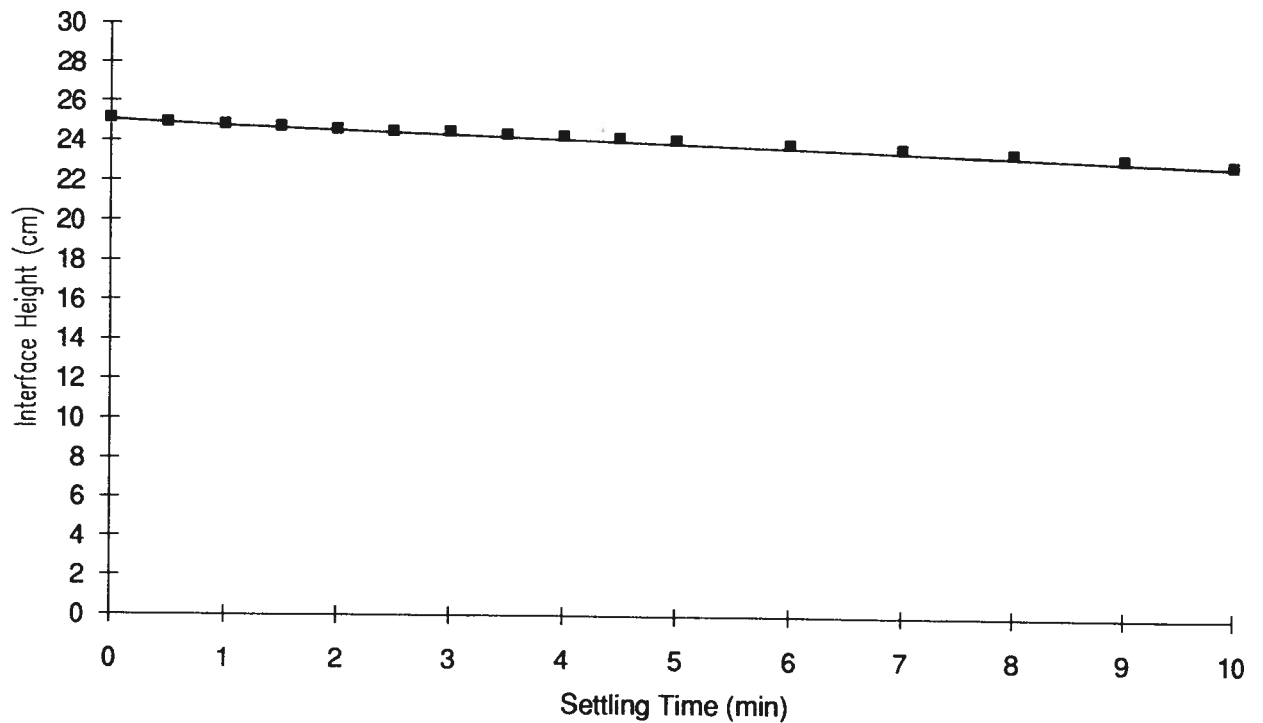


Figure AV.52 Settling curve interface height as a function of time for experimental Run #18.

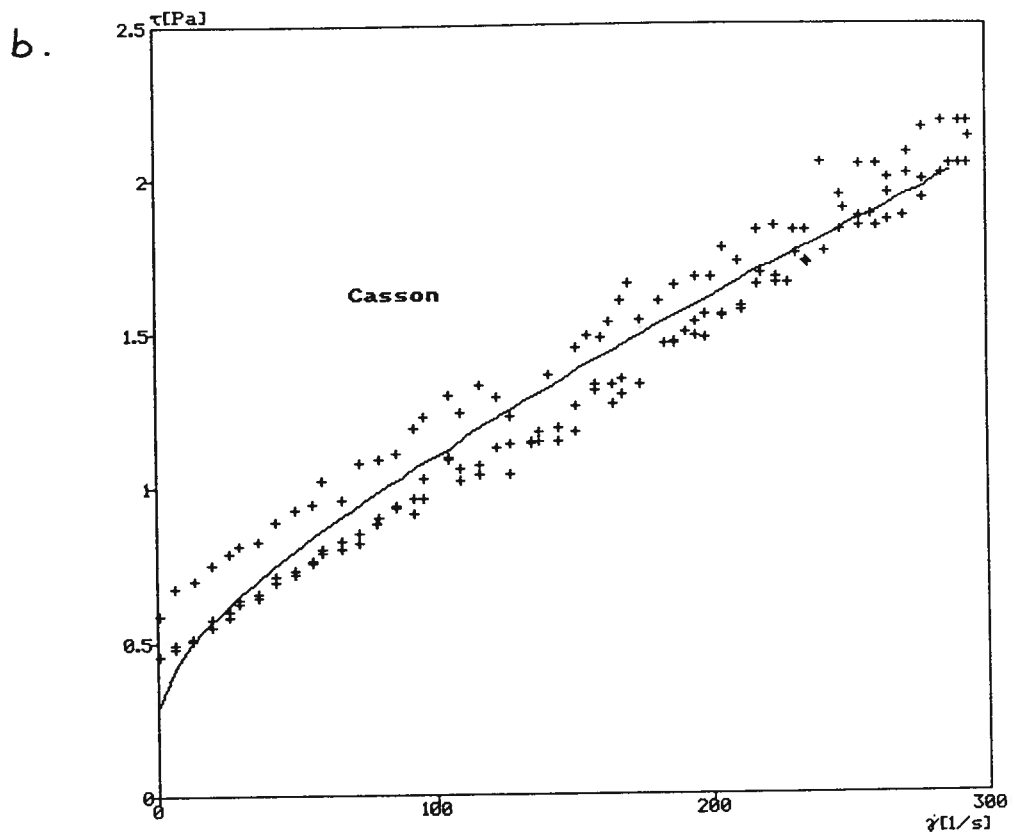
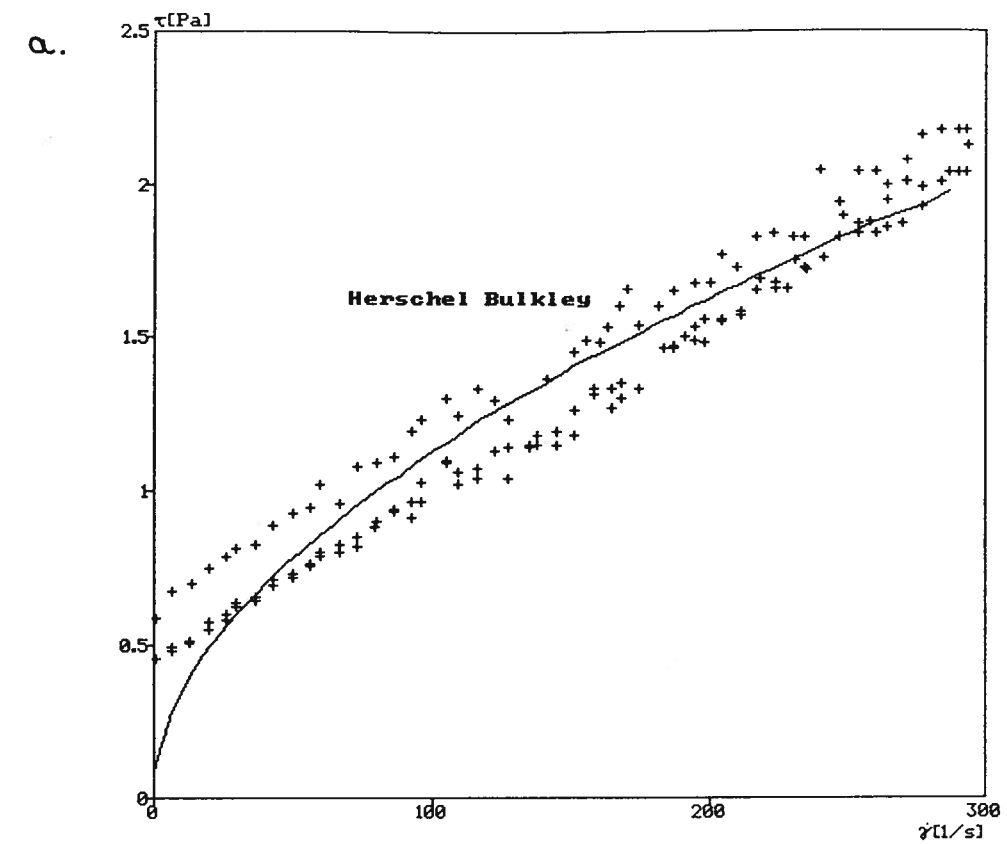


Figure AV.53 Rheological flow curve with fitted a) Herschel Bulkley and b) Casson models for experimental Run #18.

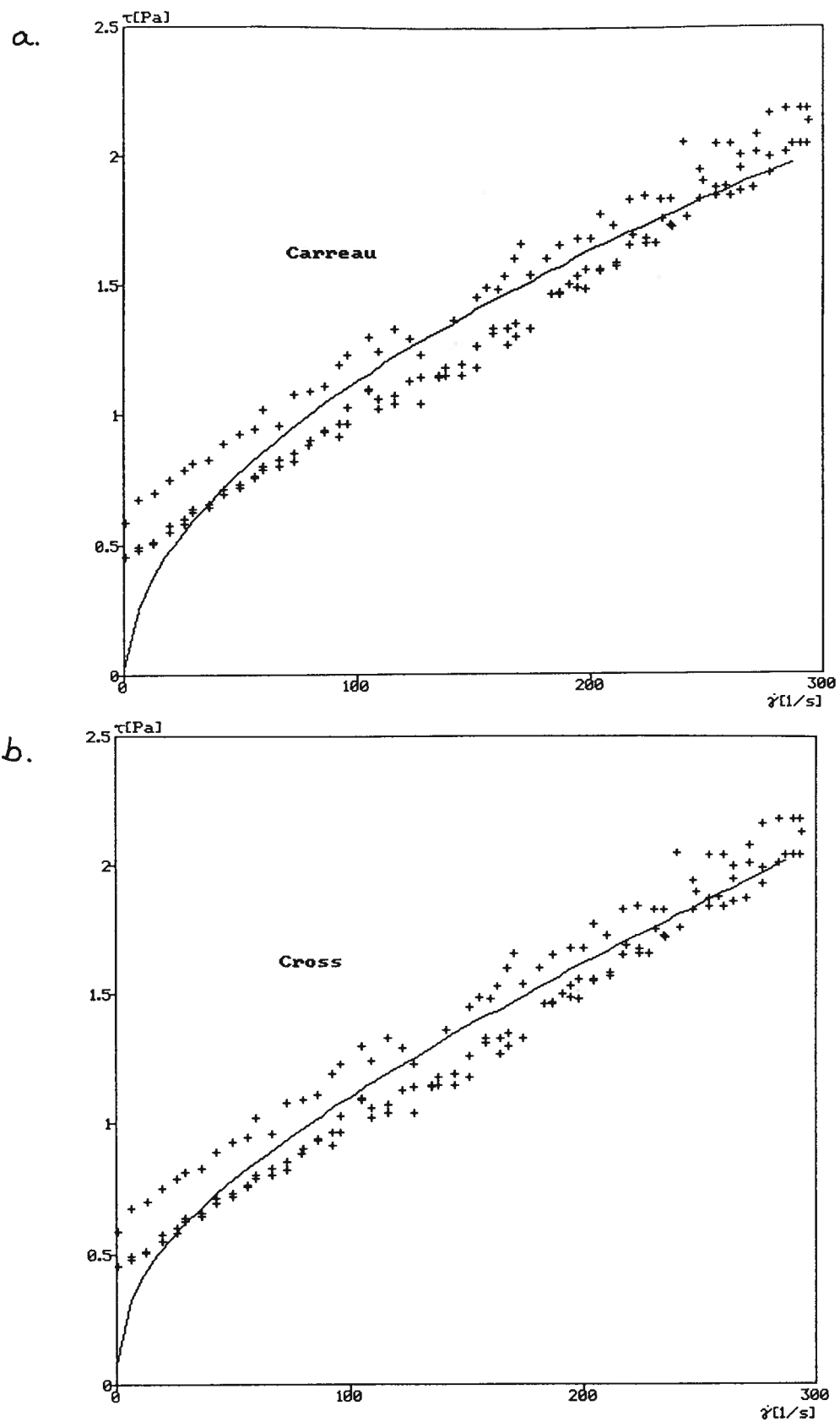


Figure AV.54 Rheological flow curve with fitted a) Carreau and b) Cross models for experimental Run #18.

Run #19: Suspension Composition

Carboxymethyl Cellulose (kg T ⁻¹):	1.00
Particle Passing Size (μm):	30.0
Solids Volume Fraction:	0.15
Magnetization:	Magnetized
Sodium Silicate (kg T ⁻¹):	0.10
Kaolinite (% w/v):	0.50
pH:	7.0
Bentonite (% w/v):	0.50
Fine Coal (% w/v):	0.50

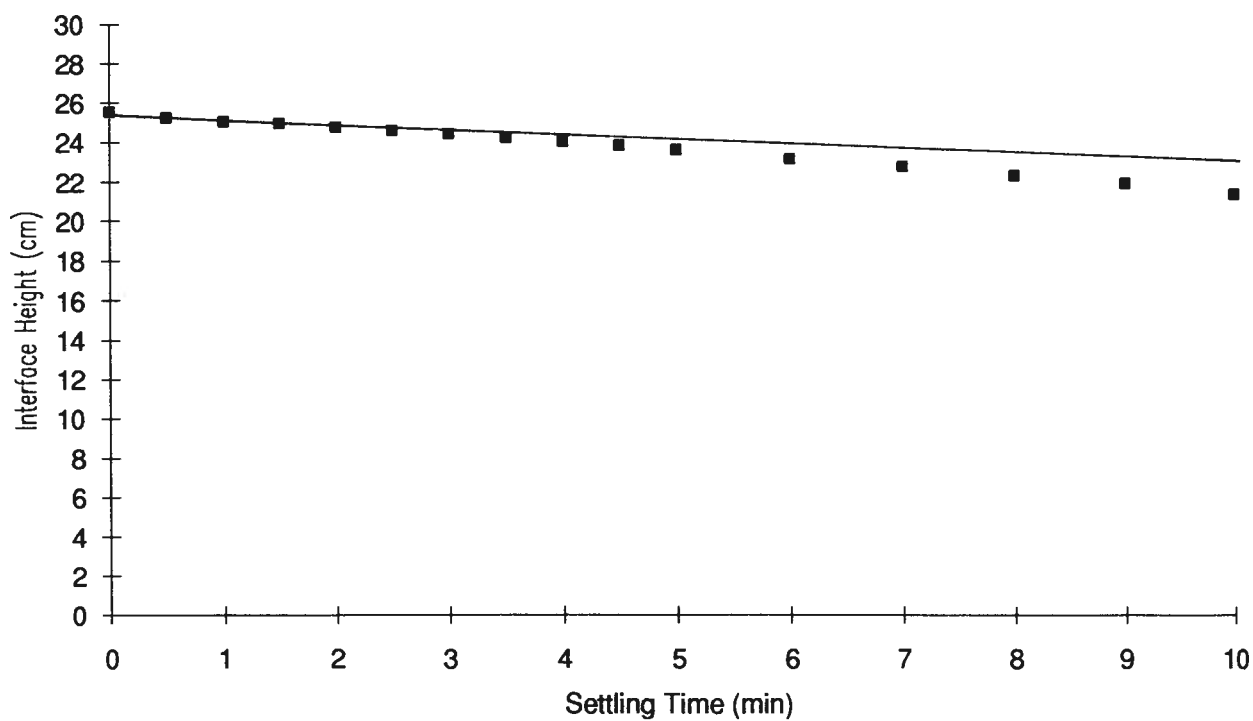


Figure AV.55 Settling curve interface height as a function of time for experimental Run #19.

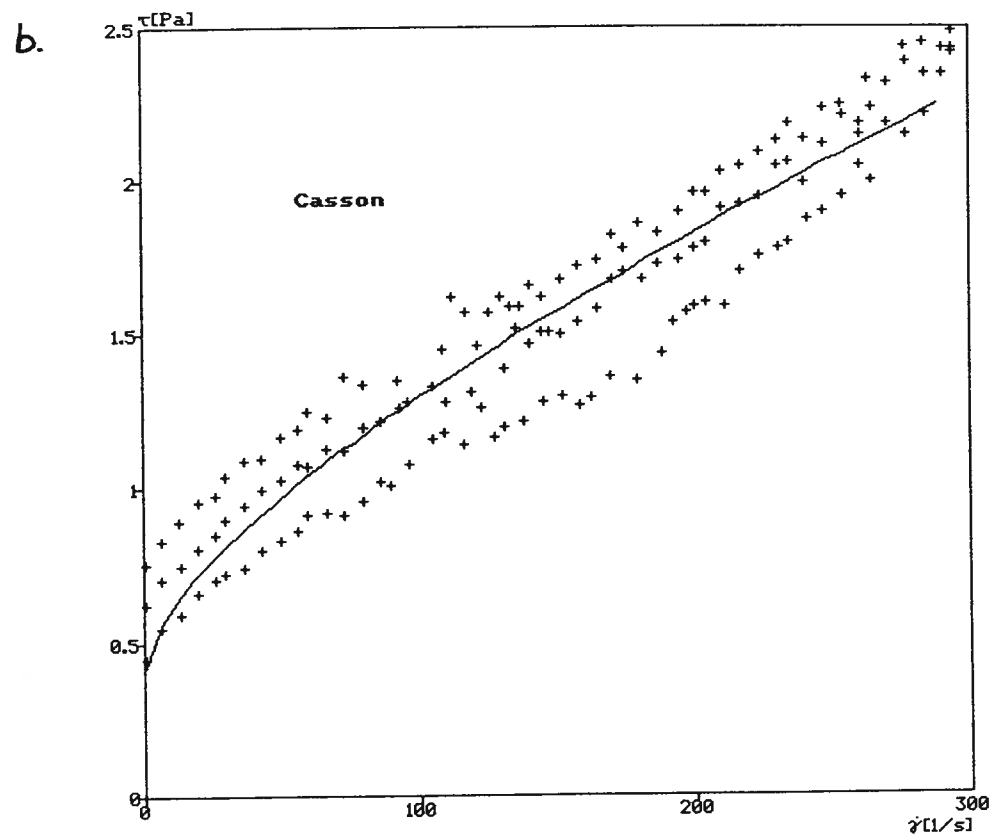
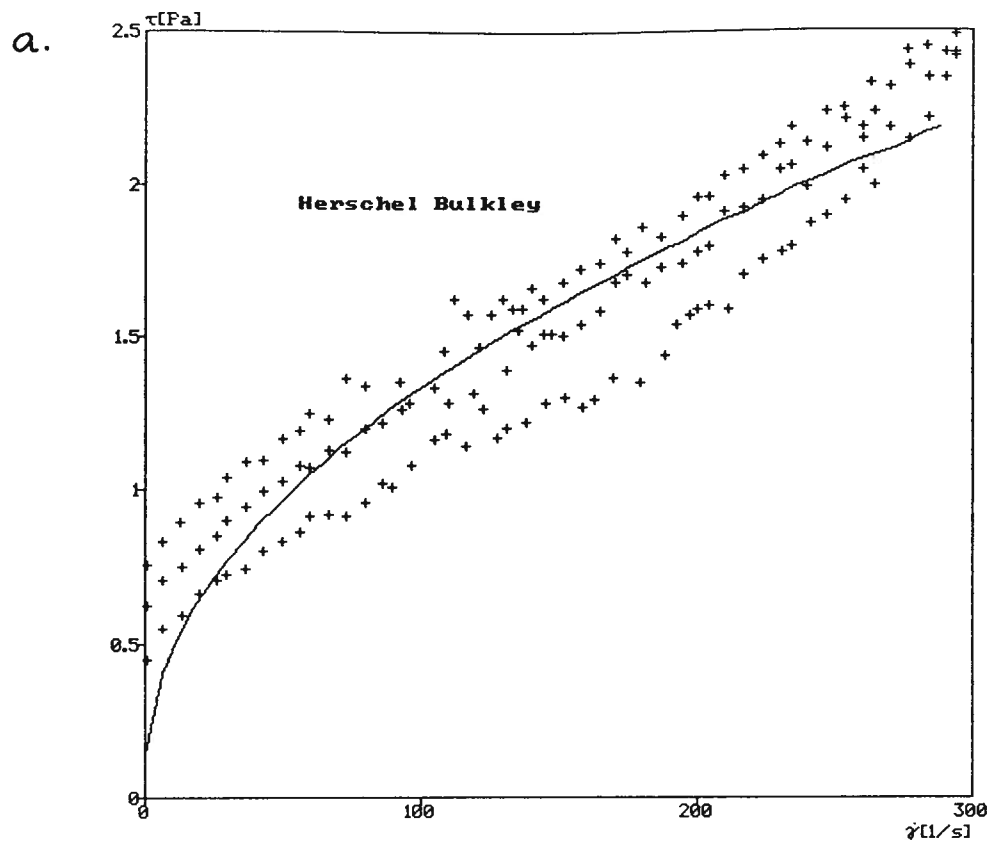


Figure AV.56 Rheological flow curve with fitted a) Herschel Bulkley and b) Casson models for experimental Run #19.

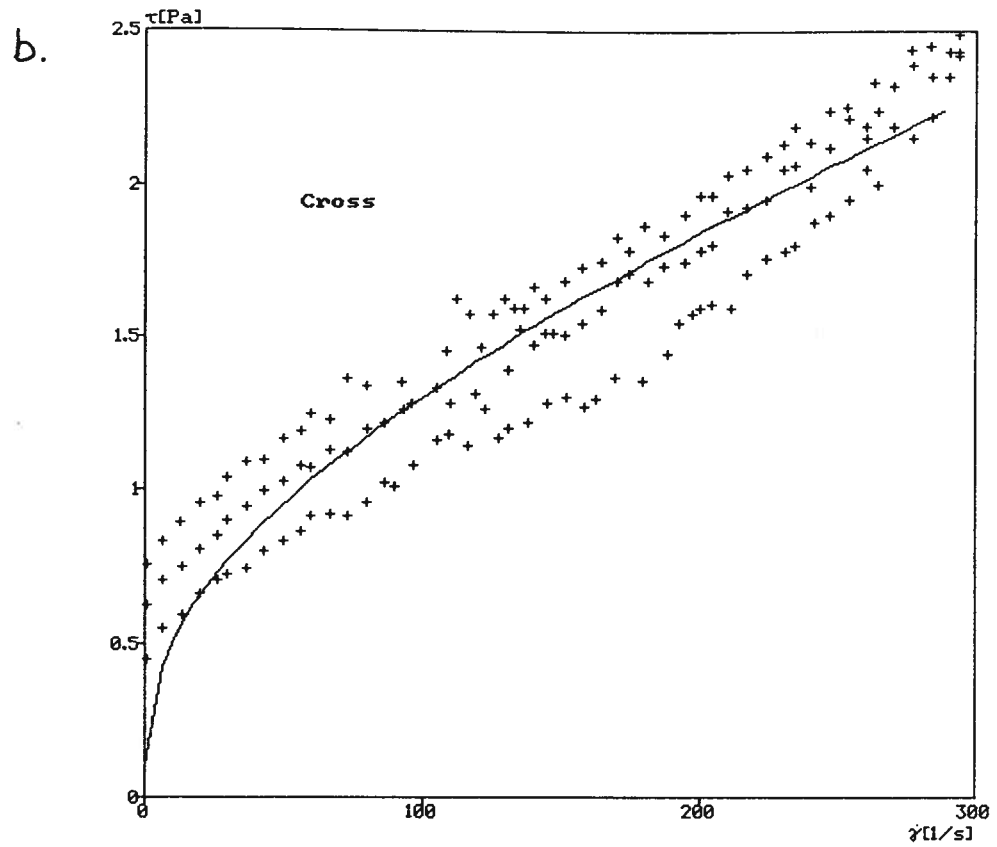
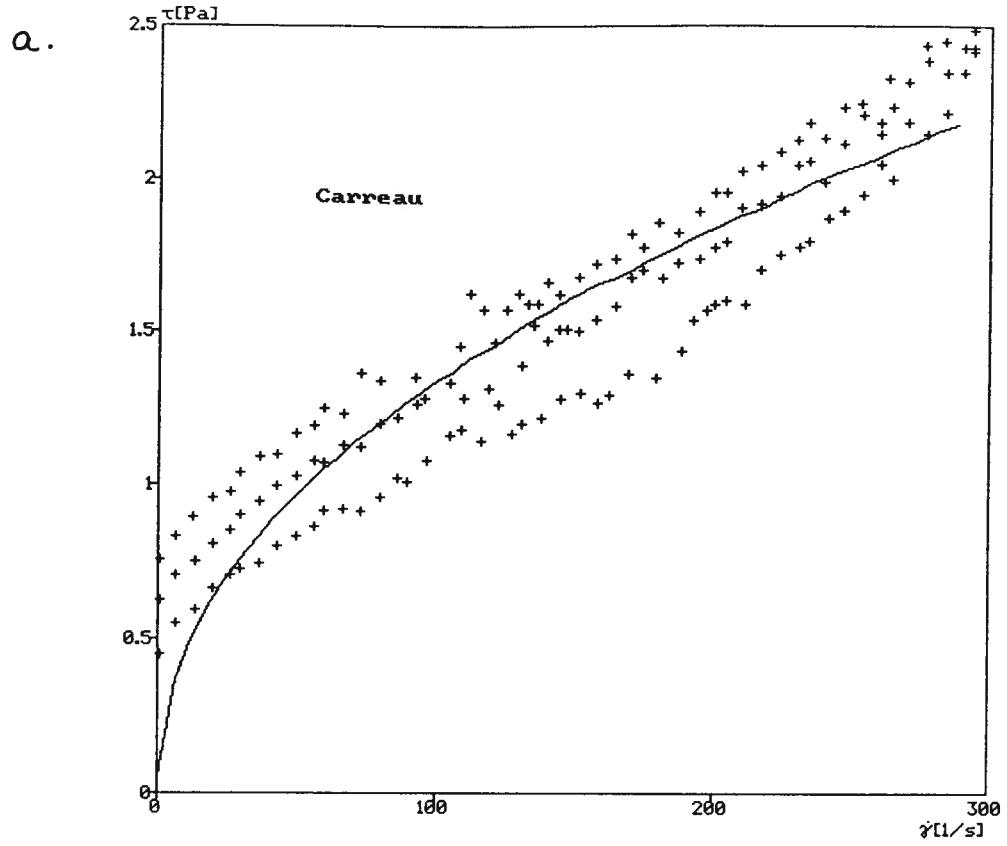


Figure AV.57 Rheological flow curve with fitted a) Carreau and b) Cross models for experimental Run #19.

Run #20: Suspension Composition

Carboxymethyl Cellulose (kg T ⁻¹):	1.00
Particle Passing Size (μm):	30.0
Solids Volume Fraction:	0.15
Magnetization:	Magnetized
Sodium Silicate (kg T ⁻¹):	0.10
Kaolinite (% w/v):	0.50
pH:	7.0
Bentonite (% w/v):	0.50
Fine Coal (% w/v):	0.50

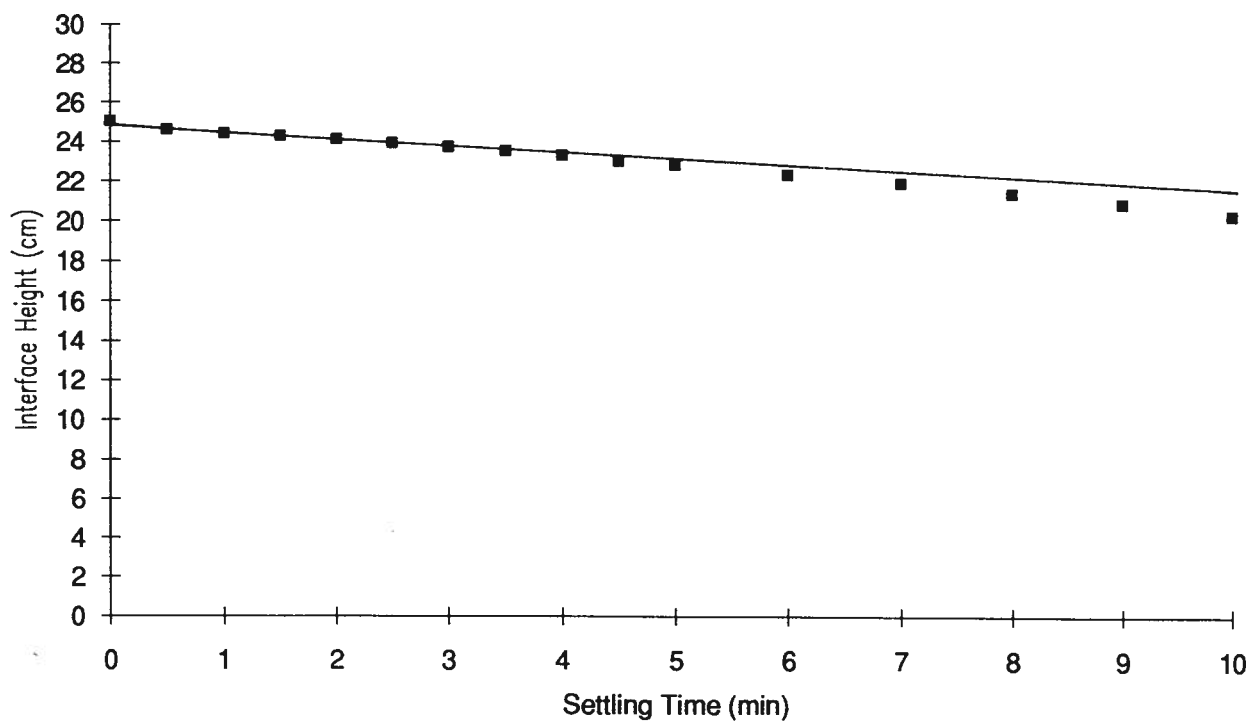


Figure AV.58 Settling curve interface height as a function of time for experimental Run #20.

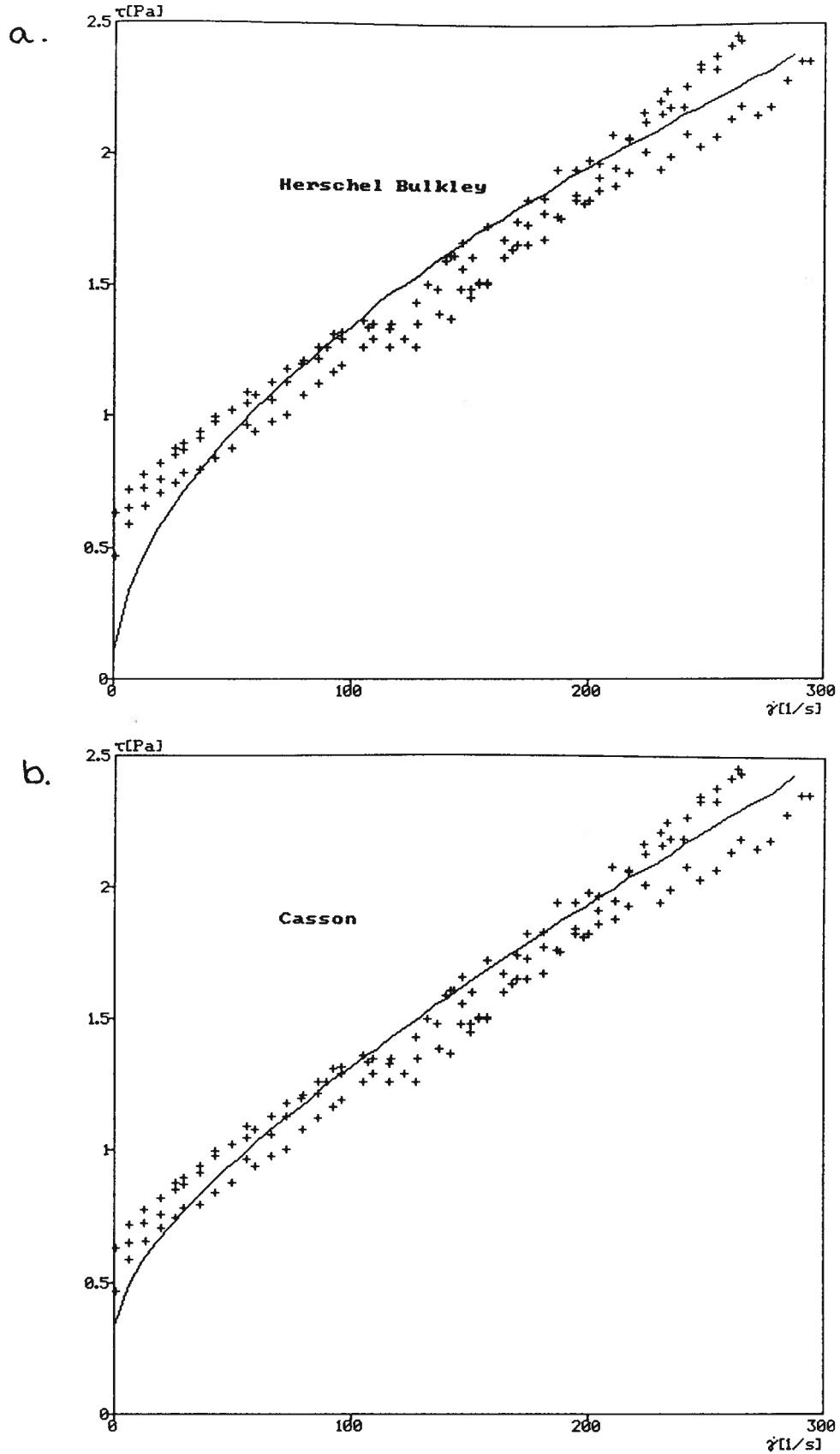


Figure AV.59 Rheological flow curve with fitted a) Herschel Bulkley and b) Casson models for experimental Run #20.

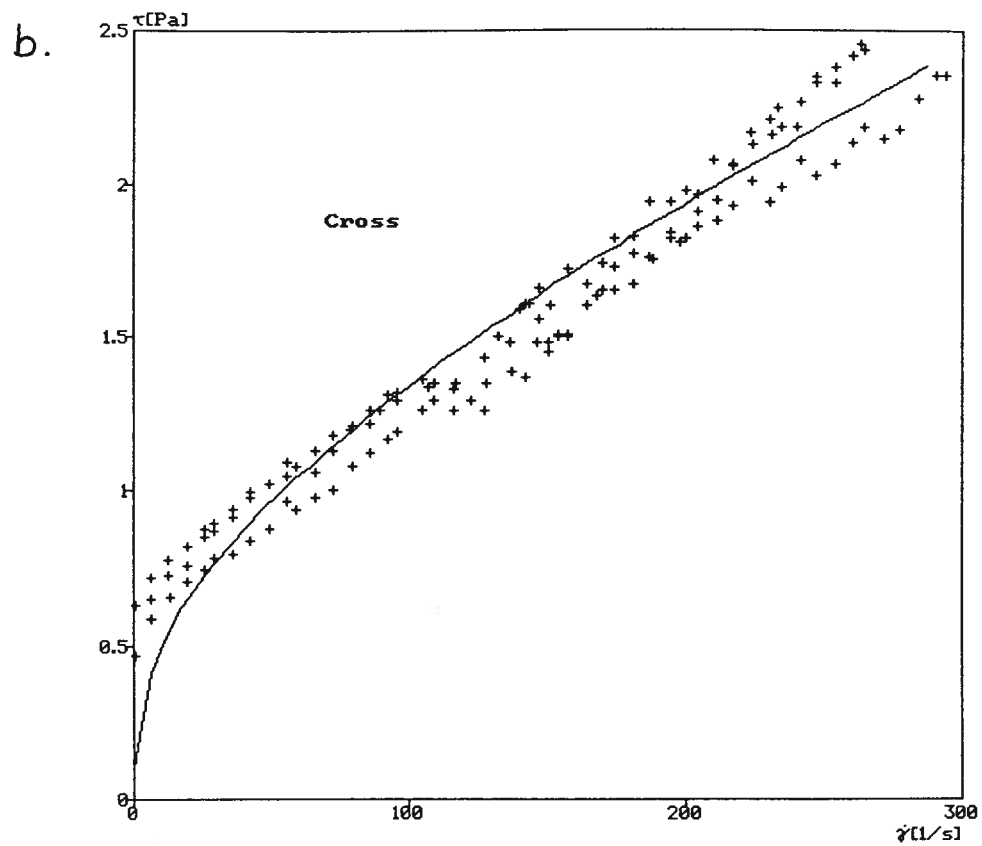
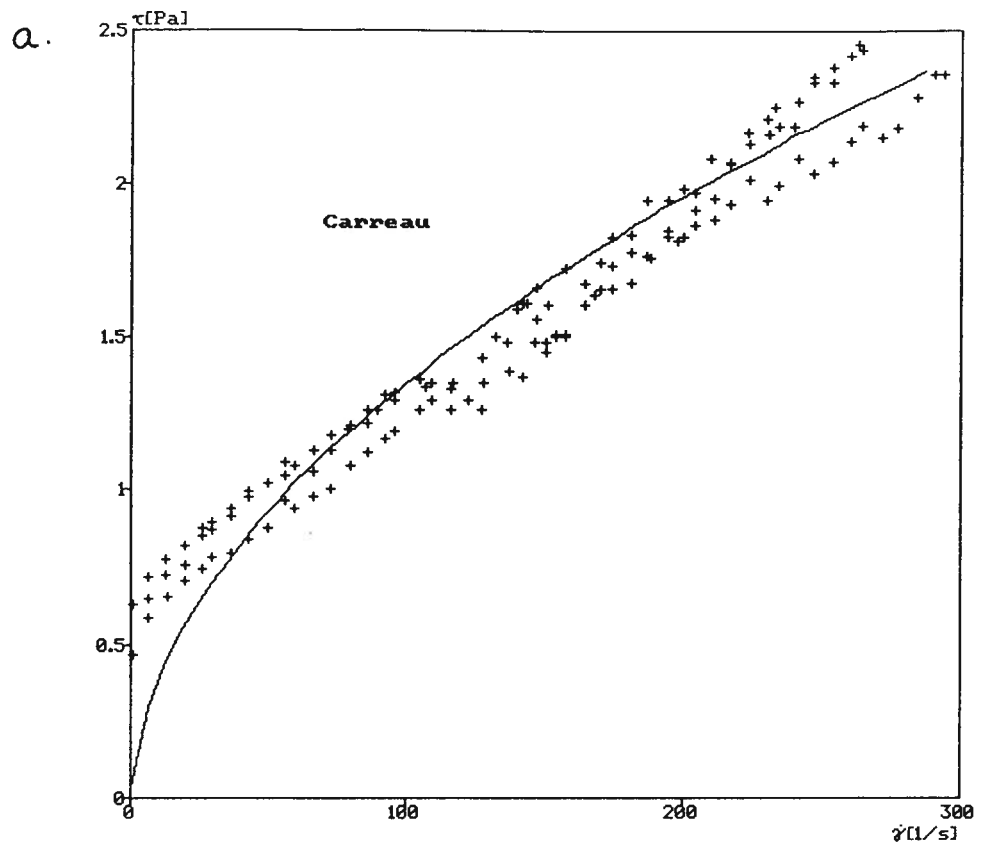


Figure AV.60 Rheological flow curve with fitted a) Carreau and b) Cross models for experimental Run #20.

APPENDIX VI

Settling Curves and Modelled Rheological

Flow Curves for Investigations into the

Effects of Particle Size Distribution on Media Properties

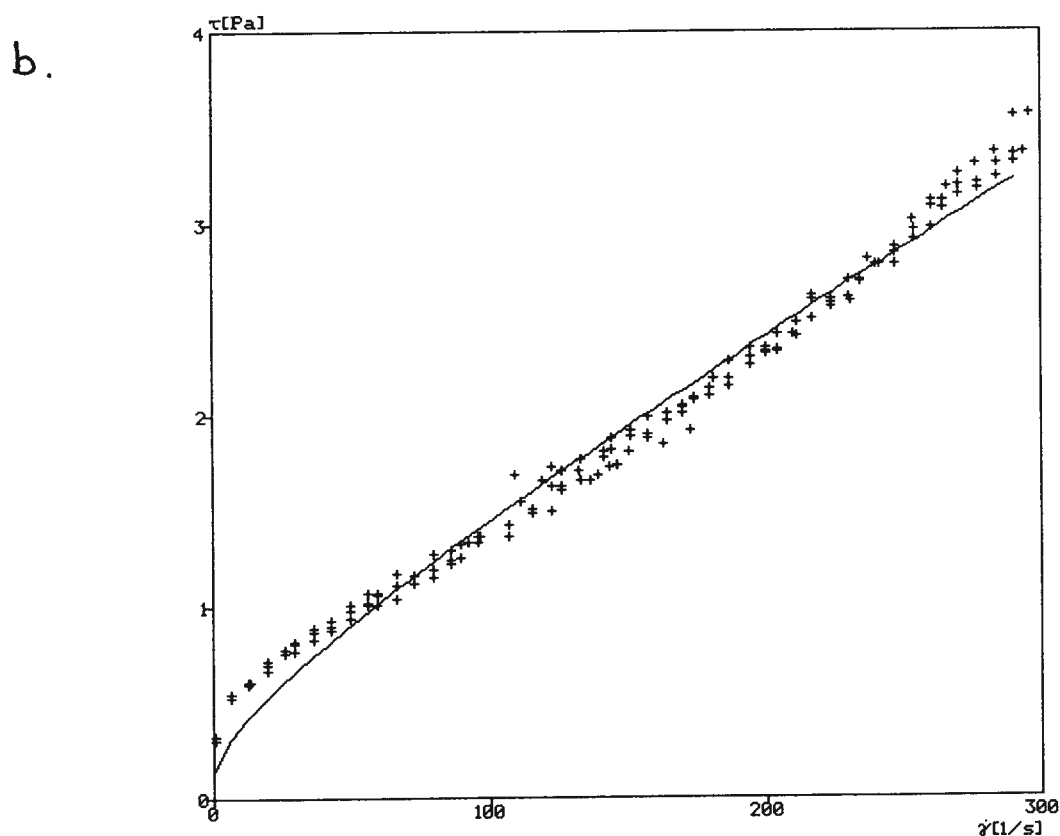
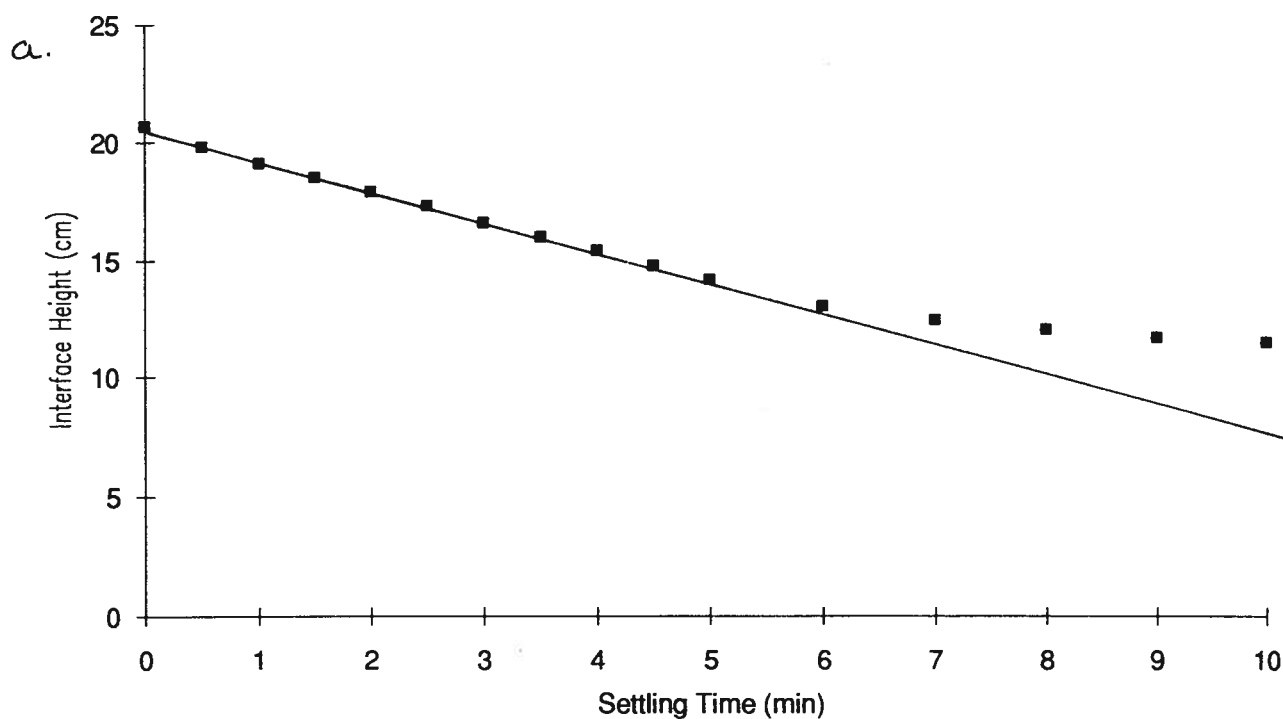


Figure AVL.1 a) Settling curve and b) fitted (Casson model) flow curve for experimental Run #1 ($\phi_{sv}=0.25$, $\phi_r=0.40$, $d_j/d_i=0.39$, pH=8.08).

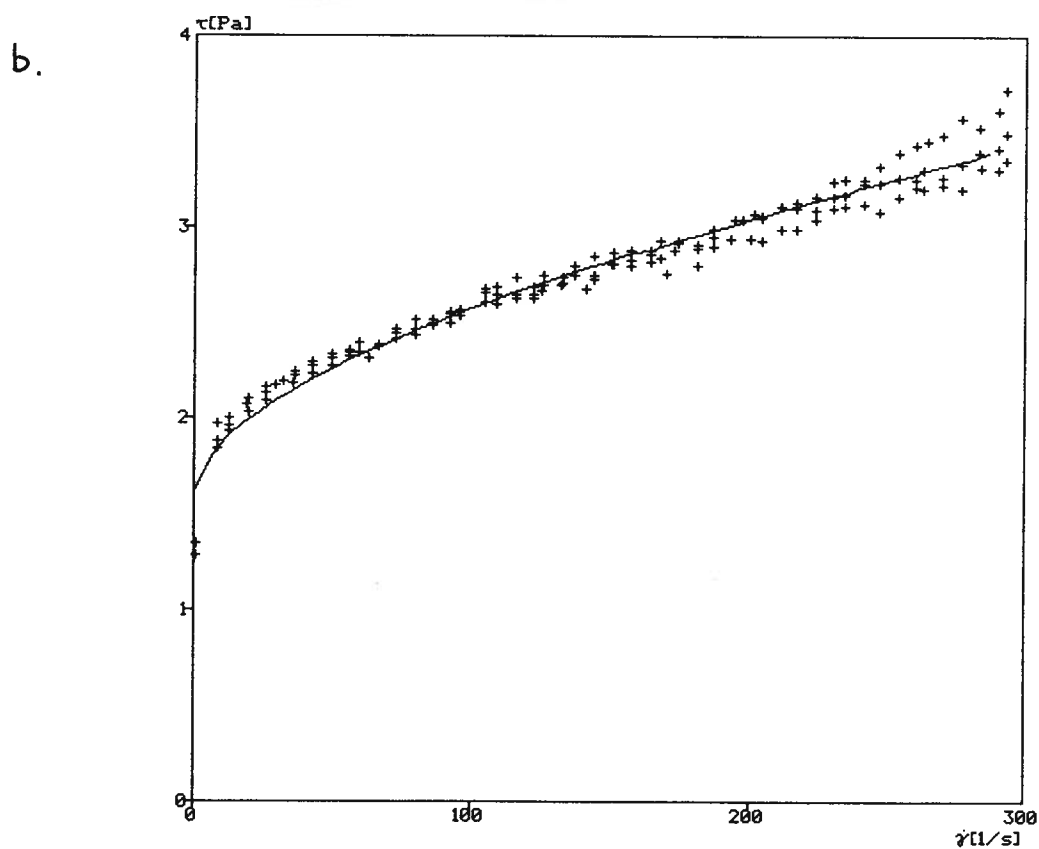
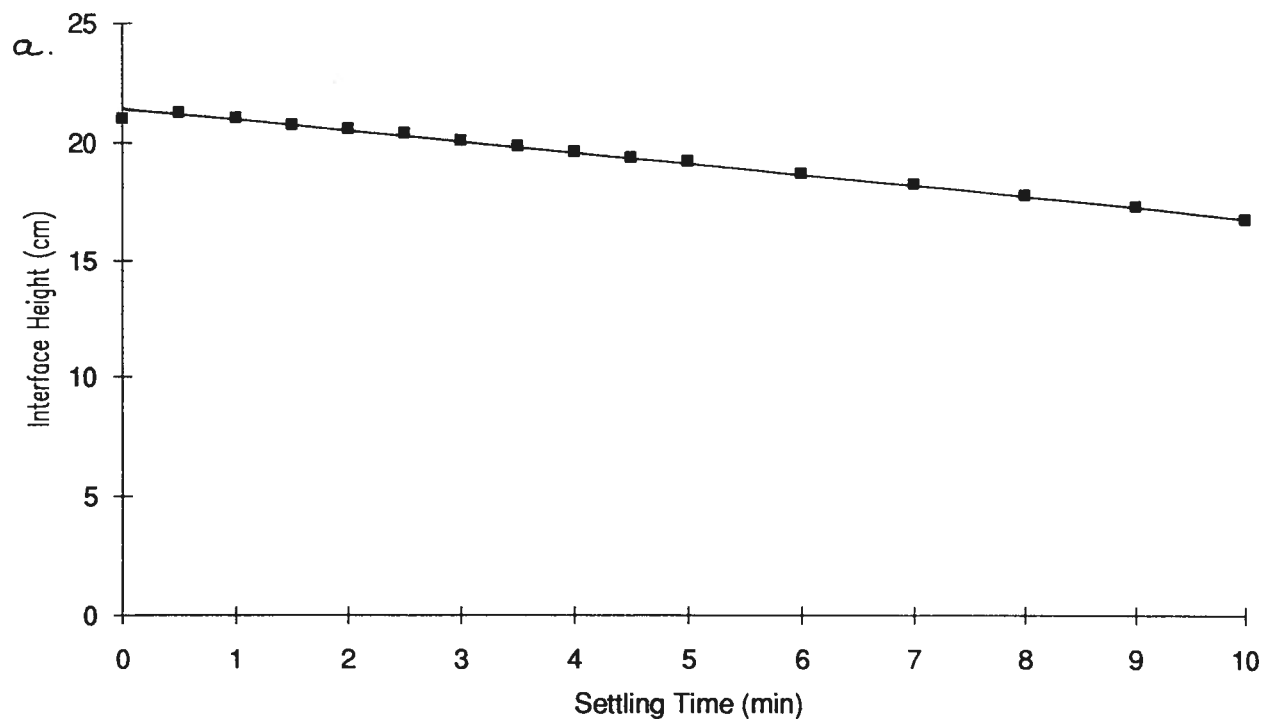


Figure AVL2 a) Settling curve and b) fitted (Casson model) flow curve for experimental Run #2 ($\phi_{sv}=0.25$, $\phi_r=0.40$, $d_v/d_l=0.13$, $pH=8.33$).

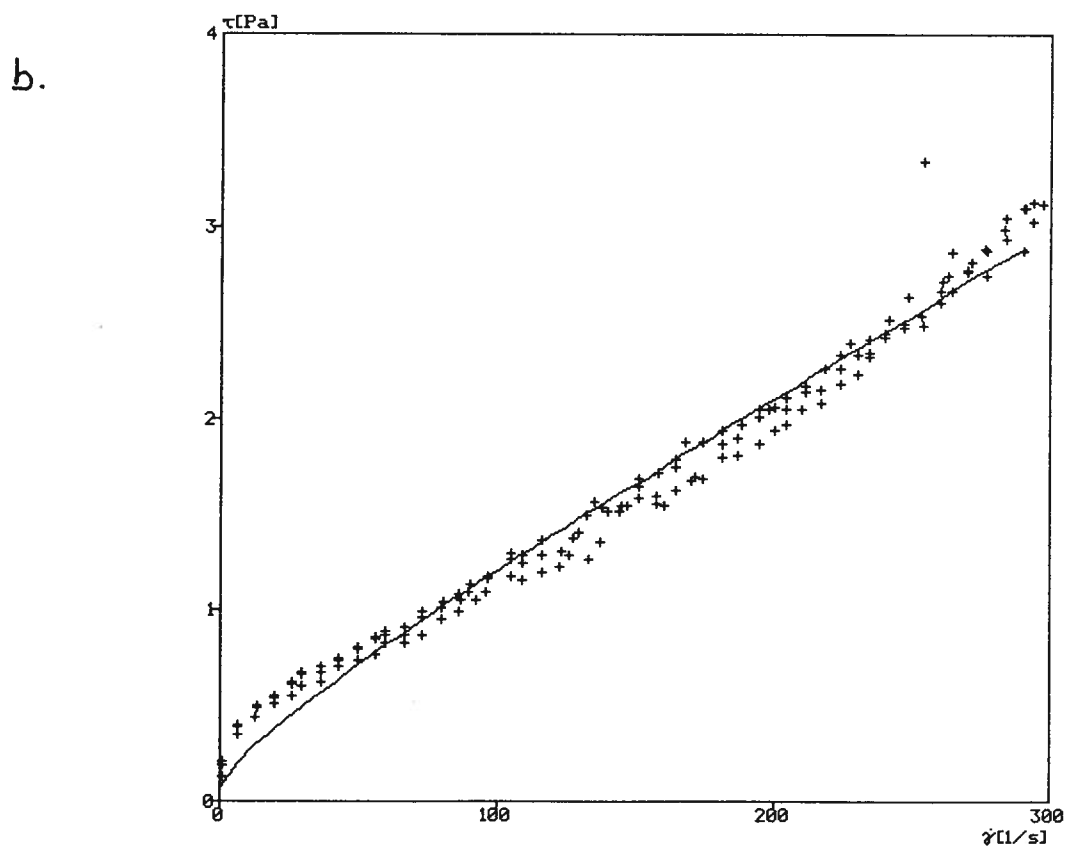
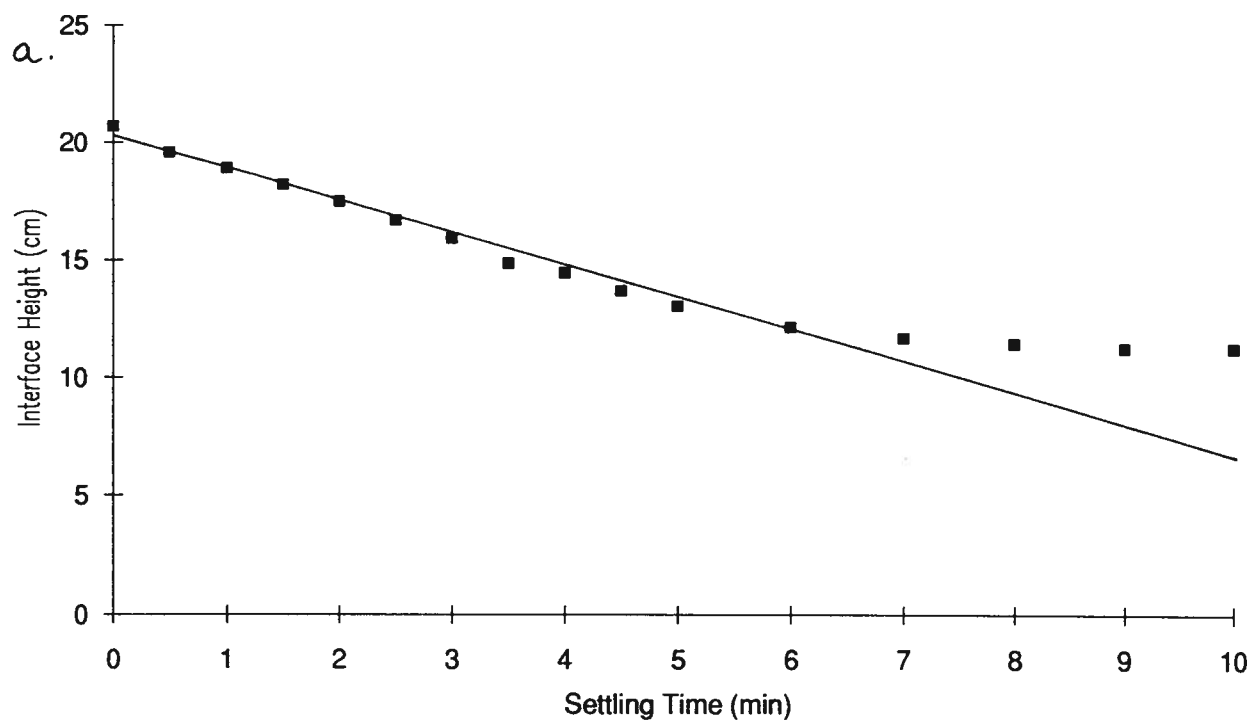


Figure AVI.3 a) Settling curve and b) fitted (Casson model) flow curve for experimental Run #3 ($\phi_{sv}=0.25$, $\phi_f=0.25$, $d_s/d_f=0.39$, $pH=8.38$).

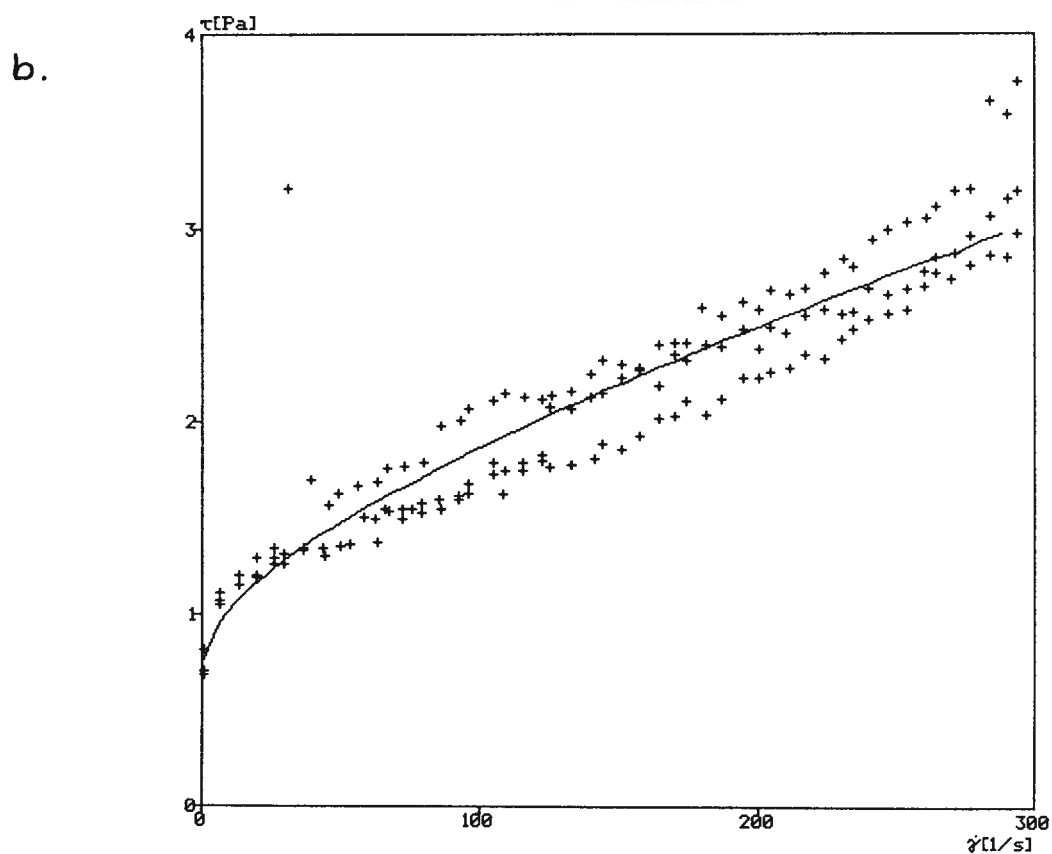
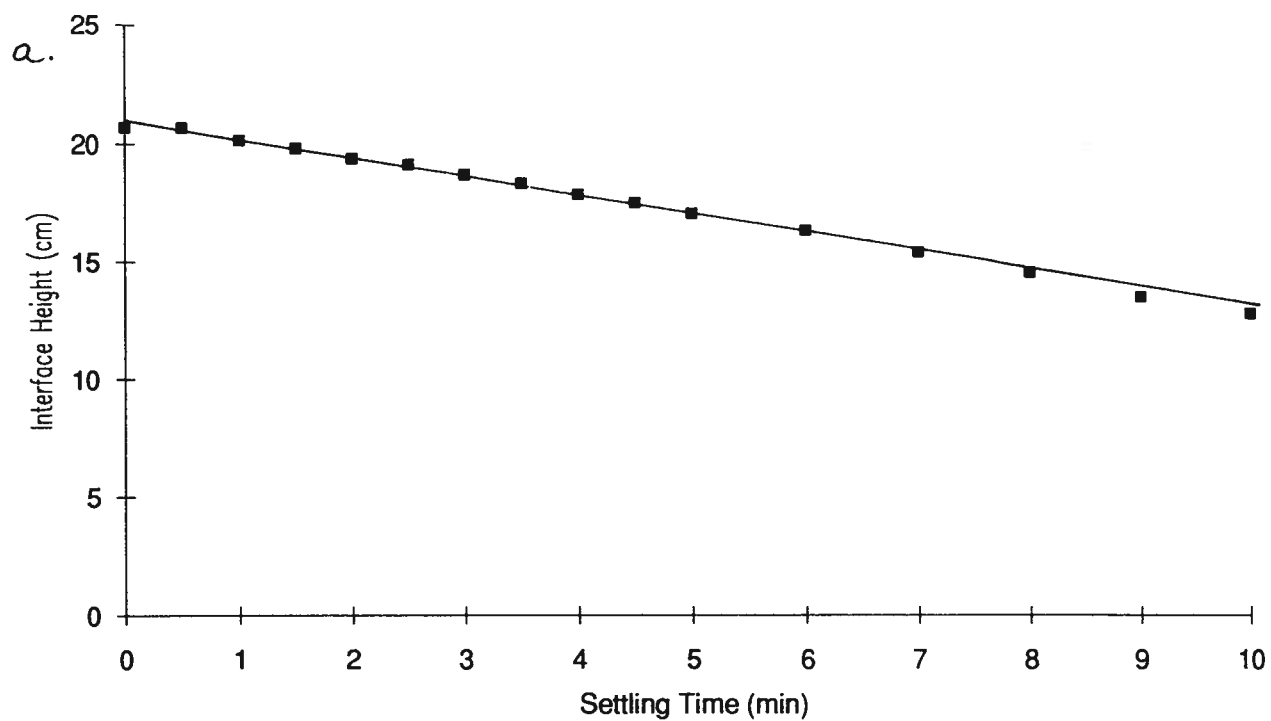


Figure AVL4 a) Settling curve and b) fitted (Casson model) flow curve for experimental Run #4 ($\phi_{sv}=0.25$, $\phi_r=0.25$, $d_v/d_l=0.13$, $pH=8.21$).

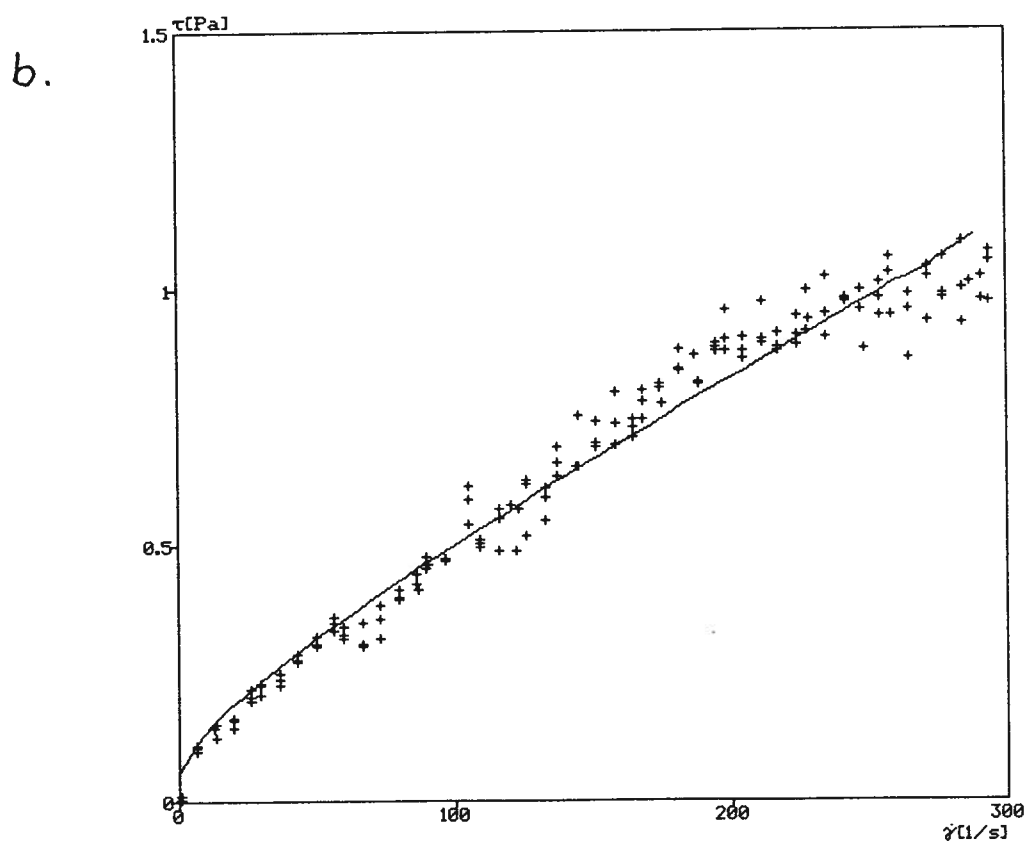
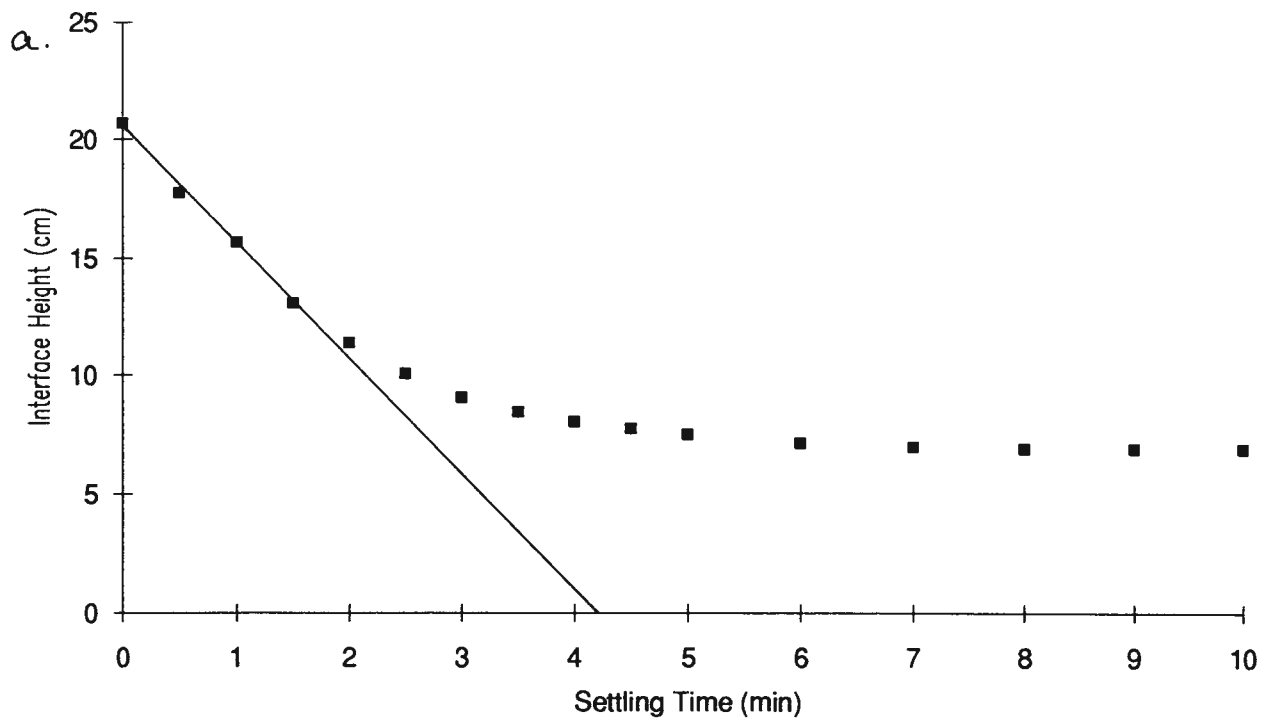


Figure AVL5 a) Settling curve and b) fitted (Casson model) flow curve for experimental Run #5 ($\phi_{sv}=0.15$, $\phi_f=0.40$, $d_s/d_f=0.39$, $pH=8.17$).

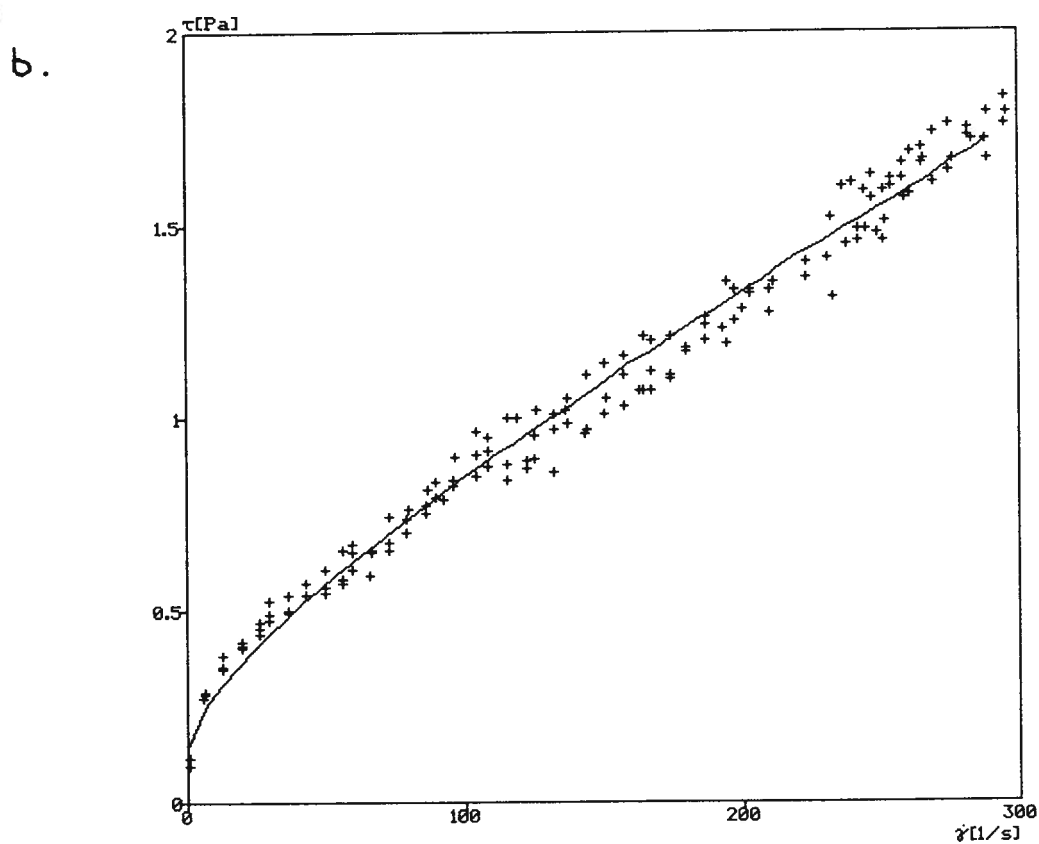
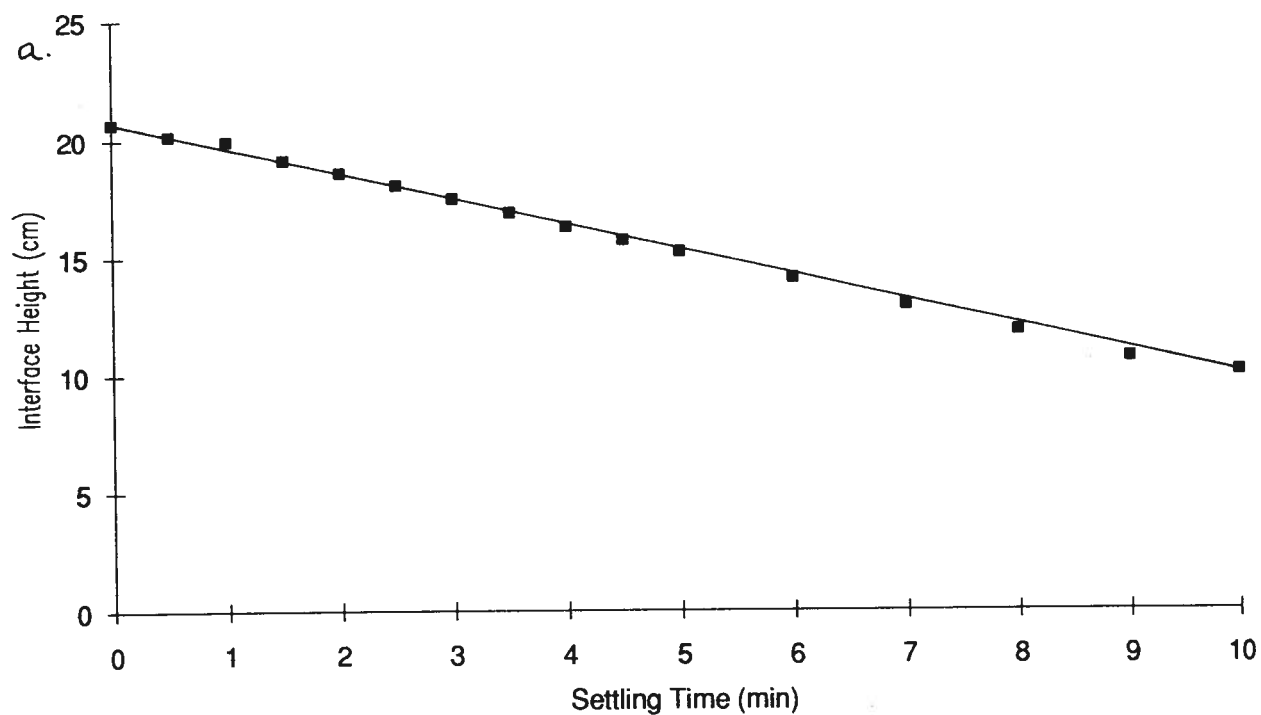


Figure AVI.6 a) Settling curve and b) fitted (Casson model) flow curve for experimental Run #6 ($\phi_{sv}=0.15$, $\phi_t=0.40$, $d_s/d_t=0.13$, $pH=8.78$).

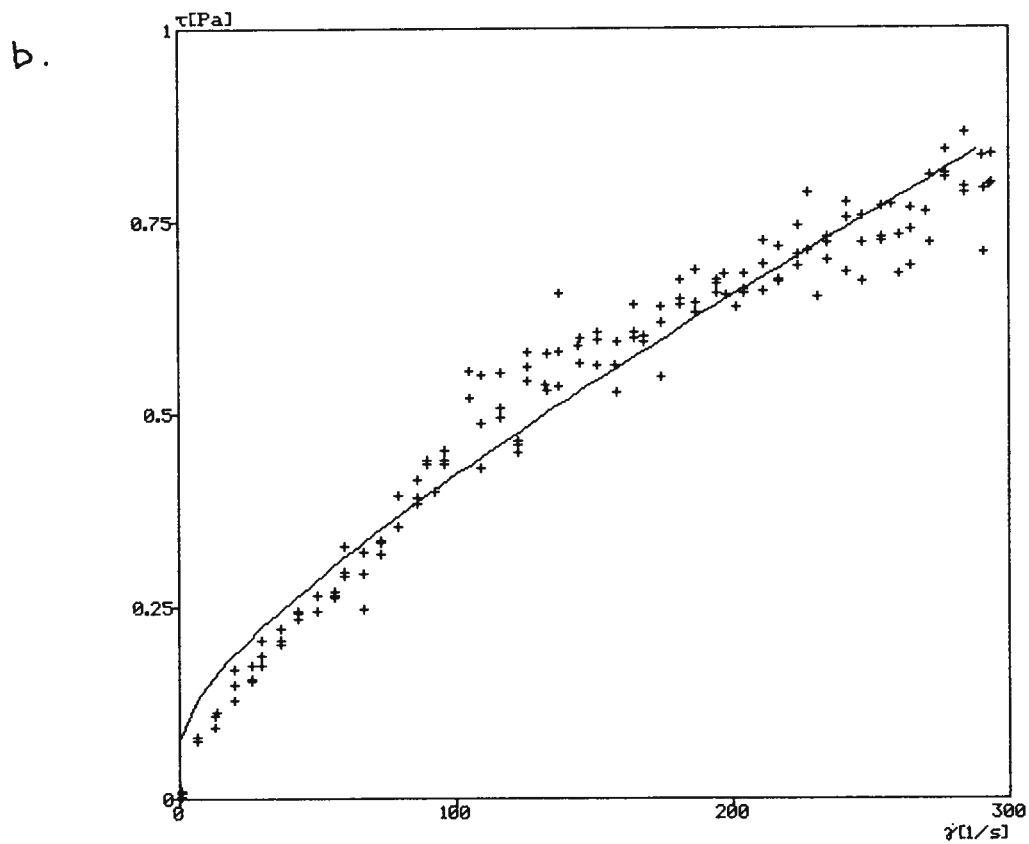
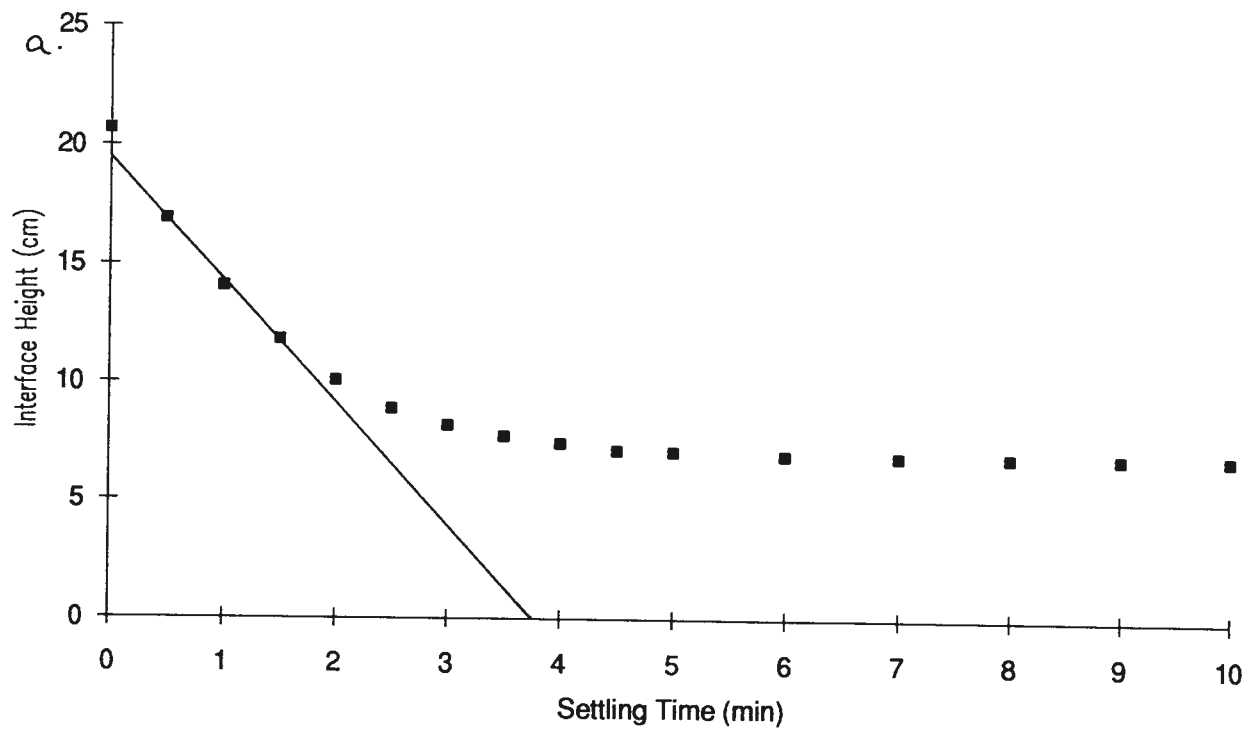


Figure AVI.7 a) Settling curve and b) fitted (Casson model) flow curve for experimental Run #7 ($\phi_{sv}=0.15$, $\phi_f=0.25$, $d_f/d_i=0.39$, pH=8.42).

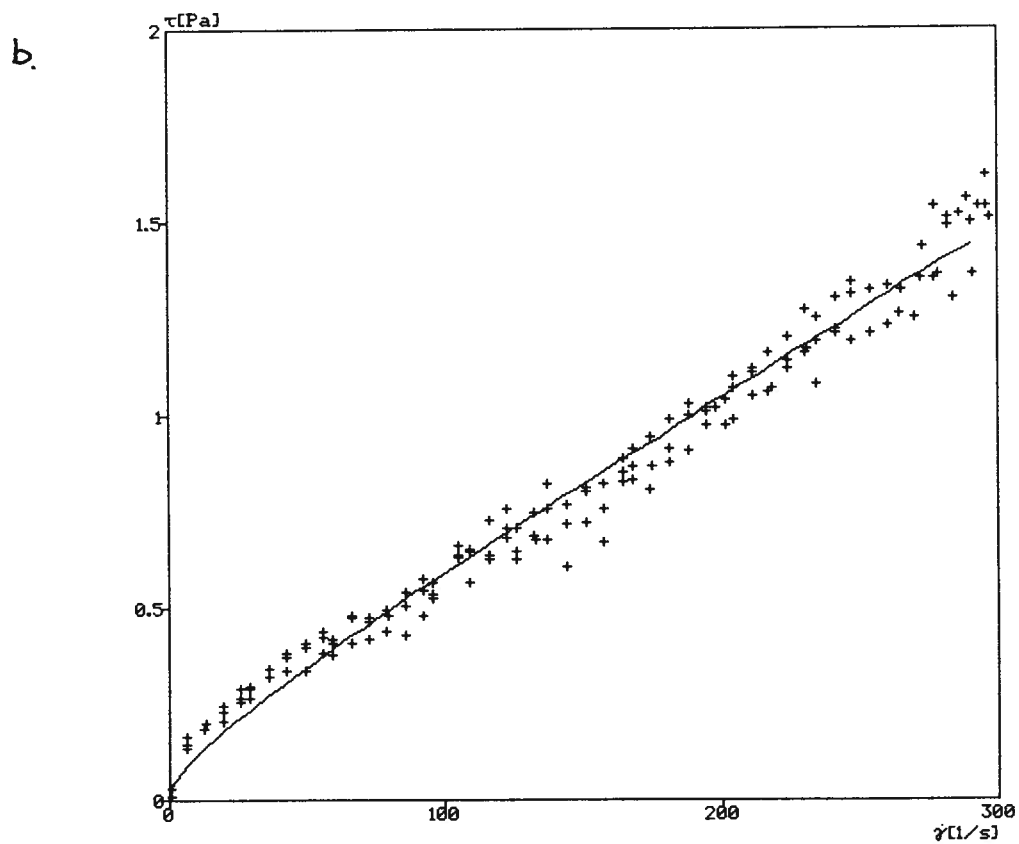
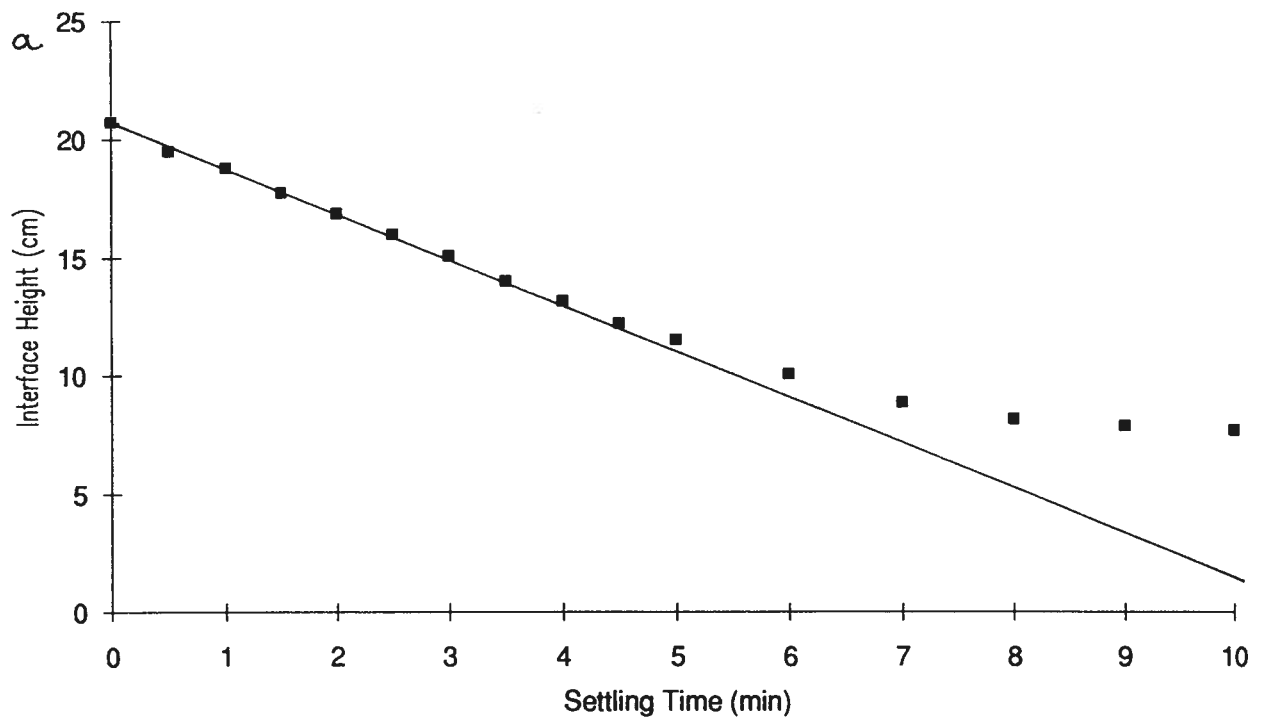


Figure AVL8 a) Settling curve and b) fitted (Casson model) flow curve for experimental Run #8 ($\phi_{sv}=0.15$, $\phi_f=0.25$, $d_s/d_l=0.13$, $pH=8.85$).

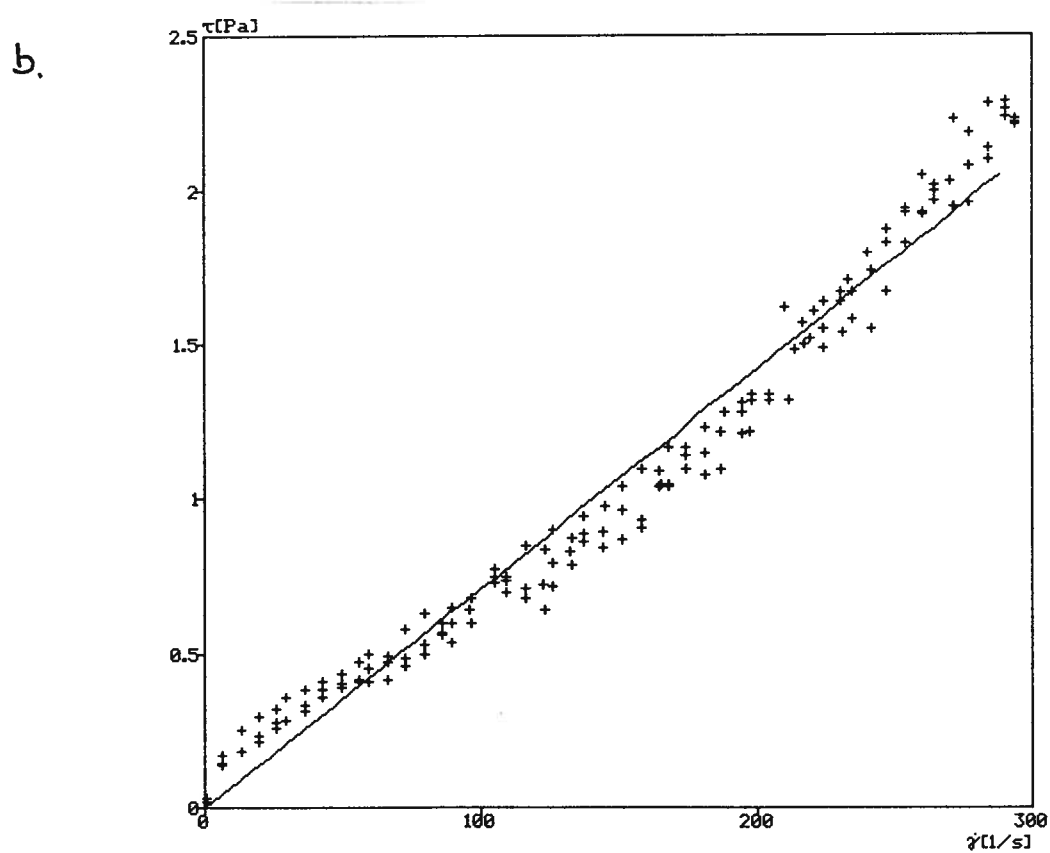
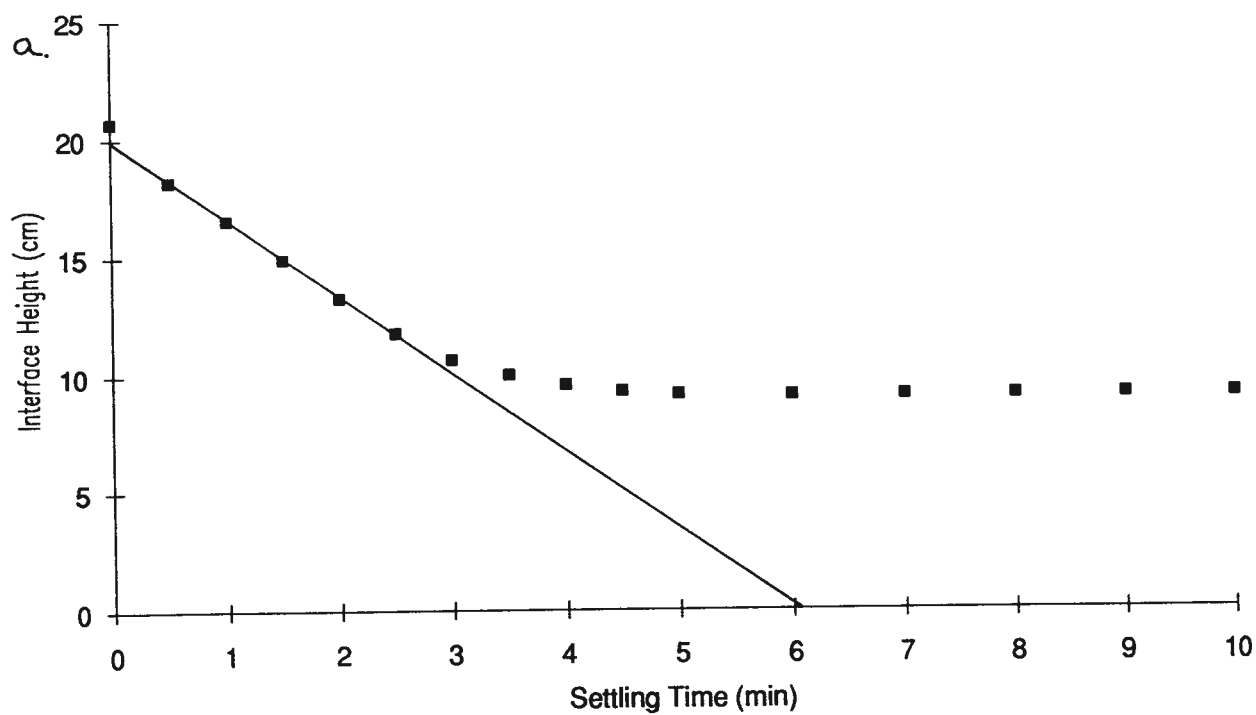


Figure AVI.9 a) Settling curve and b) fitted (Casson model) flow curve for experimental Run #9 ($\phi_{sv}=0.20$, $\phi_f=0.325$, $d_j/d_i=0.67$, $pH=8.25$).

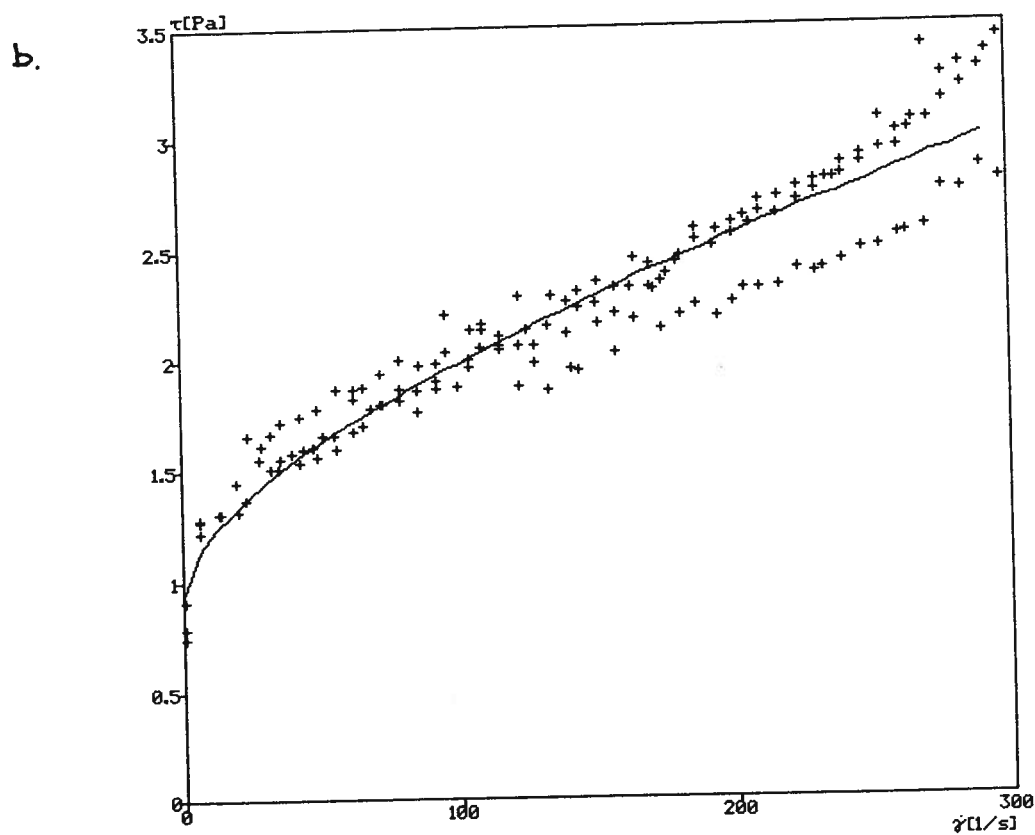
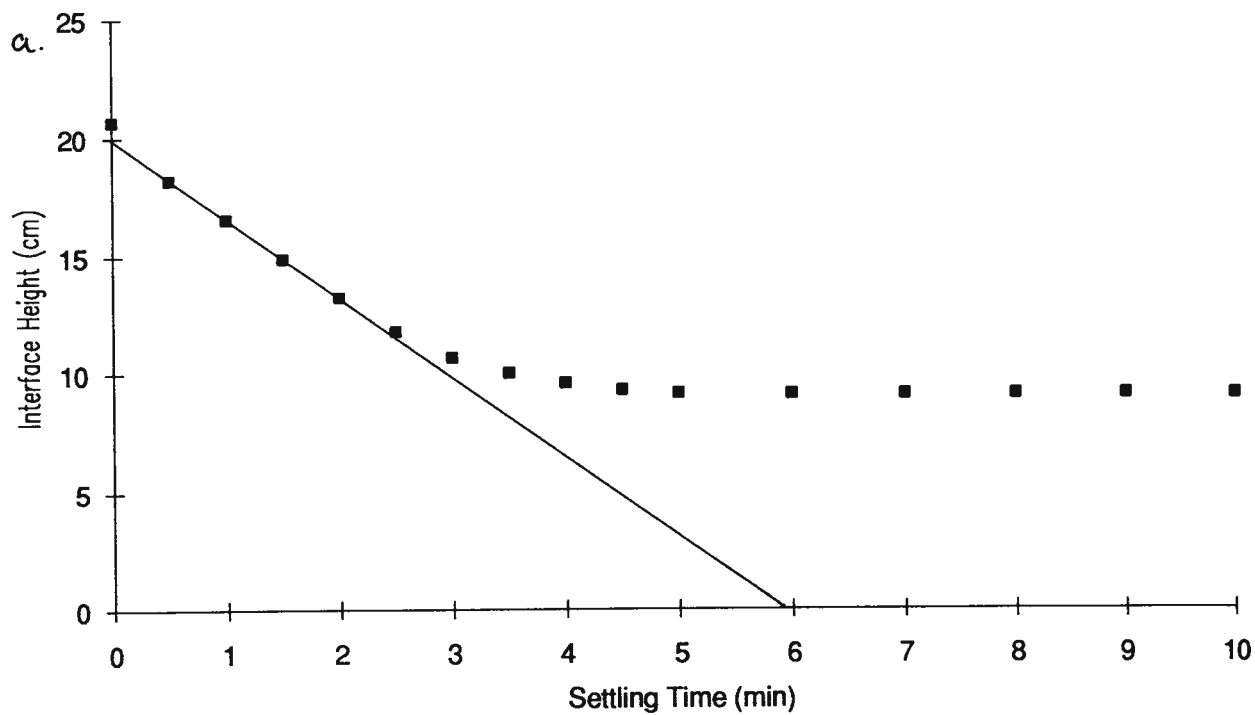


Figure AVL10 a) Settling curve and b) fitted (Casson model) flow curve for experimental Run #10 ($\phi_{sv}=0.20$, $\phi_f=0.325$, $d_s/d_f=0.09$, $pH=8.63$).

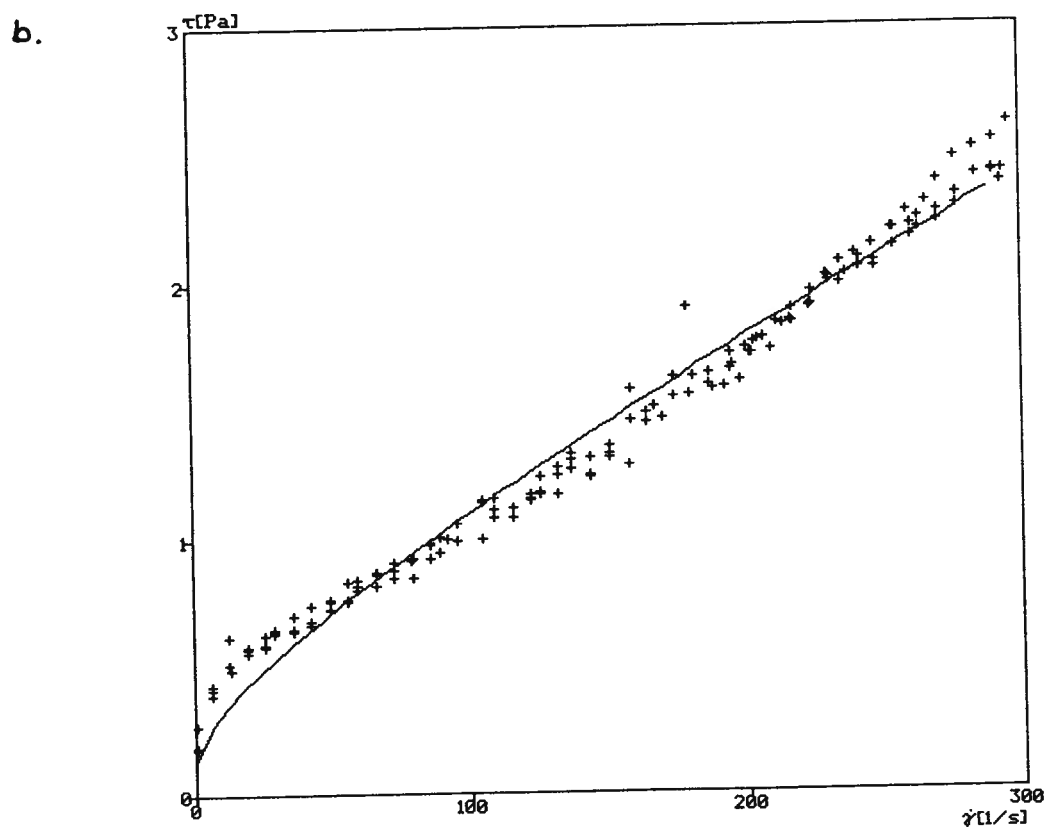
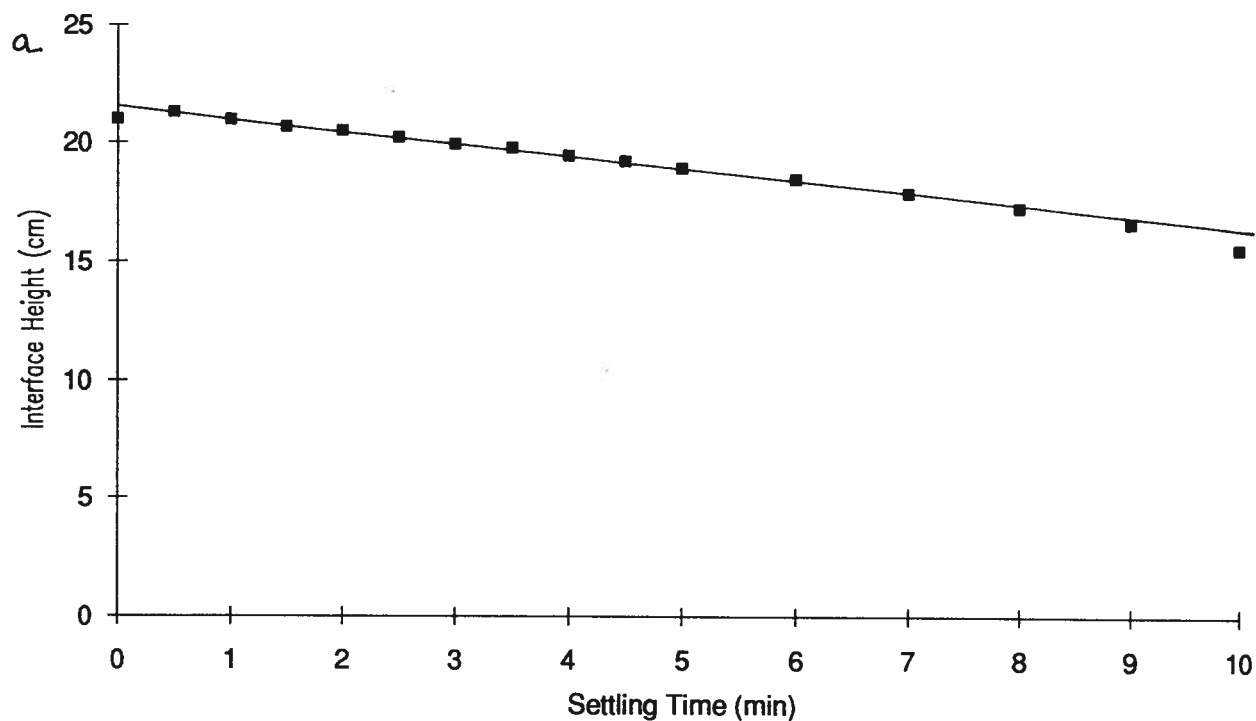


Figure AVL.11 a) Settling curve and b) fitted (Casson model) flow curve for experimental Run #11 ($\phi_{sv}=0.20$, $\phi_f=0.451$, $d_v/d_f=0.22$, $pH=8.35$).

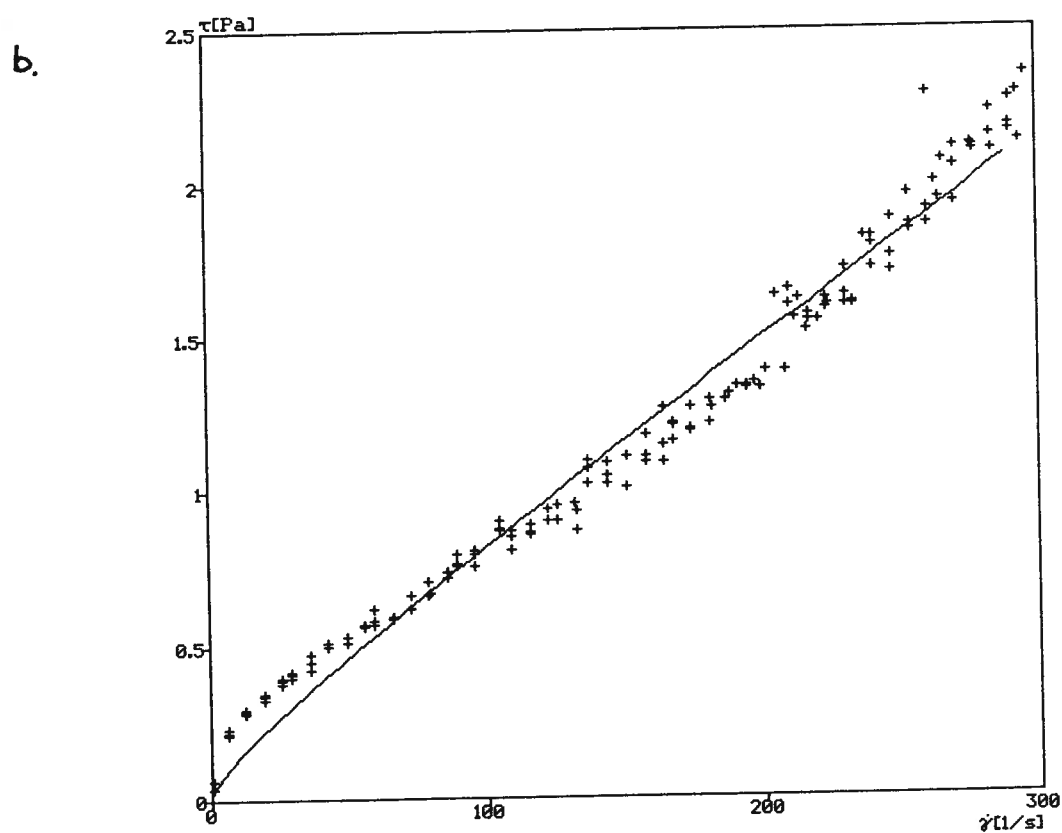
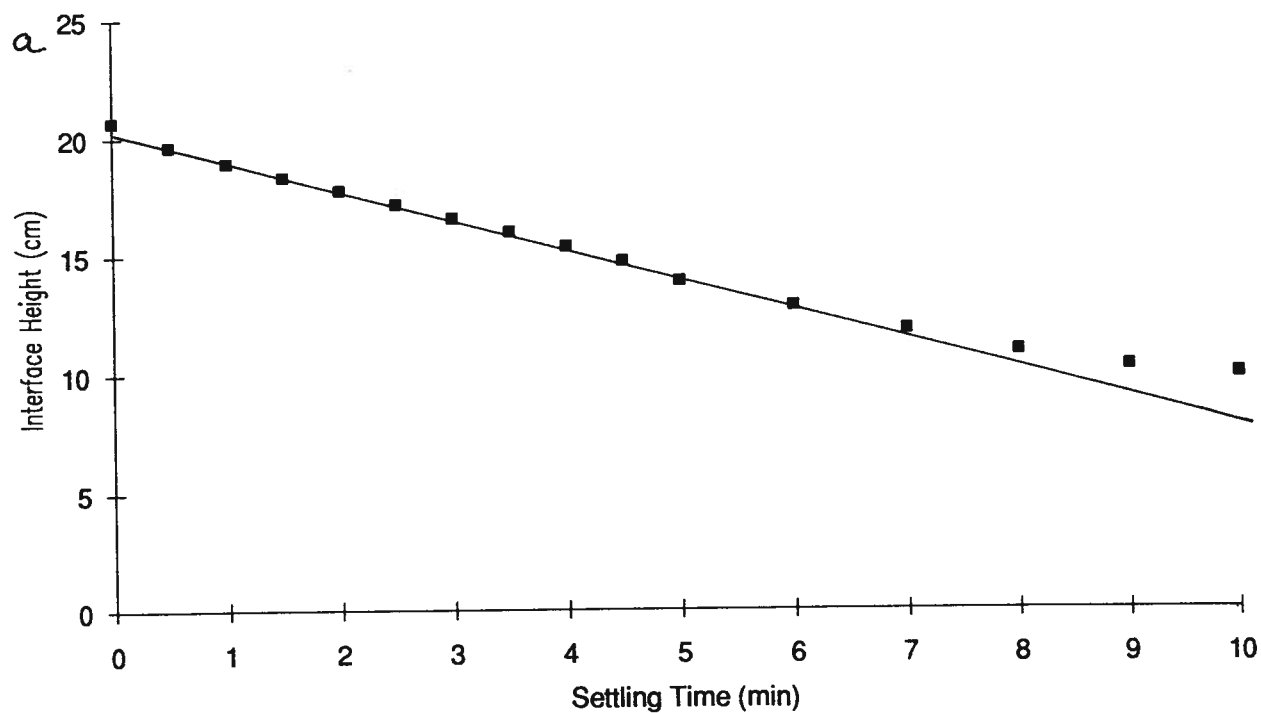


Figure AVL12 a) Settling curve and b) fitted (Casson model) flow curve for experimental Run #12 ($\phi_{sv}=0.20$, $\phi_r=0.199$, $d_v/d_l=0.22$, pH=8.29).

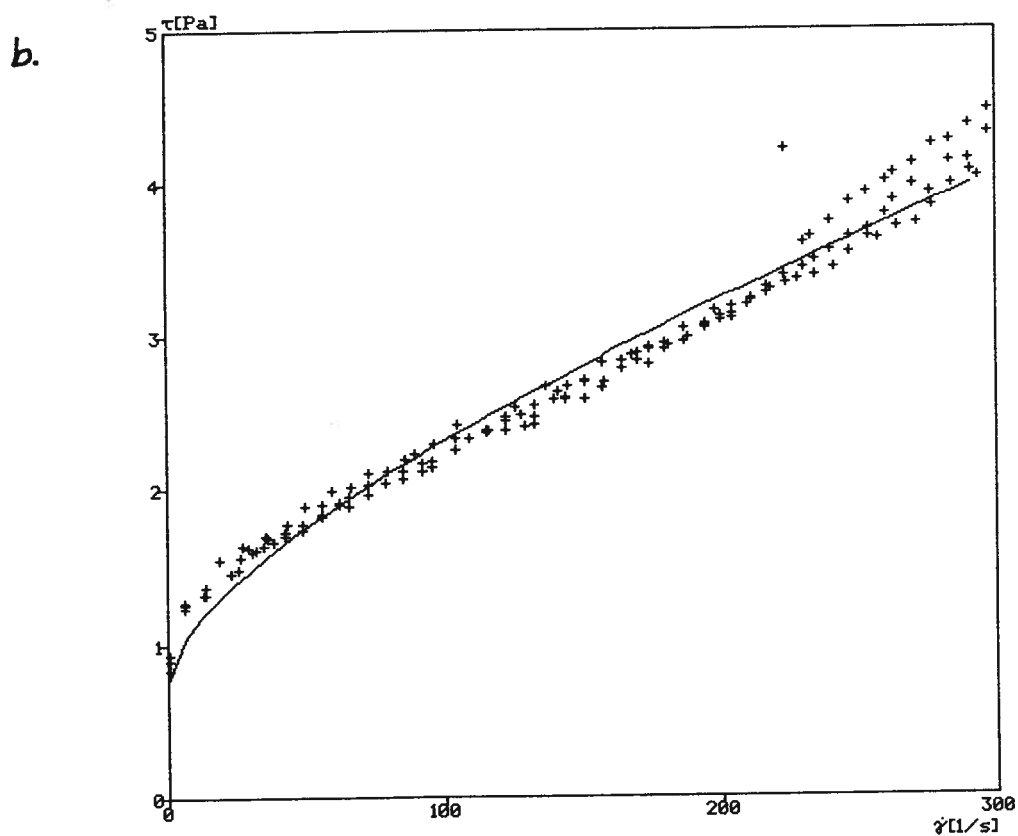
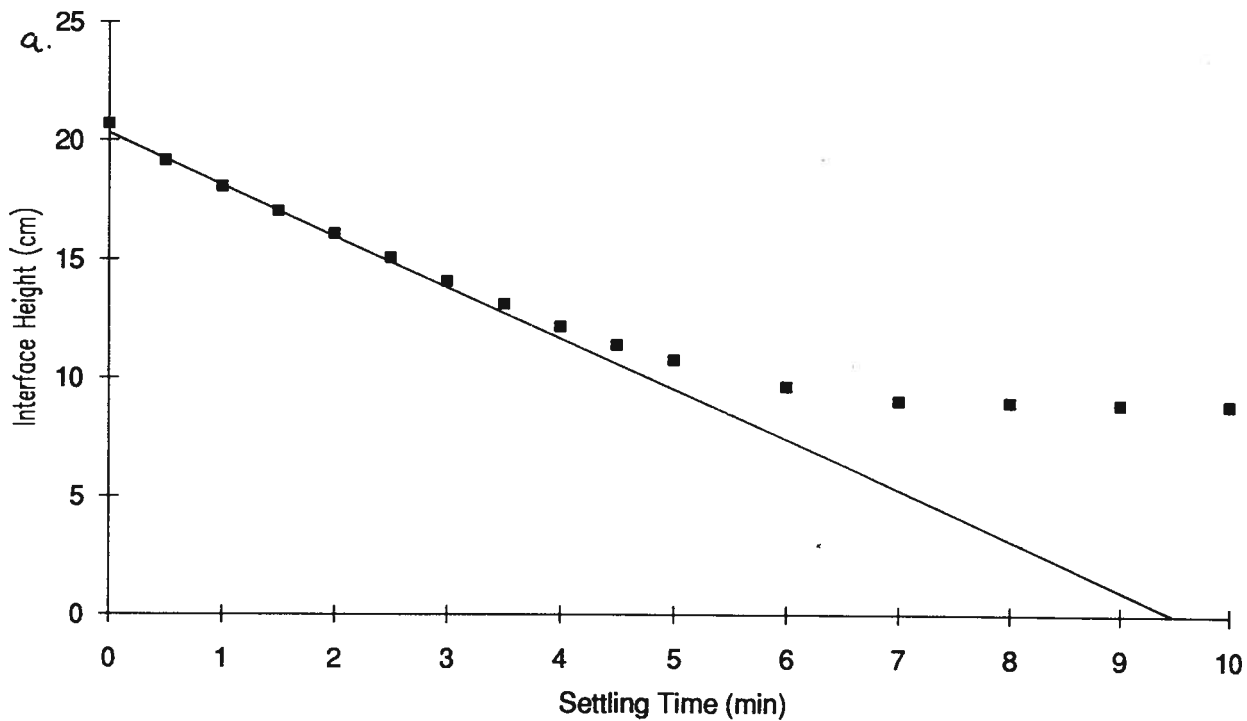


Figure AVL13 a) Settling curve and b) fitted (Casson model) flow curve for experimental Run #13 ($\phi_{sv}=0.284$, $\phi_r=0.325$, $d_v/d_l=0.22$, pH=8.27).

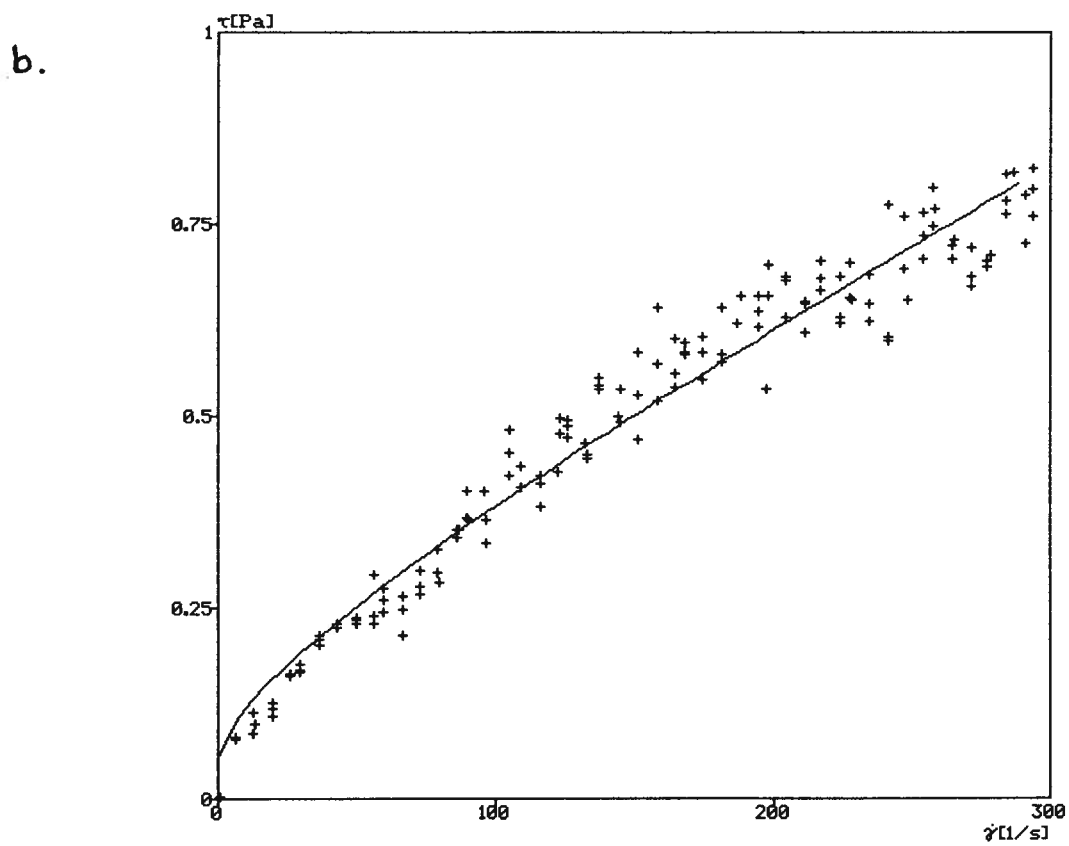
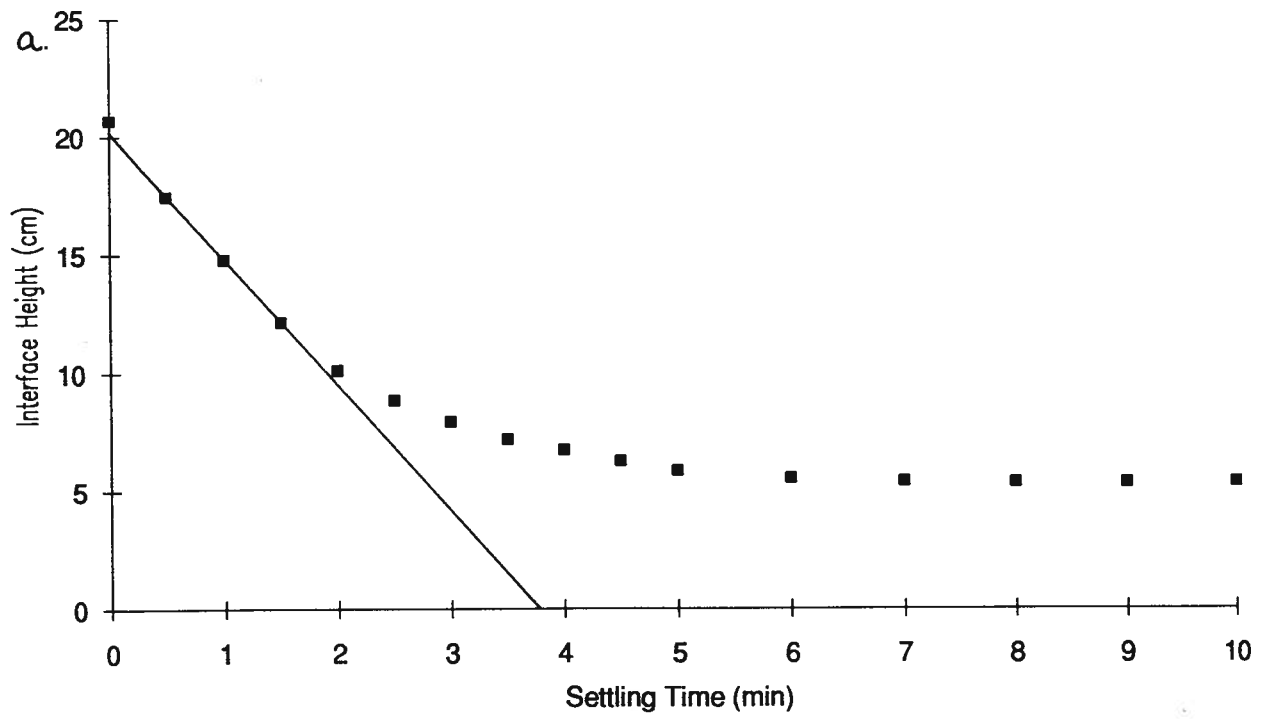


Figure AVL14 a) Settling curve and b) fitted (Casson model) flow curve for experimental Run #14 ($\phi_{sv}=0.116$, $\phi_f=0.325$, $d_f/d_i=0.22$, $pH=8.41$).

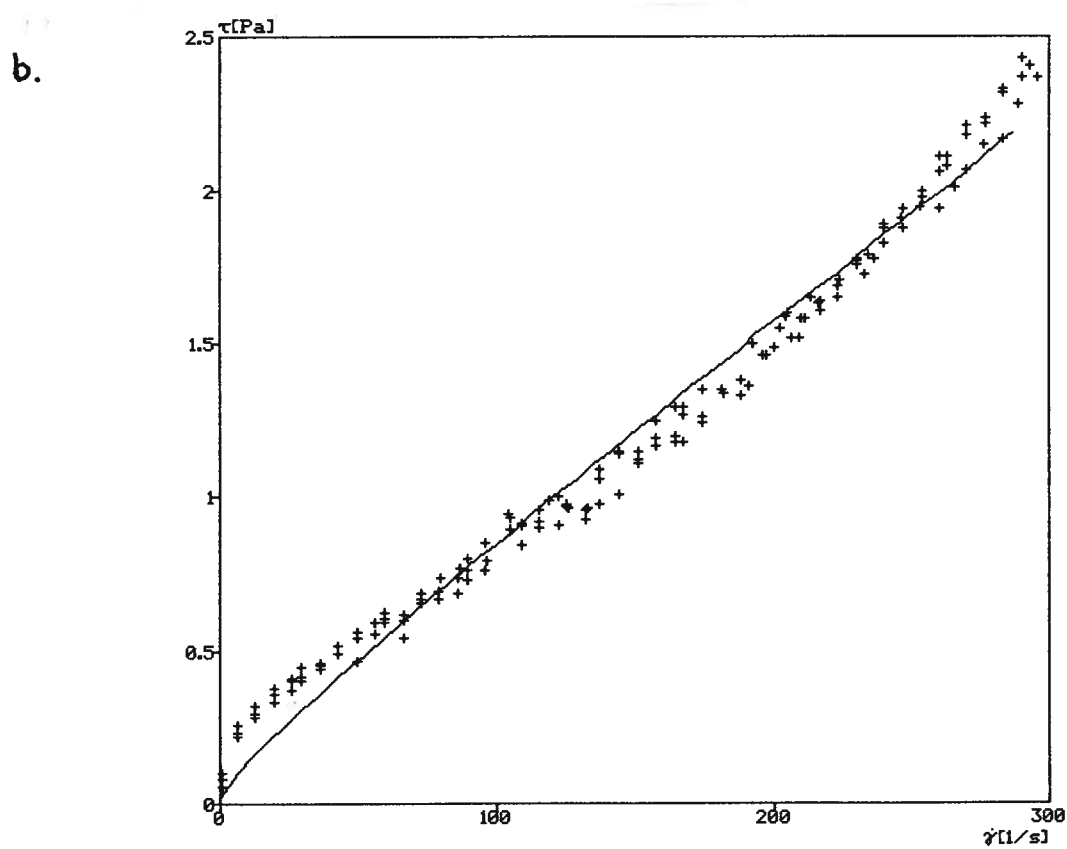
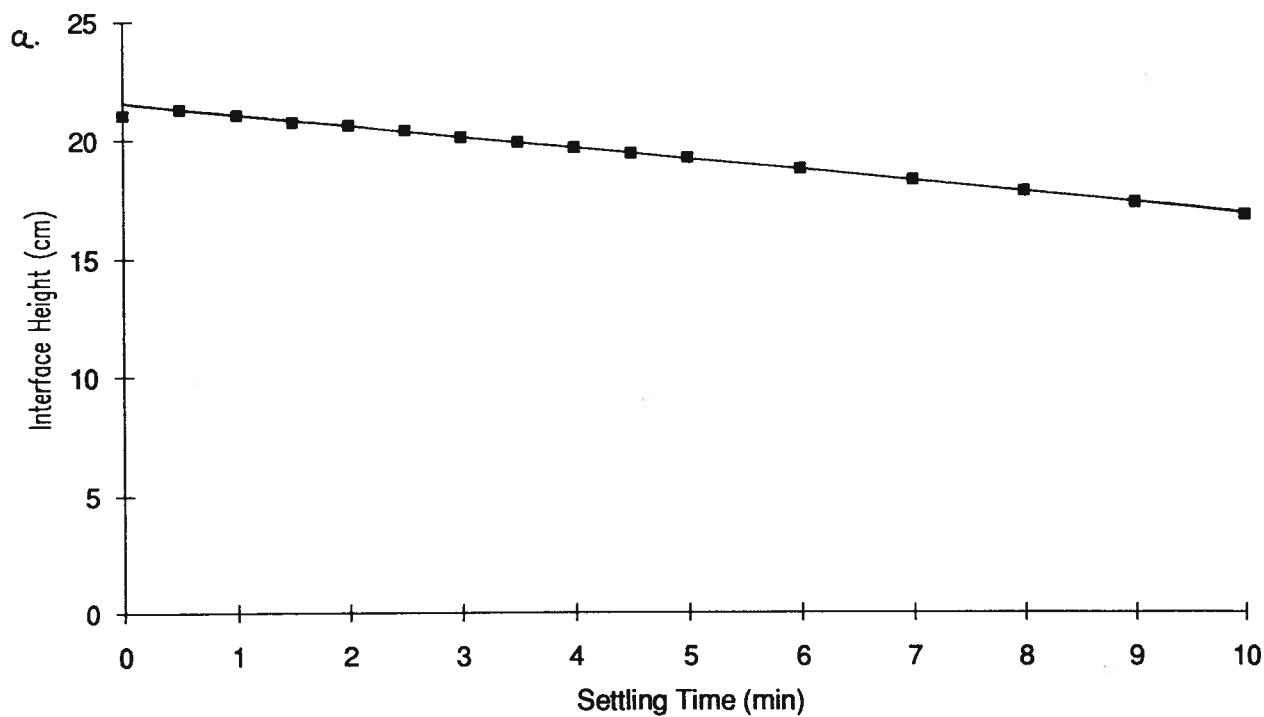


Figure AVL15 a) Settling curve and b) fitted (Casson model) flow curve for experimental Run #15 ($\phi_{sv}=0.20$, $\phi_f=0.325$, $d_f/d_i=0.22$, $pH=8.42$).

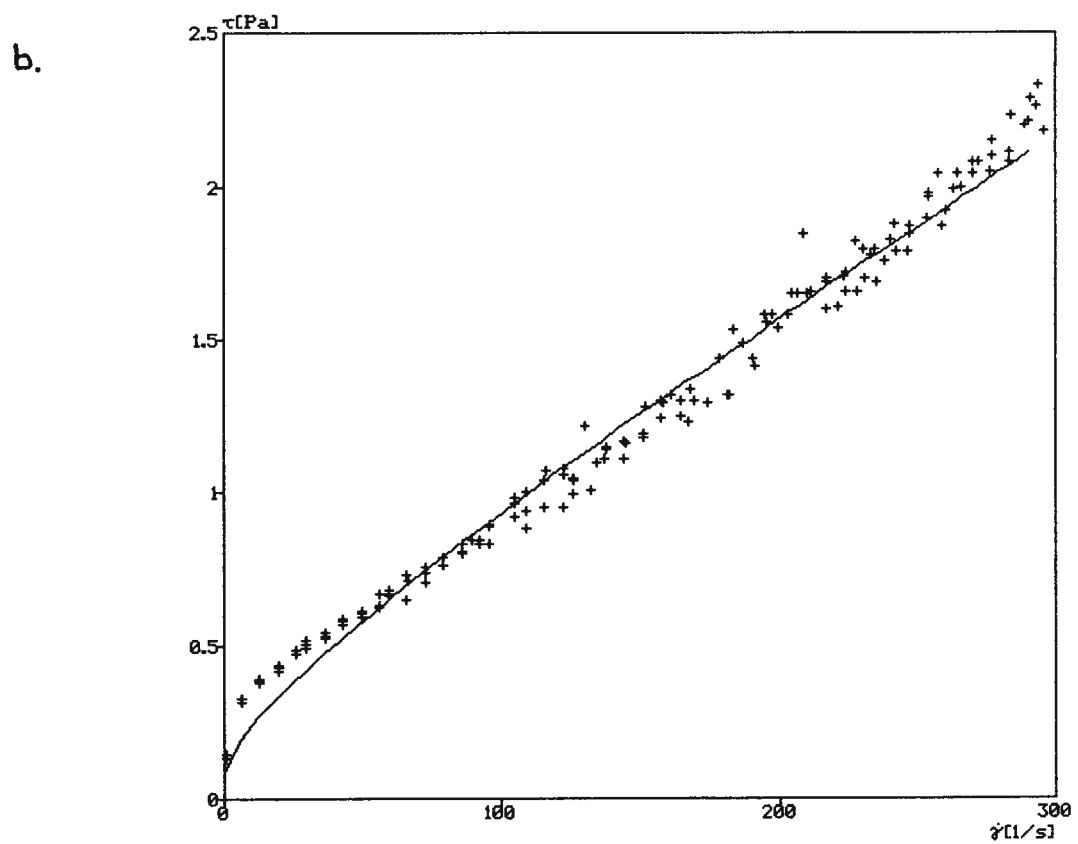
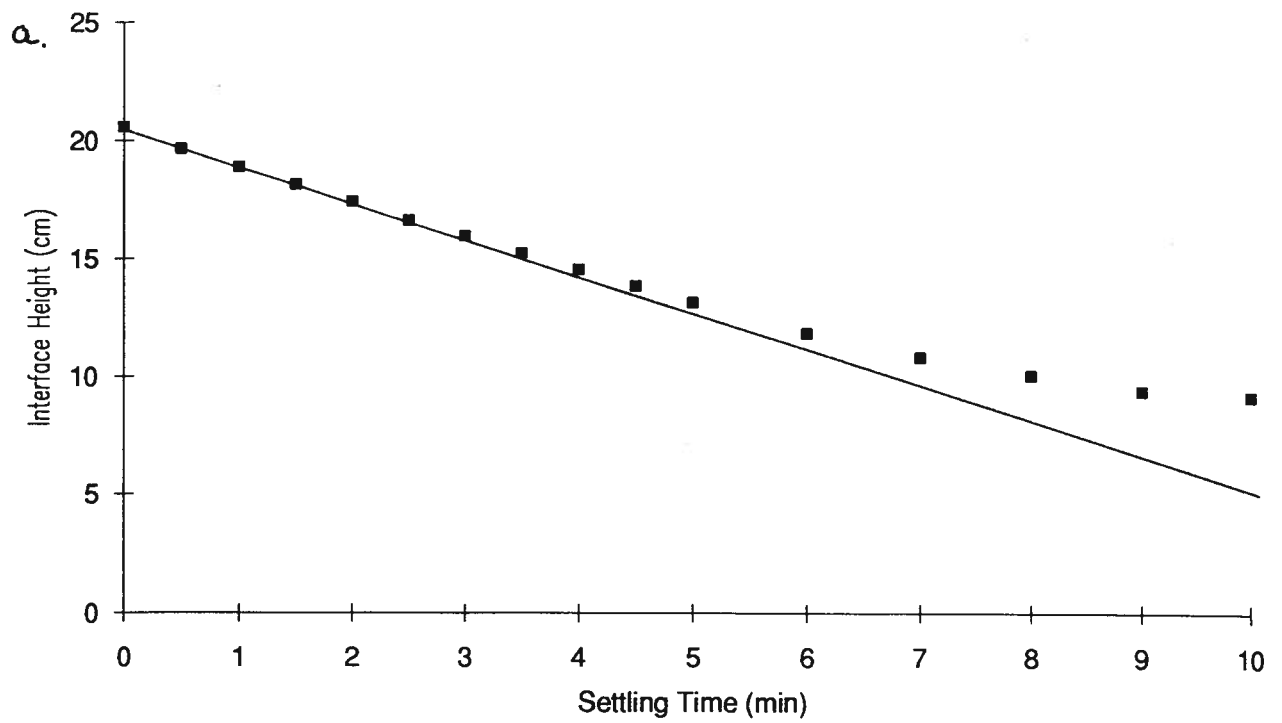


Figure AVI.16 a) Settling curve and b) fitted (Casson model) flow curve for experimental Run #16 ($\phi_{sv}=0.20$, $\phi_f=0.325$, $d_s/d_f=0.22$, $pH=8.94$).

APPENDIX VII

Statistical Analyses of

Modelled Media Properties

Table VII.1 Statistical analysis of the model for the Casson yield stress as a function of particle size distribution parameters.

Variable	Coefficient	Standard Error	T-statistic	Probability (2-Tail)
Solids	-9.53	2.20	-4.33	0.001
Fines x Solids	28.3	5.48	5.15	0.000
Ratio ²	6.12	1.51	4.06	0.002
Solids ²	31.0	6.75	4.59	0.001
Ratio x Fines x Solids	-87.7	16.5	-5.32	0.000

Multiple Index, R^2 : 0.894

Analysis of Variance				
Source	Sum of Squares	Degrees of Freedom	Mean Square	Probability
Regression	3.99	5	0.797	0.000
Residual	0.474	11	0.043	

Table VII.2 Statistical analysis of the model for the Casson viscosity as a function of particle size distribution parameters.

Variable	Coefficient	Standard Error	T-statistic	Probability (2-Tail)
Ratio	-45.6	9.85	-4.63	0.00
Solids	75.6	14.8	5.10	0.00
Ratio x Solids	261	48.4	5.41	0.00
Solids ²	-303	66.7	-4.54	0.00

Multiple Index, R^2 : 0.964

Analysis of Variance				
Source	Sum of Squares	Degrees of Freedom	Mean Square	F-ratio
Regression	331.7	4	82.9	79.2
Residual	12.6	12	1.05	
				Probability
				0.000

Table VII.3 Statistical analysis of the model for settling velocity as a function of particle size distribution parameters.

Variable	Coefficient	Standard Error	T-statistic	Probability (2-Tail)
Constant	7.84	1.99	3.93	0.003
Ratio	32.5	4.50	7.22	0.000
Fines	-3.11	1.25	-2.49	0.034
Solids	-76.1	17.3	-4.41	0.002
Ratio x Solids	-97.1	19.1	-5.08	0.001
Ratio ²	-10.4	3.25	-3.20	0.011
Solids ²	188.6	41.3	4.66	0.001

Multiple Index, R²: 0.973

Analysis of Variance				
Source	Sum of Squares	Degrees of Freedom	Mean Square	Probability
Regression	38.8	6	6.47	0.000
Residual	1.08	9	0.119	